Experimental Investigation and Finite Element Nonlinear Analysis of Continuous Composite Curved Multi-Cell Box-Girder Bridges

By

GuoQiang Xi

Dissertation submitted to the Faculty of Graduate Studies and Research
in partial fulfillment of the requirements for the degree of
Doctor of Philosophy
in Civil Engineering

Under the Supervision of
Dr. S.F. Ng and Dr. M.S. Cheung

Department of Civil Engineering
The Doctor of Philosophy Program in Civil Engineering is a joint program
with the Carleton University, administered by the Ottawa-Carleton Institute
for Civil Engineering

University of Ottawa
Ottawa, Ontario, Canada

1998

0-612-45201-8

Abstract

Studies on ultimate limit states and nonlinear behaviors of bridges will greatly enhance the understanding of bridge engineers on the moment and shear distribution and the general performance of bridges under load.

Described herein is an experimental and theoretical investigation of ultimate loads and nonlinear behaviors of two-span continuous composite curved multi-cell box-girder bridges with a single column as middle support and subjected to OHBDC design truck loadings. The curved bridges are modeled by using the finite element methods. The deck slab, webs, the bottom plate and diaphragms are modeled by 4-node shell elements while the shear connectors and the single middle column are modeled by 3-D beam elements. The existing software COSMOS/M is used for the analysis. A model test of a two-span continuous composite curved multi-cell box-girder bridge with a single column at the middle support is conducted to verify the finite element method. Idealized bridges with different parameters are also studied. Consideration is given to many of the variables that significantly influence ultimate loads and nonlinear behaviors of such bridges. Several rational suggestions are made to enhance the design of two-span continuous composite curved four-cell box-girder bridges.

Acknowledgement

I would like to express sincere gratitude to my supervisors Professor S.F. Ng and Professor M.S. Cheung for their patience, guidance and support throughout this study.

I would also like to express sincere thanks to the Ontario Government for providing me with an Ontario Graduate Scholarship for the duration of my Ph.D. program.

Sincere thanks are also due to the technical staff of the structural laboratory of the University of Ottawa in assisting me in the construction and testing of the curved bridge model.

To all professors in the committee of my thesis, who gave constructive comments, I express my sincere appreciation.

I am greatly indebted to my wife, Haiyan and my parents for their strong encouragement during the years of my study.

Dedication

This thesis is dedicated to my wife Haiyan, our daughter Monsa and my parents.

CONTENTS

List of Tables

List of Figures

Chapter 1

Introduction

1.1. General

Horizontally curved I-girder and box-girder bridges have been widely employed for more than thirty years. These bridges are mainly built as part of the modern highway system, especially as multilevel interchange structures. One single column is commonly used as the middle support according to the requirement of space limitation and aesthetics. The box section curved bridges are preferred in construction because of their capacity to resist torsion and warping. In addition, box girder bridges are often used due to their low weight and high longitudinal flexural stiffness. Curved box-girder bridges are composite structures where the deck slab is made of reinforced or prestressed concrete and the girder is made of steel. The concrete deck and the steel girder are connected by means of shear connectors.

In general, composite curved box girder bridges are much more difficult to analyze than bridges with open sections because of the highly indeterminate and complex structural interaction of the various components of the box-girder bridges. Earlier analytical efforts in box girder bridges were mostly limited to development of approximate theories. Extensive research and the use of digital computers in bridge design have resulted in the evolution of various methods of analysis and design of curved I-girder and box-girder bridges and also the development of many specialized and general purpose computer programs. Studies on horizontally curved I-girder bridges are much more common than on curved box girder bridges. In 1969, McMannus et al., cited 202 references in the study of horizontally curved bridges, out of which only four dealt with bridges with box girders. Later, the ASCE-AASHTO Committee (1978) summarized early research works on curved box-girder bridges, which included static and dynamic analytical methods and experimental studies. One hundred and six references were cited on the studies of curved box beams and box-girder bridges.

A comprehensive and systematic research effort to investigate the behavior of curved steel girder bridges was sponsored by the Federal Highway Administration between 1969 and 1976. This project, referred to as CURT (Consortium of University Research Teams) coordinated, evaluated and produced extensive information on the static and dynamic behaviors of curved girder bridges. From this extensive research it is concluded that a proper analysis and design of curved girder bridges can be accomplished only through the use of digital computers.

Many numerical analysis methods are utilized in the study of curved girder bridges, including the differential equation method, the planar grid method, the finite element method, and the finite strip method. However, the finite element method has been found to be more generally applicable. Hence, many commercial software packages of structural analysis have been implemented utilizing the finite element method.

Several analytical and numerical methods have been developed for the static linear and nonlinear analysis of curved box girder bridges. Some analytical and experimental studies of curved bridges have also been undertaken in order to develop a rational approach to analysis and design. However most of the researches conducted mainly focused on the elastic behaviors of such bridges. Few experimental and theoretical studies on the ultimate state and nonlinear behaviors of curved composite bridges had been reported.

Under service loads, horizontally curved box-girder bridges behave in the linear elastic range. However, studies on ultimate states and nonlinear behaviors of such bridges will greatly enhance the understanding of bridge engineers on the moment and shear distribution as well as the general performance of bridges under load.

1.2. Research objectives

Few experimental and theoretical studies dealt with the ultimate loads and the nonlinear responses of curved box-girder bridges. The purpose of this experimental and theoretical study is to investigate the ultimate loads and the nonlinear responses of two-span continuous composite four-cell curved box-girder bridges with a single column at the middle support under the OHBDC design truck loading system.

1.3. Scope

The study involves the experimental study and a general parametric study. A two-span continuous composite four-cell curved box-girder bridge model with a single column at the middle support is constructed and tested under the simulated OHBDC design truck loading system. The nonlinear behavior and the ultimate load of the bridge model are observed. The experimental bridge was modeled using the finite element technique. The shell element, the beam element and the truss element are utilized in the analysis model. The shear connectors and the single middle column are modeled by using 3-D beam elements. The results of the analytical model are verified by the experimental data. Various parametric studies are also carried out to determine the effect of the various parameters on the nonlinear and ultimate performance of curved box-girder bridges. Only some major parameters are investigated by using the finite element analysis. The significant parameters included in this study are the distribution of load on the bridge deck, the curvature of the curved bridges, the stiffness of the shear connectors, the stiffness of the middle support, and the location of the middle support.

Chapter 2

Literature Review

2.1. General

Experimental studies and field studies of curved box girders that are reported are relatively few. However, they are extremely important and have served to assess the adequacy of the analytical theories. Generally, field studies, although expensive to carry out, provide invaluable data on the actual performance of such bridges.

Meanwhile, many numerical analysis methods have been developed over the past decades for the analysis of the curved box-girder bridges. These methods include the planar grid method, the space frame method, the finite strip method, the finite difference method, the finite element method, and the closed form method. These methods are the basis for the computer programs that are presently used for research as well as design. However, the finite element method has been proven to be the most accurate technique to model and analyze bridges with closed sections. It has been credited as a powerful tool for presenting solutions to complex structures. Several solutions are found for the static and dynamic analysis of girders and bridges. (Chu and Pinjarkar 1971, Bazant and Nimieri 1974, Fam and Turkstra 1975, Rabizadeh and Shore 1975, Chu and Jones 1976) The bridge structures are discretized by using various elements such as annular plates, shells, trusses, and beams. A possible disadvantage may occur in the application of finite elements when applied to large structures, in that computer storage problems may arise or the computing cost may be prohibitively expensive, especially, in the case of nonlinear analysis of such large structures. However, in recently years, with the computer becoming much faster and the price of storage capacity dramatically lower, it is now feasible to conduct nonlinear finite element analysis even for relatively complicated large structures.

Studies of horizontally curved bridges were introduced by McMannus et al. in 1969, but only four research studies dealt with box girders. In 1978, the ASCE-AASHTO Committee (1978) summarized early research works on curved box-girder bridges, which included static and dynamic analytical methods and experimental studies. One hundred and six references were cited on the studies of curved box beams and box-girder bridges.

The finite element method has been chosen for the ultimate load and nonlinear analysis of curved box girder bridges in this thesis using the COSMOS/M structural analysis software package presently available at University of Ottawa.

2.2. Review of experimental studies

A few experimental studies were conducted to investigate the ultimate load and nonlinear behaviors of curved box-girder and I-girder bridges. Scordelis and Larsen (1977) reported the testing of a two-span reinforced concrete curved box girder bridge model. Both linear responses and ultimate strength of the bridge model were investigated. In the analysis of linear responses and ultimate strength, the results showed that the bending moments obtained from the finite element analysis and from the experiments were in good agreement, but the theoretical maximum deflection was 1.5 times greater than the experimental deflection. Ultimate state and nonlinear behaviors on steel-concrete composite curved I-beams were investigated by Colville, J. (1973) by using both theoretical and experimental methods. The ultimate load capacity was estimated based on the capacities of both bending and torsional moments. Although the ultimate load was predicted accurately, the deflections were again rather different between the theoretical and experiment results. Yabuki, T. et al (1995) presented a numerical method for predicting the influence of local buckling in component plates and distortional phenomenon on the ultimate strength of thin-walled, welded steel box girders curved in plan. A modified stress-strain curve allowing for local buckling of plate components was proposed. The effect of distortion was considered by incorporating additional strain in the reference stage of the incremental process in the nonlinear flexure analysis. Theoretical predictions obtained using the proposed method were compared to experimental test results. Nonlinear behavior of the test girders was illustrated and reasonable agreement between tests and theory was observed.

2.3. Review of the Finite Element Method

During the past three decades, finite element analytical methods have rapidly become a very popular technique for the computer solution of complex problems in engineering. At present, the method represents one of the most general analysis tools and is used in practically all fields of engineering analysis. In structures, the method can be regarded as an extension of earlier established analysis techniques, in which a structure is represented as an assemblage of discrete elements interconnected at a finite number of nodal points.

Development of the finite element method has followed three main lines:

1. Displacement-based formulation
2. Force-based formulation

3. Hybrid formulation

The force-based finite element formulation can be understood as an extension of the flexibility method whereas the displacement-based formulation can be regarded as a continuation of the displacement method in structural analysis both of which had been used for many years in the analysis of beams, trusses and framed structures. Although many of the concepts which pertain to the force-based formulation are, in many cases, directly applicable to the displacement formulation, the latter approach seems to be more popular in the literatures (Robert D. Cook 1981; Bathe Klaus-Jurgen 1982)

In the displacement-based formulation, the basic steps in the analysis can be summarized as follows:

1. The structure is modeled using suitable finite elements by subdividing its solution domain into discrete elements. Element type must be selected such that its structural response in terms of strains and deformation reflects, realistically, the components of the actual prototype. In case of box girder structures, plate bending or shell elements are usually selected. Furthermore, in this step one must decide upon the number, size and the arrangement of the elements in the discretized structure.

2. Since the displacement solution cannot be predicted exactly one must assume a suitable displacement function within the element to approximate the unknown solution. The assumed functions must be simple and should satisfy certain convergence requirements such as compatibility and completeness. The former requirement implies that the displacements within the elements and across the element boundaries must be continuous. The latter requirement ensures that the element can represent the rigid body displacements and the constant strain states. (Bathe Klaus-Jurgen 1982)

In general, the interpolation displacement function is taken in the form of polynomials, which merely describes the solution displacements at any point in the element space in terms of the nodal displacements.

3. From the kinematics of the problem at hand, element strains are obtained by using the appropriate strain-displacement relations. Moreover, element stresses are evaluated, depending on material model selected, by using appropriate stress-strain relationships. Once these relationships or matrices are established, the stiffness matrix [Ke] and load vector {Re} on the element level can be derived by using either equilibrium conditions or a suitable variational principle such as the minimization of total potential energy.

4. Since the structure is composed of several finite elements, the individual element stiffness matrices and load vector are to be assembled in a suitable manner taking into consideration any transformation of element local coordinates into the structure global coordinates. Hence the overall equilibrium equation can be formulated as [K]{U}={R}, where [K] denotes the assembled or global stiffness matrix and {U}, {R} denote structure nodal displacement and external force vectors respectively.

5. In this step, one modifies the overall equilibrium equations by imposing the boundary conditions and hence one solves for the unknown displacement vector.

6. Once the nodal displacements are known, one can solve for the element strains and stresses by using the element strain-displacement and stress-strain matrices respectively.

In the earliest work on the analysis of curved box girder bridges by the finite element method, the curvilinear boundaries were approximated by a series of straight ones. In most cases, the structure was idealized by rectangular elements for the webs and quadrilateral elements for the flanges.

Anija and Frederic (1971) divided their one-cell single span curved box girder into 240 panels. The flange elements were treated as flat plate elements with curved boundaries, whereas the webs, which are cylindrically curved plates, were treated as flat rectangular elements. Comparison between the finite element results and the experimental findings showed poor agreement and they concluded that flat elements cannot adequately represent the behavior of curved structures.

William and Scordelis (1972) presented a linear elastic analysis and computer program CELL for cellular structures of constant depth with arbitrary geometry in plan view. The multi-plate structure was idealized by means of improved quadrilateral or triangular elements containing both membrane and flexural stiffness. The special elements were developed using both mixed and displacement formulations. They tested their elements for a two-cell simply supported straight and a continuous highway bridge and concluded that the mixed formulations yielded more accurate results than the displacement-based models.

Bazant and EL Nimeiri (1974) attributed the problems associated with the neglect of curvilinear boundaries of the curved box beam to the loss of continuity at the end cross sections of two adjacent elements meeting at an angle. The presence of such discontinuity violates the assumptions of the classical bending theory that cross sectional planes are normal to the beam longitudinal axis. No attempt was made to remedy this problem by using curvilinear element boundaries. Instead, they developed the skew-ended finite element with shear deformation using straight elements and adopted a more accurate theory, which allows for transverse shear deformations and hence does not require the cross sections to be normal to the beam axis.

Although curvilinear boundaries may be idealized by straight edges, the number of the elements must be high enough to achieve a satisfactory solution. Such an approach is impractical especially for highly and moderately curved box bridges. The advantages of curved flat and shell elements have been demonstrated by Fam and Turkstra (1972) both at the element level and at the three dimensional structural level. In 1975, Fam and Turkstra (1975) described a finite element scheme for static and free vibration of box girders with orthogonal boundaries and arbitrary combinations of straight and horizontally curved sections. The curved top and bottom flanges of the box were idealized by a 4-node plate bending annular element with two straight radial boundaries. To idealize the general case of inclined web members in the curved box, conical elements were used. The analysis included in-plane, bending and coupling action as well as anisotropic element properties. They tested their elements against results from folded plate theory and finite strip methods with sufficient harmonics for a twin-cell simply supported curved box girder bridge and reported good agreement.

The versatility of the finite element method has attracted the attention of many researchers (Aslam and Godden 1975; Fam and Turkstra 1976; Scotrdelis and Larsen 1977; Schelling, Heins and Sikes 1978) to analyze the complex mechanics of an arbitrary girder-diaphragm-cross-beam system. The numerical effectiveness as well as the flexibility of the method in linear, nonlinear, static or dynamic types of analysis attracted many investigators to use this technique as the basis of theoretical analysis in model studies of the multi-plate curved box structure.

Chapter 3

Experimental Study

3.1. General

The lack of data on the performance of curved box girder bridges especially in nonlinear and ultimate range has spurred analytical development in the finite element method and experimental investigations. Unfortunately, as is evident in the literature review, few experimental studies have been undertaken to investigate the ultimate strength and nonlinear behaviors of such bridges. While full scale experimental investigations could be cost-prohibitive, model testing has become a suitable compromise to verify analytical predictions of the structural responses.

Most experimental model studies involve simple girder bridges and bridge models subjected to idealized single point loads. In general, a large amount of previous experimental research work concentrated almost exclusively on investigations of elastic behaviors of bridges.

Continuous composite multi-cell curved box-girder bridges with a single column as the middle support are commonly used in practice. Cyrville road over the Queensway underpass in east Ottawa sets a good example of such a structure and hence it was selected as the prototype for the current model study. The structure is 102.4 m long, 12.8 m wide and consists of two spans with a 16.8 degrees horizontal angle of curvature between extreme ends of supports. A typical cross-section of box consists of four contiguous cells. The depth of the bridge is 1.83 m with prestressed diaphragms, two of which are located at the extreme end supports and one intermediately located over the single column support. The bridge was designed to be subjected to ASHTO design truck load HS20-44 by the Ministry of Transportation and Communication and was built in1973.

In this chapter a detailed description of the bridge model and its testing is presented. This includes model geometry, material properties, loading system, support details instrumentation, as well as test setup. An outline of test procedure and test results are presented. This experimental model study is used to verify the ultimate load and the nonlinear behaviors of the finite element model. Further, various parametric studies were also carried out using a similar finite element model and will be presented in chapter 5.

3.2. Bridge model

3.2.1. Model geometry and construction

The curved bridge model was rebuilt from a bridge model previously utilized for linear experimental study at University of Ottawa. The bridge model (Figure 3.1) was made from a composite of micro-concrete deck, aluminum cylindrical webs and aluminum bottom plate. The bridge model consists of three diaphragms, two of which are placed at the extreme ends and the third placed at the middle support. These transverse diaphragms were made from aluminum U-Channels. In order to generate the curved box girder (Figure 3.4), the curved webs were clamped in position and then welded to the bottom plate. Due to the heat release as a result of welding, and to minimize the possible warping of aluminum, spot welding was utilized. However, to allow horizontal movements, rockers were installed in the end support system (Figure

3.2) of the bridge model. Aluminum shear connectors with 8 mm in diameter were installed to the top flange of the webs at 80 mm c/c spacing, so that the slab would act as an integral part of the box girder.

A scale of 1/24 was adopted for the bridge model, and the centerline radius of curvature of the model was 14.554m. The bridge model width is 0.48 m and has a depth of 0.133m (Figure 3.1). The main geometrical dimensions of the curved bridge model are listed as follows: Central angle between end supports is 16.8°. Circumferential distance between end supports along the central web is 4,267 mm. Curvature radius of the central web is 14,554 mm. Width of the deck is 480 mm. Thickness of the deck is 20 mm. Width of the bottom flange is 400 mm. Thickness of the bottom flange is 6 mm. Depth of the cylindrical webs is 110 mm. Thickness of webs is 13 mm. And thickness of the diaphragms with U-channel is 6.0 mm. The details of the bridge prototype and the bridge model were described by Ng *et al.* (1993). The curved bridge model, which was used to investigate the elastic behaviors of the continuous composite curved bridges, was reconstructed in order to investigate the nonlinear behaviors of the curved box-girder bridge model. Because the old deck was extensively cracked, the deck was rebuilt with micro concrete and 25.4mm×25.4mm×16 welded wire fabric mesh, while the aluminum parts of the bridge model (Figure 3.4) were kept. The central column was modeled as the middle support (Figure 3.3) by means of a steel column with 80 mm in diameter and 200 mm in length instead of an aluminum one because of the relatively large deflection at the central support (Ng *et al.* 1993). All strain gages were checked, the damaged ones were replaced, and a number of additional strain gages where added to the model at sections 1, 4 and 9 as shown in Figure 3.1.

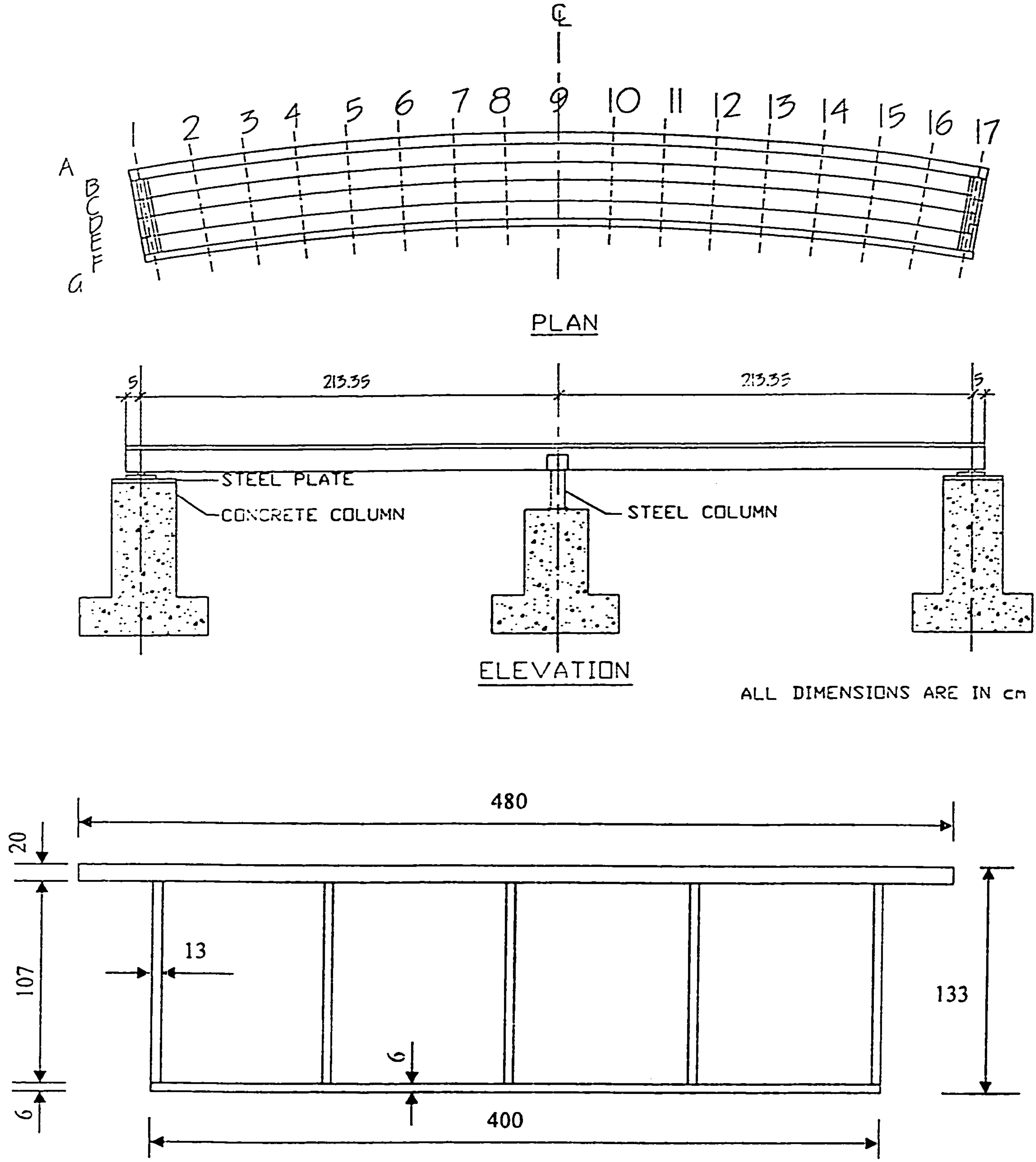

Figure 3.1 The curved bridge model

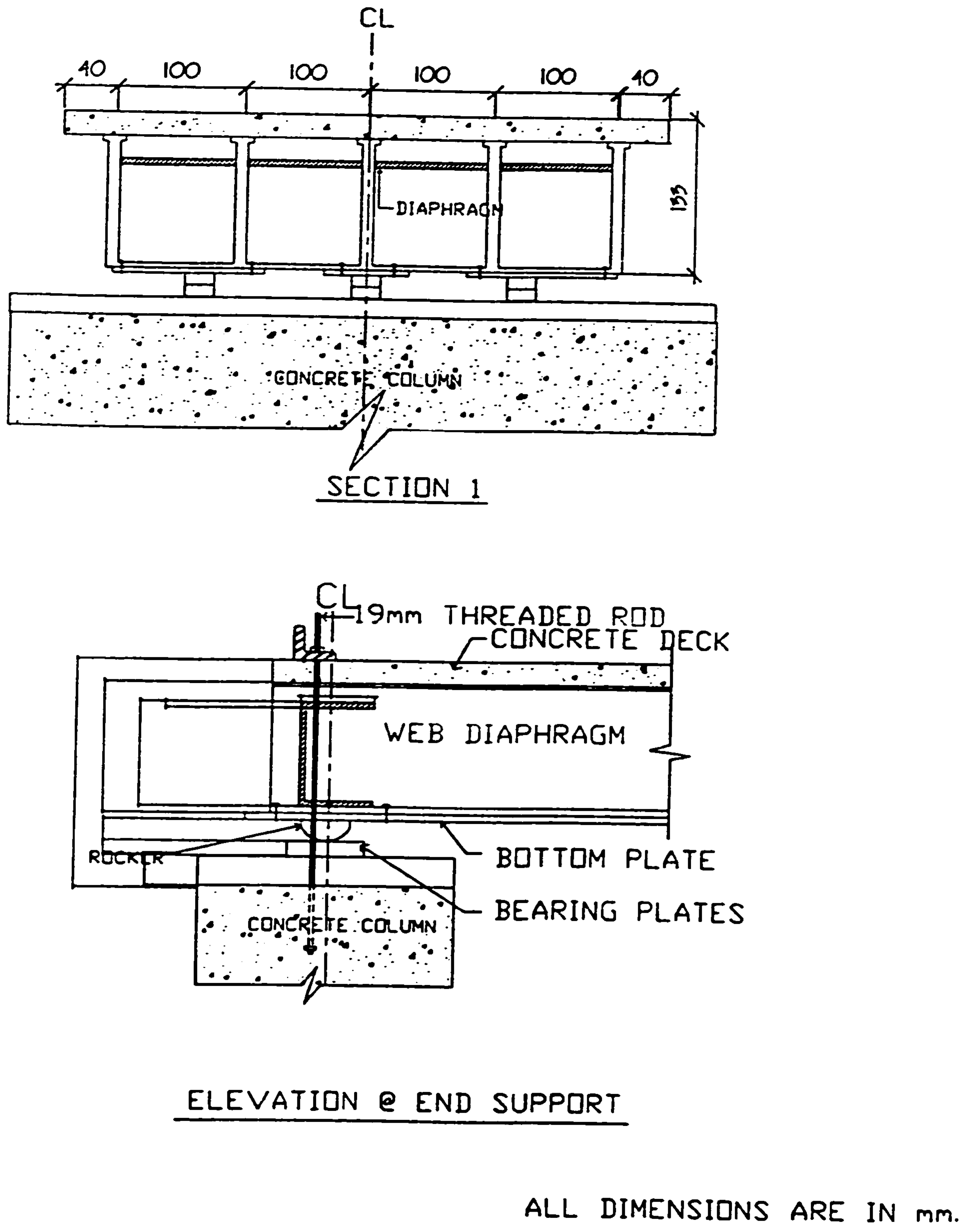

Figure 3.2 Details of the bridge model at the end support

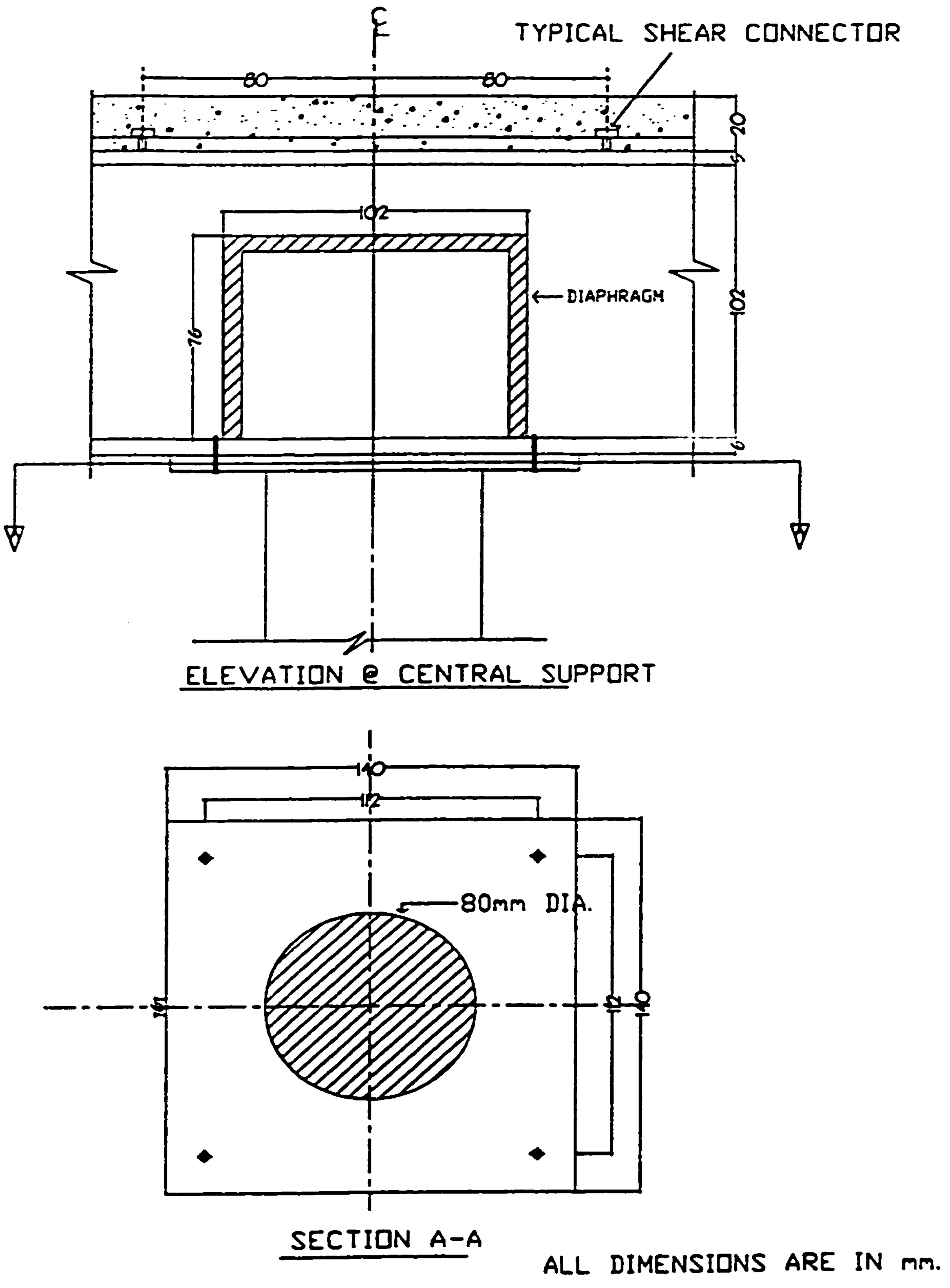

Figure 3.3 Details of the bridge model at the middle support

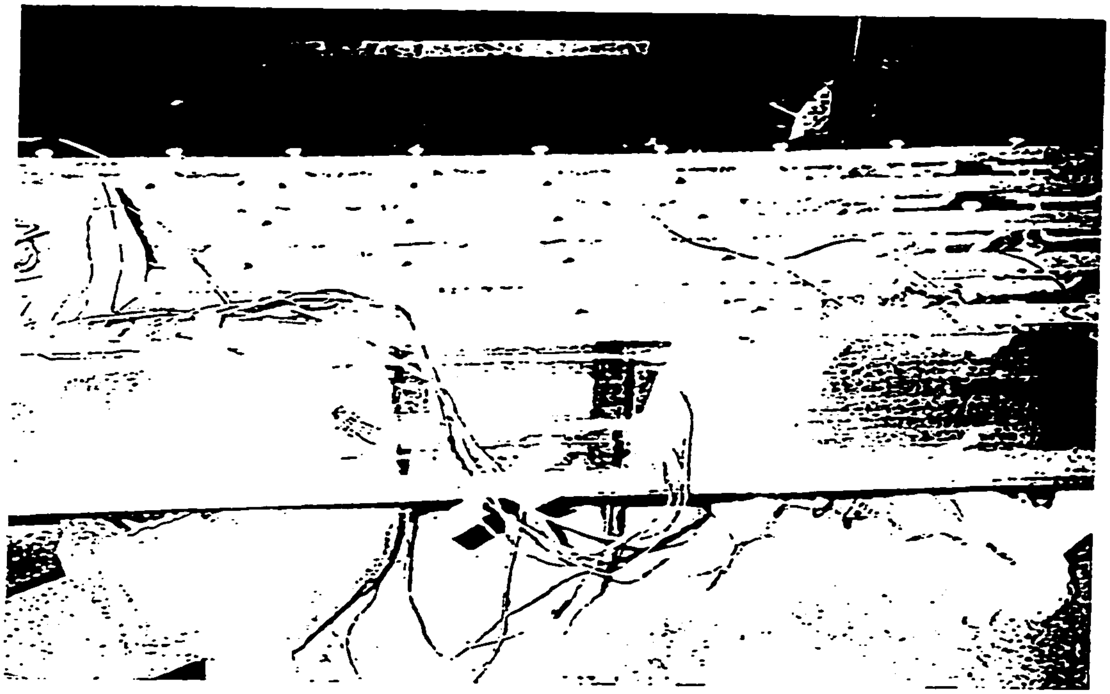

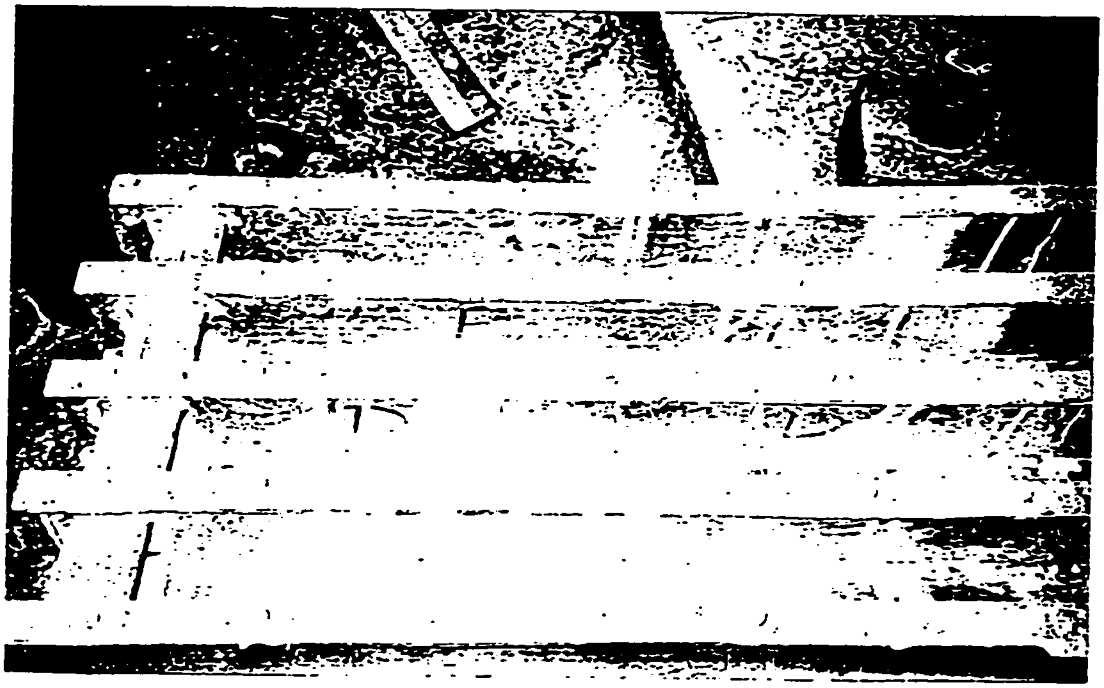

Figure 3.4 Aluminum box girder of the bridge model

The girder of the bridge model was loaded within the elastic range and all the strain gages were checked before the casting of the new bridge deck. The same stay-in-place formworks were adopted for the model's deck, except for the side formworks. Steel angles (1" × 1" L Shape) were utilized as the side formworks and bolted to the model. (Figure 3.5a)

A 1" × 1" × 16 WWF (Welded Wire Fabric) mesh was placed over the formworks as temperature and shrinkage reinforcement for the micro concrete deck. A high strength micro concrete with $f_c^{'}$= 60.0 MPa was prepared at University of Ottawa Structures Laboratory and the deck of the model was poured with thickness of 20.0 mm and cured for 28 days. (Figure 3.5b)

3.2.2. Material Properties

Regular concrete cannot be used to model the slab with the thickness of 20.0mm. Therefore, the micro concrete was chosen. The maximum aggregate size of No. 4 is used in the micro concrete mix design. An early high strength micro concrete mix design was adopted as presented in Table 3.1.

The model bridge deck was cast. At the same time, 30 cylinders (75mm × 150 mm or 3" × 6") (Figure 3.6) were also cast, to determine the mechanical properties of the micro concrete. At 7, 14 and at 28 days three cylinders were tested each time for compressive strength, as presented in Table 3.2. The other three cylinders were tested for tensile strength and the results are listed in Table 3.3. The mechanical properties of the micro concrete are as listed in Table 3.4.

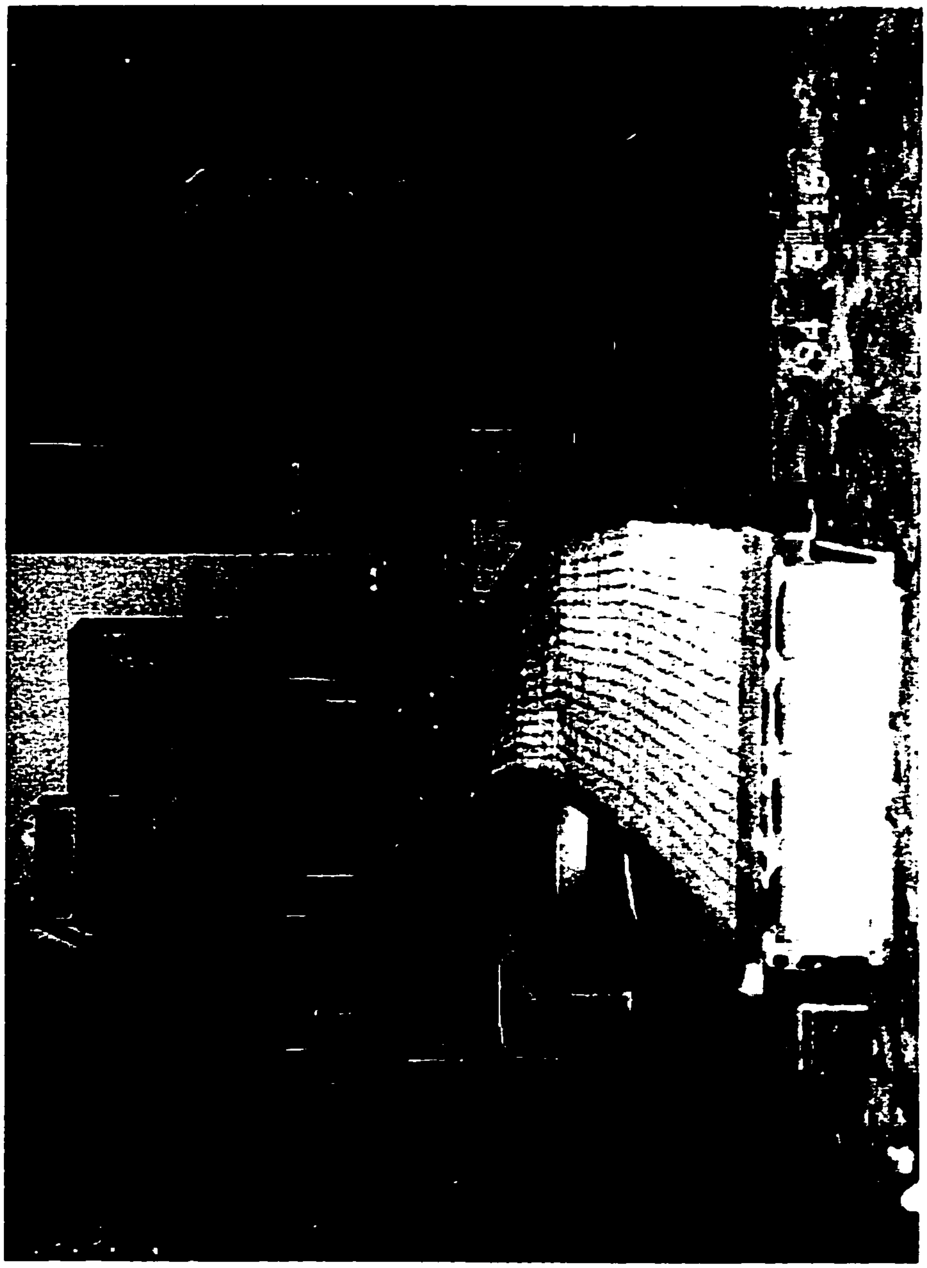

Figure 3.5a Formworks of the bridge model's deck

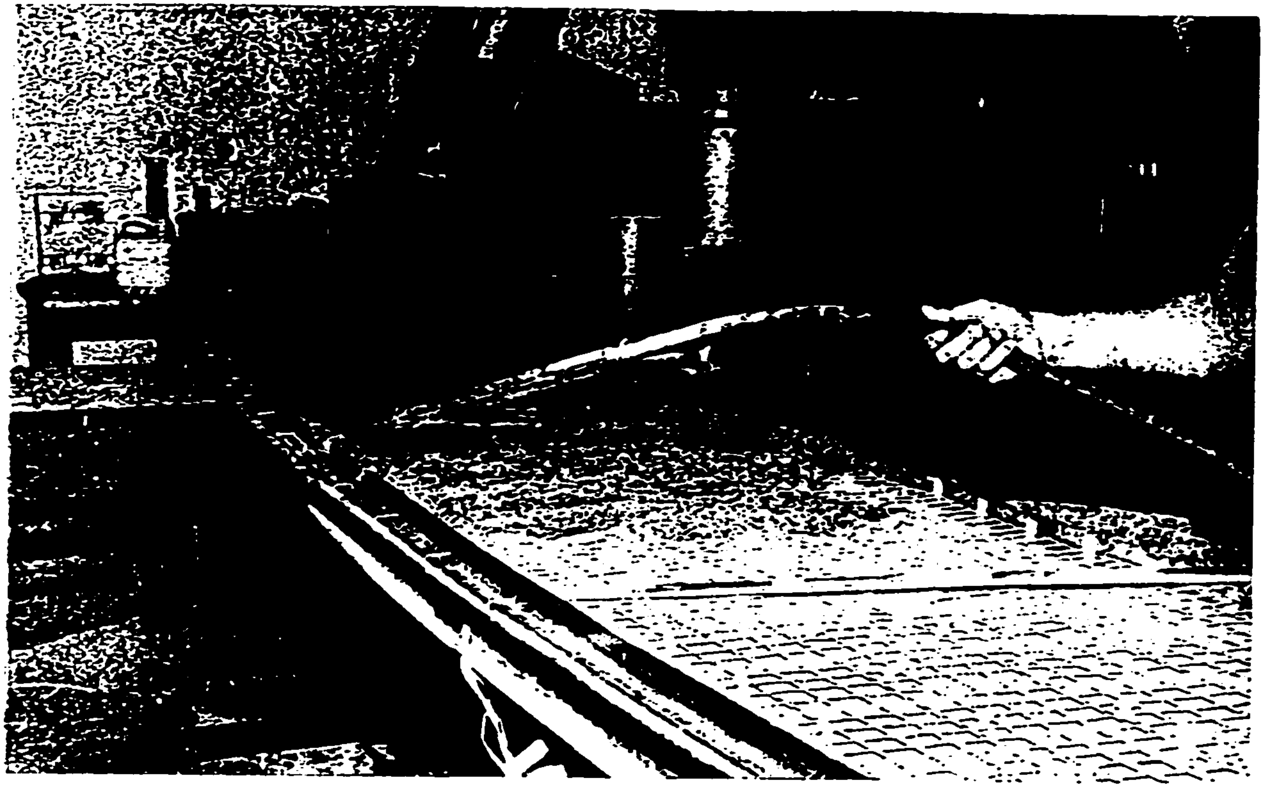

Figure 3.5b Pouring and curing of the bridge model's deck

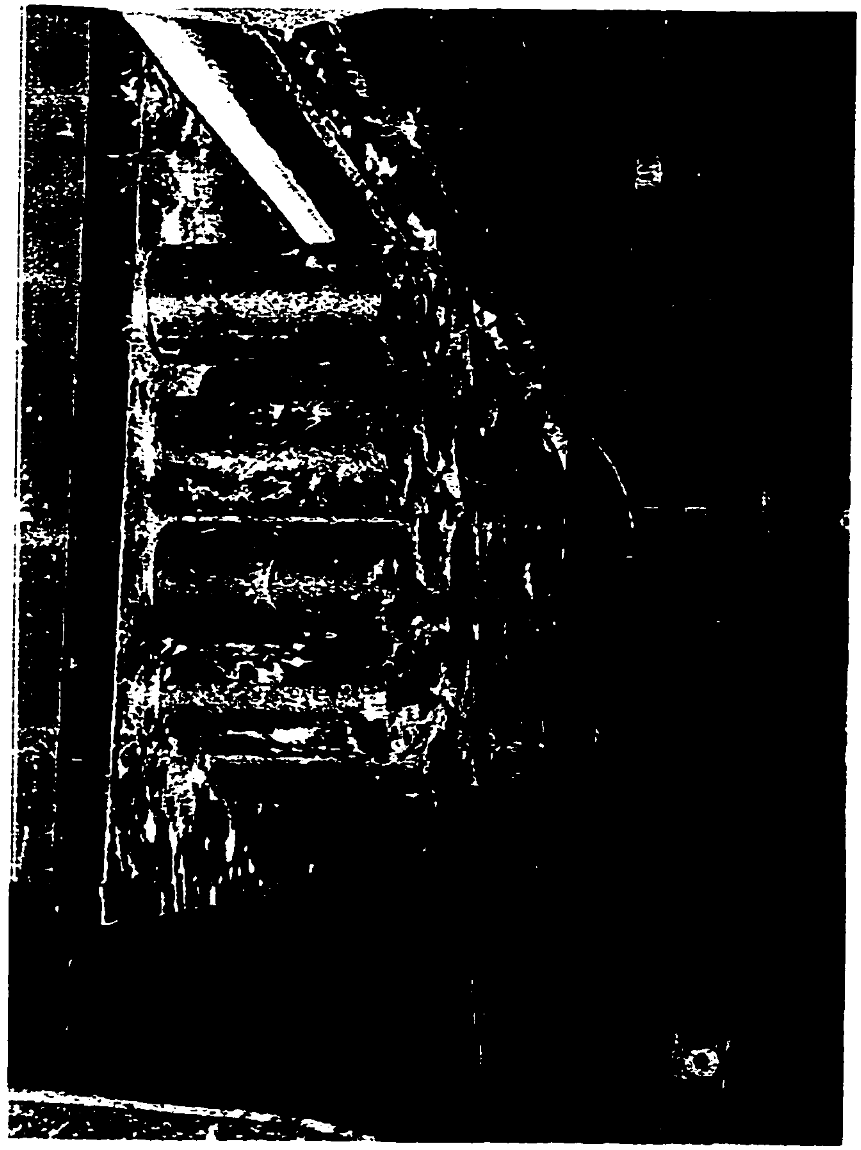

Figure 3.6   Pouring of the micro concrete cylinders

Before the nonlinear test, five cylinders were tested to verify the compressive strength of the micro concrete and to find the stress-strain relationship shown in Figure 3.7. It is found that the compressive strength of the micro concrete obtained before the nonlinear test is 10% greater than that of the micro concrete tested at 28 days. A typical stress-strain relationship of the micro concrete is presented in Figure 3.8. The secant modulus at a stress of 0.5fc' was adopted as the modulus of elasticity of the micro concrete.

Table 3.1 Micro Concrete Mix Design

Cement (Kg)	Silica Fume (Kg)	Water (Kg)	Fine Aggregates (Kg)	Super Plasticizer (Liters)	W/C
34.61	1.08	13.32	111.53	1.92	0.35

Table 3.2 Micro Concrete Compressive Strength

Cylinder	Compressive Strength (MPa)		
Number	7 days	14 days	28 days
1	46	52	58
2	38	48	53
3	50	45	56
Average	45	48	56

Table 3.3 Micro Concrete Tensile Strength

Cylinder #	Load Recorded (kN)	F'ct
1	62	3.508
2	99	5.600
3	55	3.110
Average	72	4.074

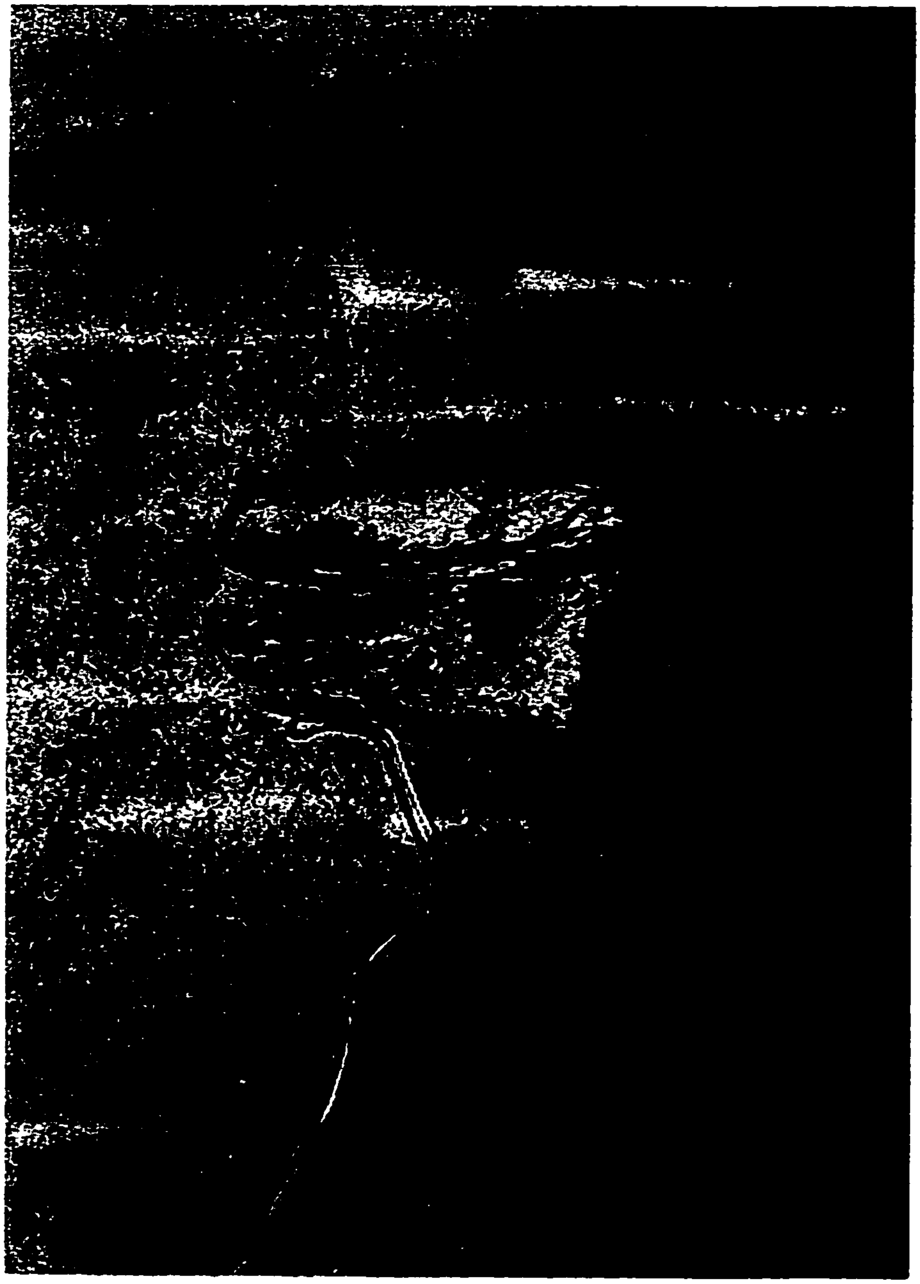

Figure 3.7 Testing of a typical micro concrete cylinder

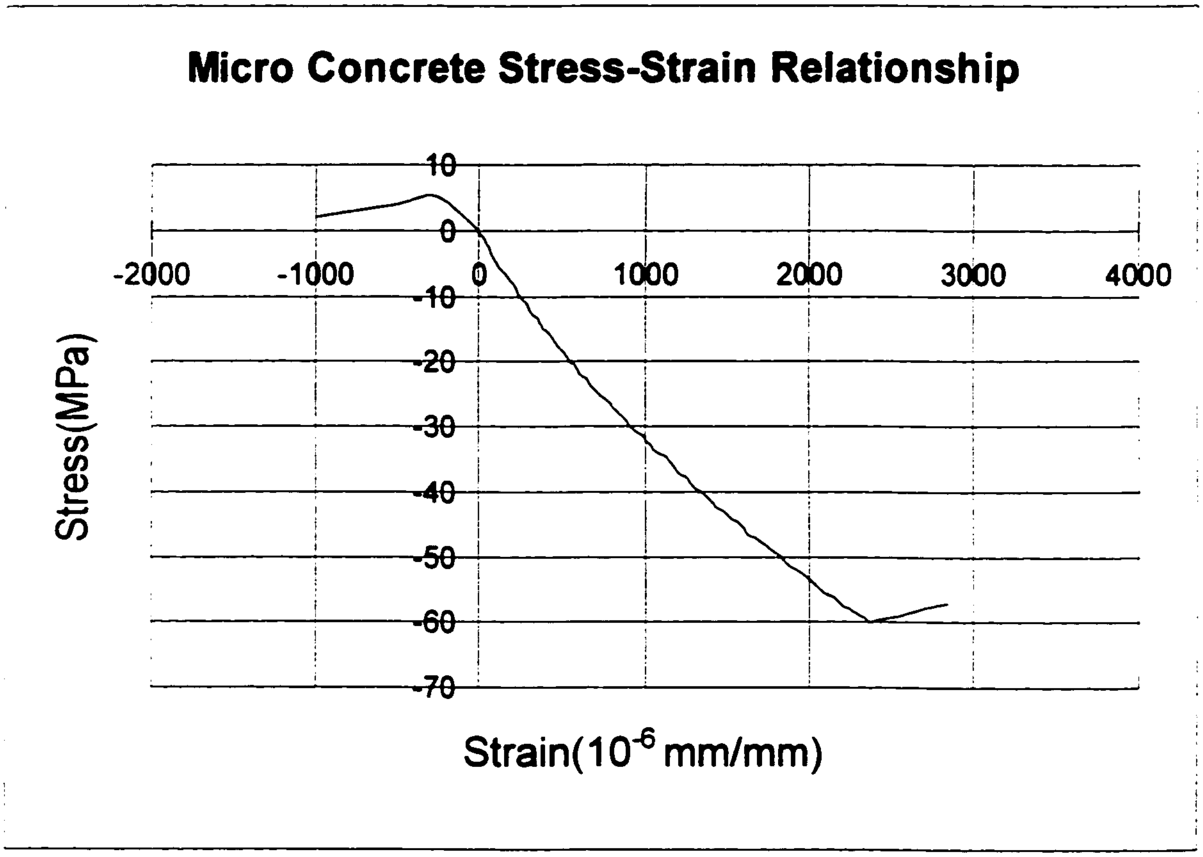

Figure 3.8 The stress-strain relationship of micro concrete

Table 3.4 Summary of the Micro Concrete

Property	Symbol	Magnitude
Compressive Strength (Mpa)	F'c	56.0
Tensile Strength (MPa)	F'ct	4.074
Modulus of elasticity(Mpa)	Ec	35,000
Poisson's Ratio	Vc	0.150

Table 3.5 Aluminum properties

Property	Symbol	Magnitude		
		Set A	Set B	Average
Ultimate Strength (MPa)	Fult	327	306	317
Yield Strength (MPa)	Fy	316	285	301
Modulus of Elasticity (MPa)	Ea	70277	72000	71100
Poisson's Ratio	Va	0.379	0.379	0.379

The aluminum alloy No. 6061-T6 was utilized for the webs, bottom plate, ends and middle diaphragms (Hachem 1988). Two sets of aluminum were tested, set A representing the bottom plate, and set B representing the webs, ends and middle supports. The results are tabulated in Table 3.5. The stress-strain relationship of the aluminum material was tested. The aluminum stress-strain relationship is shown in Figure 3.9.

3.3. Support and foundation

The bridge model was supported by means of three rockers at each end support, and by a single steel column support at the middle section. The details of the middle support and the end supports are shown in Figures 3.2 and 3.3.

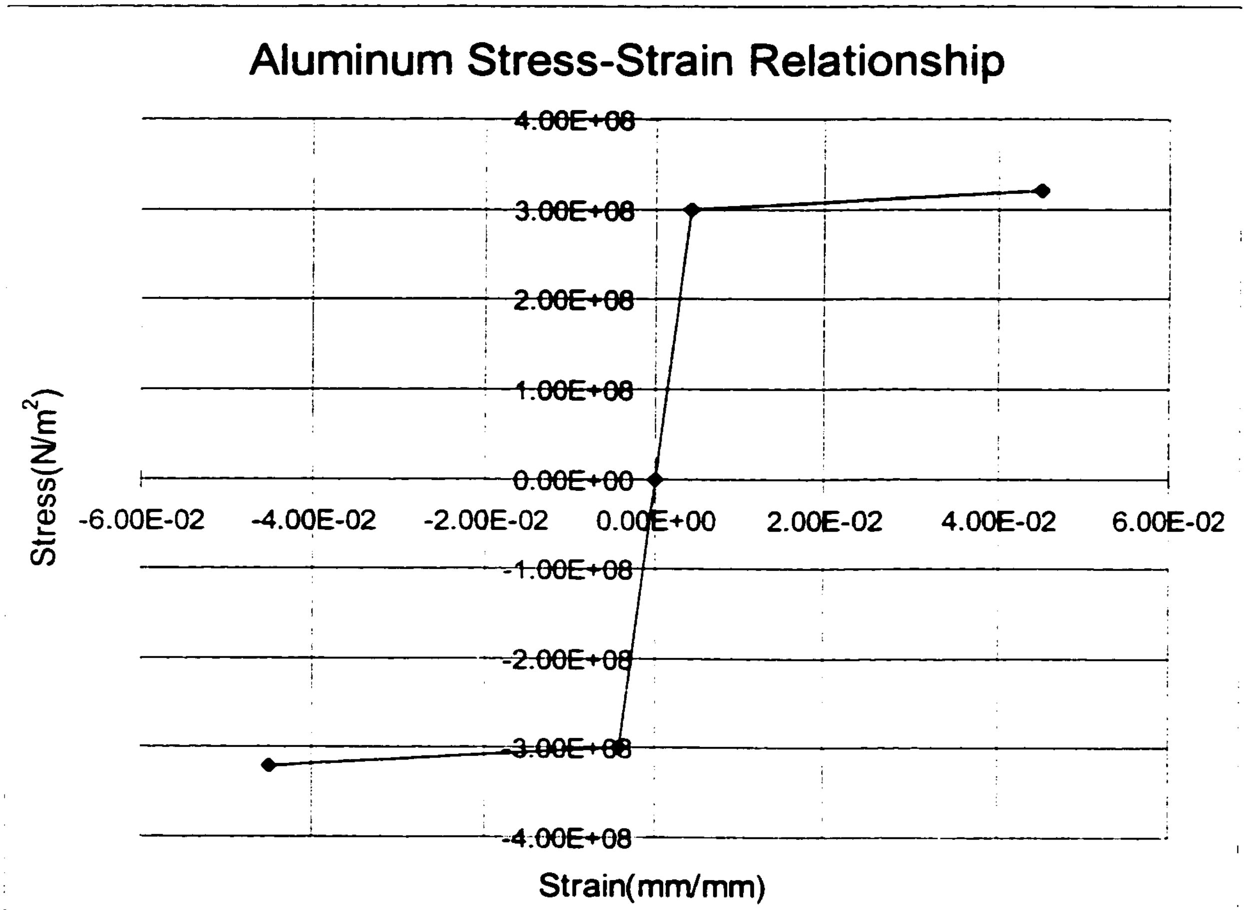

Figure 3.9 The stress-strain relationship of aluminum

Each end support consists of three rockers, made up of 25.4 mm thick steel plates having a curve with an outer diameter of 108.0 mm. These rockers were welded to 6.5 mm thick steel bearing plates. Then each set of rockers was connected to the bottom plate of the model at the appropriate location, making the rockers a part of the structure.

As for the middle column support, it was made up of a short steel column 80.0 mm in diameter. The column was welded to two bearing plates 140 mm × 140 mm and 6.35 mm in thickness at the top and bottom. The top plate of the shaft was connected to the bottom plate of the bridge by means of four screws at a distance of 112.0 mm center to center. The same kind of connection was used for the bottom plate, which was, in turn, connected to the concrete pier. The column connection is intended to simulate a pin type support.

A total of three reinforced concrete columns were constructed at University of Ottawa Structures Laboratory to support the bridge model. Two of these columns were used as end supports (Figure 3.10), which have identical dimensions of a 700 mm × 300 mm cross section, a total height of 600 mm and a base 1100 mm × 600 mm. Each column base was fixed to the floor by using the high strength bolts. As for the middle column (Figure 3.11), it has the same cross section dimensions as the end columns but with a total height of 450 mm.

Each end support column has 21 #15 bars as longitudinal reinforcement, with 6 #10 as transverse reinforcement at 100 mm c/c as shown in Figure 3.12. As for the middle support column it has 32 #15 bars as longitudinal reinforcement, with 5 #10 as transverse reinforcement at 75 mm c/c as shown in Figure 3.13. The complete column and footing reinforcement sections are shown in Figure 3.14. All reinforcements for the

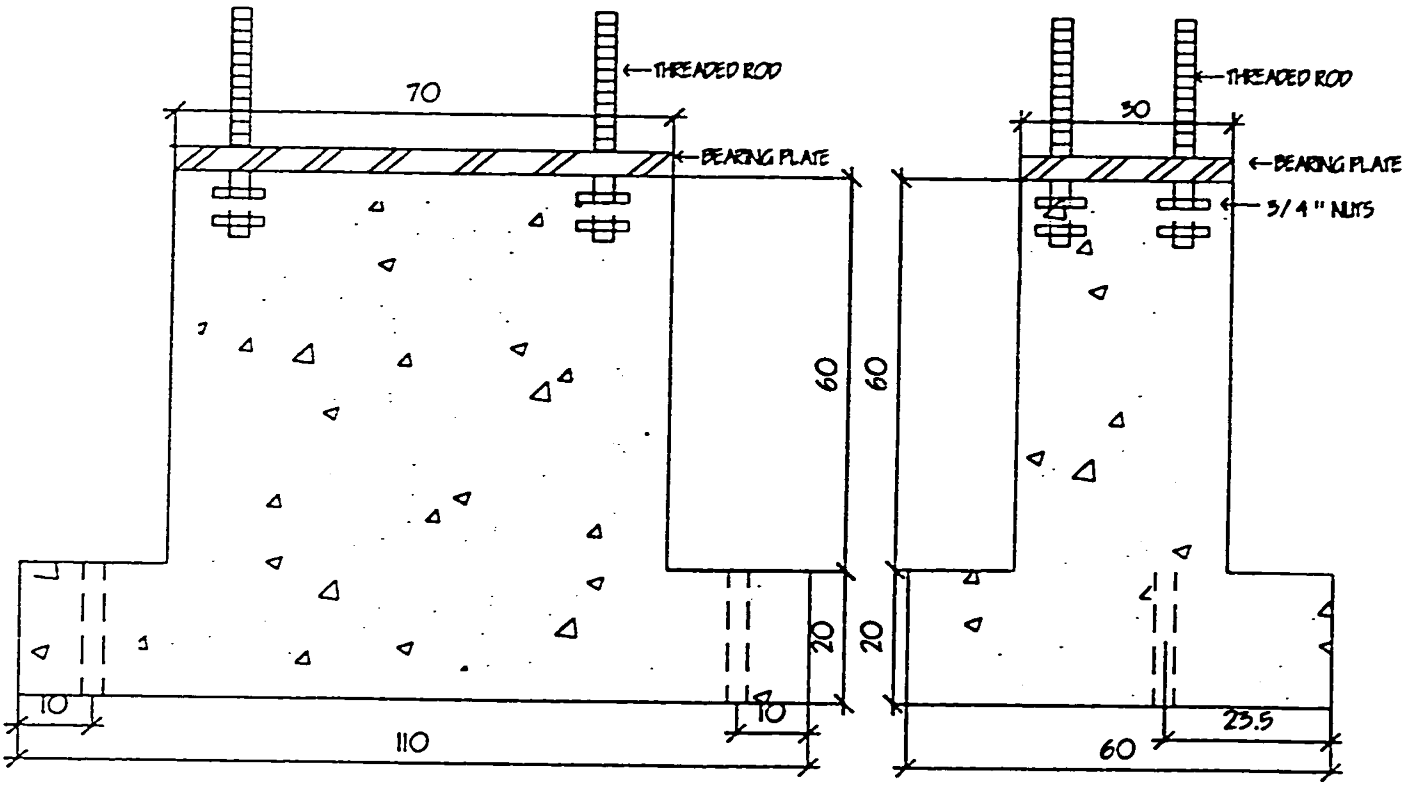

END SUPPORT

ALL DIMENSIONS ARE IN cm.

Figure 3.10 The reinforced concrete end support

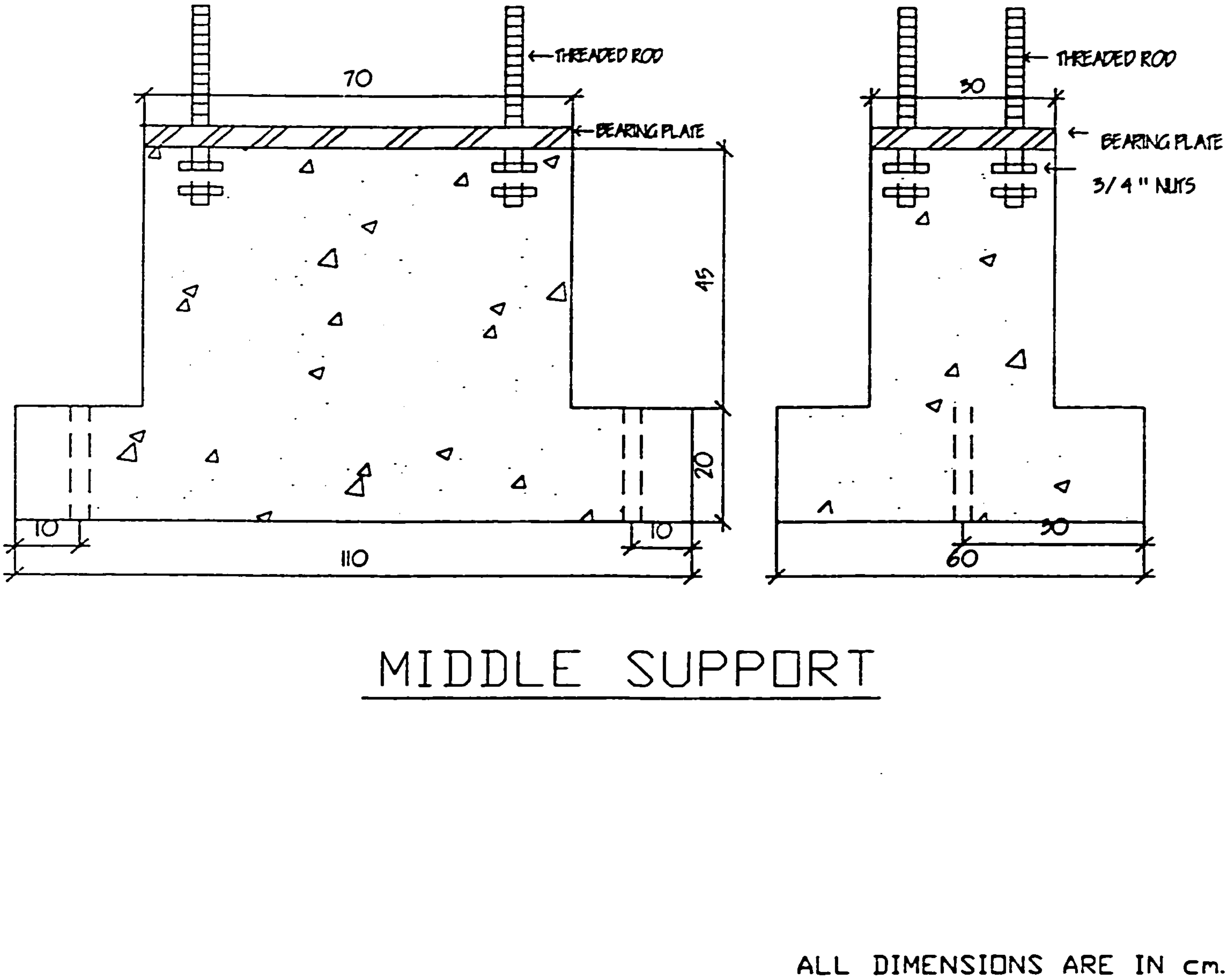

Figure 3.11 The reinforced concrete middle support

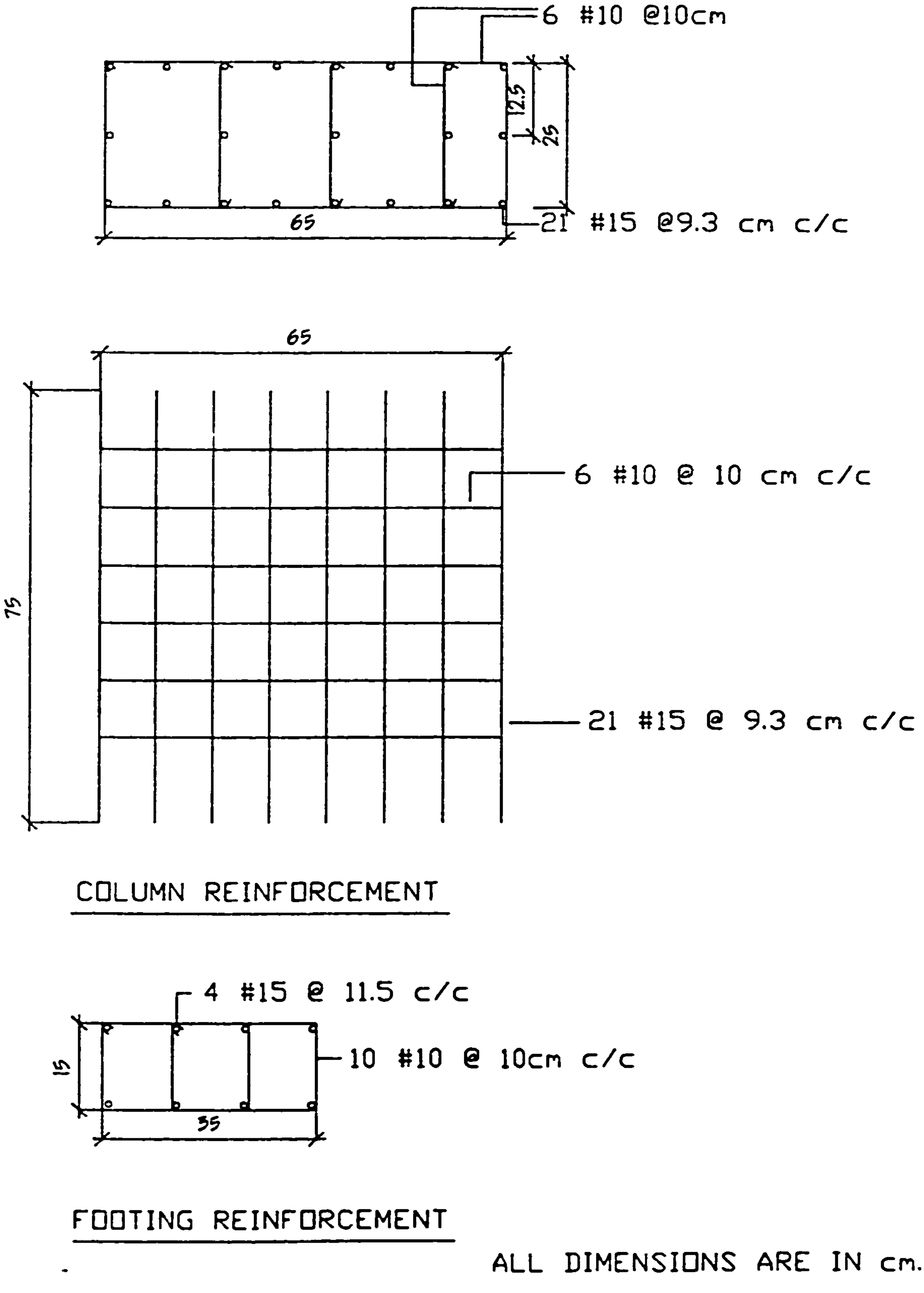

Figure 3.12 Reinforcement details of the end supports

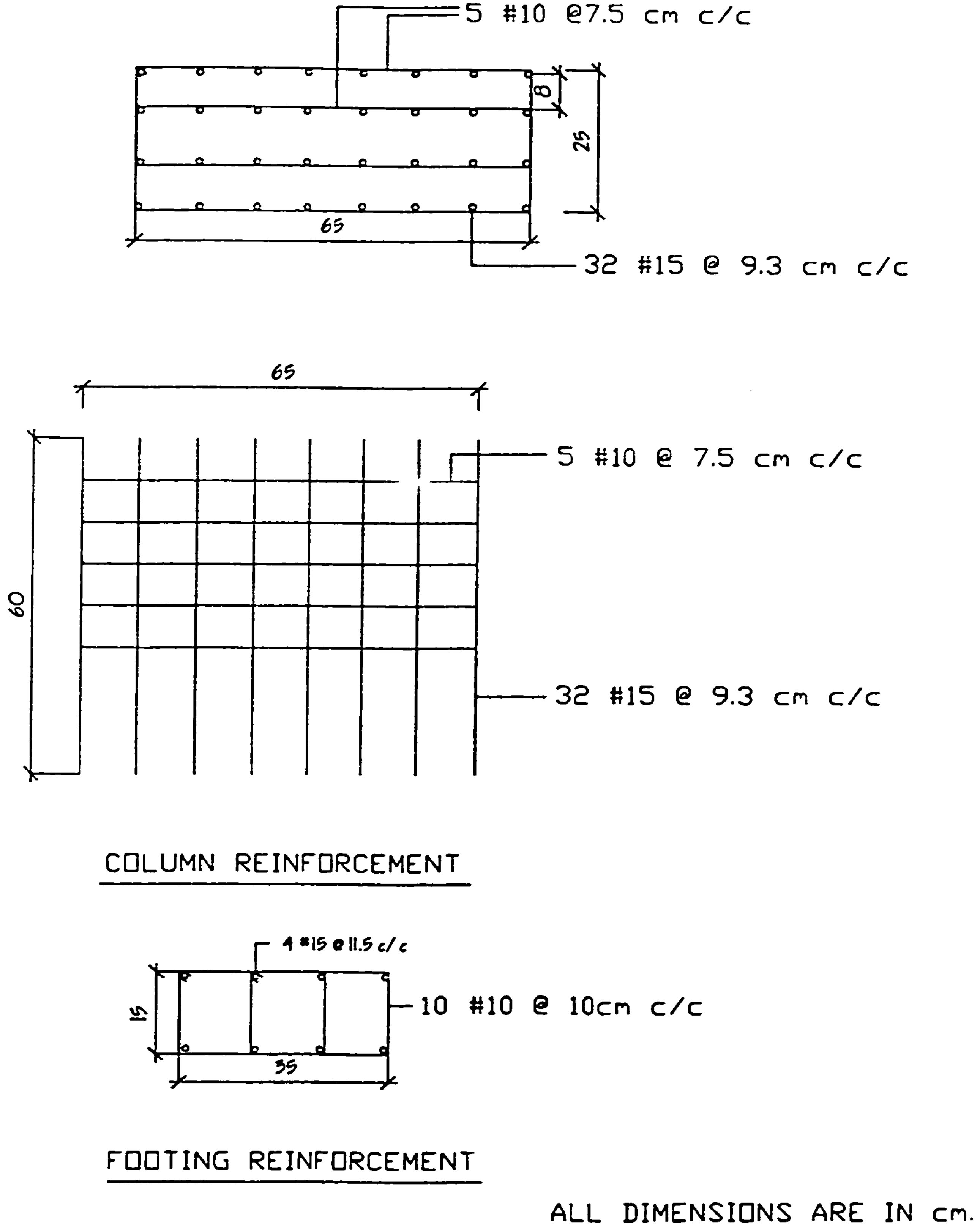

Figure 3.13 Reinforcement details of the middle support

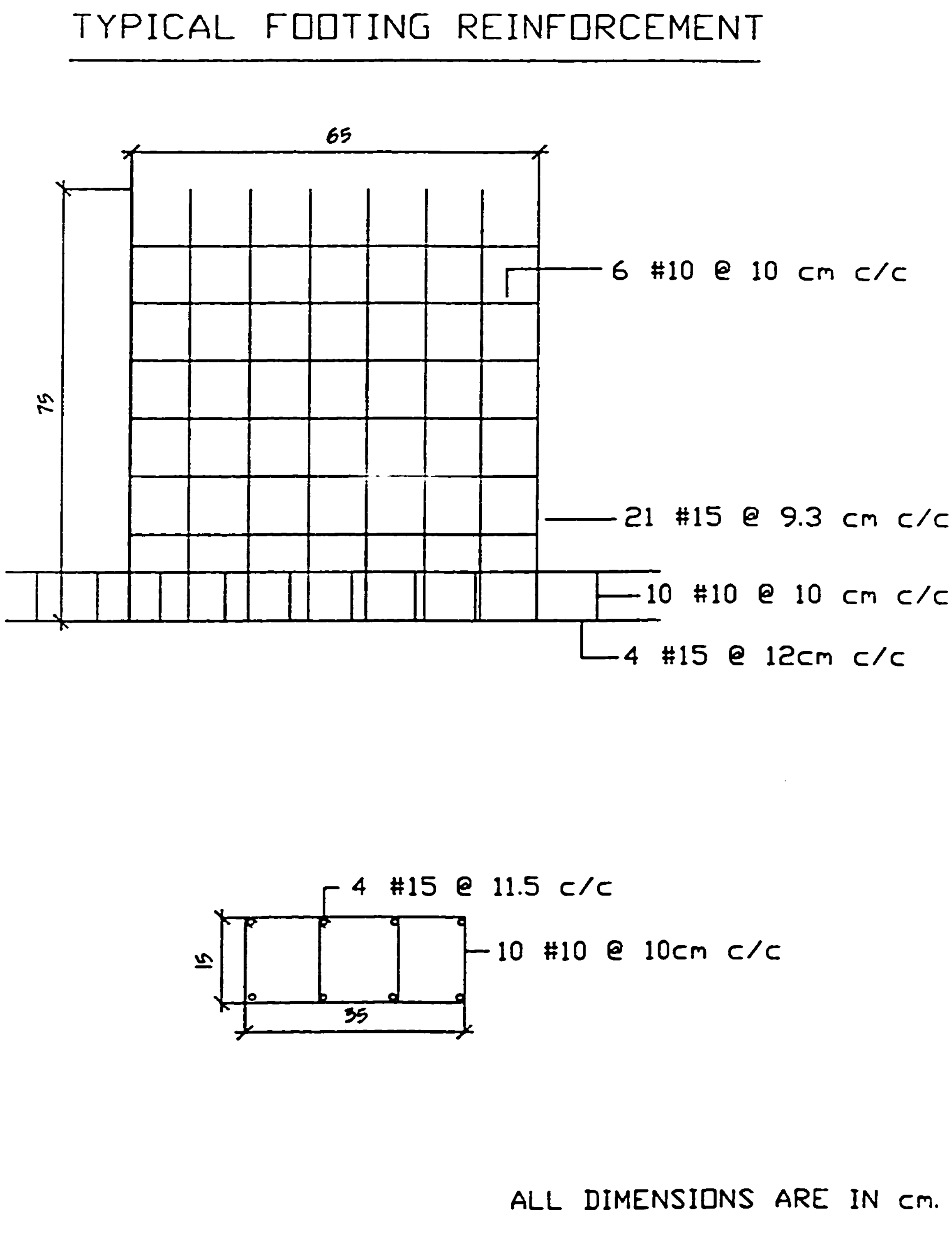

Figure 3.14 A typical footing reinforcement of the support

three columns were designed according to the CSA A23.3-M84. (CSA Standard A23.3-M84, 1984). The concrete with the strength of 60 MPa was poured and cured (Figure 3.15)

It is clear that the reinforced concrete support system was over designed, in order to ensure that during experimental testing the support system will not experience any kind of deformation.

The bridge model was supported at both ends on 700 mm × 300 mm × 13 mm thick bearing plates resting on the reinforced contact with the bearing plates. As a result, additional thin steel plates were utilized to adjust and level the bridge model, so that all rockers rest on the bearing plates.

3.4. Model loading system

An equivalent OHBDC truck loading system was simulated by the laws of similitude and dimensional analysis in the bridge model. The equivalent OHBDC truck loading system consists of a combination of steel beams. The method and principle of the simulation were the same as the ones used by Ng *et al.* (1987). To establish the equivalent OHBD truck, the laws of similitude and dimensional analysis were employed. The basic similitude used in this analysis was the simulation of the longitudinal strains, i.e. the equivalent OHBD truck must produce the same normal strain (ε^m) in the model as (ε^p) in the prototype. Hence

$$\varepsilon^m = \varepsilon^p \qquad (3\text{-}1)$$

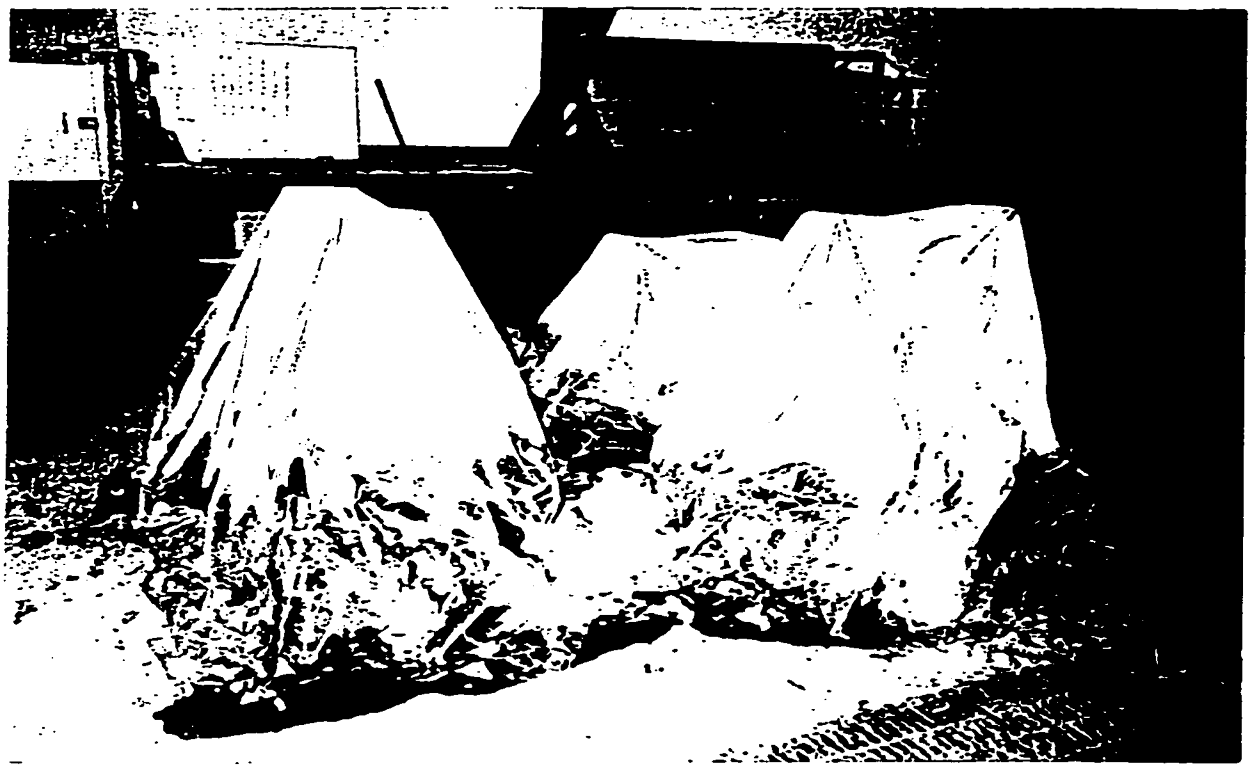

Figure 3.15 Pouring and curing of the supports

Ignoring Poisson's effect, we have

$$\frac{\sigma^m}{E^m} = \frac{\sigma^p}{E^p} \qquad (3\text{-}2)$$

Where

E: Young's Modulus

σ: the longitudinal bending stress

m: denotation of the model

p: denotation of the prototype

However, the normal stress at any section is given by:

$$\sigma = \frac{MY}{I} \qquad (3\text{-}3)$$

Where

M: the bending moment at the section

Y: the distance from the neutral axis of the cross section

I: moment of inertia of the section about the neutral axis.

Furthermore; M, the bending moment can be expressed in the form of

$$M=FX \qquad (3\text{-}4)$$

Where

F: the external force

X: linear dimension along the longitudinal axis of the structure

After substituting Eq. 3.4 into Eq. 3.3 and Eq. 3.2, the new equation will be

$$\frac{F^m X^m Y^m}{E^m I^m} = \frac{F^p X^p Y^p}{E^p I^p} \qquad (3\text{-}5)$$

Or

$$F^m = \frac{E^m I^m X^p Y^p}{E^p I^p X^m Y^m} F^p \qquad (3\text{-}6)$$

A constant linear scale (L_f) was used for the two linear dimensions X, Y:

$$L_f = \frac{X^p}{X^m} = \frac{Y^p}{Y^m} \qquad (3\text{-}7)$$

$$I_f = \frac{I^p}{I^m} \qquad (3\text{-}8)$$

$$E_f = \frac{E^p}{E^m} \qquad (3\text{-}9)$$

Substituting Eqs. 3.7,3.8 and 3.9 into Eq. 3.6, we have

$$F^m = \frac{L_f^2}{E_f I_f} F^p \qquad (3\text{-}10)$$

Or

$$F^p = F_f F^m \qquad (3\text{-}11)$$

Where F_f, the static linear force is given by

$$F_f = \frac{E_f I_f}{L_f^2} \qquad (3\text{-}12)$$

Eq. 3.11 shows the relationship between the prototype force (F_p) and the equivalent model force (F_m) that would satisfy the normal strain similarities. The prototype bridge is a reinforced concrete bridge and it was modeled by a composite bridge model in this study. The stiffness properties that were used in the calculation of the force scale factor are as follows:

Ip = 310520100 cm^4

Im = 2871 cm^4

Ep = 27700 Mpa

Em = 71100 Mpa

With a linear scale factor L_f =24 and substituting Ip, Im, Ep, Em, and L_f into Eq. 3.6, the force scale factor can be calculated as

$$F_f = 73 \qquad (3\text{-}13)$$

Applying this factor, the model truck simulating one OHBD truck (Ontario Highway Bridge Design Code, 1991) was calculated and the results are shown in Table 3.6. The total load of an equivalent OHBDC model design truck load is equal to 10.138 kN. Each set of parallel truck loading system has 20.276 kN (Figure 3.16).

In general, the model truck load consists of four axles instead of five due to the fact that, axles number 2 and 3 were lumped together because of the short distance between these two axles. This model truck loading system is made up of a number of steel bars that are assembled on top of each other to form what is called a tree loading system, such that when a concentrated jack load is applied, the load is distributed between the four axles to the wheels as shown in Figure 3.17. At this stage it is important to note that the wheel loads are located exactly on the webs in order to avoid the damage of the micro concrete deck. The capacity of the load system was verified (Figure 3.18) before the formal load test was carried out. The location of the loading system is shown in Figure 3.19.

Table 3.6 OHBD Truck Load vs. Model Load

Axle Number	Axle Load (kN)	
	Prototype	Model
1	60	0.822
2	160	2.192
3	160	2.192
4	200	2.740
5	160	2.192
Gross Load	740	10.138

Table 3.7 Single Model Truck Weight

Beam ID	Beam Dimension (cm)	Mass/Beam (Kg)	Number of Beams	Mass (Kg)
A	10×10×50	39.25	1	39.25
B	5×5×16.5	3.24	2	6.48
C	5×6.4×23.5	5.90	2	11.80
D	5×6.4×36.5	9.17	2	18.34
E	3.2×5×9.5	1.19	8	9.52
Total mass of One model Truck85.39				

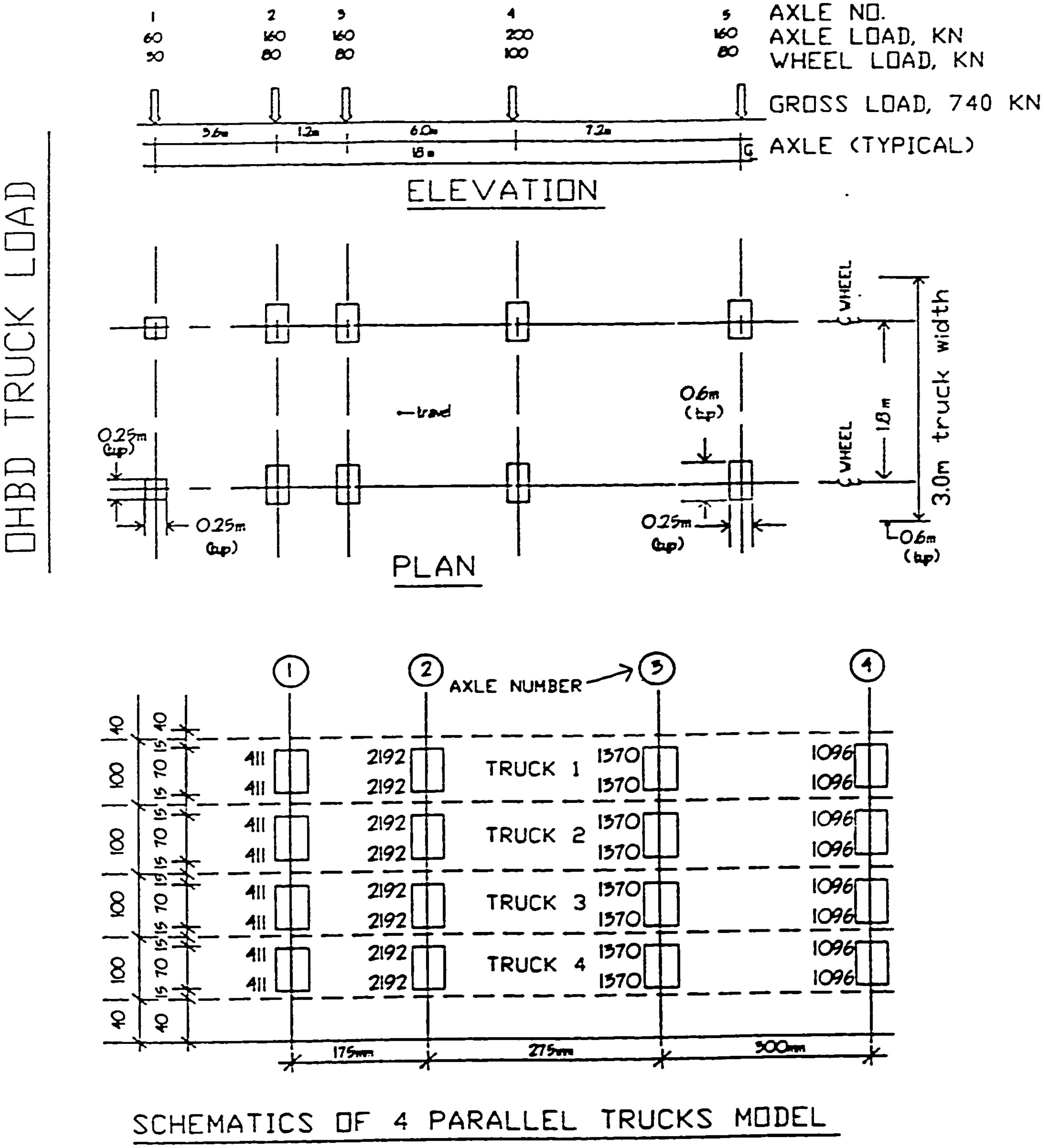

Figure 3.16 OHBD truck and parallel model truck loading system

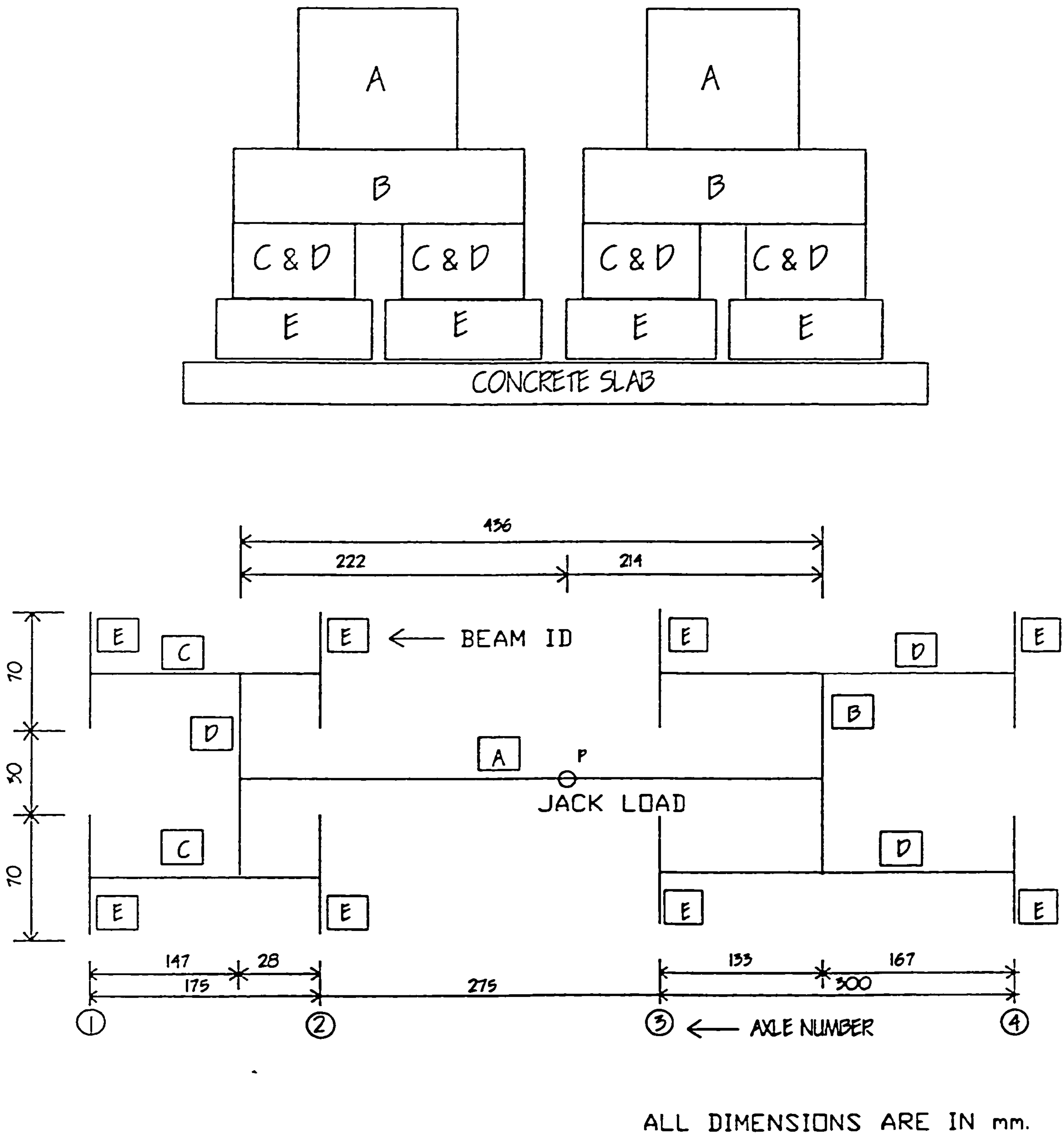

Figure 3.17 Truck loading system

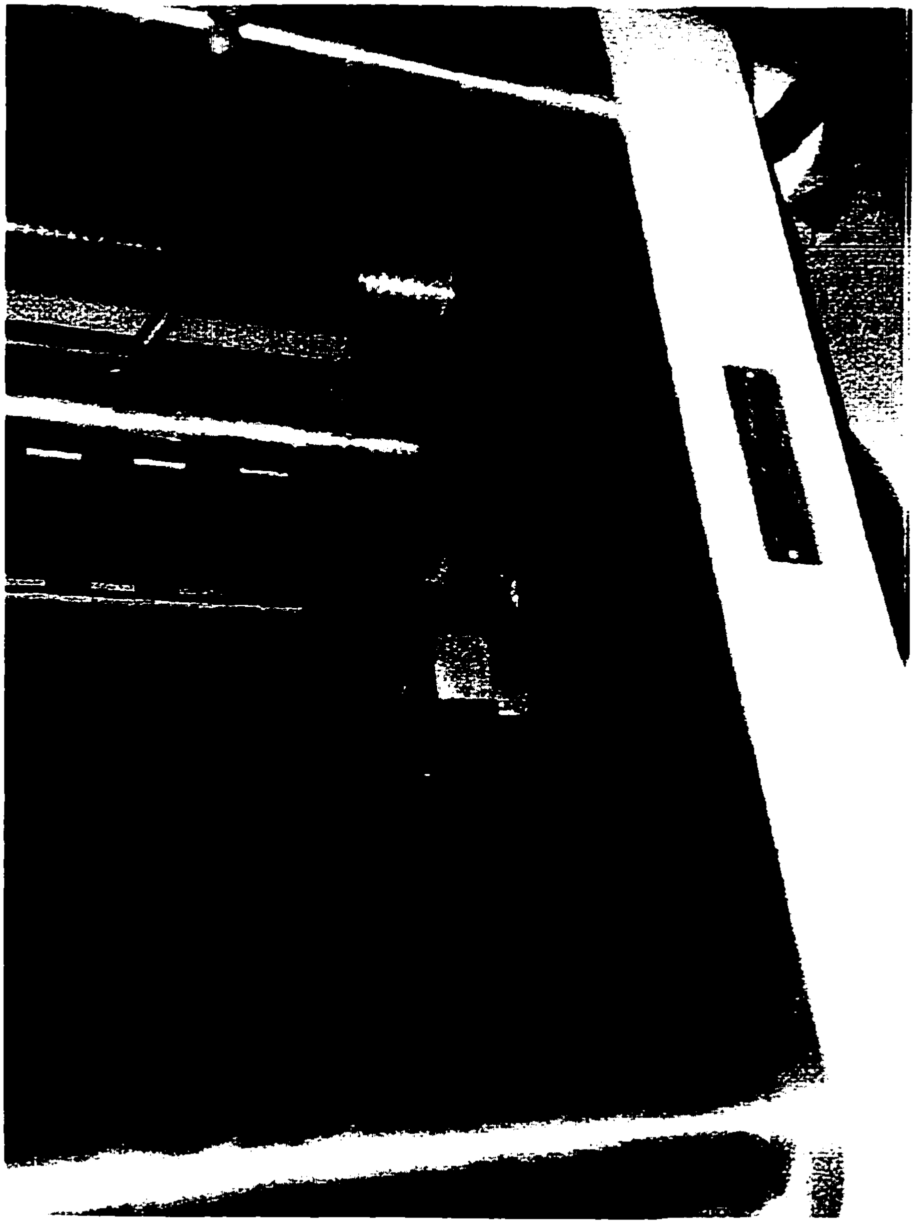

Figure 3.18 Testing of the loading system

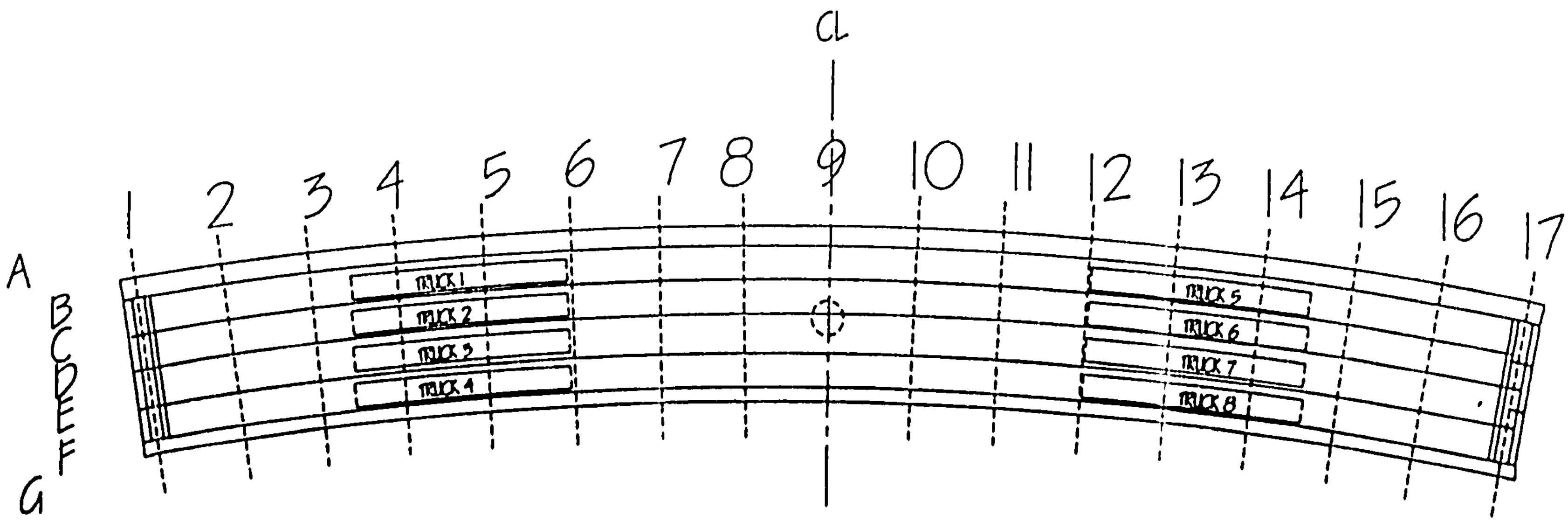

Figure 3.19 The location of the loading system

3.5. Test Setup and test procedure

3.5.1. Test setup and instruments

The setup of the bridge model is shown in Figure 3.20. To prevent the model from uplift at the end supports, both end supports were restrained against torsional movements by bolting a 2" × 2" L shape angle to two 3/4" threaded rods that form part of the end support system for the reinforced concrete columns as shown in Figure 3.21. The middle support was fixed at the end by the reinforced concrete foundation.

The curved bridge model was mounted on the supports. The RC foundations of the middle and end supports and the two box-section loading reaction frames were fixed on the floor. Four hydraulic jacks with the capacity of 500 kN were used. They were mounted on the two reaction frames respectively. The load cells were installed on the loading system. The setup of the load system is shown in Figure 3.22.

Four LVDTs are used to measure the deflections of the external webs A and E at sections 4 and 14, where the maximum predicted deflections would occur. The installation of the LVDTs is shown in Figure 3.23.

A total of 10 dial gages with sensitivity 0.01 mm were mounted vertically under the bottom flange of several sections including section 4, section 14, and the sections at the middle support and the end supports shown in Figure 3.24. Those dial gages were mainly used to measure the deflection of the bridge model at the supports and check the LVDTs' readings in the previous load stages.

Dial gages were supported by 3/8" threaded rods bolted to steel angles that were clamped onto a separated steel frame underneath the bridge model.

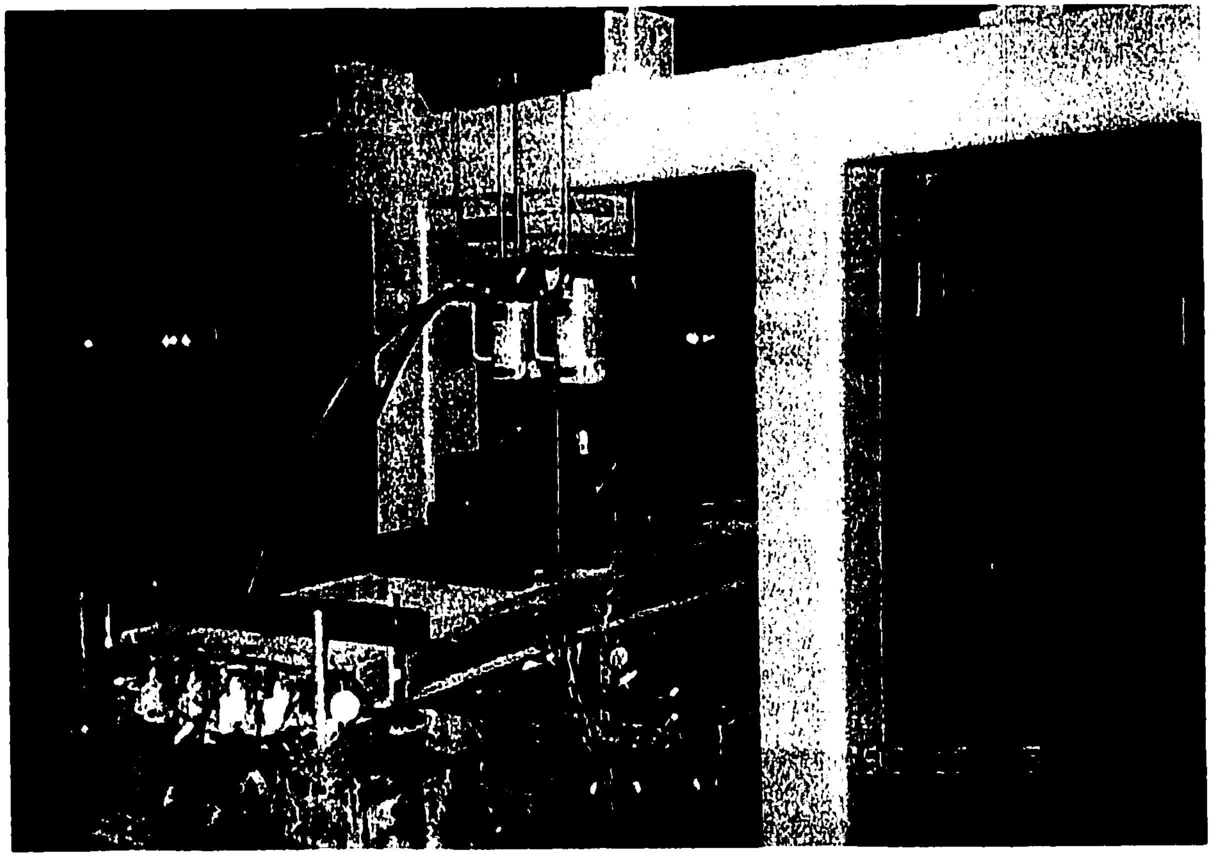

Figure 3.20 Test setup of the bridge model

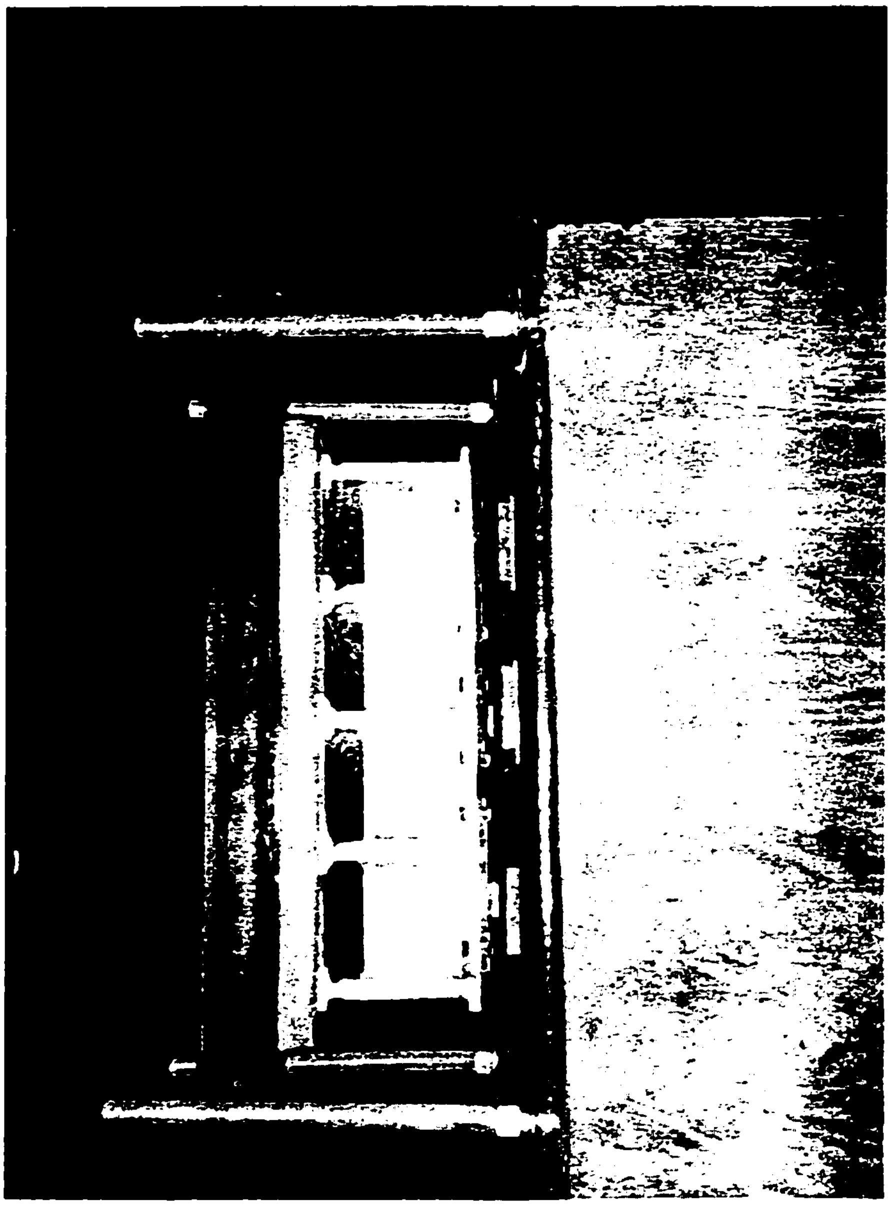

Figure 3.21 Detailed setup of the end support

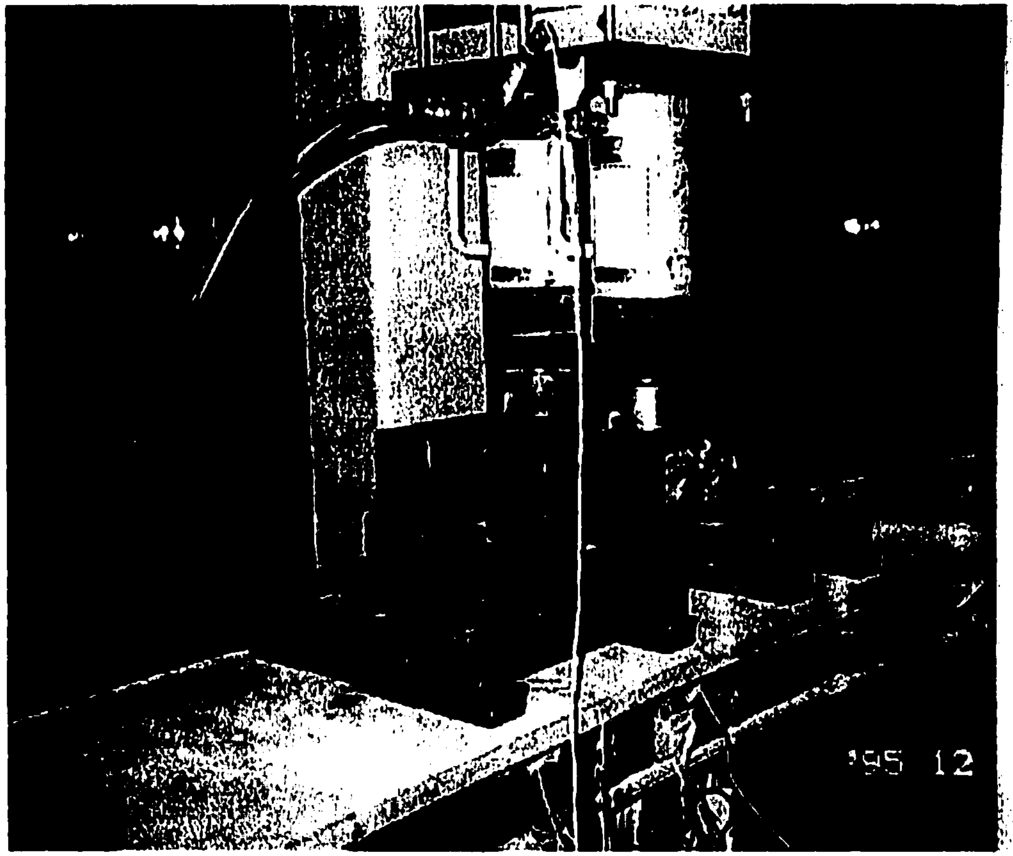

Figure 3.22 Detailed setup of the loading system

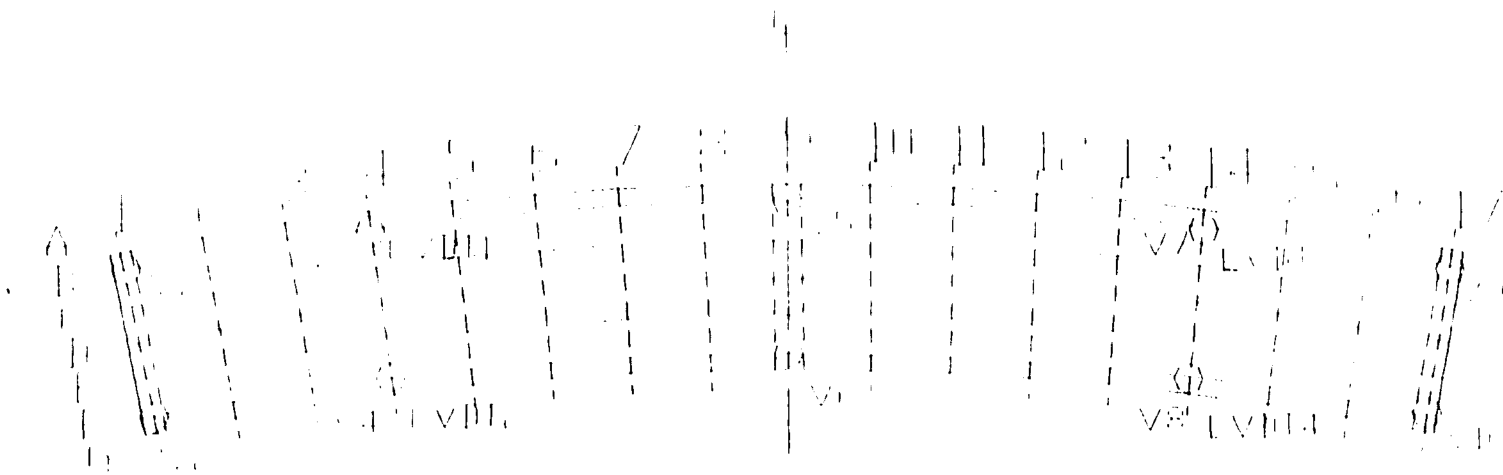

Figure 3.23 The location of LVDTs and dial gages

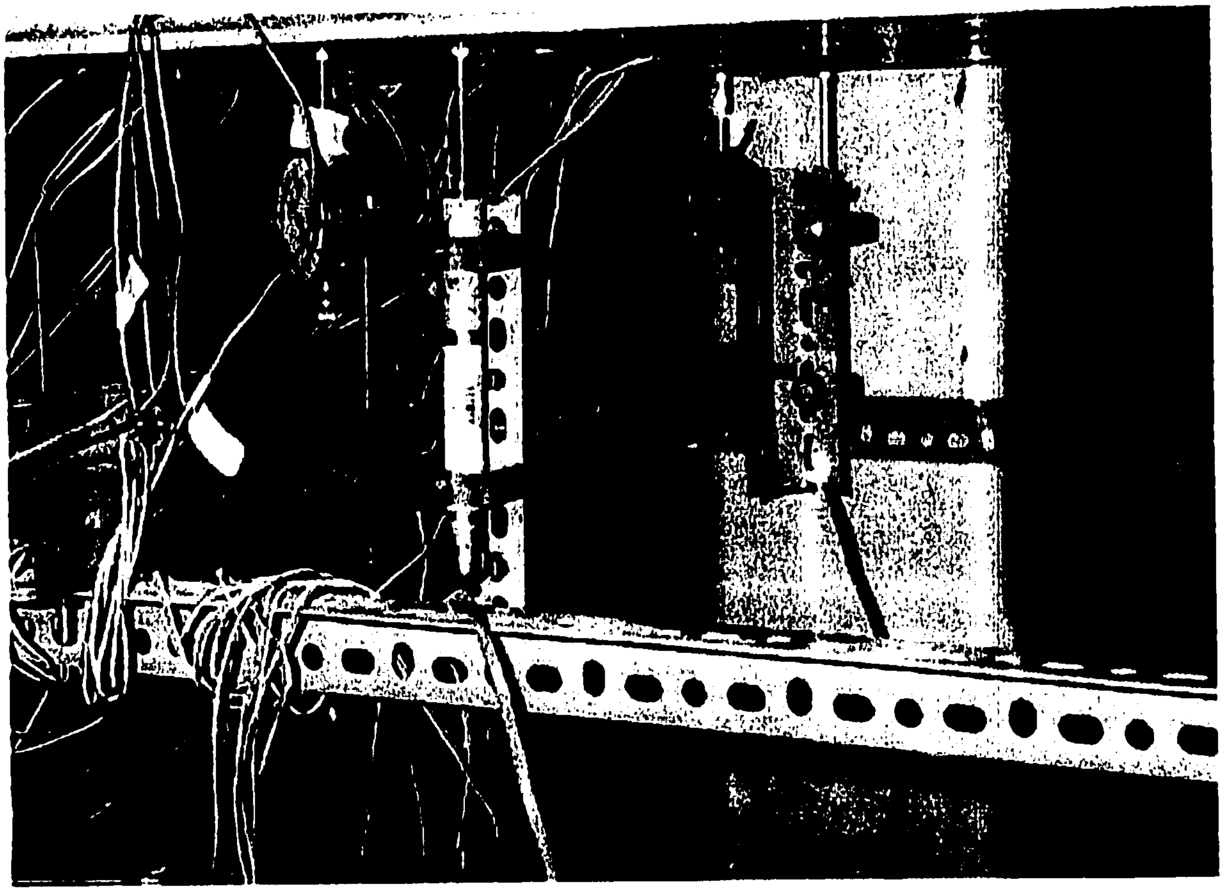

Figure 3.24 Detailed setup of LVDTs

The bridge model was divided transversely into seven distinct tangential lines, namely A, B, C, D, E, F, and G. Lines A and G representing the bridge model extreme edges, and the other five line B, C, D, E, and F represent the center lines of the webs. Figure 3.25 shows the location and identification of dial gages and LVDTs.

A data acquisition system (Figure 3.26) with 64 channels, which was connected to the computer, was used to collect the experimental data. In the 64 channels of the data acquisition system, 8 channels may be used for load cells, 52 channels for strain gages and 4 channels for LVDTs. All load cells, strain gages and LVDTs were connected to the data acquisition system. All readings were collected automatically every five seconds by the data acquisition system.

A total of three types of foil strain gages were utilized in this experimental study to measure the strains. Types of the strain gages are shown as:

1. 45 three-gage rosette strain gages, aluminum type EA-13-125RA-120
2. Uniaxial "linear" strain gage, aluminum type KEC-5-C1-11
3. A linear strain gage for the micro concrete type EA-06-500GB-120

All the above mentioned strain gages have a gage factor of 2.10 and have been installed and wired. Micro-Measurement M-Bond 200 adhesive was used to glue the strain gages to either the micro concrete or the aluminum.

A total of 82 strain gages were installed, at five chosen sections, namely sections 1, 4, 5, 8 and 9. Strain gages inside the deck were all made waterproof before casting of the micro concrete deck. Eight linear strain gages with the type EA-06-500GB-120 were installed at the model's deck surface of sections 4, 8 and 9 shown in Figure 3.27. Ten

45° three-gage rosette strain gages type EA-13-125RA-120 were installed on the outer surface of aluminum at sections 1, 4, 5 and 8 shown in Figure 3.28. Finally, forty four linear strain gages type KEC-5-C1-11 were installed on the outer and inner surfaces of aluminum at sections 1, 4, 5, 8 and 9 as shown in Figures 3.29 and 3.30. Because there are only 64 channels available in the data acquisition system, 34 linear strain gages and 6 rosette gages were measured at various sections of the bridge model. Two rosette strain gages at section 1, all strain gages at section 4, rosette strain gages and linear strain gages for the concrete deck at section 8, and all strain gages at section 9 are used in the load test. The last eight were sensors and two of them were used to measure the load generated by the jacks.

Each strain gage has an identification symbol as follows:

$A_{ij}{}^{L}$: A linear strain gages type KEC-5-C1-11 located on the outer or inner surfaces of the aluminum at section j and i refers to the gage number within section j.

$A^{RX}ij$: A 45 three-gage rosette strain gage type EA-13-125RA-120 located on the outer surface of the aluminum at section j and I refers to the gage number within section j.

Where x refers to the axis in the plane of the rosette as follows:

x=L defines longitudinal axis of the bridge model

x=T defines perpendicular axis to L in rosette plane

x=D defines the 45 axis between L and T.

$C^{l}ij$: A linear strain gage type EA-06-500GB-120 located on deck surface at section j, and i refers to the gage number within section j.

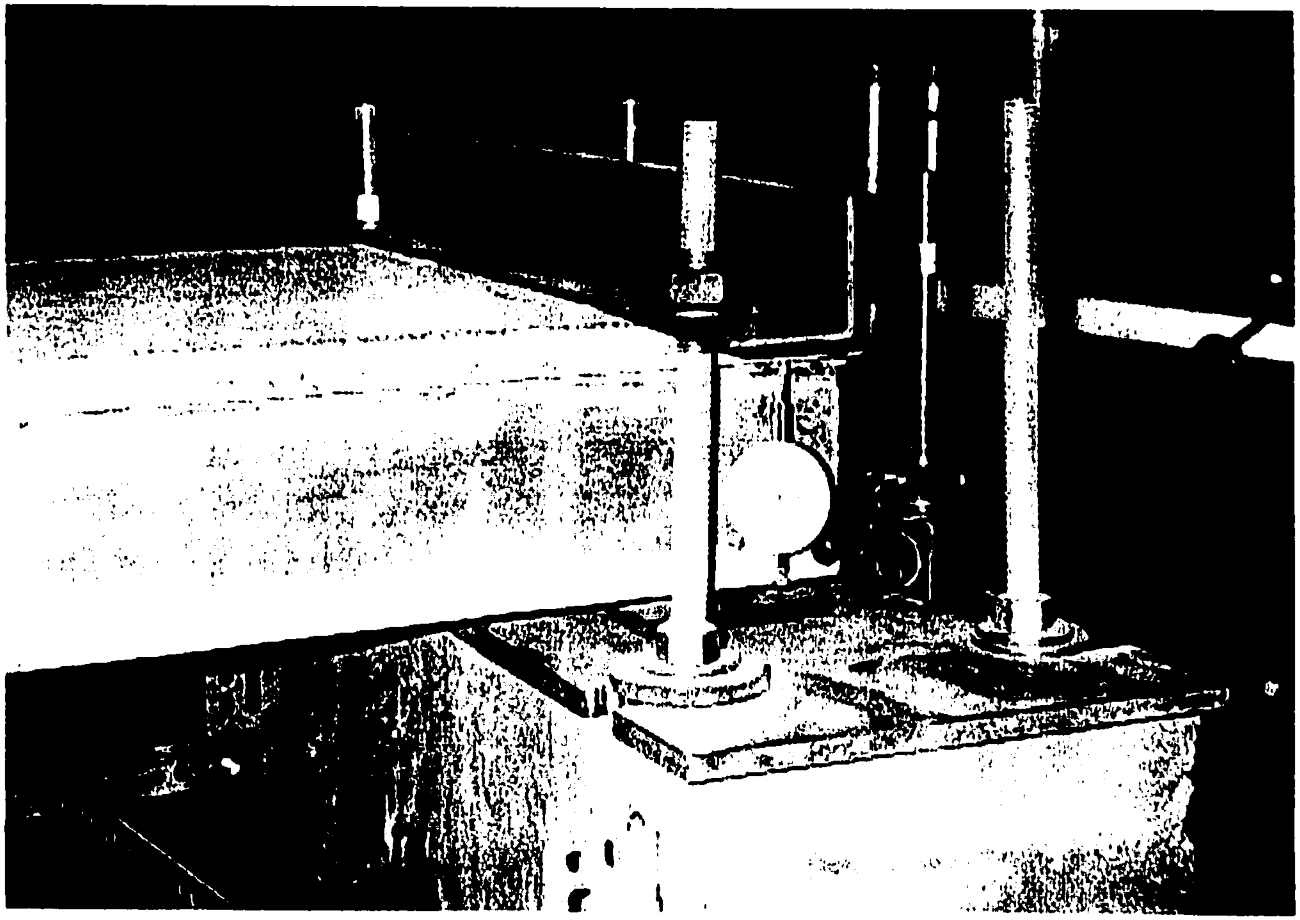

Figure 3.25 Detailed setup of a typical dial gage at the end support

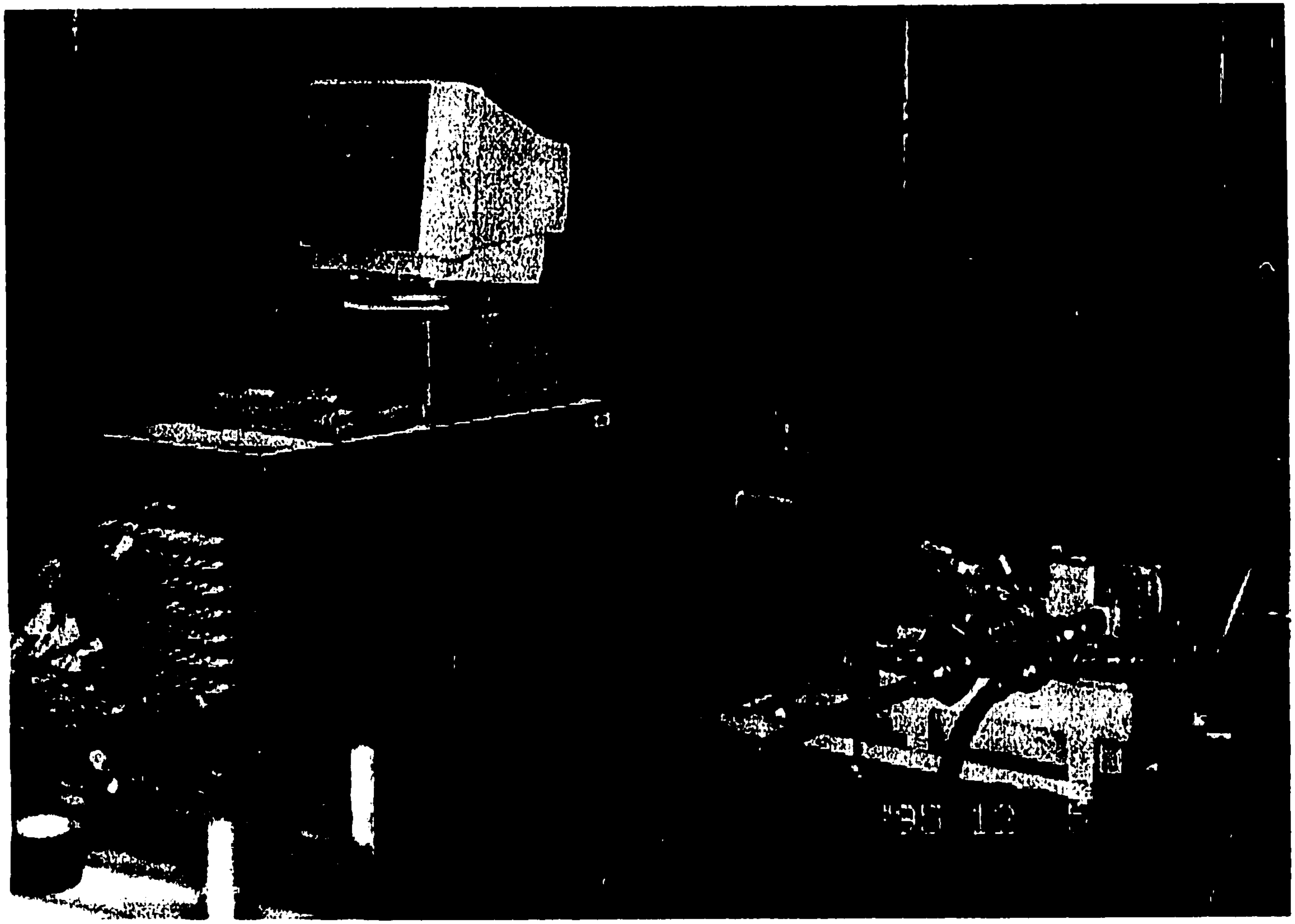

Figure 3.26 Data acquisition system and the pump

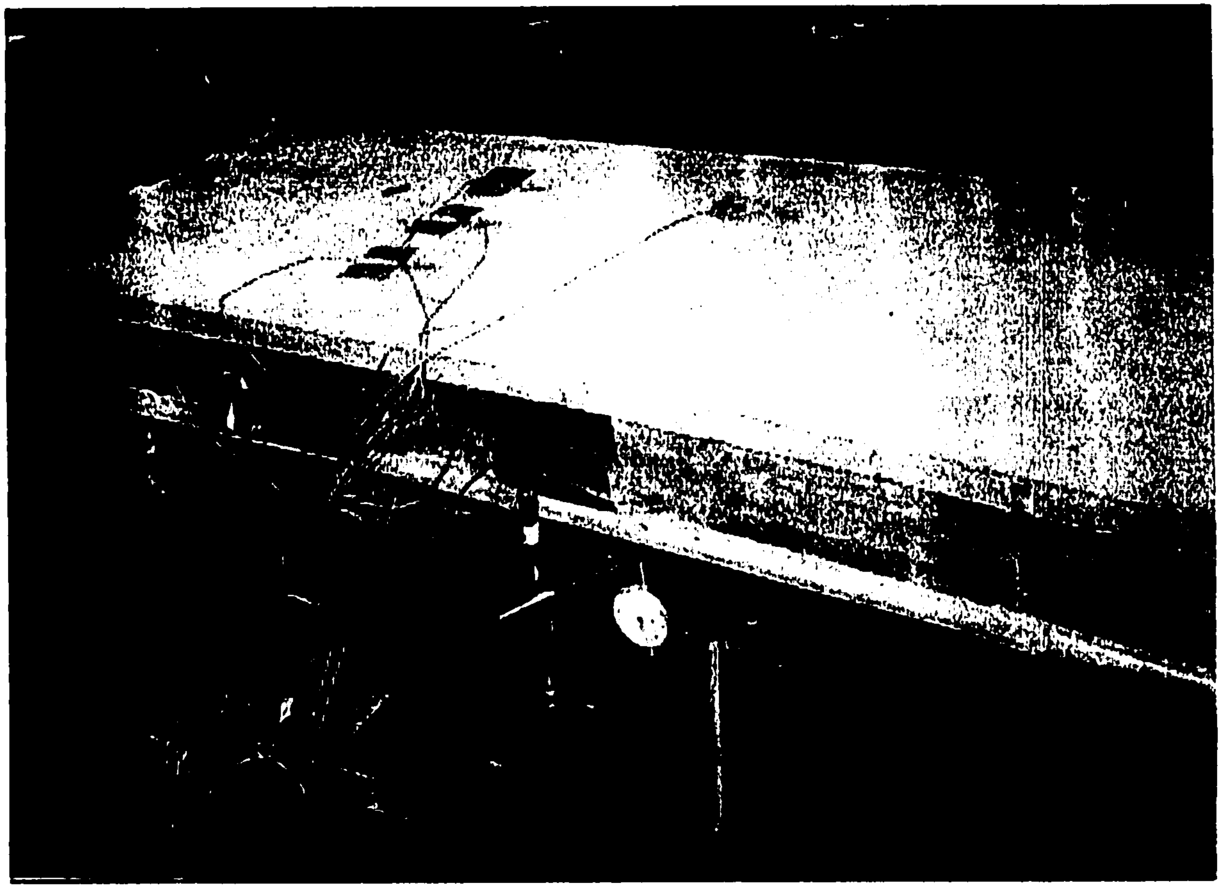

Figure 3.27 Strain gages for the concrete deck

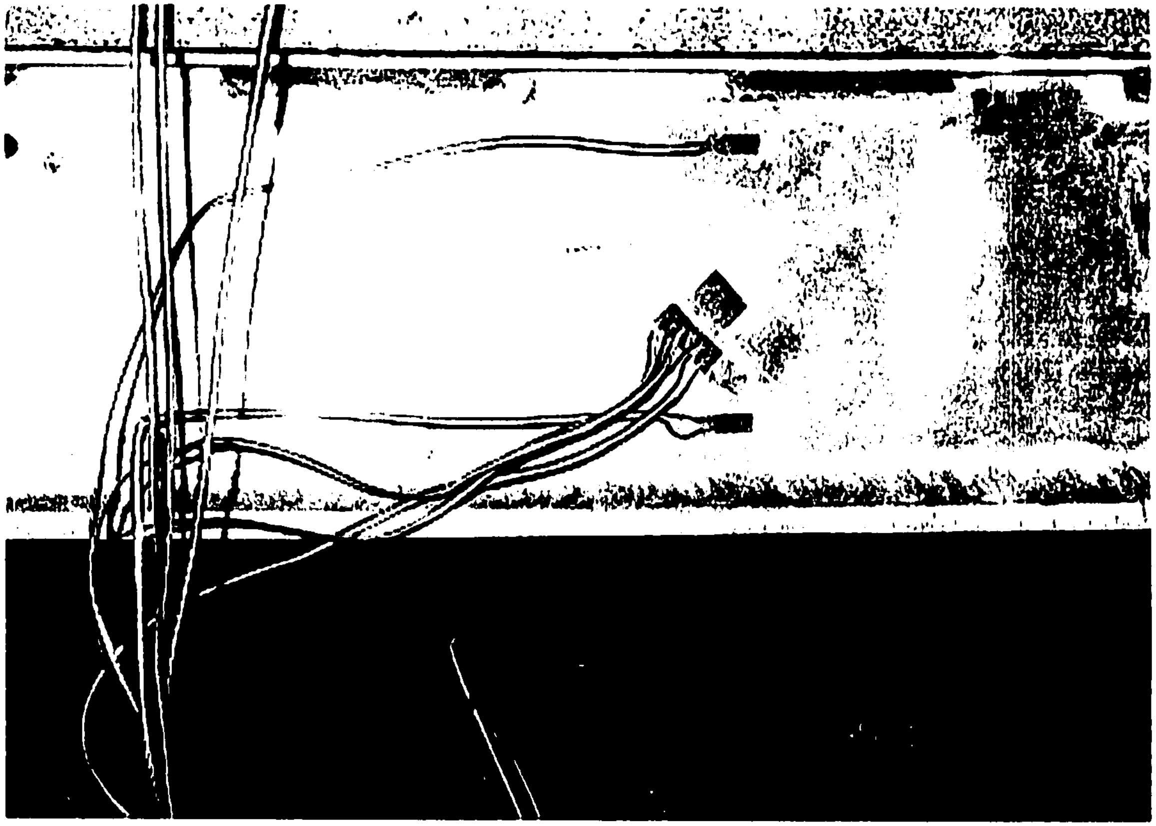

Figure 3.28 Strain gages for the aluminum girder

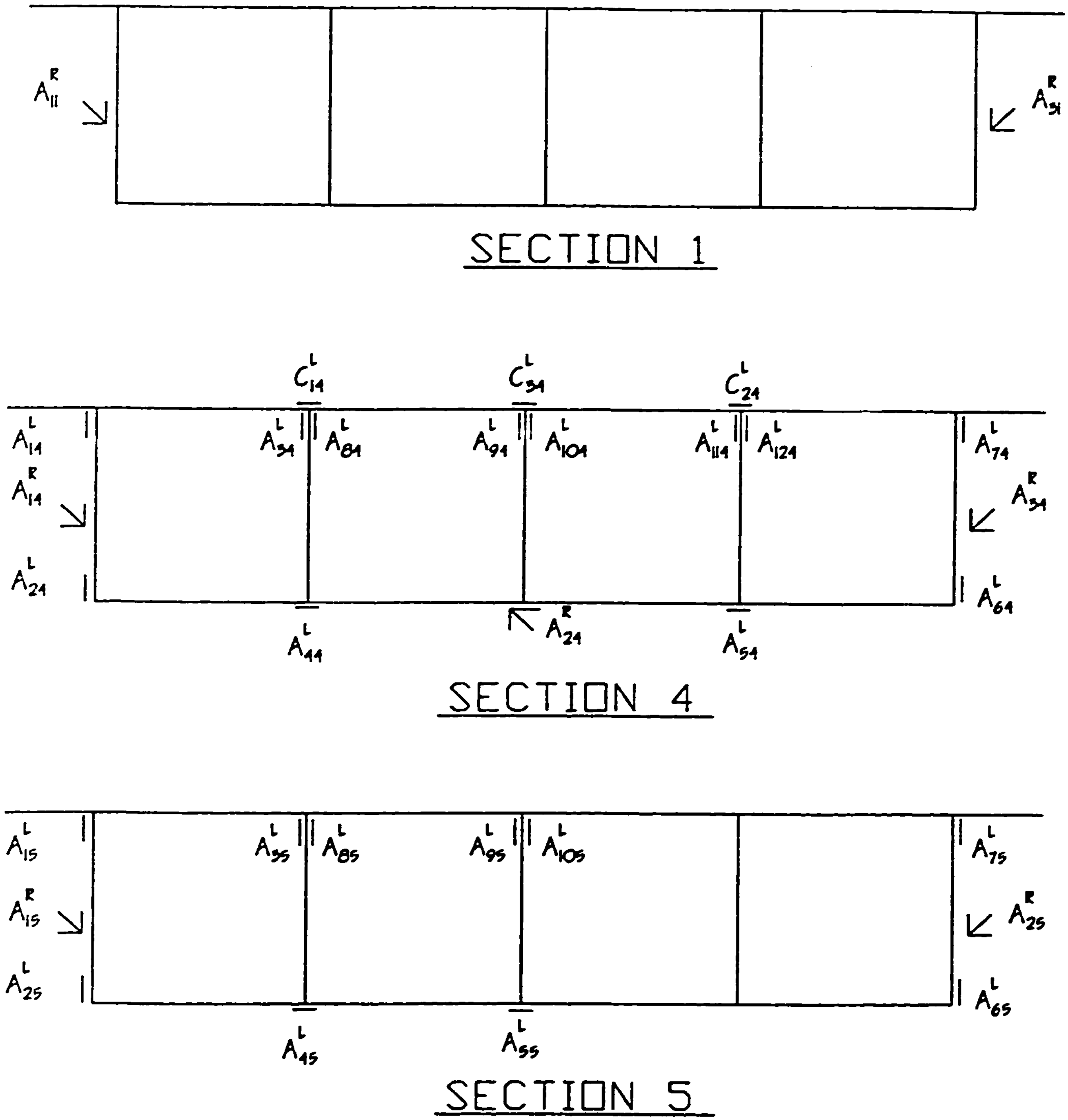

Figure 3.29 Strain gauges location at sections 1, 4, and 5

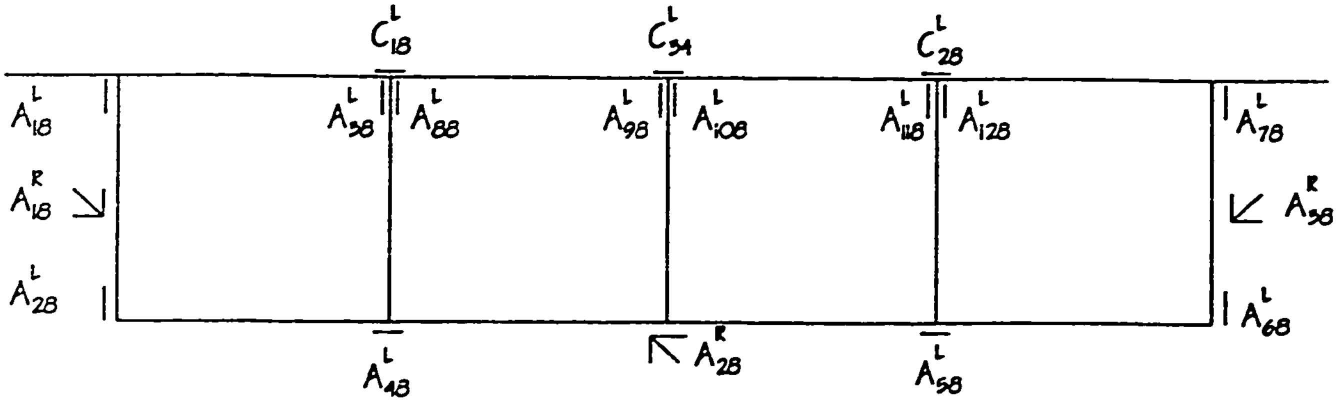

SECTION 8

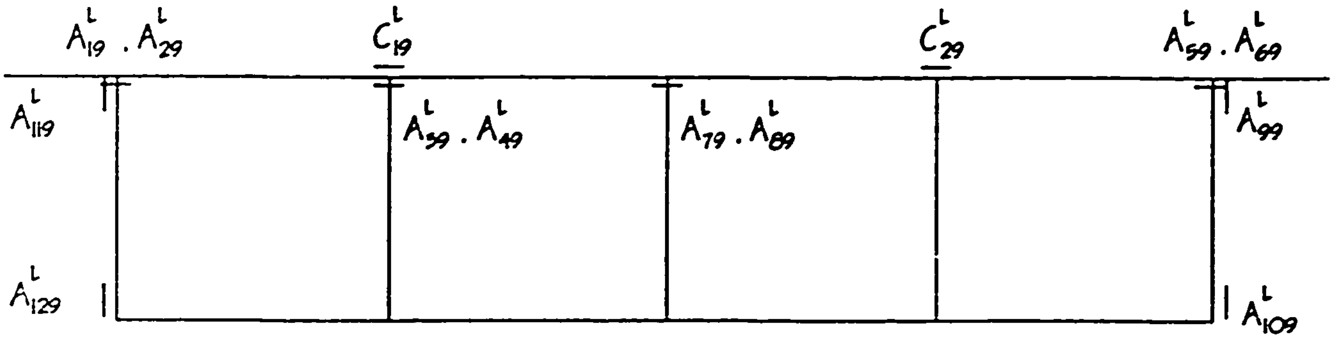

SECTION 9

Figure 3.30 Strain gauges location at sections 8 and 9

For example:

Strain gage number A^L_{39} refers to the 3rd linear strain gage type KEC-5-C1-11 located on the outer or inner surface of the aluminum at section 9.

Similarly C^L_{18} refers to the1st linear strain gage type EA-06-500GB-120 located on the deck surface at section 8.

COPILOT is a system of integrated data acquisition and management modules that are designed to collect, display, and manage scientific and engineering monitoring data. These integrated modules form a system that allows the collection and analysis of a large amount of data.

COPILOT operates sensors and Electronic Measurement System equipment (EMS Equipment) or Electronic Measurement and Control System equipment (EMCS Equipment) to the exact specification that one defines. Data read by the sensors are automatically processed and stored into a disk for future analysis. With COPILOT one can conduct monitoring over a period of hours or years and for a large number of locations. Once the data acquisition is completed, COPILOT can display data on the screen, or print data tables and graphs. Furthermore, COPILOT manages data so it can be exported to other programs for further analysis.

COPILOT consists of three independent programs called modules. The COPILOT module is a program that acts as an entry to the COPILOT package that consists of the following: (COPILOT 1987)

1. CONFIGURE

The configure module allows the user to define a monitoring task that will tell COPILOT what data acquisition equipment and sensors to use, what data to gather, and how to process and save that data.

2. MONITOR

The monitor module performs real-time data acquisition using the monitoring task that was specified using the CONFIGURE module. This module operates the data acquisition system, measures sensors, performs calculations, and displays and stores data.

3. DISPLAY

The display module allows the user to view data, which the MONITOR has stored on a disk, in tables or graphs and export the stored data to a spreadsheet.

COPILOT utilizes pop-up menus that allow the user to get around the program and chooses task configuration, monitoring, and display options. All the available options are displayed on the screen. However, when configuring a task, COPILOT prompts the user with parameter names and explanations and often offers the user options of using default parameter values.

3.5.2. Test Procedure

Before the ultimate load test started, Strain gages, load cells, and wires were checked and gage factors were set to their appropriate values. In addition, dial gages were checked for proper locations. Zeros reading for strain and dial gages were taken. Parallel trucks loading system was setup at the proper location. The jacks were then aligned vertically. The instruments and the setup were checked by a few loading and unloading tests in the elastic range before the ultimate load test was carried out.

In the ultimate load test, the load was increased by 5% of the predicted ultimate load in the beginning steps. After the cracking of the concrete deck in the maximum negative moment region, the load was increased by 2% of the ultimate load until the failure of the curved bridge model. During the experiment, the load and the deflections were observed and recorded at all load steps.

3.6. Experimental Results

3.6.1. Displacements and Strains

All the experimental strain data recorded using the data acquisition system COPILOT were exported into spreadsheet format, and the software MS Excel were employed to read these exported data.

The fact that the data acquisition system COPILOT was recording data every five seconds made the amount of data collected very huge. To overcome the difficulty of working with such a huge amount of data, an average of each load step along with its corresponding strain were calculated using the software Excel.

As for the deflections, all the dial gages readings were recorded manually, while the LVDTs' data were collected by using COPILOT.

3.6.2. Stresses

Normal stresses (σ) and shear stresses (τ) were computed from the experimental strain data collected. Due to the curvilinear nature of the model geometry, it is convenient to adopt cylindrical coordinate system shown in Figure 3.31

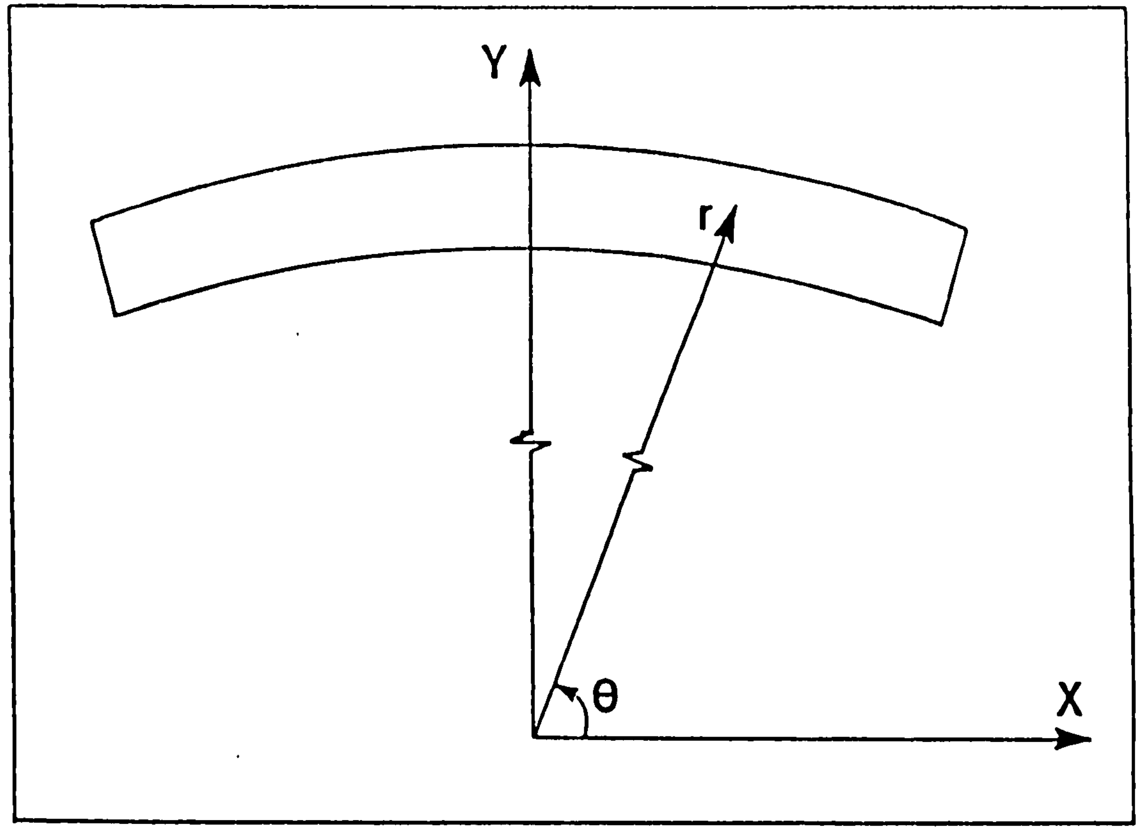

Figure 3.31 The cylindrical coordinate system

From the experimental strain data the following stress components can be identified:

1. Normal stress components.

   Tangential stress ($\sigma_{\theta\theta}$)

   Radial stress (σ_{rr})

2. Shear stress components

   Torsional shear stress ($\tau_{\theta r}$)

   Vertical shear stress ($\tau_{\theta z}$)

In the elastic region, normal shear stresses were computed using the classical Hook's Law relations namely based on the stress-strain relationships of the materials:

$$\sigma = E\varepsilon_L$$

$$\tau = G\gamma$$

Where E, G denote Young's modulus and Shear modulus respectively. γ Denote shear strain computed from the rosette gage readings as follows:

$$\gamma = 2\varepsilon_D - \varepsilon_L - \varepsilon_T$$

where ε_L, ε_T, ε_D denote longitudinal, transverse, and diagonal strain components in the rosette plane.

In the plastic region, stresses of the bridge model are calculated based on the stress-strain relationships of the materials used

3.6.3. Results

The bridge model was tested by using a manual pump and was observed at every stage. The transverse cracks of the model deck near section 9 over the middle support were found at the load of 120 kN. The cracks extended and the longitudinal cracks of the deck were observed near the section 9 at load of 450 kN shown in Figure 3.32. The shear connectors started to fail near the maximum negative moment region at the total load of 520 kN (Figure 3.33). The cracks were developing with the increment of the applied load. The longitudinal cracks were extending to the middle of spans, which can be seen in Figure 3.34, while the failure of shear connectors were extending to the positive moment region before the bridge model collapsed under the maximum applied load of 550 kN. Figure 3.35 shows the bridge model after its failure. The large plastic deformation was found over the middle support shown in Figure 3.36.

After the test, the micro concrete deck of the bridge model was removed. The middle diaphragm and the webs were observed. The cracks of the middle diaphragm and the middle web over the middle support were found (Figures 3.37 and 3.38). It may be surmised that the failure of the middle diaphragm induced the load redistribution among the webs with the middle web taking a significantly larger portion of the load and hence failure of the middle diaphragm. With the failure of the middle diaphragm the outer webs lost the supports at the middle support and then the shear connector at this region failed. The failure of the bridge model could be attributed to the failure of the middle diaphragm and insufficient shear connectors in the maximum negative moment region.

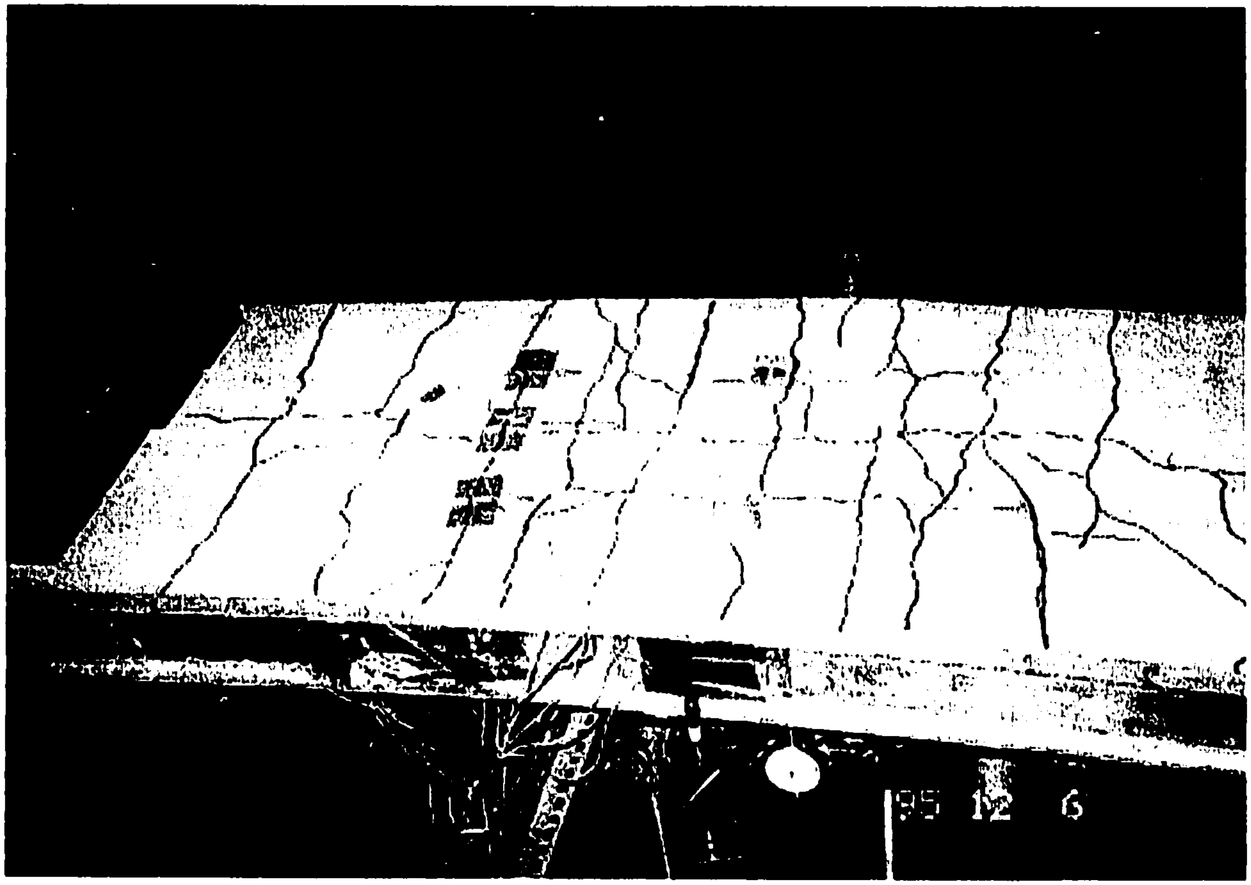

Figure 3.32 The concrete deck over the middle support

at the load of 450 kN

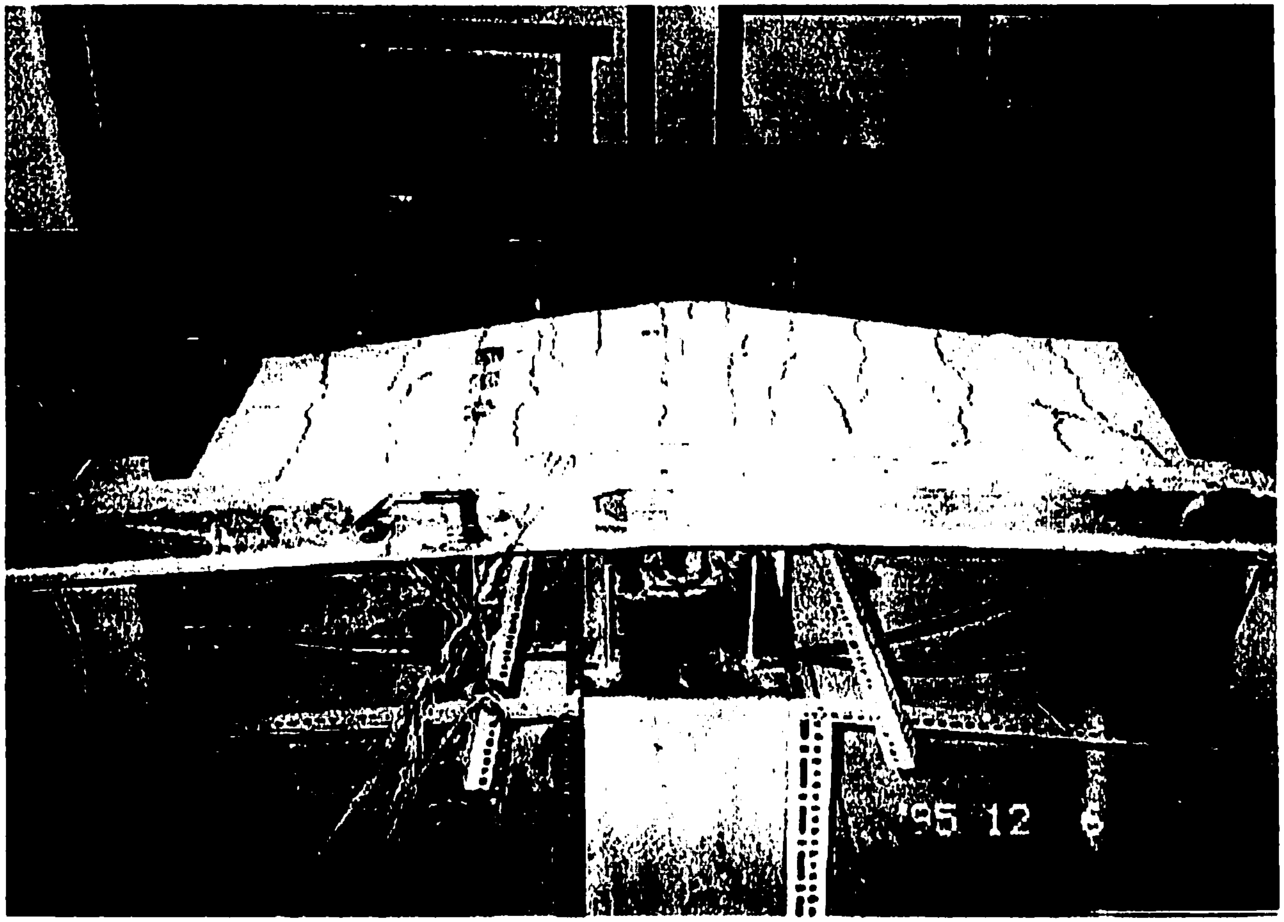

Figure 3.33a The concrete deck over the middle support

at the load of 520 kN

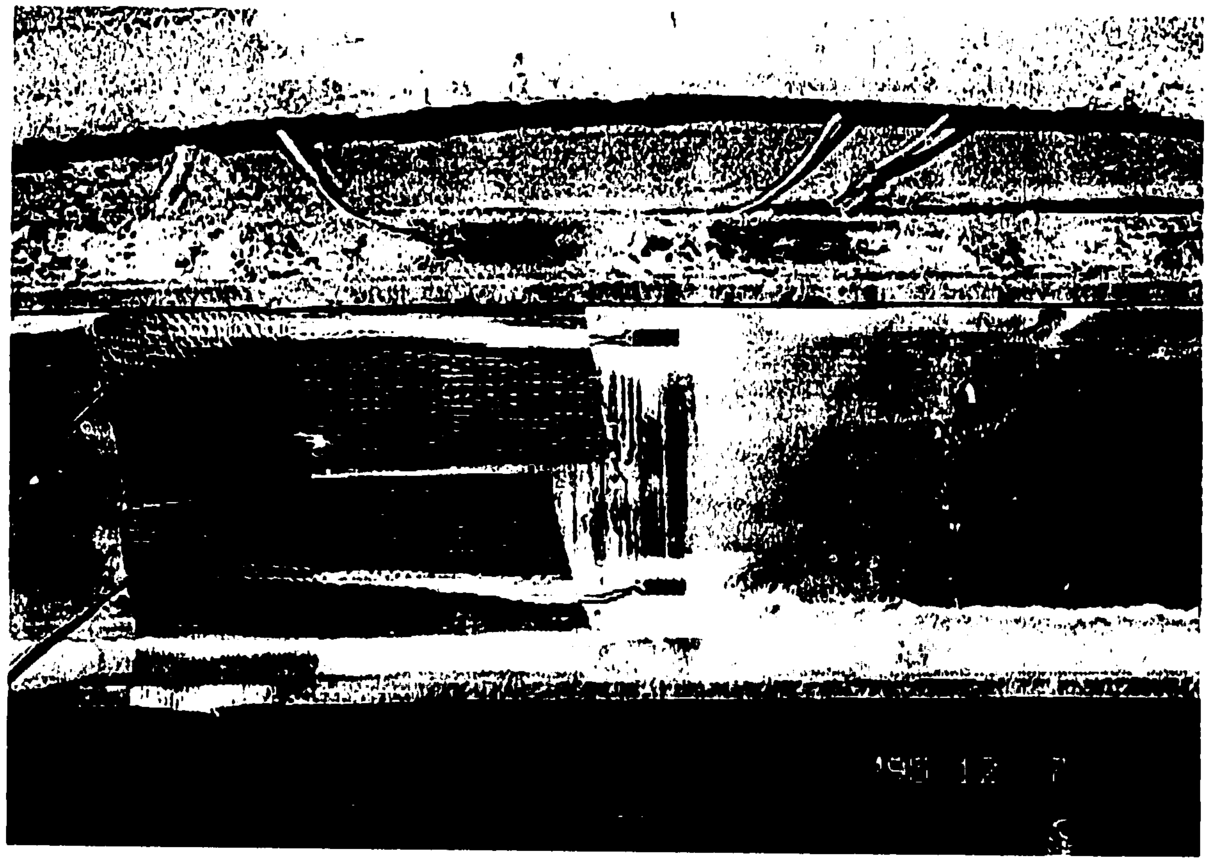

Figure 3.33bThe failure of the shear connectors near the middle support

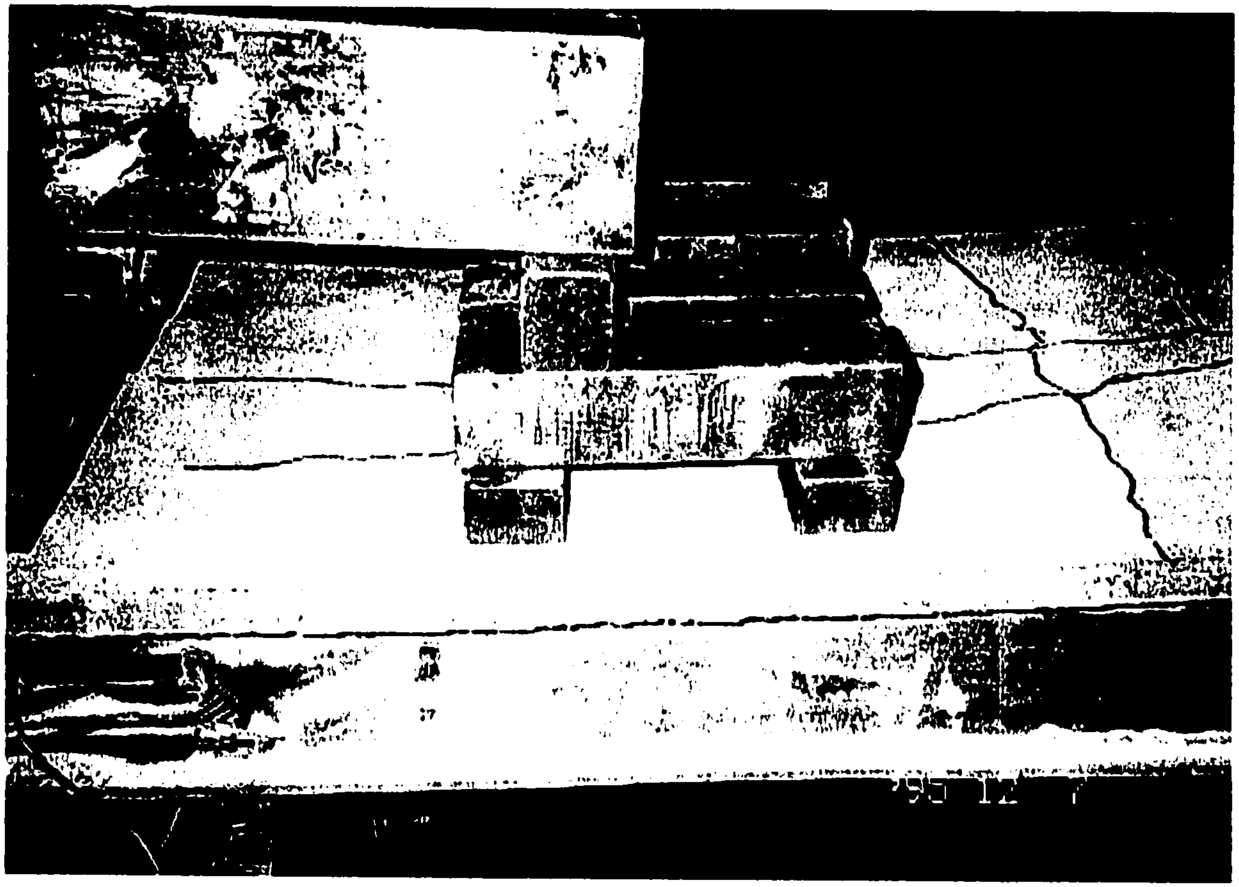

Figure 3.34 The cracks at the positive moment region

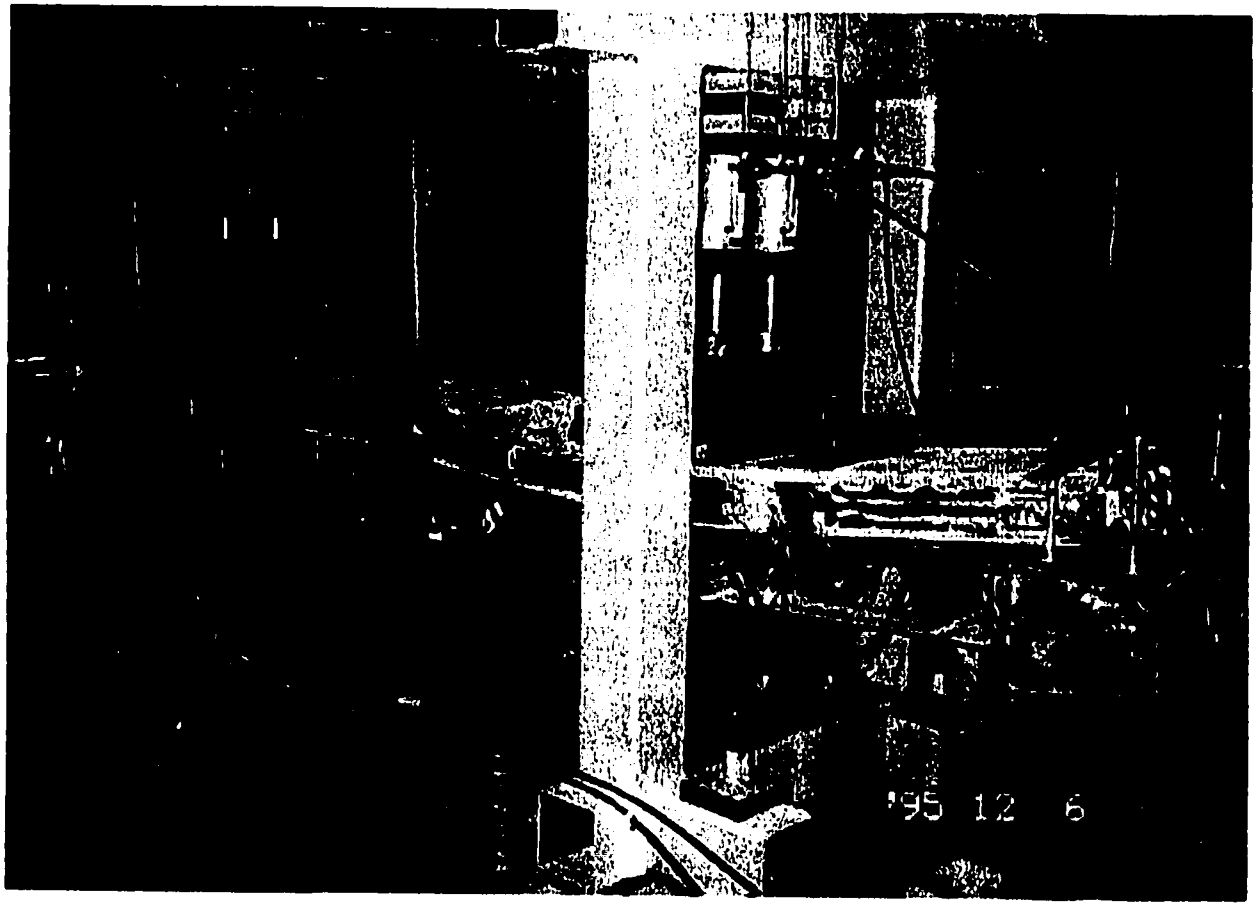

Figure 3.35 The bridge model after its failure

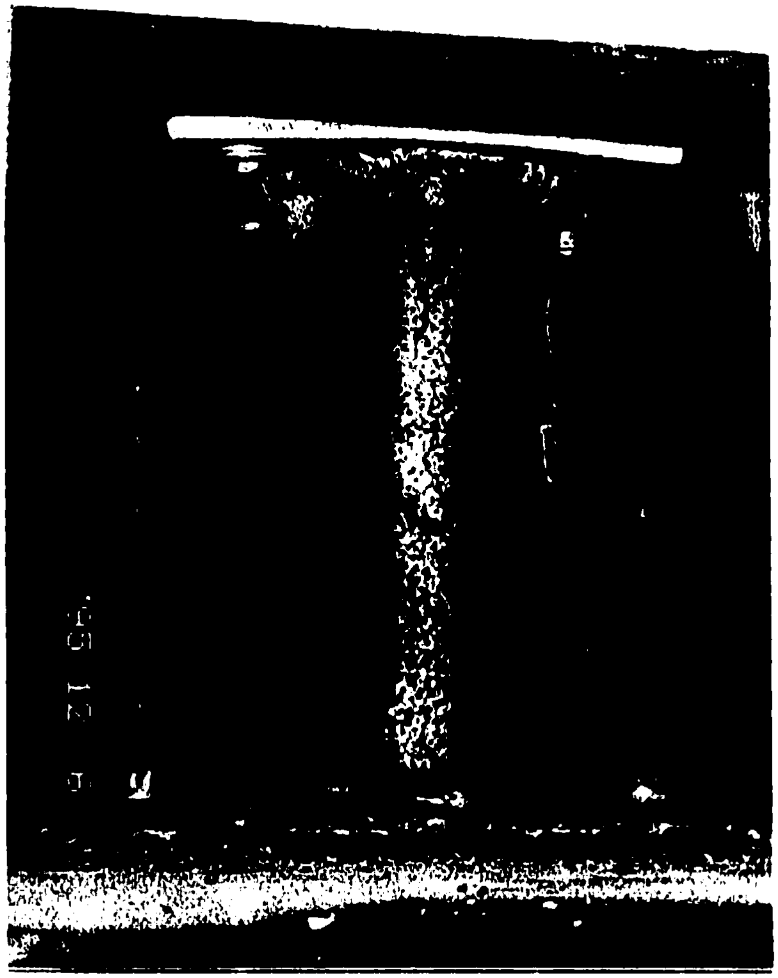

Figure 3.36 The deformation at the middle support

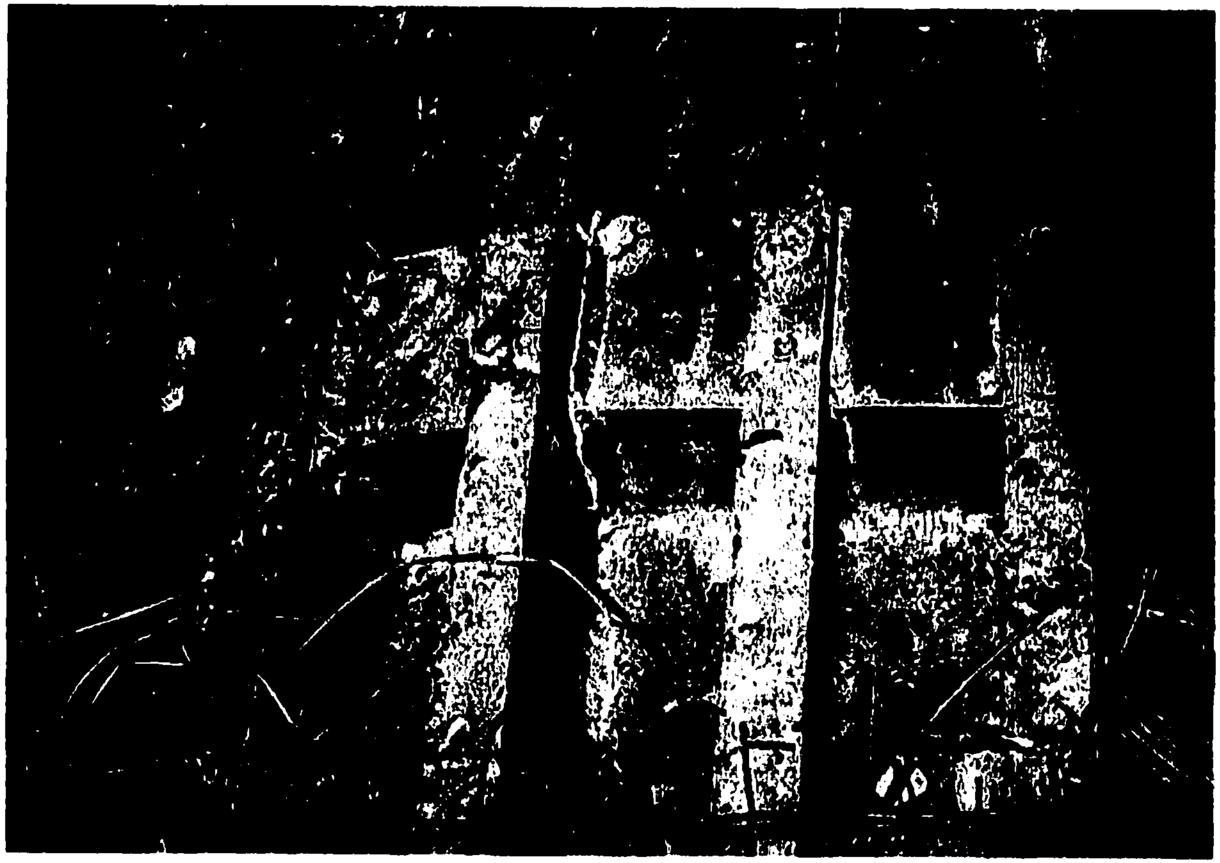

Figure 3.37 The failure of the middle diaphragm

Figure 3.38 The failure of the middle web at the middle diaphragm

The strain-load relationships of stain gages and deflection-load relationships of LVDTs are shown in Appendix C. Stresses are calculated based on their strain-load relationships and used in the comparison with the analytical results in Chapter 4.

Chapter 4

Finite Element Analysis of the Experimental Model

4.1. General

The fundamental aspect, prior to analysis, in any bridge design lies in the proper or most realistic structural idealization of the actual prototype in terms of its geometry, material, boundary conditions, as well as applied loads. In the analysis phase the mathematical idealization is further simplified by means of assumptions which establish the relation between the behavior of single elements and the integrated structure. The accuracy of such solutions depends on the validity of the assumptions made.

In this chapter, the COSMOS/M program was used to analyze the curved box-girder bridge model. Prior to analyzing the bridge model, a brief description about the finite element method and the commercially available COSMOS/M program are presented along with some modeling requirements which are specific to curved box-girder bridges.

4.2. The finite element method and COSMOS/M program

The potential energy Πp of a body can be expressed as

(4.2.1) $$\Pi_p = \int_V \left(\frac{1}{2}\{\varepsilon\}^T[E]\{\varepsilon\}\right)dV - \int_V \{u\}^T\{F\}dV - \int_S \{u\}^T\{\Phi\}dS - \{U\}^T\{P\}$$

where

$\{u\} = [u \;\; v \;\; w]^T$, the displacement field

$\{\varepsilon\} = [\varepsilon_x \;\; \varepsilon_y \;\; \varepsilon_z \;\; \gamma_{xy} \;\; \gamma_{yz} \;\; \gamma_{zx}]^T$, the strain field

$[E]$ = the material property matrix

$\{F\} = [Fx \;\; Fy \;\; Fz]^T$, body forces

$\{\Phi\} = [\Phi x \;\; \Phi y \;\; \Phi z]^T$, surface tractions

$\{U\}$ = nodal d.o.f. of the structure

$\{P\}$ = loads applied to d.o.f. by external agencies

S, V = surface area and volume of the structure.

Equation (4.2.1) can be used in finite element analysis to approximate the body as an assemblage of discretized elements interconnected at nodal points as the element boundary. By assuming the displacements, and hence the strains of the elements as a function of the finite number of nodal displacements, and $\left\{\dfrac{\partial \Pi_p}{\partial U}\right\} = \{\mathbf{0}\}$, then the equilibrium equations of the element assemblage corresponding to the nodal displacements can be written as:

(4.2.2) $$[K]\{U\} = \{R\}$$

In general, for a time-independent problem symbolized as $[K]\{U\}=\{R\}$, in linear analysis both $[K]$ and $\{R\}$ are regarded as independent of $\{U\}$, whereas in nonlinear analysis $[K]$ and/or $\{R\}$ are regarded as functions of $\{D\}$. Therefore, incremental control technique, iteration method, and convergence control schemes must be used to solve the nonlinear problems.

4.2.1 Incremental control techniques

Different control techniques have been devised to perform nonlinear analysis. These techniques can be classified as:

a) Force control

In this strategy, the loads applied to the system are used as the prescribed variables. Each state (point) on the equilibrium path is determined by the intersection of a surface (F = constant) with the path to determine the deformation parameters. In adapting this technique for finite element analysis, the loads are incrementally applied according to their associated "time" curves.

b) Displacement control

In this technique, a point on the equilibrium path is determined by the intersection of a surface defined by a constant deformation parameter (U = constant) with the solution curve. To incorporate this technique in finite element analysis, the pattern of the applied loads is proportionally incremented (using a single load multiplier) to achieve equilibrium under the control of a specified degree of freedom. The controlled DOF is incremented through the use of a "time" curve.

c) Arc-Length control

In this strategy, a special parameter is prescribed by means of a constraint (auxiliary) equation, which is added to the set of equations governing the equilibrium of the system. In the geometric sense, the control parameter can be viewed as an 'arc length' of the equilibrium path. To use this technique in finite element analysis, the pattern of the applied loads is proportionally incremented (using a single load multiplier) to achieve equilibrium under the control of a specified length (arc-length) of the equilibrium path. The arc-length will be automatically calculated by the program. No "time" curve is required.

4.2.2 Iterative solution methods

In nonlinear static analysis, the basic set of equations to be solved at any "time" step, t+Δt, is:

$$^{t+\Delta t}\{R\} - {}^{t+\Delta t}\{F\} = 0$$

where

$^{t+\Delta t}\{R\}$ =Vector of externally applied nodal loads

$^{t+\Delta t}\{F\}$ = Vector of internally generated nodal forces

Since the internal nodal forces $^{t+\Delta t}\{F\}$ depend on nodal displacements at time t+Δt, $^{t+\Delta t}\{U\}$, an iterative method must be used.

The following equations represent the basic outline of an iterative scheme to solve the equilibrium equations at a certain time step, t+Δt,

$$\{\Delta R\}^{(i-1)} = {}^{t+\Delta t}\{R\} - {}^{t+\Delta t}\{F\}^{(i-1)}$$

$${}^{t+\Delta t}[K]^{(i)}\{\Delta U\}^{(i)} = \{\Delta R\}^{(i-1)}$$

$${}^{t+\Delta t}\{U\}^{(i)} = {}^{t+\Delta t}\{U\}^{(i-1)} + \{\Delta U\}^{(i)}$$

$${}^{t+\Delta t}\{U\}^{(0)} = {}^{t}\{U\}\,; \quad {}^{t+\Delta t}\{F\}^{(0)} = {}^{t}\{F\}$$

where

${}^{t+\Delta t}\{R\}$ = Vector of externally applied nodal loads

${}^{t+\Delta t}\{F\}^{(i-1)}$ = Vector of internally generated nodal forces at iteration (i)

$\{\Delta R\}^{(i-1)}$ = The out-of-balance load vector at iteration (i)

$\{\Delta U\}^{(i)}$ = Vector of incremental nodal displacements at iteration (i)

${}^{t+\Delta t}\{U\}^{(i)}$ = Vector of total displacements at iteration (i)

${}^{t+\Delta t}[K]^{(i)}$ = The Jacobian (tangent stiffness) matrix at iteration (i)

There exist different schemes to perform the above iteration. In the following, a brief description of three methods of the Newton type will be furnished.

a) Newton-Raphson (NR) Scheme

In this scheme, the tangential stiffness matrix is formed and decomposed at each iteration within a particular step. The NR method has a high convergence rate and its rate of convergence is quadrate. However, since the tangential stiffness is formed and decomposed at each iteration, the method can be prohibitively expensive for large systems. Hence, for analyzing large systems it may be advantageous to use another iterative method.

b) Modified Newton-Raphson (MNR) Scheme

In this scheme, the tangential stiffness matrix is formed and decomposed at the beginning of each step and used throughout the iterations.

c) Quasi-Newton (QN) Schemes

Unlike the NR and MNR iterative schemes, the QN family of schemes employs a lower-rank matrix to update the stiffness matrix (or its inverse) to provide secant approximation from iteration (i-1) to iteration (i). Defining a displacement increment as:

$$\{\delta\}^{(i)} = {}^{t+\Delta t}\{U\}^{(i)} - {}^{t+\Delta t}\{U\}^{(i-1)}$$

and an increment in the out-of-balance loads;

$$\{\gamma\}^{(i)} = \{\Delta R\}^{(i-1)} - \{\Delta R\}^{(i)}$$

the updated iterative matrix should satisfy the QN equation:

$${}^{t+\Delta t}[K]^{(i)}\{\delta\}^{(i)} = \{\gamma\}^{(i)}$$

The BFGS (Broyden-Fletcher-Goldfarb-Shanno) update formula are widely used with the QN algorithm.

4.2.3. Convergence control schemes

For any incremental procedure, based on iterative methods, to be effective, practical termination schemes should be provided. At the end of each iteration, a check should be made to test if the iteration converges within realistic tolerances or it is diverging. Very loose tolerance will initiate inaccurate results, while very strict tolerance can needlessly make the computational cost prohibitive. On the other hand, bad divergence can end the iterative process when the solution is diverging or the process is allowed to continue searching for unrealizable solutions.

A number of procedures have been introduced as convergence criteria for terminating an iterative process. In the following, three convergence criteria will be discussed.

a) Displacement convergence

This criterion is based on the displacement increments during iterations. It is given by:

$$\left|\{\Delta U\}^{(i)}\right| \le \varepsilon_d \left|^{t+\Delta t}\{U\}^{(i)}\right|$$

where $|\{\alpha\}|$ denotes the Euclidean norm of $\{\alpha\}$, and εd is the displacement tolerance.

b) Force Convergence

This criterion is based on the out-of-balance (residual) loads during iterations. It requires that the norm of the residual load vector to be within a tolerance ε_f of the applied load increment, i.e.,

$$\left|{}^{t+\Delta t}\{R\}-{}^{t+\Delta t}\{F\}^{(i)}\right| \le \varepsilon_f \left|{}^{t+\Delta t}\{R\}-{}^{t+\Delta t}\{F\}\right|$$

where ε_f is the energy tolerance.

c) Energy Tolerance

In this criterion, the increment in the internal energy during each iteration, which is the work done by the residual forces through the incremental displacements, is compared with the initial energy increment. Convergence is assumed satisfactory when the following is satisfied:

$$\left(\{\Delta U\}^{(i)}\right)^T \left({}^{t+\Delta t}\{R\}-{}^{t+\Delta t}\{F\}^{(i-1)}\right) \le \varepsilon_e \left(\Delta U^{(1)}\right)^T \left({}^{t+\Delta t}\{R\}-{}^{t+\Delta t}\{F\}\right)$$

where ε_e is the energy tolerance.

4.3. Finite Element Analytical Model

In the analysis of nonlinear behaviors of the two-span horizontally curved composite continuous four-cell box-girder bridge model, the 4-node nonlinear quadrilateral thick shell element was chosen to model the reinforced micro concrete slab deck and the aluminum webs, bottom plate and diaphragms, while the 3-D beam element was used to model the aluminum stud shear connectors and the middle steel column. Six degrees of freedom per node are considered in the analysis. Some 3-D truss elements with enough stiffness were also put with the 3-D beam element together under the concentrated loads to prevent the large deformation of the 3-D beam element in the analysis. Transverse shear deformations were considered in the shell element. The shell element is assumed to be isotropic with constant thickness. The directions of force and moment components per unit length for thick shells are shown in Figure 4.6. The main geometrical parameters of the curved bridge model used in the finite element analysis are similar to those of the bridge test model. The two end diaphragms were modeled as plates for simplicity. The equivalent thickness of the end diaphragm is modeled as 11.0 mm.

The finite element analysis model of the curved bridge model is shown in Figure 4.1. The nonlinear material behaviors were used to model the micro concrete deck and all aluminum components of the curved bridge model based on the testing results of micro concrete, aluminum materials, and the steel middle column. The elasto-plastic stress-strain relationship with strain hardening was used to model the aluminum components and the steel column. The yielding stress of the aluminum is 300 MPa with Young's modulus E of 71000 MPa in the elastic region and a strain hardening modulus 0.05E, while the yielding stress of the steel is 350 MPa with Young's modulus E of 200000 MPa in the elastic region and a strain hardening modulus 0.1E. Figure 3.9 shows the aluminum stress-strain relationship, while the typical stress-strain relationship of steel is shown in Figure 4.2. The micro concrete stress-strain relationship with the strength of the micro concrete of 60 MPa is shown in Figure 3.8. Because the 25.4mm×25.4mm×16 welded wire fabric mesh was used in the micro concrete slab deck, its effects were also taken into account in the tensile region of the micro concrete stress-strain curve. The aluminum stud shear connectors were modeled by means of the 3-D beam element with the elasto-plastic stress-strain relationship. The details of derivation of the equivalent shear connector from 3-D element are presented in the next section. For the boundary conditions in analysis, only vertical translation was restrained at the three bottom nodes for each end support while all translations and rotations were restrained at the foundation end of the middle support. As for the boundary conditions between the bottom plate of the bridge girder and the middle support, a hinge is used. That is, all translations are not allowed between them and all rotations are allowed. However, translations in both plane directions and rotation in the plane direction are restricted in the analysis. The normal stresses in the midsurface of elements and the deflections were used to compare with experimental results.

In finite element analysis, two sets of the parallel truck loading systems were employed and the concentrated loads were used as wheel loads of the truck model. The axial loads at axle No. 2 and axle No. 3 were lumped together because they are very close in the model (Figure 3.16). The equivalent load system (Figure 4.7) are used in the finite element analysis. In Figure 4.7, it is shown that two adjacent wheel loads between two adjacent model trucks are lumped together; and approximate distances are used between the adjacent axles because node loads are used in the analysis.

A 3-D beam element was used to model nonlinear behaviors of a stud shear connector. The elasto-plastic stress-strain relationship was associated with the 3-D beam element. In 1968 and 1972, Chapman and Yam used an empirical nonlinear equation to represent the shear force-slip relationship based on test results of the inelastic behaviors of simply supported and continuous composite beams. Close agreements were obtained when compared with experimental results. In 1986, Oehlers and Coughlor presented the shear force-slip relationship based on a large number of tests with different diameters of stud shanks and different concrete strengths. A typical shear-slip relationship of a stud shear connector is shown in Figure 4.3, which is based on the findings of Oehlers and Coughlor (1986). In the figure, the shear force P is represented as a fraction of the maximum static strength P_u of a stud shear connector and the slip S is represented as a fraction of the diameter of the stud shank d.

The deformation of a shear connector was assumed to be the same as a fixed-ended beam with a lateral slip (Figure 4.4). In figure 3.3, L refers to half of the thickness of the concrete slab and S refers to the slip of the shear connector or the lateral displacement of the 3-D beam. According to the typical shear-slip relationship of a stud shear connector and the assumed deformation of a shear connector, the bilinear shear-slip relationship of the shear connectors in the bridge model may be represented by means of elasto-plastic stress-strain relationship of the 3-D beam element (Figure 4.5).

For deriving the stress-strain relationship of an equivalent shear connector element, some assumptions are made as follows:

1. The shear force-slip relationship is assumed as a bilinear model. When the slip S reaches S_y, the shear connector yields ($P = P_y$) and the yielding shear force P_y is assumed to be equal to the ultimate shear force P_u at that time.

(4.3.1) $Py = Fu\ A$

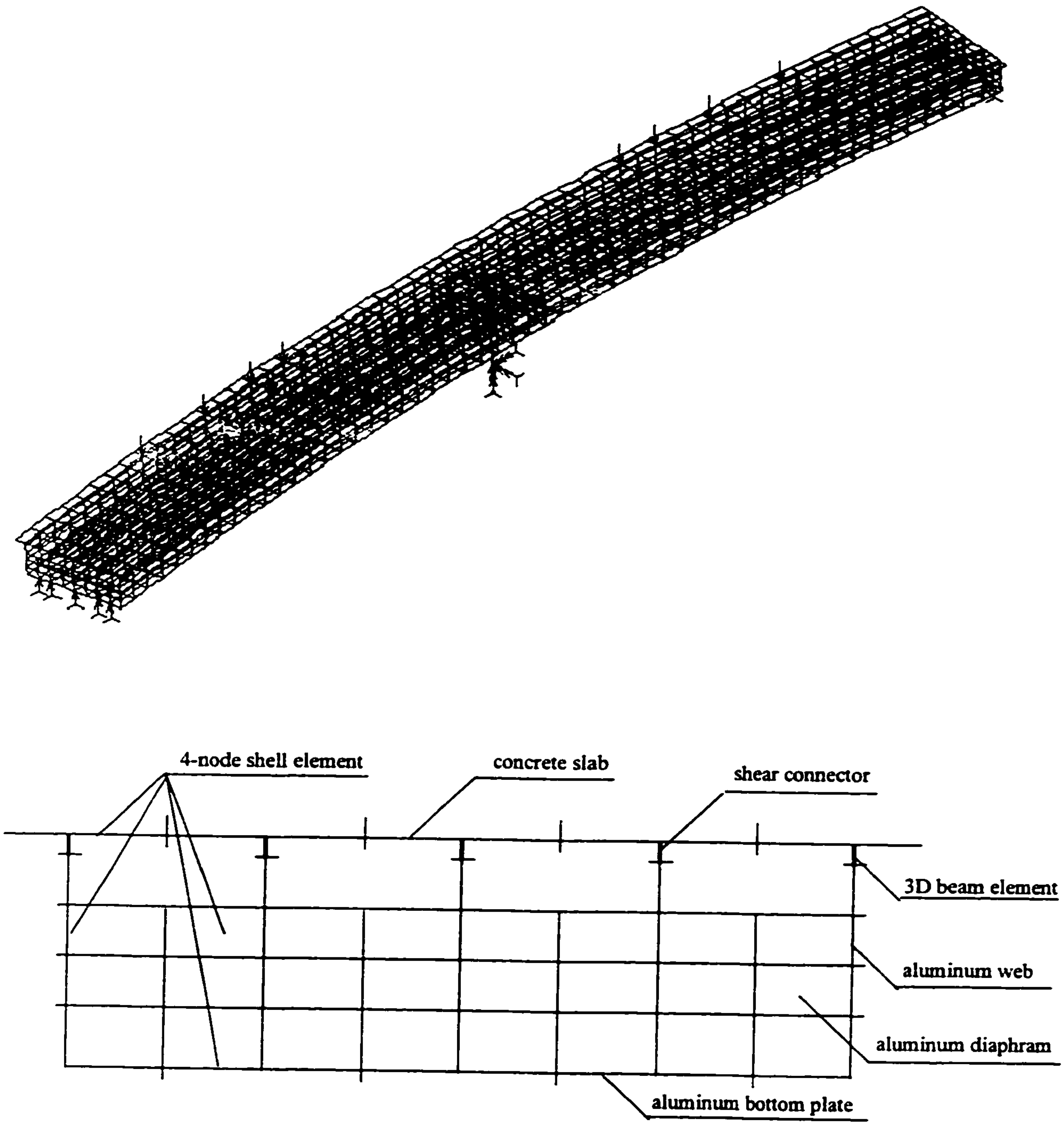

Figure 4.1 The finite element curved bridge model

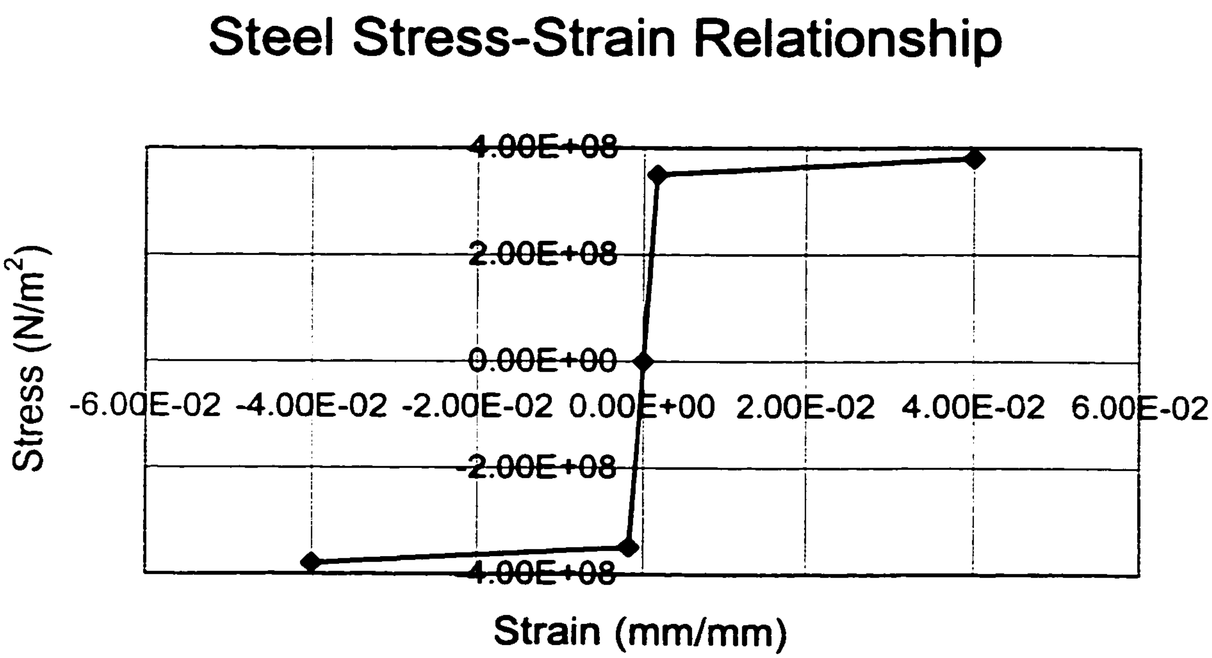

Figure 4.2 Stress-strain relationship of steel

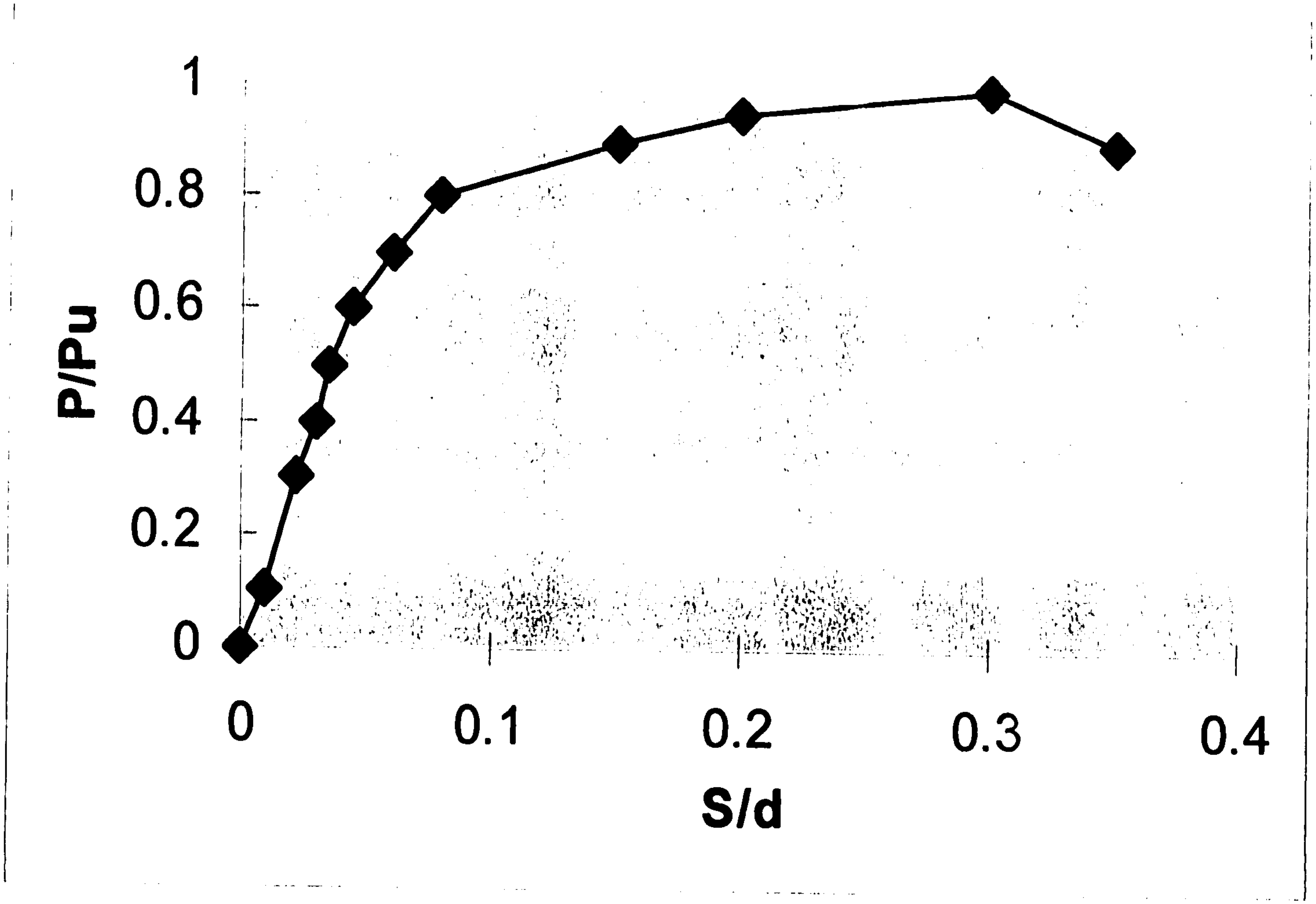

Figure 4.3 A typical force-slip relationship of a shear connector

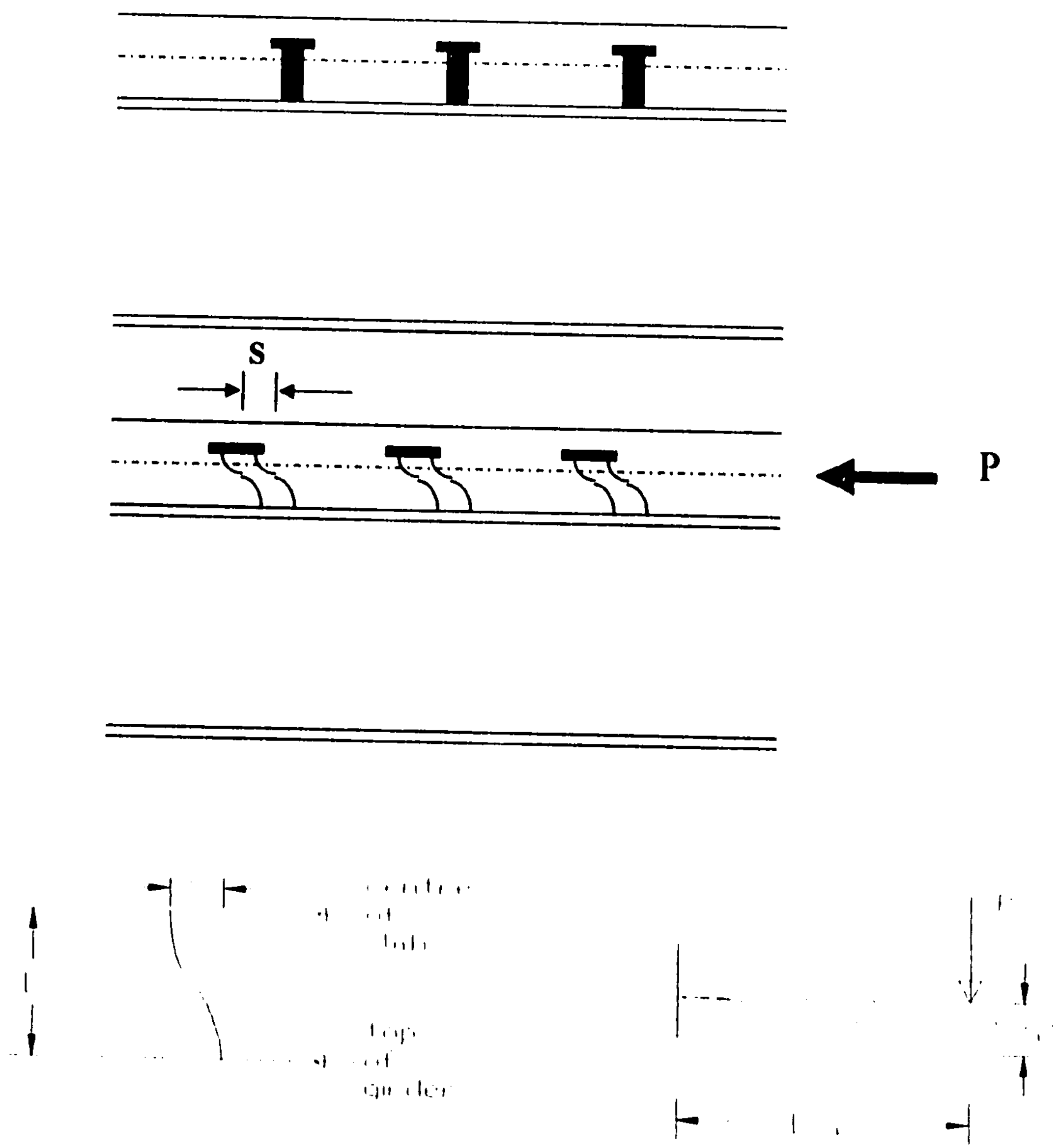

Figure 4.4 Assumed deformation of a shear connector

2. When the shear connector yields, the yielding slip equals to 0.05 of the shank diameter of stud shear connector according to the study by Oehlers and Coughlor (1986), that is

(4.3.2) $S_y = 0.05\ d$

3. The stiffness of a shear connector K_s is equal to its yielding shear force P_y divided by its yielding slip S_y, that is

(4.3.3) $$K_s = \frac{P_y}{S_y}$$

4. The slip S of the shear connector equals the lateral displacement of the 3-D beam element in the nonlinear behavior.

5. The stiffness of the shear connector and the 3-D beam element are equal in the elastic region.

6. When the shear connector yields, the 3-D beam element starts to yield. In other words, the 3-D beam element reaches its yielding moment at both of its ends. That is when $S = S_y$ and $P = P_y$ in the shear connector, $\varepsilon = \varepsilon_y$ and $\sigma = \sigma_y$ in the 3-D beam element.

Based the above assumptions, from Appendix B, we can respectively express the yielding stress and the yielding strain of an equivalent 3-D beam element as

(4.3.4) $$\sigma_y = \frac{P_y L c}{2I} = \frac{16 P_y L}{\pi D^3}$$

and

$$(4.3.5) \qquad \varepsilon_y = \frac{1.5S_y c}{L^2} = \frac{3S_y D}{L^2}$$

Therefore, the yielding shear force and the yielding slip may be determined from equations 4.3.1 and 4.3.2 respectively. If a certain value of the yielding stress of the 3-D beam element is given, then the diameter of the 3-D element will be obtained from equation 4.3.4 and the yielding strain will be calculated from equation 4.3.5. In this bridge model, L is equal to 10 mm and d is equal to 8 mm. Therefore, S_y is equal to 0.05d = 0.4 mm. According to OHBDC, F_u = 300 MPa. The yielding stress of the equivalent shear connector element σ_y = 600 MPa was also employed in the analysis. Therefore, using equations 4.3.4 and 4.3.5, the equivalent diameter D of 10.8 mm and the yielding strain ε_y of 0.13 of the shear connector may be obtained. The elasto-plastic stress-strain relationship of the equivalent shear connector element is shown in Figure 4.5.

3-D truss elements with high stiffness are also put together with 3-D beam elements under the concentrated loads such that the 3-D beam element will be prevented from deformation in the axial direction.

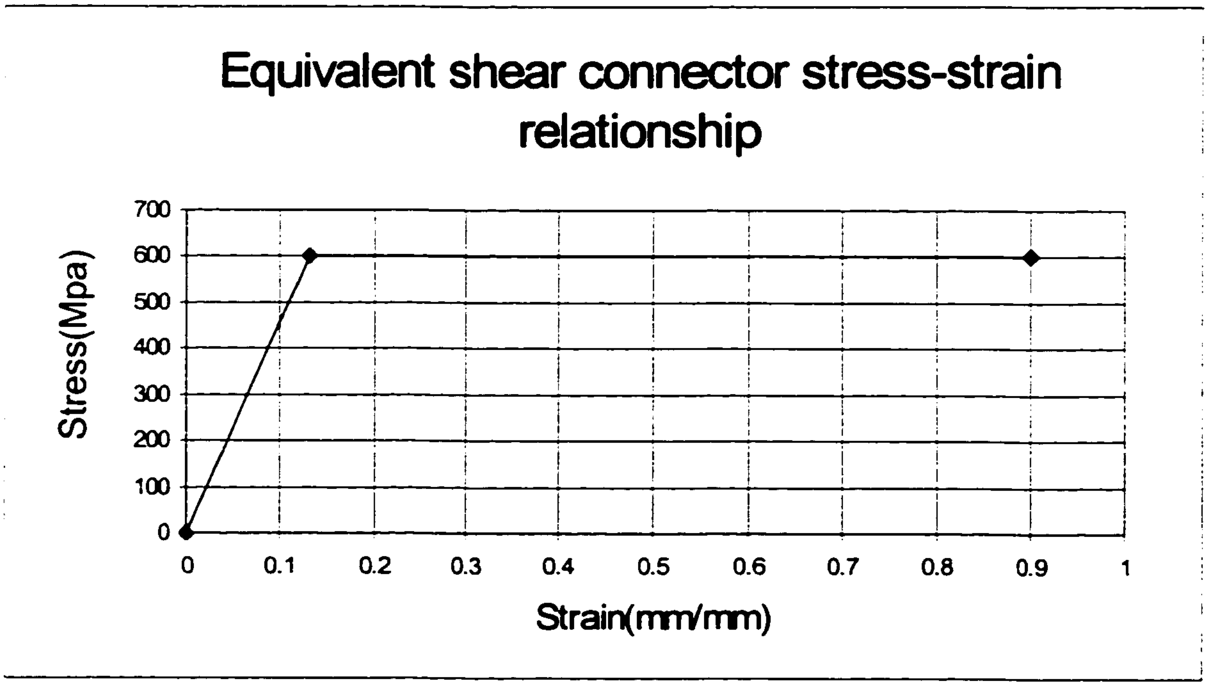

Figure 4.5 The stress-strain relationship of a 3-D beam element

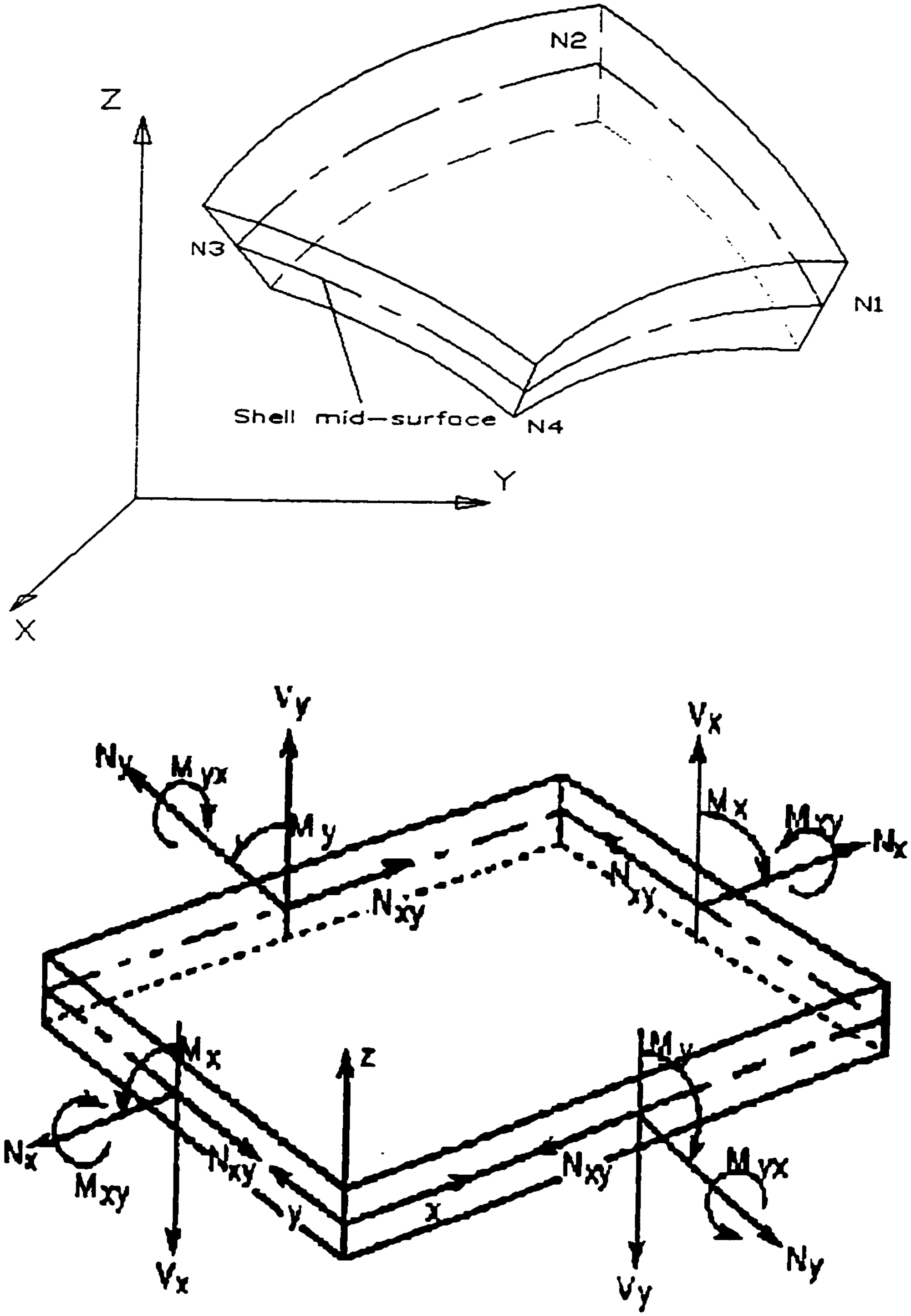

Figure 4.6   4-node thick shell element

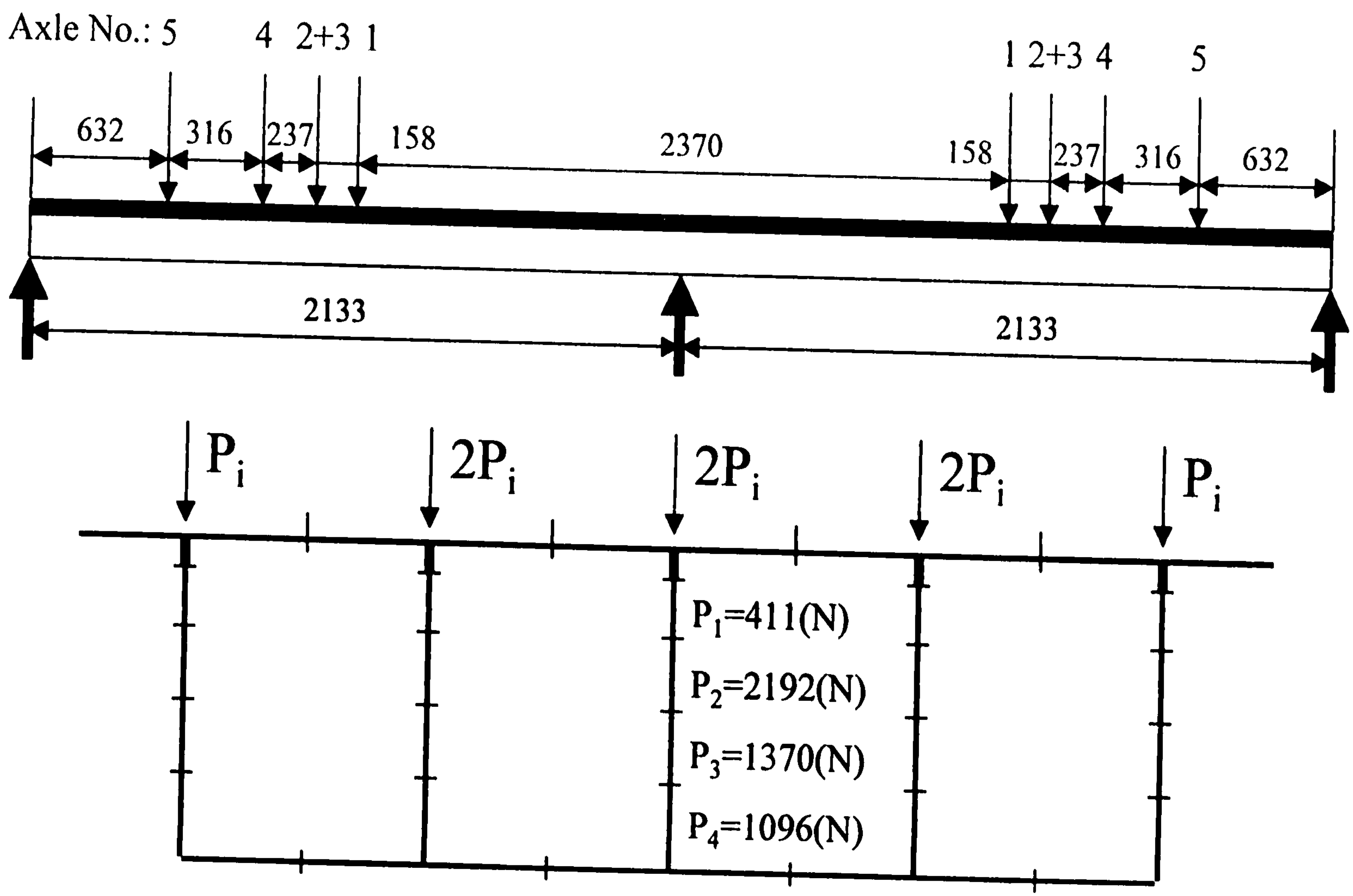

P_i refers to wheel load of truck model at axle No. i

Figure 4.7 Equivalent load system in FEM

4.4. Nonlinear Finite Element Analysis

The COSMOS/M finite element analysis program was employed for the analysis of the nonlinear behaviors of the two-span horizontally curved composite continuous four-cell box-girder bridge model with a single column at the middle support. The material nonlinear responses of the curved bridge model were solved by using Newton-Raphson method. The arc-length control technique was also used to achieve the convergence. The elasto-plastic material yielding was assumed to be determined by the Von Mises yielding criterion. The stresses and deflections were calculated at all load steps.

4.5. Comparisons and Results

Nonlinear behaviors of the bridge model were calculated and analyzed step by step using COSMOS/M software program until its ultimate state is reached. The deformation of the bridge model at the load of 410kN is shown in Figure 4.8. The overall stresses of the bridge model's deck and girder at the total load of 410kN are respectively shown in Figures 4.10 and 4.11. At that time, the middle diaphragm starts to yield first. The detailed stresses of the bridge girder at the maximum negative and positive moment regions at this load stage are respectively shown in Figures 4.12 and 4.13. In the analysis the bridge model reaches its ultimate state at the total applied load of 601 kN. Figure 4.9 shows the deformation of the bridge model at its ultimate state. The large deformation of the bridge model at the middle support can be seen. Overall stresses of the bridge model's deck and girder are respectively shown in Figure 4.14 and 4.15. When the bridge model reaches the ultimate state, the yielding stresses occur in the middle web at the middle support. The detailed normal stresses of the bridge model's girder at the maximum negative moment region are shown in Figures 4.16 and 4.17. It can be seen from Figure 4.17 that the normal stresses of the bridge model's girder do not reach the yielding stresses at the maximum negative moment region.

The deflections under web A and web F at section 4 are used to compare with the experimental results, which are shown in Figures 4.18 and 4.19 respectively. It is quite evident that there is good agreement of the maximum deflections between the analytical and experimental results until the bridge model starts to yield. The maximum difference of the deflections is about 10%. Figures 4.20 and 4.21 show the deflections under web A and web F at section 9. It shows that the middle diaphragm starts to yield at the applied load of around 450 kN in the experiment, compared with a corresponding load of 410 kN in the theoretical analysis. The deflections of sections 4 and 9 at different load stages are also shown in Figure 4.25 and 4.26 respectively.

The normal stresses of sections 4 and 9 are also compared with the experimental results. Figure 4.22 and 4.24 show the normal stresses of section 4 at the load of 80 kN and 500 kN, while the normal stresses of section 9 at the load of 80 kN and 500 kN are shown in Figures 4.23 and 4.24. It can be observed that good agreements of the normal stresses at load levels in both positive and negative moment regions are obtained. In general, at all load stages the normal stresses of the bridge girder are virtually uniform at the maximum positive moment region although the normal stresses of the inner web are larger than those of the outer web. At the maximum negative moment region, the middle web is subjected to 50% more stresses than any other web not only in the lower load level but also in the higher load level. It is also found from the theoretical analysis that the shear connectors start to yield over web D at sections 7 and 11 at the load of 430 kN.

The above comparisons show that the theoretical analysis results are in good agreements with the experimental results in both deflections and normal stresses. The failure of the middle diaphragm can be found not only in the experiment but also in the nonlinear theoretical analysis. The curved bridge model could only carry an ultimate load of 550 kN due to the failure of the middle diaphragm and the fracture failure of the shear connectors, compared with the ultimate load of 601 kN as predicted from theoretical analysis where the shear connectors had sufficient ductility.

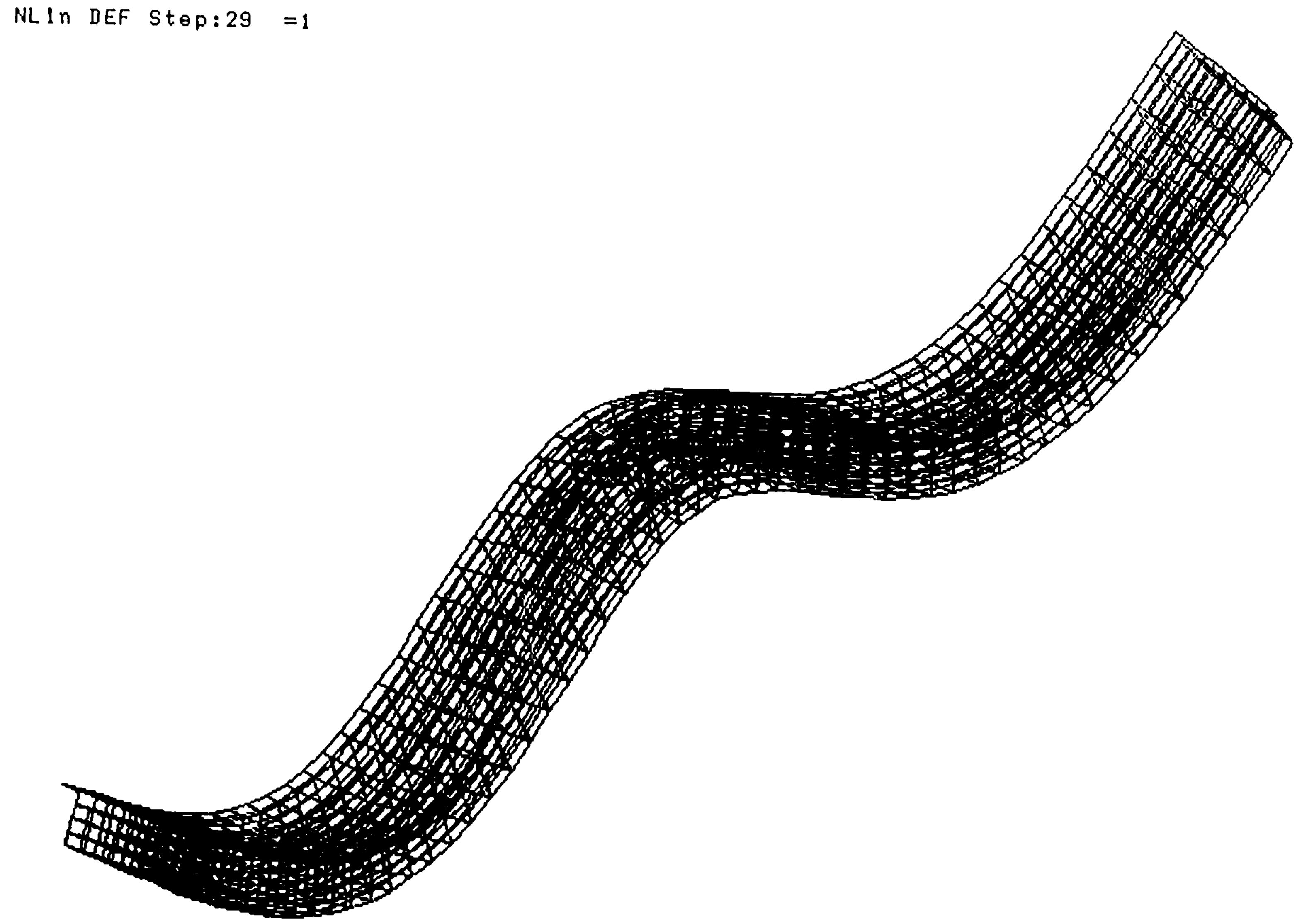

Figure 4.8 Deformation of the bridge model at the load of 410 kN

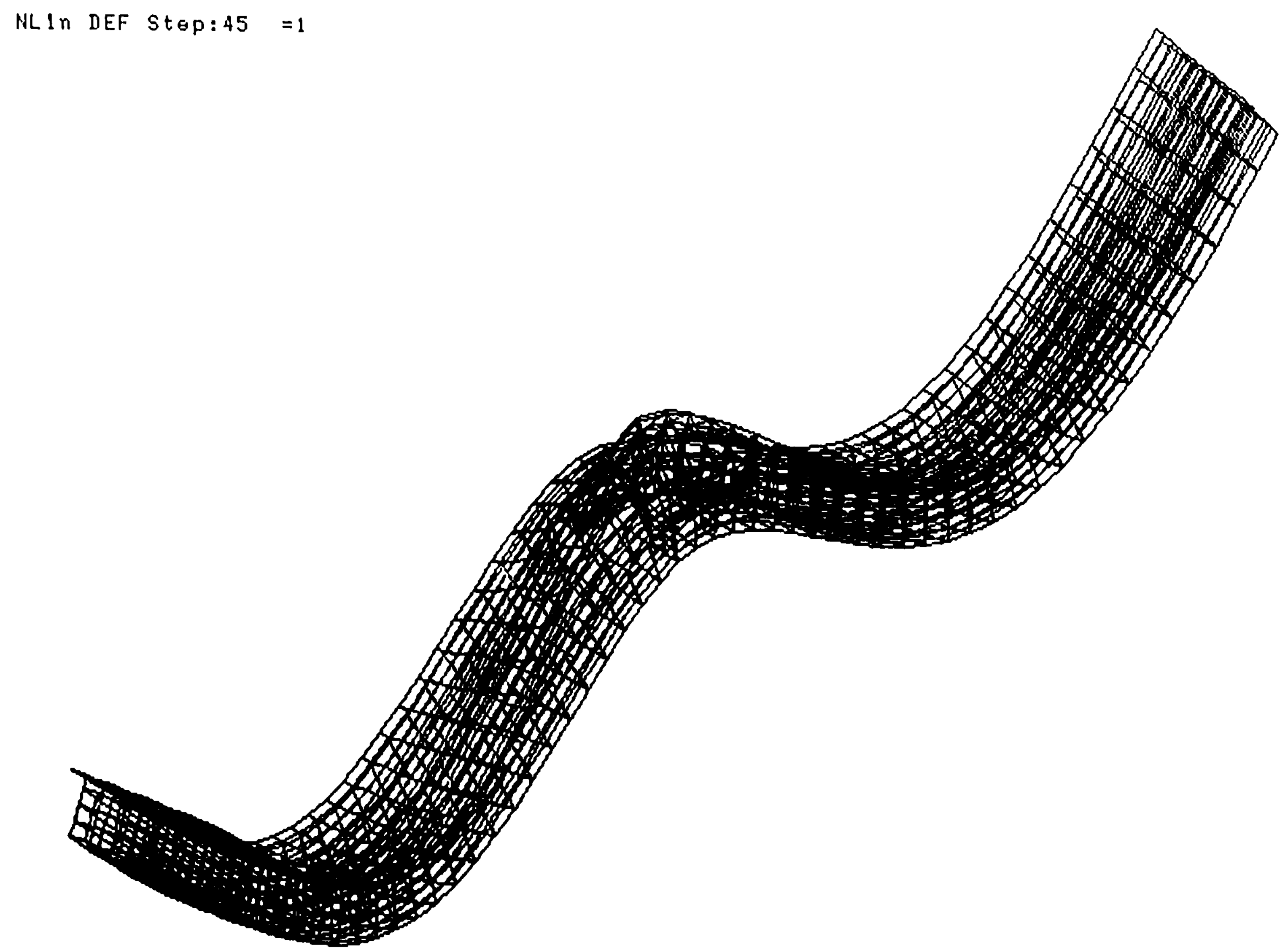

Figure 4.9 Deformation of the bridge model at the ultimate state

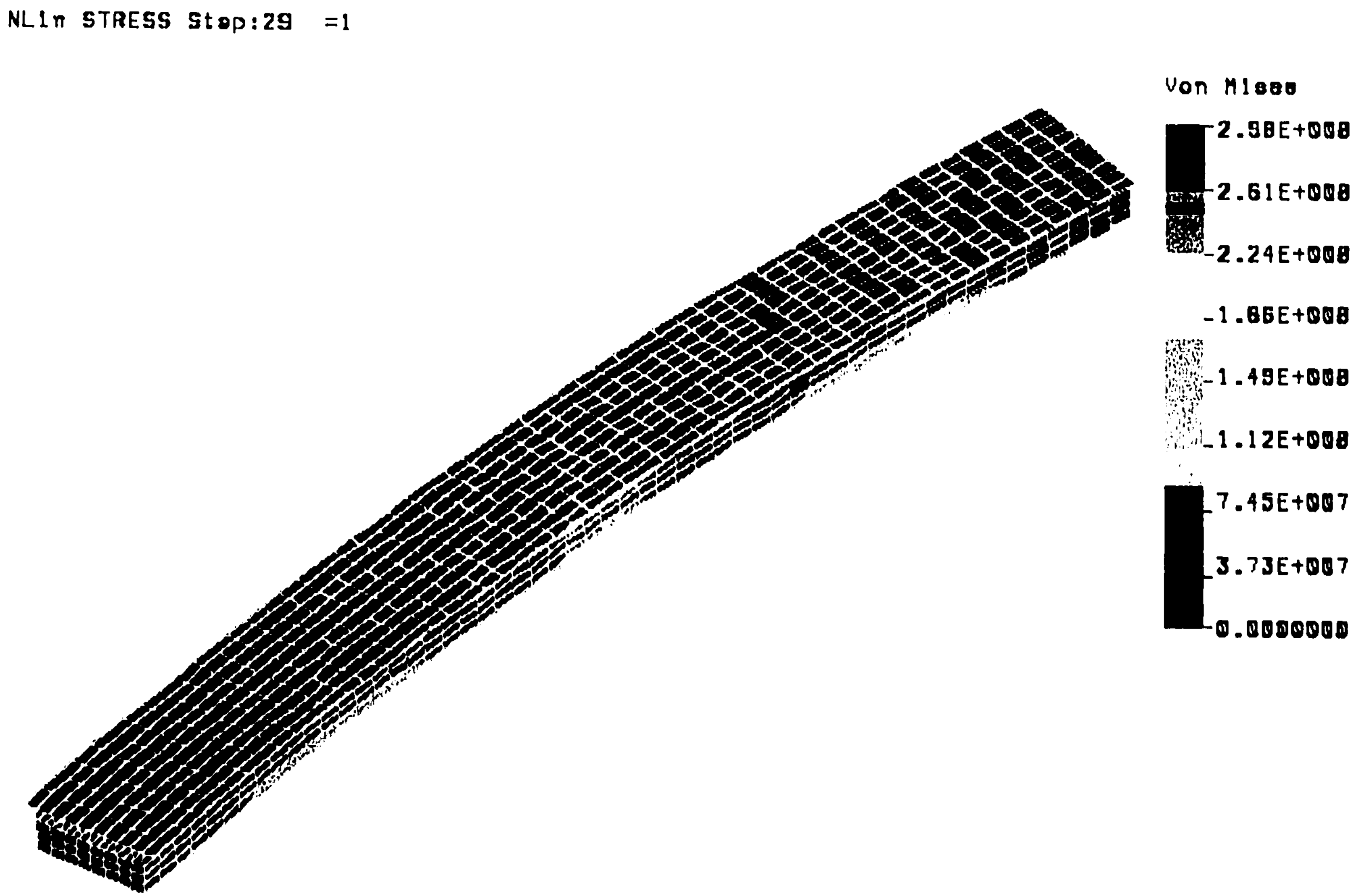

Figure 4.10 Overall stresses of the bridge model's deck

at the load of 410 kN

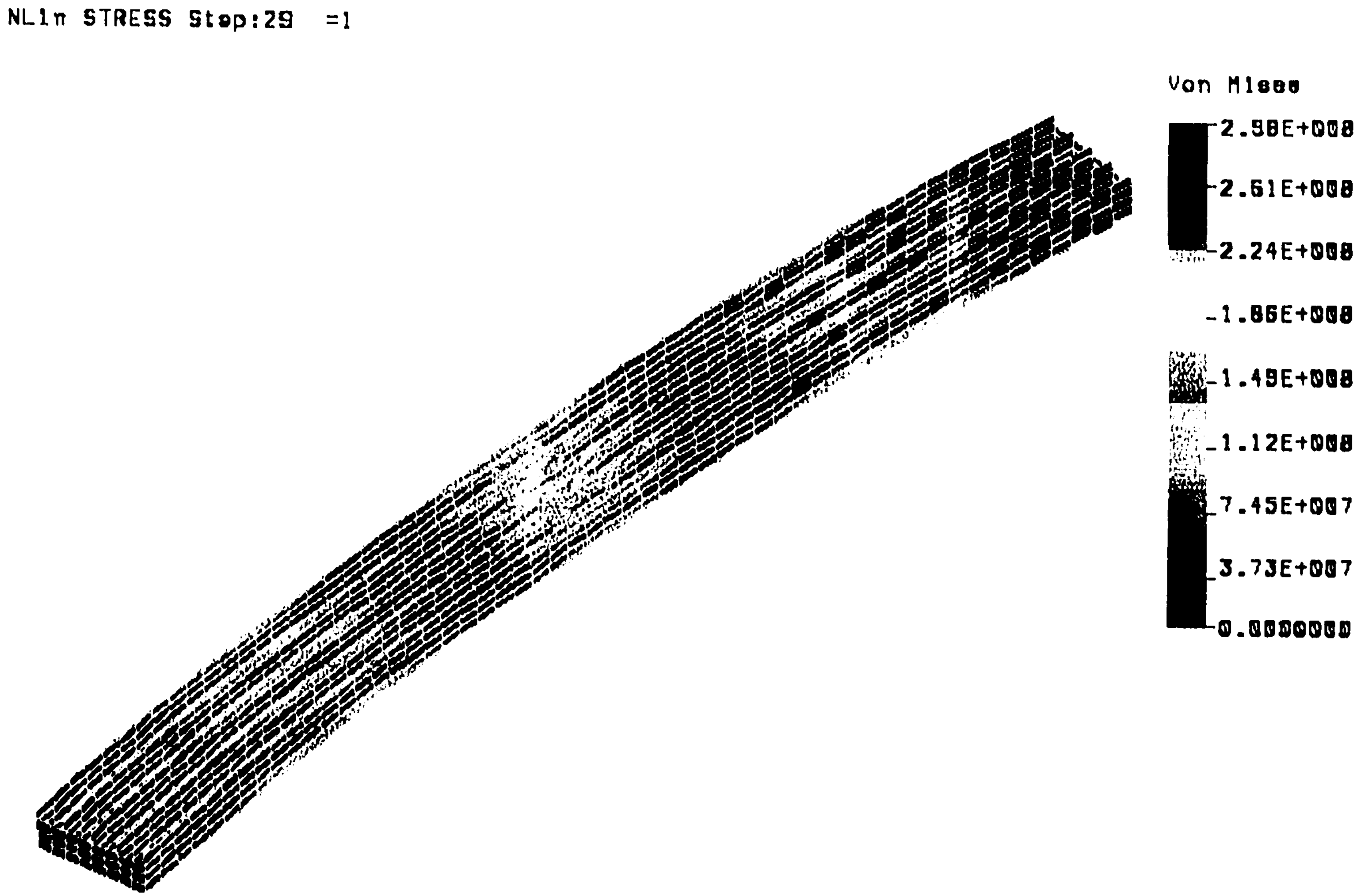

Figure 4.11 Overall stresses of the bridge model's girder

at the load of 410 kN

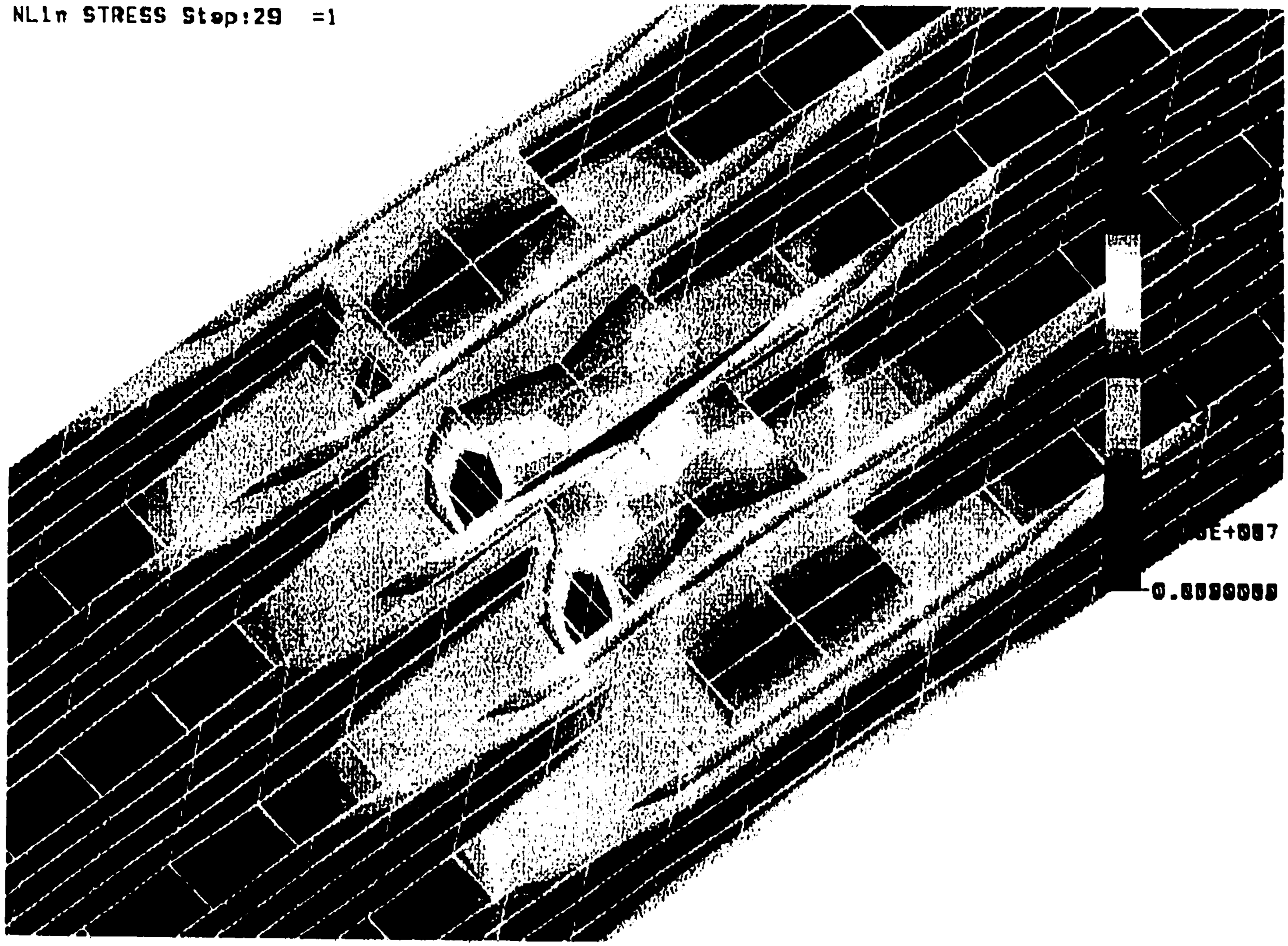

Figure 4.12 Stresses of the bridge model's girder at the maximum negative moment region at the load of 410 kN

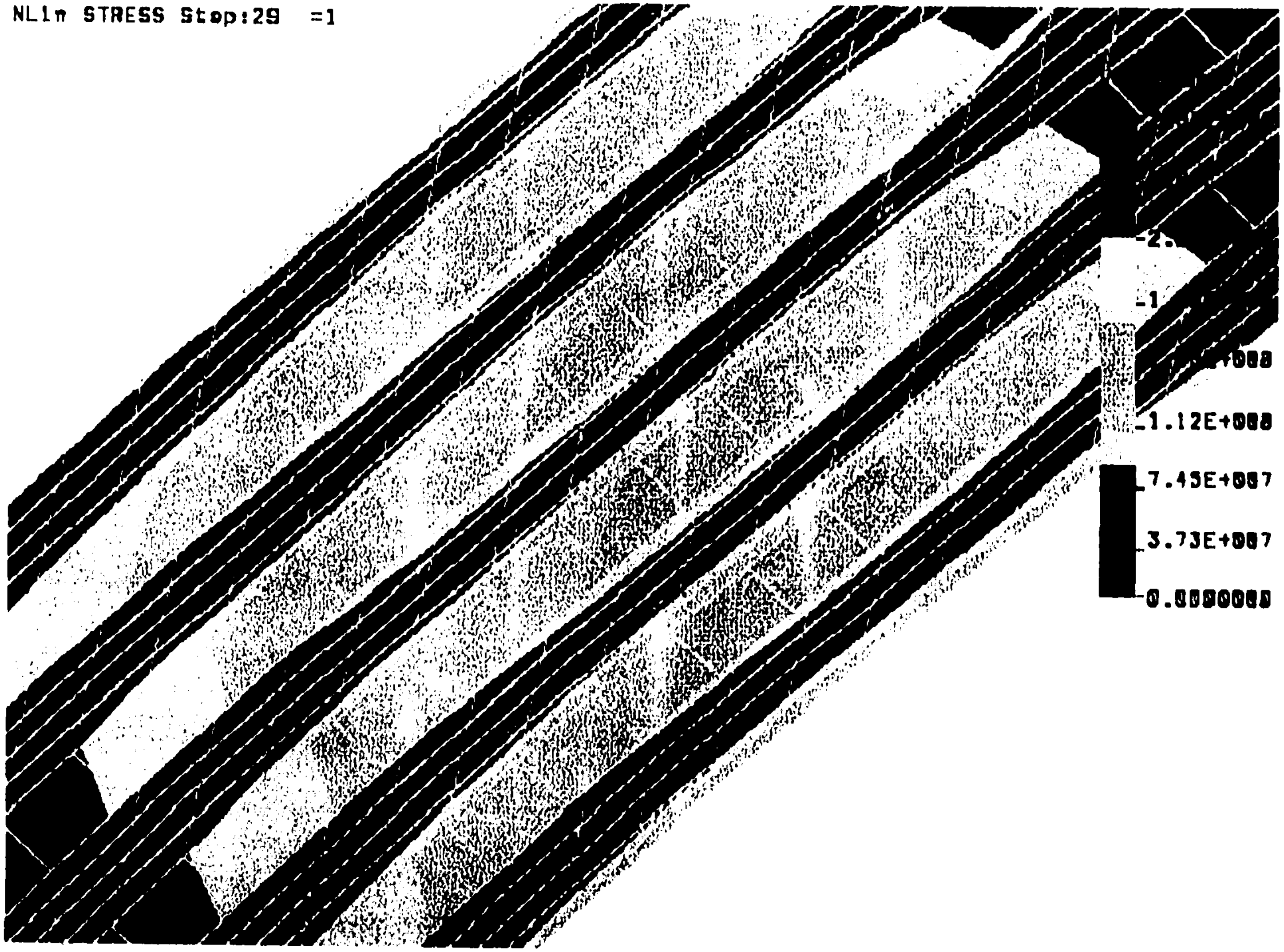

Figure 4.13 Stresses of the bridge model's girder at the maximum positive moment region at the load of 410 kN

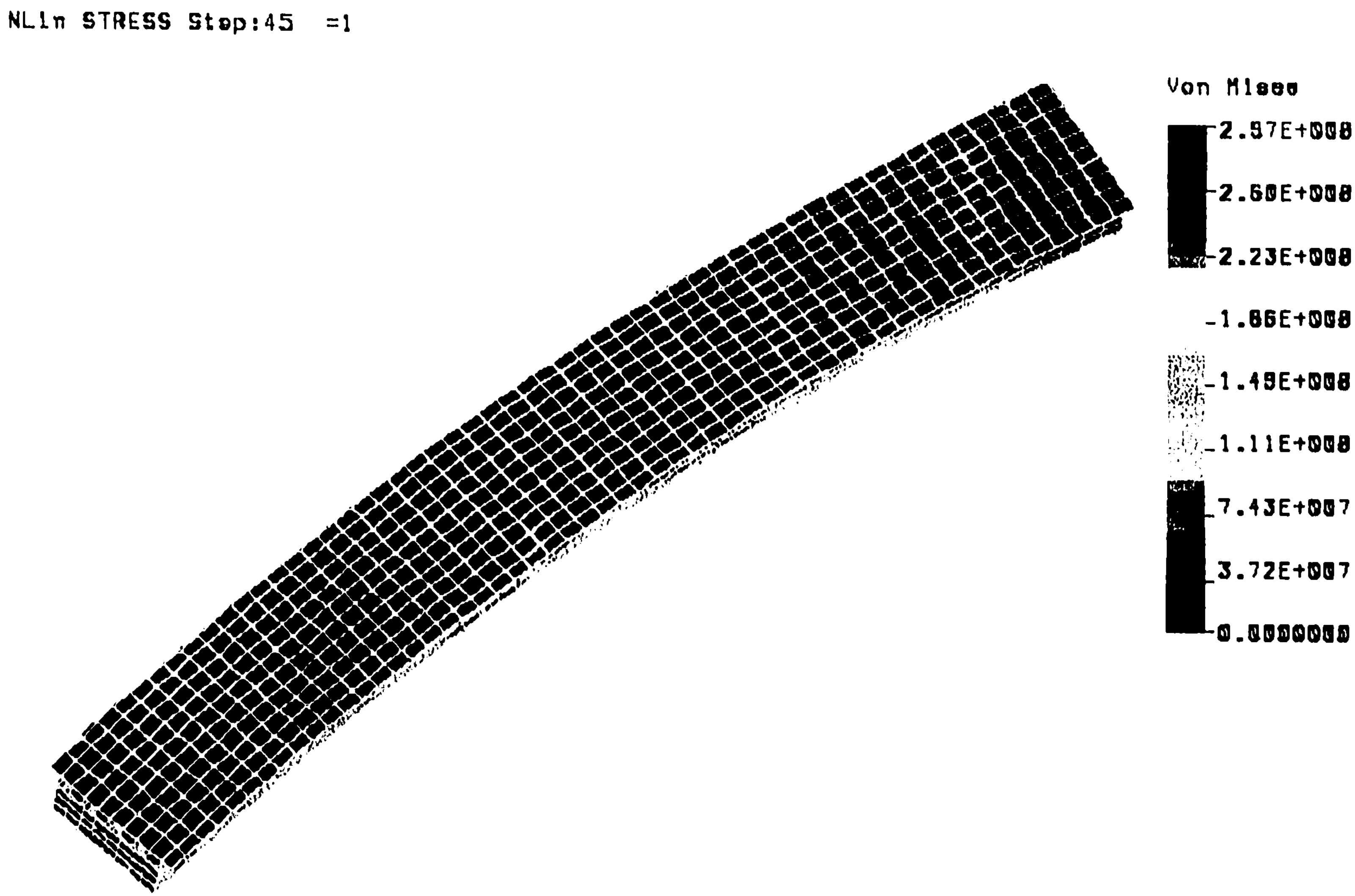

Figure 4.14 Overall stresses of the bridge model's deck

at the maximum load

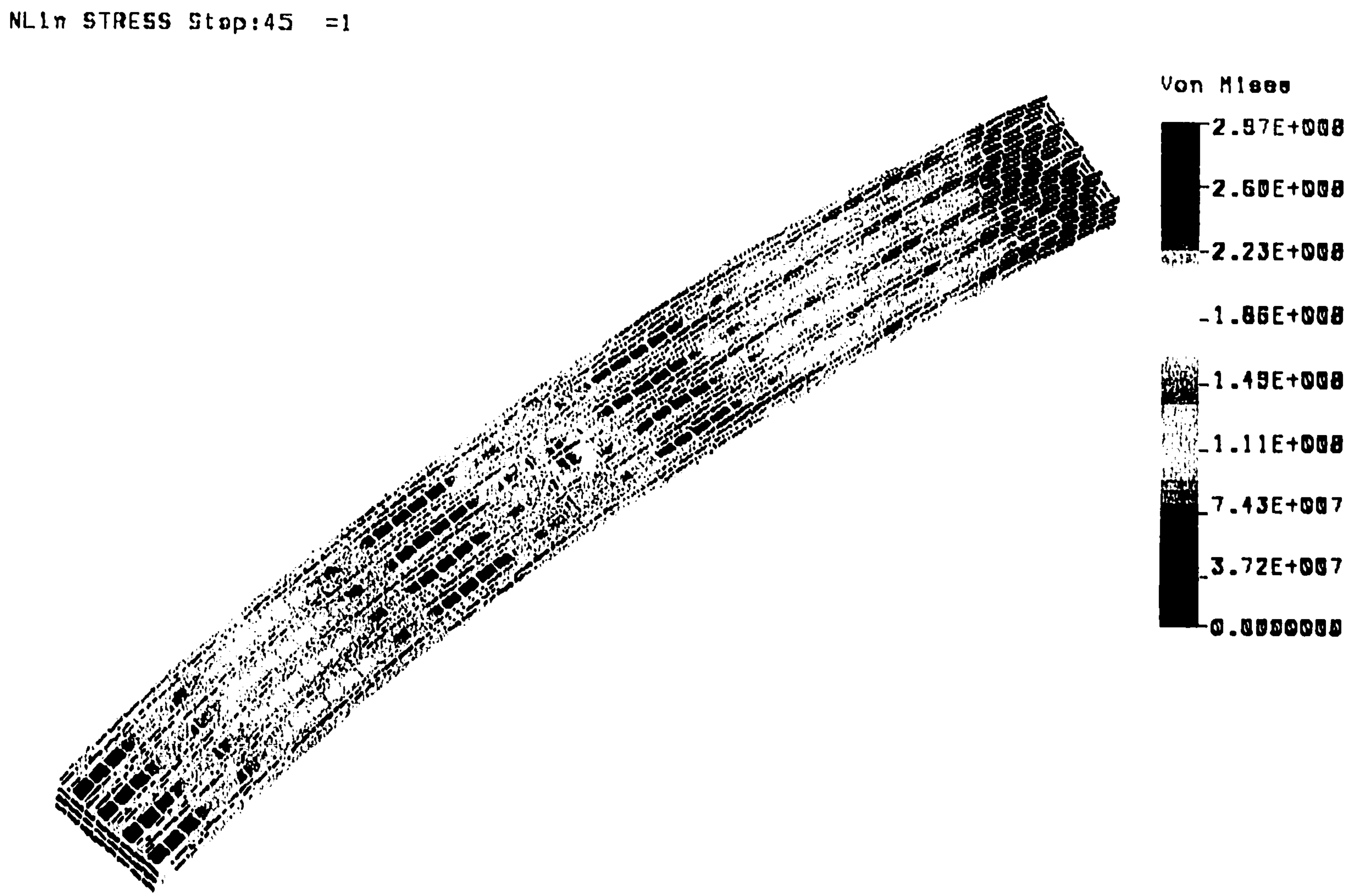

Figure 4.15 Overall stresses of the bridge model's girder

at the maximum load

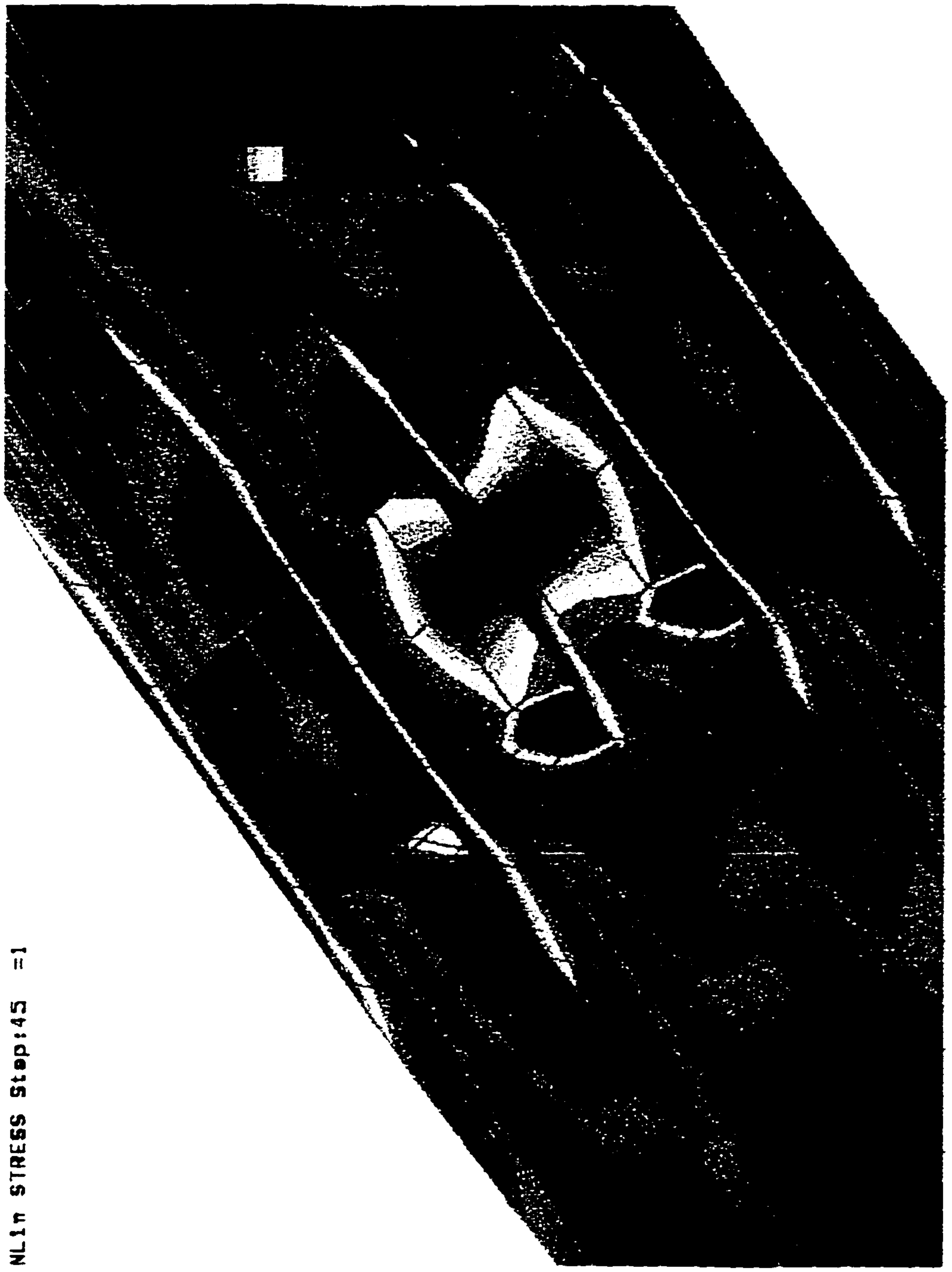

Figure 4.16 Stresses of the bridge model's girder at the maximum negative moment region at the maximum load

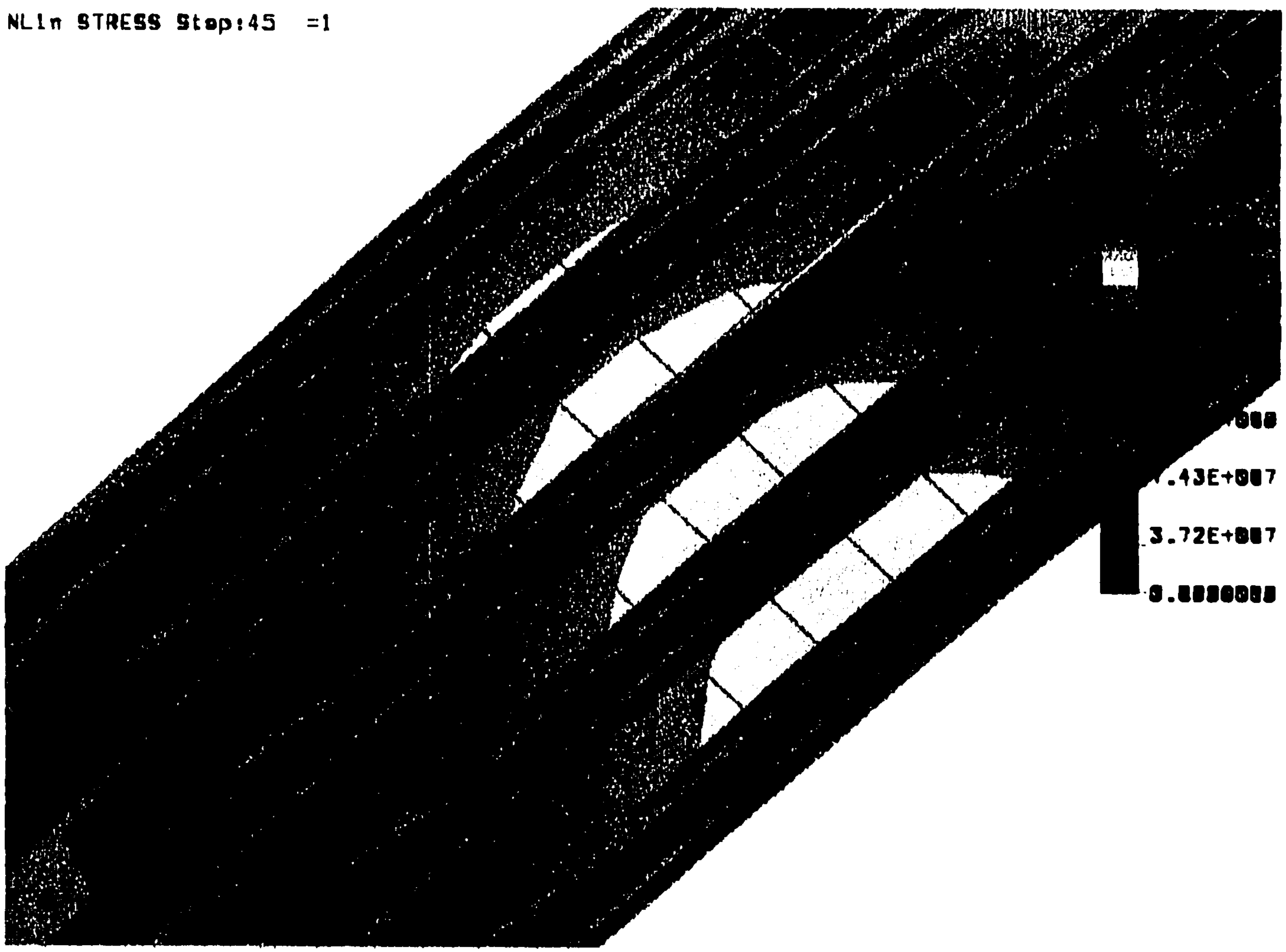

Figure 4.17 Stresses of the bridge model's girder at the maximum positive moment region at the maximum load

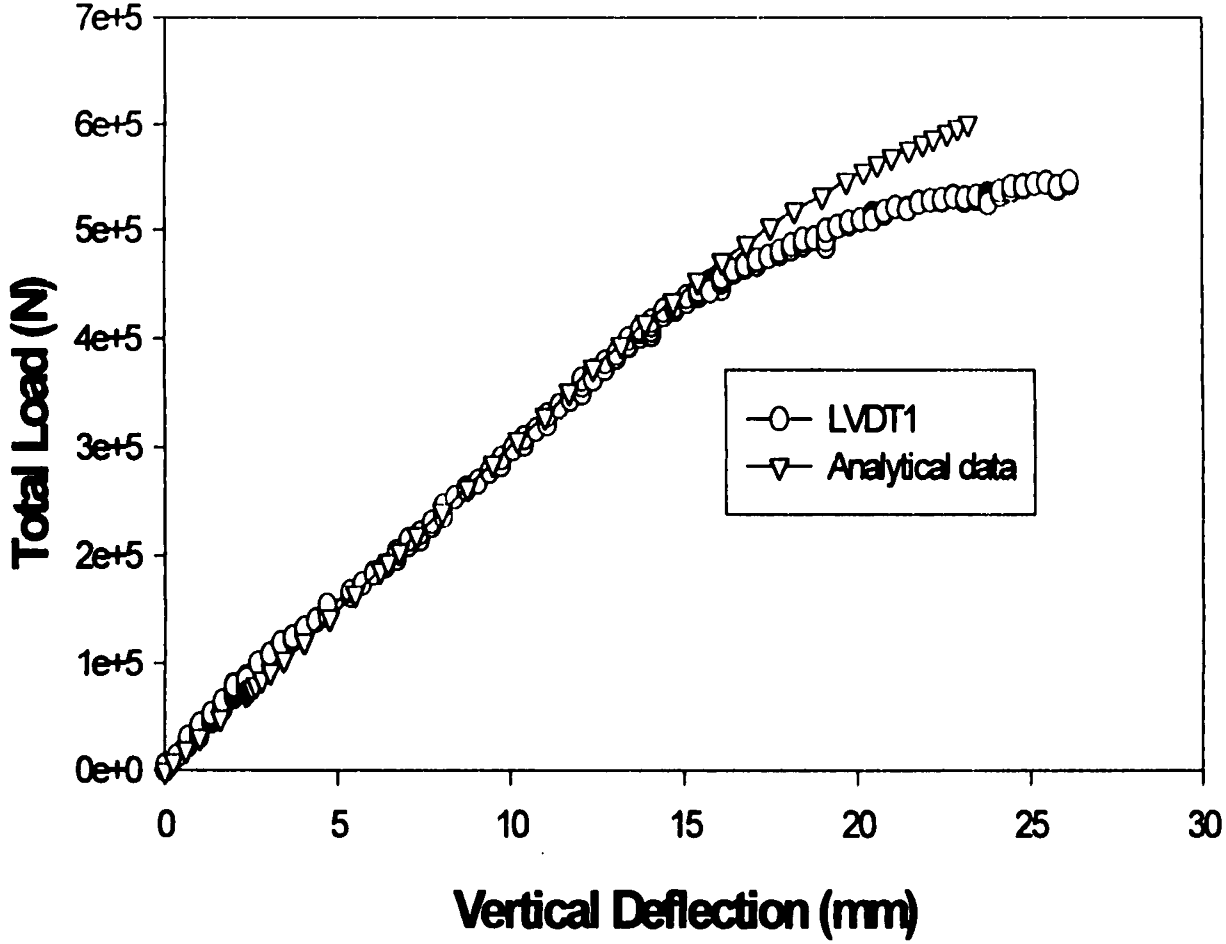

Figure 4.18 The relationship of the load vs. the deflection

under web A at section 4

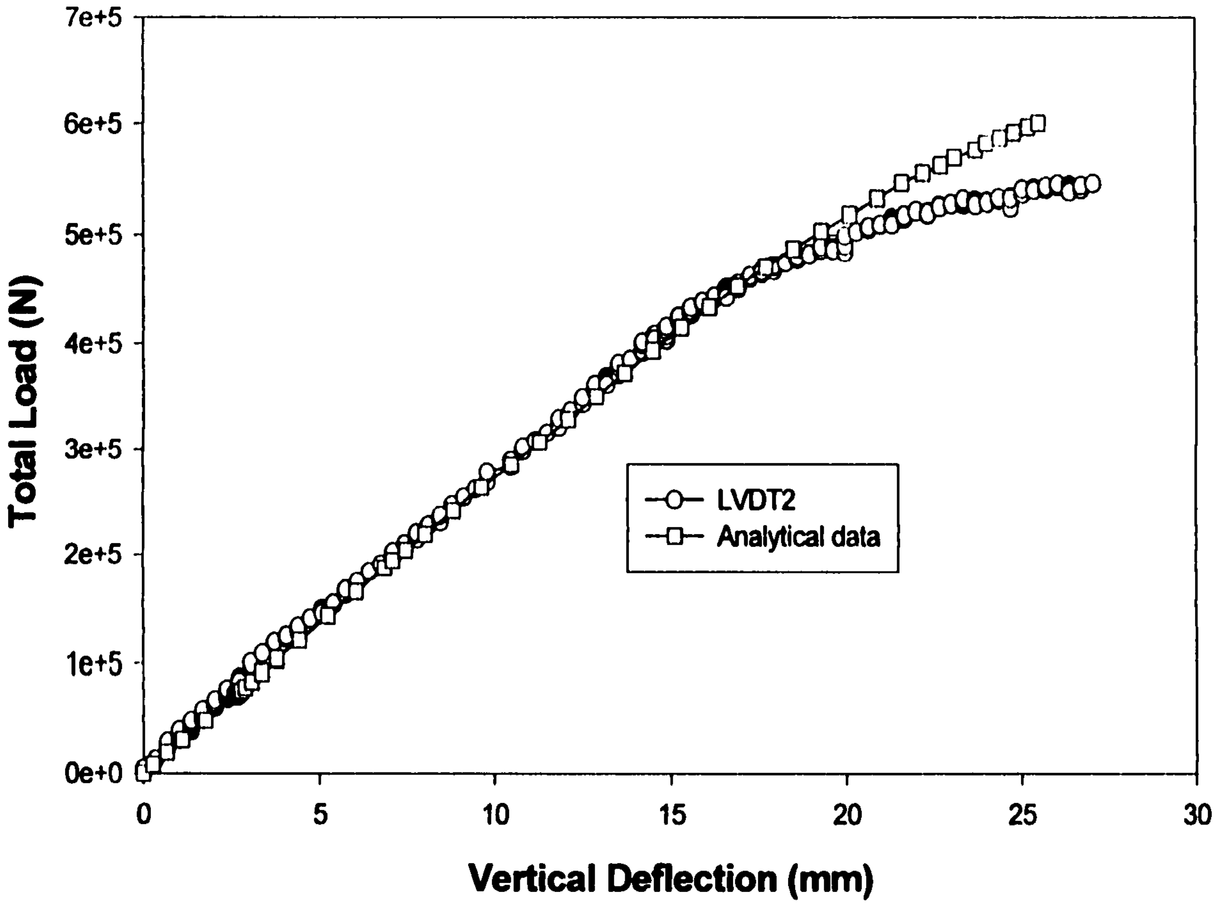

Figure 4.19 The relationship of the load vs. the deflection under web F at section 4

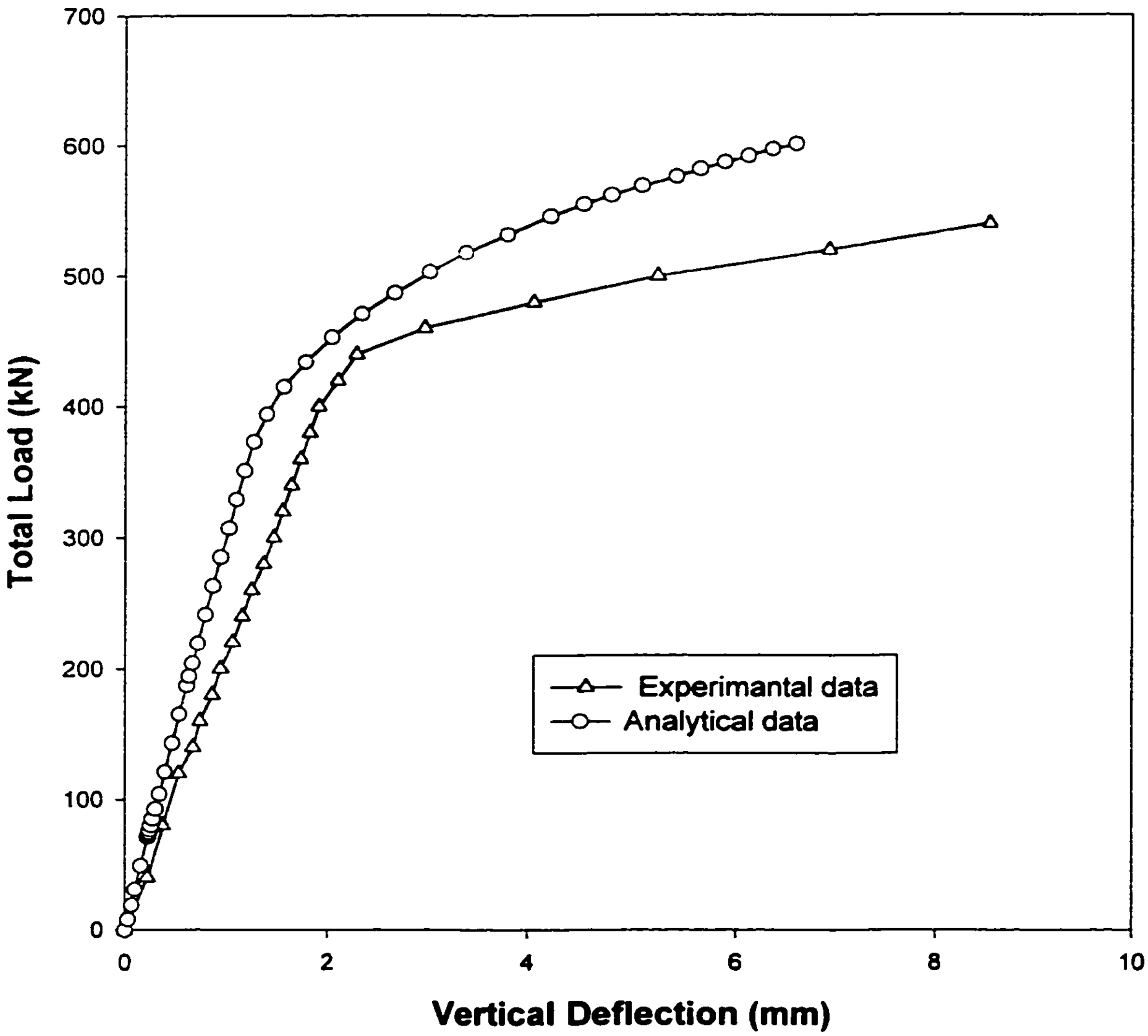

Figure 4.20 The relationship of the load vs. the deflection under web A at section 9

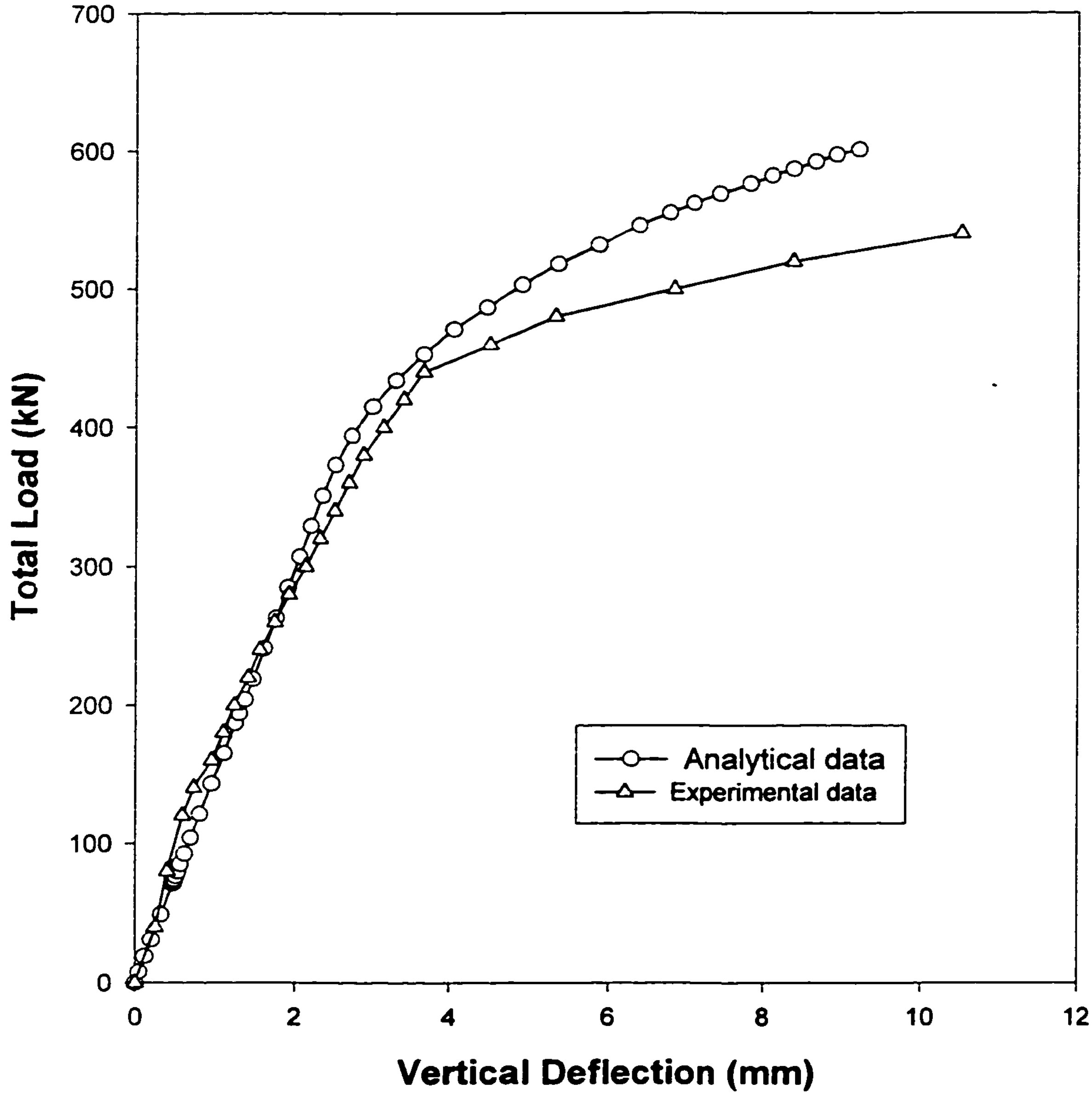

Figure 4.21 The relationship of the load vs. the deflection

under web F at section 9

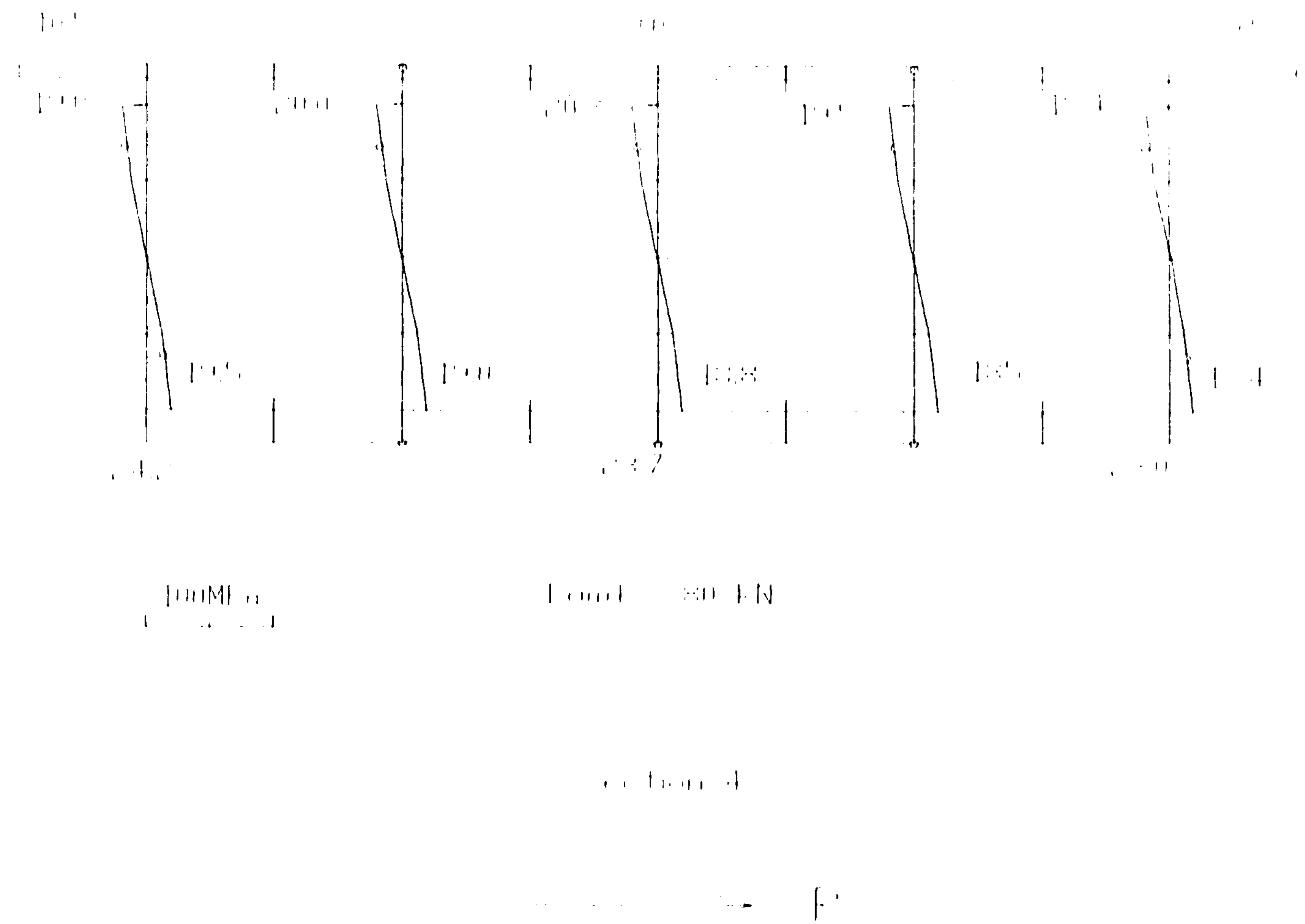

Figure 4.22 Distribution of stresses at section 4 under the load of 80 kN

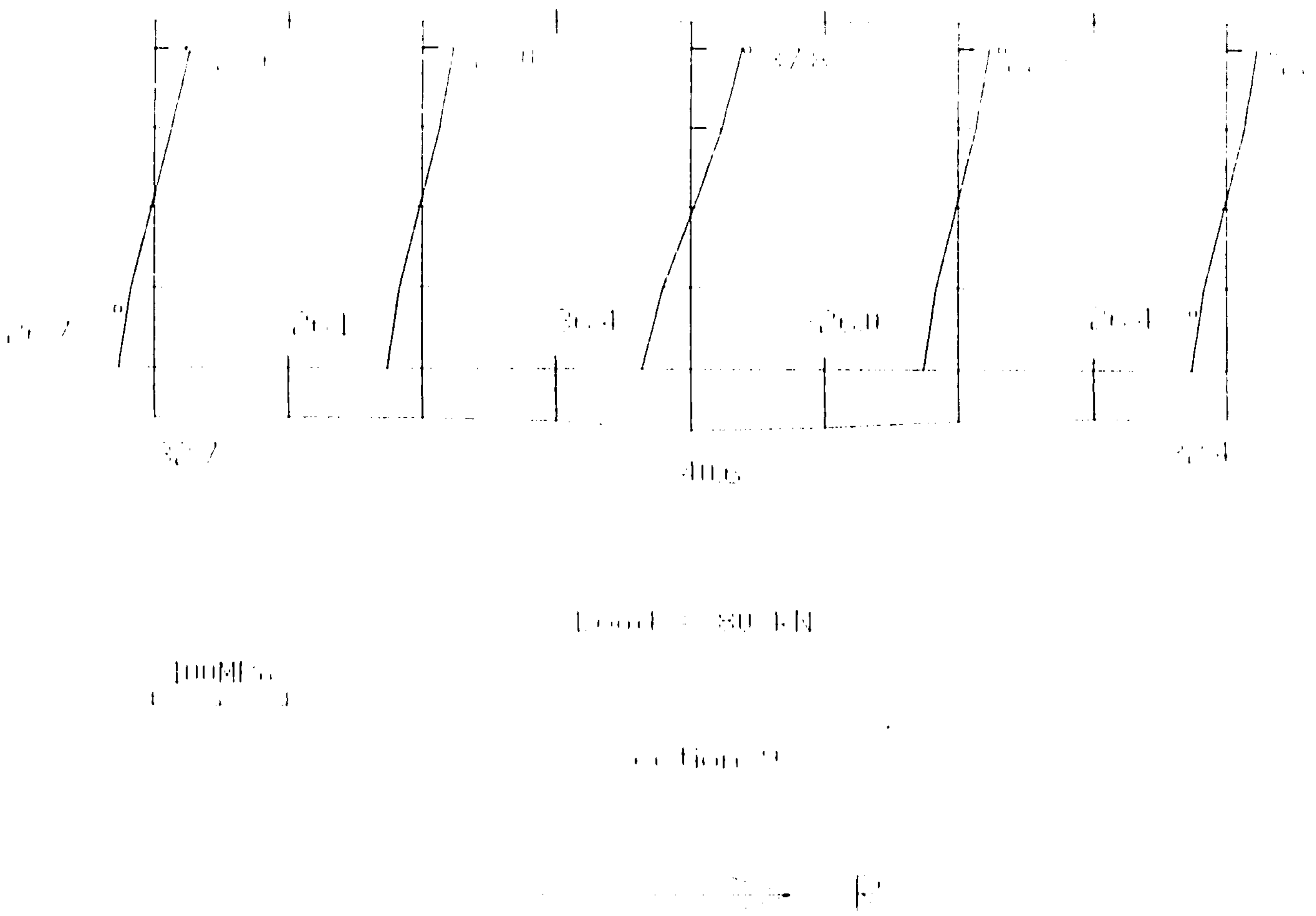

Figure 4.23 Distribution of stresses at section 9 under the load of 80 kN

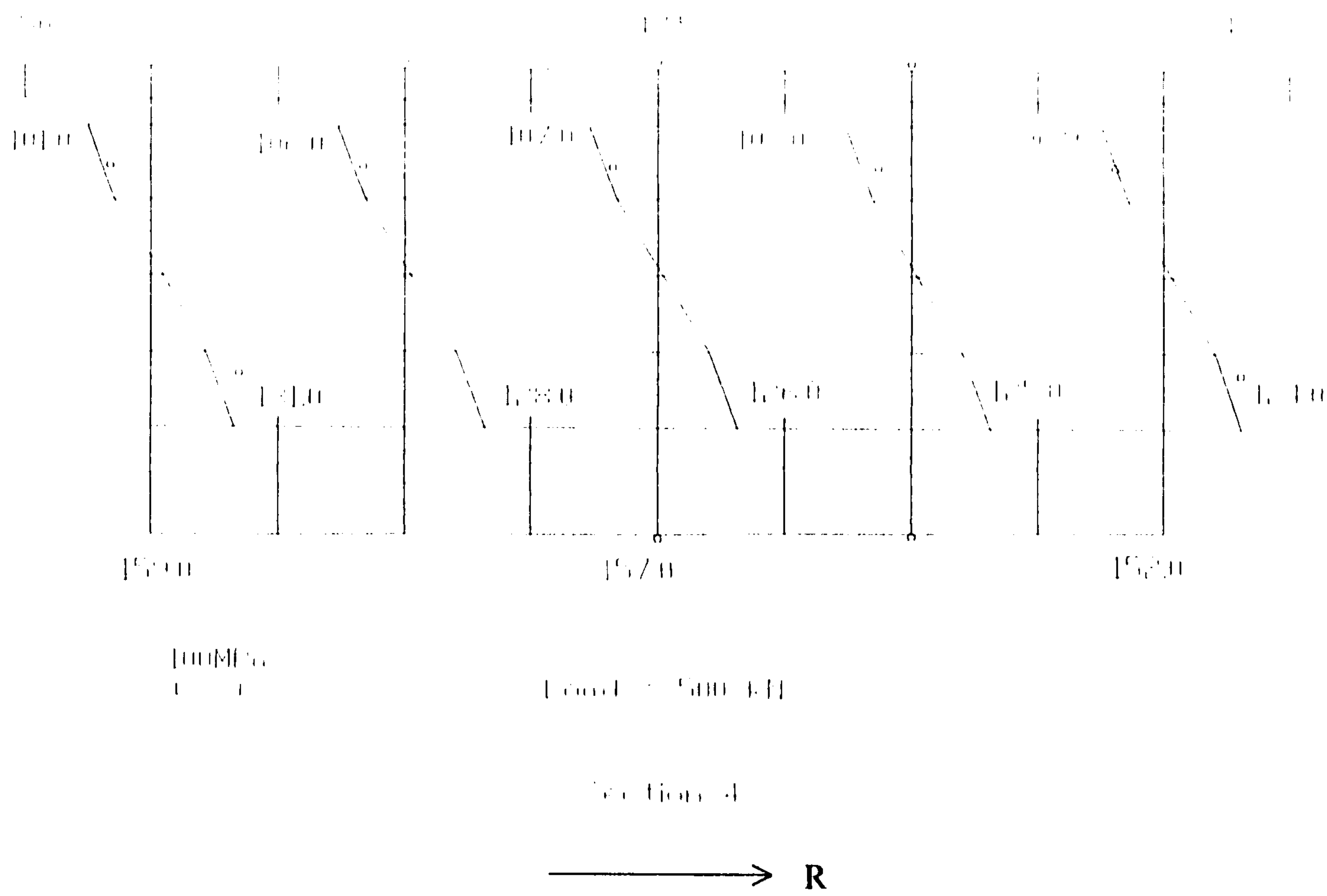

Figure 4.24 Distribution of stresses at section 4 under the load of 500 kN

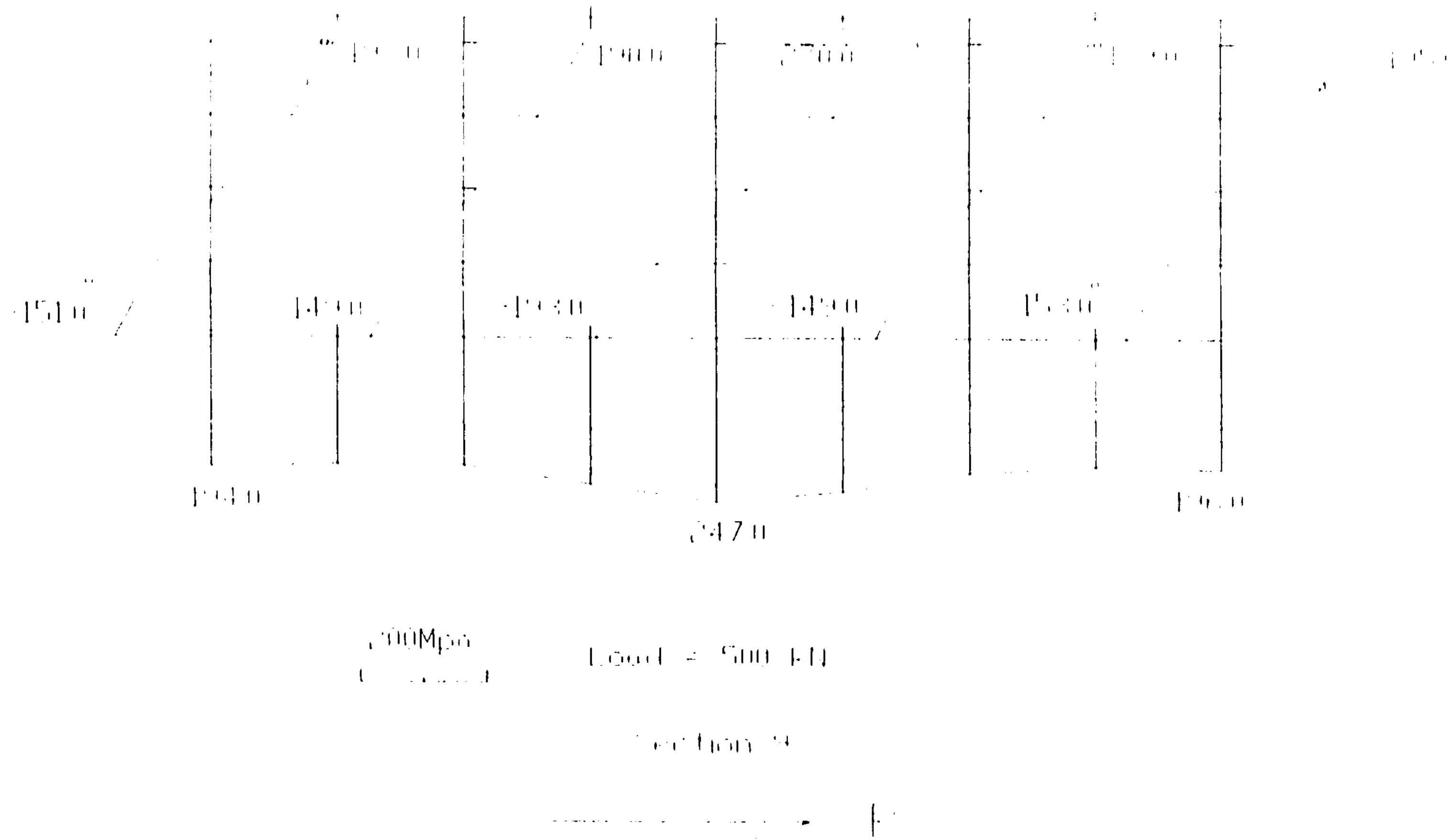

Figure 4.25 Distribution of stresses at section 9 at the load of 500 kN

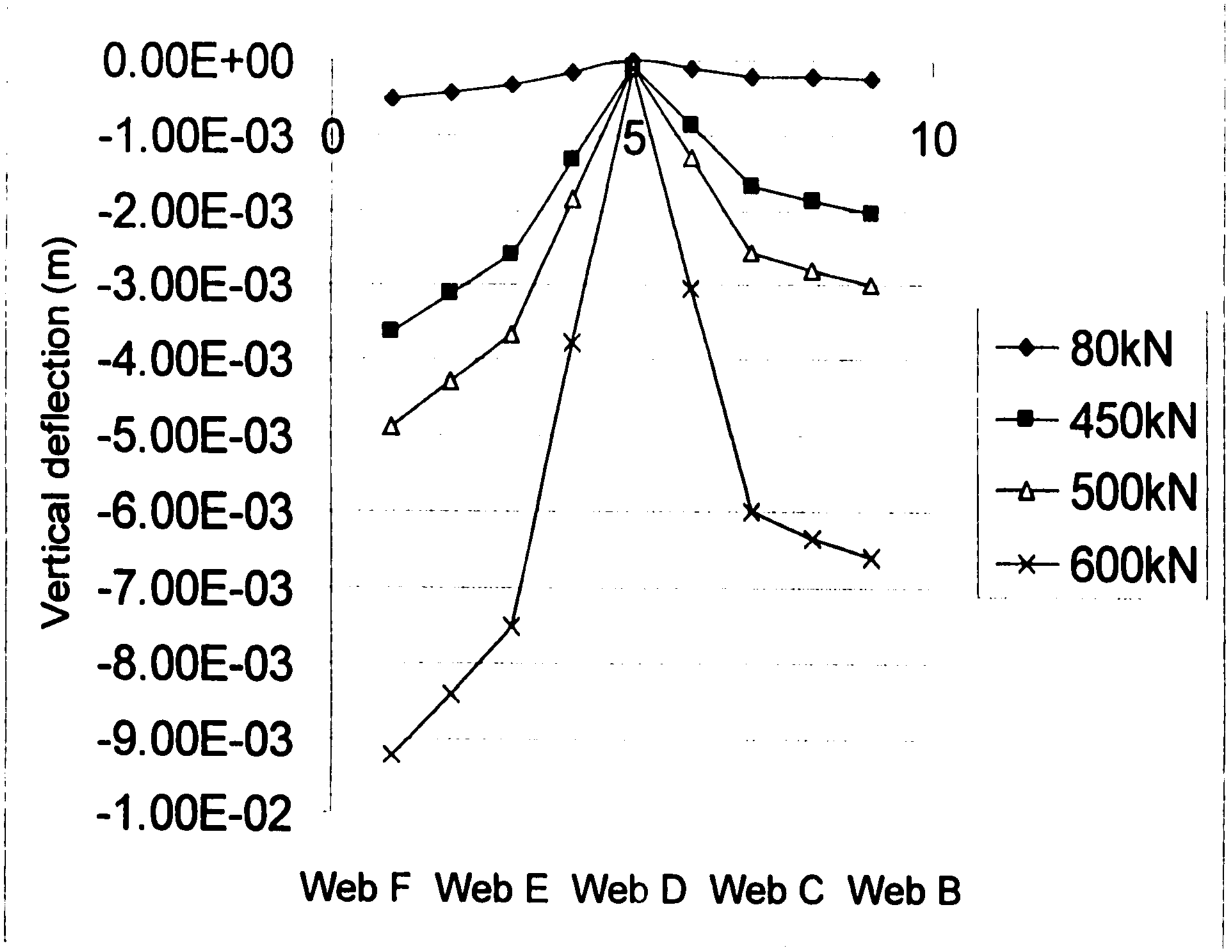

Figure 4.26 Deflection at section 9

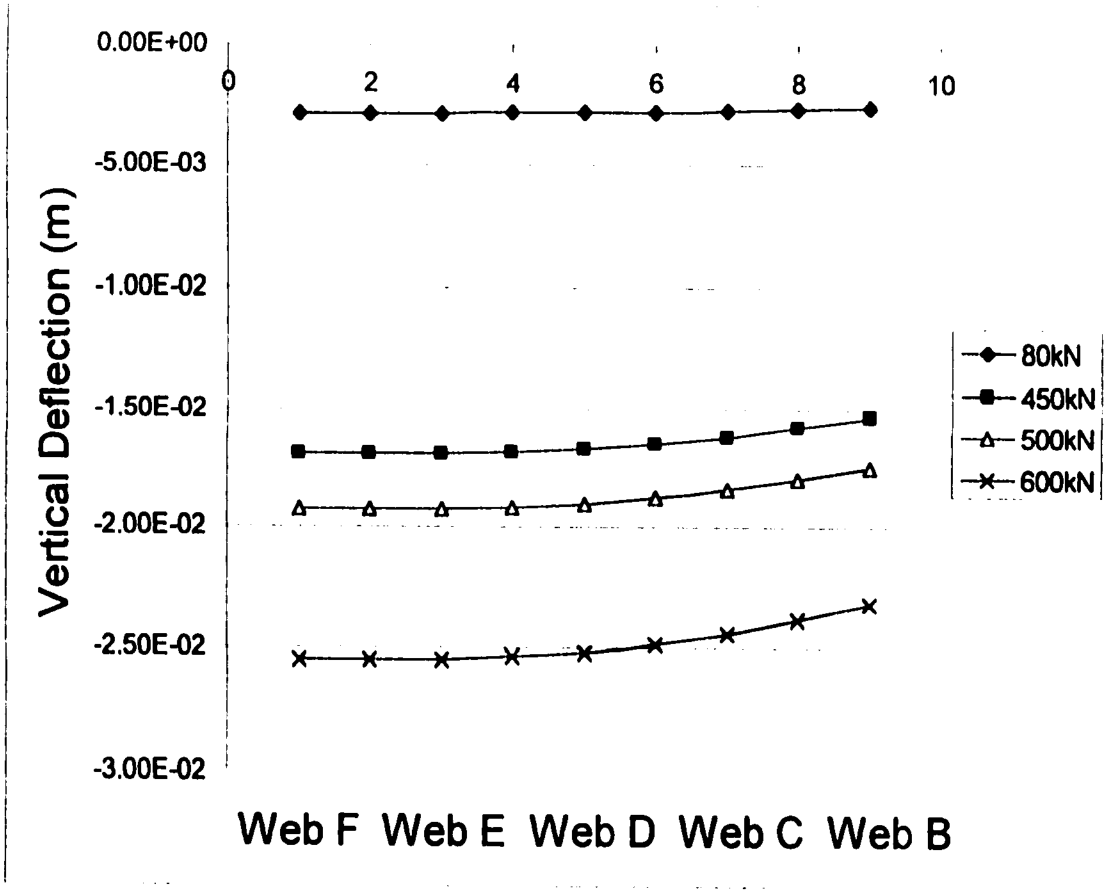

Figure 4.27 Deflection at section 4

Chapter 5

Parametric Study of Curved Bridges

5.1. General

To further accomplish the objectives of this research, extensive parametric studies on curved box-girder bridges are carried out. Generally, a two-span continuous multi-cell composite curved box-girder bridge consisted of a reinforced concrete deck, a steel box-girder with diaphragms, and shear connectors. A single column is normally used as the middle support due to the utilization of the space and the requirements of aesthetics. The ultimate load capacity of such box-girder bridges changes with different properties of these components used. Different locations of the applied truck load will also induce different behavior of the curved bridges. Many parameters were expected to affect significantly the ultimate load capacity and nonlinear behaviors of two-span continuous curved box-girder bridges with a single column middle support. Such parameters include the curvature of the bridge, the properties of the middle diaphragm, the properties of the shear connectors, the stiffness of the middle column and its location, the stiffness of intermediate diaphragms, and the location of the load. The effects of these parameters on nonlinear behaviors and ultimate states of curved box-girder bridges are included in this thesis and are studied by using the finite element method with the COSMOS/M software package.

5.2.Ideal curved bridge model

Dimensions of the idealized bridge sample are generated for the nonlinear analysis based on real box-girder parameters given in the reference (Heins, C. P. 1978). A total of fifty-four four-cell curved box girder bridge analytical models are utilized in the parametric study.

Symmetric structures have been selected for the curved bridges. The typical dimensions of the ideal bridge models are shown in Figure 5.1. Typically, the total longitudinal length of all bridge models is 72 meters from end to end with each span length of 36 meters. The width of the reinforced concrete deck is 15m. The width of the bottom plate is 12m. The height of the web plates is 1.3m. The width of the flange plates is 0.4m. The plate middle and intermediate diaphragms were used. The height of the diaphragms is 1.3m. The interval distance of the intermediate diaphragms is 7.2m. The reinforced concrete deck has a thickness of 0.25m, the web plates a thickness of 0.01m, the flange plates a thickness of 0.015m, the bottom plate a thickness of 0.01m, and the end diaphragms a thickness of 0.04m. Shear connectors are chosen and verified in terms of the OHBDC. Following Appendix B, the equivalent shear connector was calculated and the 3-D beam element with a length of 0.125m and a diameter of 0.115m was used in bridge models.

For the parametric study, the following parameter variables were used: curvature radii (50 m, 100 m, 200 m, and 500 m, that is, L/R ratios of 0.72, 0.36, 0.18, and 0.072), thicknesses of the plate middle diaphragm (0.02m, 0.04m, and 0.08m), stiffnesses of the middle column (1.26×10^{7} N/m, 1.26×10^{8} N/m, 1.26×10^{9} N/m, 1.26×10^{10} N/m, and 1.26×10^{11} N/m) for various locations of the middle column (Figure 5.2), and thickness of the plate intermediate diaphragms (0.0m, 0.0002m, 0.0006m, 0.002m, and 0.02m). Effects of various locations of the middle column and four load cases were also investigated.

The nonlinear behaviors of bridge models were investigated using the above parameter variables under various load cases. The rigid shear connectors and regular shear connectors were used to verify the difference of two kinds of situations in the analysis. The typical finite element analytical model is shown in Figure 5.3. The shear connectors are modeled by the equivalent 3-D beam element. The concrete deck, steel webs, flanges, bottom plate and diaphragm are modeled by the 4-node thick shell element. The shear deformation of the shell element was taken into account. The middle support column is modeled by the 3-D beam element. The 3-D truss element is used to put with the 3-D beam element together under the concentrated loads in order to limit the vertical deformation of the 3-D beam elements.

Typical stress-strain relationships of concrete and steel are used for the deck and the bridge girder and shown in Figures 5.4 and 5.5 respectively. The special stress-strain relationship is calculated for the equivalent shear connectors following Appendix B and is shown in Figure 5.6. The elastic middle column is used throughout the analysis because it is supposed that the middle column never failed.

At both extreme ends of a bridge model, only the vertical translation under each web was restricted; As for the boundary conditions between the bottom plate of the bridge girder and the middle support, a hinge is used. That is, all translations are not allowed between them and all rotations are allowed. However, translations in both plane directions and rotation in the plane direction are restricted in the analysis because enough requirements must be applied to prevent the bridge model free movements. At the other end of the middle column, all six translations are restricted.

The bridge models have four lanes. The width of each lane equals to 3.5 m following the requirements of OHBDC. The OHBDC design truck (Figure 5.7) was used in the nonlinear analysis. Four types of truck loadings were applied to the bridge models. The central longitudinal locations of these truck loadings are shown in Figure 5.8. Transverse locations of the eight-truck loading with four-truck symmetrically located on each span, Load Case 1, and the four-truck loading located on one span, Load Case 2, are shown in Figure 5.9. Transverse locations of the four-truck loading with two-truck symmetrically located at outer side of bridges on each span, Load Case 3; is shown in Figure 5.10. And Transverse locations of the four-truck loading with two-truck symmetrically located at inner side of bridges on each span, Load Case 4, is shown in Figure 5.11. Each type of these truck loadings was applied in one of three circumferential paths: inner, concentric and outer edge paths. These circumferential paths were selected to simulate locations of truck loadings, which were expected to produce maximum possible static effects on the bridge system. Load Factor is a factor used to measure the load level of total OHBDC design trucks applied on a bridge model, that is

$$\text{Load Factor} = \frac{\text{the total applied load}}{\text{the total basic truck load}}$$

where the total basic truck load refers to the total load of all basic design trucks applied on a bridge model in each load case. That is, the total basic truck load equals to 5920 kN for Load Case 1, and equals to 2960 kN for Load Case 2, Load Case 3, and Load Case 4.

In the finite element analysis, section A of the bridge models was selected in the analysis. Node 127, Node 131 and Node 135 of section A (Figure 5.12) were used to verify the deflections of bridge models. Rotation of section A refers to the difference between Node 127 and Node 135 divided by the bottom width of the bridge model, that is,

$$Rotation = \frac{\text{(Deflection of Node 127 - Deflection of Node 135)}}{\text{The bottom width of the bridge box girder}}$$

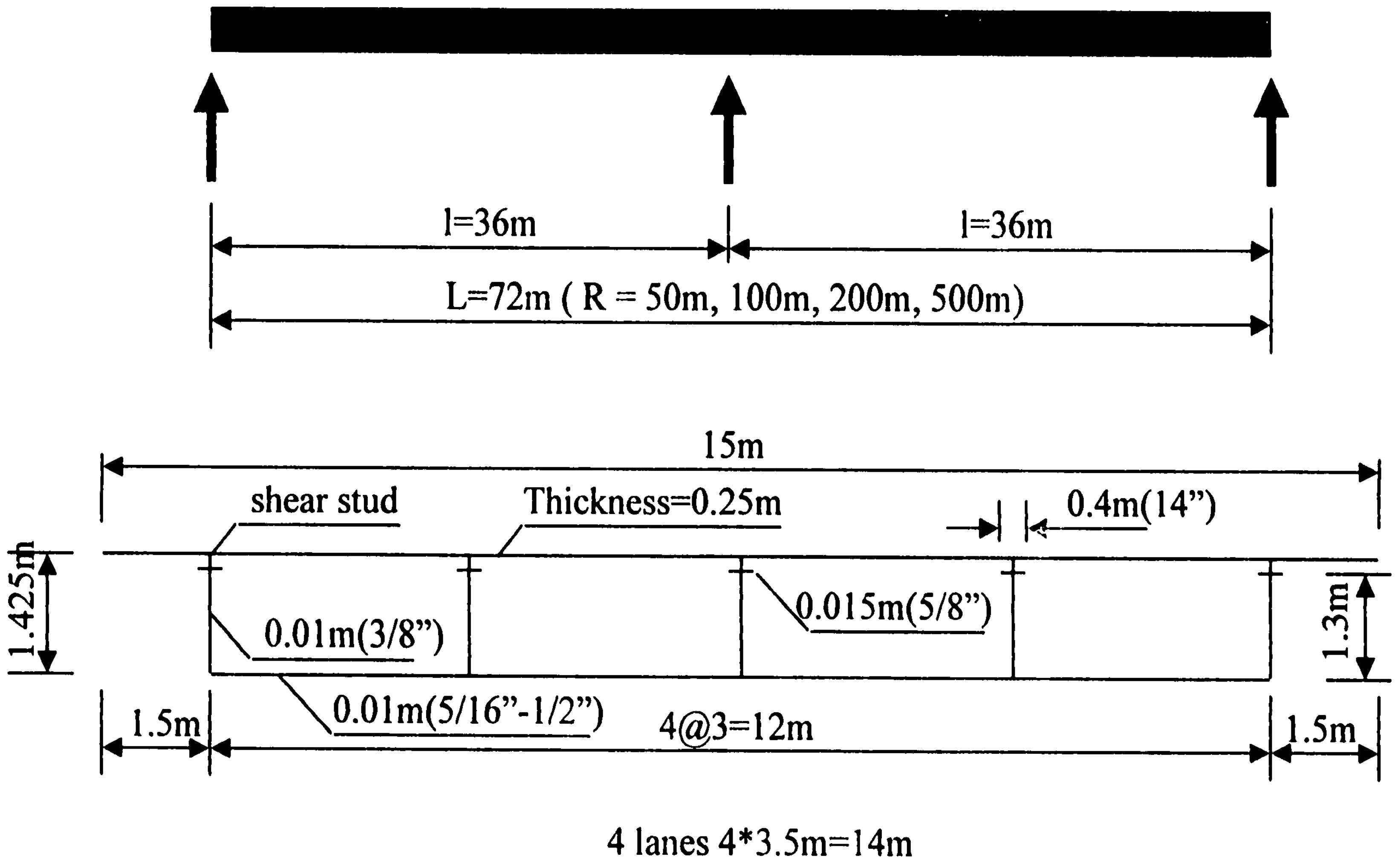

Figure 5.1. Dimensions of a bridge model

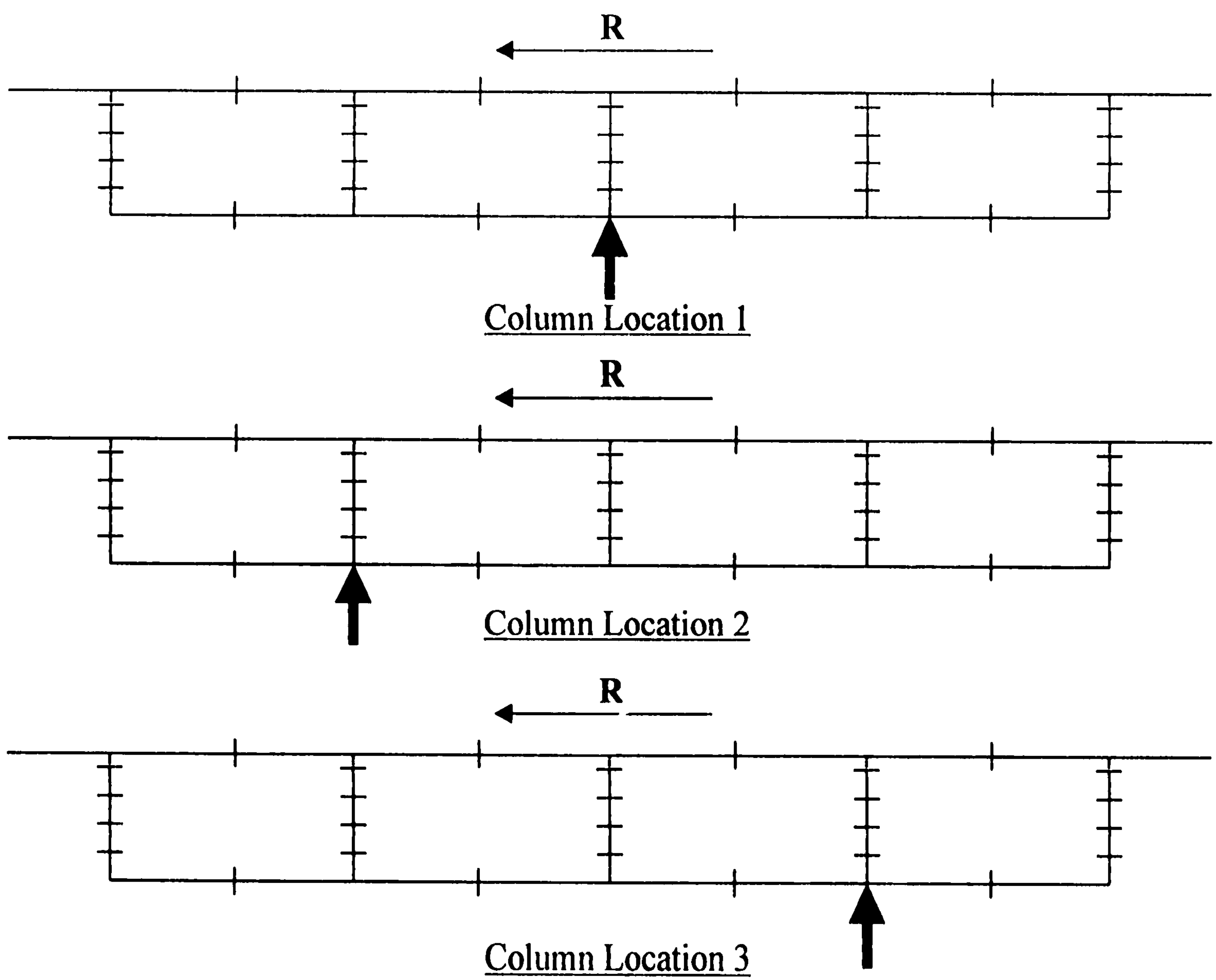

Figure 5.2. Locations of the middle column

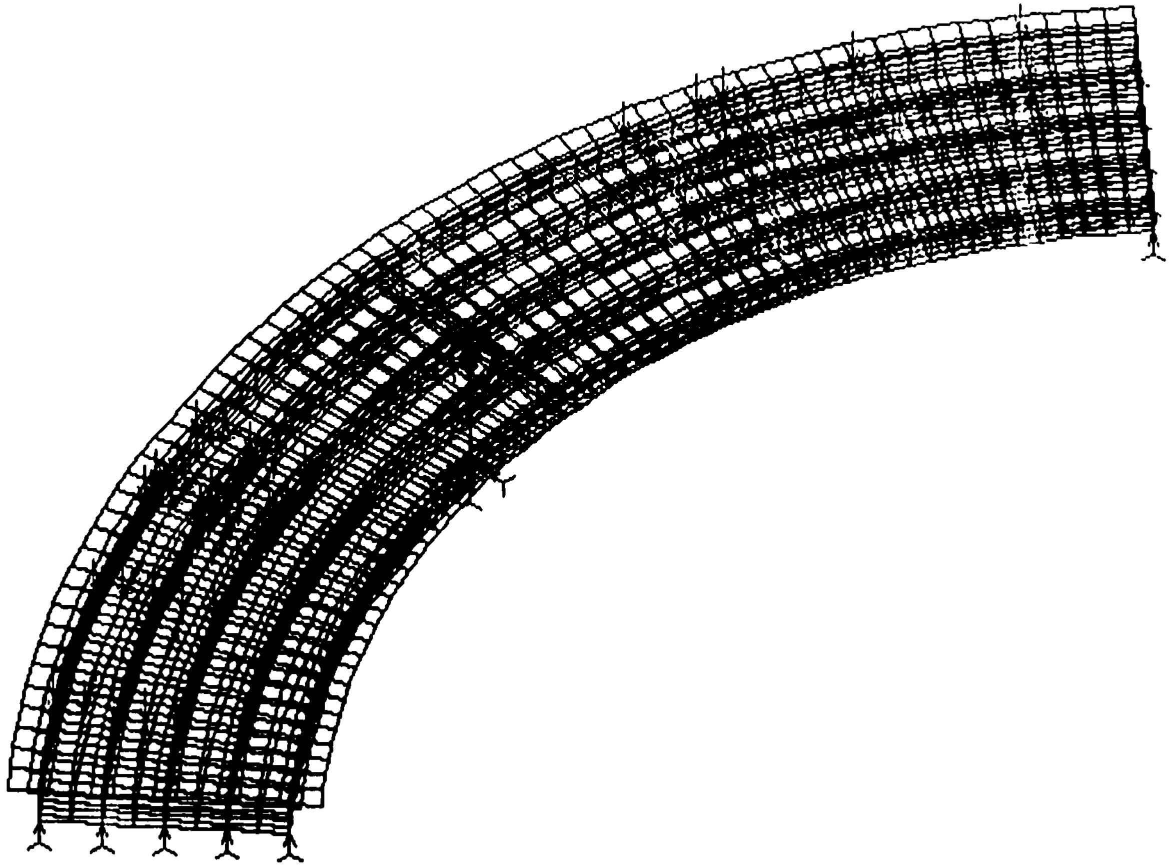

Figure 5.3. A typical finite element analytical model

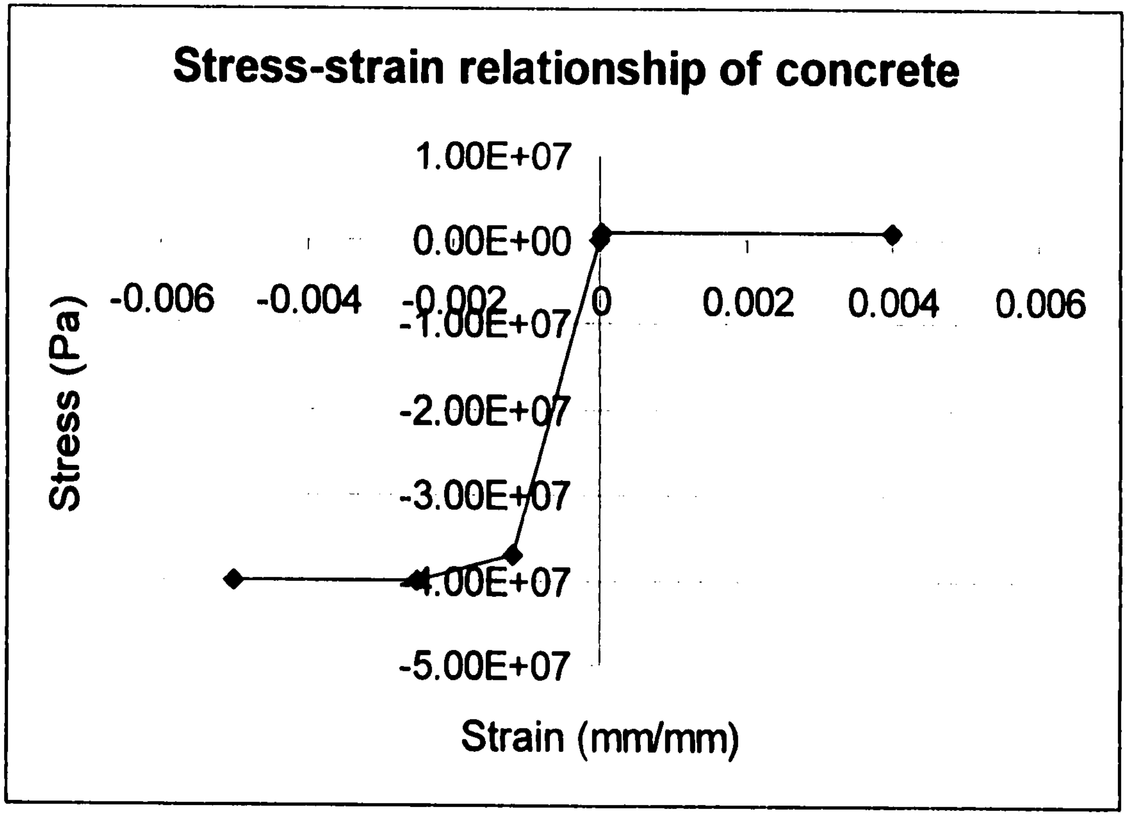

Figure 5.4. Stress-strain relationship of concrete

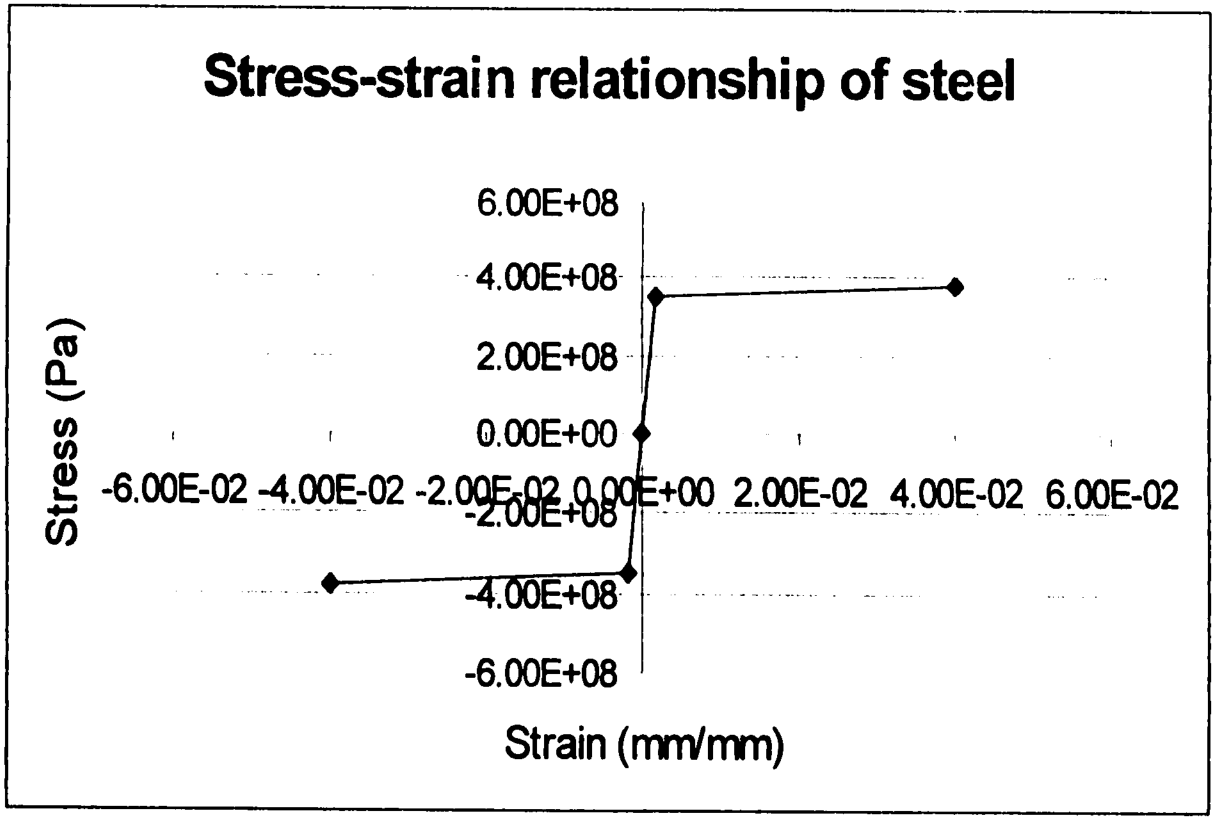

Figure 5.5. Stress-strain relationship of steel

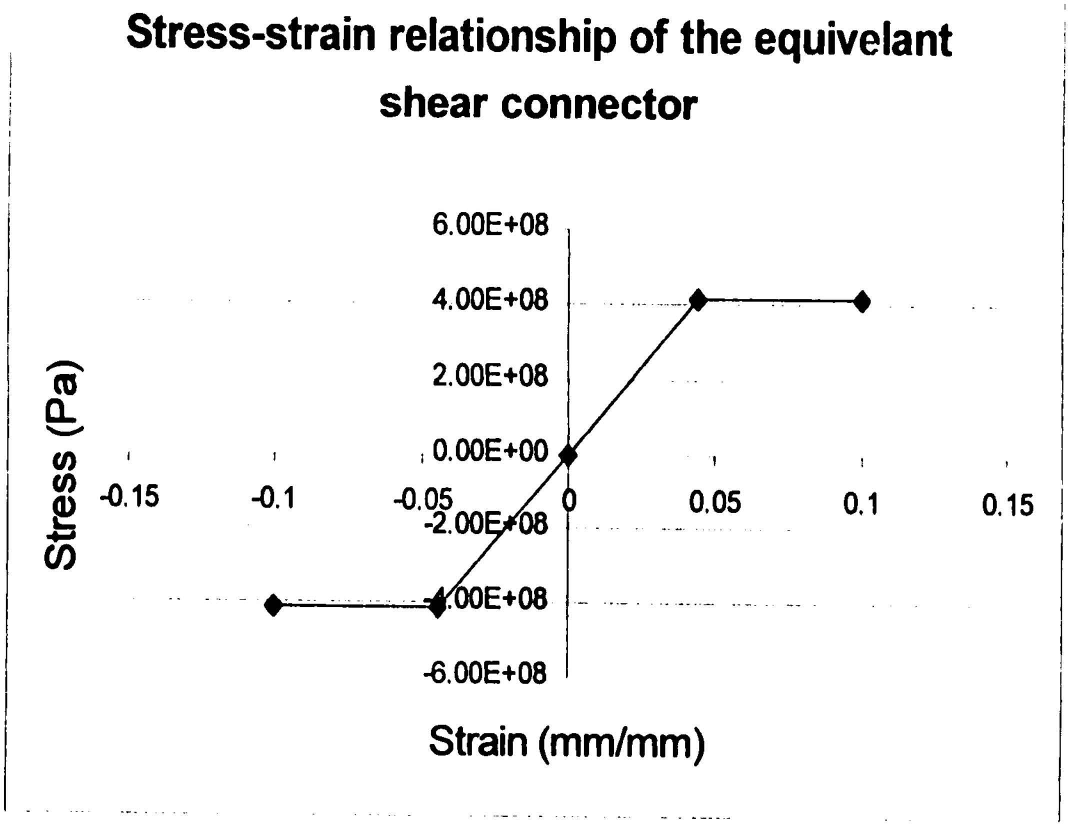

Figure 5.6. Stress-strain relationship of an equivalent shear connector

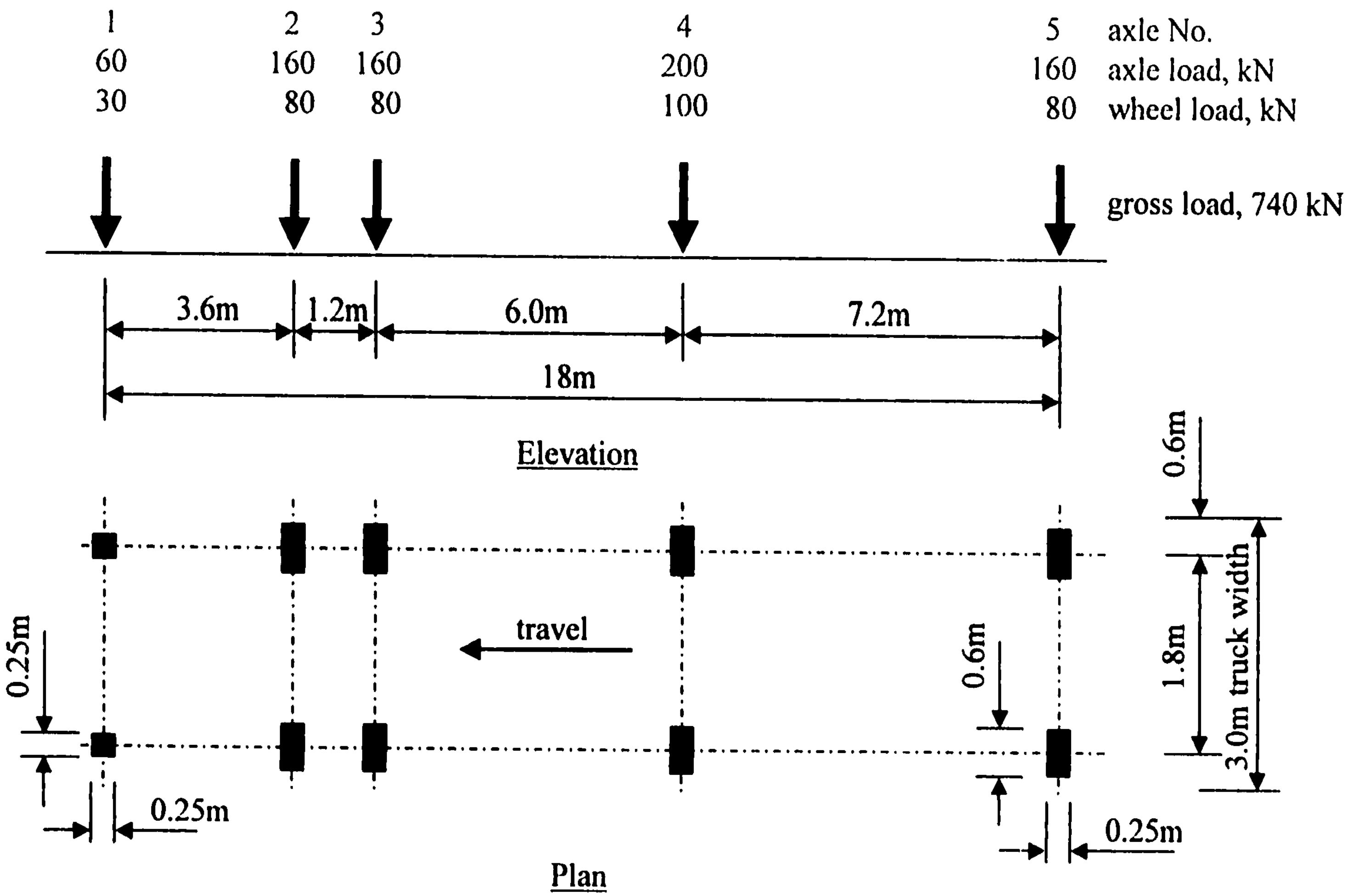

OHBDC design truck

Figure 5.7. OHBDC design truck

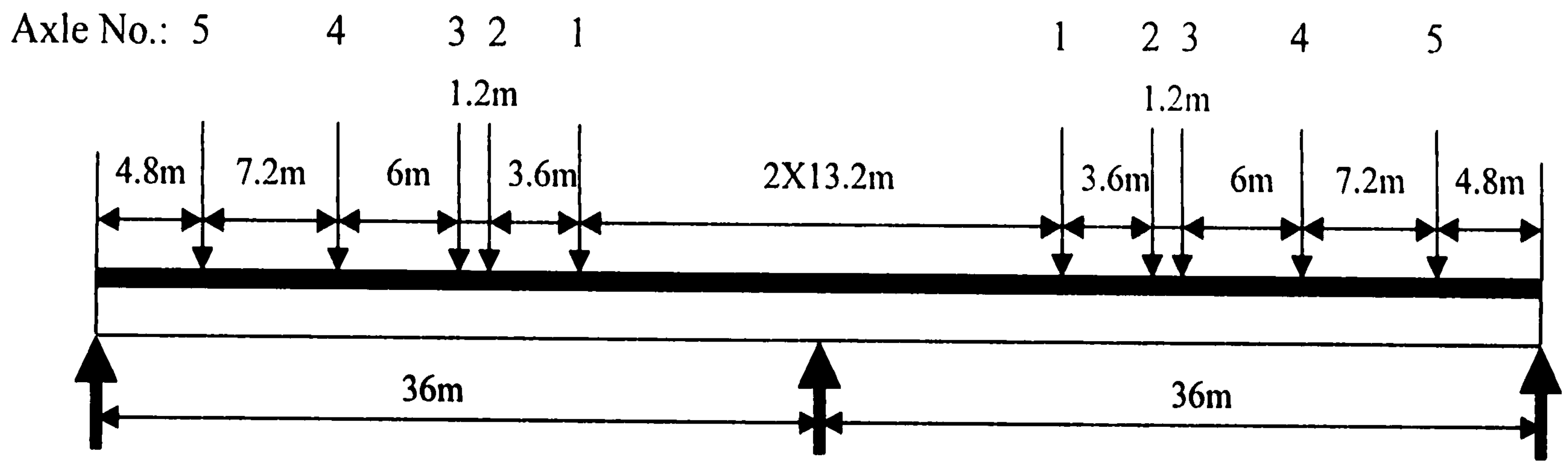

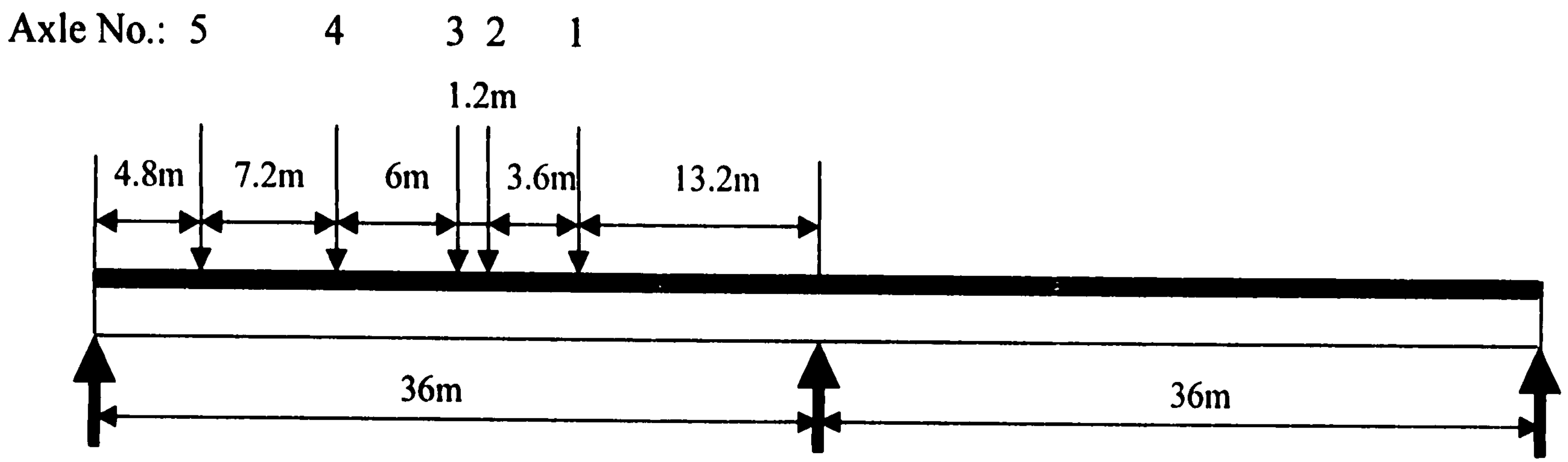

Figure 5.8. Longitudinal locations of load cases

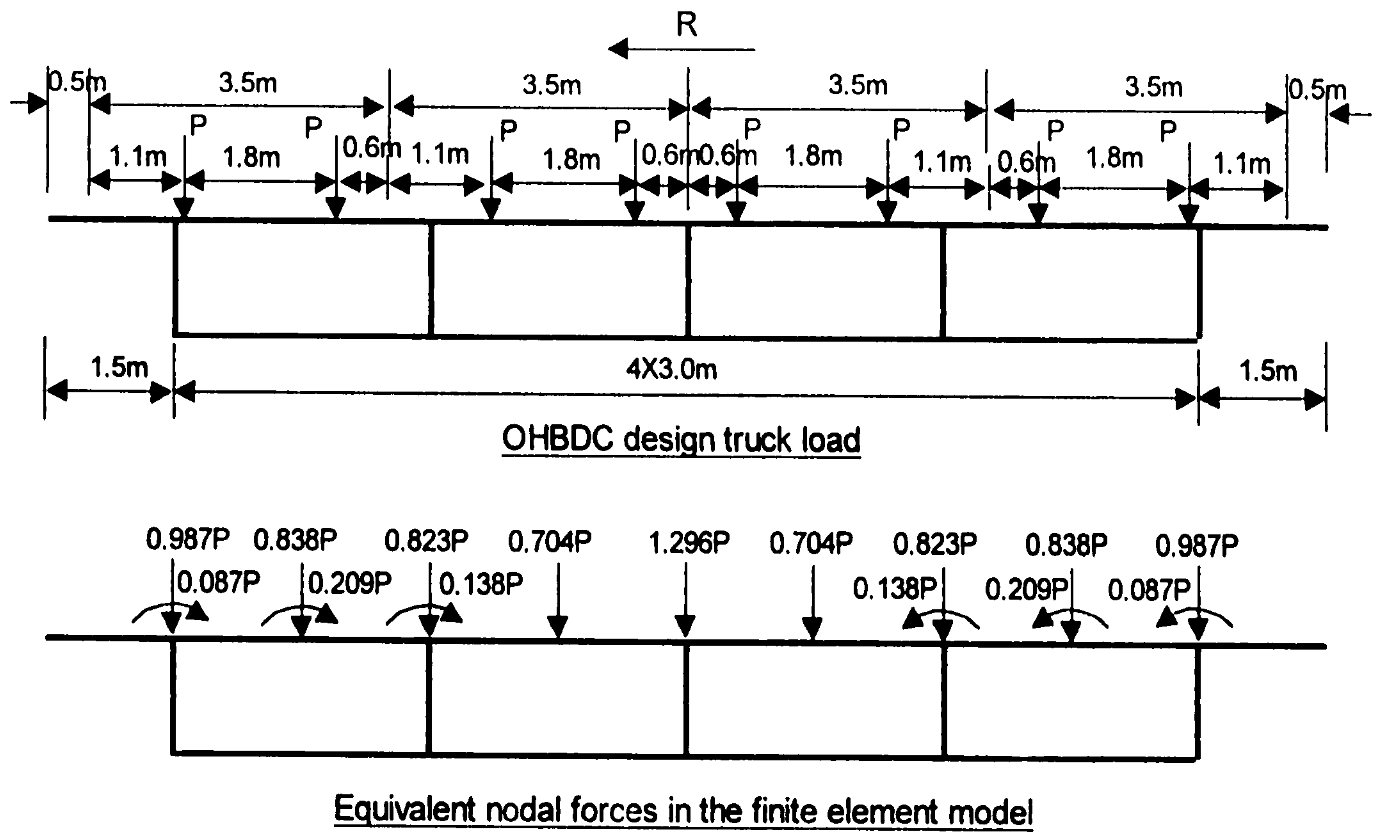

Figure 5.9. Equivalent loading system of Load Cases 1 and 2

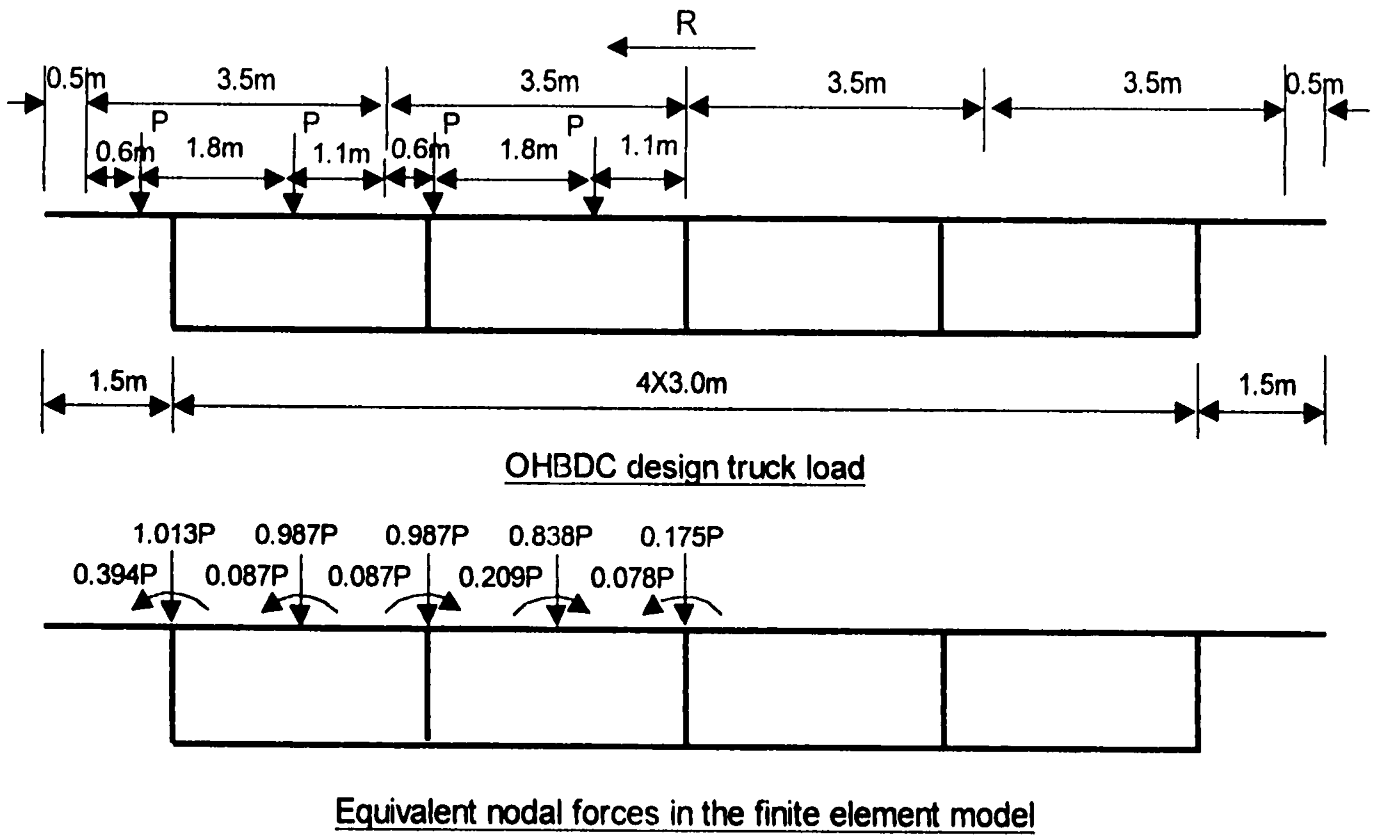

Figure 5.10. Equivalent loading system of Load case 3

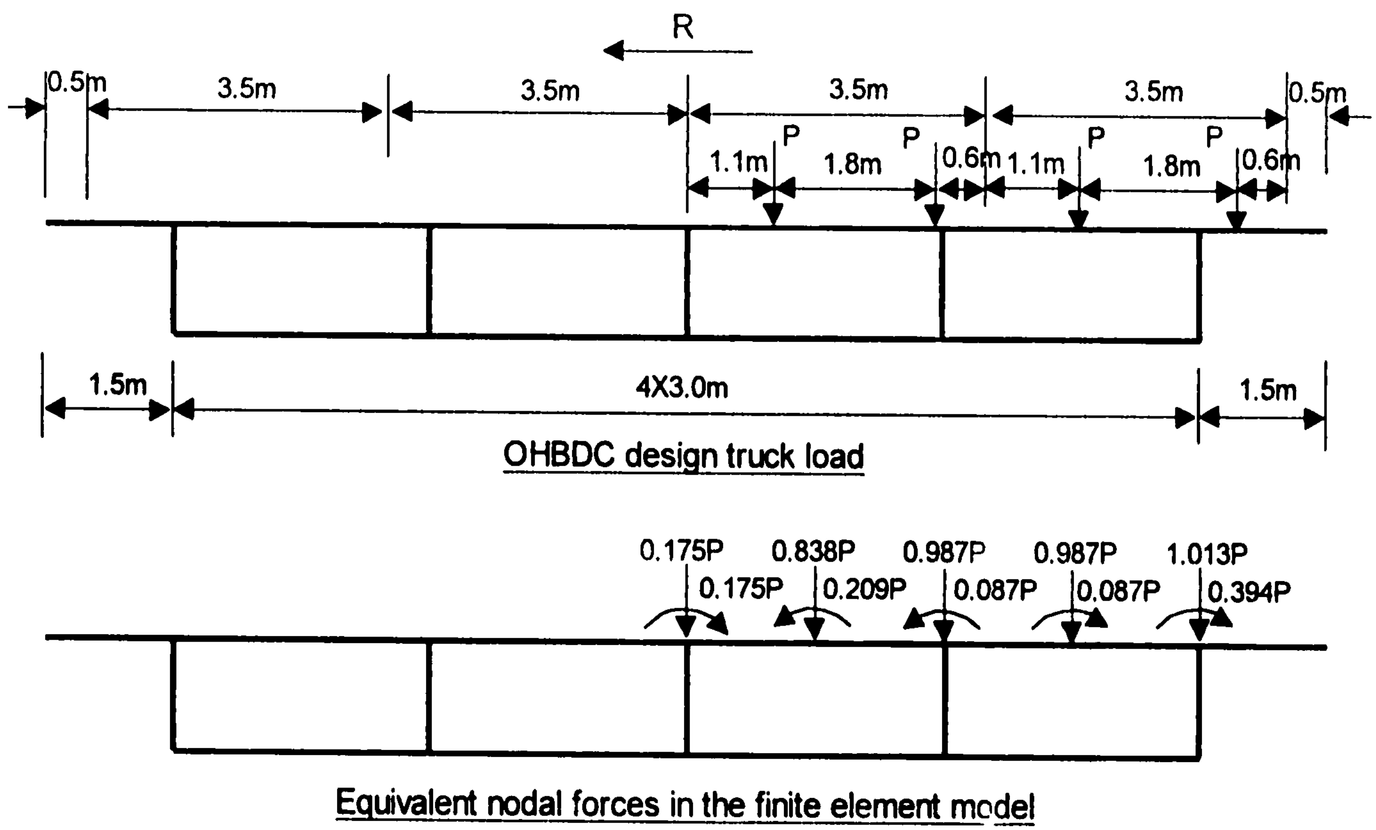

Figure 5.11. Equivalent loading system of Load case 4

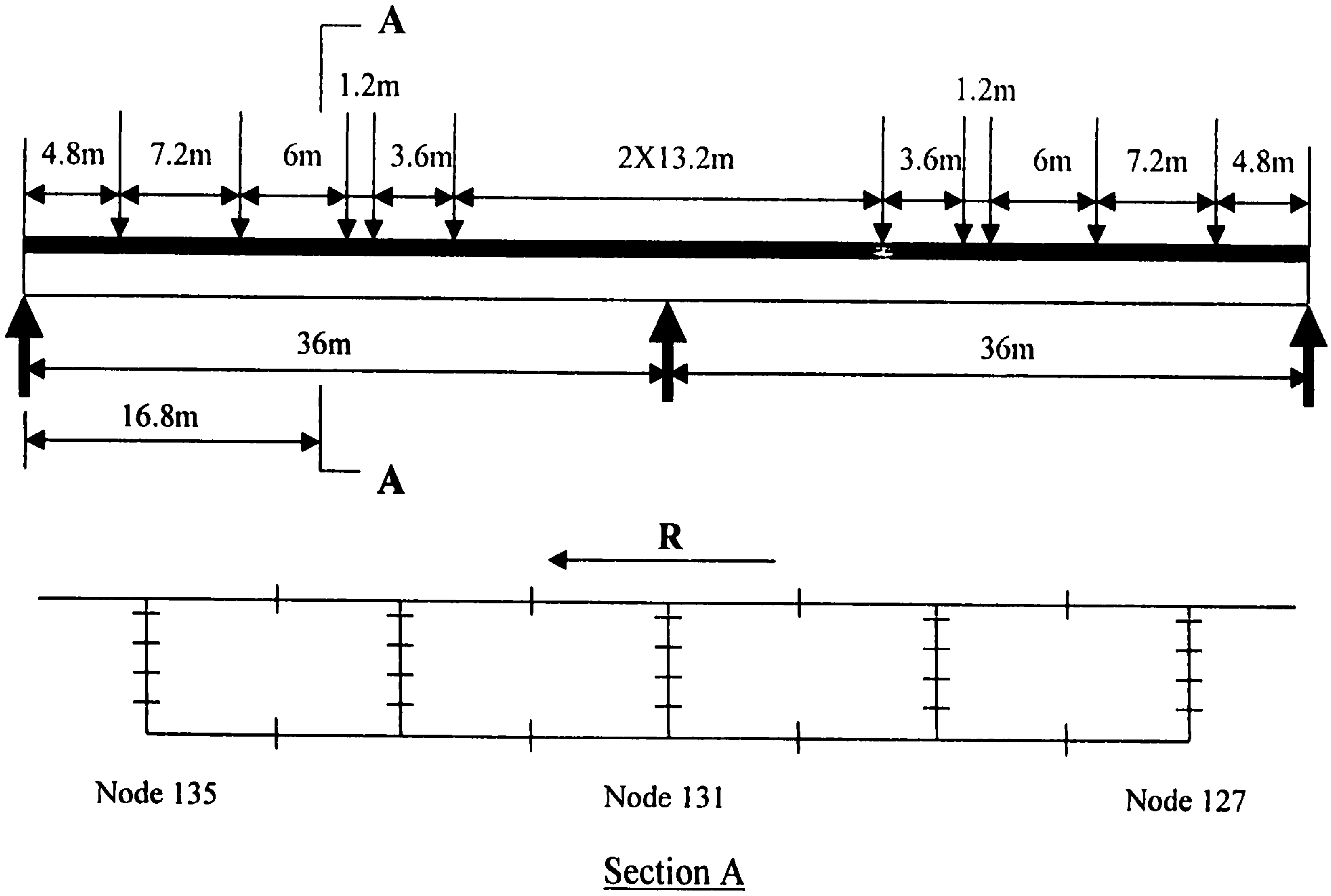

Figure 5.12. Cross-section of section A

5.3.Influence of load distribution

Four types of truck loadings are applied to the bridge models without intermediate diaphragms described in section 5.2. Various locations of the middle column (Figure 5.2), namely, Column Location 1, Column Location 2 and Column Location 3, were used in the analysis. But the stiffness of the middle column is kept unchanged as 1.26×10^{11} N/m. The thickness of the middle diaphragm of 0.08 m for Load Case 1 and 0.02 m for Load Cases 2, 3, and 4 were used. Two radii of curvature of 50m and 500m were used to compare the effects of load cases in different radii of curvature. The stiffness of regular shear connectors was used. The effects of the various loading are presented based on various locations of the middle column. The deflections and the rotations at section A of bridge models are presented. The distributions of overall stresses of bridge girders are also shown in this section.

Column Location 1

For bridge models with curvature radius of 50m, vertical deflections at nodes 127, 131 and 135 under four load cases are shown in Figures 5.13a, 5.13b and 5.13c. The maximum deflections of the bridge model at section A are shown in Figure 5.14. The rotations of section A of the bridge models are shown in Figure 5.15. From Figure 5.13 to Figure 5.15, it can be seen that the lowest ultimate load factor is about 4.0 for the bridge model with the middle column at Column Location 1 under Load Case 1. In the elastic region, Load Case 2 induces a larger maximum vertical deflection than any other load case. But under Load Case 2, the ultimate load factor appears to be almost the same as that under Load Case 1. There is no obvious yielding point for the bridge model under all load cases.

The stress distributions of the bridge model under Load Case 1 and Load Case 2 before yielding are shown in Figures 5.16 and 5.18 respectively. In Figures 5.16 and 5.18, it can be observed that the webs start to yield at the maximum negative moment region and the inner webs and the inner bottom plate are subjected to larger stresses than the outer parts at the maximum positive moment region. The stress distributions of the bridge model under Load Case 1 and Load Case 2 at the ultimate states are also shown in Figures 5.17 and 5.19 respectively. It should be noted in Figures 5.17 and 5.19 that the outer webs and the outer part of the bottom plate are still in the elastic region while the inner webs and the inner part of the bottom plate fail at the maximum positive moment region under both load cases. However, from the figure of rotations, yielding points for the bridge model under Load Cases 1 and 2 are seen much clearer than from the figures of the vertical deflections. The bridge model starts to yield at the load factor of near 3.0 under Load Cases 1 and 2. Although the bridge model has a larger rotation at section A under Load Cases 3 and 4, larger load factors of about 5.5 are needed to induce the failure of the bridge model. The stress distributions of the bridge model under Load Case 3 and Load Case 4 at the ultimate states are also shown in Figures 5.20 and 5.21 respectively. It can be seen that the parts under the loading location fail first while other parts of the bridge model still remain in the elastic region.

For bridge models with curvature radius of 500m, vertical deflections at nodes 127, 131 and 135 under four load cases are shown in Figures 5.22a, 5.22b and 5.22c. The rotation of section A is shown in Figure5.24. The maximum deflection of the bridge model at section A is shown in Figure 5.23. From the figures, it can be observed that load cases 1 and 2 induce the failure of the bridge model at almost the same ultimate load factor with the lowest ultimate load factors being approximately 5.0 under both load cases. There are two yielding points occurred in the bridge model under Load Case 1. One at the load factor of about 3.0 where the bridge girder starts to yield at the maximum negative moment region, and other at the load factor of about 4.5 where the bridge model starts to yield at the maximum positive moment region. It can also be seen clearly in Figure 5.24 that the bridge model starts to fail at the load factor of about 4.5 under Load Cases 1 and 2.

The stress distributions of the bridge model under Load Case 1 and Load Case 2 before yielding are shown in Figures 5.25 and 5.27 respectively. In Figures 5.25 and 5.27, it can be seen that the webs start to yield at the maximum negative moment region. All webs are subjected to almost the same stresses; and the stresses of the bottom plate are much more uniformly distributed at the maximum positive moment region under both load cases. The stress distributions of the bridge model under Load Case 1 and Load Case 2 at the ultimate states are also shown in Figures 5.26 and 5.28 respectively. It should be noted in Figures 5.26 and 5.28 that the inner and outer parts of the bottom plate fail simultaneously at the maximum positive moment region under both load cases. For load cases 3 and 4, the larger ultimate load factors are needed to induce the bridge model to fail. The stress distributions of the bridge model under Load Case 3 and Load Case 4 at the ultimate states are shown in Figures 5.29 and 5.30 respectively. It can be seen that the parts of the bridge model under the loading location fail first while other parts of the bridge model still remain in the elastic region.

Column Location 2

For bridge models with curvature radius of 50m, vertical deflections at nodes 127, 131 and 135 under four load cases are shown in Figures 5.31a, 5.31b and 5.31c. The rotation of section A is shown in Figure 5.33. The maximum deflection of the bridge model at section A is shown in Figure 5.32. The bridge model starts to yield at the load factor of about 2.5 under both load cases 1 and 2, although load case 2 induces a larger vertical deflection at section A of the bridge model. From Figures 5.32 and 5.33, it can be observed that Load cases 1 and 2 induce the failure of the bridge model at almost the same load factor of about 4.0, which is the lowest ultimate load factor in both load cases. The stress distributions of the bridge model under Load Case 1 and Load Case 2 at the ultimate states are also shown in Figures 5.34 and 5.35 respectively. It can be noted in Figures 5.34 and 5.35 that the outer webs and the outer part of the bottom plate are still in the elastic region while the inner webs and the inner part of the bottom plate fail at the maximum positive moment region under both load cases. It can also be seen the bridge model has the greatest ultimate load factor of 7.0 under Load Case 3. The stress distributions of the bridge model under Load Case 3 and Load Case 4 at the ultimate states are also shown in Figures 5.36 and 5.137 respectively. It can be seen that the parts under the loading location fail first while other parts of the bridge model still remain in the elastic region.

For bridge models with curvature radius of 500m, vertical deflections at nodes 127, 131 and 135 under four load cases are shown in Figures 5.38a, 5.38b and 5.38c. The rotation of section A is shown in Figure 5.40. The maximum deflection of the bridge model at section A is shown in Figure 5.39. It can be seen that load case 1 induces the bridge model to fail at the lowest ultimate load factor of about 4.3 from the figures. The bridge model has the smallest rotation at section A under Load Case 2. The stress distributions of the bridge model under Load Case 1 and Load Case 2 at the ultimate states are also shown in Figures 5.41 and 5.42 respectively. It can be noted in Figures 5.41 and 5.42 that the inner webs and the inner part of the bottom plate fail at the maximum positive moment region under both load cases before the outer webs and the outer part of the bottom plate. It can also be noted in Figure 5.39 that the bridge model has the highest ultimate load factor of 7.0 under Load Case 3. The stress distributions of the bridge model under Load Case 3 and Load Case 4 at the ultimate states are also shown in Figures 5.43 and 5.44 respectively. It can be seen that the parts under the loading location fail first and other parts of the bridge model still remain in the elastic region.

Column Location 3

For bridge models with curvature radius of 50m, vertical deflections at nodes 127, 131 and 135 under four load cases are shown in Figures 5.45a, 5.45b and 5.45c. The rotation of section A is shown in Figure 5.47. The maximum deflection of the bridge model at section A is shown in Figure 5.46. It can be seen that Load Case 1 induces the bridge model to fail at the lowest ultimate load factor of about 3.2. The stress distributions of the bridge model under Load Case 1 and Load Case 2 at the ultimate states are also shown in Figures 5.48 and 5.49 respectively. It can be noted that the outer webs and the outer part of the bottom plate are still in the elastic region while the inner webs and the inner part of the bottom plate fail at the maximum positive moment region under both load cases. The bridge model has the smallest rotation at section A under Load Case 2. It is shown in Figure 5.46 that the bridge model has the highest ultimate load factor of about 6.0 under Load Case 4. The stress distributions of the bridge model under Load Case 3 and Load Case 4 at the ultimate states are also shown in Figures 5.50 and 5.51 respectively. It can be seen that the parts under the loading location fail first and other parts of the bridge model still remain in the elastic region.

For bridge models with curvature radius of 500m, vertical deflections at nodes 127, 131 and 135 under four load cases are shown in Figures 5.52a, 5.52b and 5.52c. The rotation of section A is shown in Figure 5.54. The maximum deflection of the bridge model at section A is shown in Figure 5.53. It can be noted that load case 1 induces the bridge model to fail at the lowest ultimate load factor of about 4.5. The bridge model has the smallest rotation at section A under load case 2. The stress distributions of the bridge model under Load Case 1 and Load Case 2 at the ultimate states are also shown in Figures 5.55 and 5.56 respectively. It can be noted that the inner webs and the inner part of the bottom plate fail at the maximum positive moment region under both load cases before the outer webs and the outer part of the bottom plate. The bridge model has the highest ultimate load factor of about 7.0 under Load case 4. The stress distributions of the bridge model under Load Case 3 and Load Case 4 at the ultimate states are also shown in Figures 5.57 and 5.58 respectively. It can be seen that the parts under the loading location fail first while other parts of the bridge model still remain in the elastic region.

Based on above observations, it can be noted that the bridge model with the middle column at Column Locations 1, 2 and 3 and with any radius of curvature has the lowest ultimate load factor under Load Case 1. Section A has the smallest rotation in all load stages under Load Case 2.

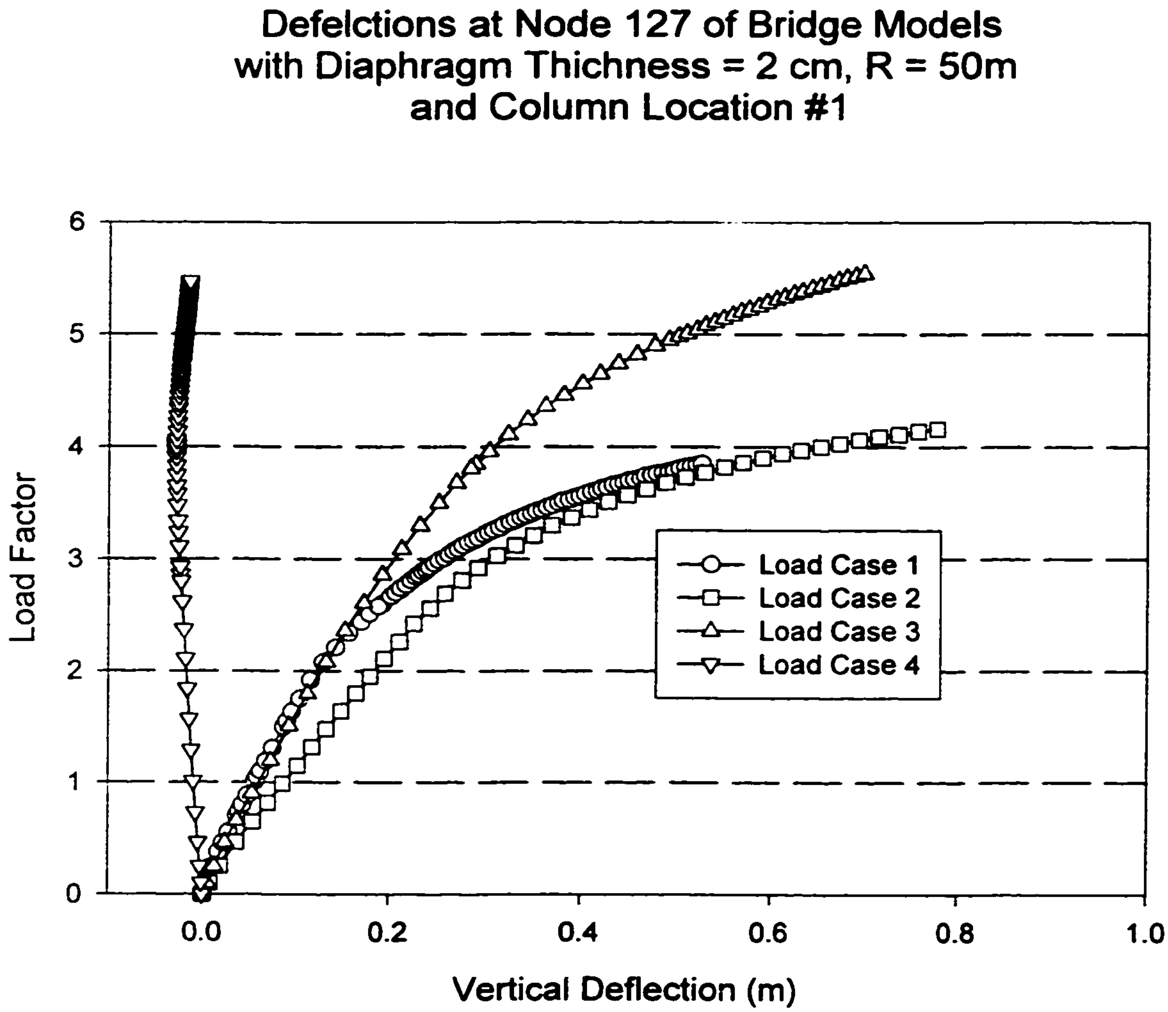

Figure 5.13a Deflections of Node 127 of Bridge Models with R=50m and Column Location #1 under Various Load Cases

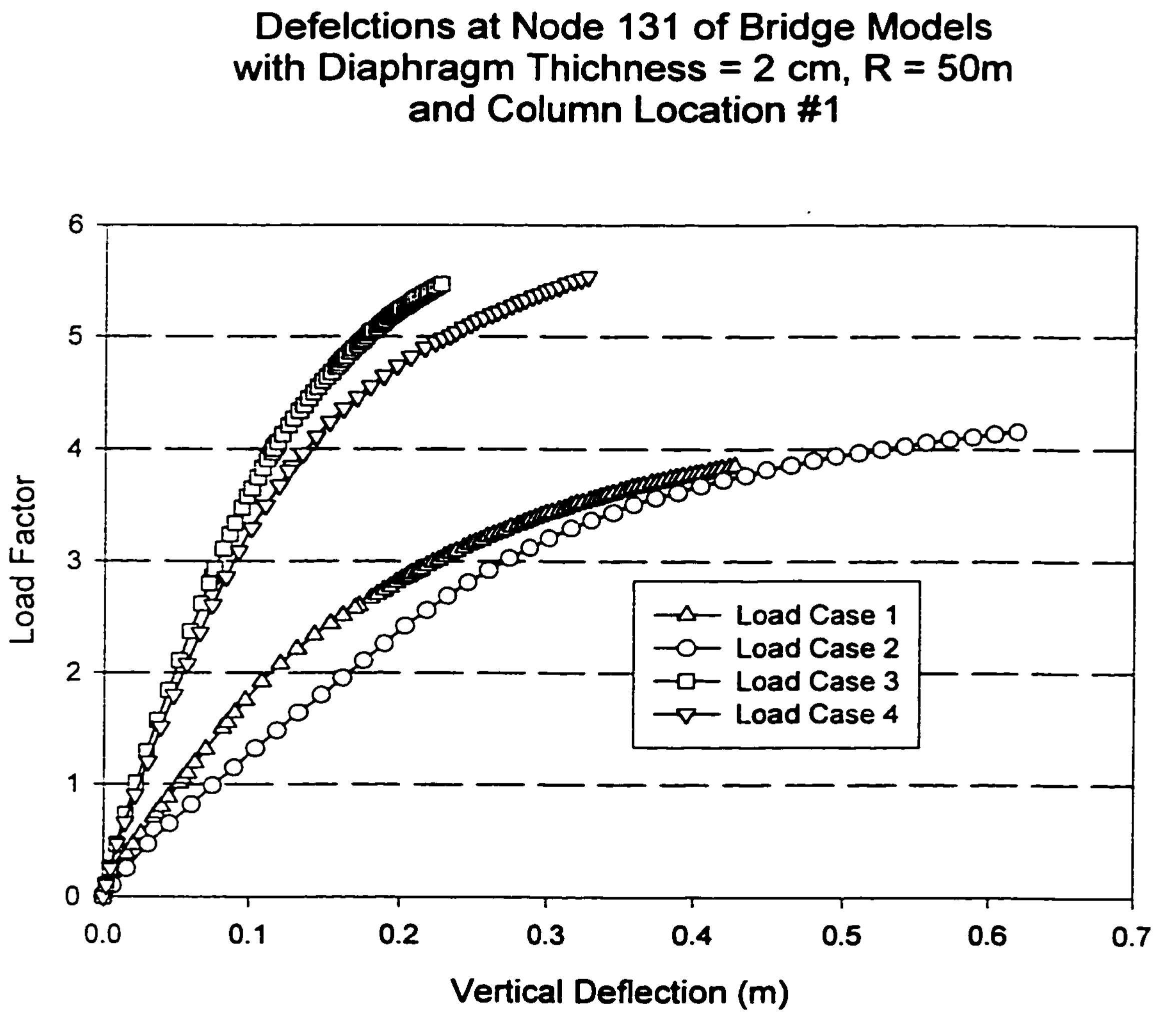

Figure 5.13b Deflections of Node 131 of Bridge Models with R=50m and Column Location #1 under Various Load Cases

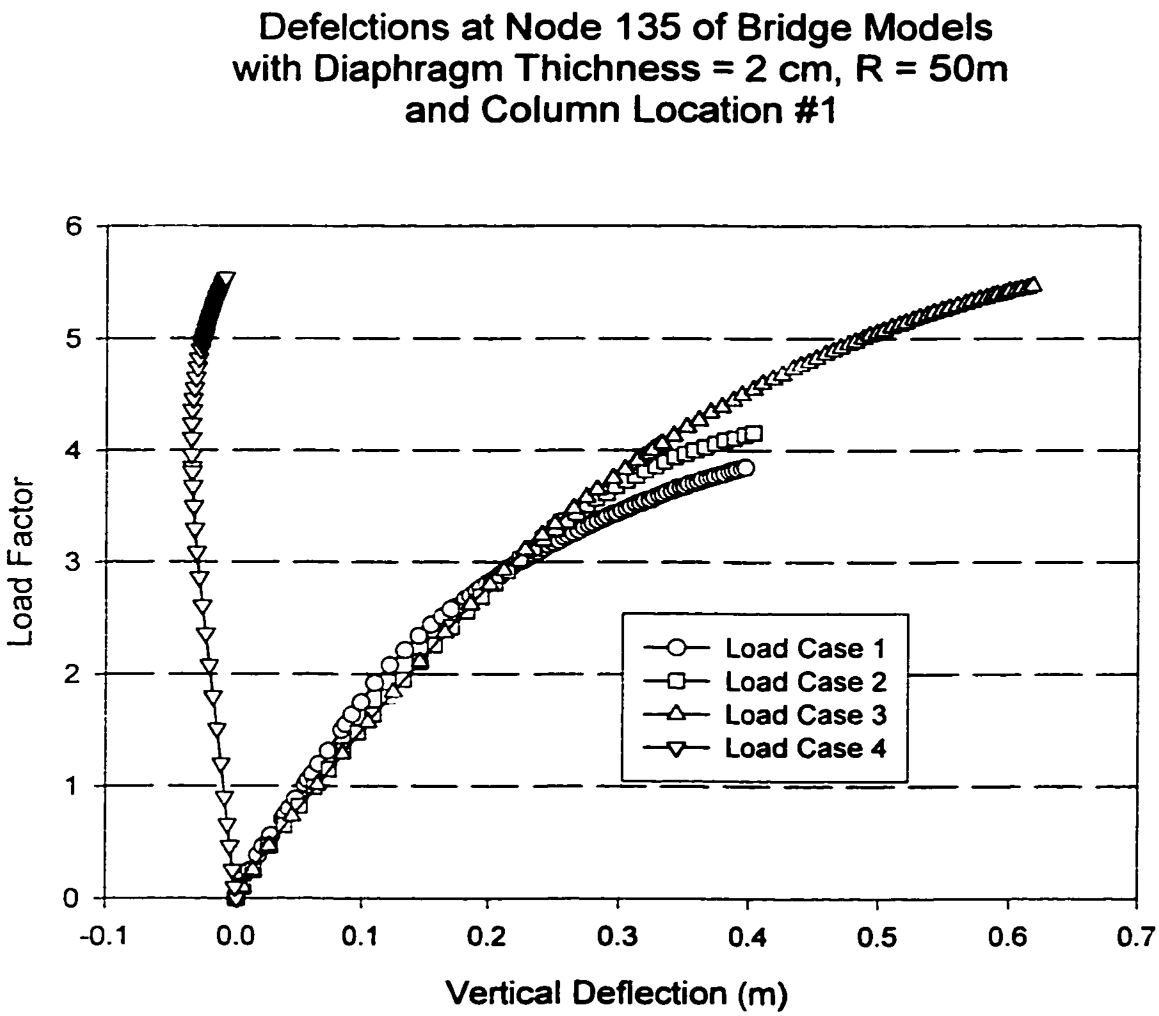

Figure 5.13c Deflections of Node 135 of Bridge Models with R=50m and Column Location #1 under Various Load Cases

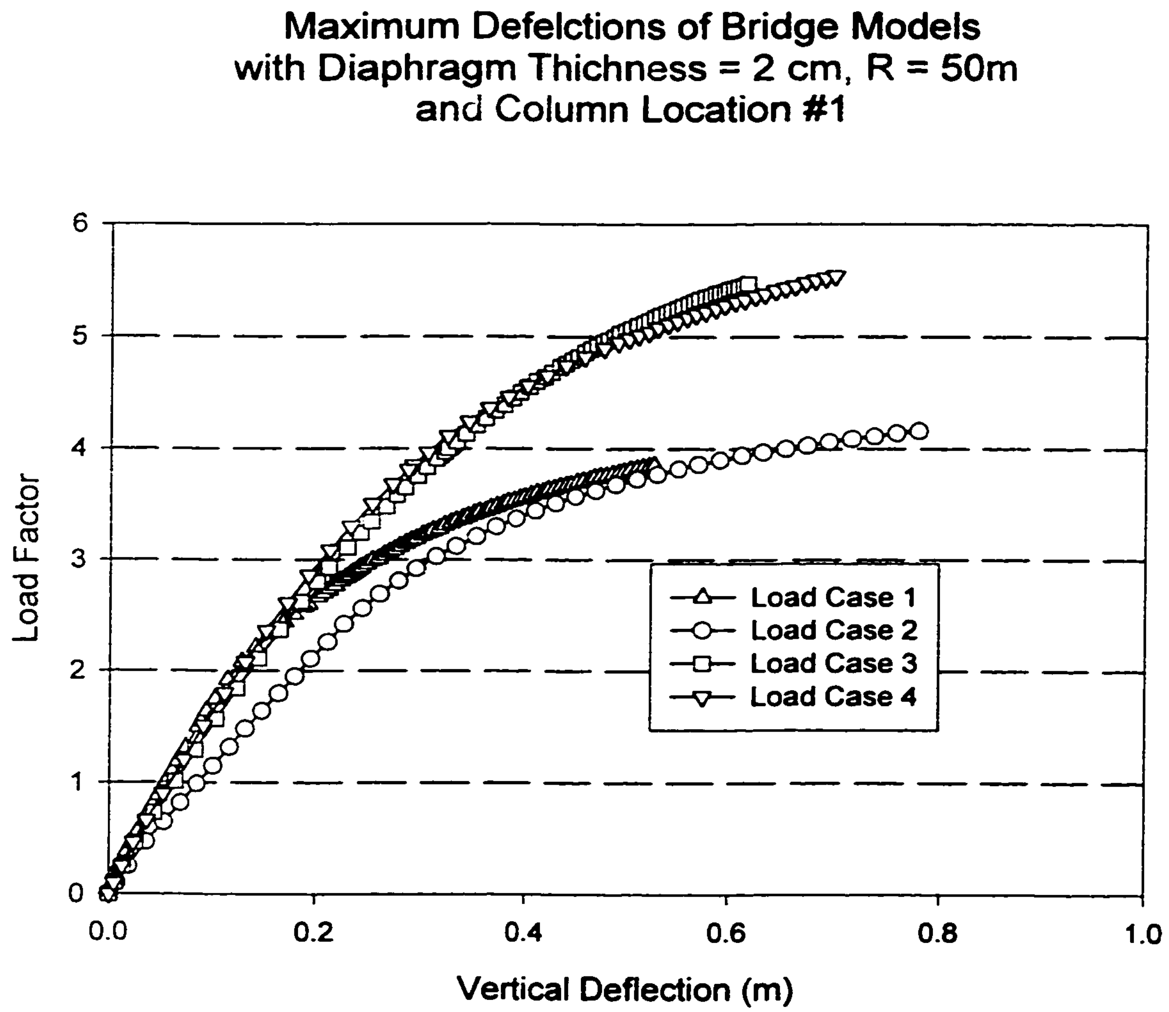

Figure 5.14 Maximum Deflections at Section A of Bridge Models with R=50m and Column Location #1 under Various Load Cases

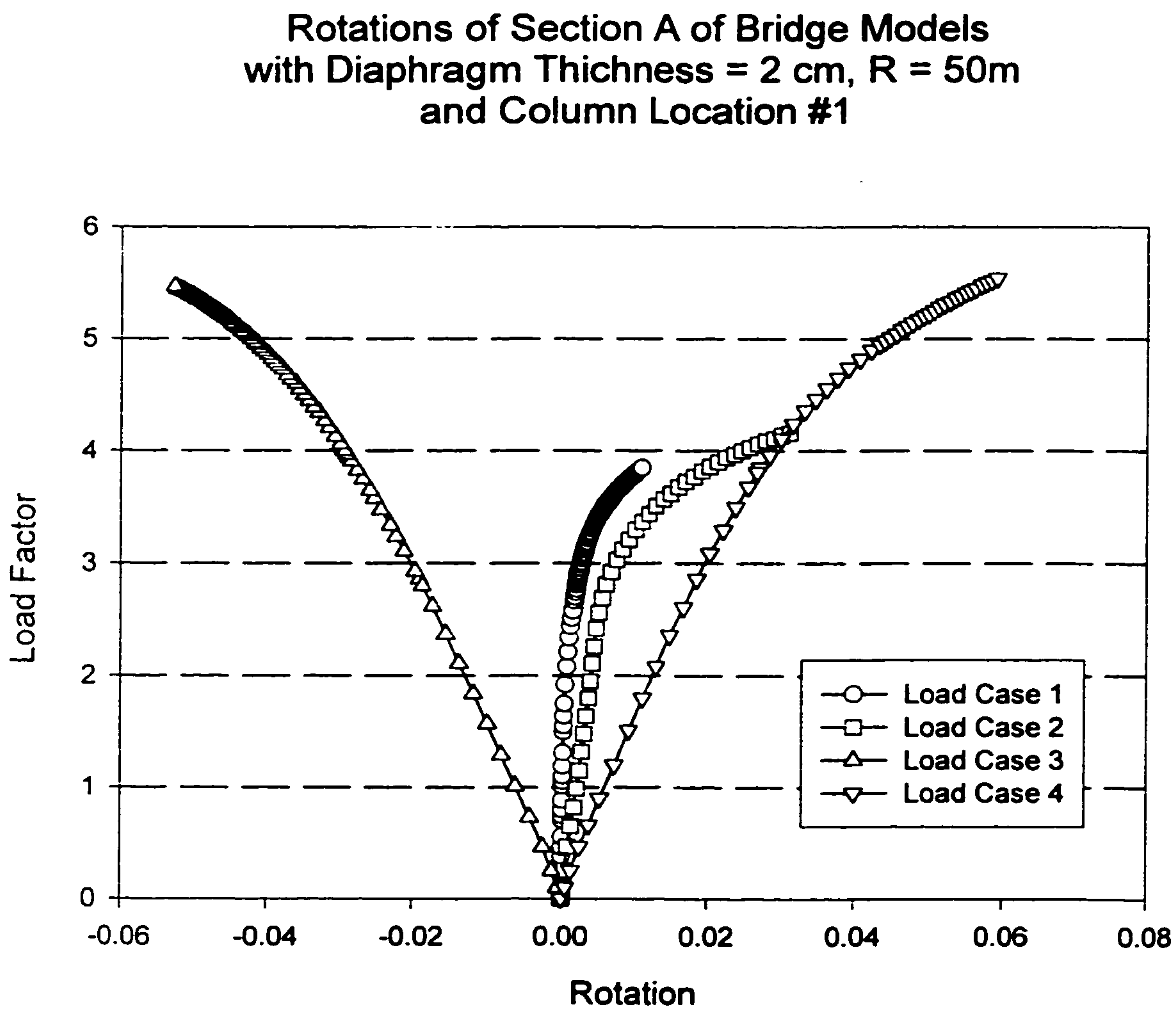

Figure 5.15. Rotations at Section A of Bridge Models with R=50m and Column Location #1 under Various Load Cases

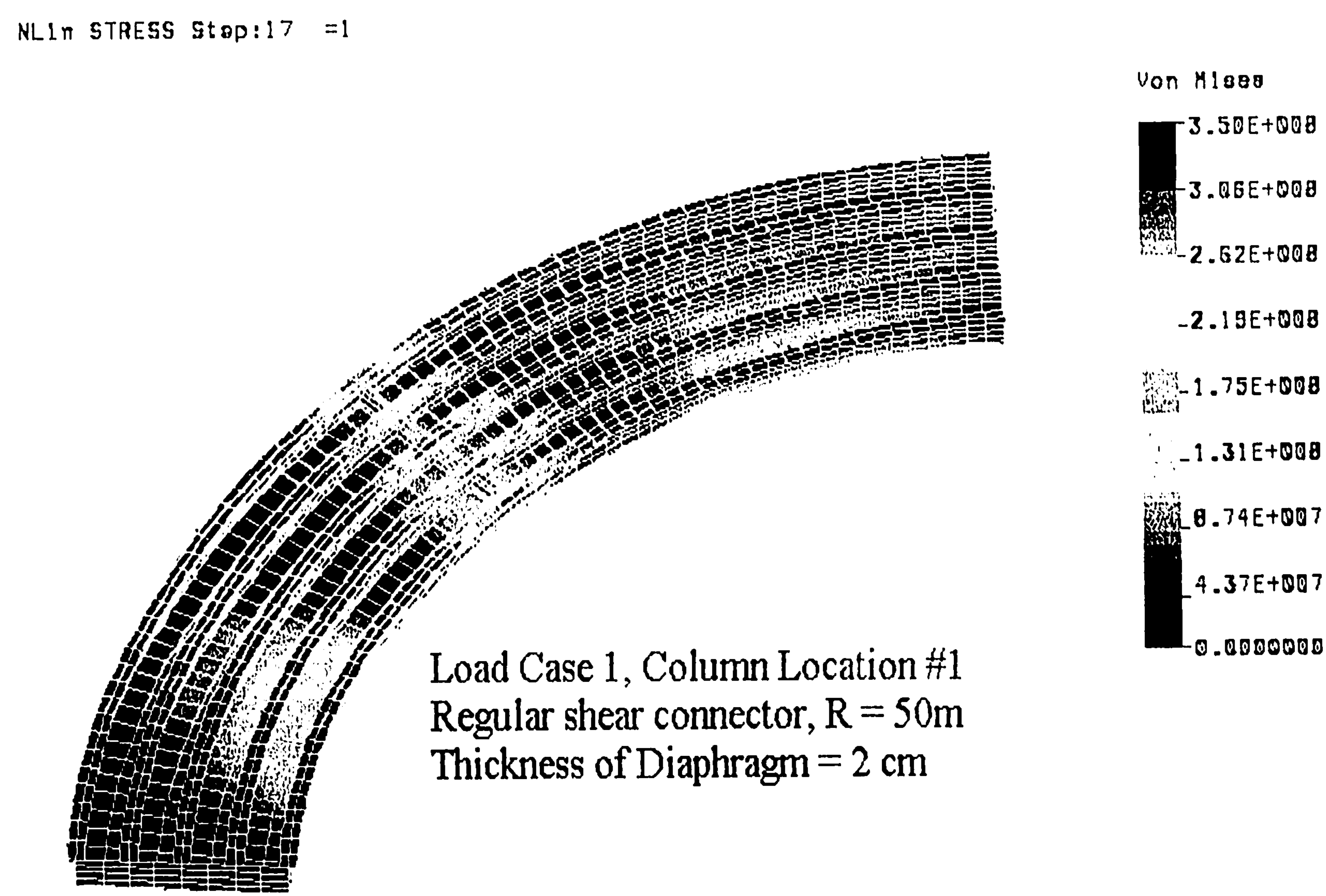

Figure 5.16 Stress Distribution of the Bridge Model with R = 50 m and Column Location 1 at Yielding State under Load Case 1

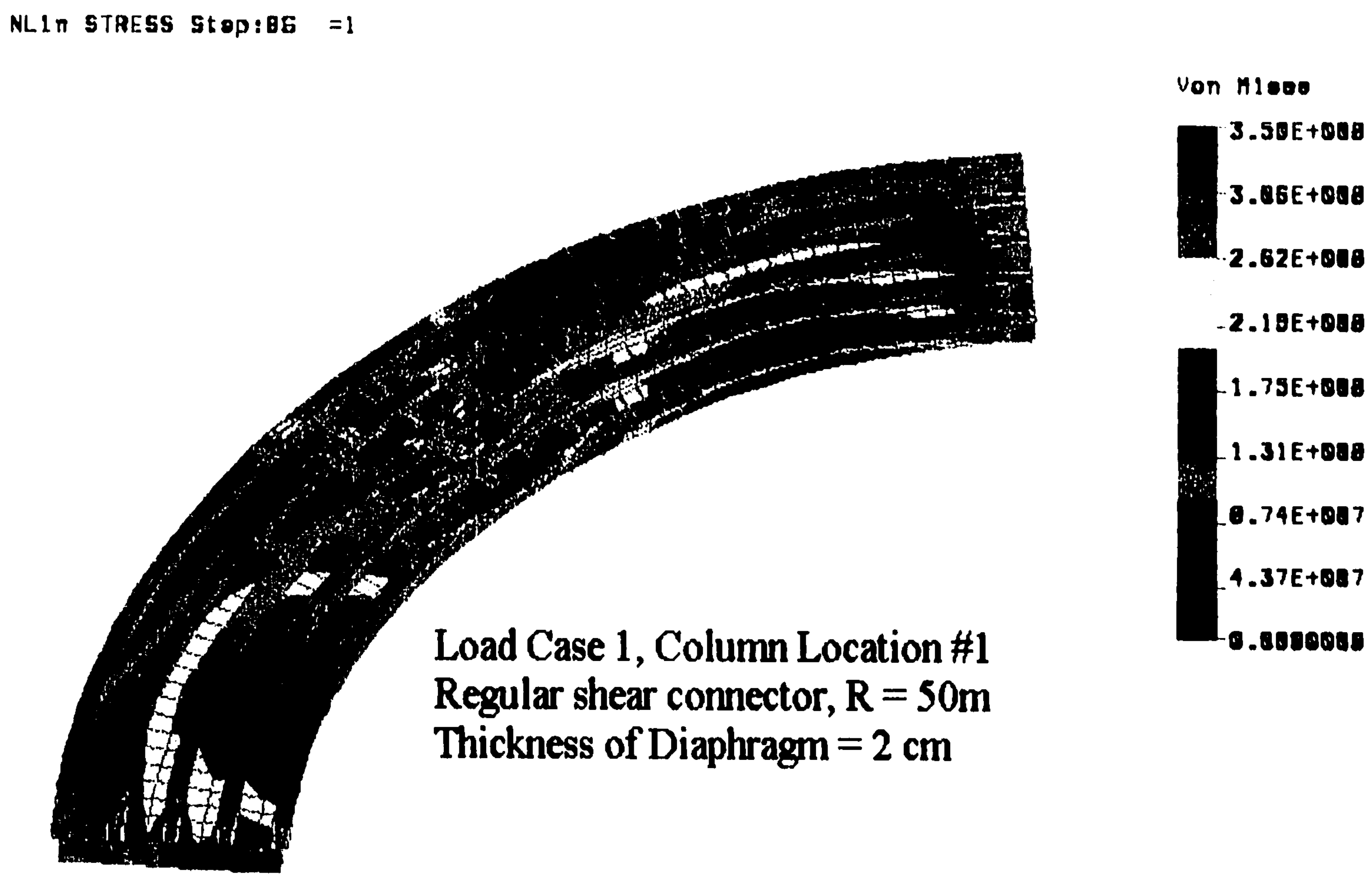

Figure 5.17 Stress Distribution of the Bridge Model with R = 50 m and Column Location 1 at Ultimate State under Load Case 1

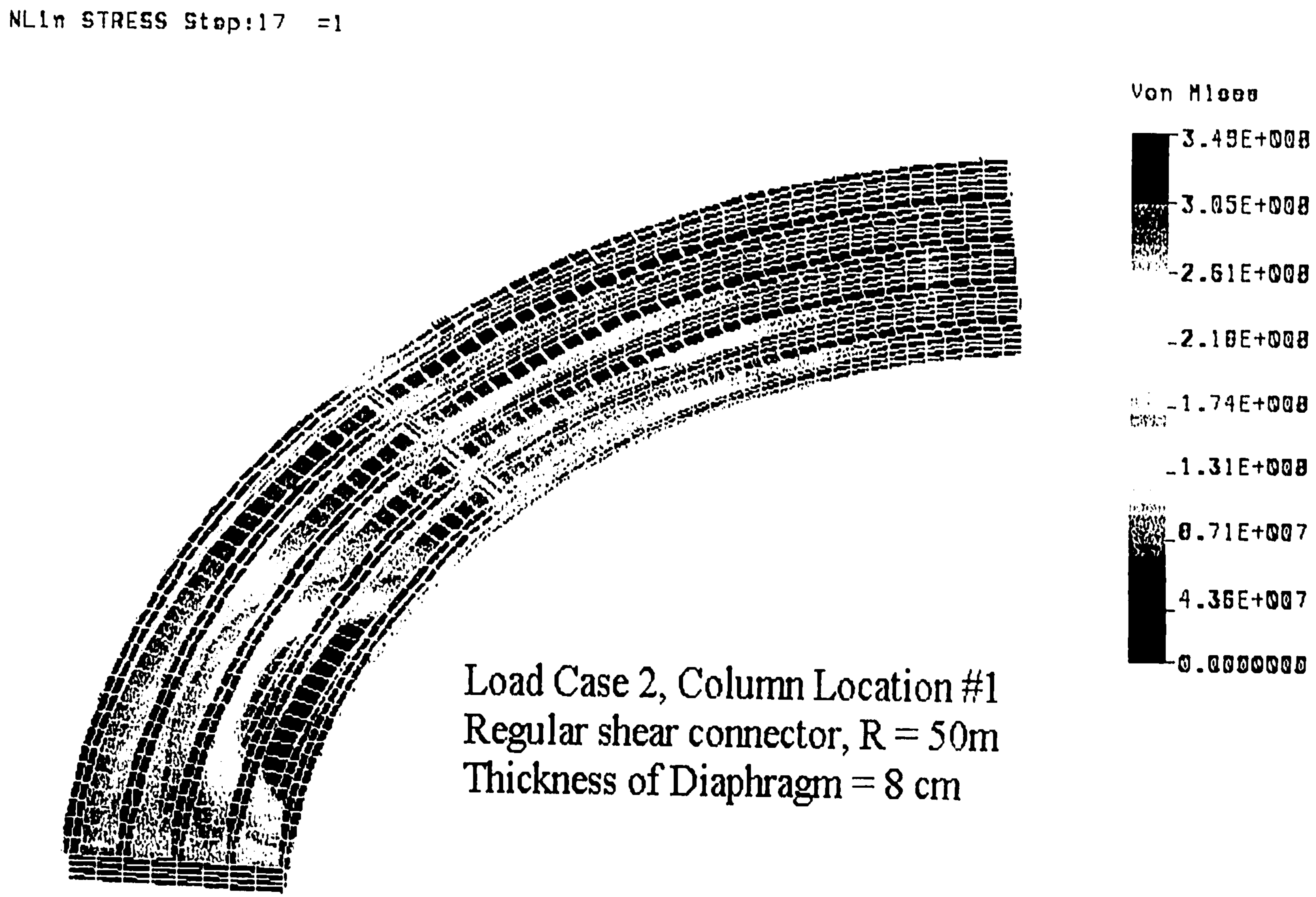

Figure 5.18 Stress Distribution of the Bridge Model with R = 50 m and Column Location 1 at Yielding State under Load Case 2

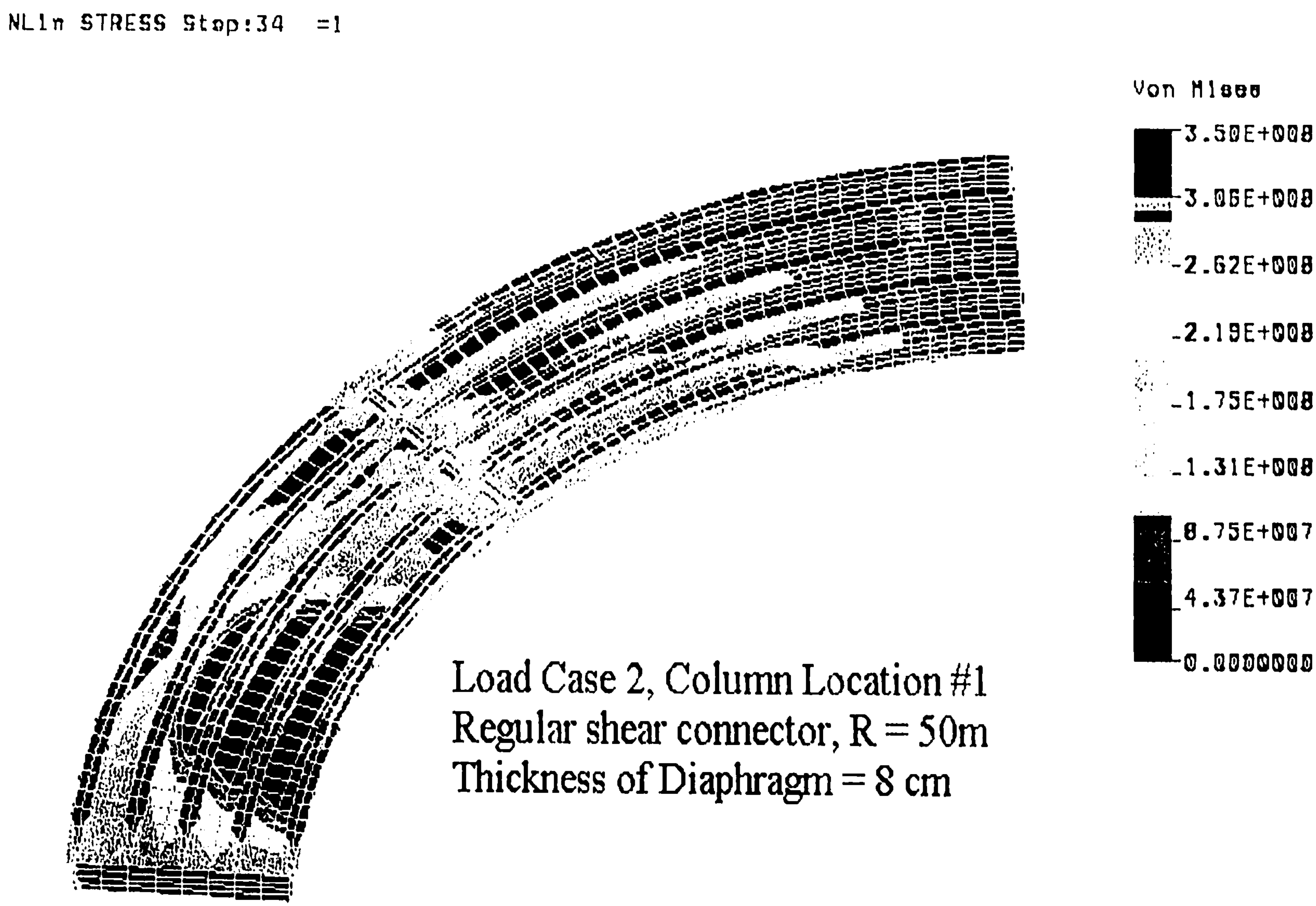

Figure 5.19 Stress Distribution of the Bridge Model with R = 50 m and Column Location 1 at Ultimate State under Load Case 2

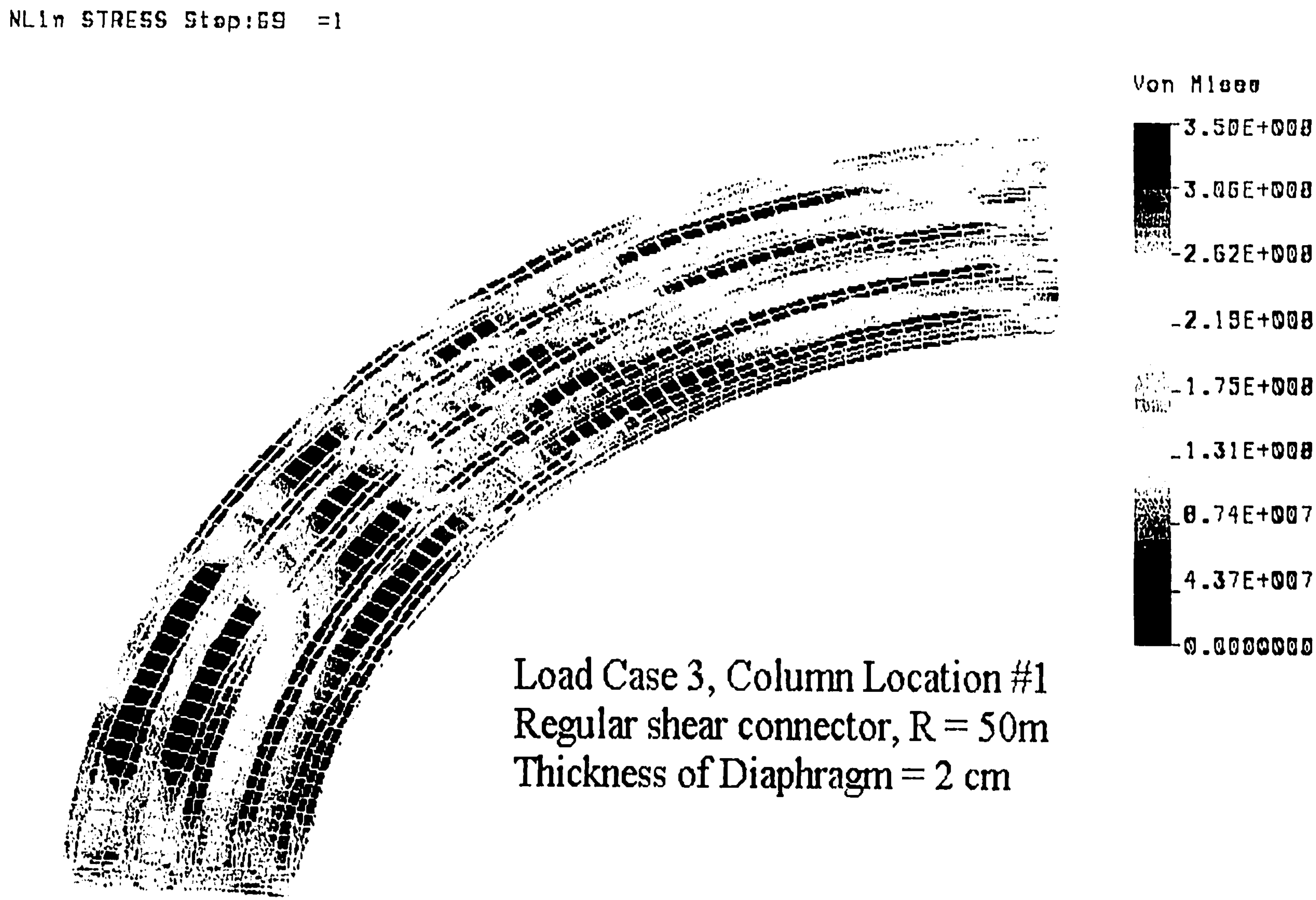

Figure 5.20 Stress Distribution of the Bridge Model with R = 50 m and Column Location 1 at Ultimate State under Load Case 3

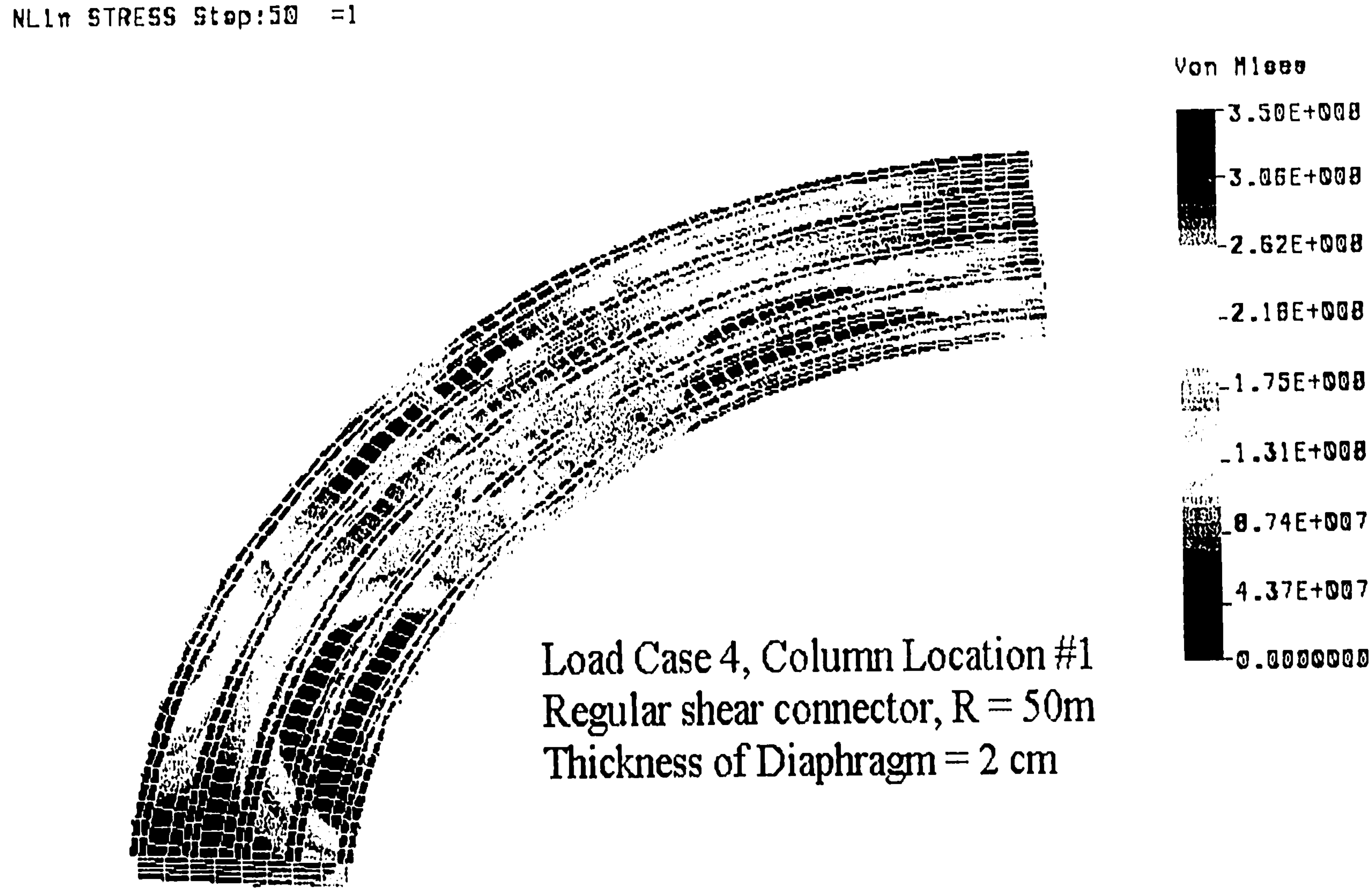

Figure 5.21 Stress Distribution of the Bridge Model with R = 50 m and Column Location 1 at Ultimate State under Load Case 4

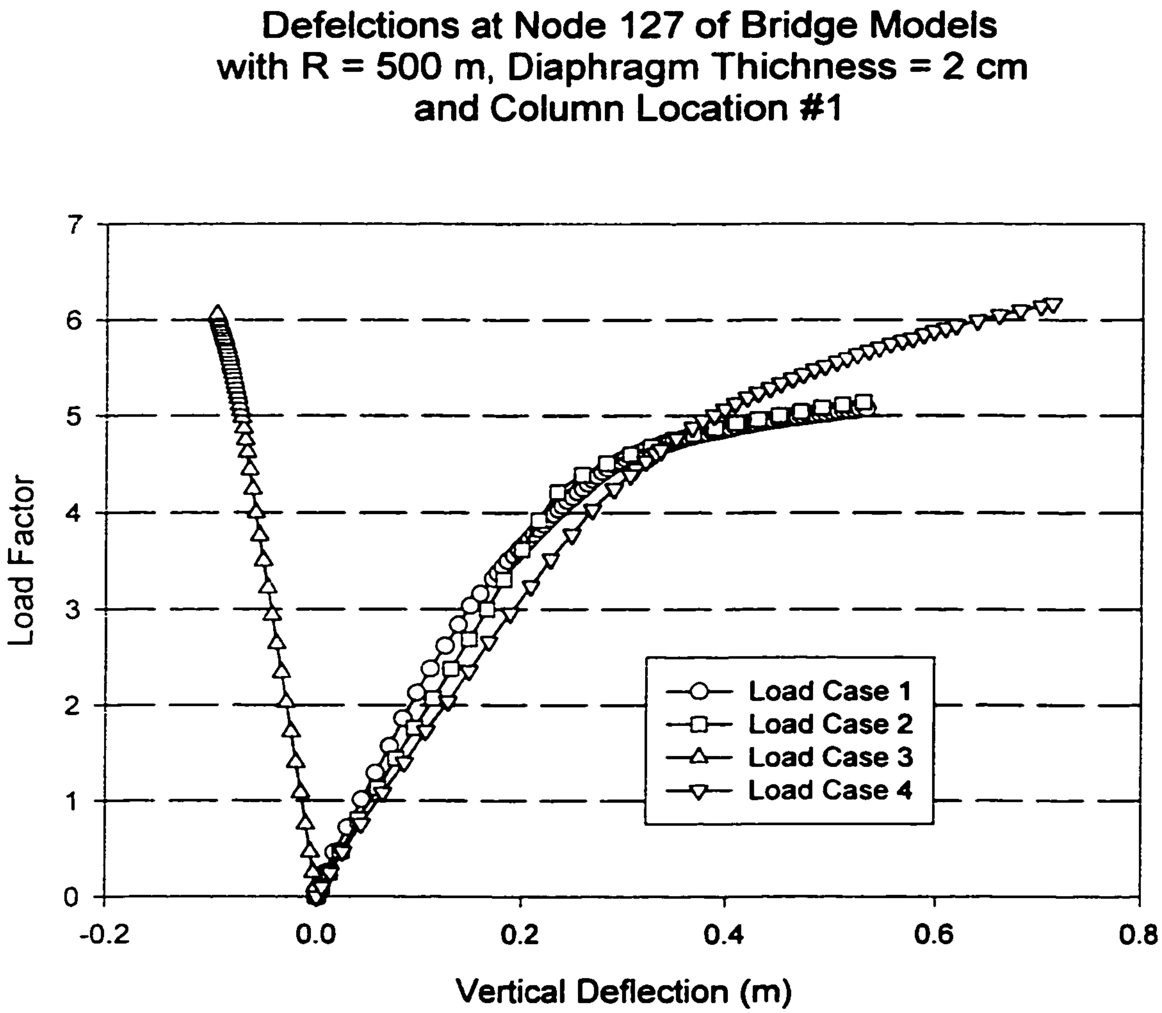

Figure 5.22a Deflections of Node 127 of Bridge Models R=500m and Column Location #1 under Various Load Cases

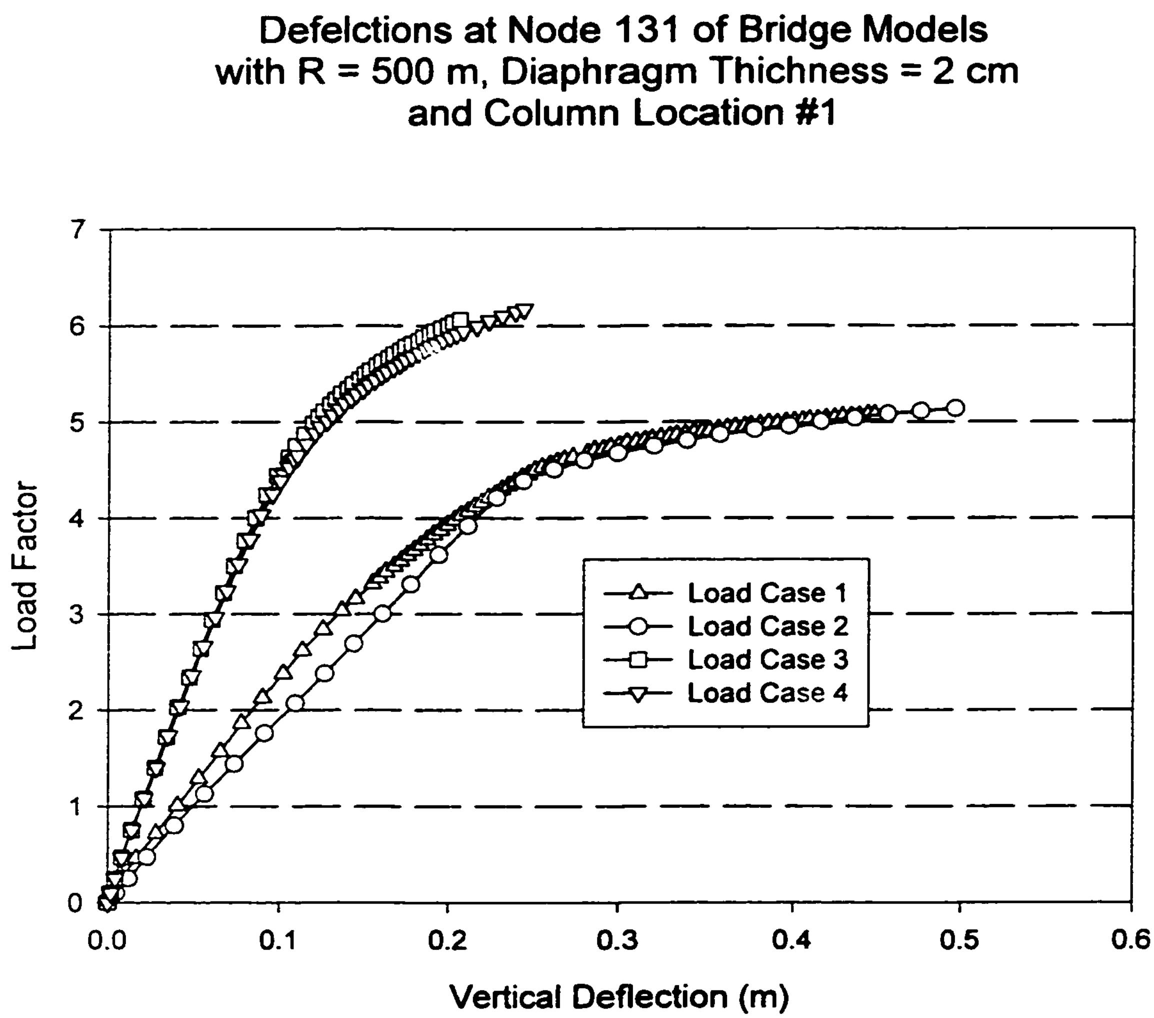

Figure 5.22b Deflections of Node 131 of Bridge Models R=500m and Column Location #1 under Various Load Cases

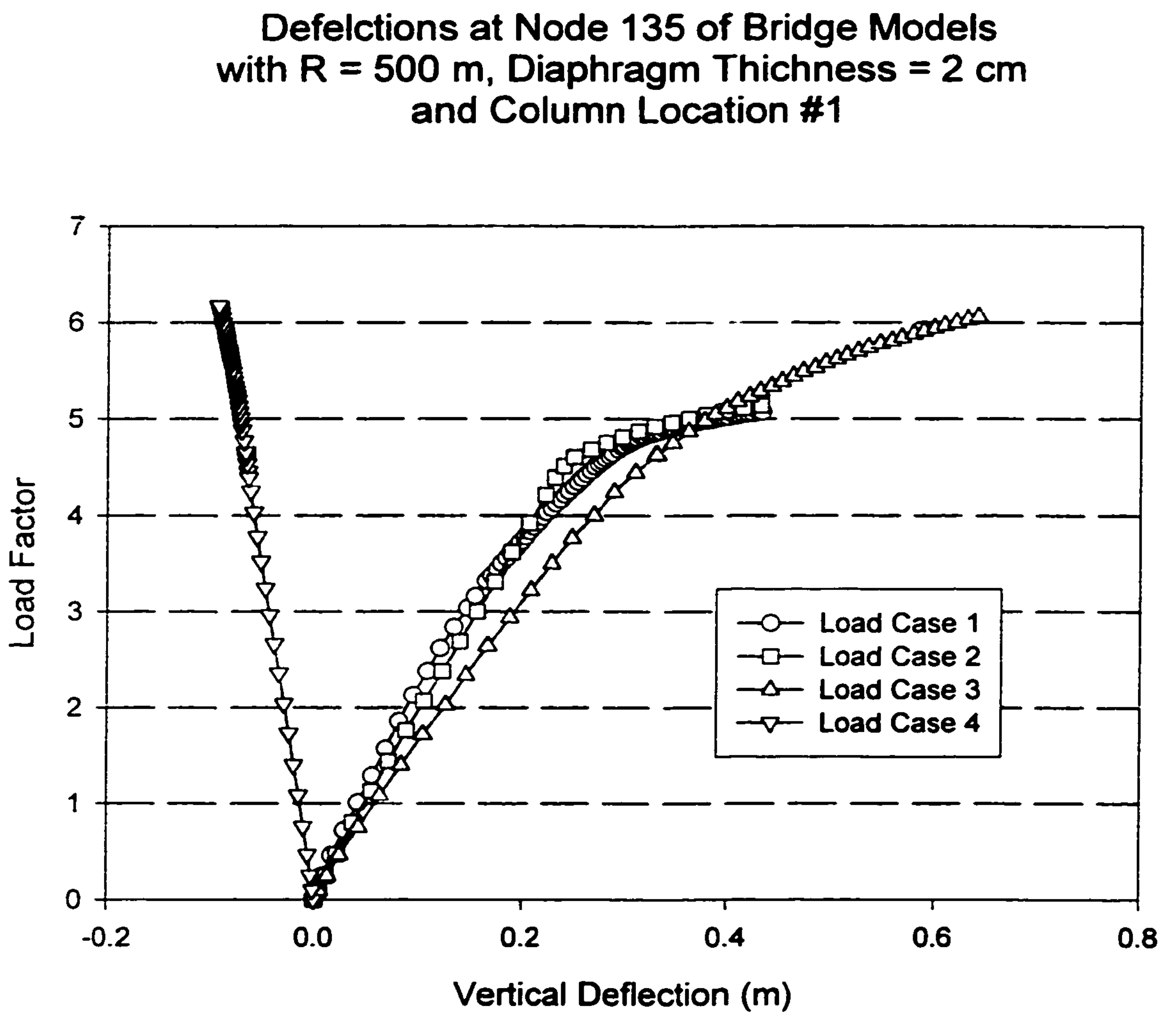

Figure 5.22c Deflections of Node 135 of Bridge Models with R=500m and Column Location #1 under Various Load Cases

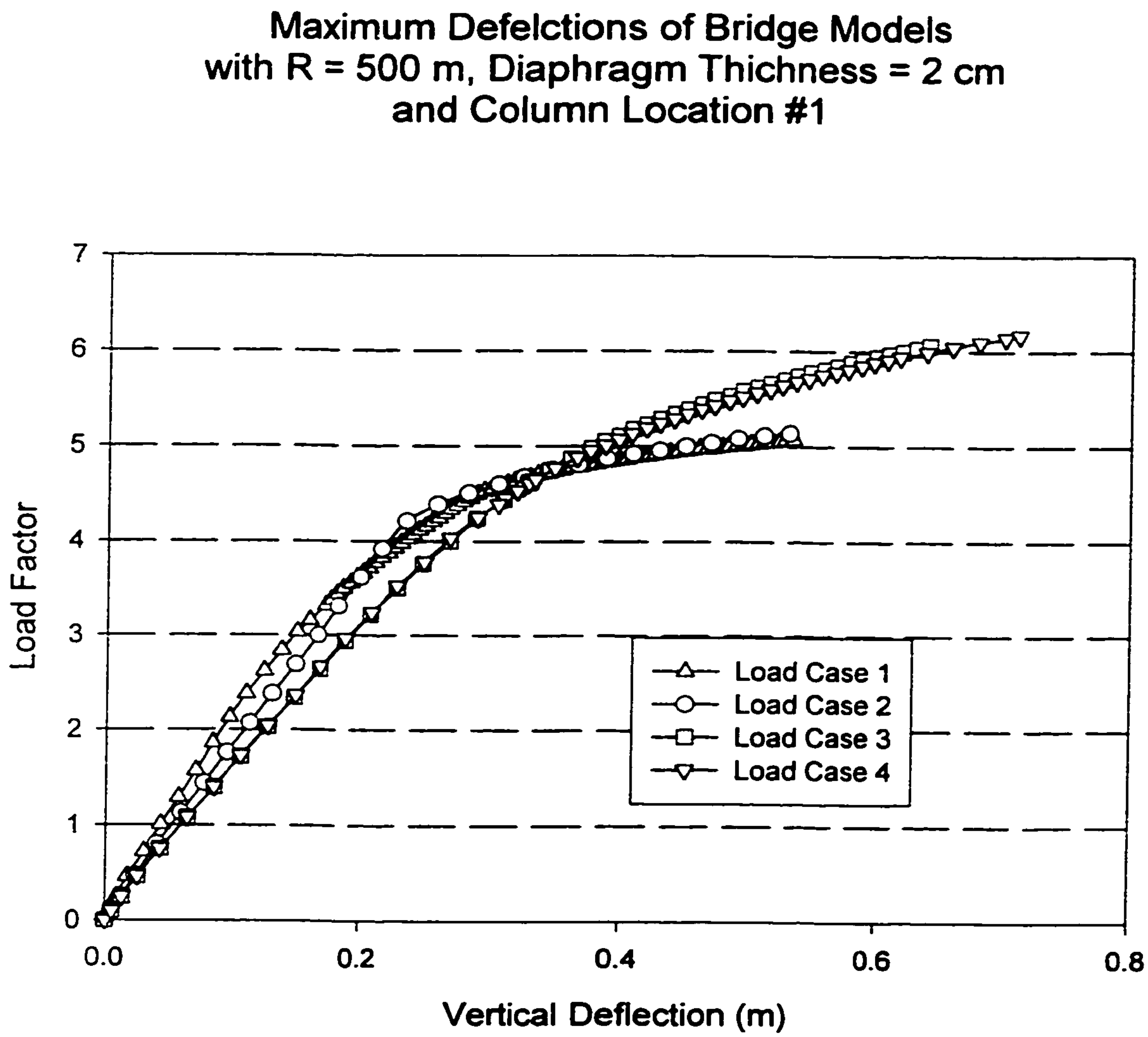

Figure 5.23 Maximum Deflections at Section A of Bridge Models with R=500m and Column Location #1 under Various Load Cases

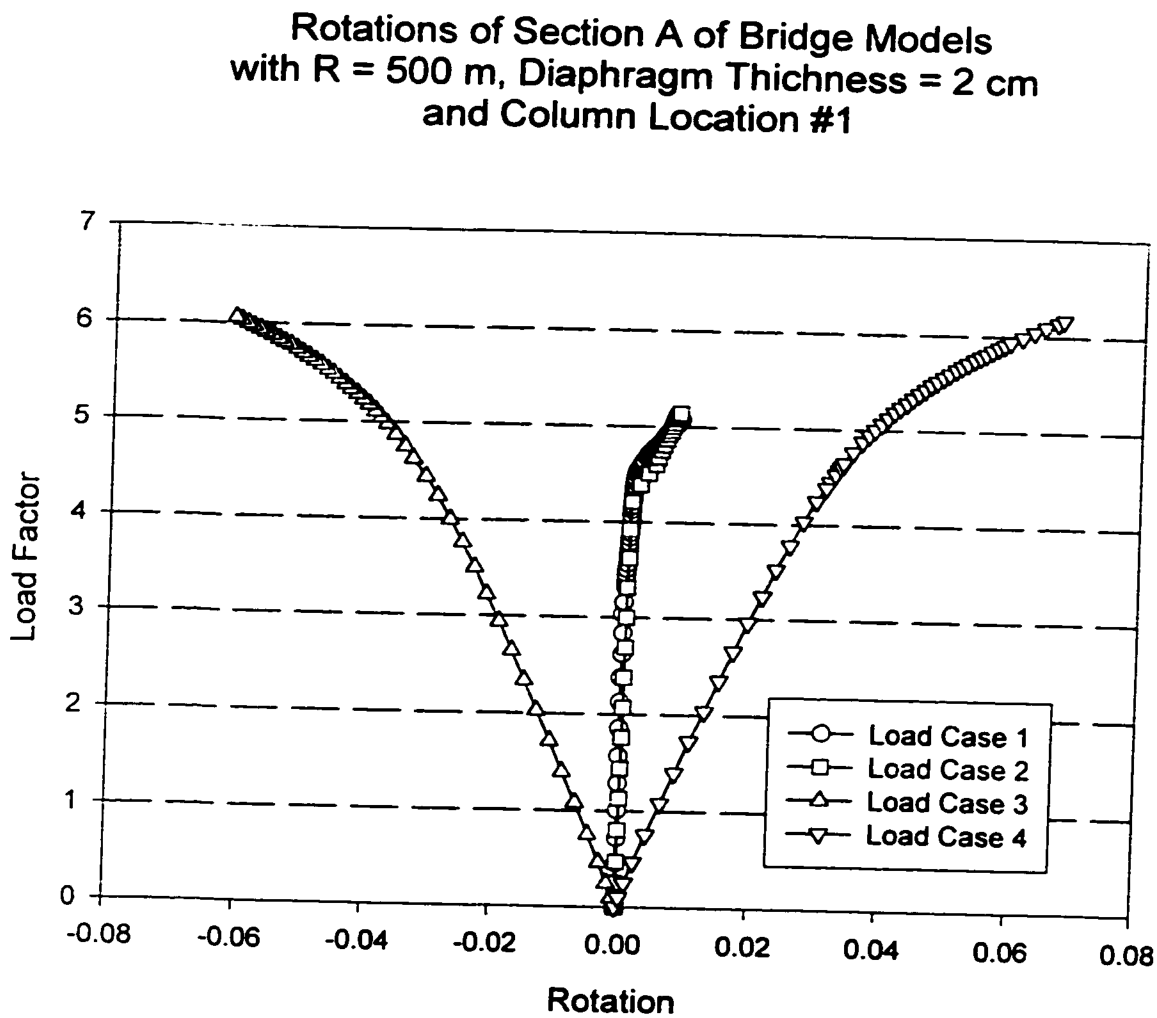

Figure 5.24. Rotations at Section A of Bridge Models with R=500m and Column Location #1 under Various Load Cases

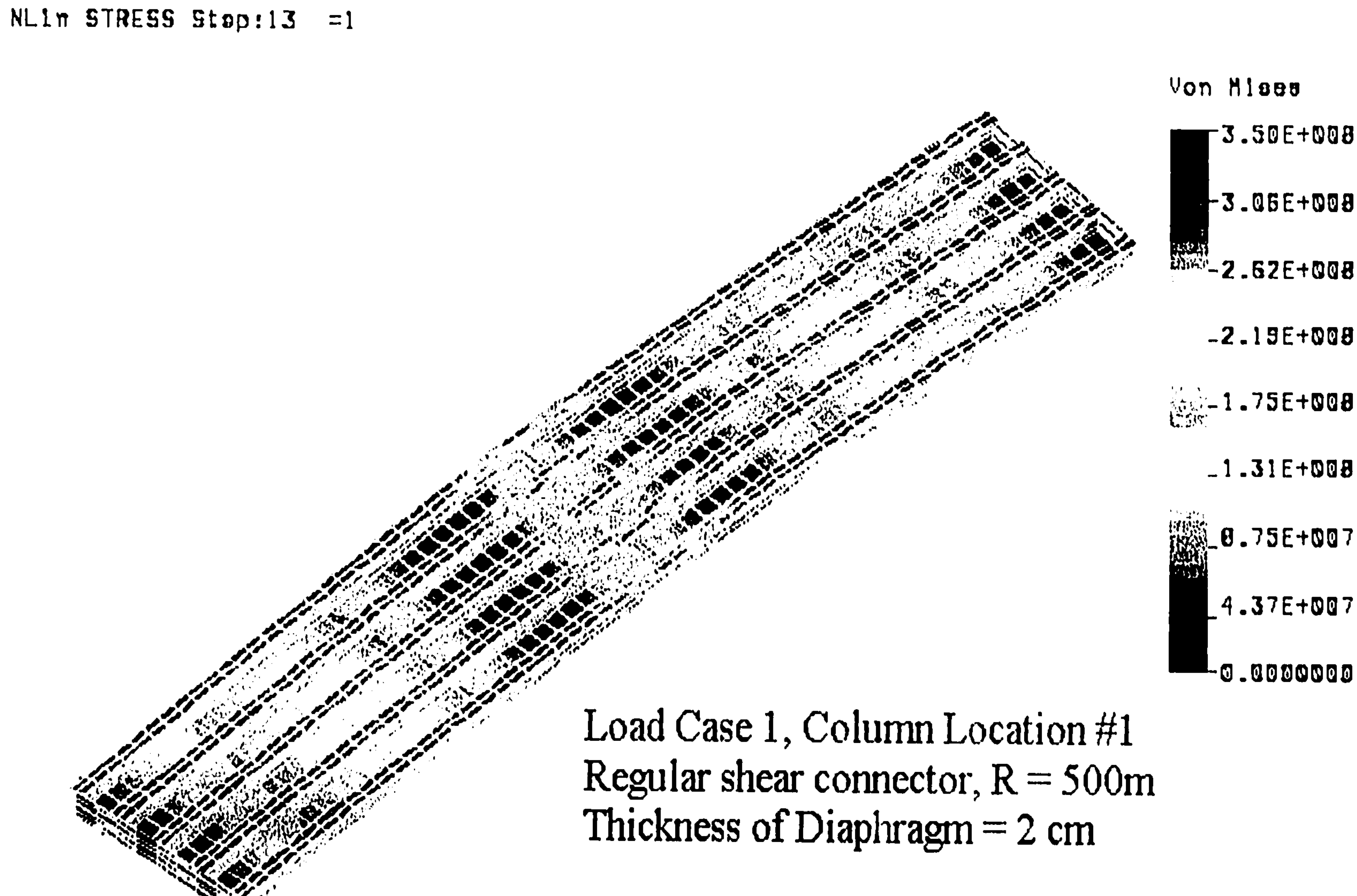

Figure 5.25 Stress Distribution of the Bridge Model with R = 500 m and Column Location 1 at Yielding State under Load Case 1

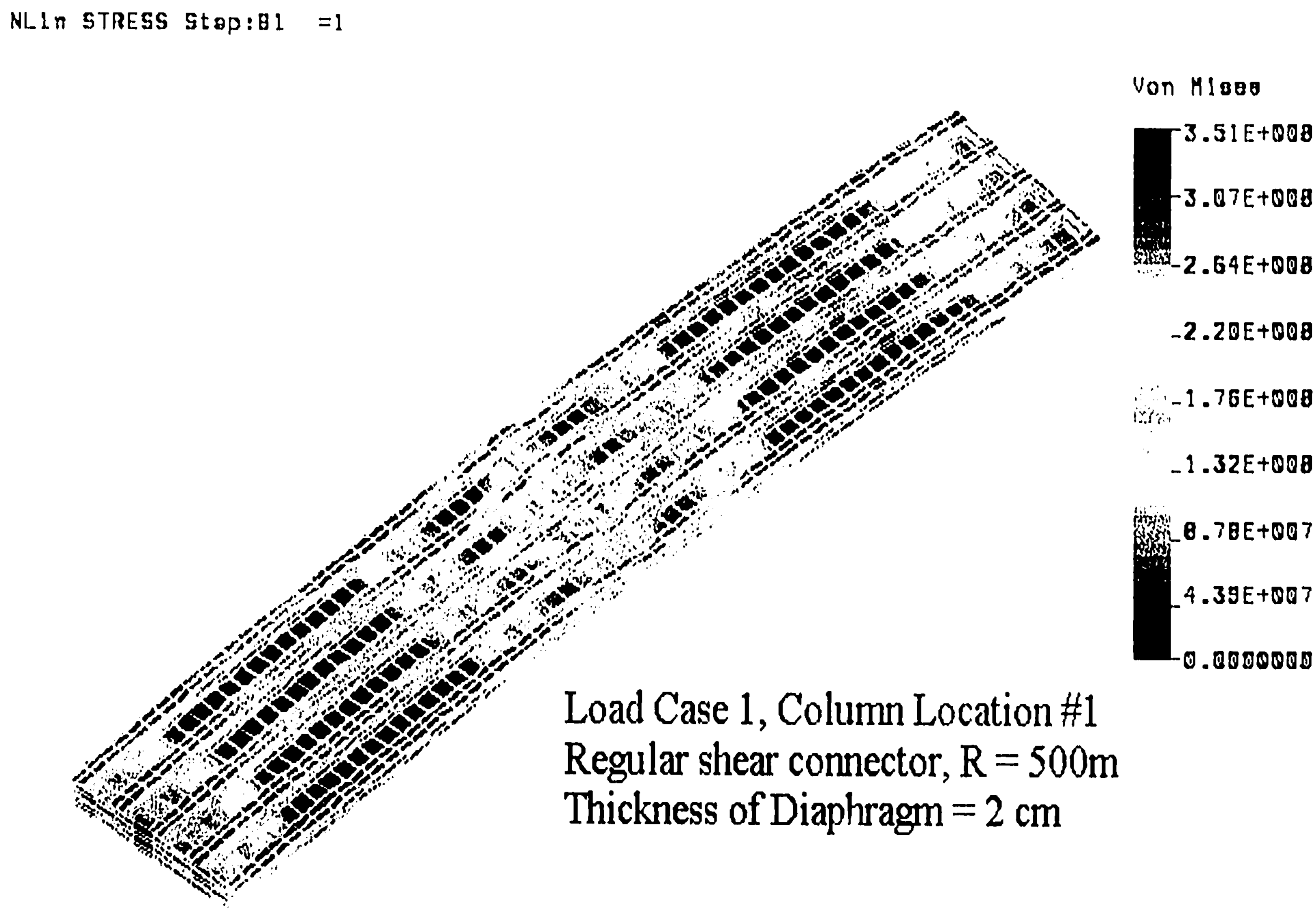

Figure 5.26 Stress Distribution of the Bridge Model with R = 500 m and Column Location 1 at Ultimate State under Load Case 1

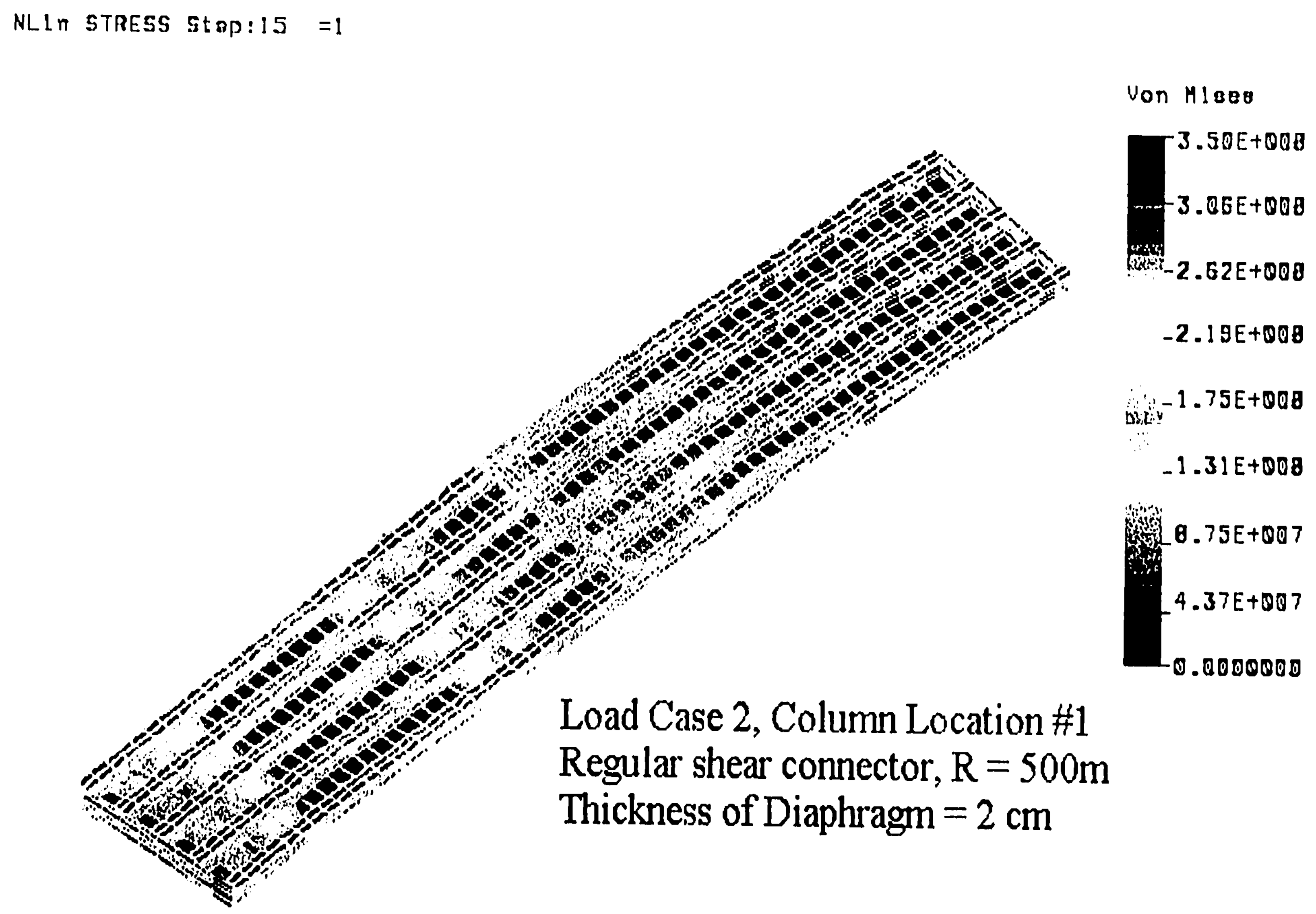

Figure 5.27 Stress Distribution of the Bridge Model with R = 500 m and Column Location 1 at Yielding State under Load Case 2

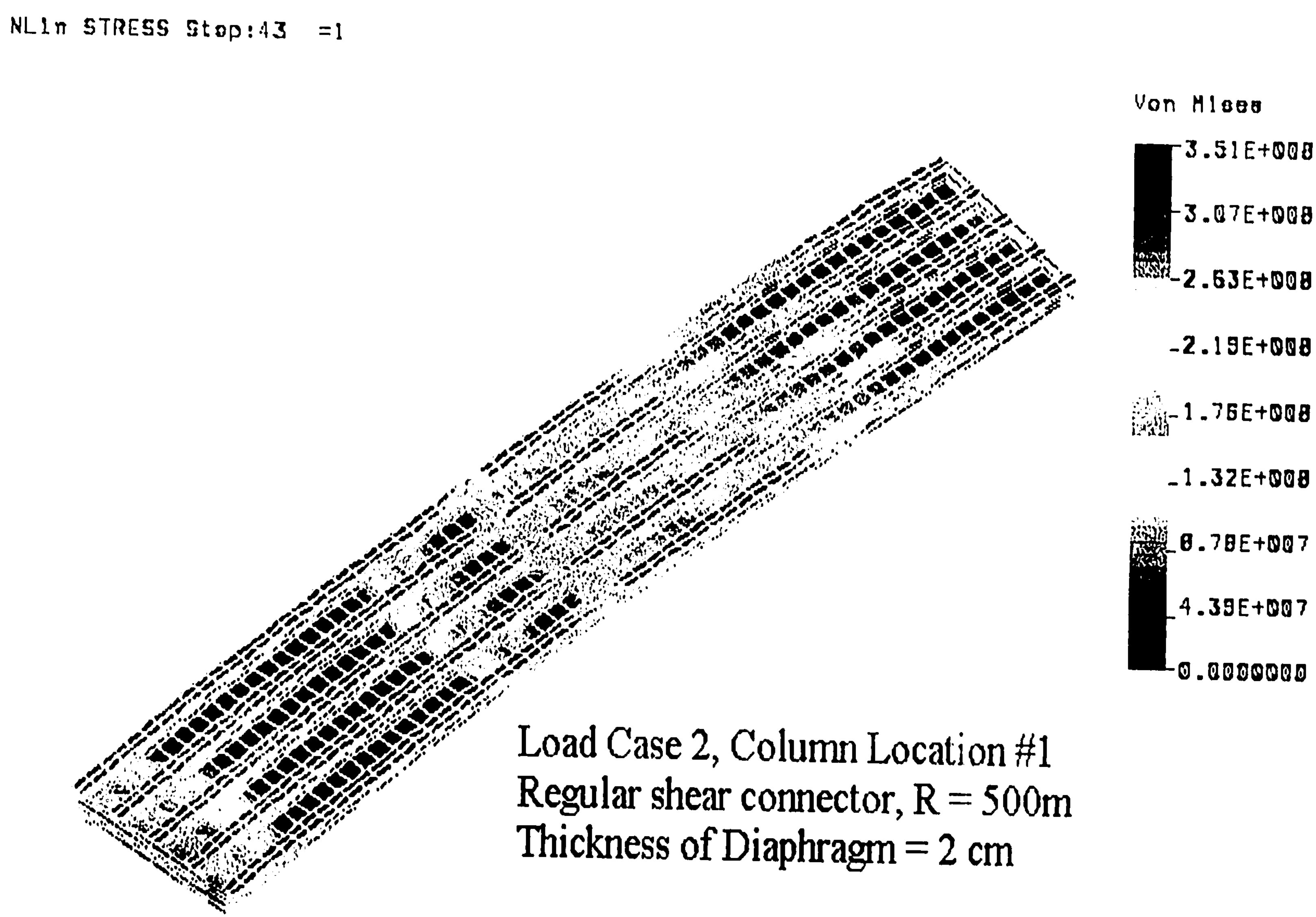

Figure 5.28 Stress Distribution of the Bridge Model with R = 500 m and Column Location 1 at Ultimate State under Load Case 2

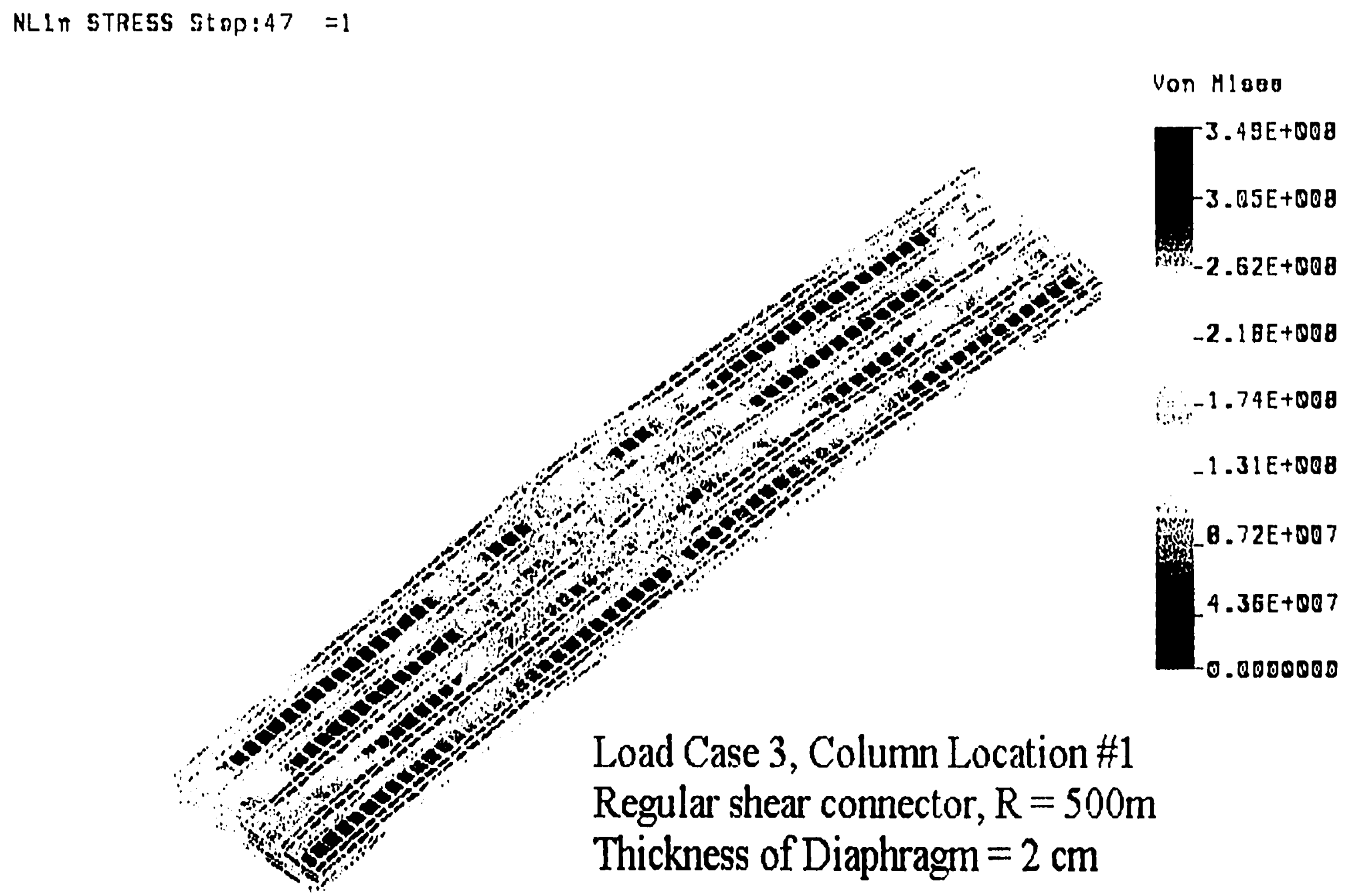

Figure 5.29 Stress Distribution of the Bridge Model with R = 500 m and Column Location 1 at Ultimate State under Load Case 3

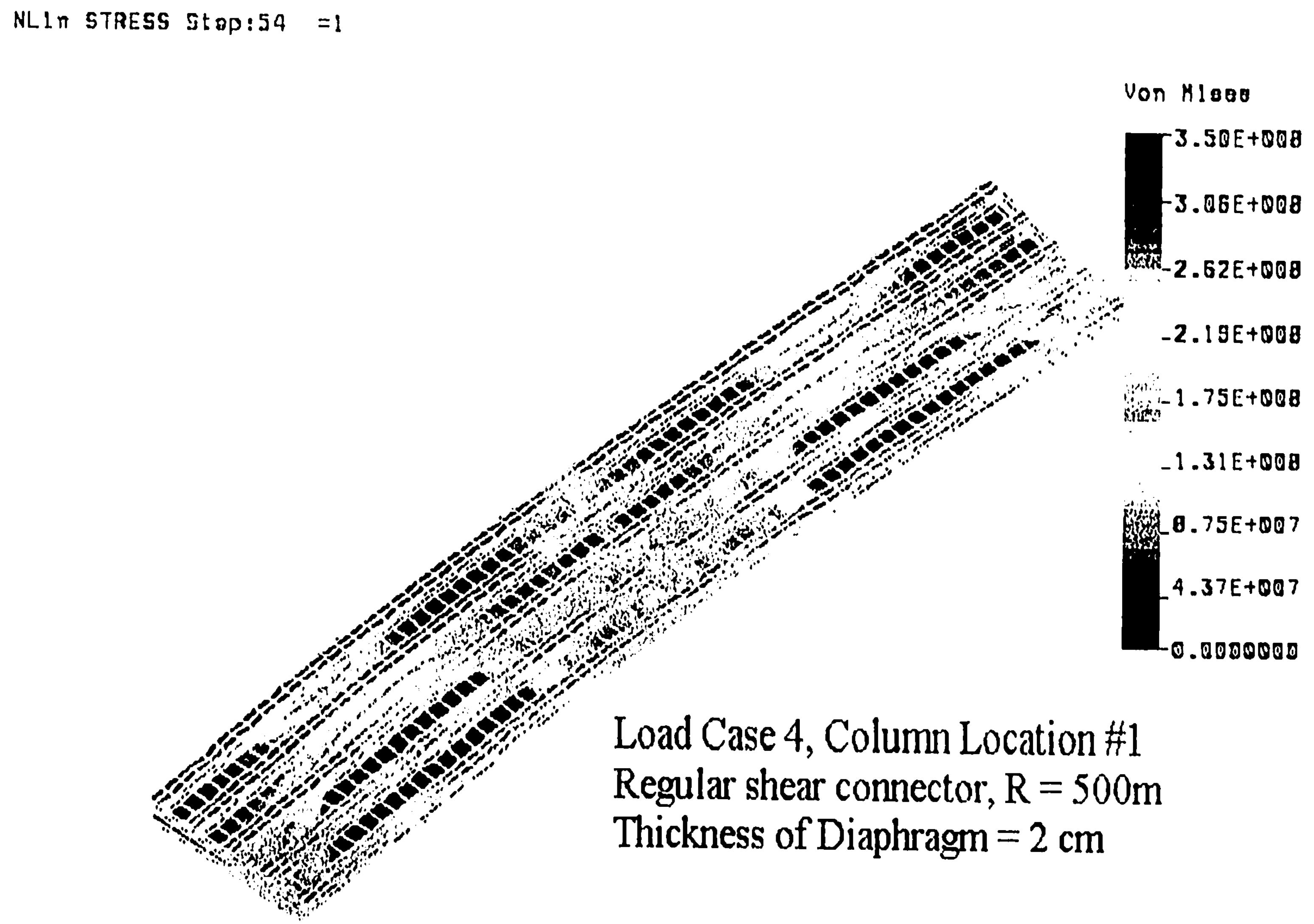

Figure 5.30 Stress Distribution of the Bridge Model with R = 500 m and Column Location 1 at Ultimate State under Load Case 4

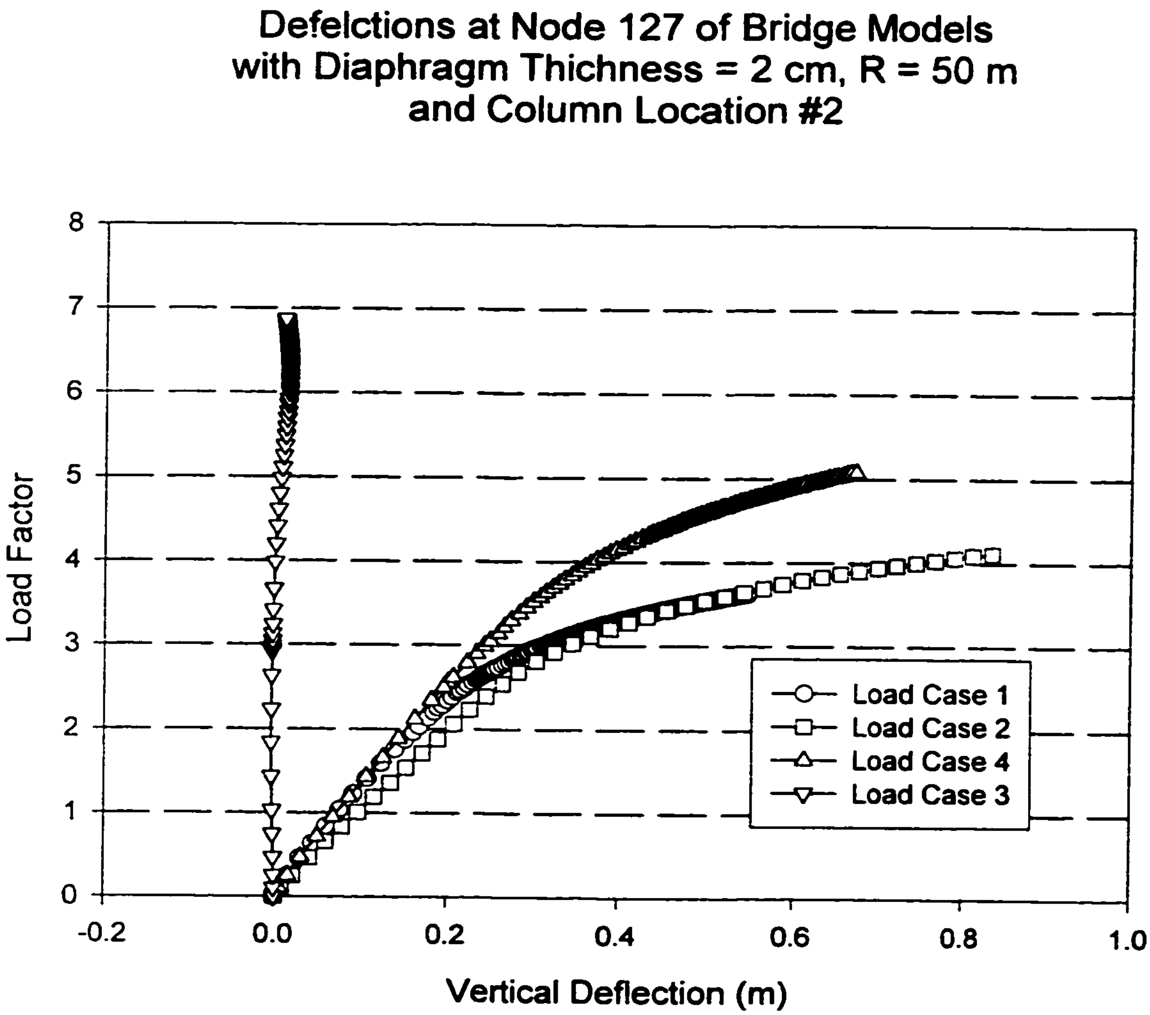

Figure 5.31a Deflections of Node 127 of Bridge Models with R=50m and Column Location #2 under Various Load Cases

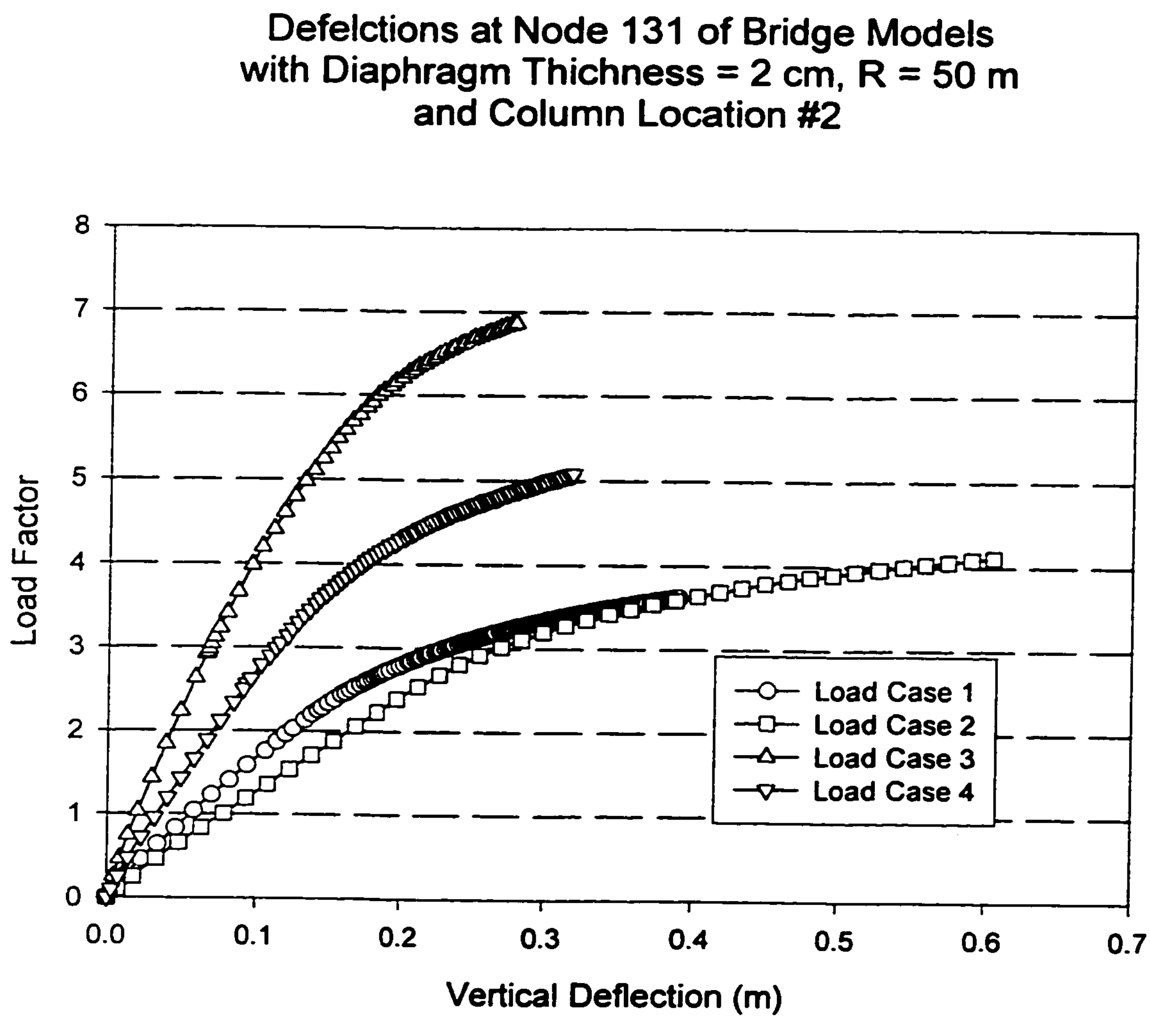

Figure 5.31b Deflections of Node 131 of Bridge Models with R=50m and Column Location #2 under Various Load Cases

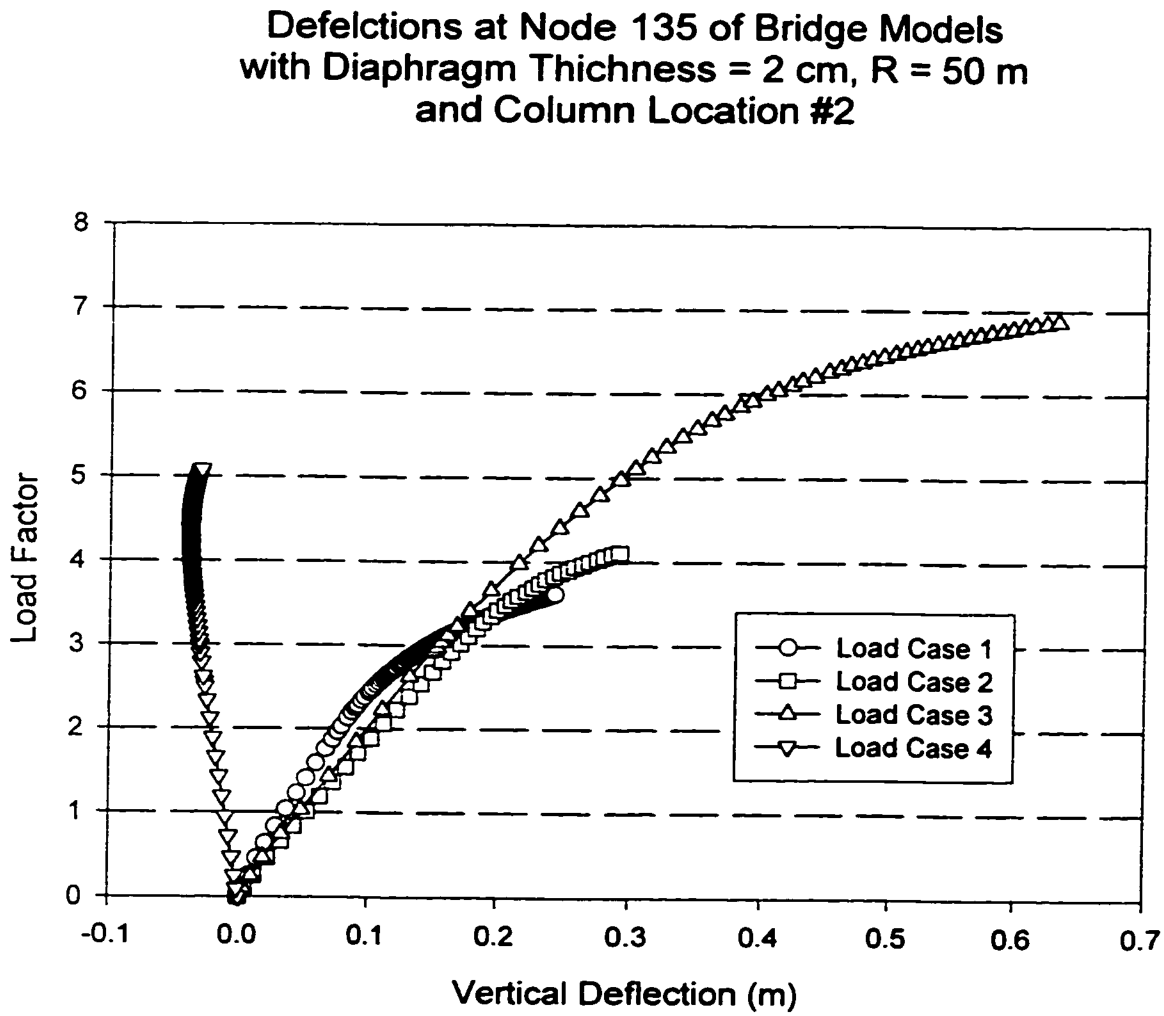

Figure 5.31c Deflections of Node 135 of Bridge Models with R=50m and Column Location #2 under Various Load Cases

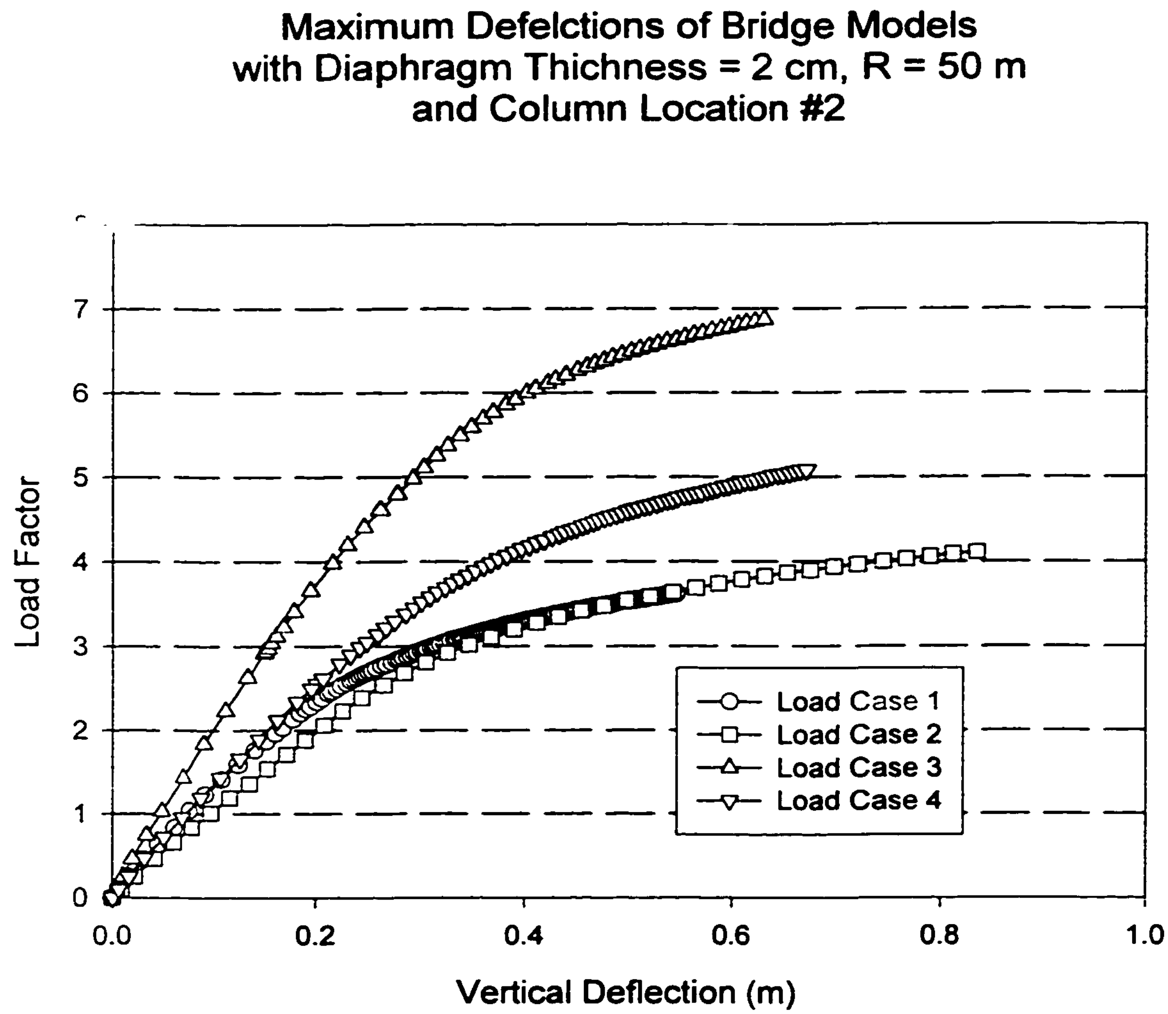

Figure 5.32 Maximum Deflections at Section A of Bridge Models with R=50m and Column Location #2 under Various Load Cases

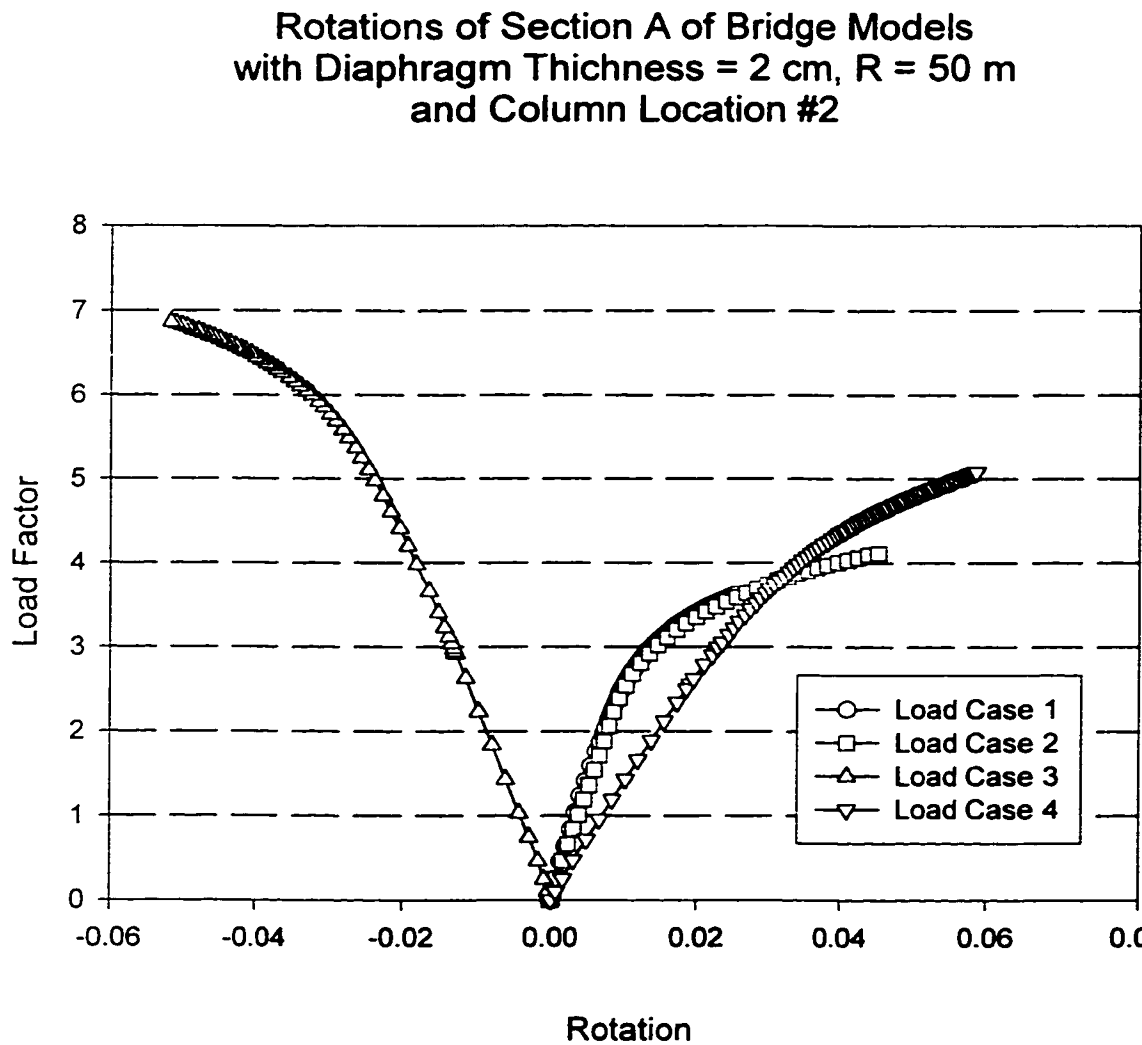

Figure 5.33. Rotations at Section A of Bridge Models with R=50m and Column Location #2 under Various Load Cases

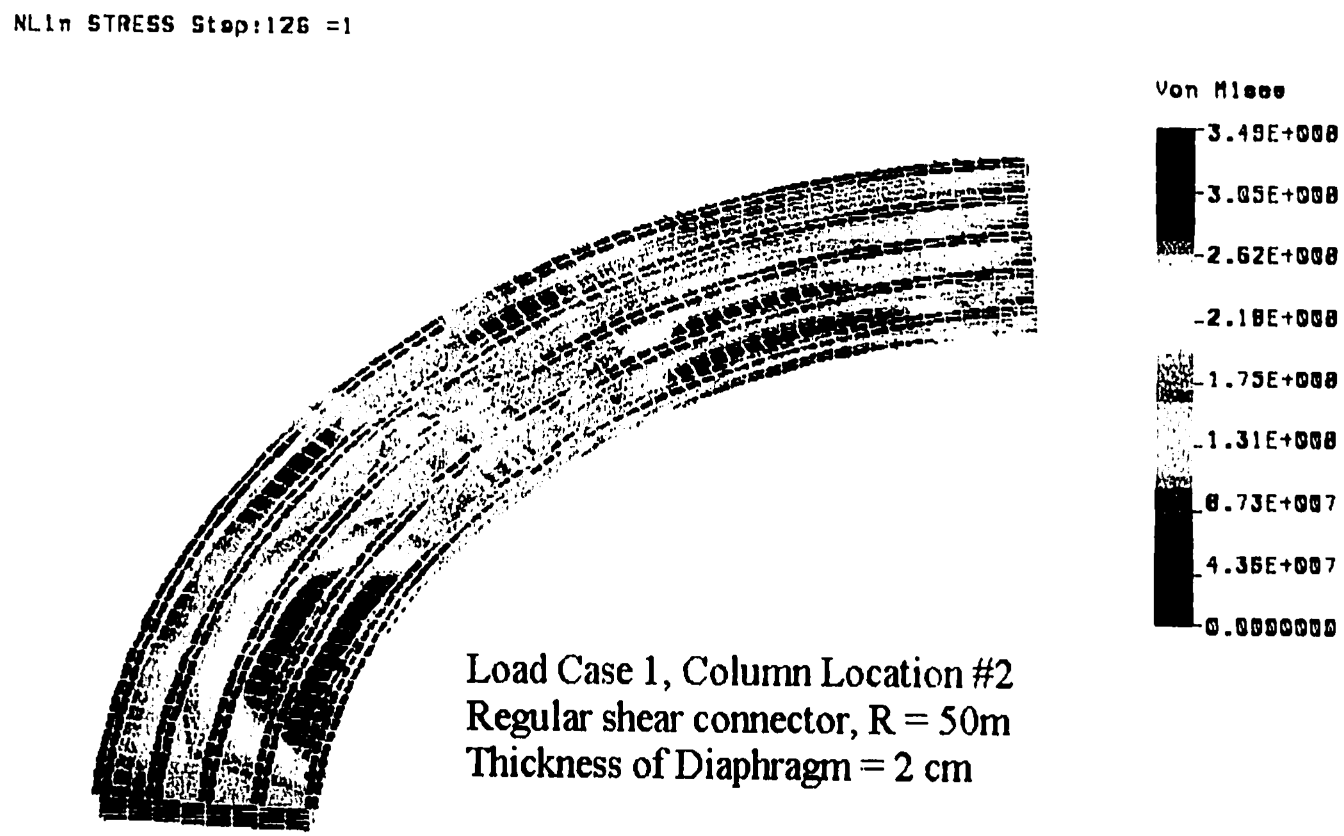

Figure 5.34 Stress Distribution of the Bridge Model with R = 50 m and Column Location 2 at Ultimate State under Load Case 1

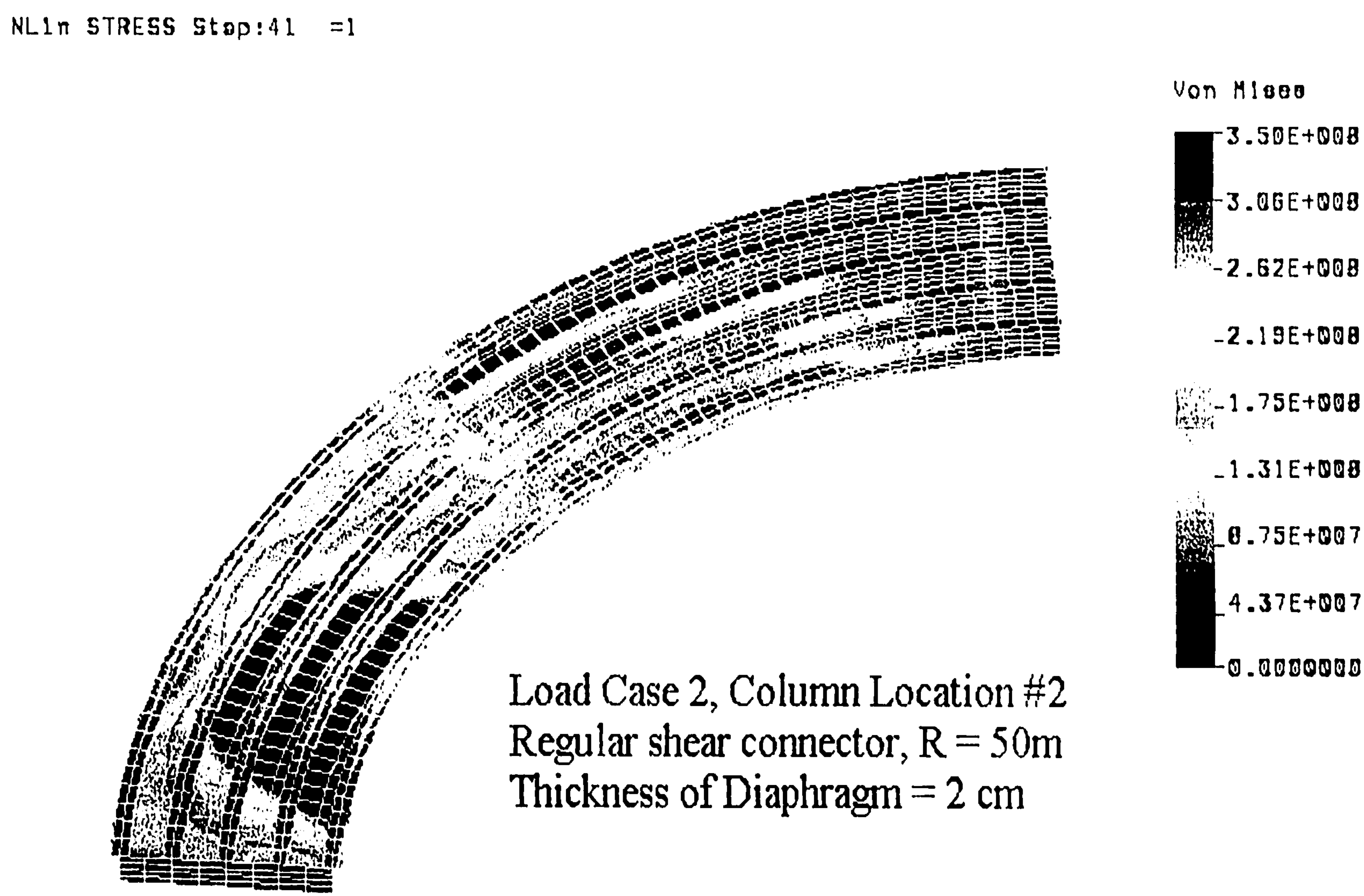

Figure 5.35 Stress Distribution of the Bridge Model with R = 50 m and Column Location 2 at Ultimate State under Load Case 2

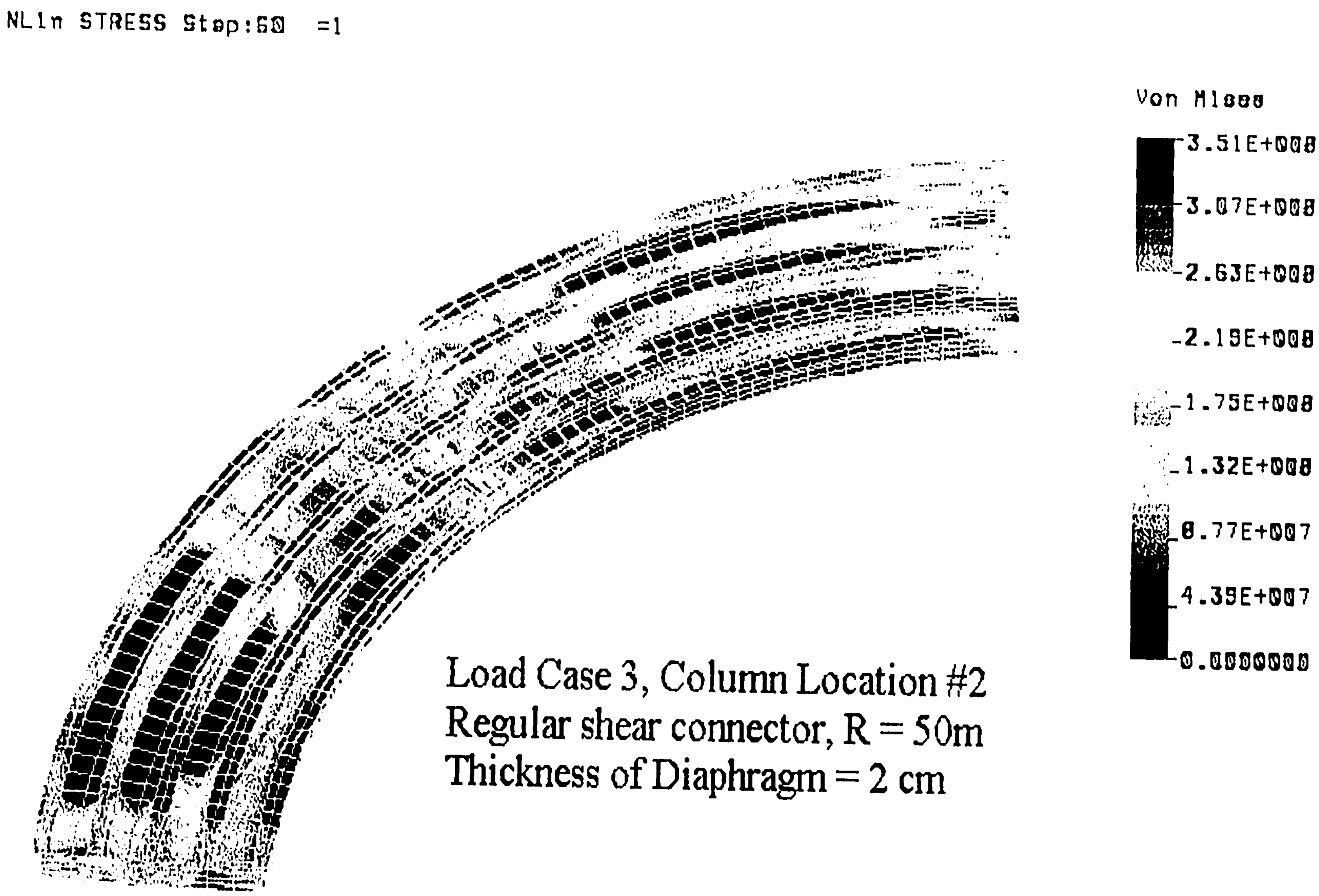

Figure 5.36 Stress Distribution of the Bridge Model with R = 50 m and Column Location 2 at Ultimate State under Load Case 3

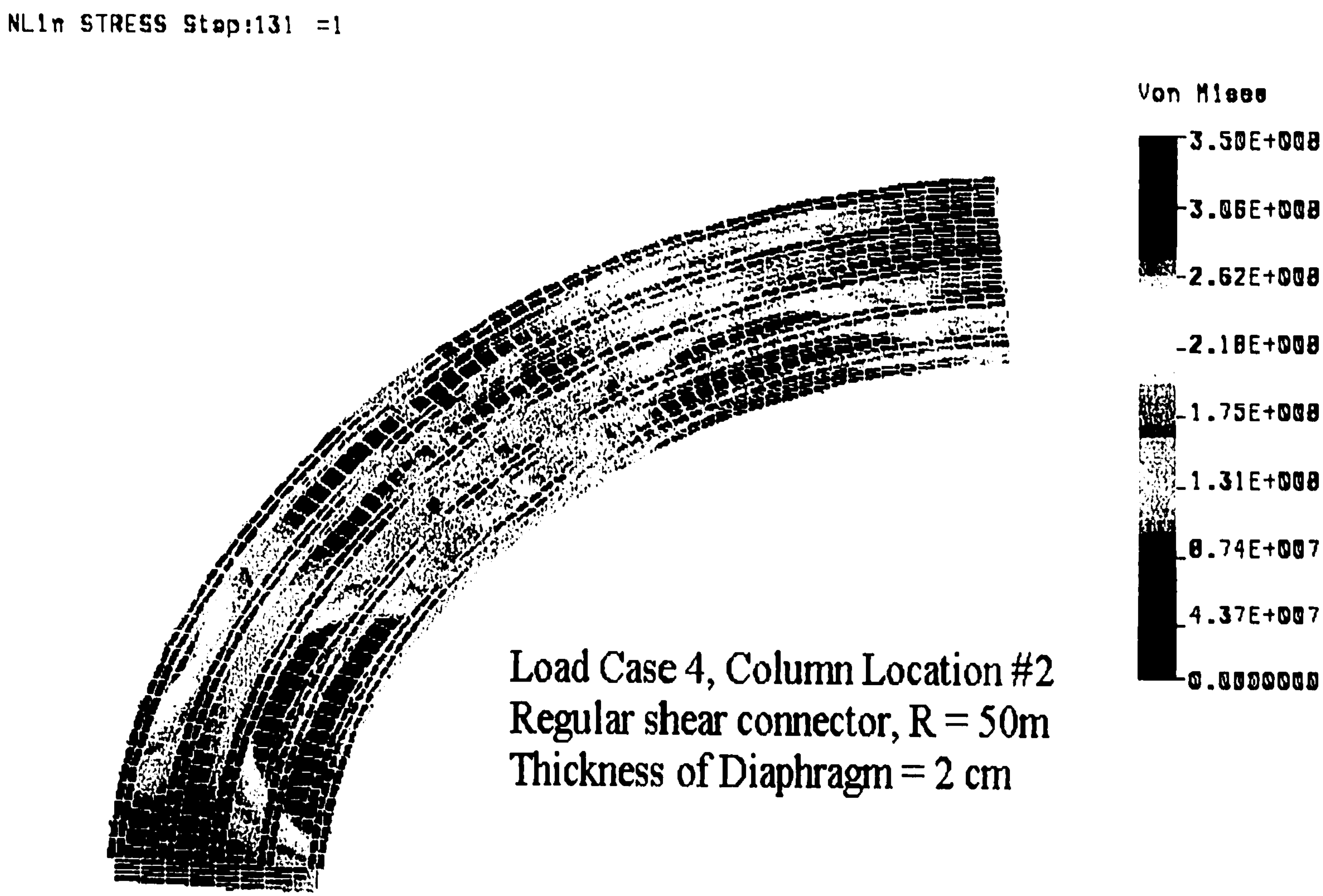

Figure 5.37 Stress Distribution of the Bridge Model with R = 50 m and Column Location 2 at Ultimate State under Load Case 4

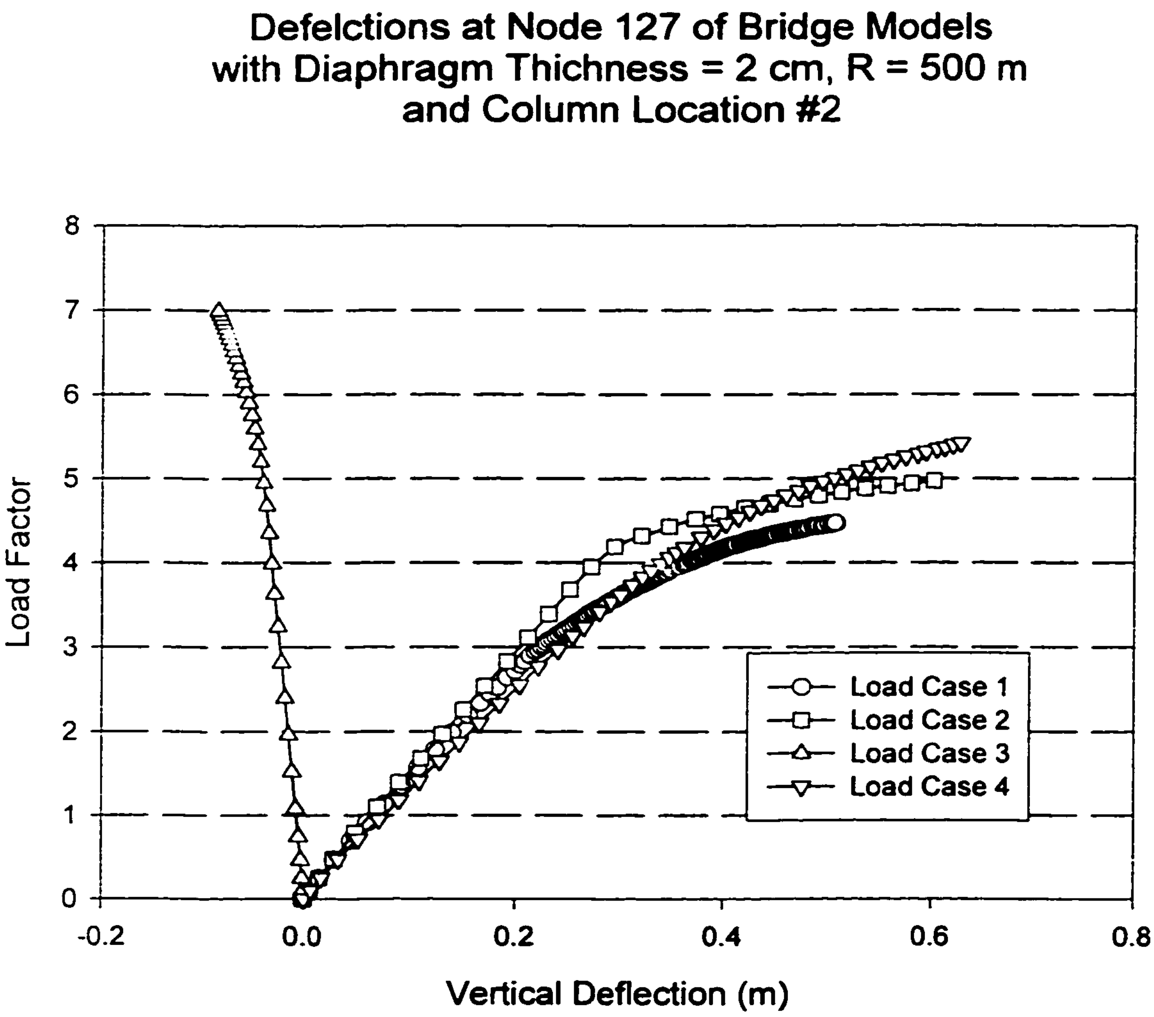

Figure 5.38a Deflections of Node 127 of Bridge Models with R=500m and Column Location #2 under Various Load Cases

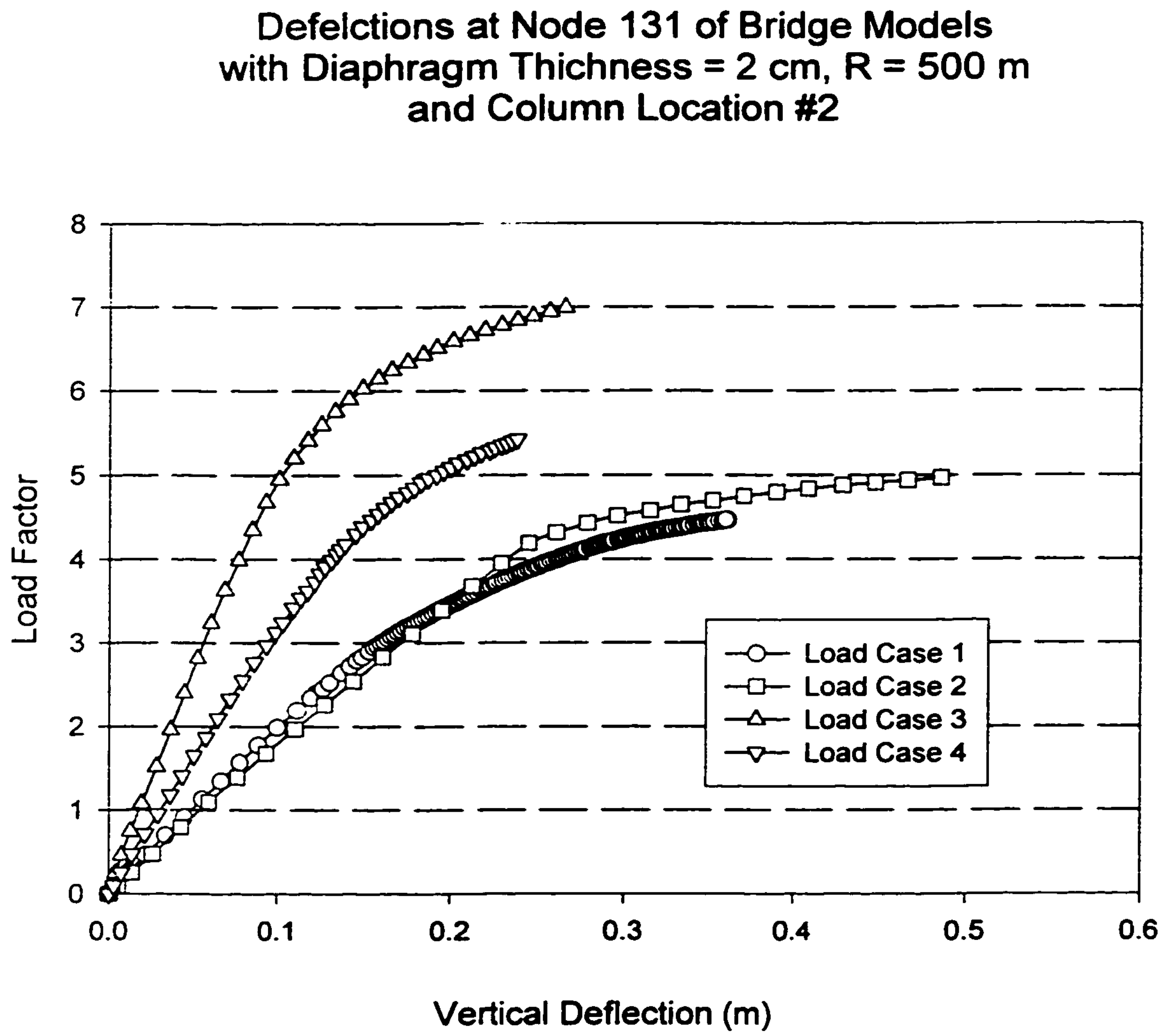

Figure 5.38b Deflections of Node 131 of Bridge Models with R=500m and Column Location #2 under Various Load Cases

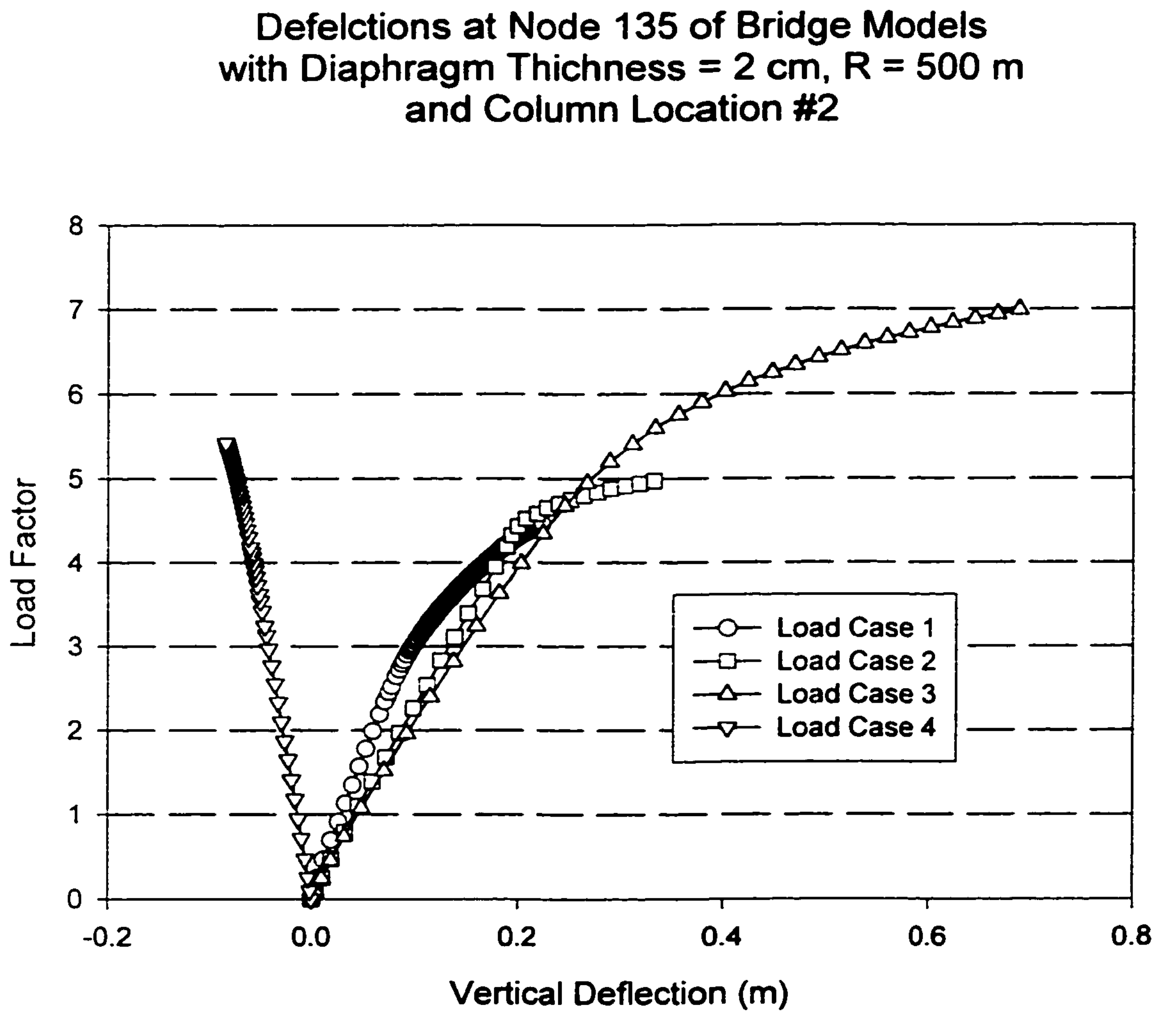

Figure 5.38c Deflections of Node 135 of Bridge Models with R=500m and Column Location #2 under Various Load Cases

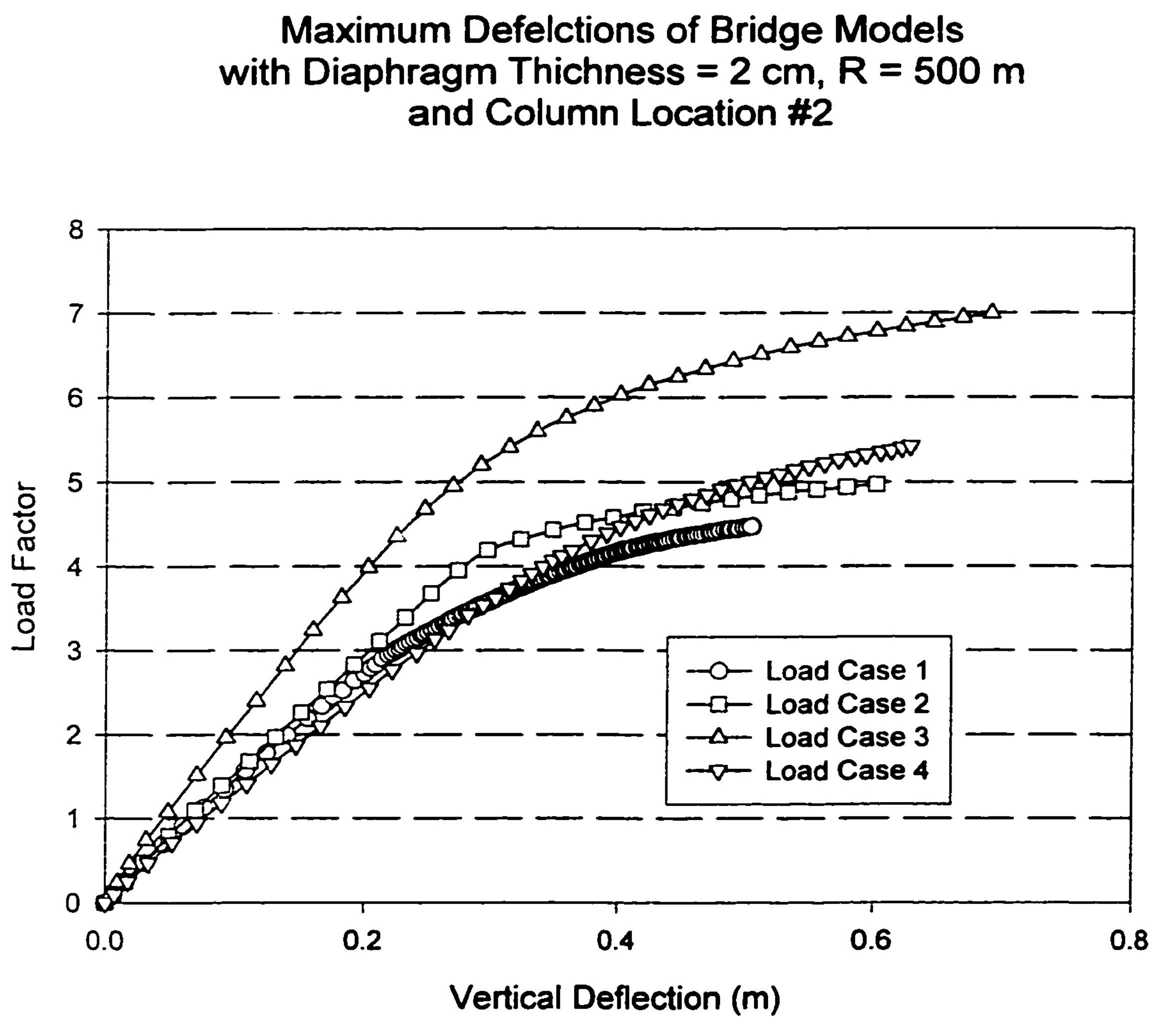

Figure 5.39 Maximum Deflections at Section A of Bridge Models R=500m and Column Location #2 under Various Load Cases

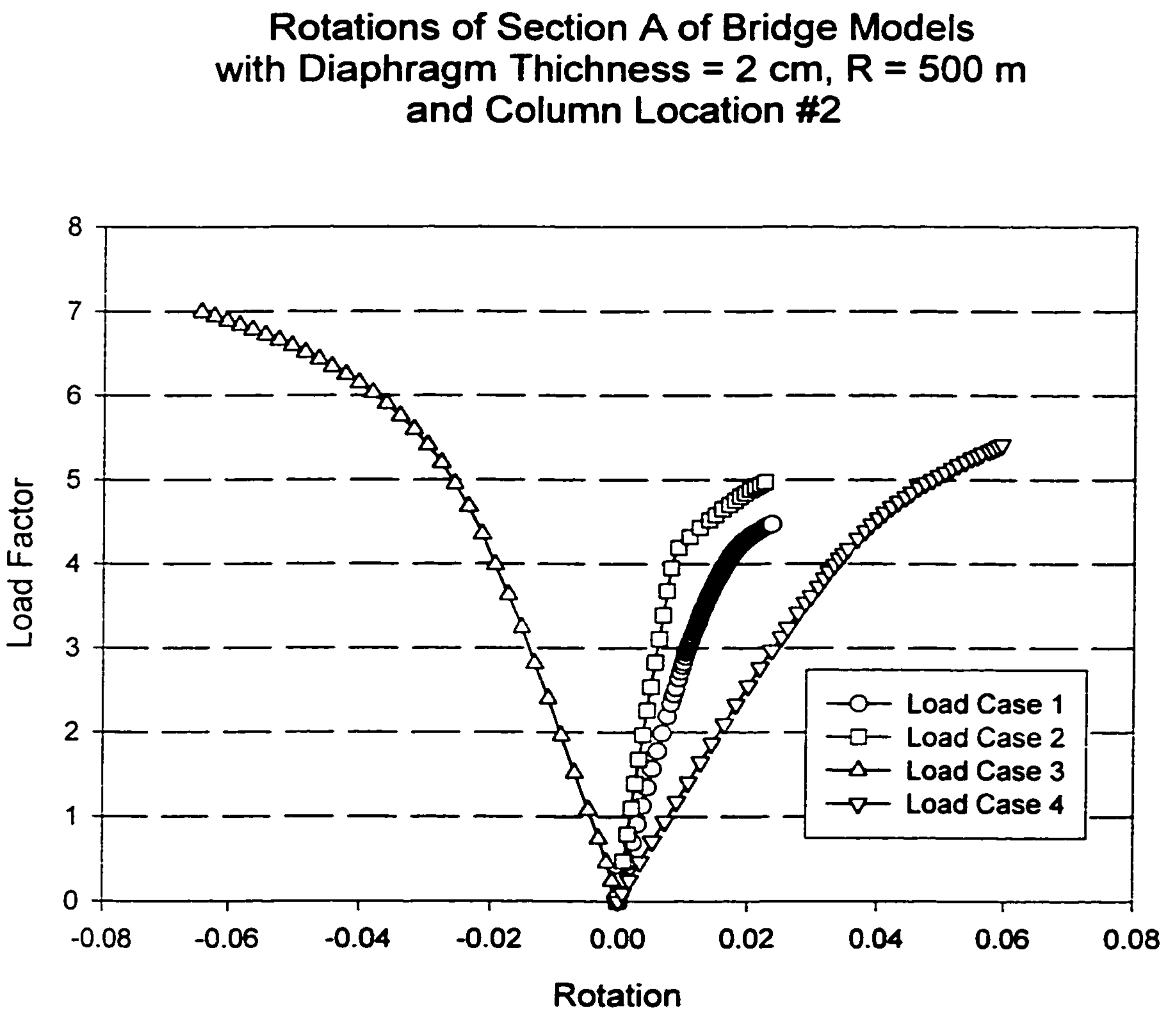

Figure 5.40. Rotations at Section A of Bridge Models with R=500m and Column Location #2 under Various Load Cases

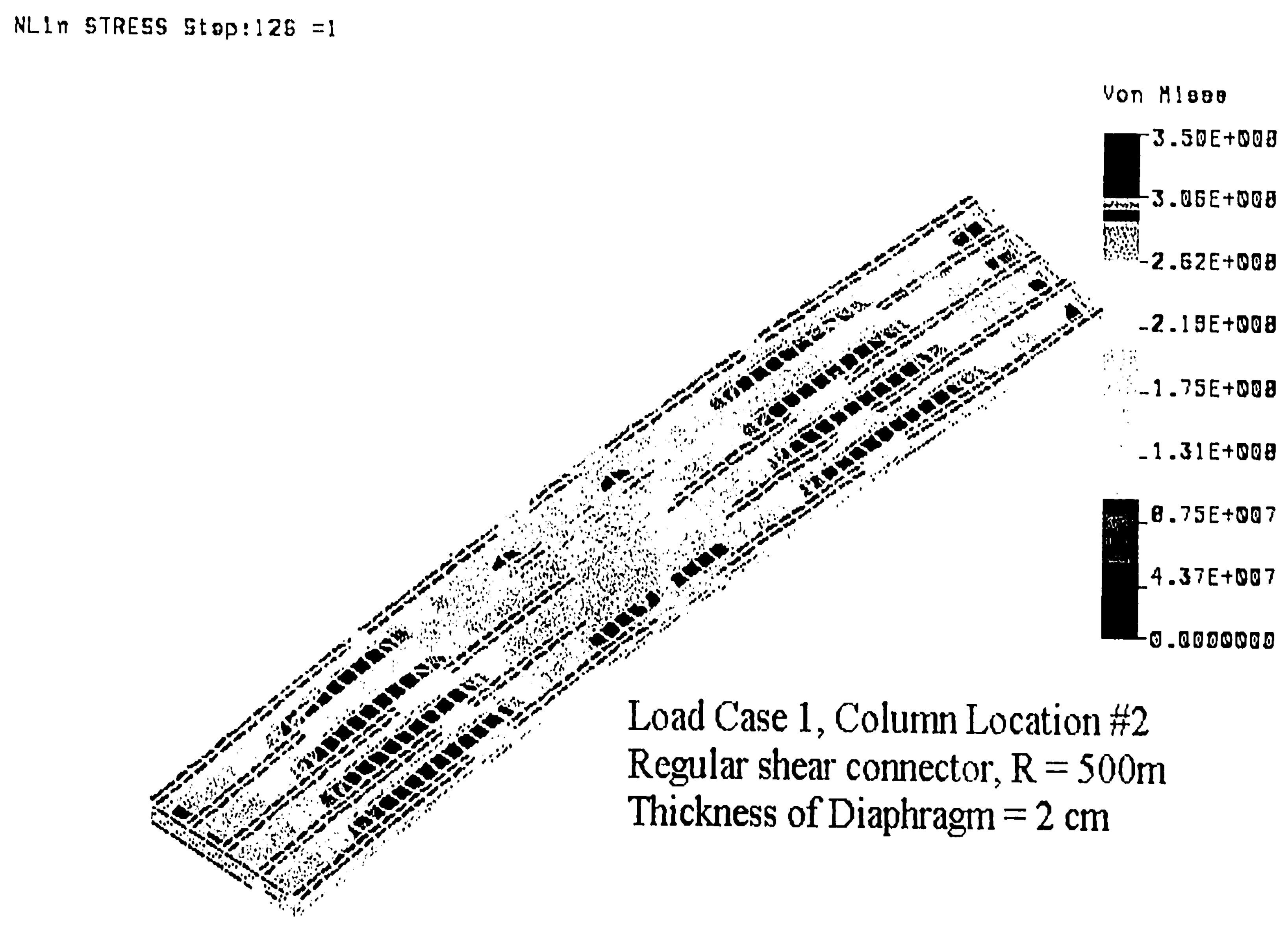

Figure 5.41 Stress Distribution of the Bridge Model with R = 500 m and Column Location 2 at Ultimate State under Load Case 1

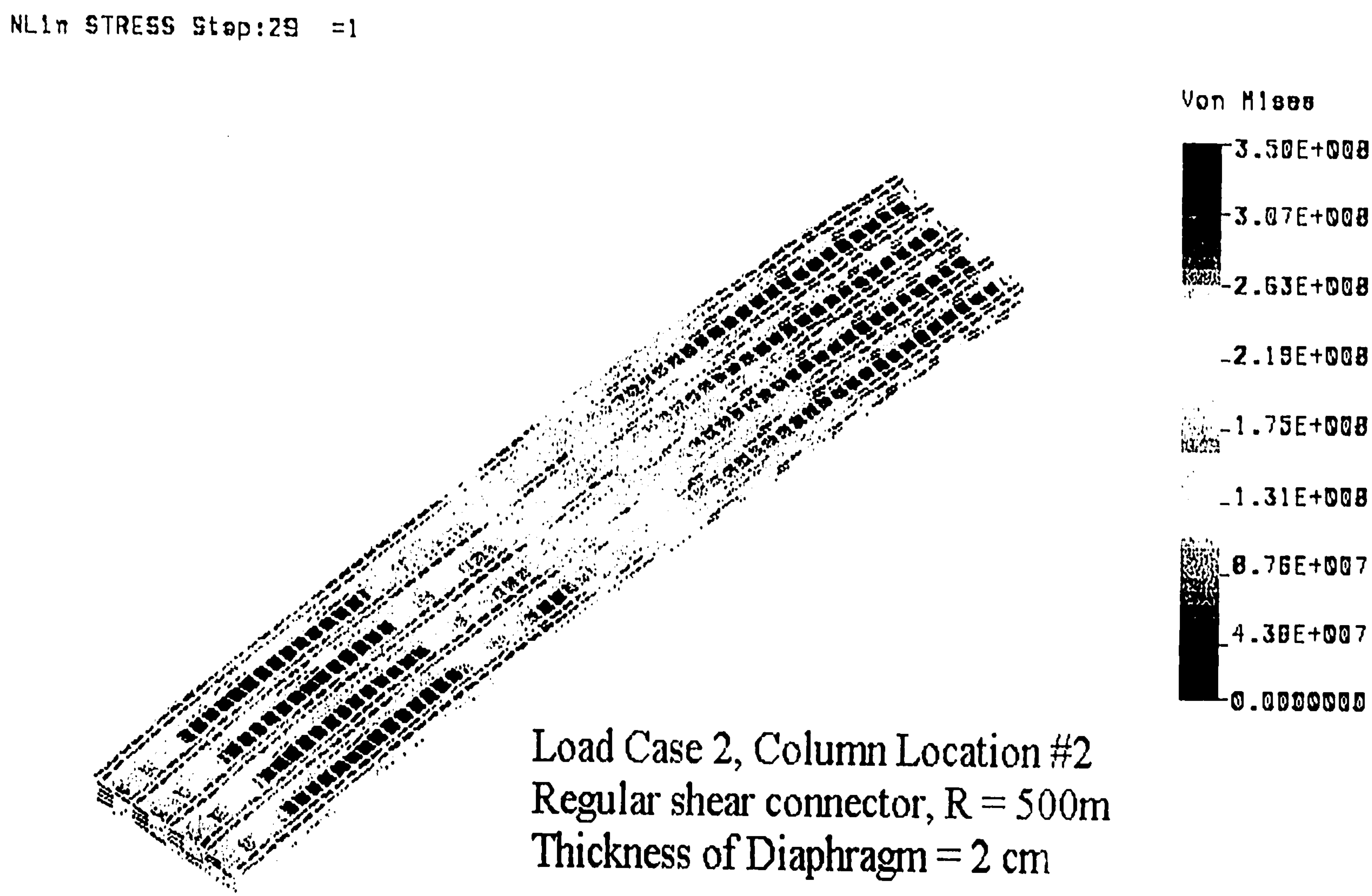

Figure 5.42 Stress Distribution of the Bridge Model with R = 500 m and Column Location 2 at Ultimate State under Load Case 2

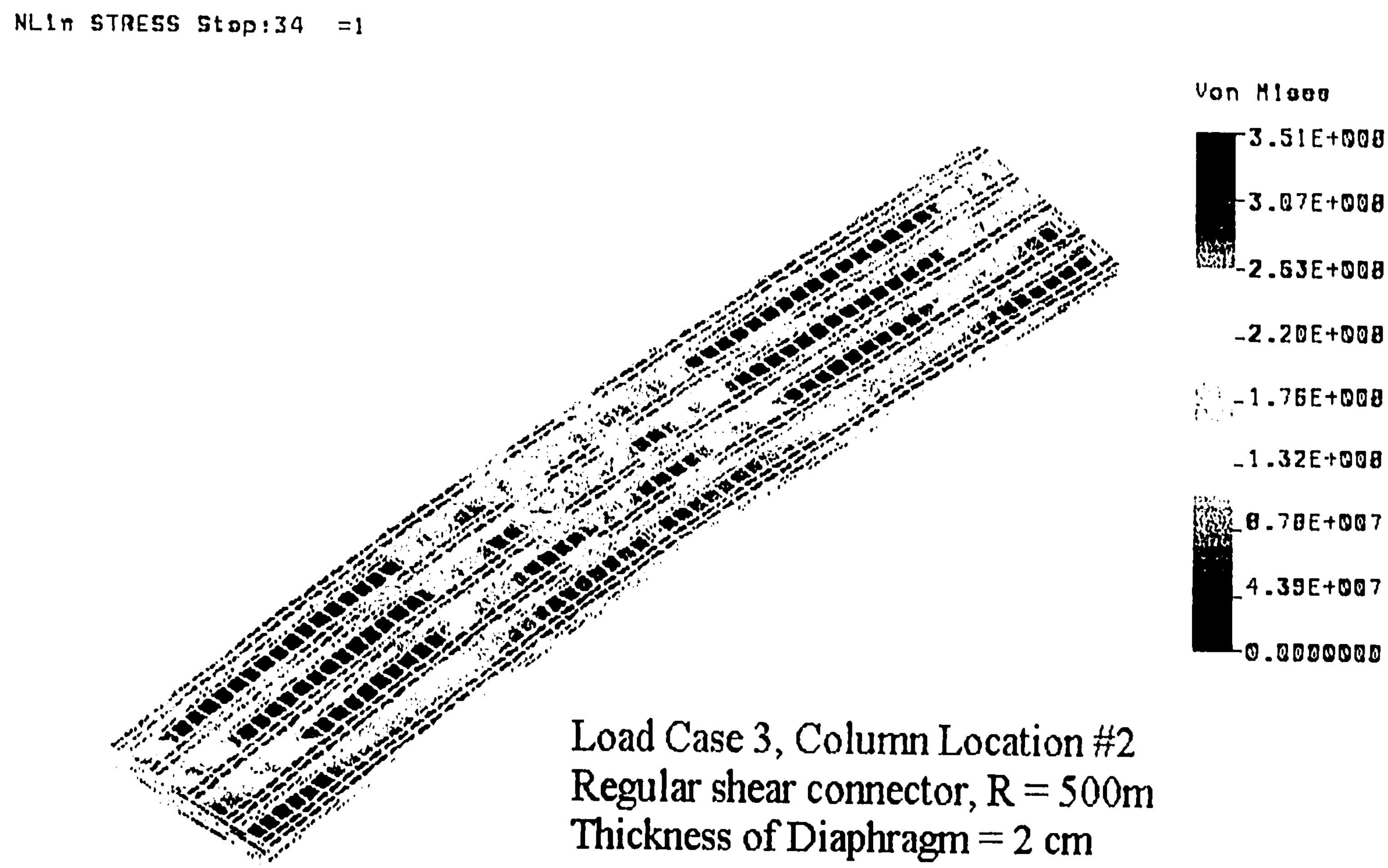

Figure 5.43 Stress Distribution of the Bridge Model with R = 500 m and Column Location 2 at Ultimate State under Load Case 3

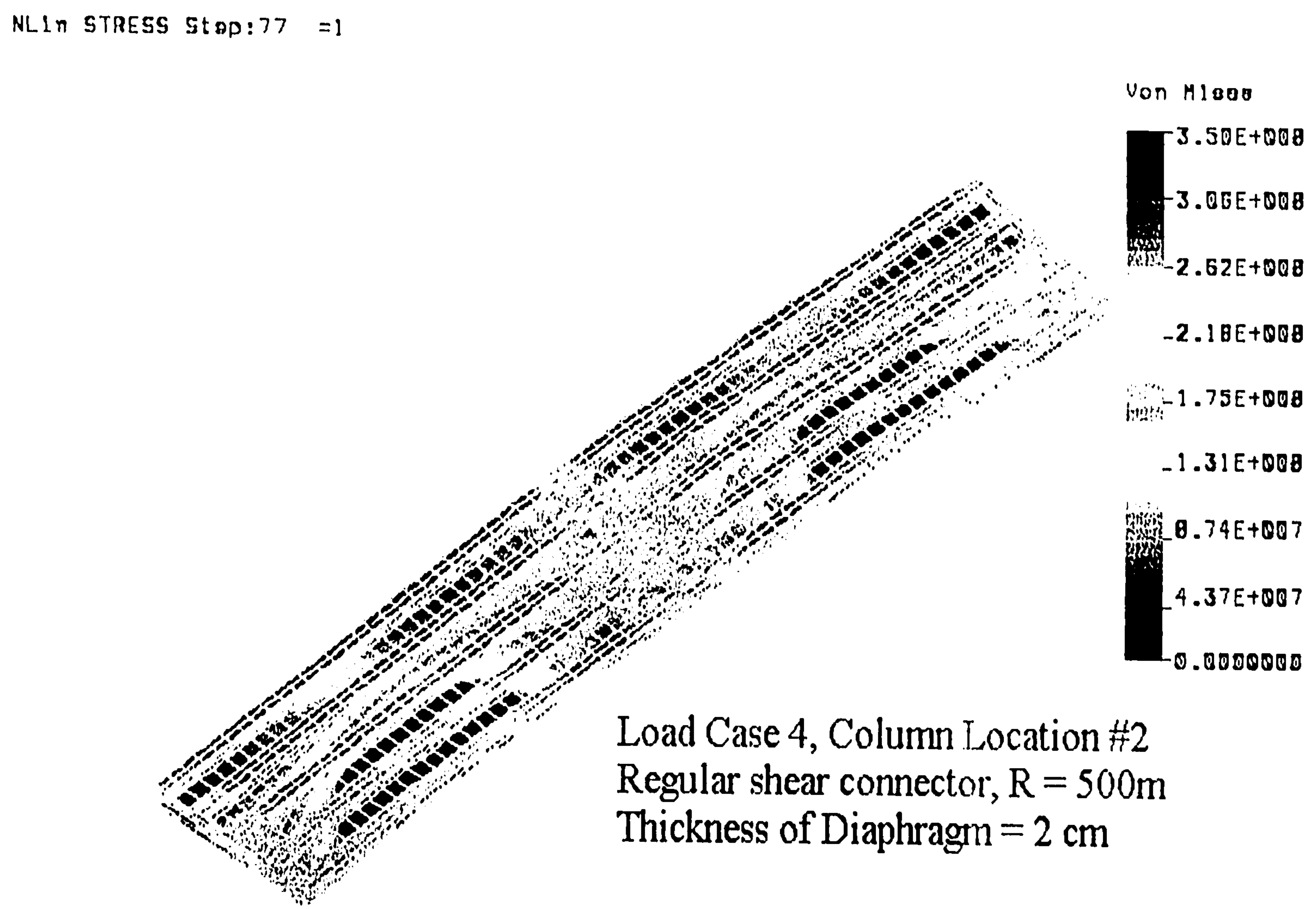

Figure 5.44 Stress Distribution of the Bridge Model with R = 500 m and Column Location 2 at Ultimate State under Load Case 4

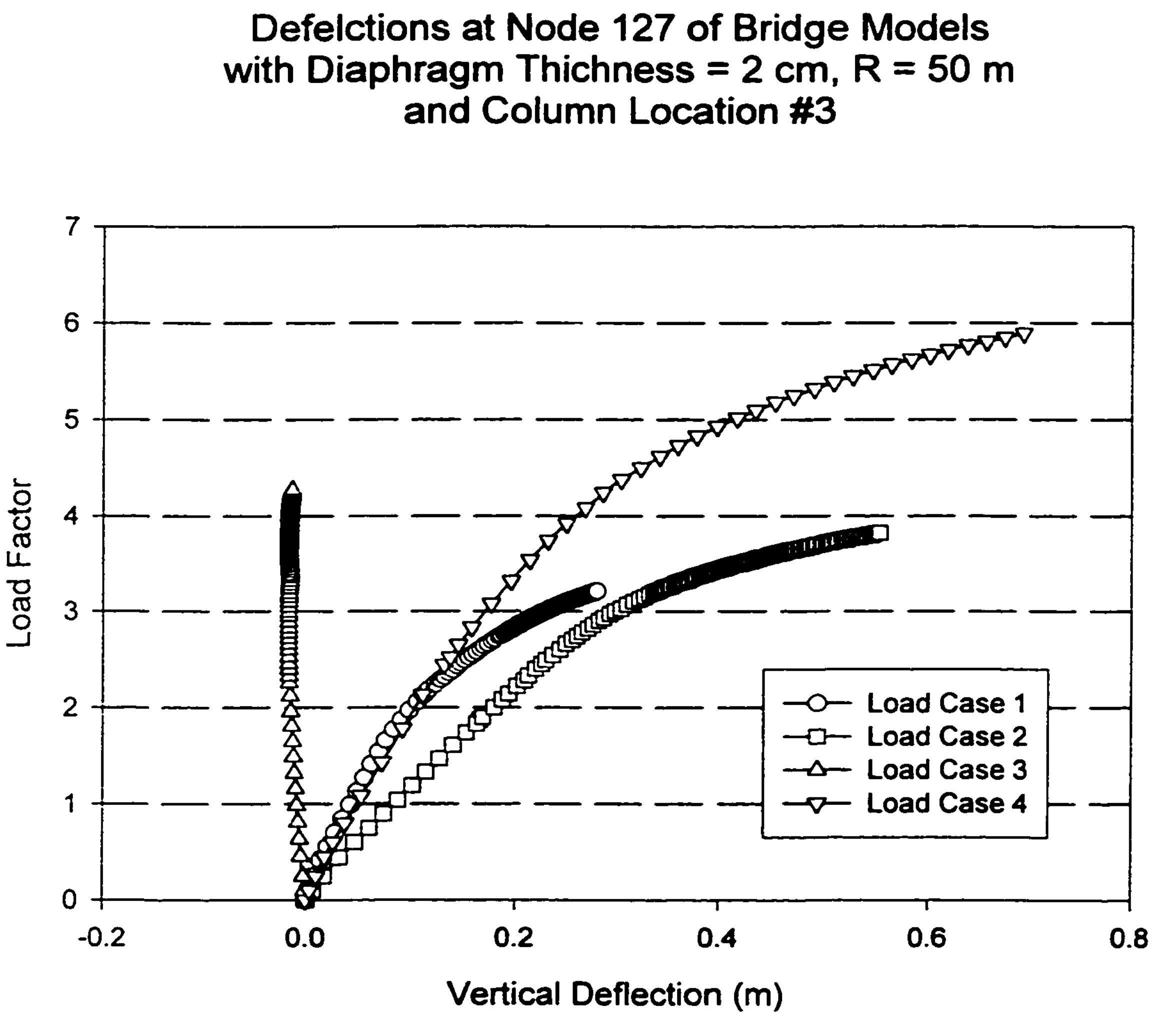

Figure 5.45a Deflections of Node 127 of Bridge Models with R=50m and Column Location #3 under Various Load Cases

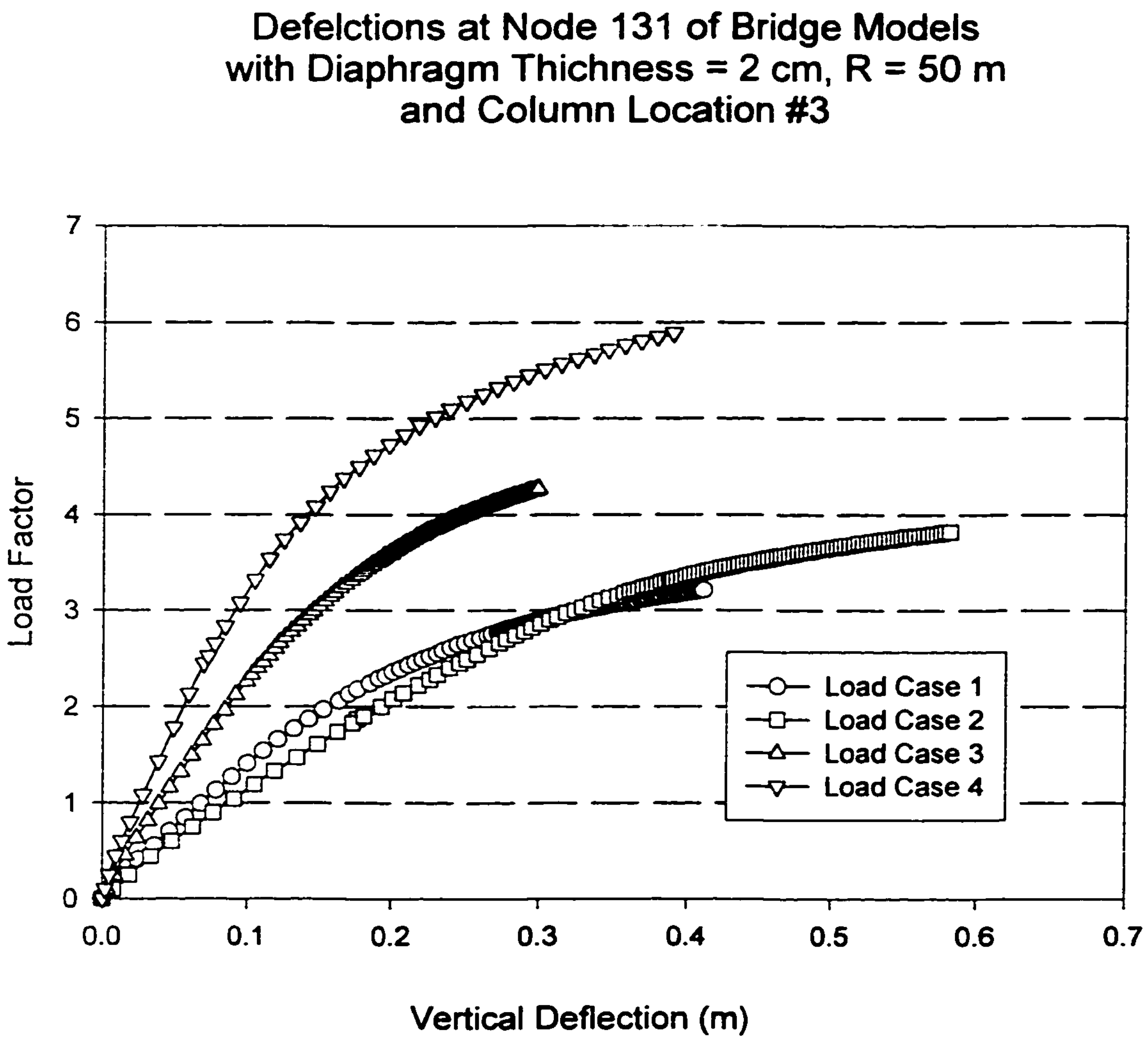

Figure 5.45b Deflections of Node 131 of Bridge Models with R=50m and Column Location #3 under Various Load Cases

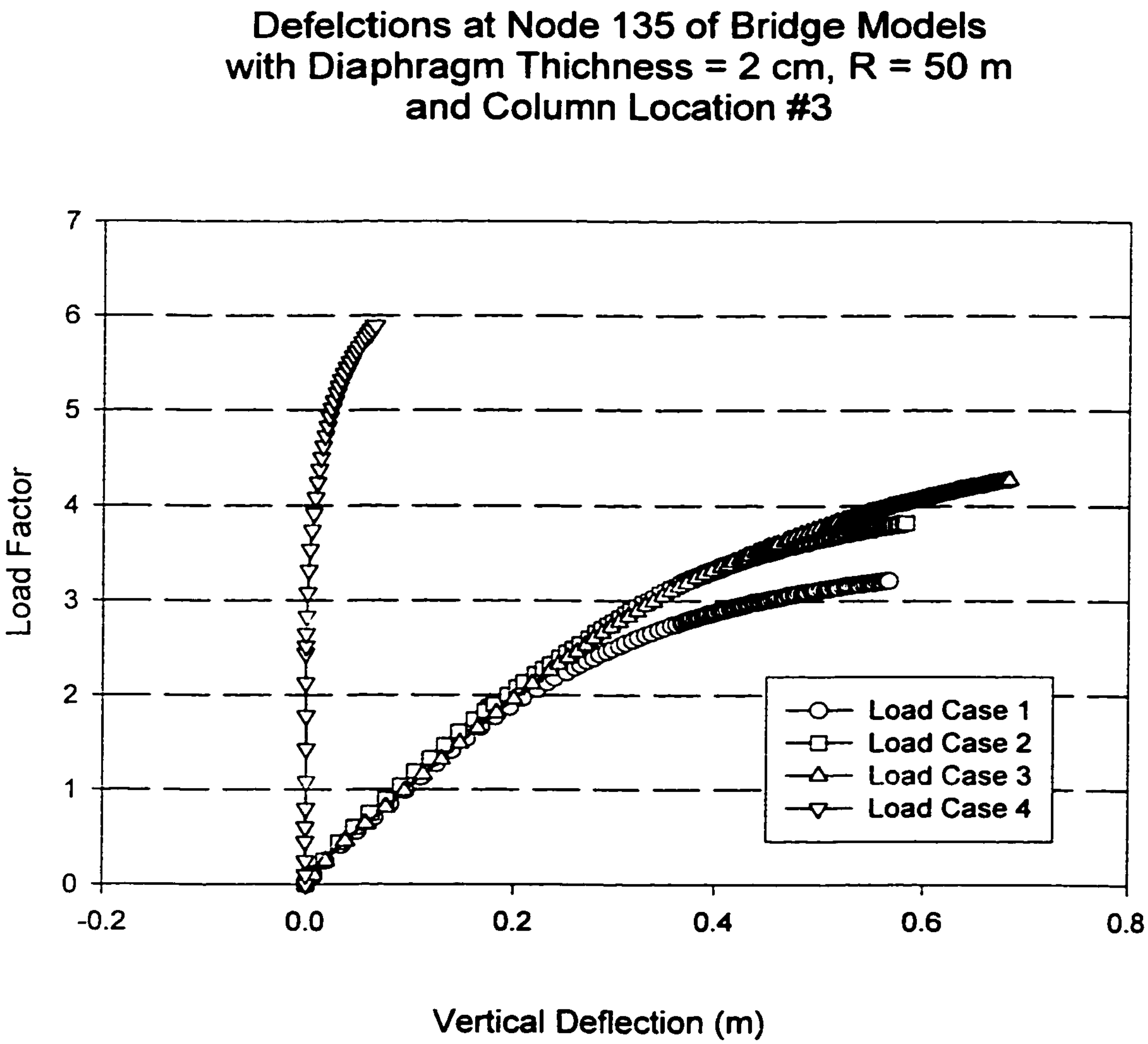

Figure 5.45c Deflections of Node 135 of Bridge Models with R=50m and Column Location #3 under Various Load Cases

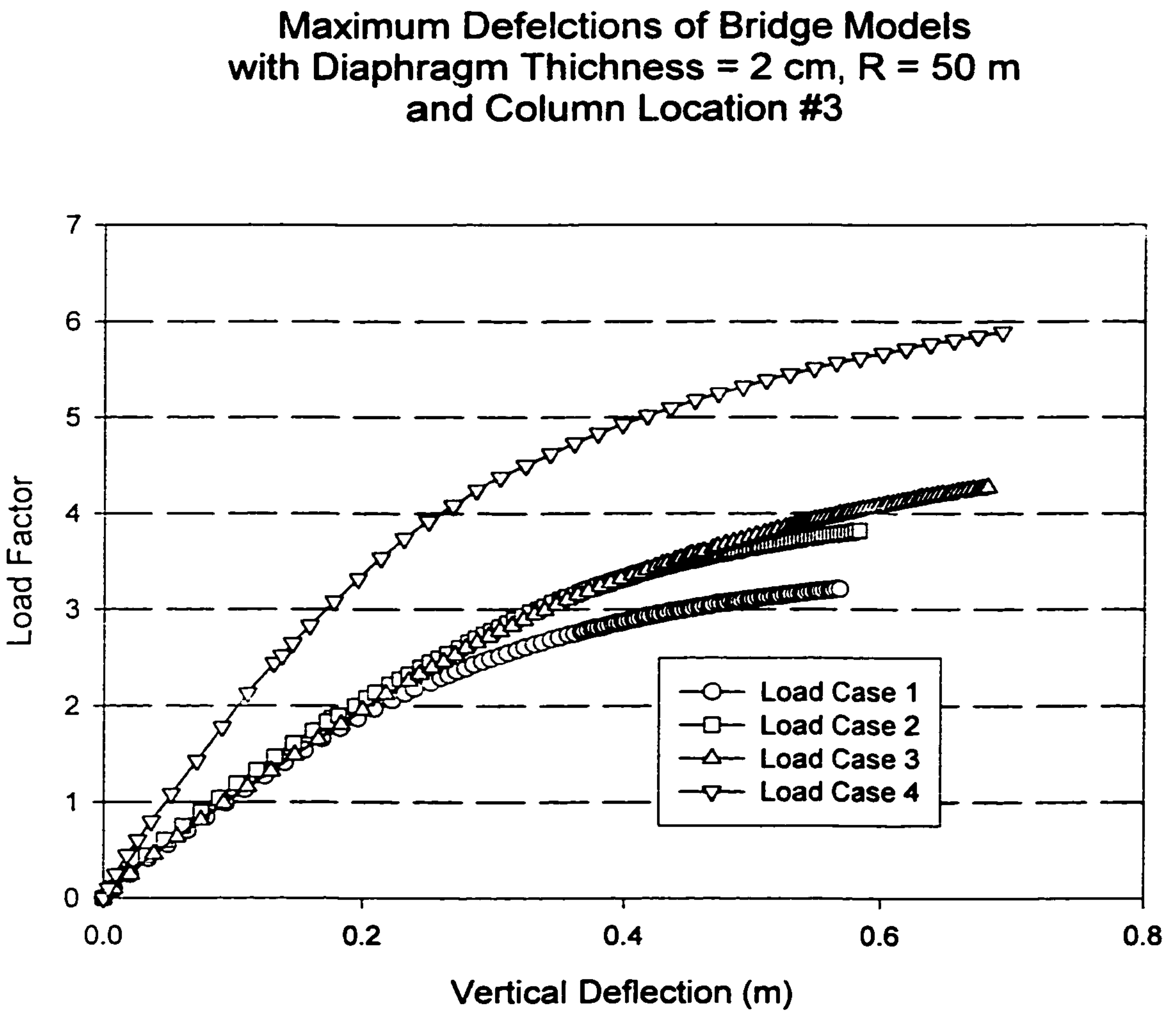

Figure 5.46 Maximum Deflections at Section A of Bridge Models with R=50m and Column Location #3 under Various Load Cases

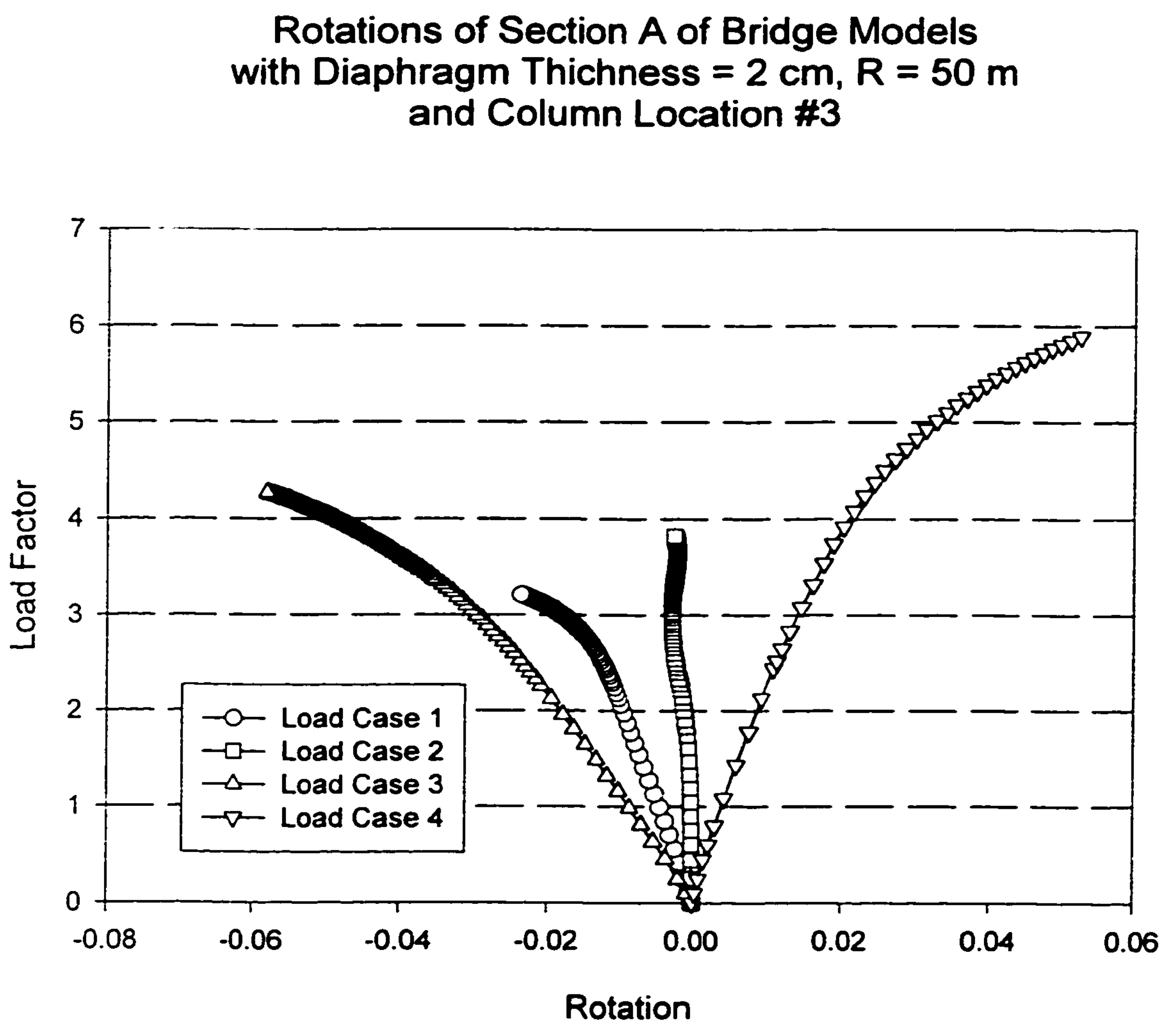

Figure 5.47. Rotations at Section A of Bridge Models with R=50m and Column Location #3 under Various Load Cases

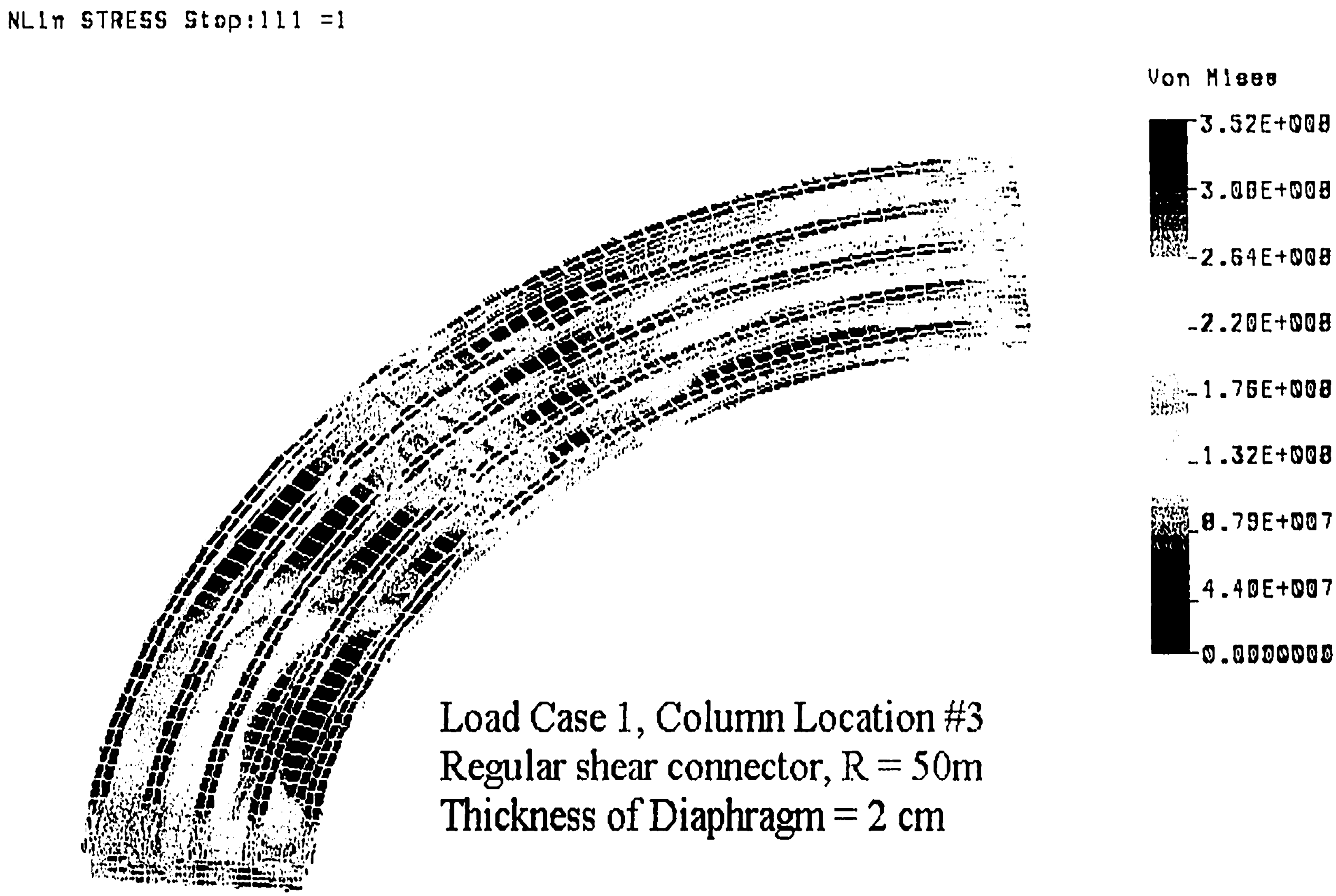

Figure 5.48 Stress Distribution of the Bridge Model with R = 50 m and Column Location 3 at Ultimate State under Load Case 1

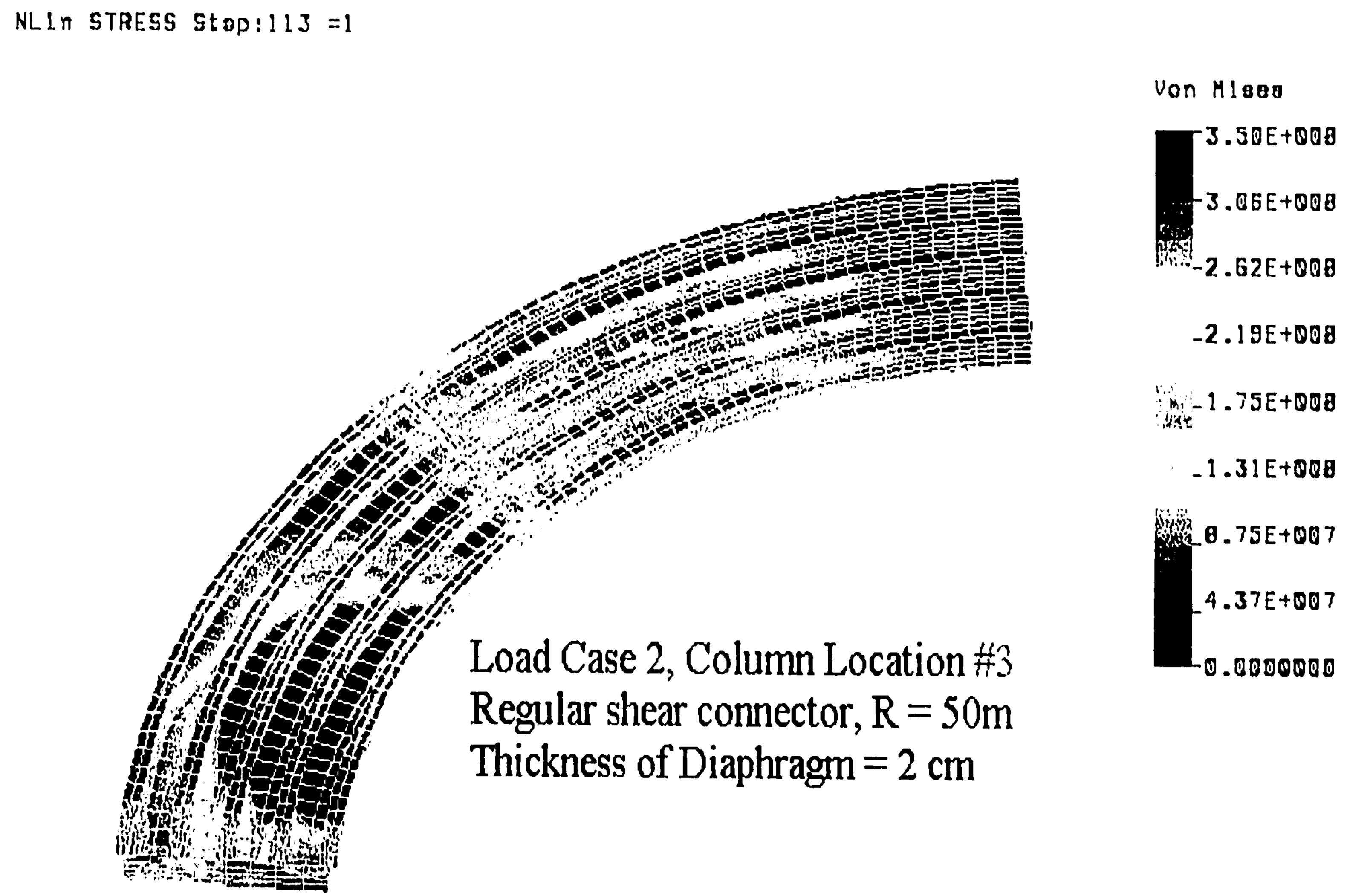

Figure 5.49 Stress Distribution of the Bridge Model with R = 50 m and Column Location 3 at Ultimate State under Load Case 2

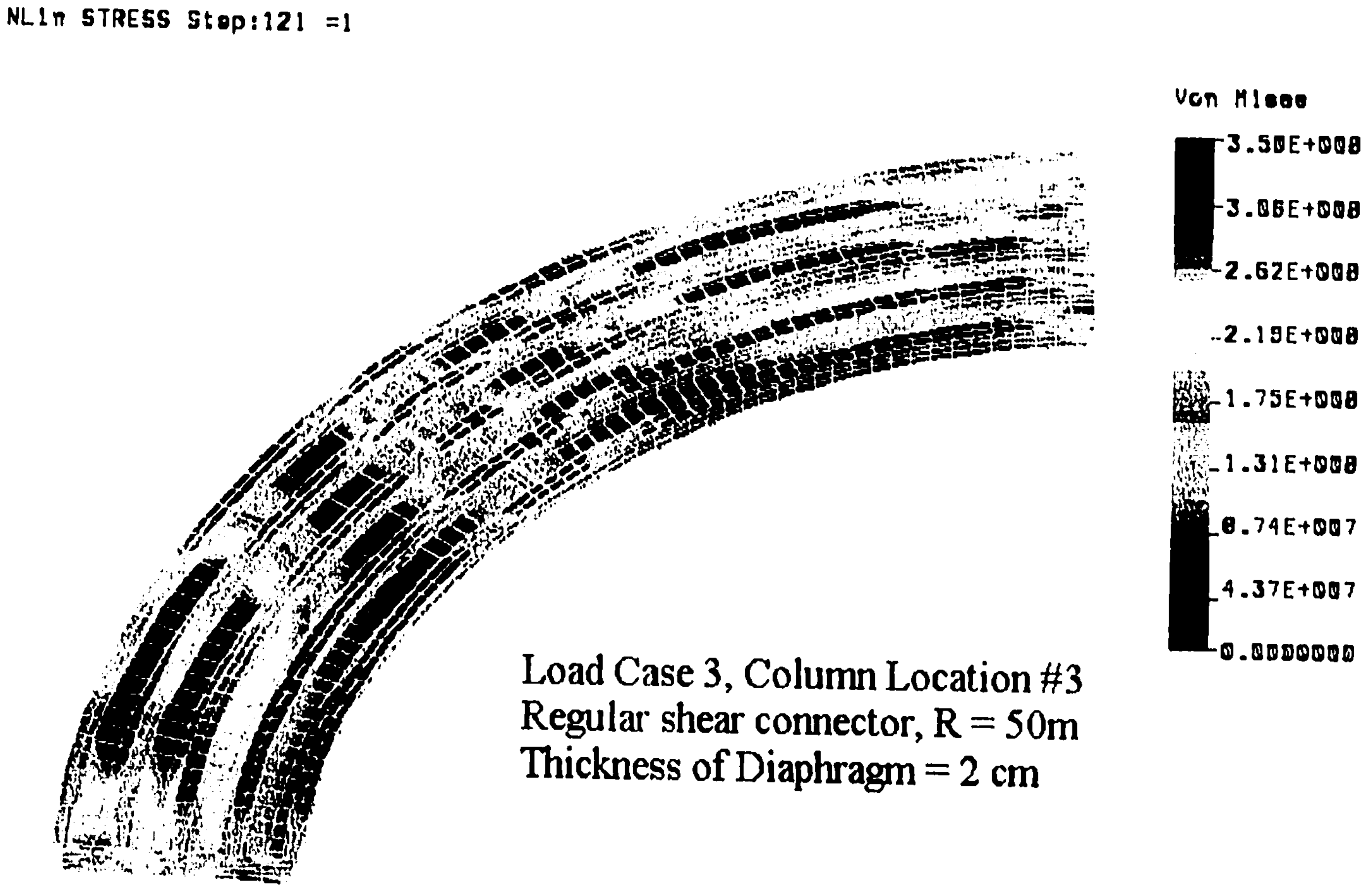

Figure 5.50 Stress Distribution of the Bridge Model with R = 50 m and Column Location 3 at Ultimate State under Load Case 3

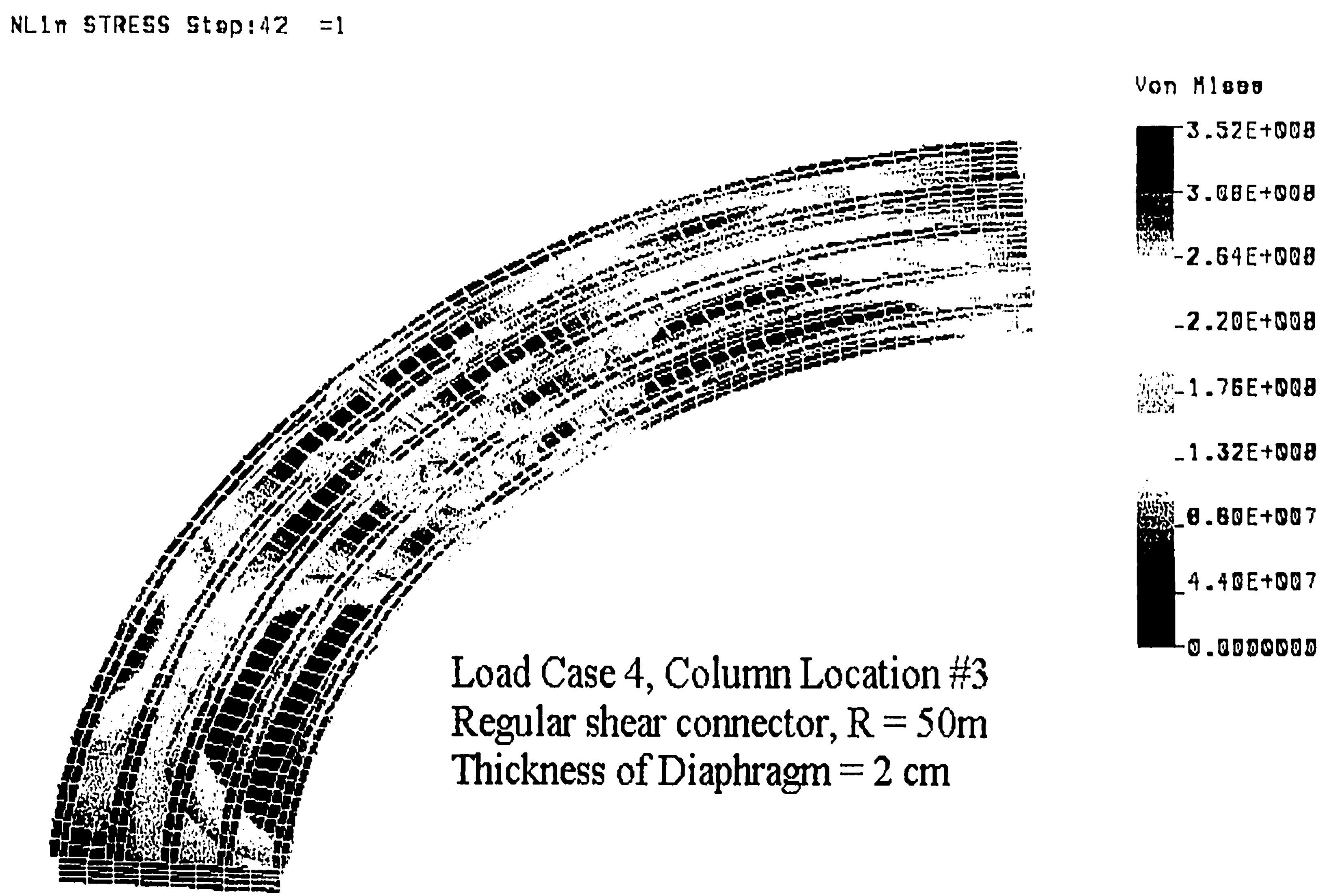

Figure 5.51 Stress Distribution of the Bridge Model with R = 50 m and Column Location 3 at Ultimate State under Load Case 4

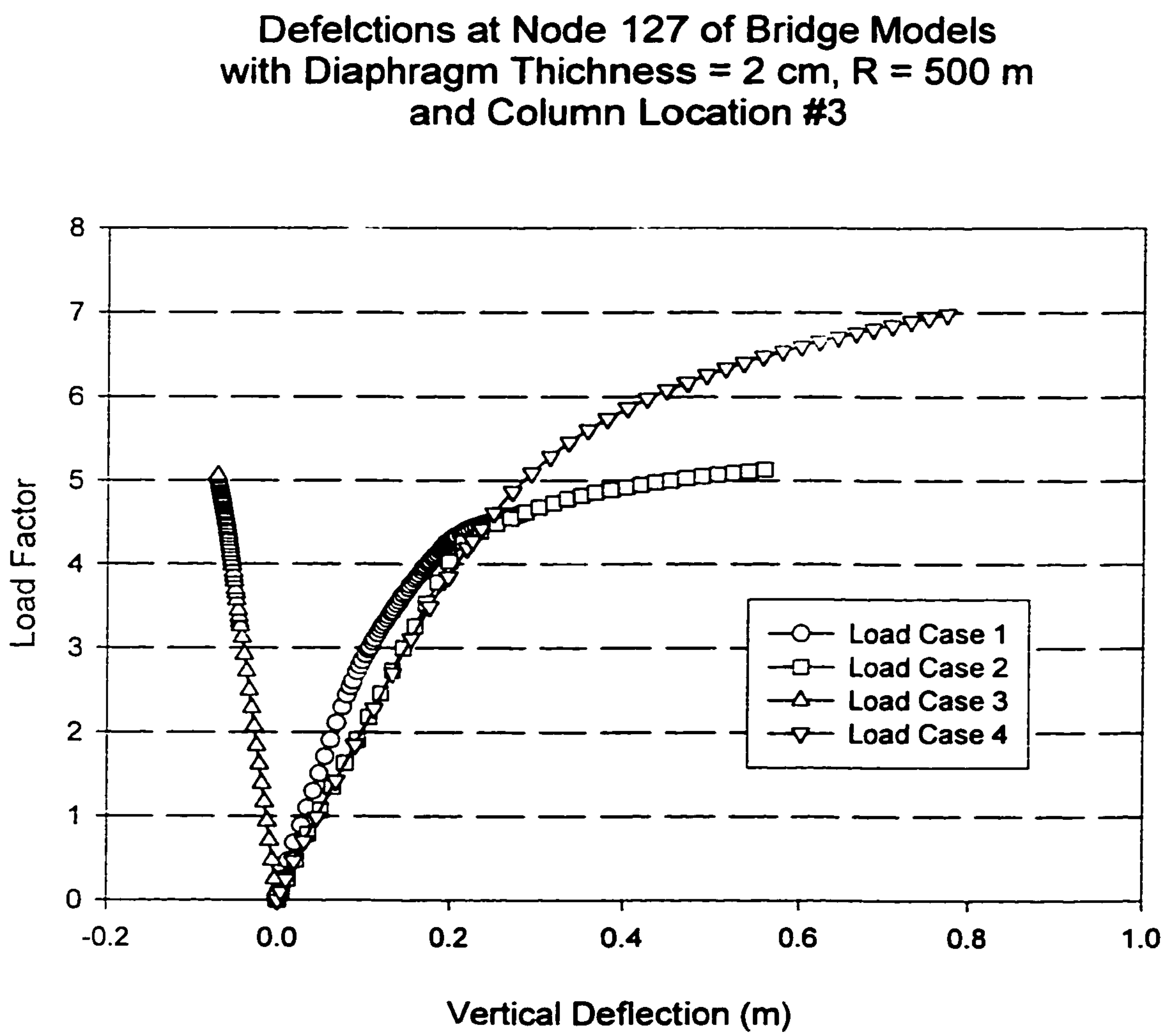

Figure 5.52a Deflections of Node 127 of Bridge Models with R=500m and Column Location #3 under Various Load Cases

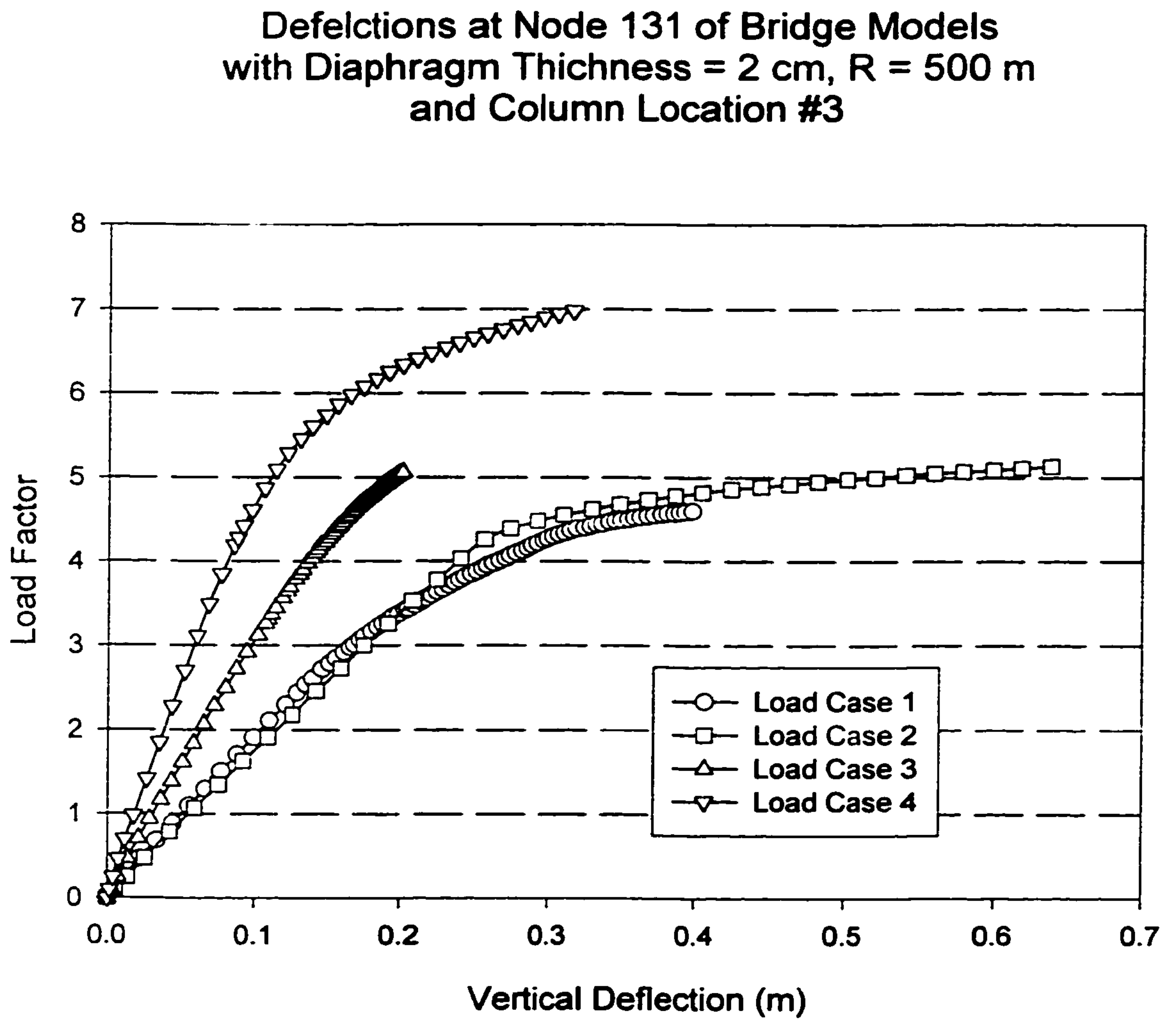

Figure 5.52b Deflections of Node 131 of Bridge Models with R=500m and Column Location #3 under Various Load Cases

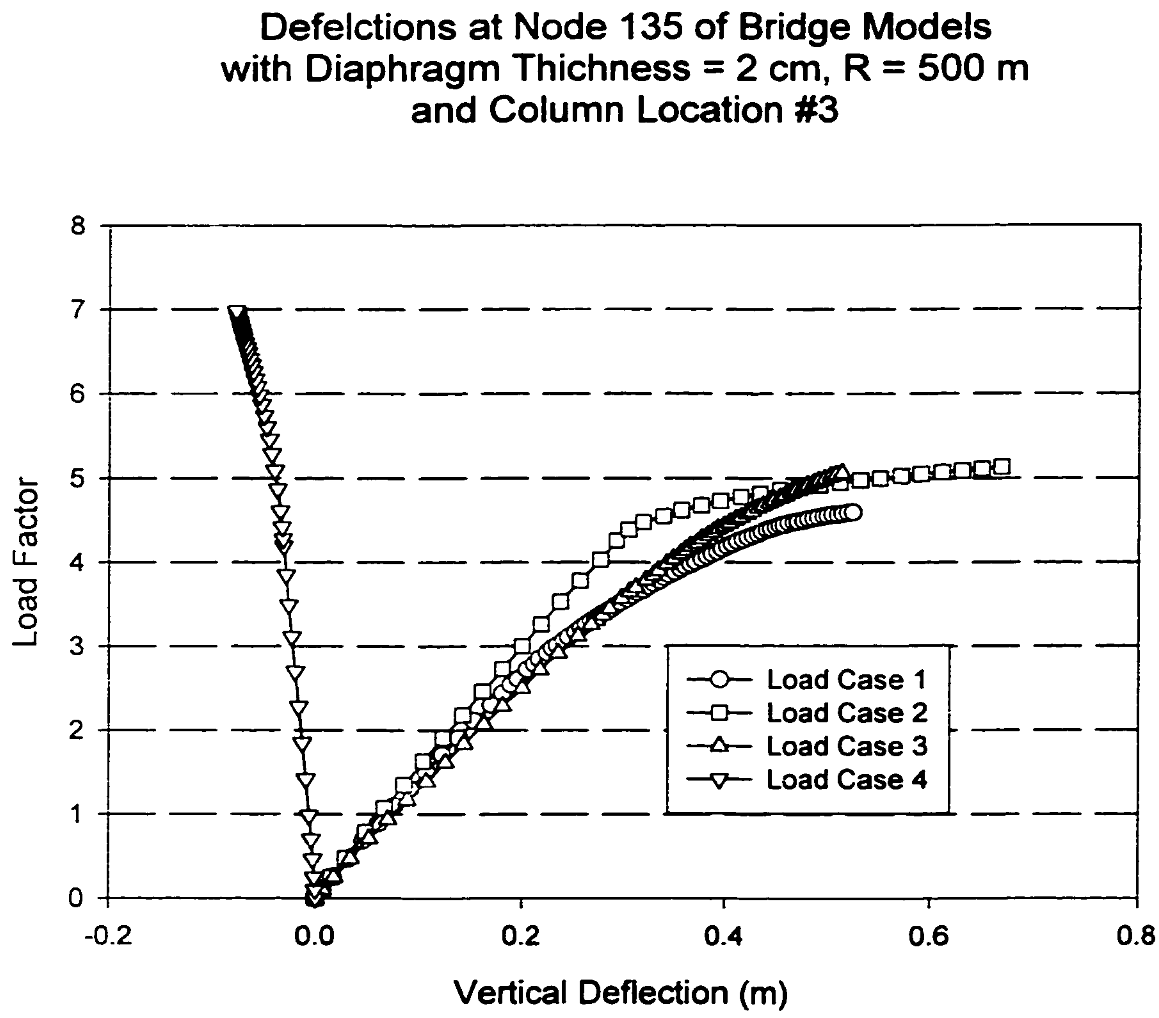

Figure 5.52c Deflections of Node 135 of Bridge Models with R=500m and Column Location #3 under Various Load Cases

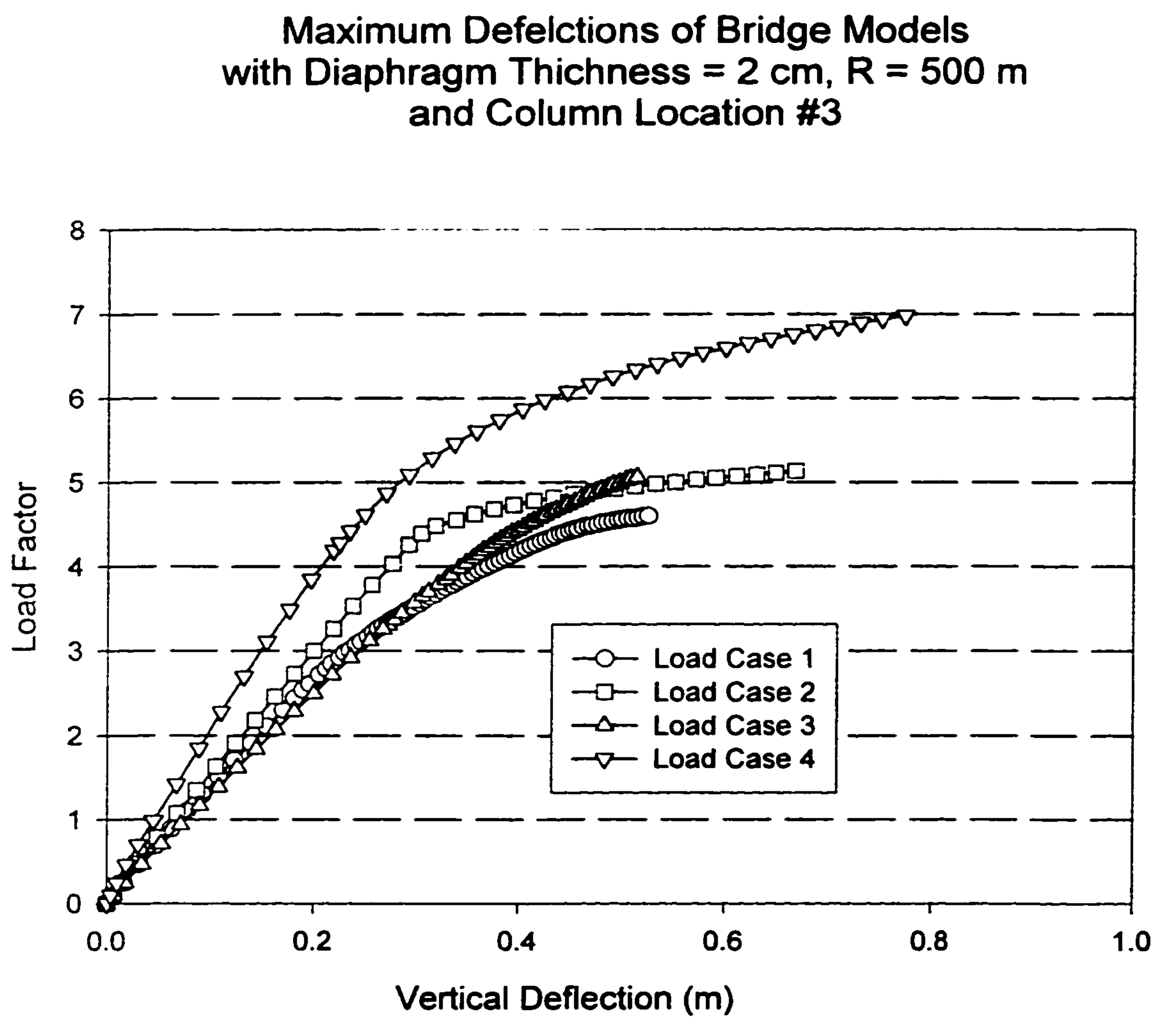

Figure 5.53 Maximum Deflections at Section A of Bridge Models with R=500m and Column Location #3

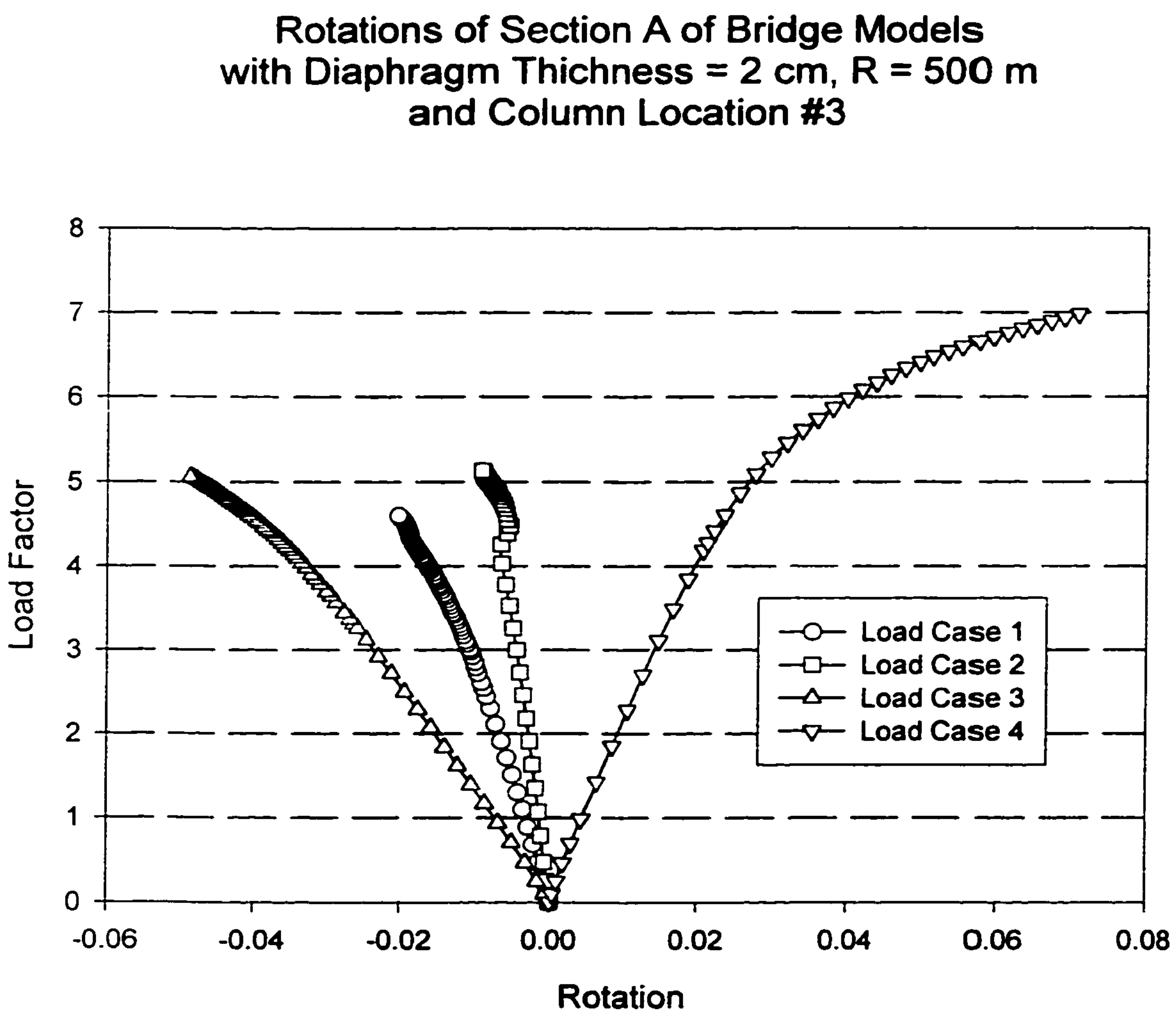

Figure 5.54. Rotations at Section A of Bridge Models with R=500m and Column Location #3 under Various Load Cases

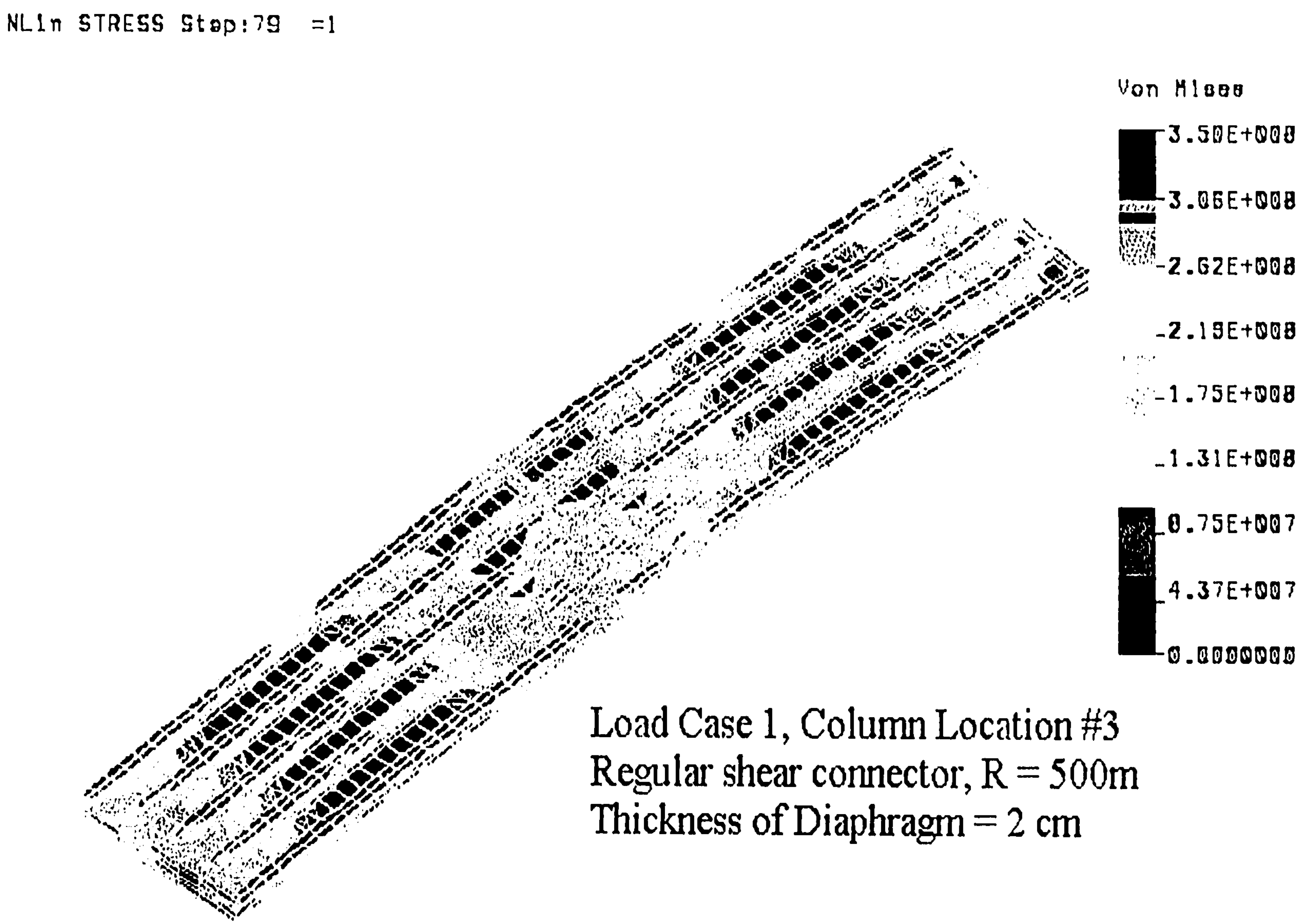

Figure 5.55 Stress Distribution of the Bridge Model with R = 500 m and Column Location 3 at Ultimate State under Load Case 1

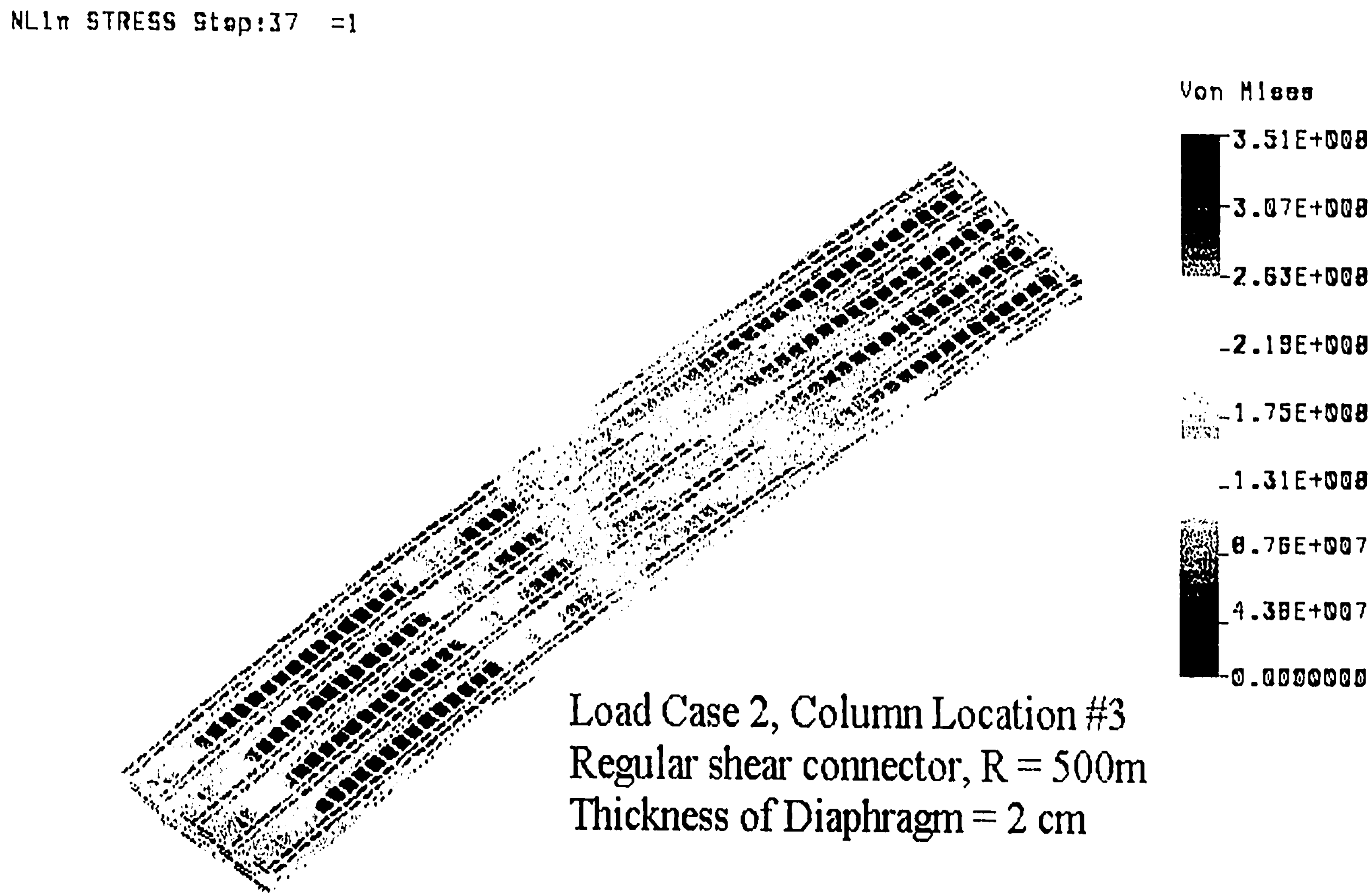

Figure 5.56 Stress Distribution of the Bridge Model with R = 500 m and Column Location 3 at Ultimate State under Load Case 2

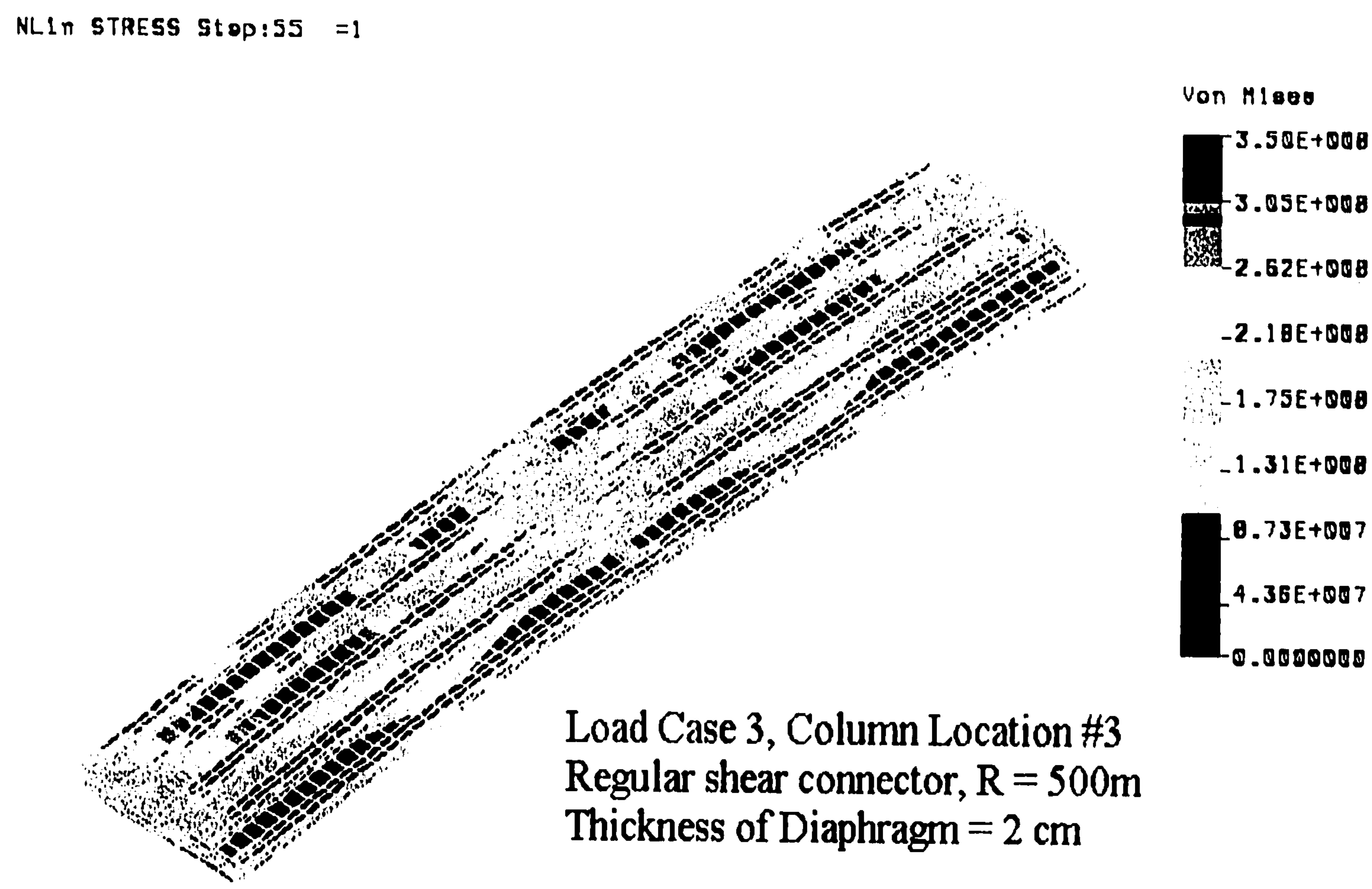

Figure 5.57 Stress Distribution of the Bridge Model with R = 500 m and Column Location 3 at Ultimate State under Load Case 3

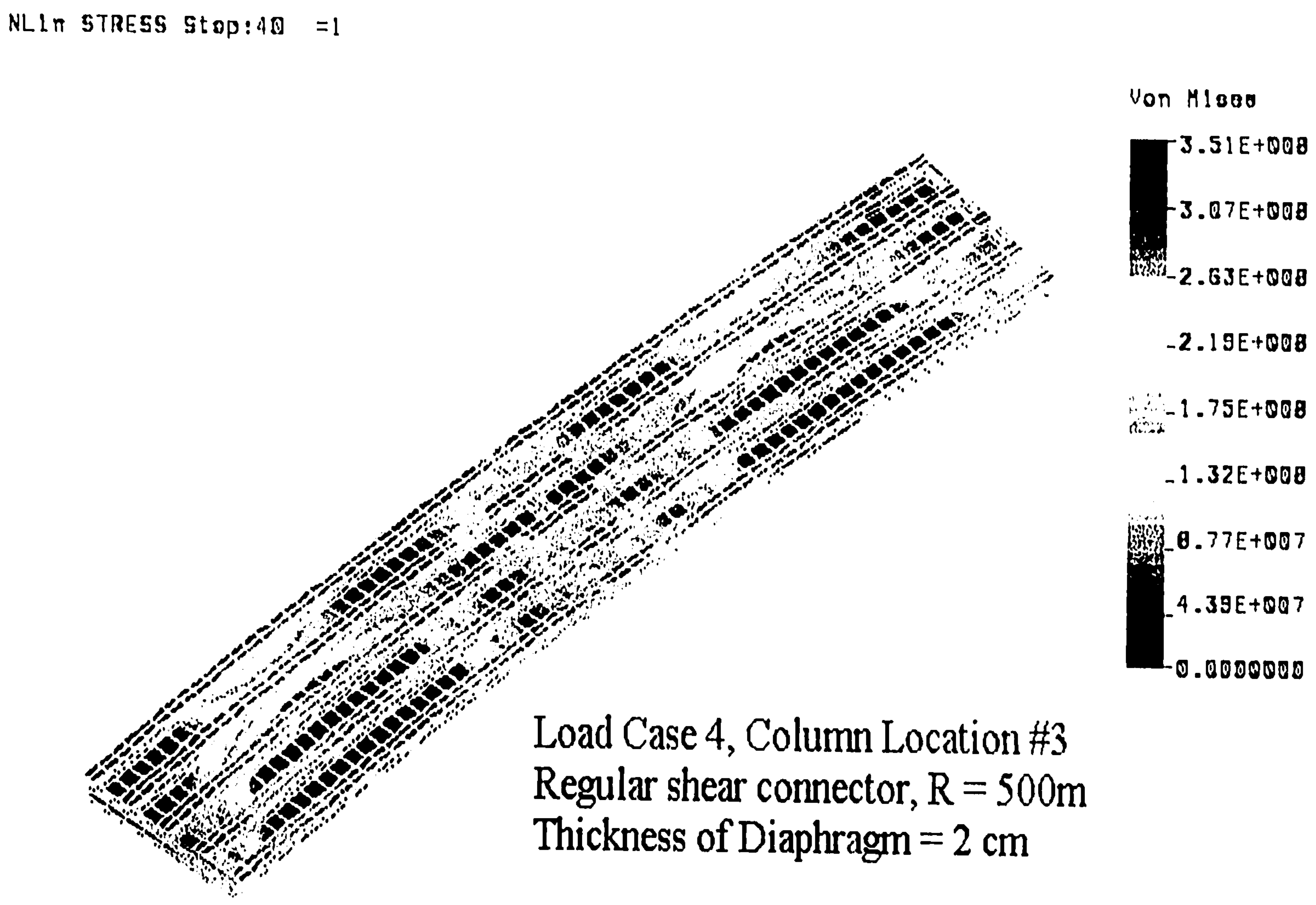

Figure 5.58 Stress Distribution of the Bridge Model with R = 500 m and Column Location 3 at Ultimate State under Load Case 4

5.4 Influence of the location of the middle support column

Three different locations of the middle column (Figure 5.2) are used in the nonlinear analysis of the bridge models without intermediate diaphragms. They include inter (Column Location 3), concentric (Column Location 1), and outer (Column Location 2) locations. For each bridge model, the nonlinear analyses are carried out using various load cases and locations of the middle column.

In the analysis, two radii of curvature are used, namely, 50m and 500m. Two thicknesses of the middle diaphragm, namely, 0.02m and 0.08m are used. The stiffness of regular shear connectors and the stiffness of the middle column of 1.26×10^{11} N/m are also used. The bridge models are analyzed under four load cases, which are Load Cases 1, 2, 3 and 4. The effects on the bridge models are presented as follows based on each load case:

Load Case 1

For bridge models with curvature radius of 50m and various location of the middle column, vertical deflections at nodes 127, 131 and 135 under Load Case 1 are shown in Figures 5.59a, 5.59b and 5.59c. The rotation of section A is shown in Figure 5.61. The maximum deflection of the bridge model at section A is shown in Figure 5.60. It can be seen from Figure 5.60 that the bridge model with the middle column at Column Location 1 has the greatest ultimate load factor of about 3.9 and the bridge model with the middle column at Column Location 3 has the lowest ultimate load factor of about 3.2. It can also be observed in Figure 5.61 that the bridge models with the middle column at Column Location 1 have the lowest rotation in both elastic and inelastic regions.

For bridge models with curvature radius of 500m and various location of the middle column, vertical deflections at nodes 127, 131 and 135 under Load Case 1 are shown in Figures 5.62a, 5.62b and 5.62c. The rotation of section A is shown in Figure 5.64. The maximum deflection of the bridge model at section A is shown in Figure 5.63. It can be observed from Figures 5.63 and 5.64 that the bridge model with the middle column, which is at Column Location 1, has the greatest ultimate load factor of about 5.1 and the lowest rotation in both elastic and inelastic regions. It can also be observed that the bridge model with the middle column at Column Location 1 starts to yield at the load factor of about 4.5. The bridge model with the middle column at Column Location 2 or 3 has almost the same lowest ultimate load factor of about 4.5. It can also be observed in Figure 5.64 that the bridge models with the middle column at Column Location 1 have the lowest rotation in both elastic and inelastic regions.

Based on above observations, it can be noted that the bridge model with the middle column at Column Locations 1 and with radii of curvature of 50m and 500m has the greatest ultimate load factor and the smallest rotation at section A in all load stages under Load Case 1.

Load Case 2

For bridge models with curvature radius of 50m and various location of the middle column, vertical deflections at nodes 127, 131 and 135 under Load Case 2 are shown in Figures 5.65a, 5.65b and 5.65c. The rotation of section A is shown in Figure 5.67. The maximum deflection of the bridge model at section A is shown in Figure 5.66. In Figure 5.66, it can be seen that the bridge model has the greatest ultimate load factor of about 4.2 with the middle column at Column Location 1 and the lowest ultimate load factor of about 4.1 with the middle column at Column Location 2. The bridge model almost starts to yield at the load factor of about 2.5 with both Column Locations 1 and 2 (Figure 5.67). In both elastic and inelastic regions, the bridge model with the middle column at Column Location 3 has the smallest rotation at section A.

For bridge models with curvature radius of 500m and various location of the middle column, vertical deflections at nodes 127, 131 and 135 under Load Case 2 are shown in Figures 5.68a, 5.68b and 5.68c. The rotation of section A is shown in Figure 5.70. The maximum deflection of the bridge model at section A is shown in Figure 5.69. In Figure 5.69, it can be seen that the bridge model has the greatest ultimate load factor of about 5.2 with the middle column at Column Location 1 and the lowest ultimate load factor of about 4.9 with the middle column at Column Location 2. The bridge model almost starts to yield at the load factor of about 4.2 with Column Locations 1, 2 and 3 (Figure 5.70). In both elastic and inelastic regions, the bridge model with the middle column at Column Location 1 has the smallest rotation at section A.

Based on above observations, it can be noted that the bridge model with the middle column at Column Locations 1 and with radii of curvature of 50m and 500m has the greatest ultimate load factor and the smallest rotation at section A in all load stages under Load Case 2.

Load Case 3

For bridge models with curvature radius of 50m and various location of the middle column, vertical deflections at nodes 127, 131 and 135 under Load Case 3 are shown in Figures 5.71a, 5.71b and 5.71c. The rotation of section A is shown in Figure 5.72. The maximum deflection of the bridge model at section A is found at Node 135 with all locations of the middle column under Load Case 3. In Figure 5.71c, it can be seen that the bridge model has the greatest ultimate load factor of about 6.8 with the middle column at Column Location 2 and the lowest ultimate load factor of about 4.2 with the middle column at Column Location 3. The bridge model with the middle column at Column Location 1 has the ultimate load factor of about 5.5. In the elastic regions (Figure 5.72), the bridge model with the middle column at Column Location 2 has the smallest rotation at section A.

For bridge models with curvature radius of 500m and various location of the middle column, vertical deflections at nodes 127, 131 and 135 under Load Case 3 are shown in Figures 5.73a, 5.73b and 5.73c. The rotation of section A is shown in Figure 5.74. The maximum deflection of the bridge model at section A is found at Node 135 with all locations of the middle column under Load Case 3. In Figure 5.73c, it can be seen that the bridge model has the greatest ultimate load factor of about 7.0 with the middle column at Column Location 2 and the lowest ultimate load factor of about 5.1 with the middle column at Column Location 3. The bridge model with the middle column at Column Location 1 has the ultimate load factor of about 6.1. In the elastic regions, the bridge model with the middle column at Column Location 2 has the smallest rotation at section A (Figure 5.74).

Based on above observations, it can be noted that the bridge model with the middle column at Column Locations 2 and with radii of curvature of 50m and 500m has the greatest ultimate load factor and the smallest rotation at section A in all load stages under Load Case 3.

Load Case 4

For bridge models with curvature radius of 50m and various location of the middle column, vertical deflections at nodes 127, 131 and 135 under Load Case 4 are shown in Figures 5.75a, 5.75b and 5.75c. The rotation of section A is shown in Figure 5.76. The maximum deflection of the bridge model at section A (Figure 5.75a) is found at Node 127 with all locations of the middle column under Load Case 4. In Figure 5.75a, it can be seen that the bridge model has the greatest ultimate load factor of about 5.9 with the middle column at Column Location 3 and the lowest ultimate load factor of about 5.1 with the middle column at Column Location 2. The bridge model with the middle column at Column Location 1 has the ultimate load factor of about 5.5. In the elastic regions (Figure 5.76), the bridge model with the middle column at Column Location 3 has the smallest rotation at section A.

For bridge models with curvature radius of 500m and various location of the middle column, vertical deflections at nodes 127, 131 and 135 under Load Case 4 are shown in Figures 5.77a, 5.77b and 5.77c. The rotation of section A is shown in Figure 5.78. The maximum deflection of the bridge model at section A is found at Node 127 with all locations of the middle column under Load Case 4. In Figure 5.77a, it can be seen that the bridge model has the greatest ultimate load factor of about 6.9 with the middle column at Column Location 3 and the lowest ultimate load factor of about 5.5 with the middle column at Column Location 2. The bridge model with the middle column at Column Location 1 has the ultimate load factor of about 6.2. In the elastic regions, the bridge model with the middle column at Column Location 3 has the smallest rotation at section A (Figure 5.78).

Based on above observations, it can be noted that the bridge model with the middle column at Column Locations 3 and with one of two radii of curvature 50m and 500m has the greatest ultimate load factor and the smallest rotation at section A in all load stages under Load Case 4.

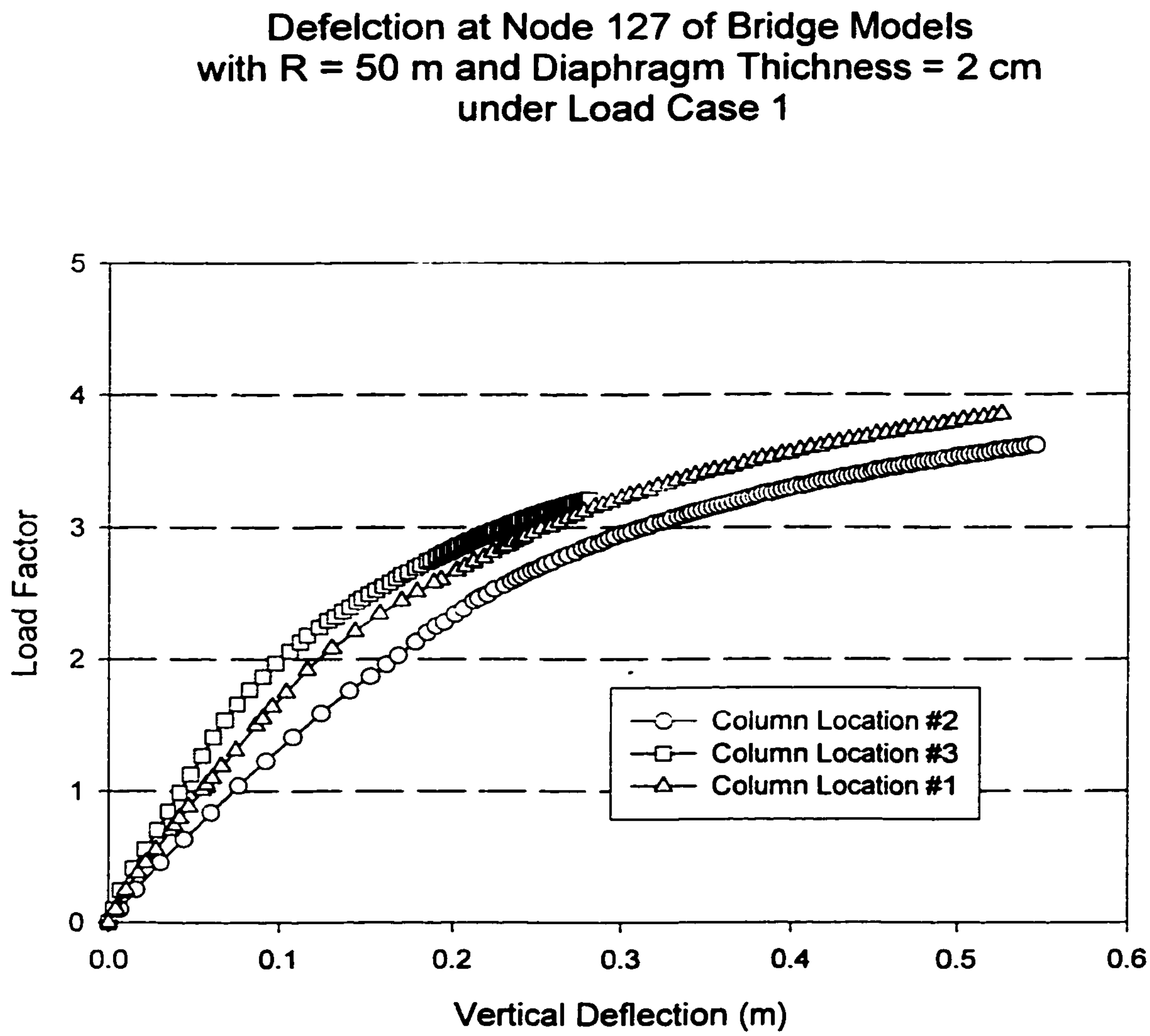

Figure 5.59a Deflections of Node 127 of Bridge Models with Various Column Locations and R=50m under Load Case 1

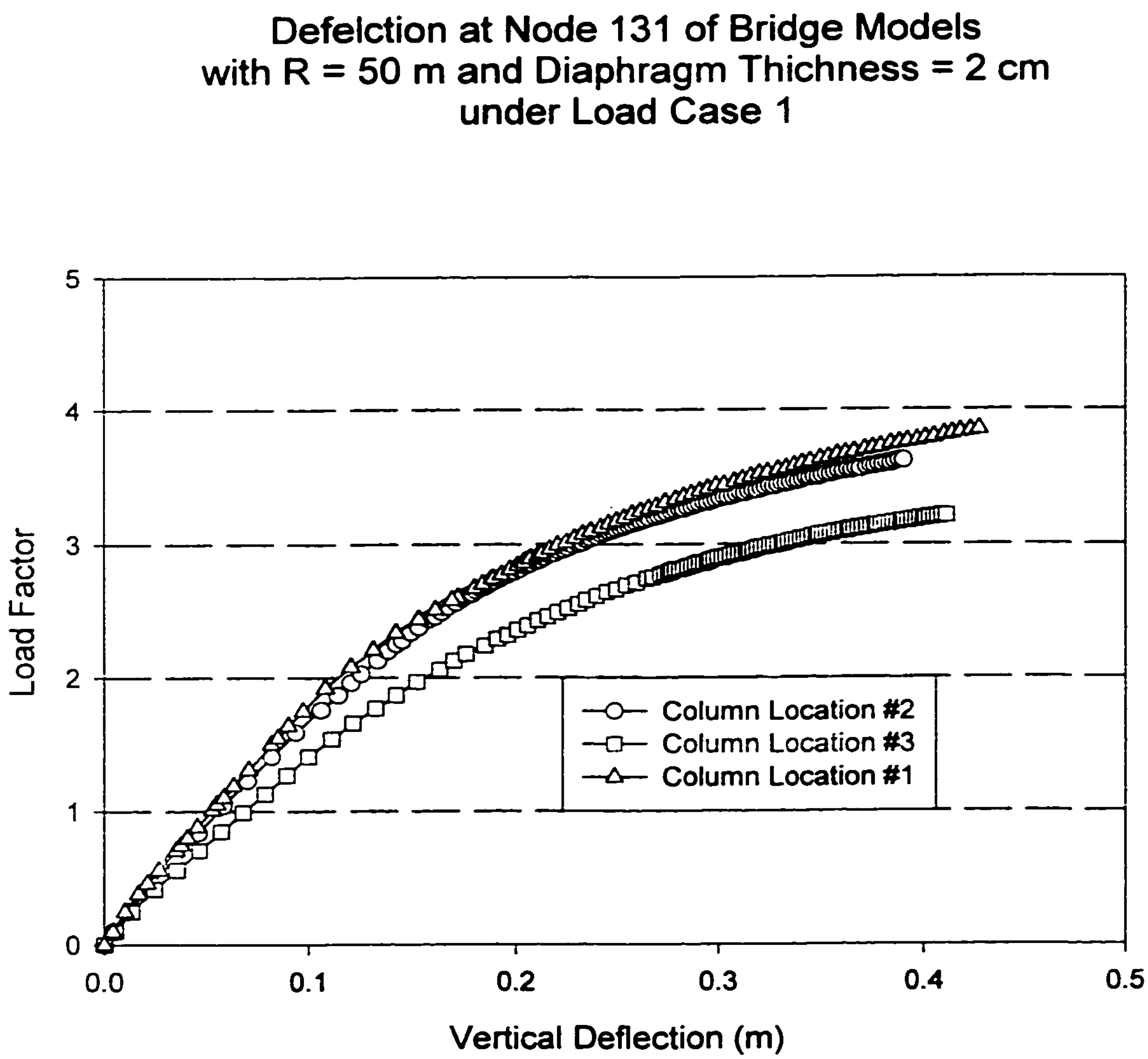

Figure 5.59b Deflections of Node 131 of Bridge Models with Various Column Locations and R=50m under Load Case 1

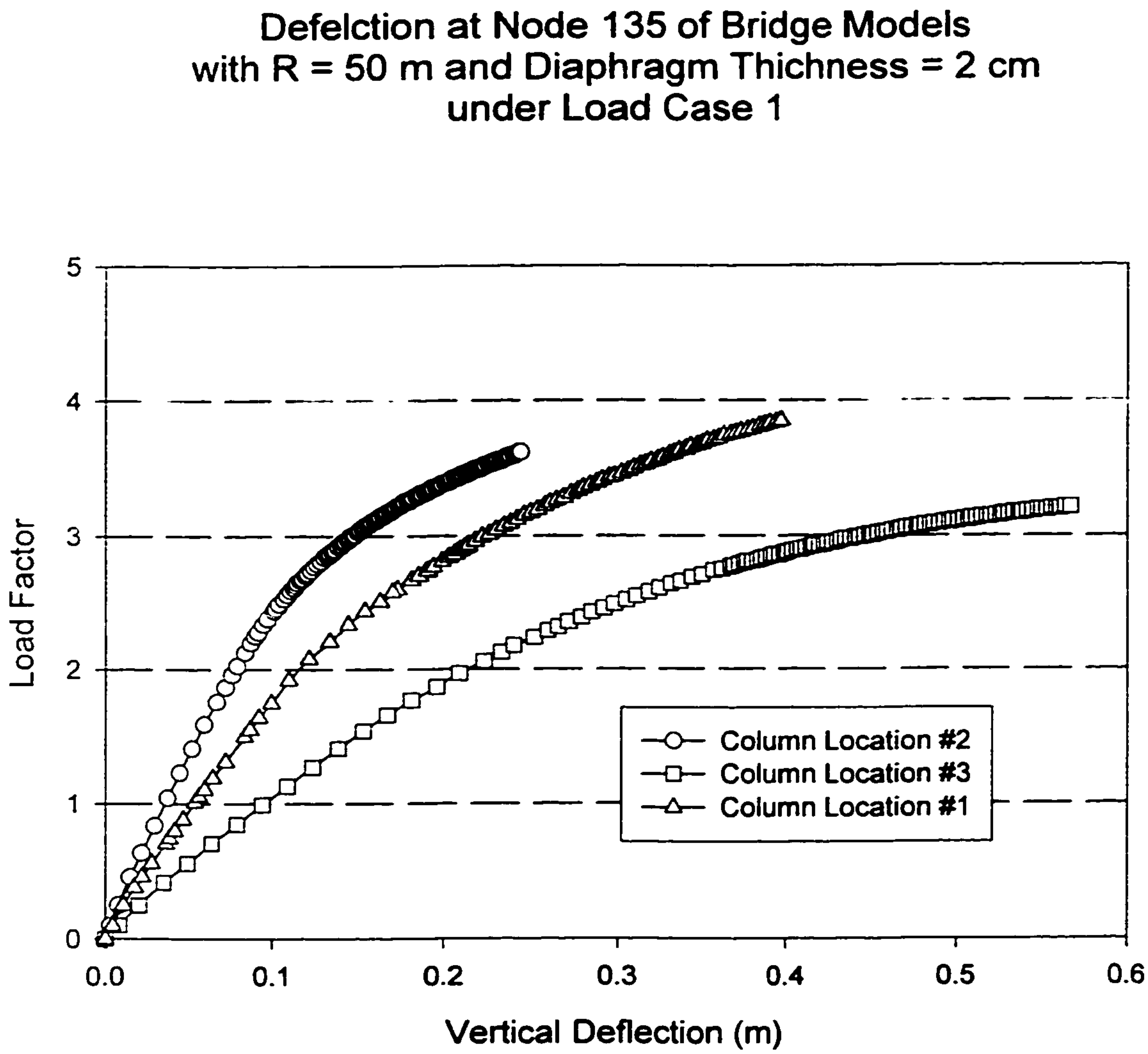

Figure 5.59c Deflections of Node 135 of Bridge Models with Various Column Locations and R=50m under Load Case 1

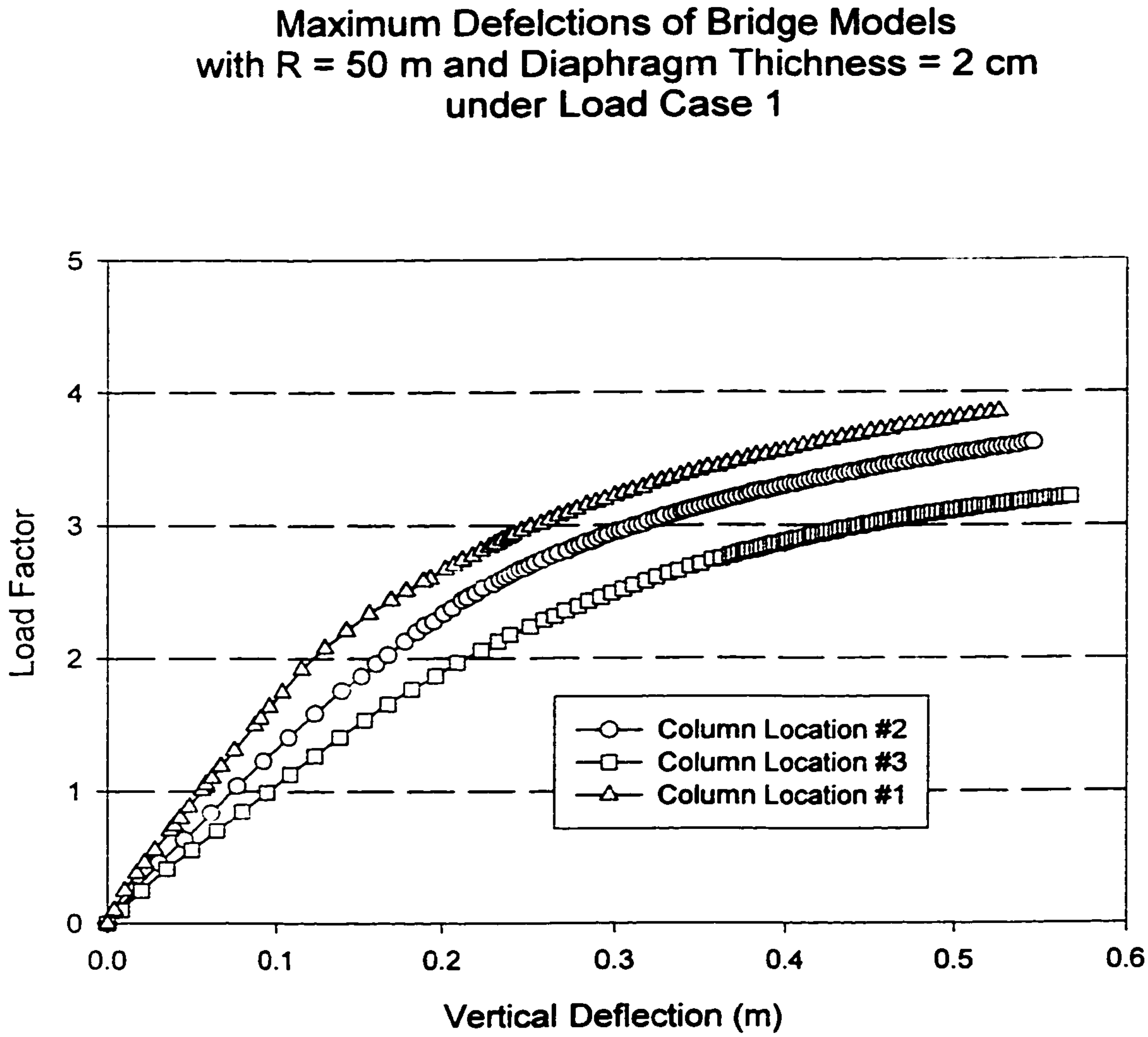

Figure 5.60 Maximum Deflections at Section A of Bridge Models with Various Column Locations and R=50m under Load Case 1

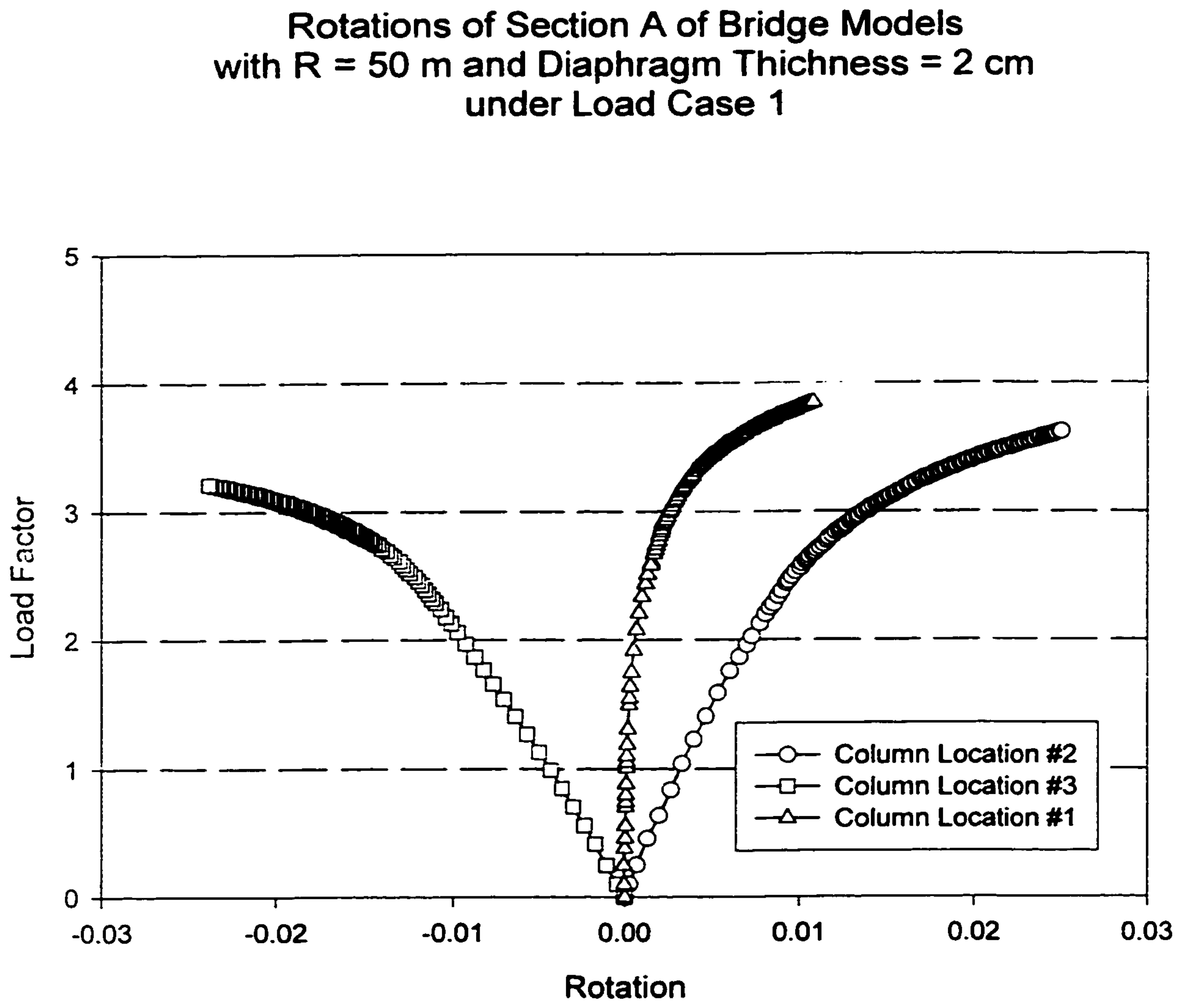

Figure 5.61. Rotations at Section A of Bridge Models with Various Column Locations and R=50m under Load Case 1

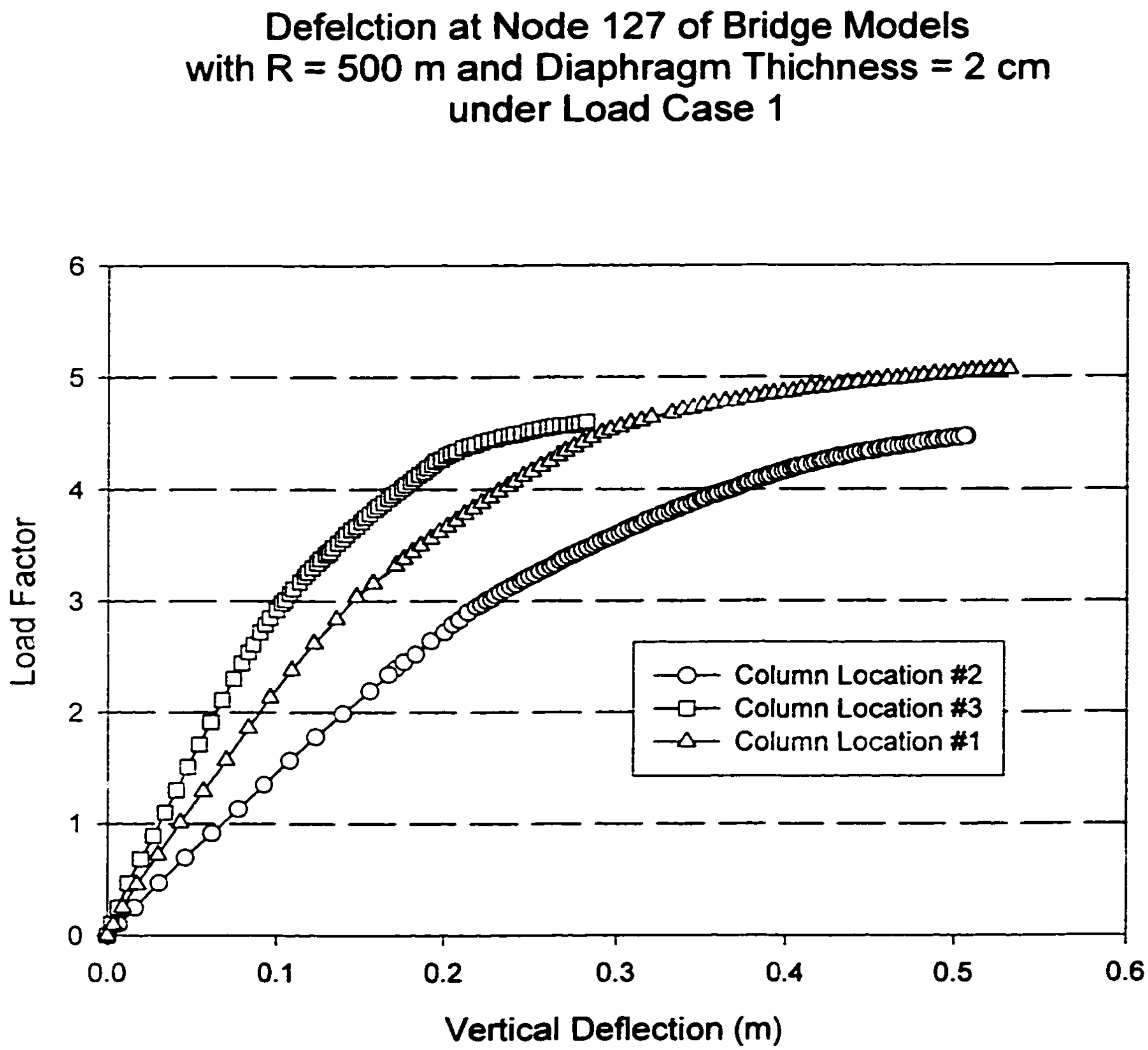

Figure 5.62a Deflections of Node 127 of Bridge Models with Various Column Locations, and R=500m under Load Case 1

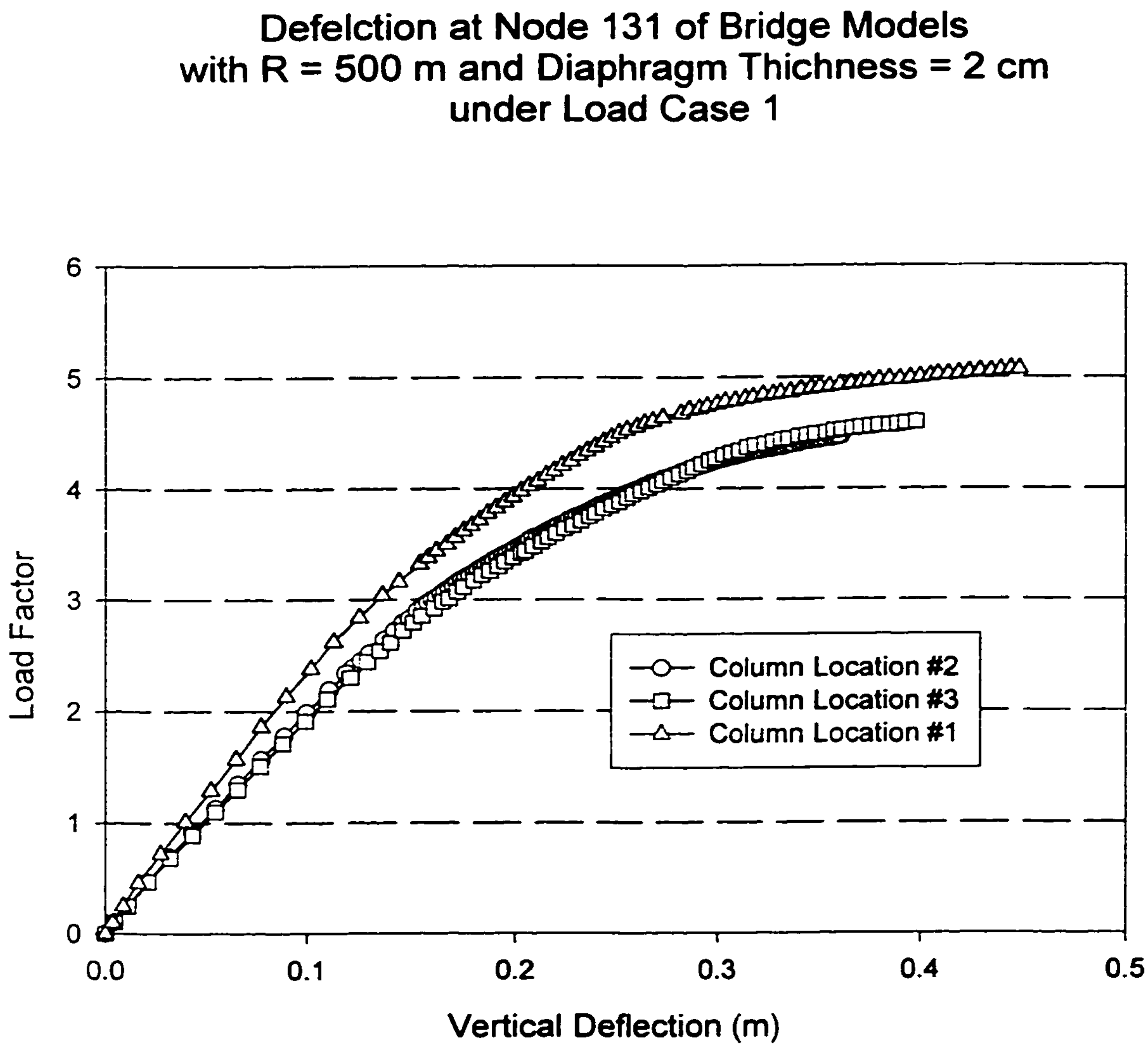

Figure 5.62b Deflections of Node 131 of Bridge Models with Various Column Locations and R=500m under Load Case 1

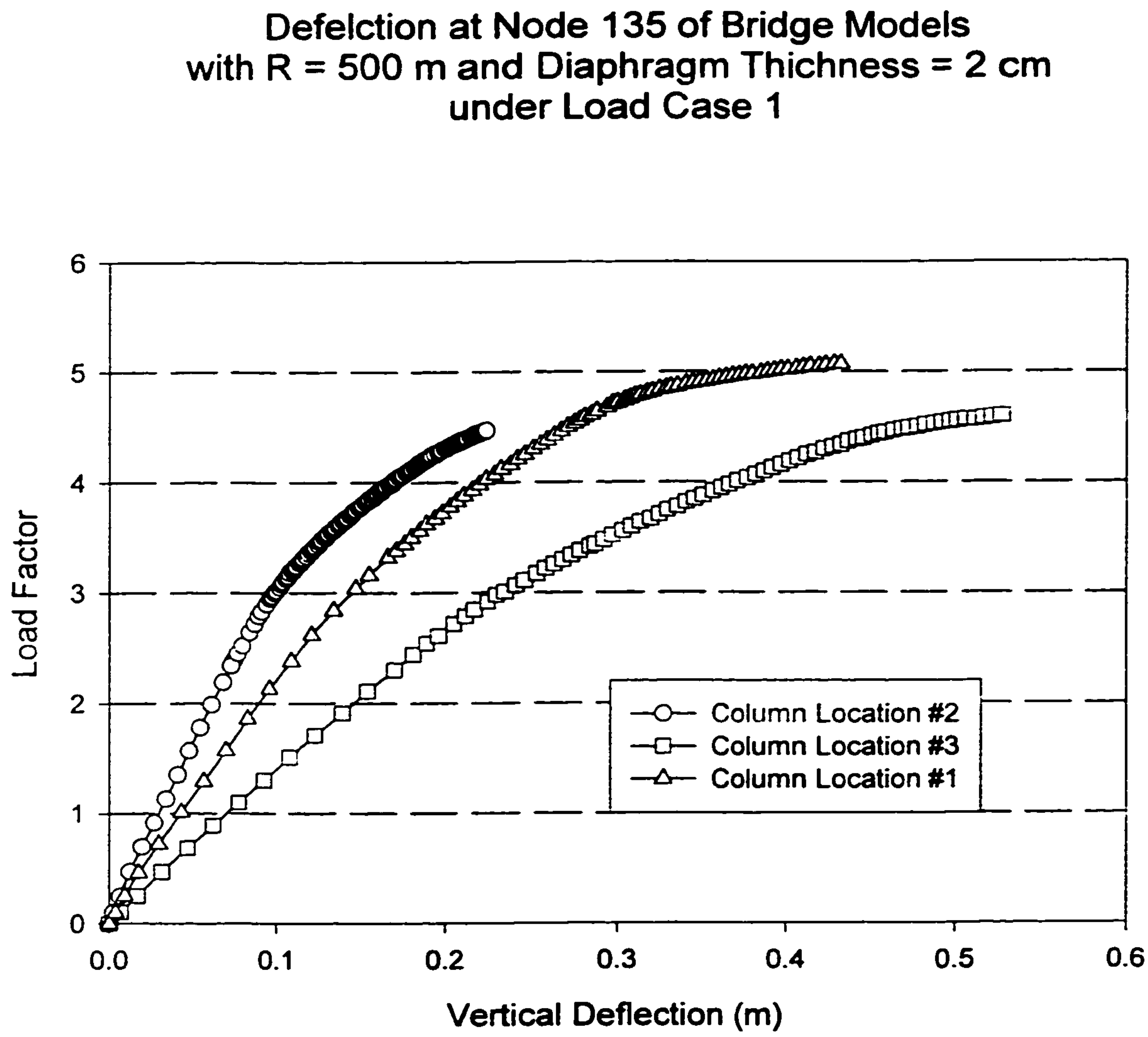

Figure 5.62c Deflections of Node 135 of Bridge Models with Various Column Locations and R=500m under Load Case 1

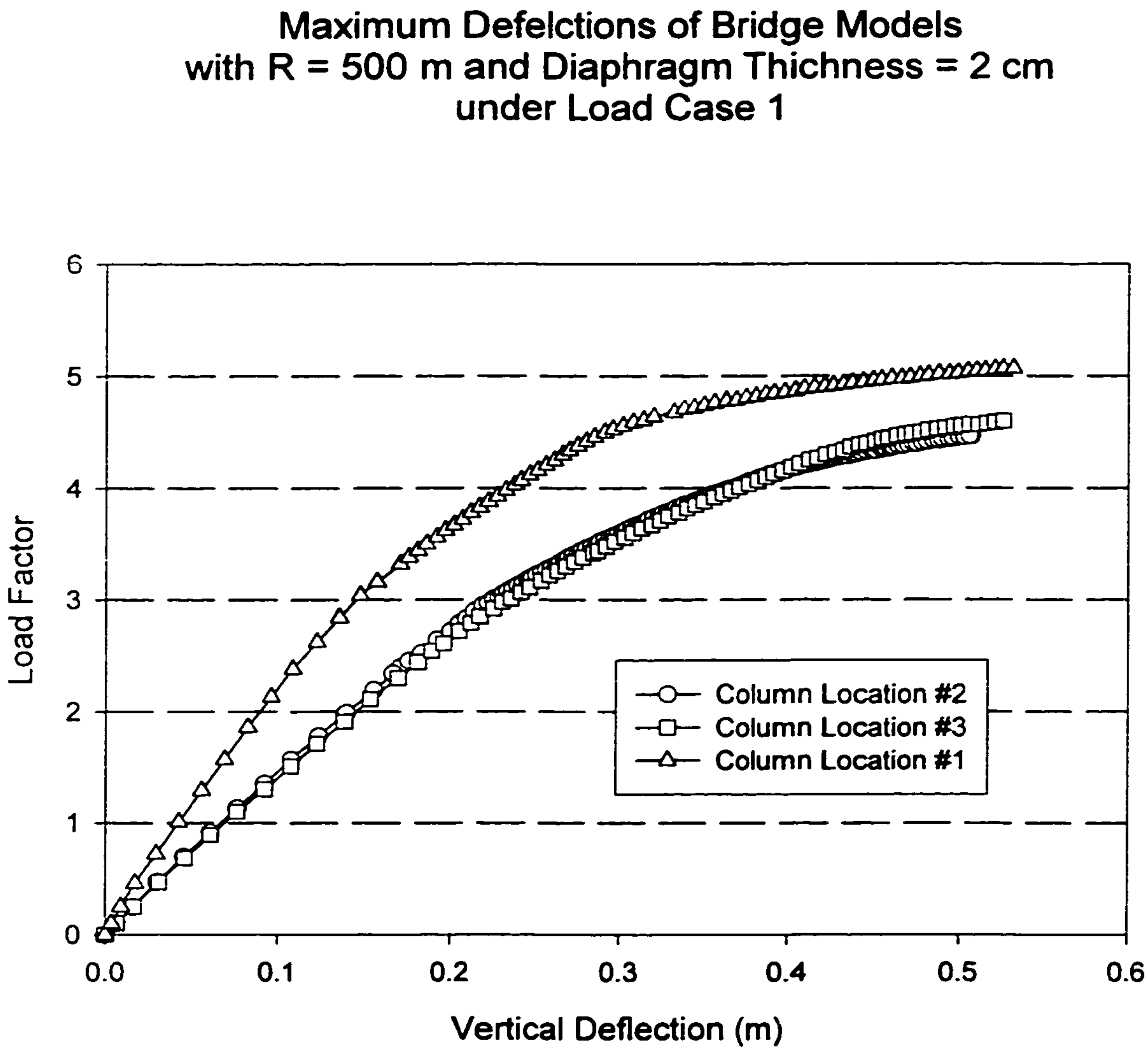

Figure 5.63 Maximum Deflections at Section A of Bridge Models with Various Column Locations and R=500m under Load Case 1

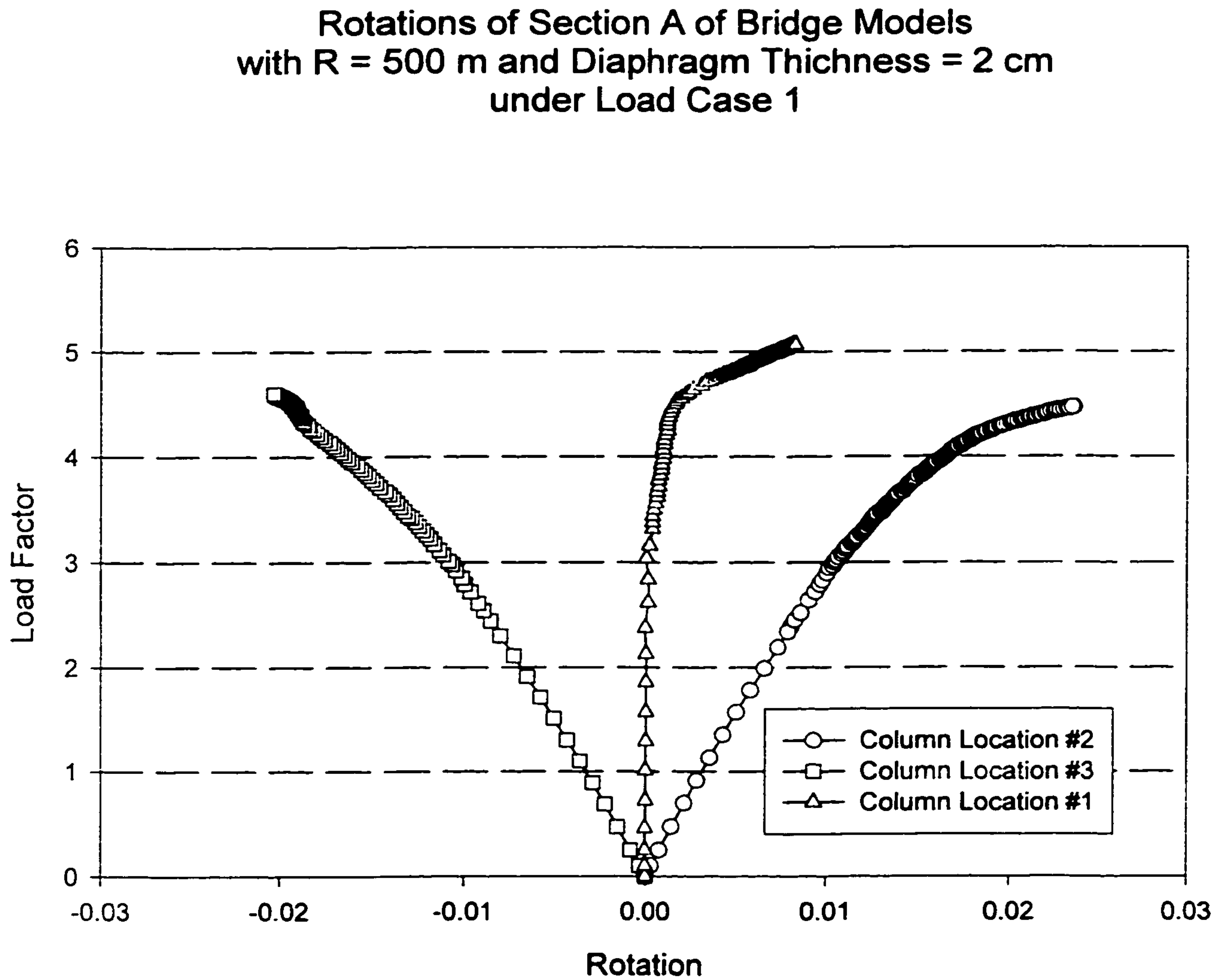

Figure 5.64. Rotations at Section A of Bridge Models with Various Column Locations and R=500m under Load Case 1

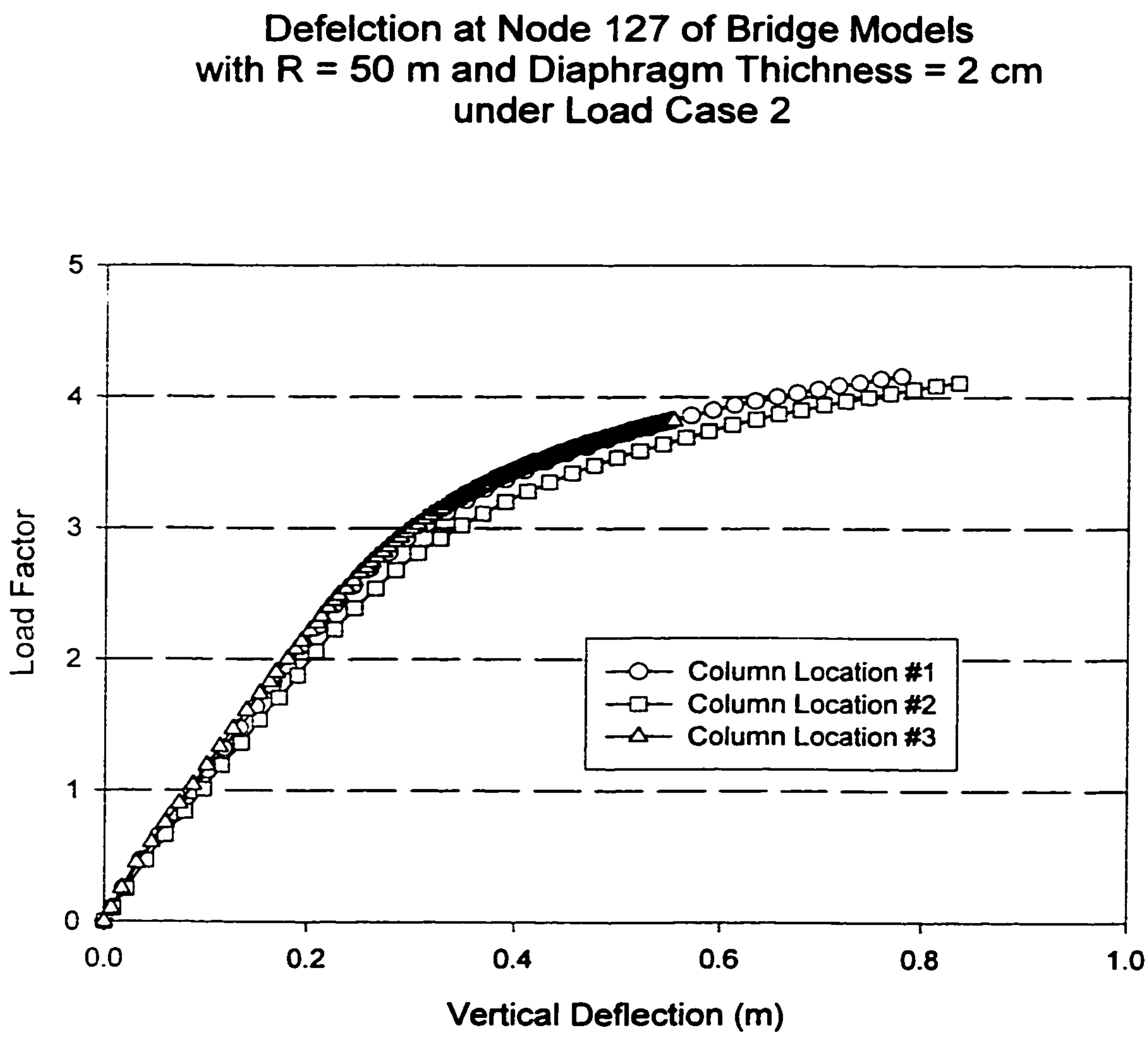

Figure 5.65a Deflections of Node 127 of Bridge Models with Various Column Locations and R=50m under Load Case 2

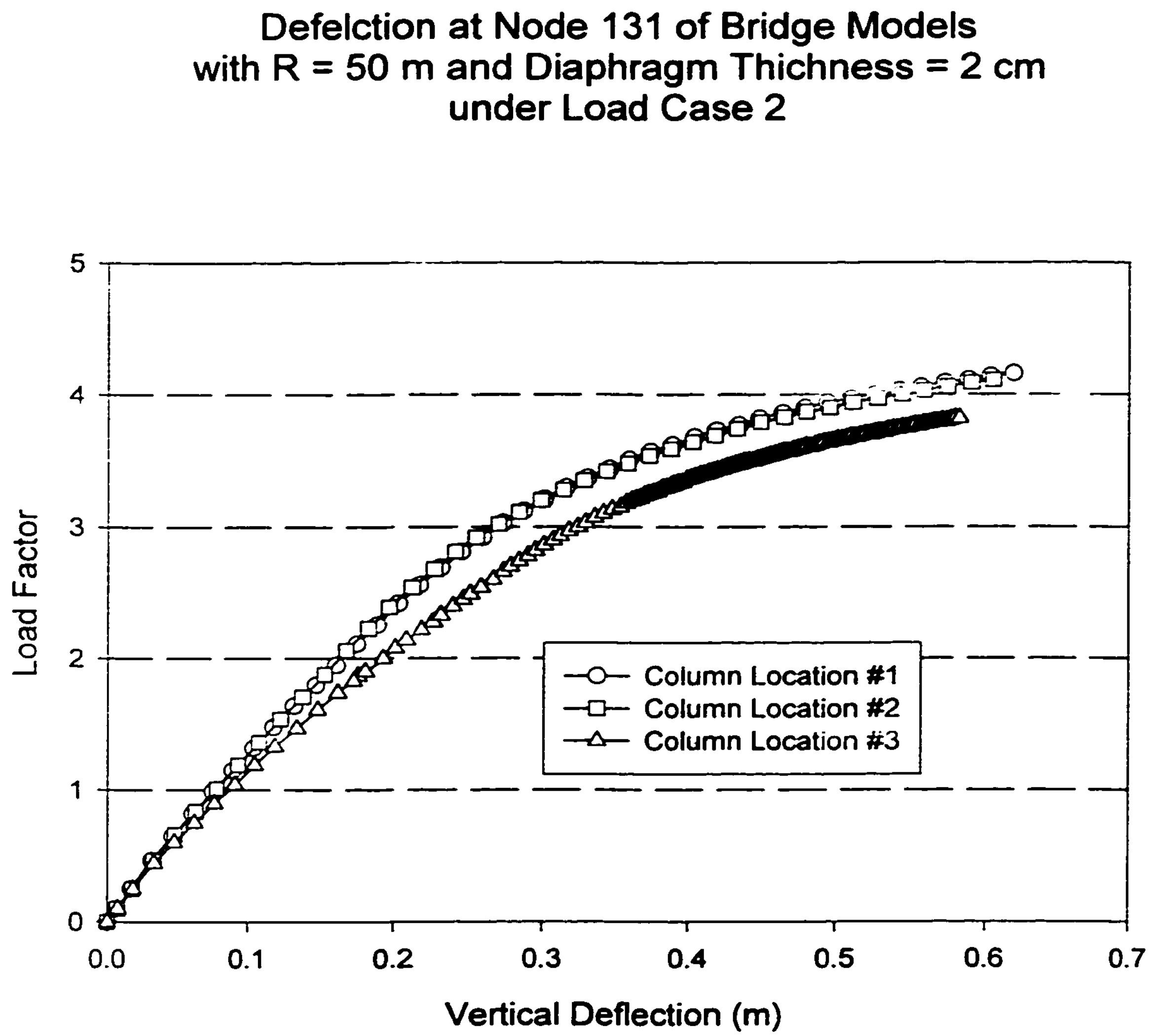

Figure 5.65b Deflections of Node 131 of Bridge Models with Various Column Locations and R=50m under Load Case 2

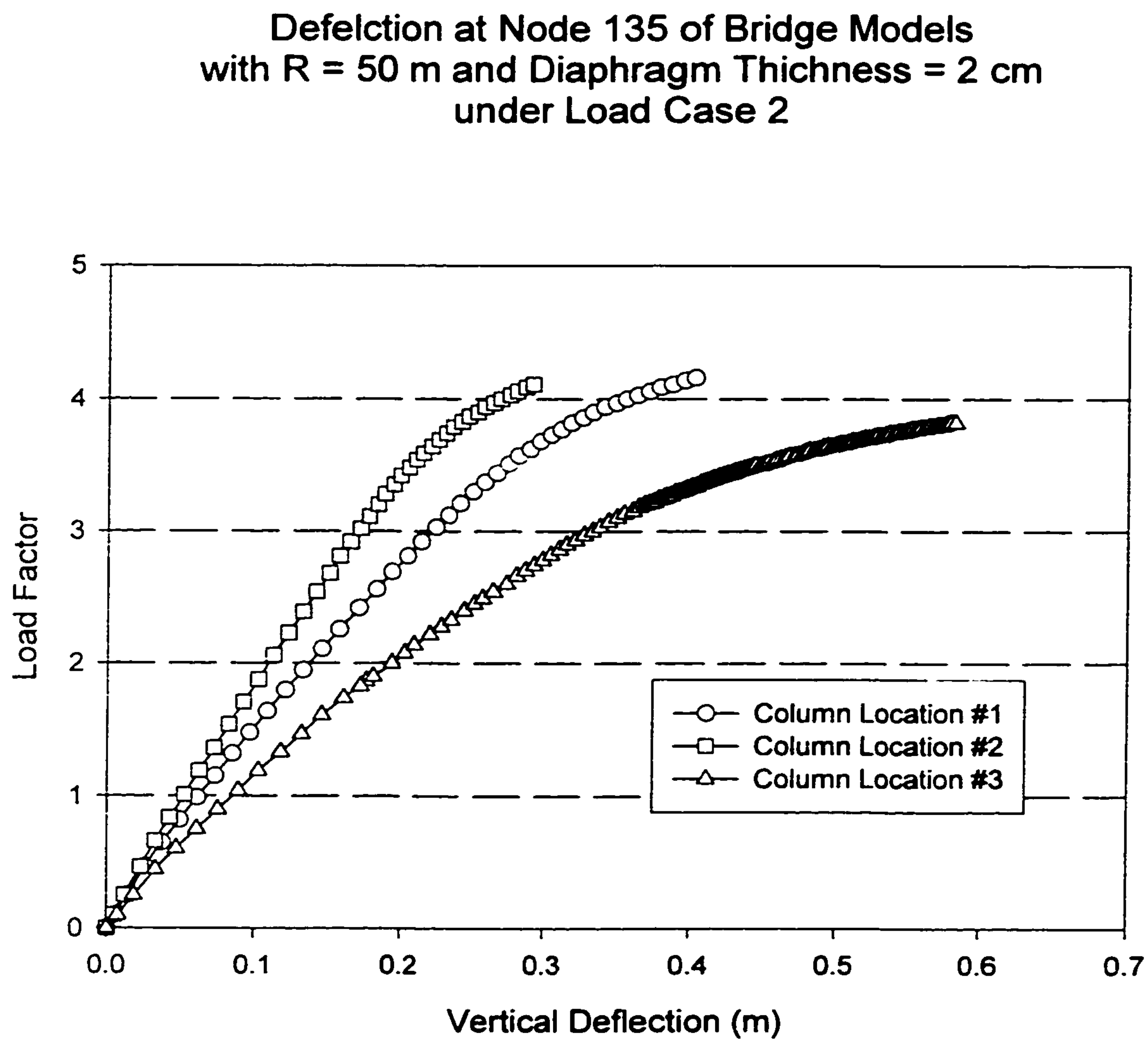

Figure 5.65c Deflections of Node 135 of Bridge Models with Various Column and R=50m under Load Case 2

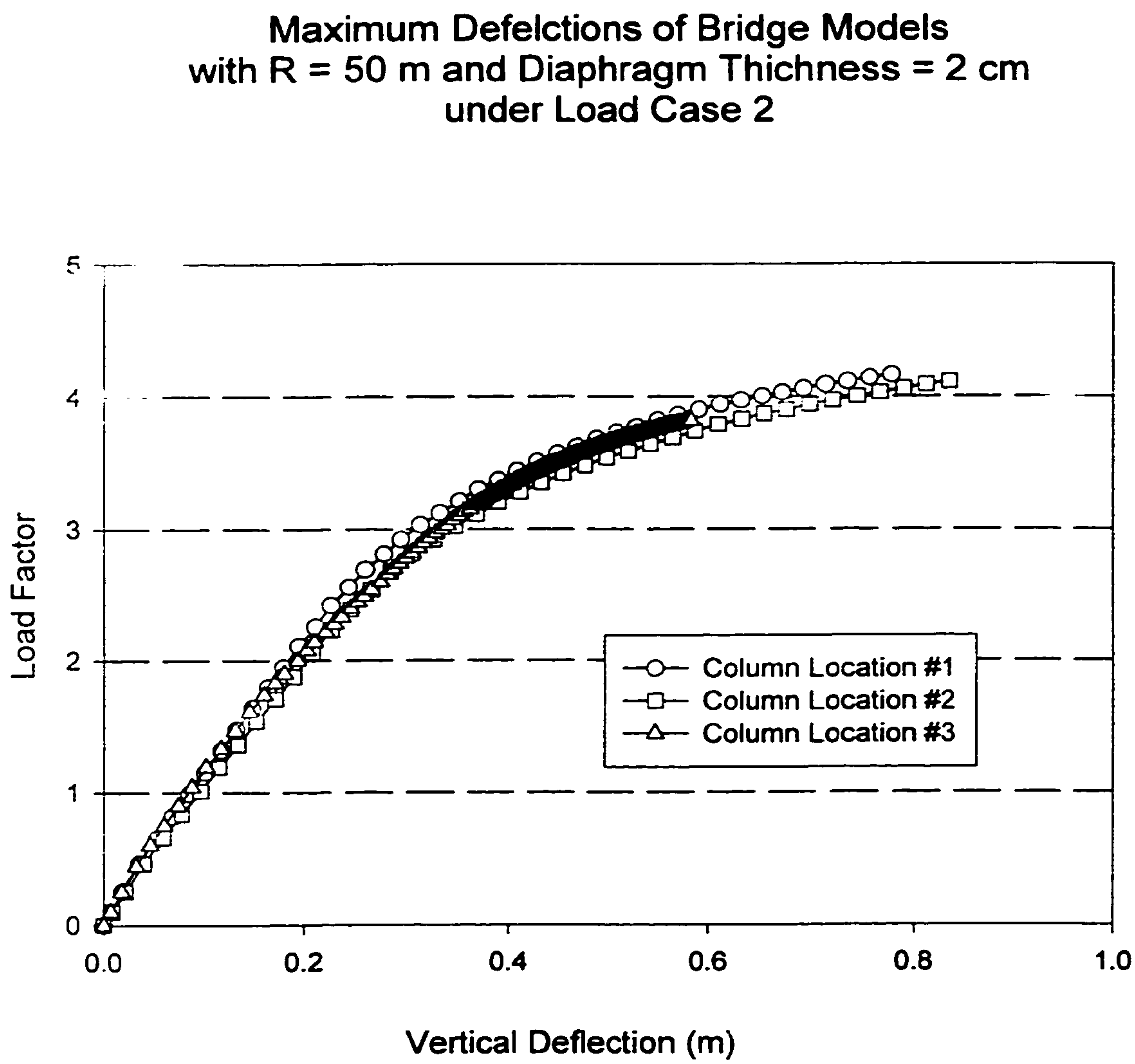

Figure 5.66 Maximum Deflections at Section A of Bridge Models with Various Column Locations and R=50m under Load Case 2

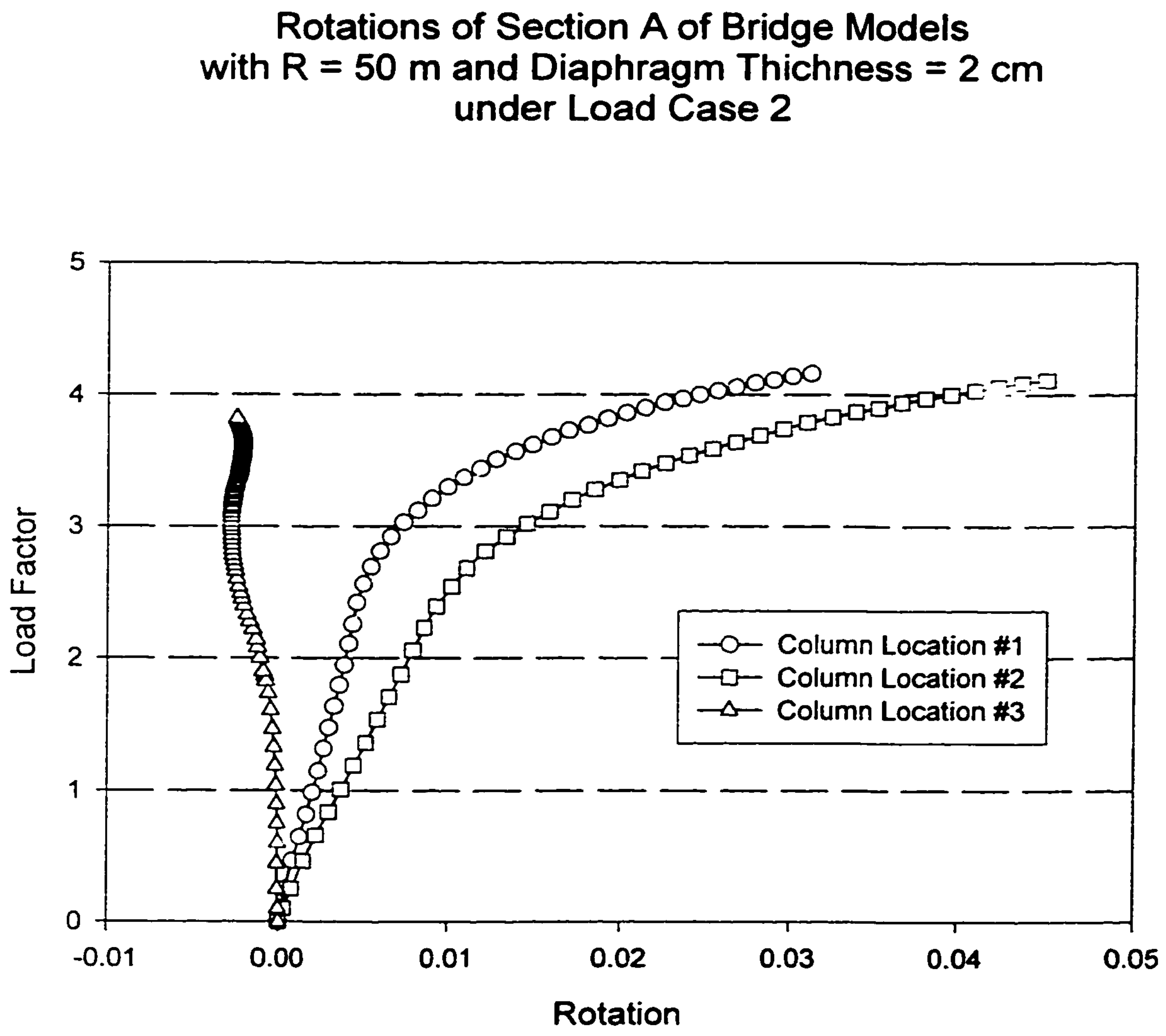

Figure 5.67. Rotations at Section A of Bridge Models with Various Column Locations and R=50m under Load Case 2

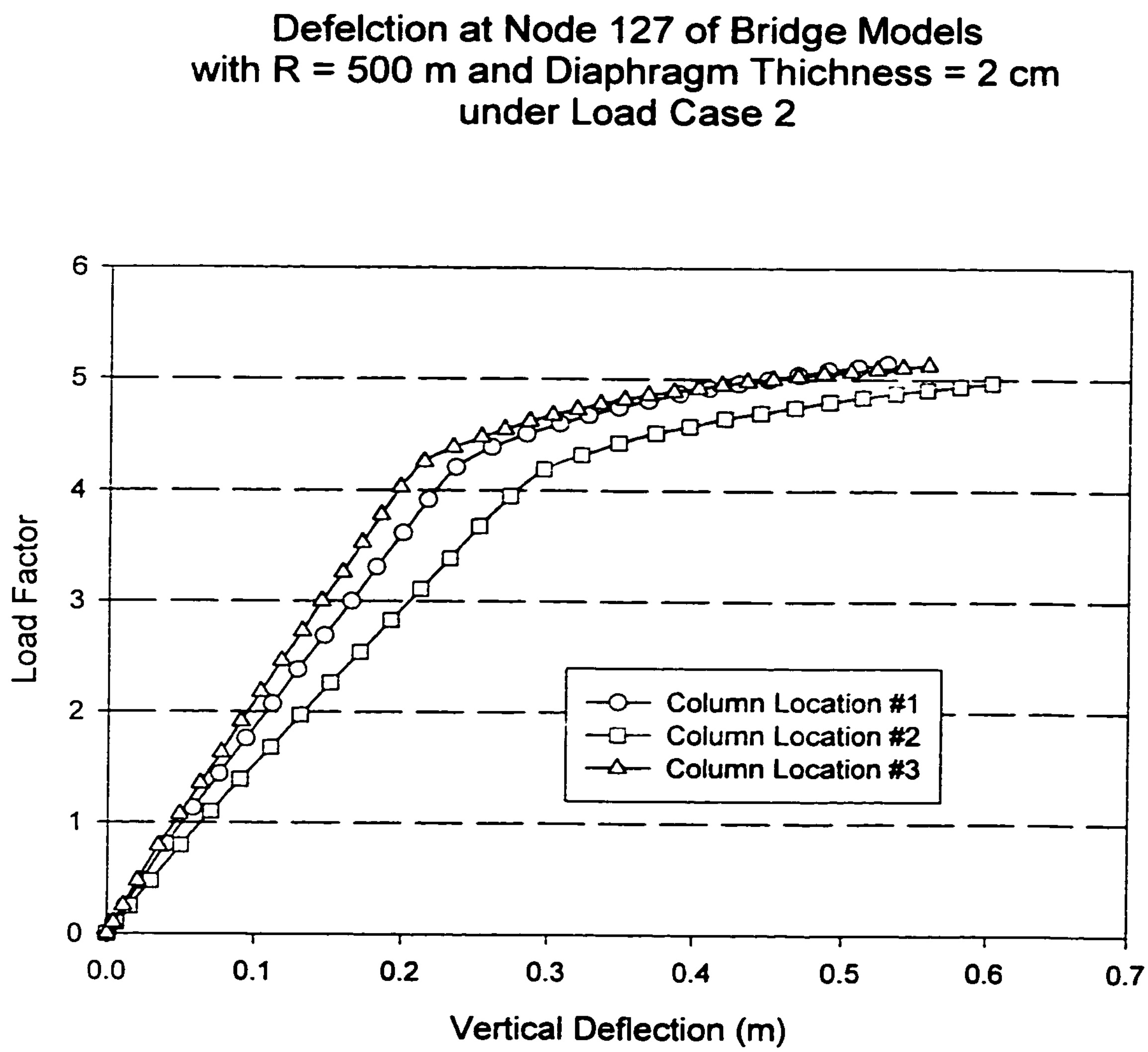

Figure 5.68a Deflections of Node 127 of Bridge Models with Various Column Locations and R=500m under Load Case 2

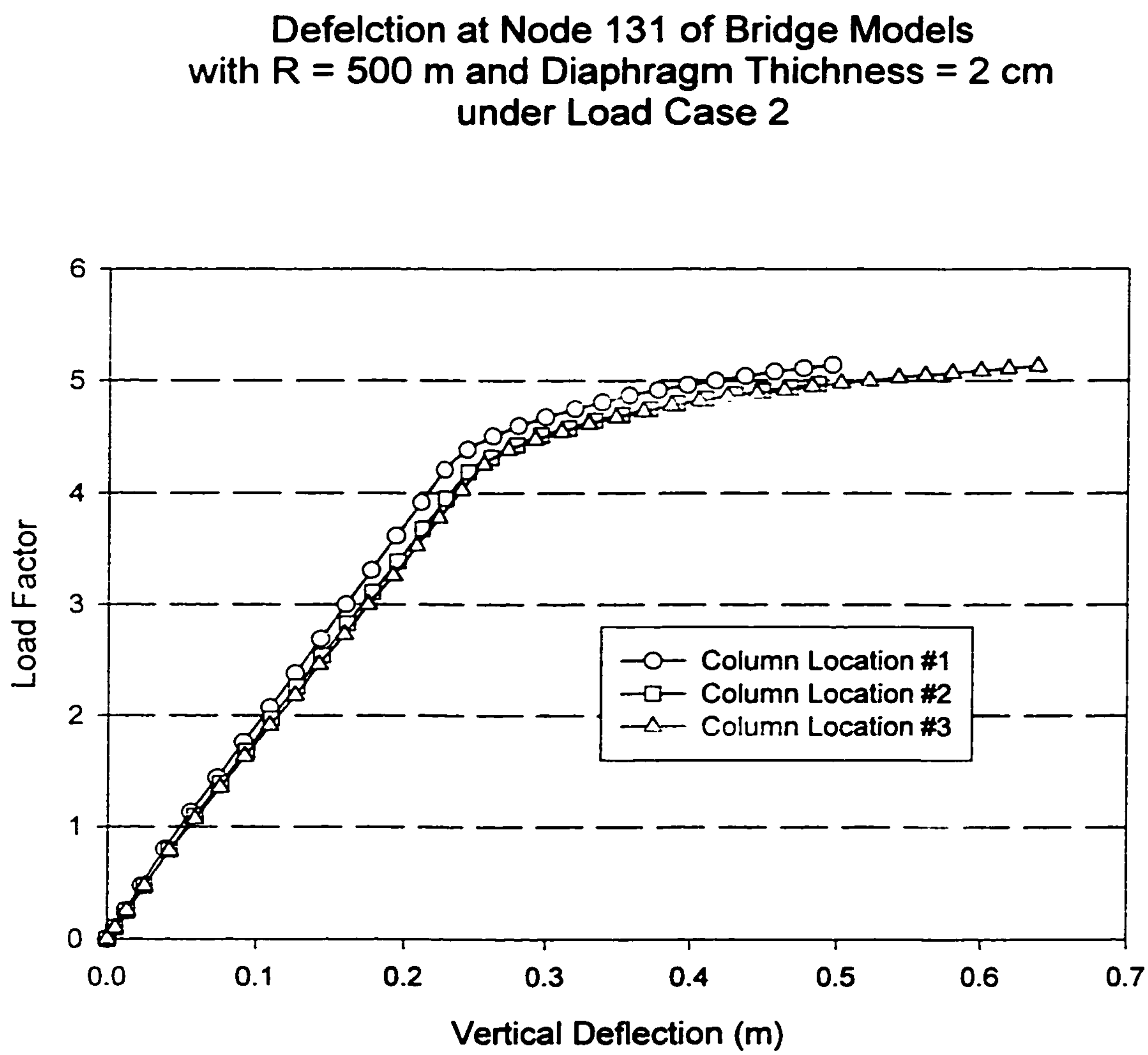

Figure 5.68b Deflections of Node 131 of Bridge Models with Various Column Locations and R=500m under Load Case 2

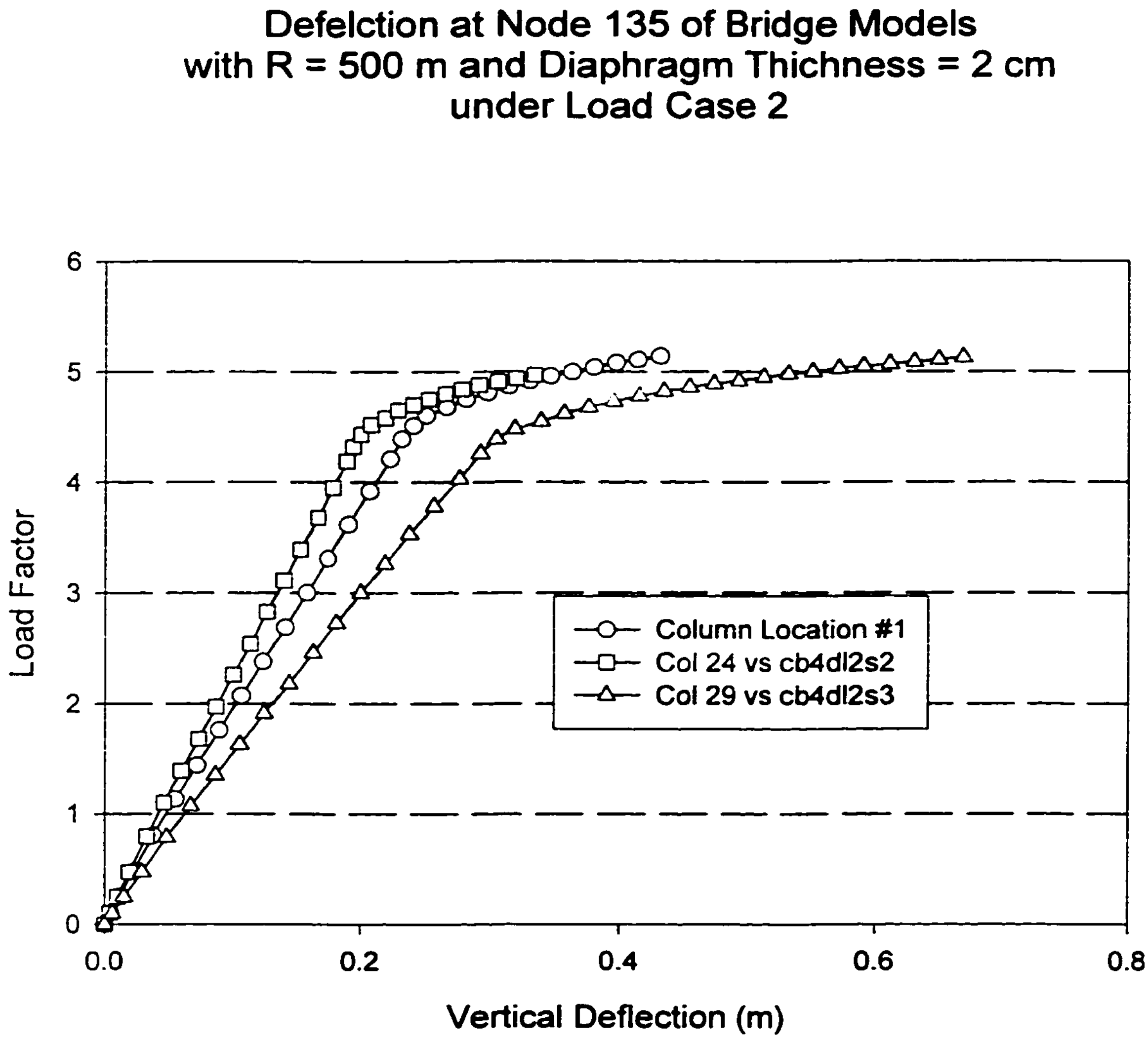

Figure 5.68c Deflections of Node 135 of Bridge Models with Various Column Locations and R=500m under Load Case 2

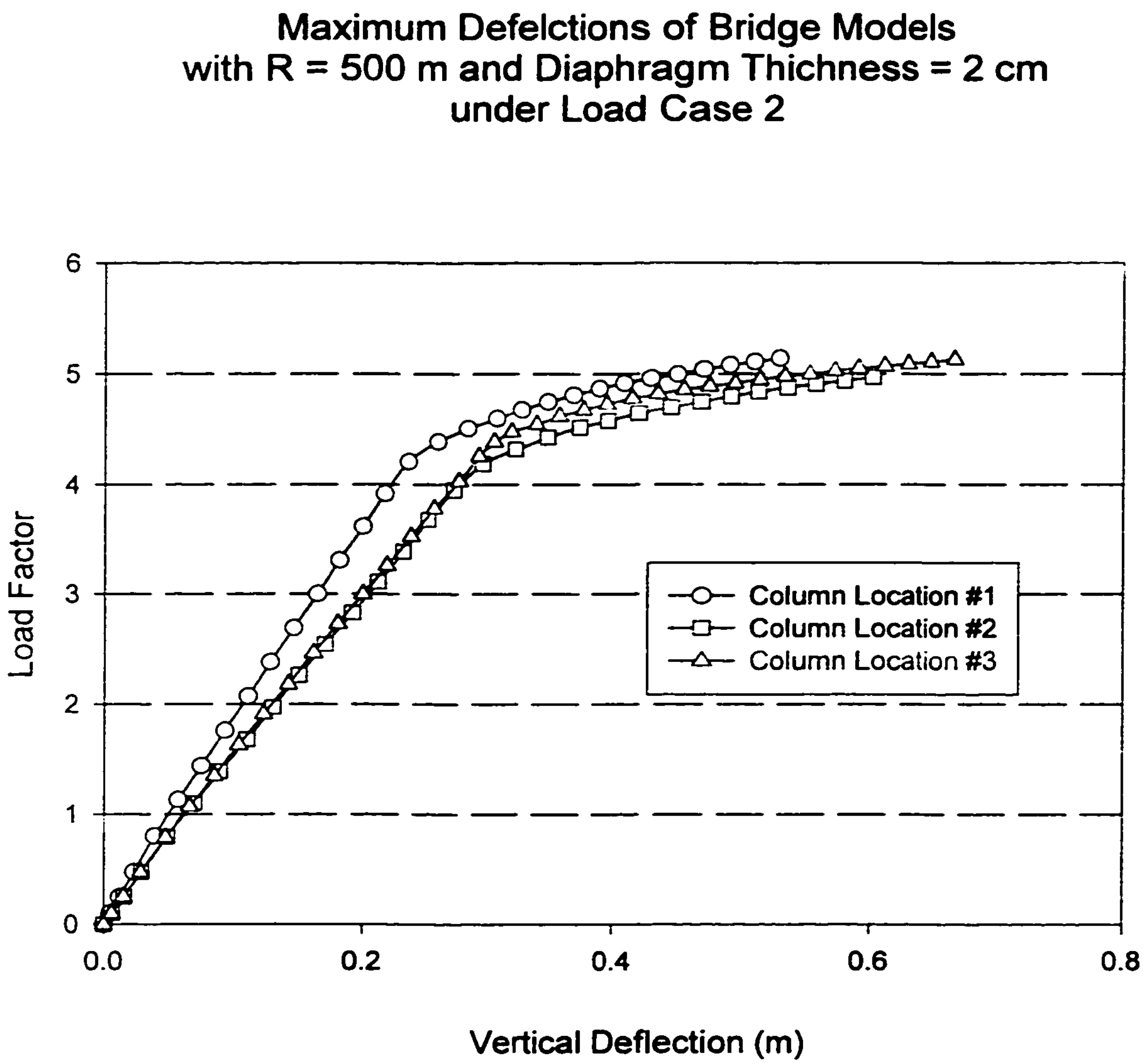

Figure 5.69 Maximum Deflections at Section A of Bridge Models with Various Column Locations and R=500m under Load Case 2

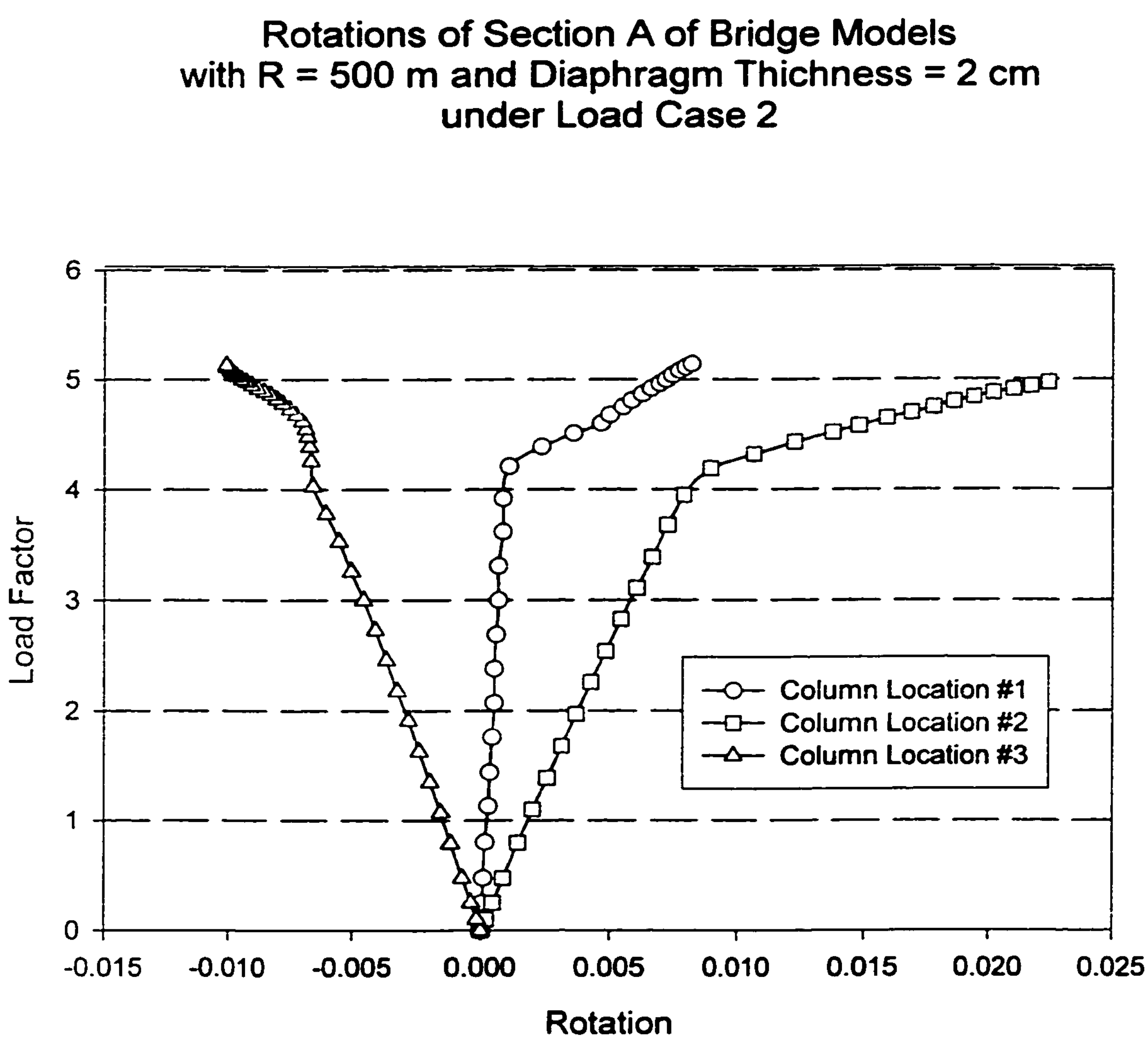

Figure 5.70. Rotations at Section A of Bridge Models with Various Column Locations and R=500m under Load Case 2

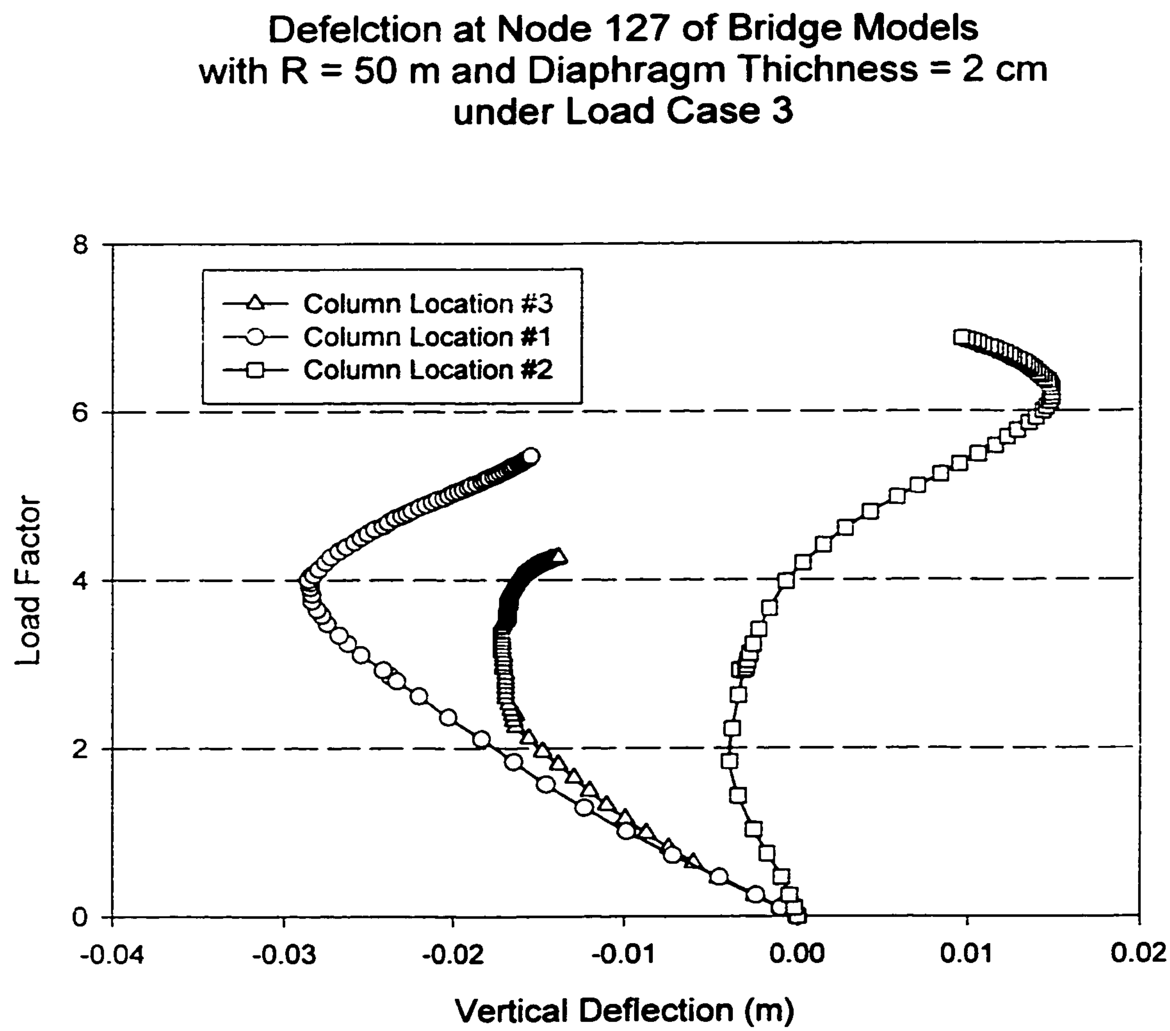

Figure 5.71a Deflections of Node 127 of Bridge Models with Various Column Locations and R=50m under Load Case 3

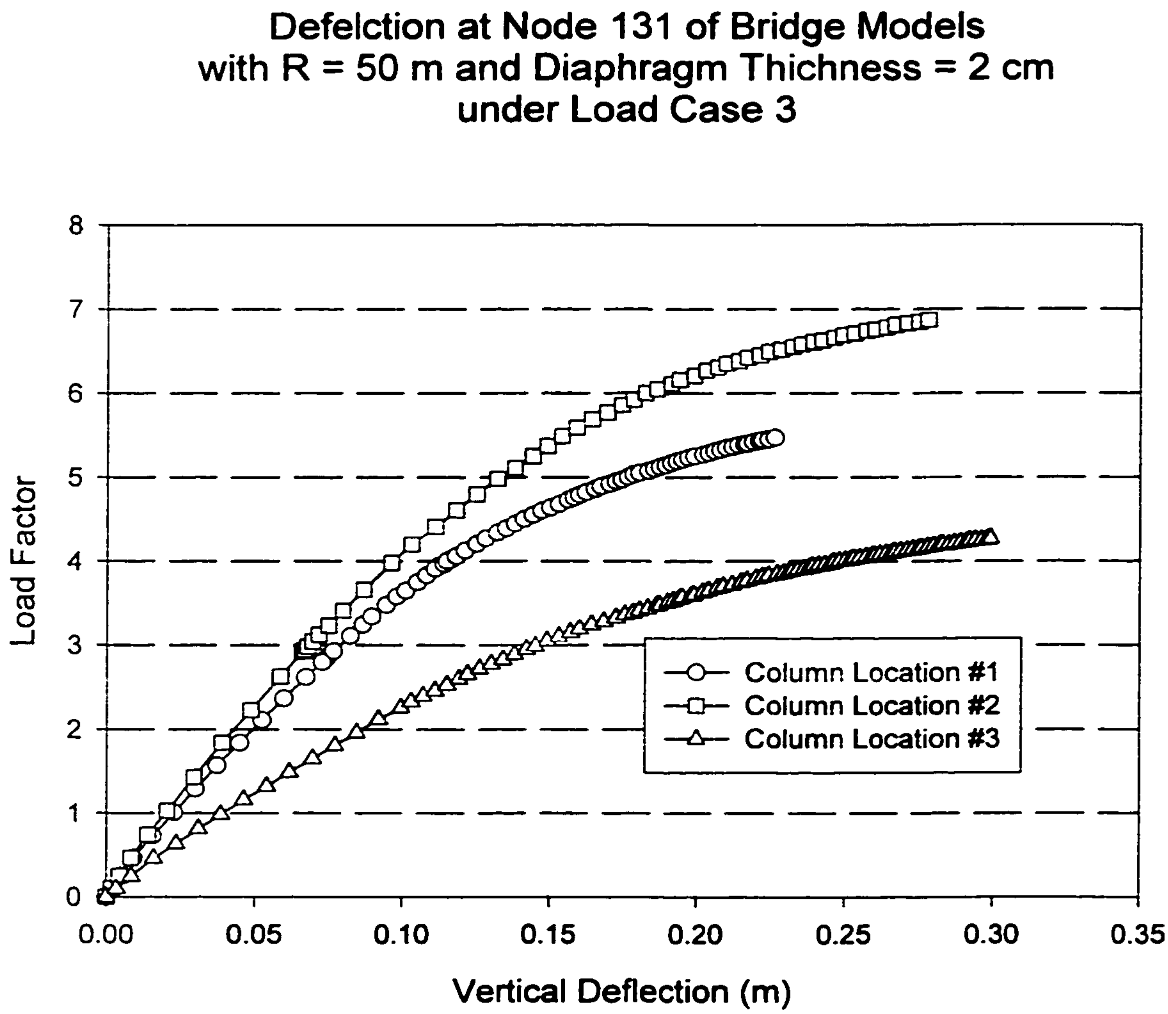

Figure 5.71b Deflections of Node 131 of Bridge Models with Various Column Locations and R=50m under Load Case 3

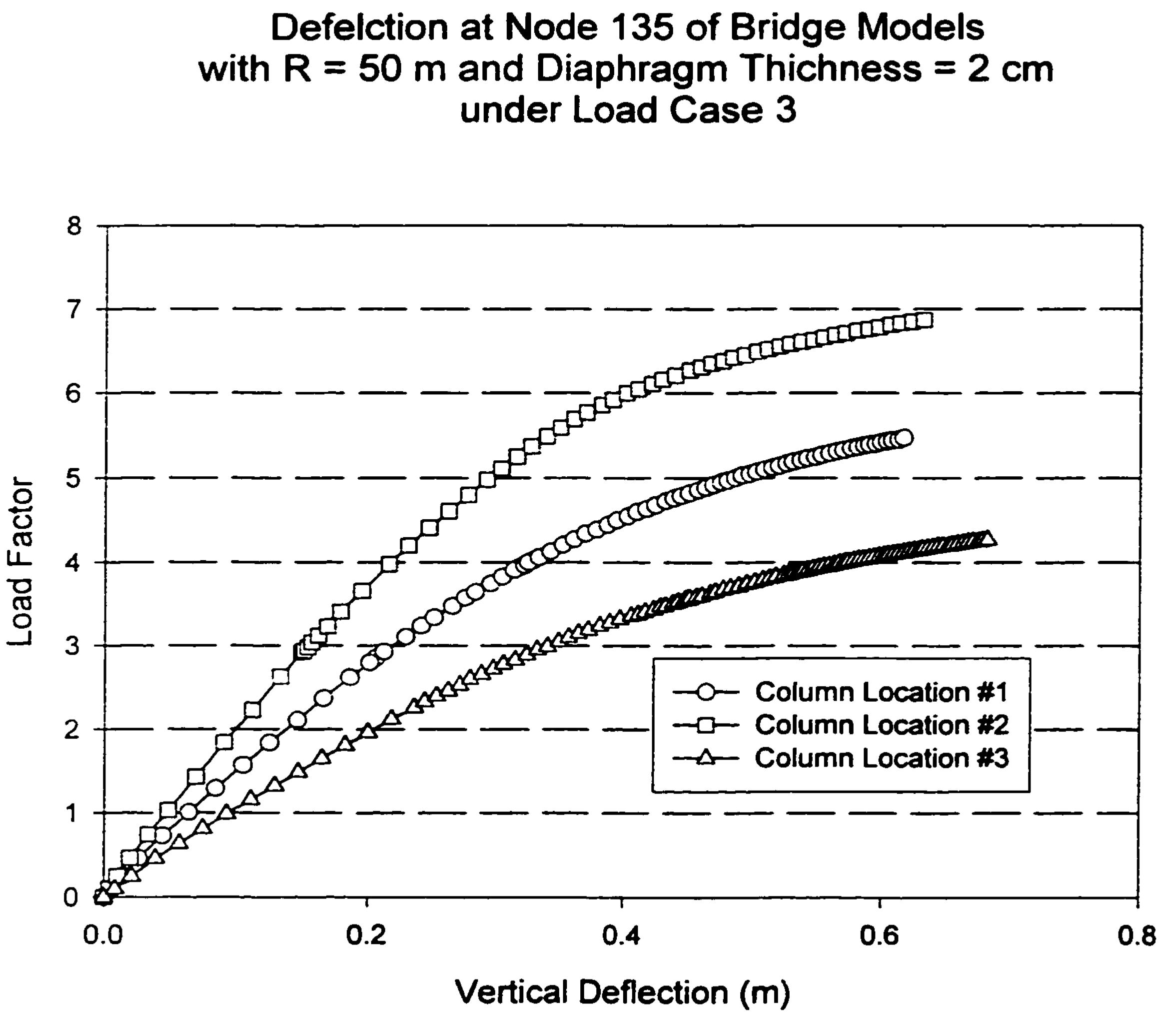

Figure 5.71c Deflections of Node 135 of Bridge Models with Various Column Locations and R=50m under Load Case 3

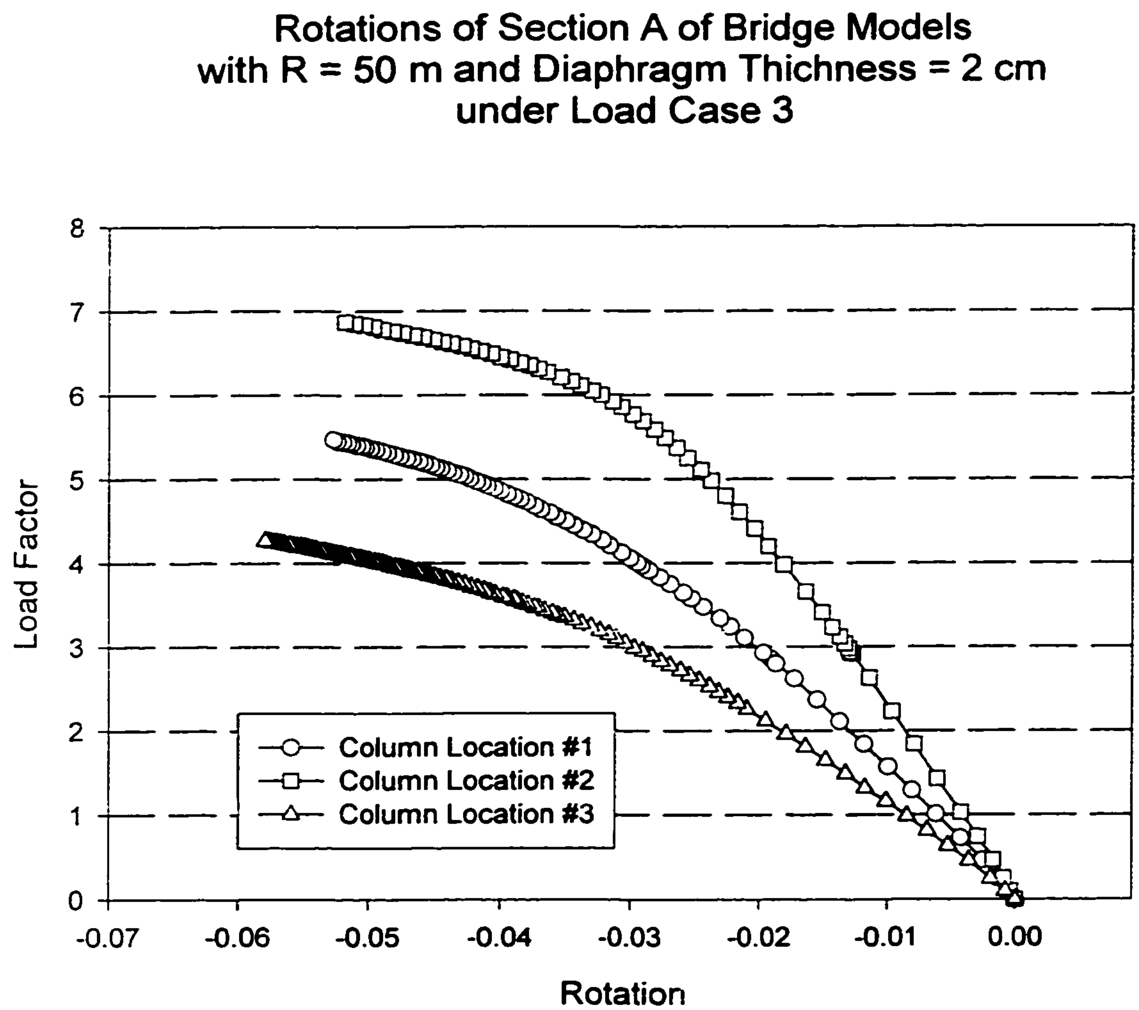

Figure 5.72. Rotations at Section A of Bridge Models with Various Column Locations and R=50m under Load Case 3

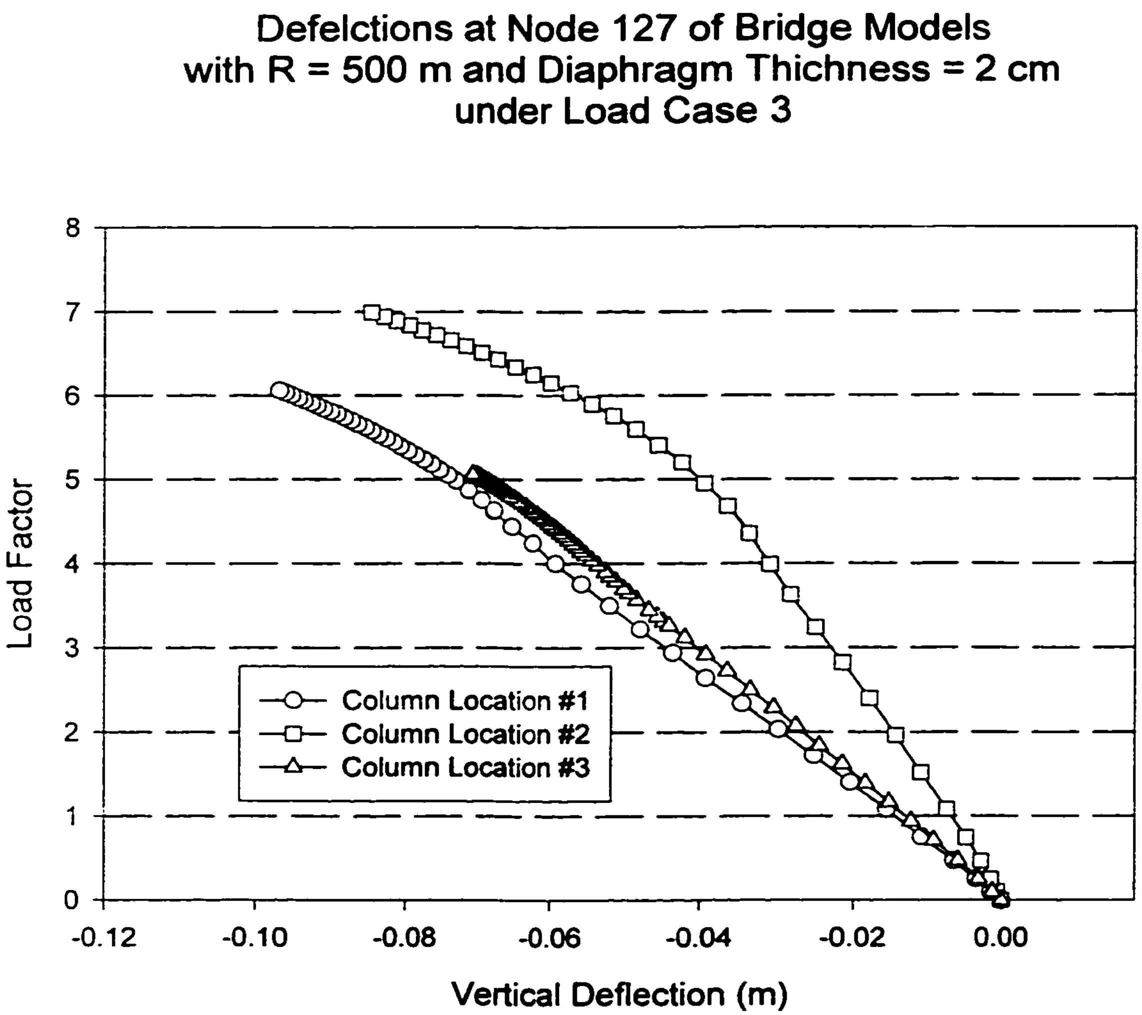

Figure 5.73a Deflections of Node 127 of Bridge Models with Various Column Locations and R=500m under Load Case 3

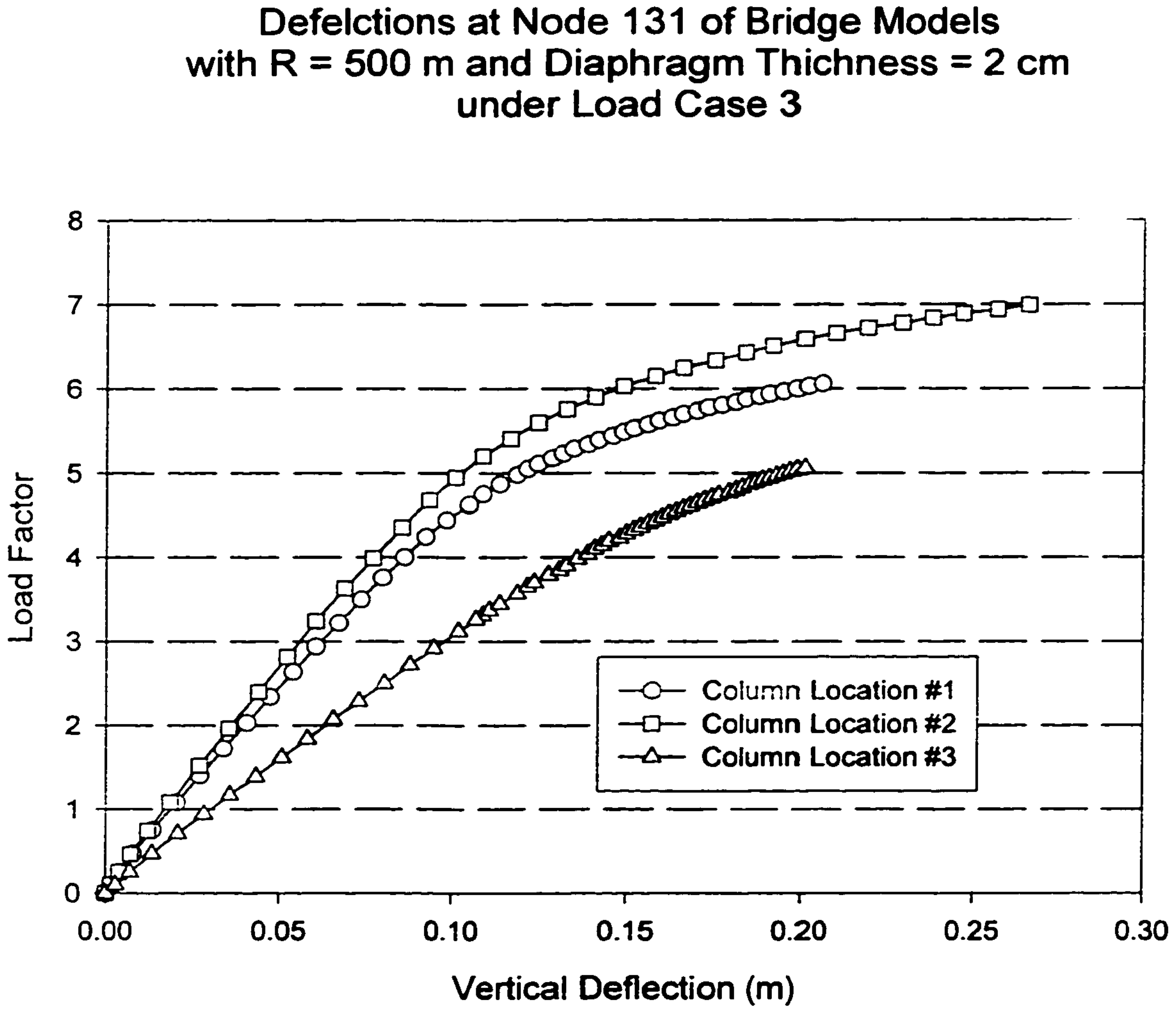

Figure 5.73b Deflections of Node 131 of Bridge Models with Various Column Locations and R=500m under Load Case 3

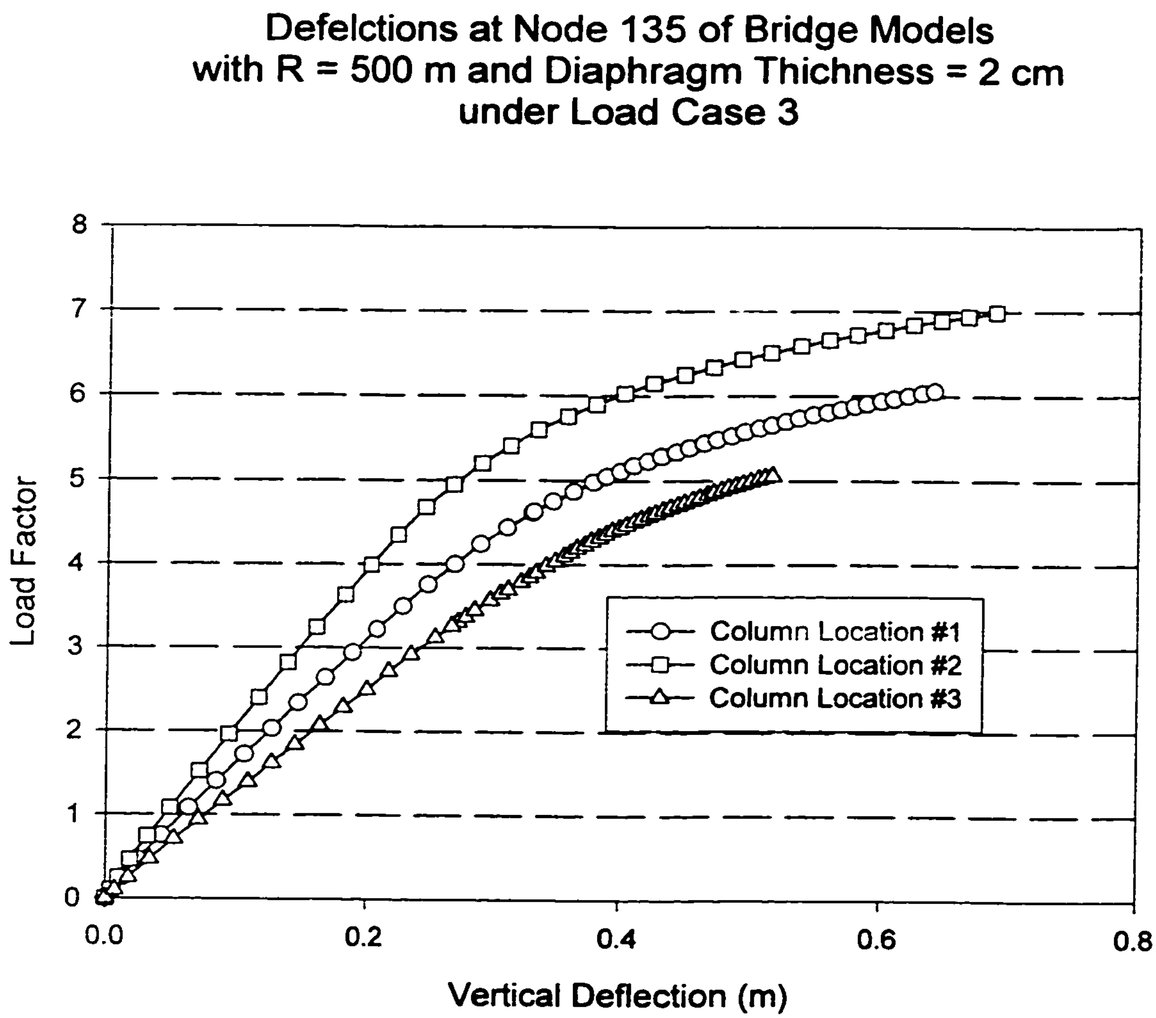

Figure 5.73c Deflections of Node 135 of Bridge Models with Various Column Locations and R=500m under Load Case 3

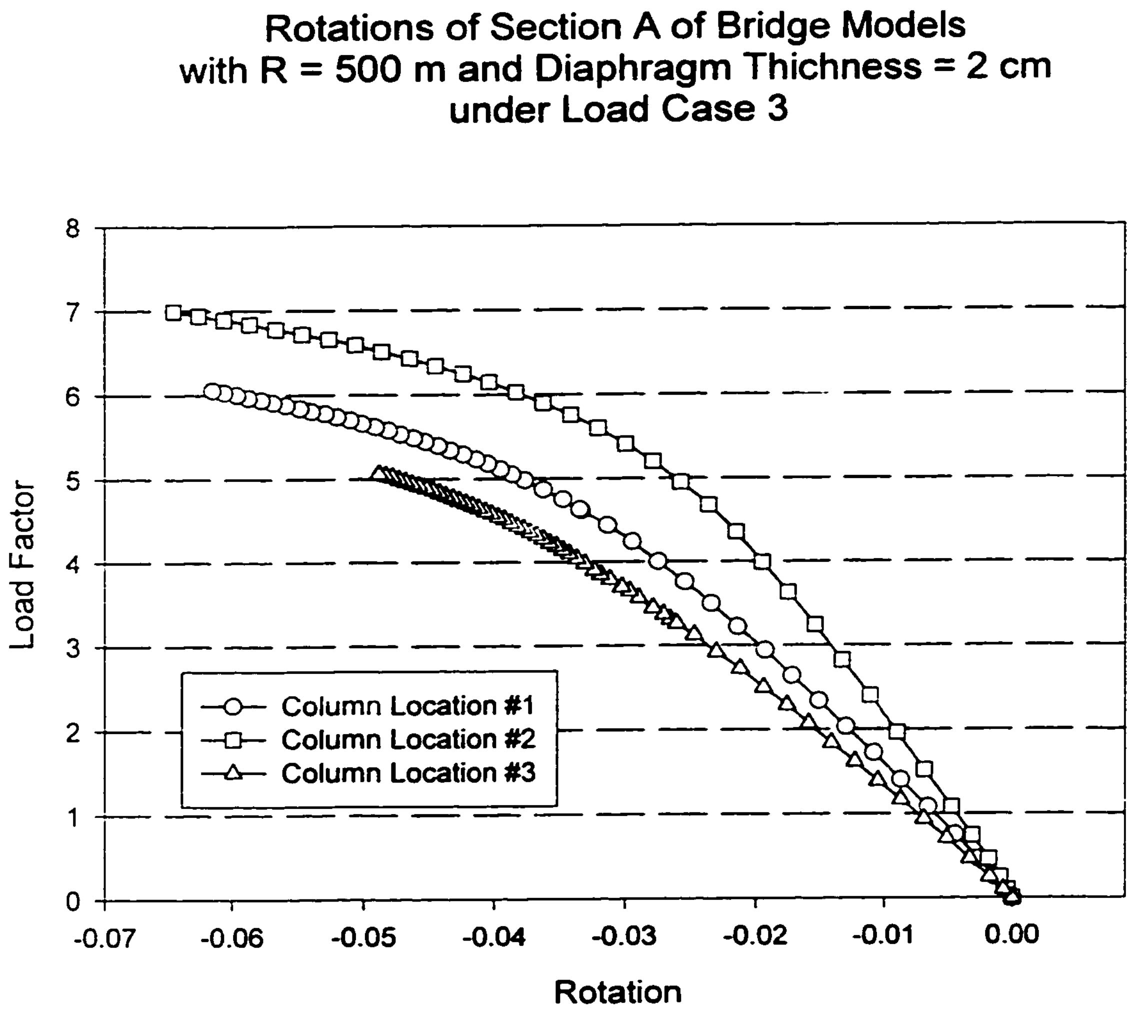

Figure 5.74. Rotations at Section A of Bridge Models with Various Column Locations and R=500m under Load Case 3

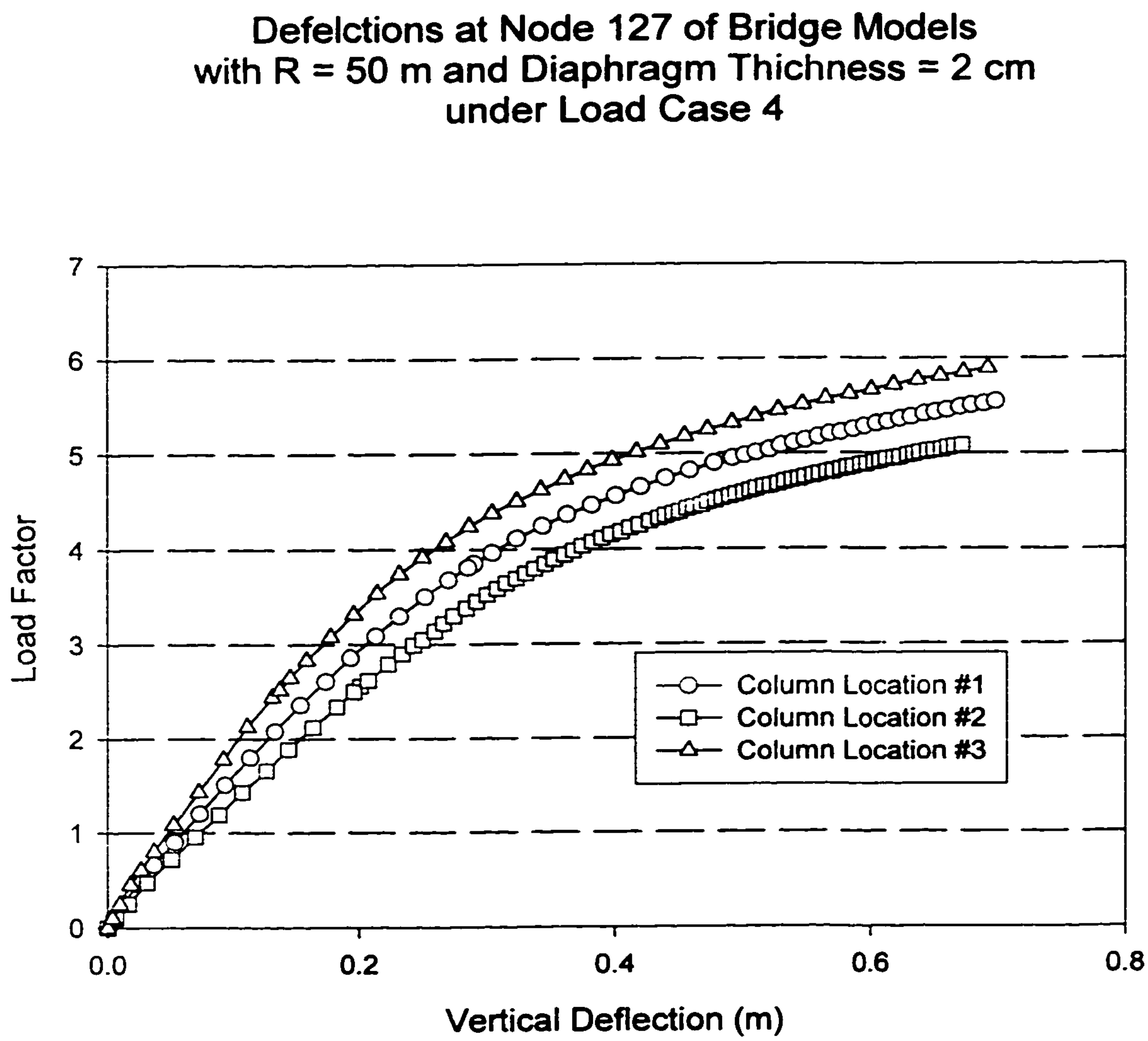

Figure 5.75a Deflections of Node 127 of Bridge Models with Various Column Locations and R=50m under Load Case 4

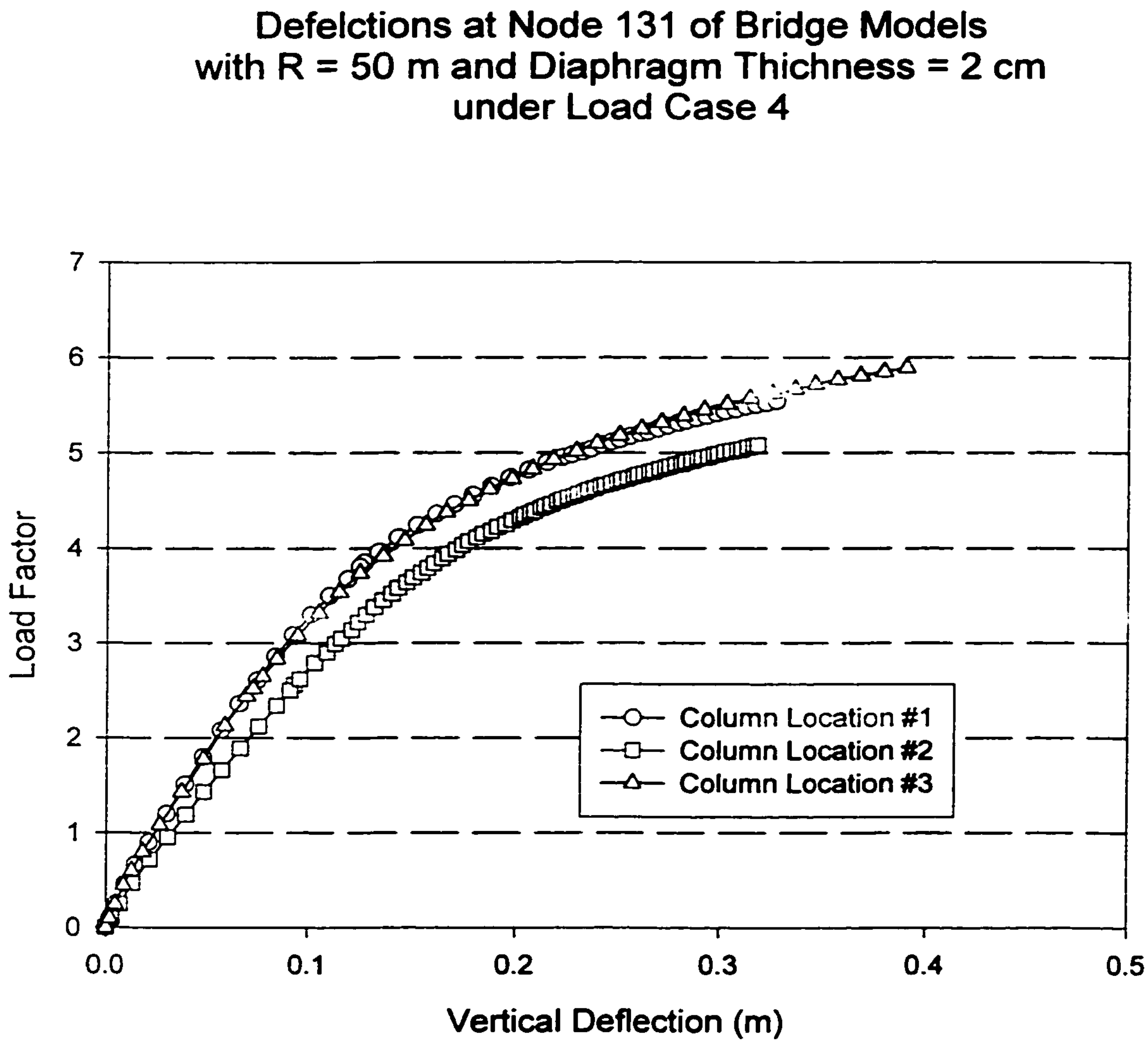

Figure 5.75b Deflections of Node 131 of Bridge Models with Various Column Locations and R=50m under Load Case 4

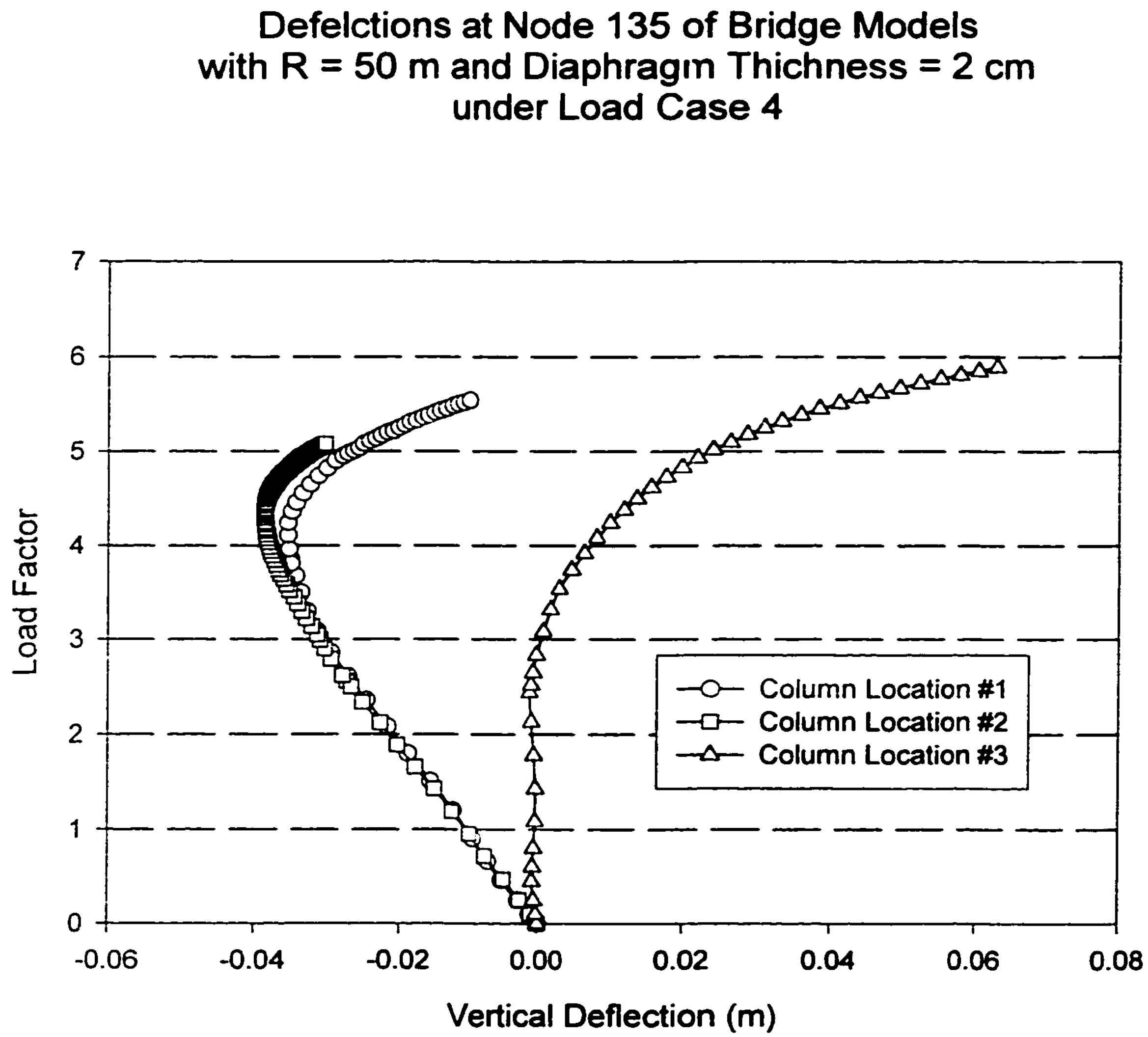

Figure 5.75c Deflections of Node 135 of Bridge Models with Various Column Locations and R=50m under Load Case 4

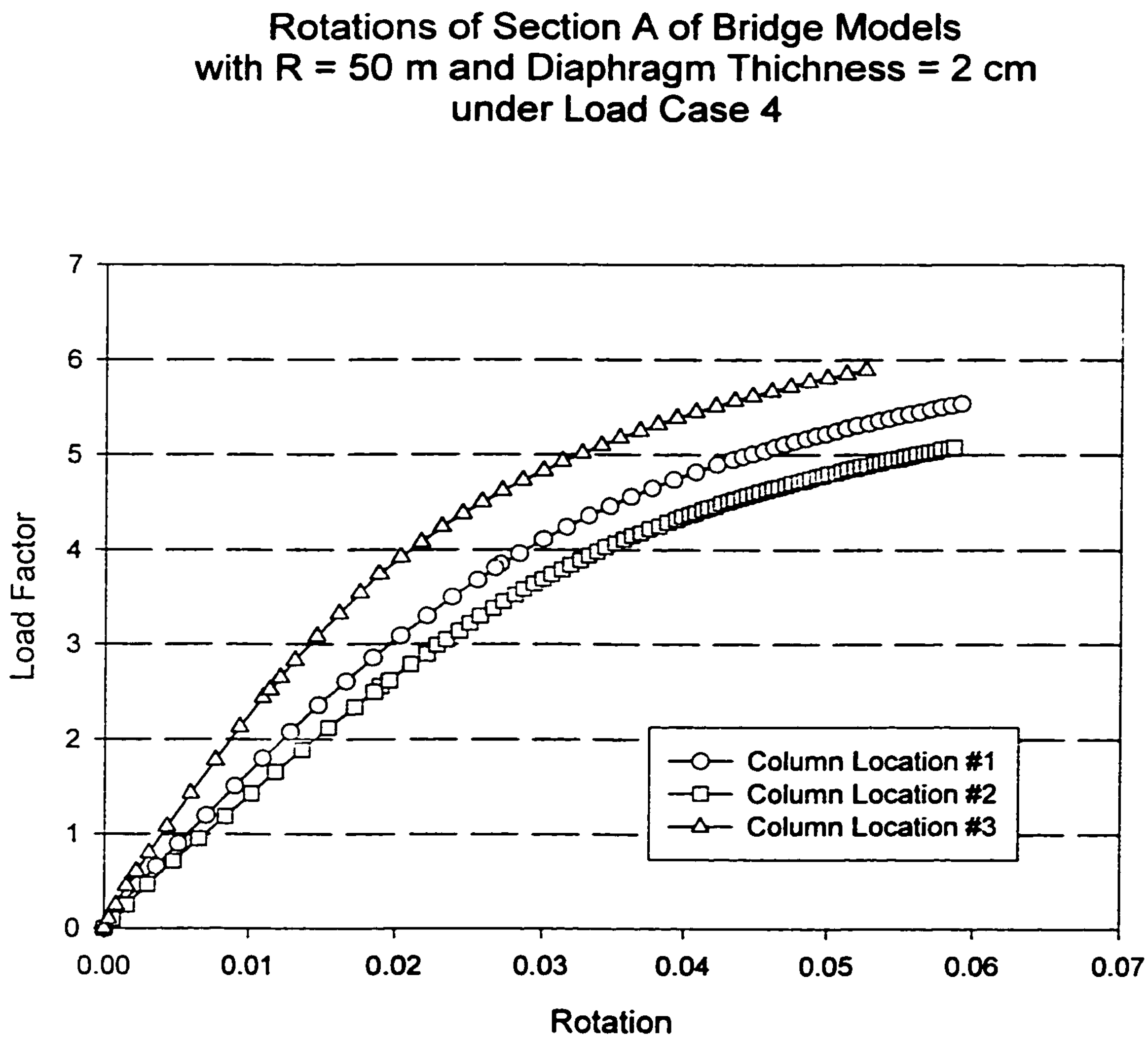

Figure 5.76. Rotations at Section A of Bridge Models with Various Column Locations and R=50m under Load Case 4

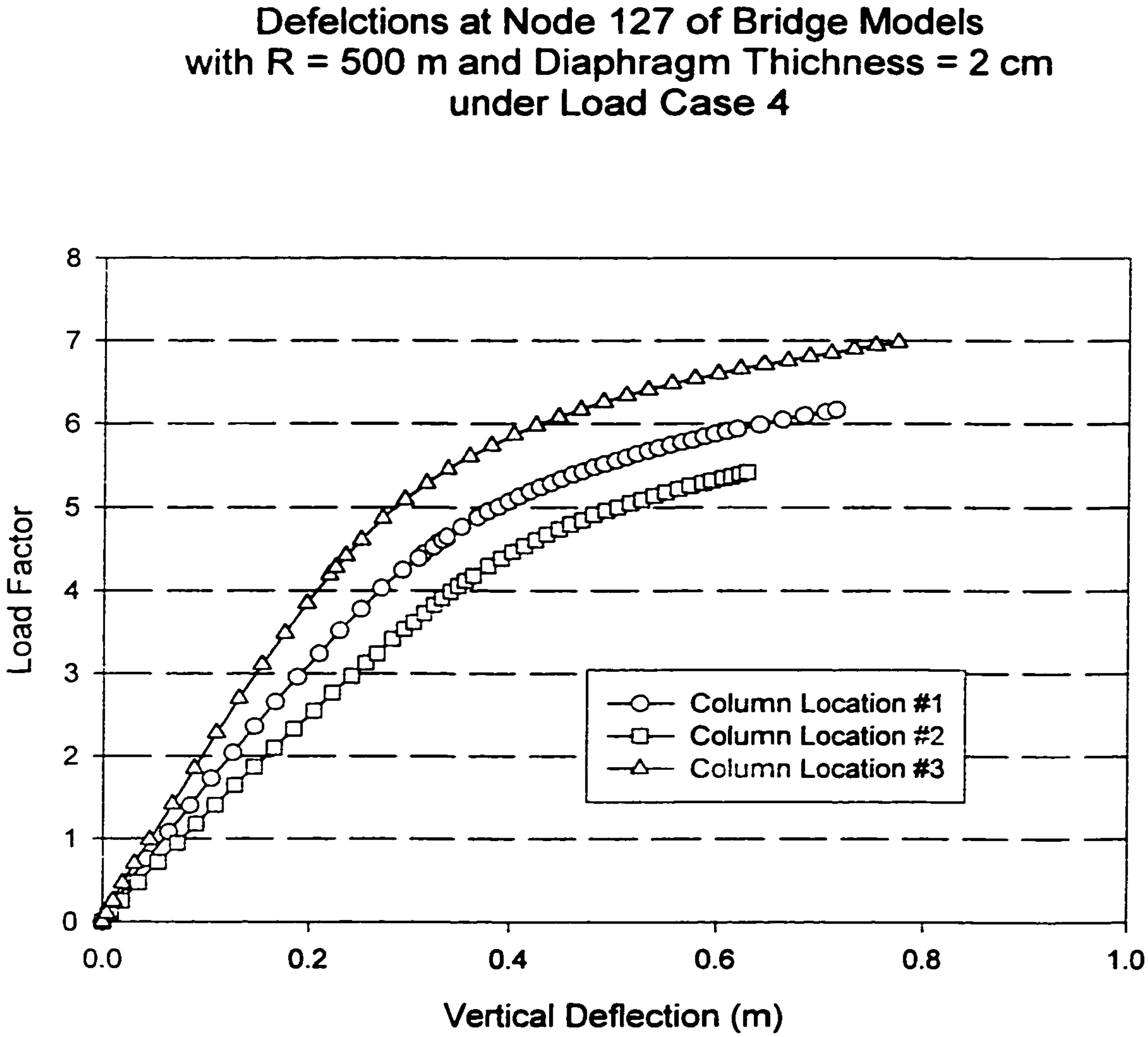

Figure 5.77a Deflections of Node 127 of Bridge Models with Various Column Locations and R=500m under Load Case 4

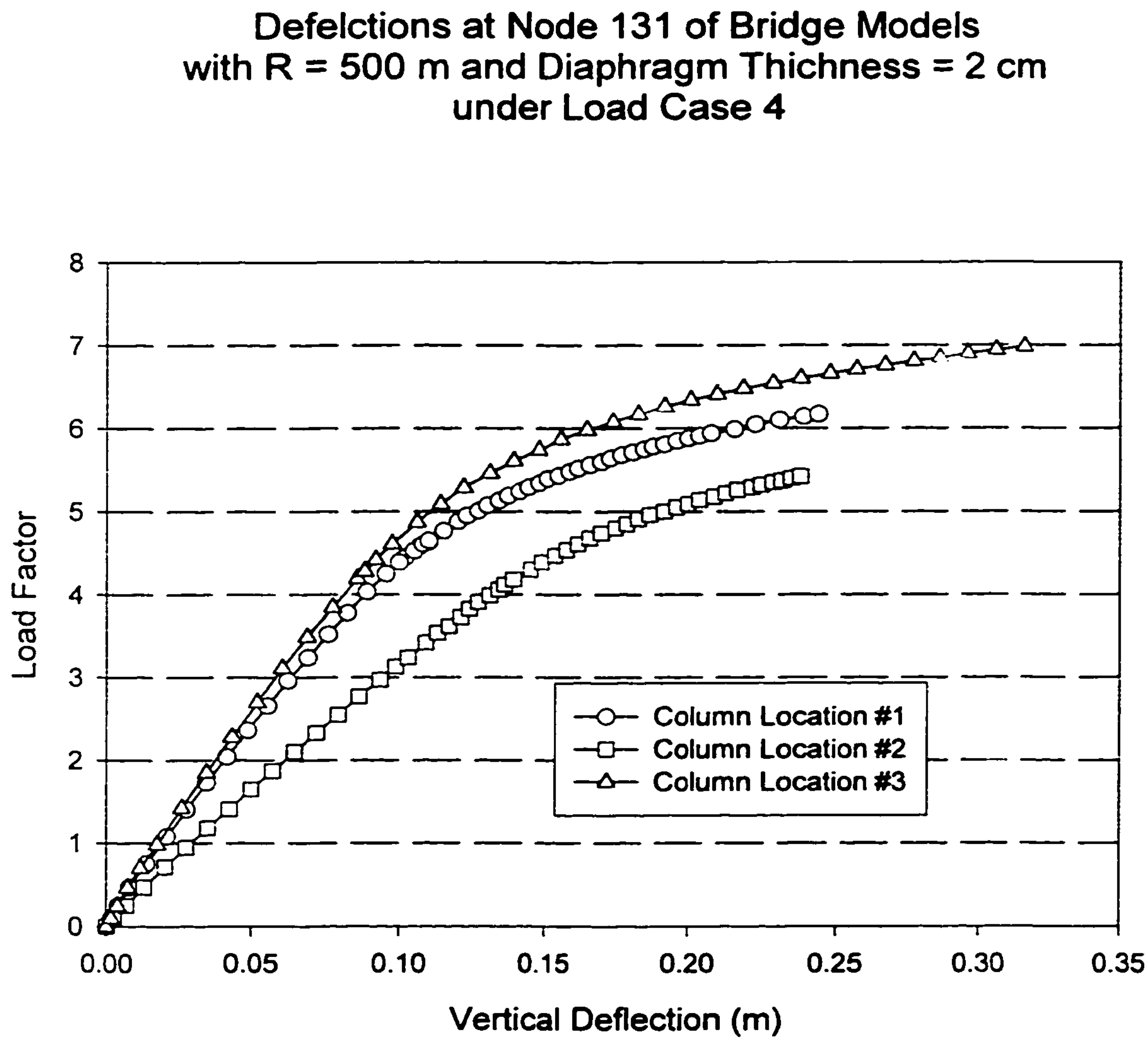

Figure 5.77b Deflections of Node 131 of Bridge Models with Various Column Locations and R=500m under Load Case 4

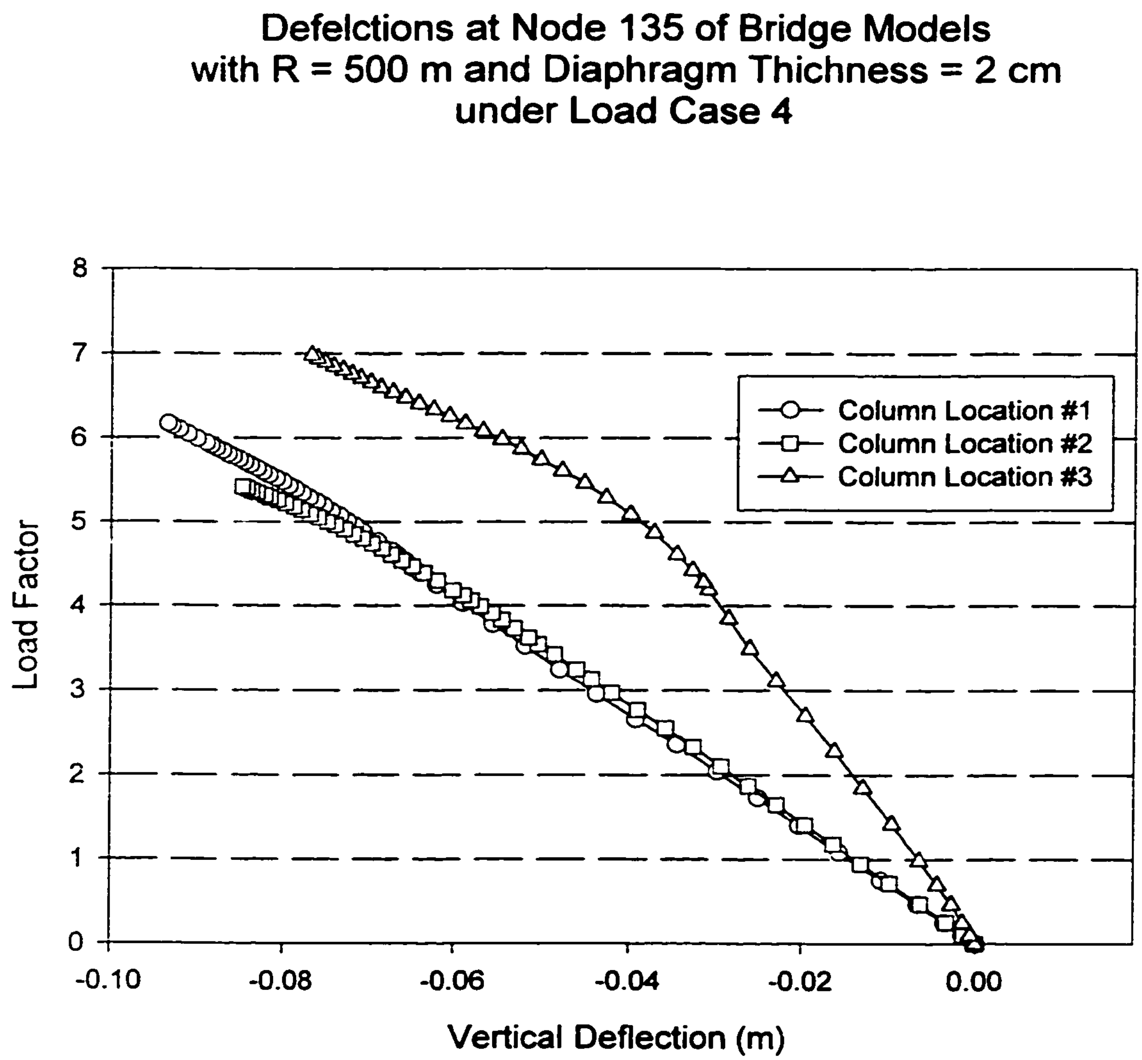

Figure 5.77c Deflections of Node 135 of Bridge Models with Various Column Locations and R=500m under Load Case 4

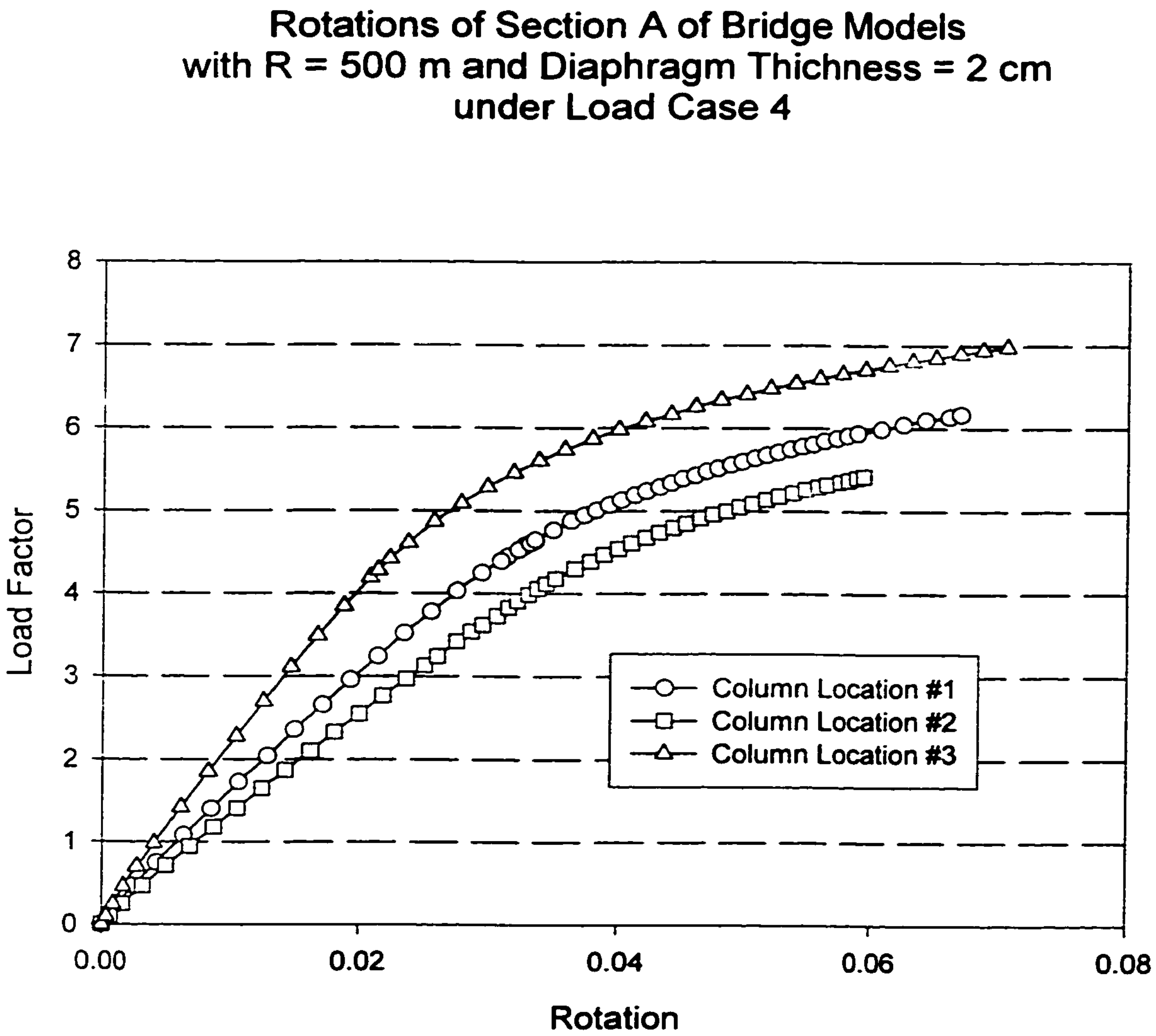

Figure 5.78. Rotations at Section A of Bridge Models with Various Column Locations and R=500m under Load Case 4

5.5. Influence of the bridge curvature and the L/R ratio

Four different radii of curvature of bridge models without intermediate diaphragms, namely, 50m, 100m, 200m, and 500m, were utilized in the analysis. The bridge longitudinal length from end to end is 72m with each span length of 36m. Therefore, their L/R ratios are 0.72, 0.36, 0.18, and 0.072 respectively. The middle column is located at Column Location 1. The thickness of the middle diaphragm is 0.02m for Load Cases 2 and is 0.08m for Load Case 1, the stiffness of the middle column is 1.26×10^{11} N/m, and the stiffness of regular shear connectors are used in the analysis. The effects on the bridge models are presented as follows based on two load cases.

Load Case 1

For bridge models with four radii of curvature under Load Case 1, vertical deflections at nodes 127, 131 and 135 are shown in Figures 5.79a, 5.79b and 5.79c. The rotation of section A is shown in Figure 5.80. The maximum deflection of the bridge model at section A is found at Node 127 of all bridge models with different curvature radii under Load Case 1. In Figure 5.79a, it can be seen that the bridge model with the curvature radius of 500m has the greatest ultimate load factor of about 5.4 and the bridge model with the curvature radius of 50m has the lowest ultimate load factor of about 4.5. In the elastic and inelastic regions, the bridge model with the curvature radius of 500m has the smallest rotation at section A under Load Case 1 (Figure 5.80). Figure 5.81 shows the relationship of curvature radii and load factors at the yielding point and the ultimate state of bridge models. When L/R is less than 0.3, The changes of both the ultimate load factor and the yielding load factor are within 5% compared with the straight bridge.

When L/R is larger than 0.3, the ultimate load of the bridge model decreases rapidly as evidenced from Figure 5.81. When L/R reaches 0.7, the ultimate load of the bridge model drops by 20% in comparison with the ultimate load of the straight bridge.

Load Case 2

For bridge models with four radii of curvature under Load Case 2, vertical deflections at nodes 127, 131 and 135 are shown in Figures 5.82a, 5.82b and 5.82c. The rotation of section A is shown in Figure 5.83. The maximum deflection of the bridge model at section A is found at Node 127 of all bridge models with different curvature radii under Load Case 2. In Figure 5.82a, it can be seen that the bridge model with the curvature radius of 500m has the greatest ultimate load factor of about 5.3 and the bridge model with the curvature radius of 50m has the lowest ultimate load factor of about 4.0. In the elastic and inelastic regions, the bridge model with the curvature radius of 500m has the smallest rotation at section A (Figure 5.83) at the same load level under Load Case 2. From Figure 5.82a, it can also be seen that the bridge models with the curvature radii of 50m, 100m, 200m and 500m start to yield at the load factors of about 2.6, 3.3, 3.8 and 4.2. Figure 5.84 shows the relationship of curvature radii and load factors at the yielding point and the ultimate state of the bridge model. When L/R is less than 0.2, The change of the ultimate load factor is within 5% compared with the straight bridge, although the yielding load factor of the bridge model decreases by 10%. When L/R is larger than 0.2, the ultimate load of the bridge model decreases faster, as can be seen from Figure 5.84. When L/R reaches 0.7, the ultimate load of the bridge model drops by about 30%, in comparison with the ultimate load of the straight bridge.

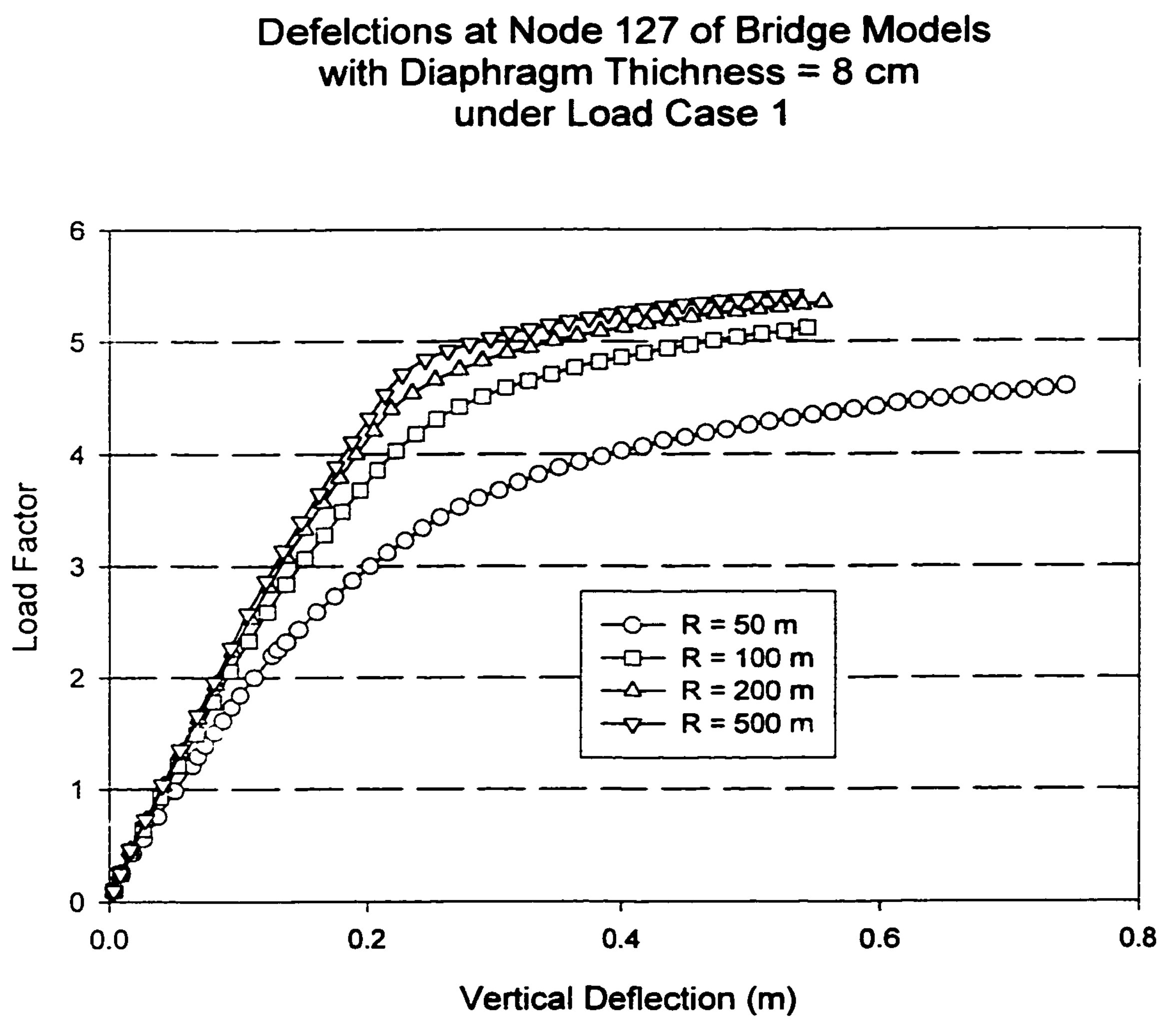

Figure 5.79a Deflections of Node 127 of Bridge Models with Various Radii of Curvature and Diaphragm Thickness=0.08m under Load Case 1

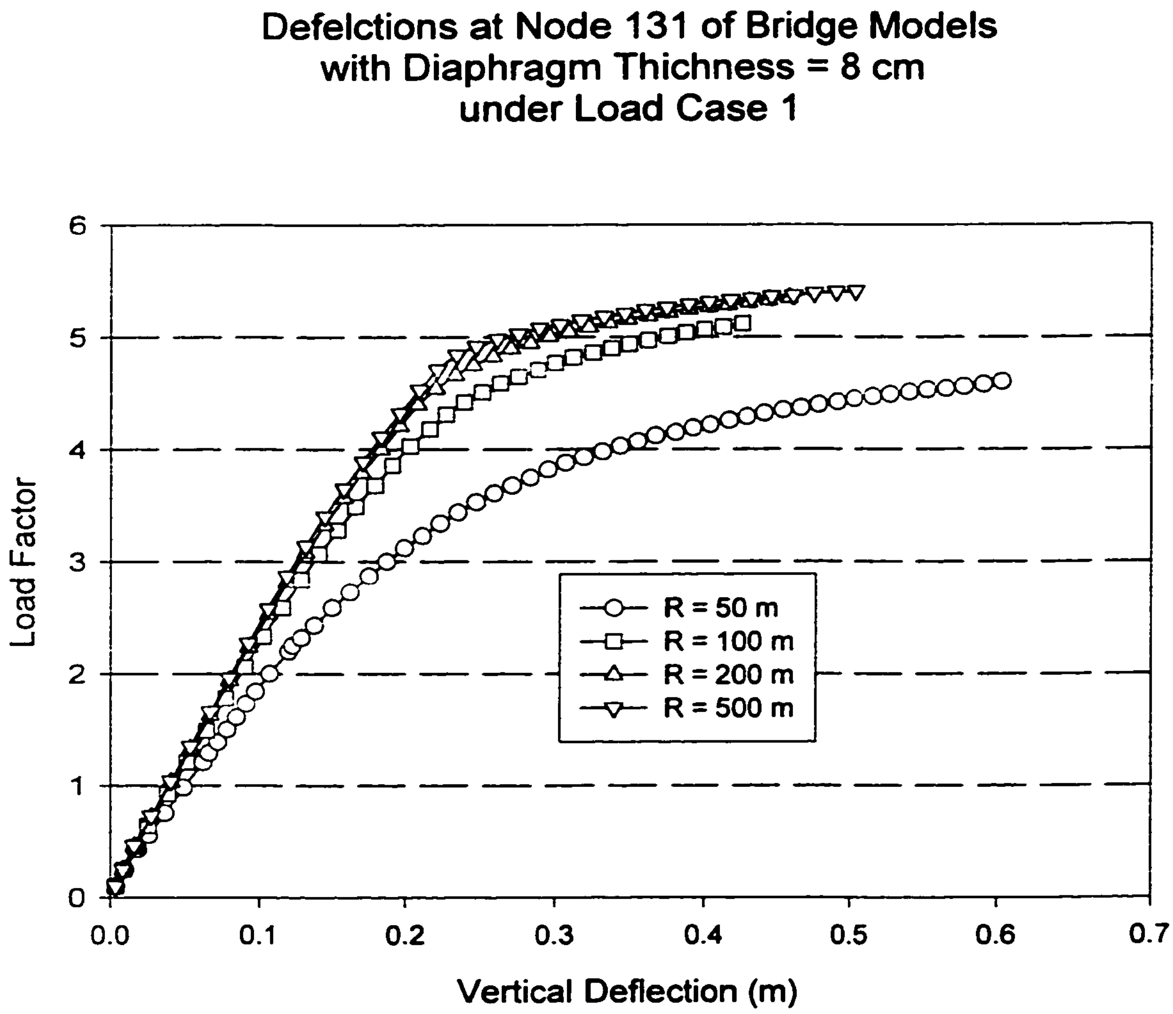

Figure 5.79b Deflections of Node 131 of Bridge Models with Various Radii of Curvature and Diaphragm Thickness=0.08m under Load Case 1

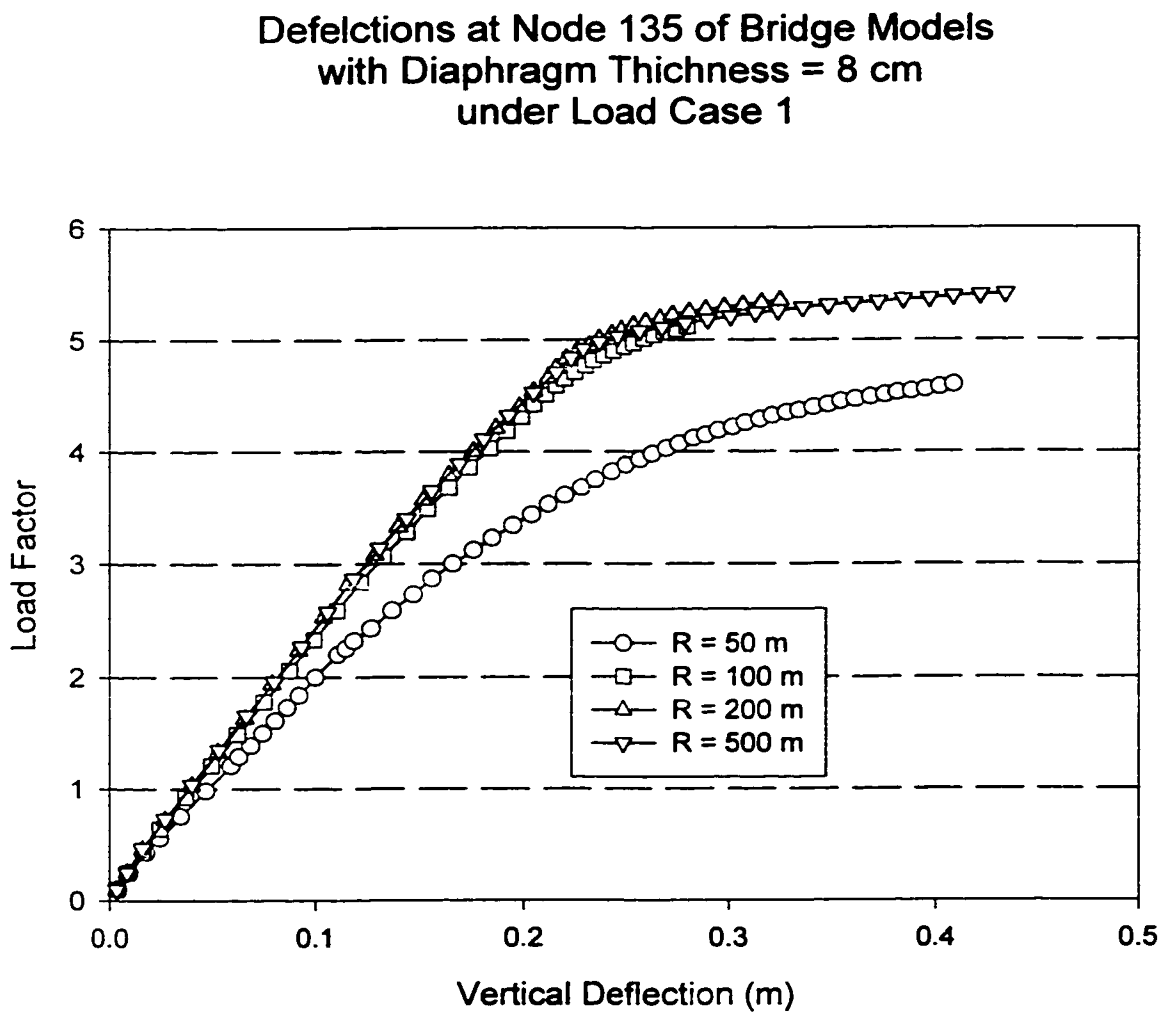

Figure 5.79c Deflections of Node 135 of Bridge Models with Various Radii of Curvature and Diaphragm Thickness=0.08m under Load Case 1

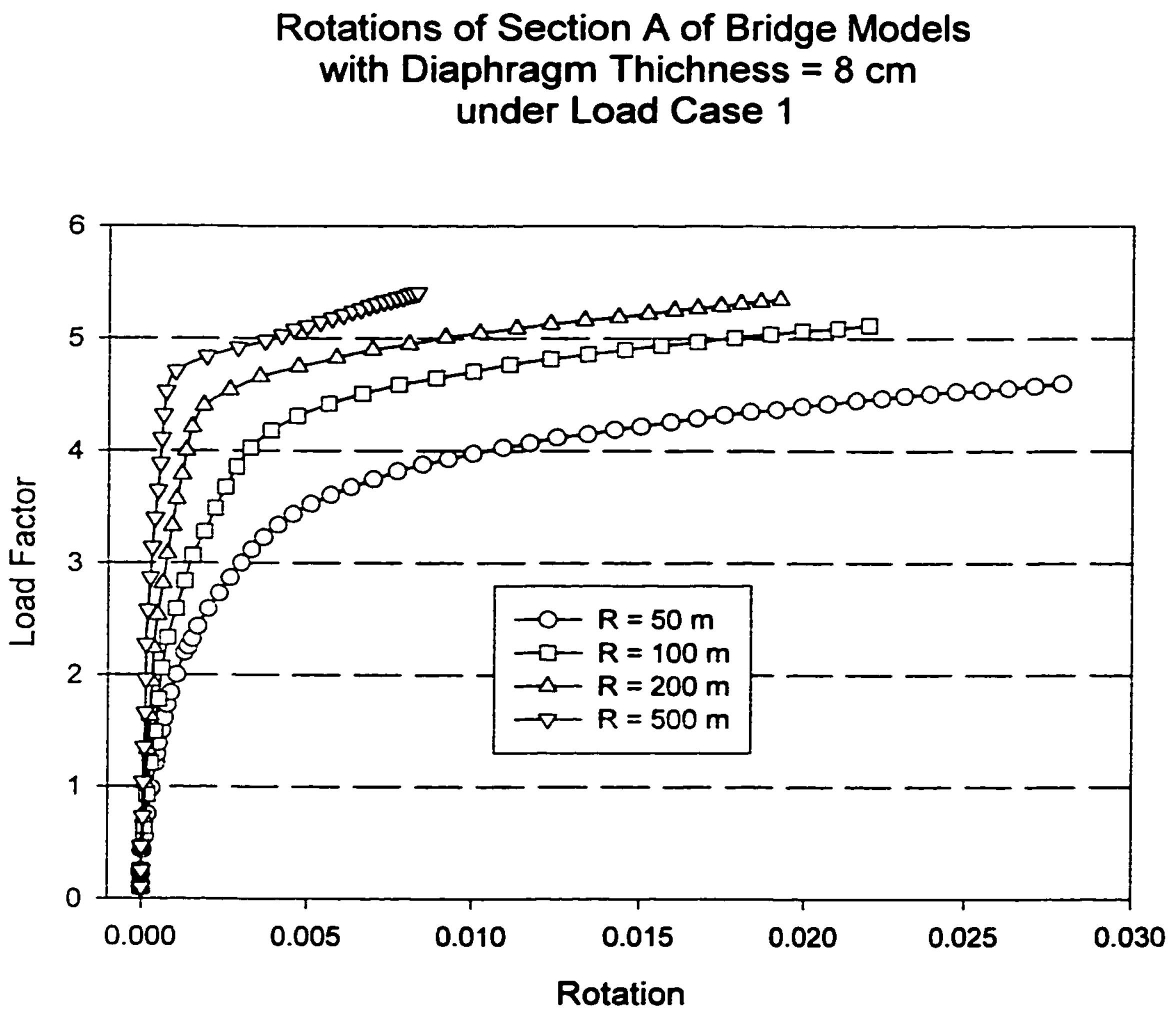

Figure 5.80. Rotations at Section A of Bridge Models with Various Radii of Curvature and Diaphragm Thickness=0.08m under Load Case 1

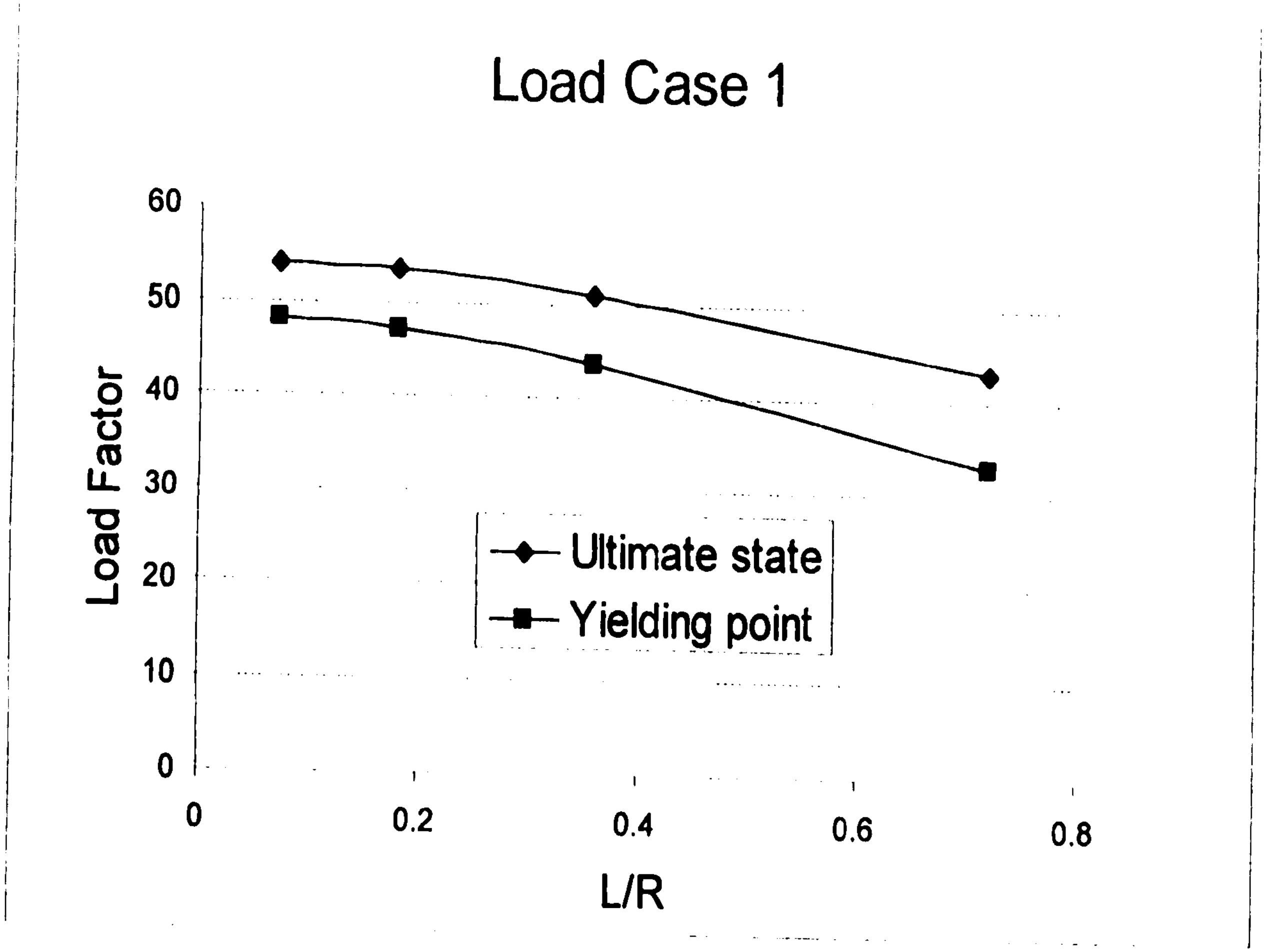

Figure 5.81 The relationship of L/R and Load Factor of the bridge models under Load Case 1

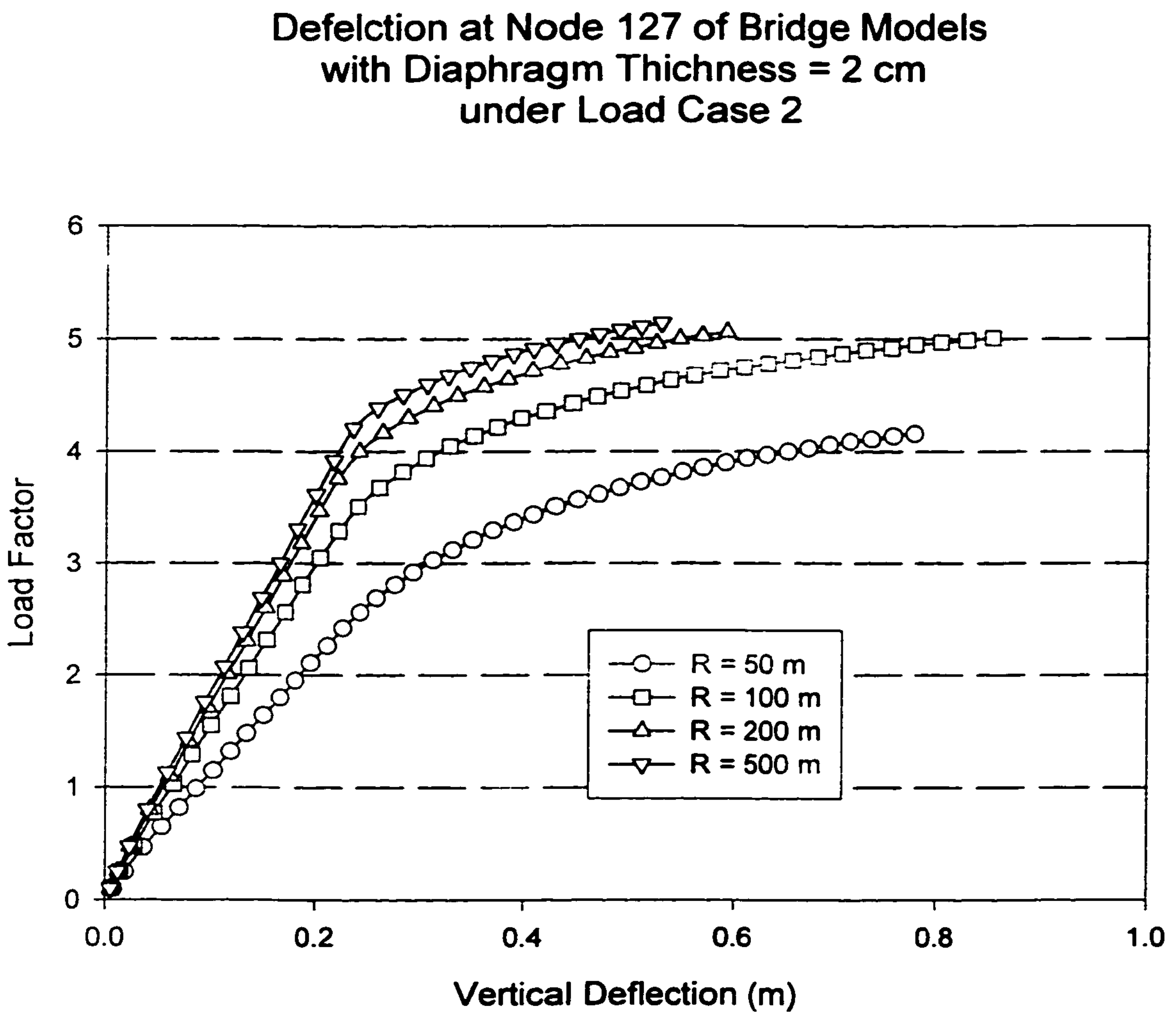

Figure 5.82a Deflections of Node 127 of Bridge Models with Various Radii of Curvature and Diaphragm Thickness=0.02m under Load Case 2

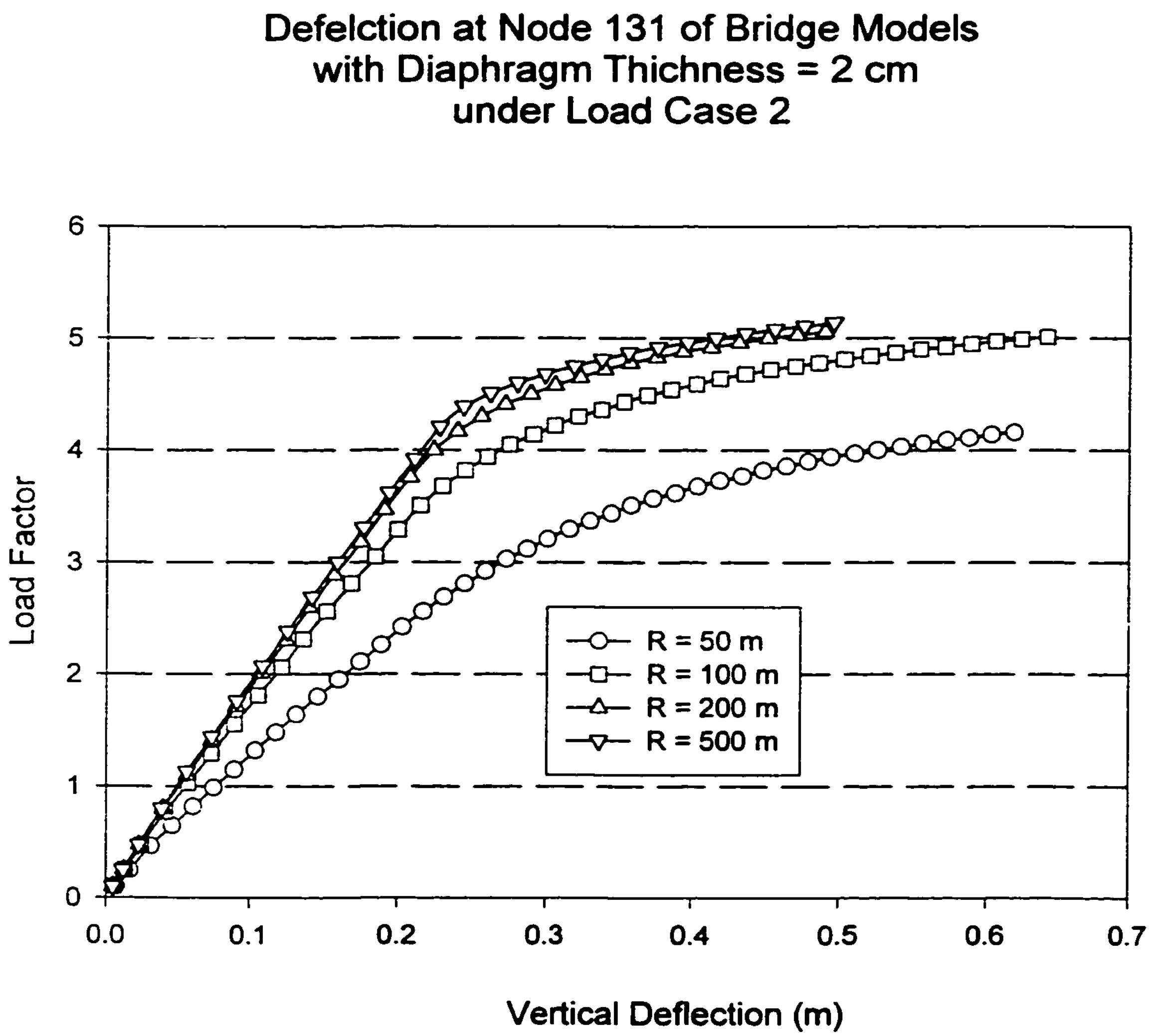

Figure 5.82b Deflections of Node 131 of Bridge Models with Various Radii of Curvature and Diaphragm Thickness=0.02m under Load Case 2

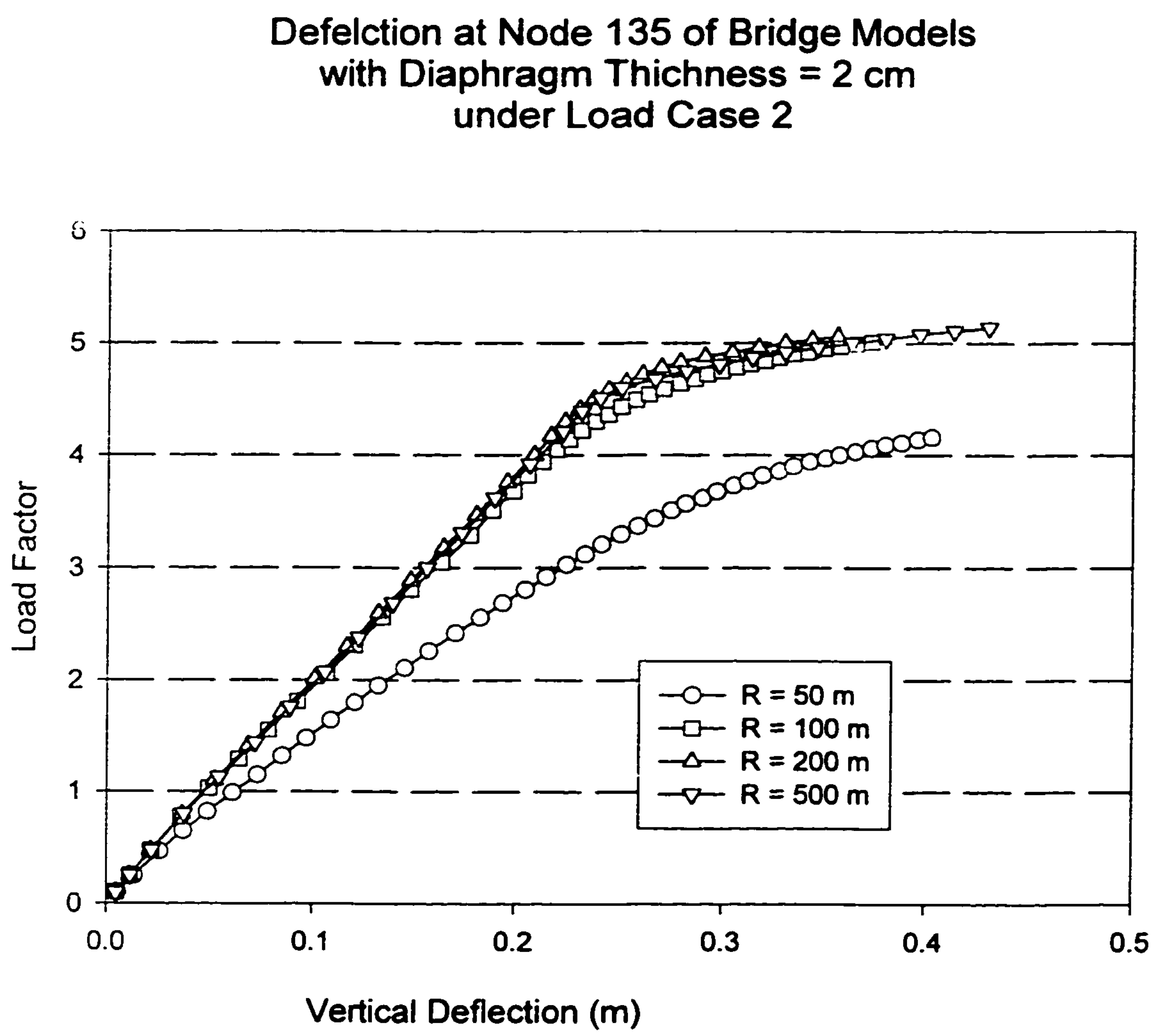

Figure 5.82c Deflections of Node 135 of Bridge Models with Various Radii of Curvature and Diaphragm Thickness=0.02m under Load Case 2

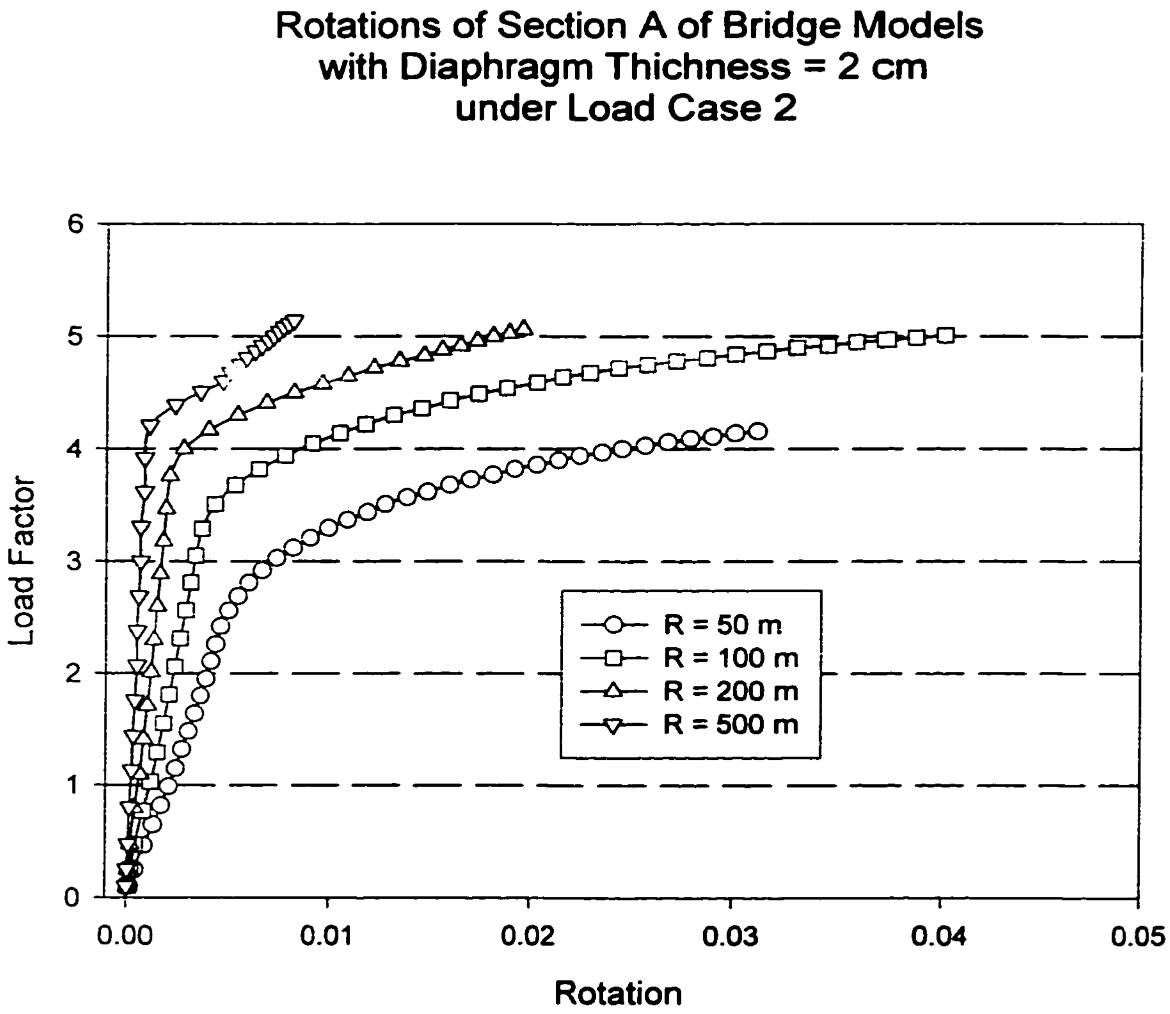

Figure 5.83. Rotations at Section A of Bridge Models with Various Radii of Curvature and Diaphragm Thickness=0.02m under Load Case 2

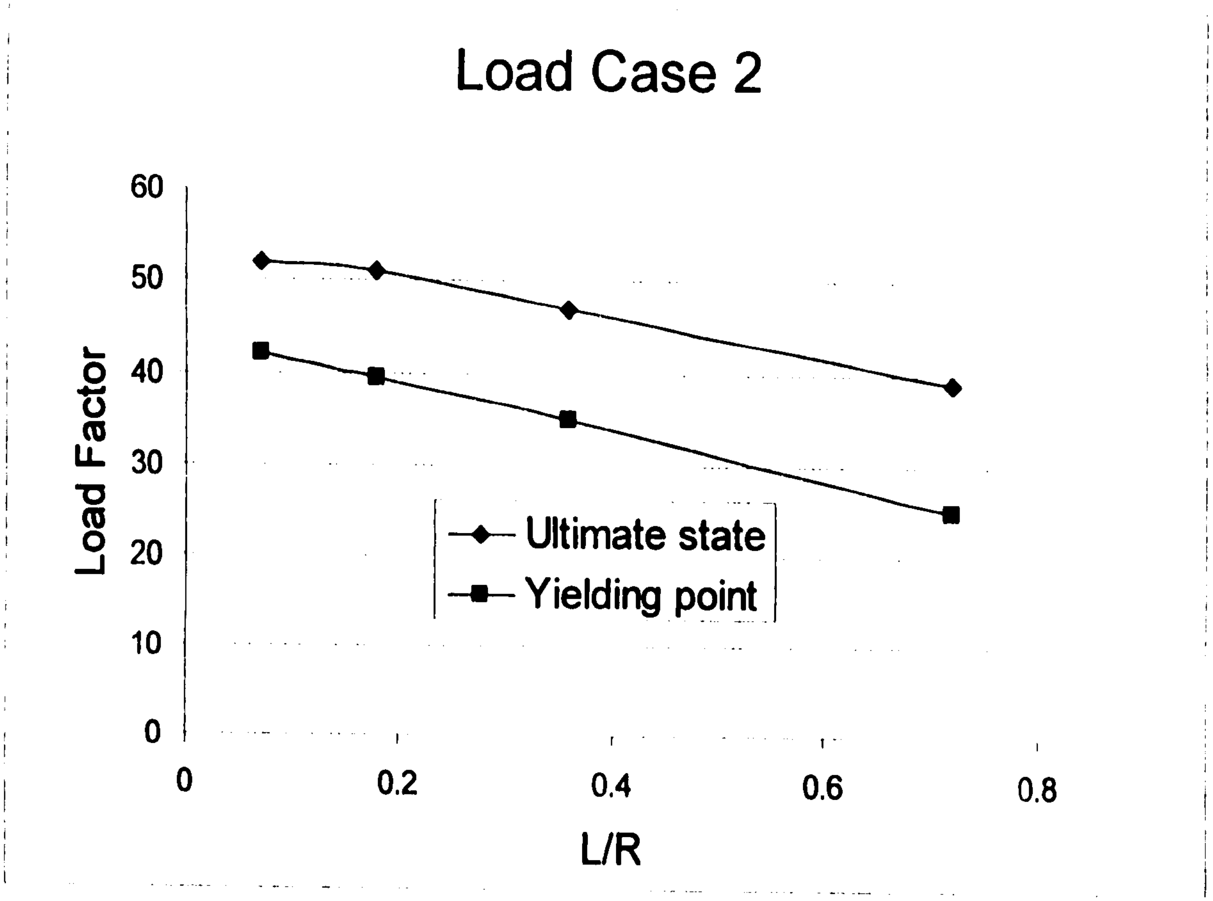

Figure 5.84 The relationship of L/R and Load Factor of the bridge models under Load Case 2

5.6.Influence of the stiffness of shear connectors

Two different connections were used between the deck and the box-girder of the bridge models without intermediate diaphragms. One was the rigid connection. The other was the connection by the regular shear connectors, which were designed and verified based on the OHBDC. Two radii of curvature of bridge models were used, which were 50m and 500m. The purpose is to observe the behaviors of bridge models with different radii of curvature. The thickness of 0.08m of the middle diaphragm was used for Load Case 1, while the thickness of 0.02m of the middle diaphragm was used for Load Case 2. The stiffness of the middle column is 1.26×10^{11} N/m. Also, Column Location 1 of the middle column, and Load Cases 1 and 2 were used in the analysis. The effects on the bridge models are given as follows based on the two Load Cases.

Load Case 1

For bridge models with curvature radius of 50m, vertical deflections at node 127 under Load Case 1 are shown in Figure 5.85. The rotations of section A of the bridge models are shown in Figure 5.86. The maximum deflections of the bridge model at section A are found at Node 127 of all bridge models with different stiffness of shear connectors under Load Case 1. In Figure 5.85, it can be seen that the bridge model with rigid shear connectors has the greatest ultimate load factor of about 4.4. However, the bridge model with the regular shear connectors has the ultimate load factor of about 4.3. Therefore, the ultimate load of the bridge model under Load Case 1 is almost unaffected by these two different kinds of shear connectors. In the elastic and inelastic regions, the bridge model with the regular shear connectors has the smallest rotation at section A at the same load level under Load Case 1 (Figure 5.86).

For bridge models with curvature radius of 500m, vertical deflections at node 127 under Load Case 1 are shown in Figure 5.87. The rotation of section A is shown in Figure 5.88. The maximum deflection of the bridge model at section A is found at Node 127 of all bridge models with different stiffness of shear connectors under Load Case 1. In Figure 5.87, it can be seen that the bridge model with the rigid shear connectors has the greatest ultimate load factor of about 5.6. However, the bridge model with the regular shear connectors has the ultimate load factor of about 5.4. Therefore, the ultimate load of the bridge model under Load Case 1 is almost unaffected by these two different kinds of shear connectors. It can also be seen that the bridge model with the rigid shear connectors and the regular shear connectors starts to yield at the load factors of 4.8 and 4.6 respectively. In the elastic region, the bridge model with the regular shear connectors has the smallest rotation at section A at the same load level under Load Case 1 (Figure 5.88). However, in the inelastic region, the bridge model with the rigid shear connectors has the smallest rotation at section A at the same load level under Load Case 1.

Load Case 2

For bridge models with curvature radius of 50m, vertical deflections at node 127 under Load Case 2 are shown in Figure 5.89. The rotation of section A is shown in Figure 5.90. The maximum deflection of the bridge model at section A is found at Node 127 of all bridge models with different stiffness of shear connectors under Load Case 2. In Figure 5.89, it can be seen that the bridge model with the rigid shear connectors has the greatest ultimate load factor of about 4.2. However, the bridge model with the regular shear connectors has the ultimate load factor of about 4.1. Therefore, the ultimate load of the bridge model under Load Case 2 is again almost unaffected by these two different kinds of shear connectors. It can also be seen that the bridge model with the rigid shear connectors and the regular shear connectors starts to yield at the load factors of 2.8 and 2.7 respectively. In the elastic and inelastic regions (Figure 5.90), the bridge model with the regular shear connectors has the smallest rotation at section A at the same load level under Load Case 2.

For bridge models with curvature radius of 500m, vertical deflections at node 127 under Load Case 2 are shown in Figure 5.91. The rotation of section A is shown in Figure 5.92. The maximum deflection of the bridge model at section A is found at Node 127 of all bridge models with different stiffness of shear connectors under Load Case 2. In Figure 5.91, it can be seen that the bridge model with rigid shear connectors has the greatest ultimate load factor of about 5.2. However, the bridge model with the regular shear connectors has the ultimate load factor of about 5.1. Therefore, the ultimate load of the bridge model under Load Case 2 is almost unaffected by these two different kinds of shear connectors. It can also be seen that the bridge model with the rigid shear connectors and the regular shear connectors starts to yield at the load factors of 4.2 and 4.1 respectively. In the elastic region (Figure 5.92), the bridge model with the regular shear connectors has the smallest rotation at section A at the same load level under Load Case 2. However, in the inelastic region, two bridge models have the same rotation at section A at the same load level under Load Case 2.

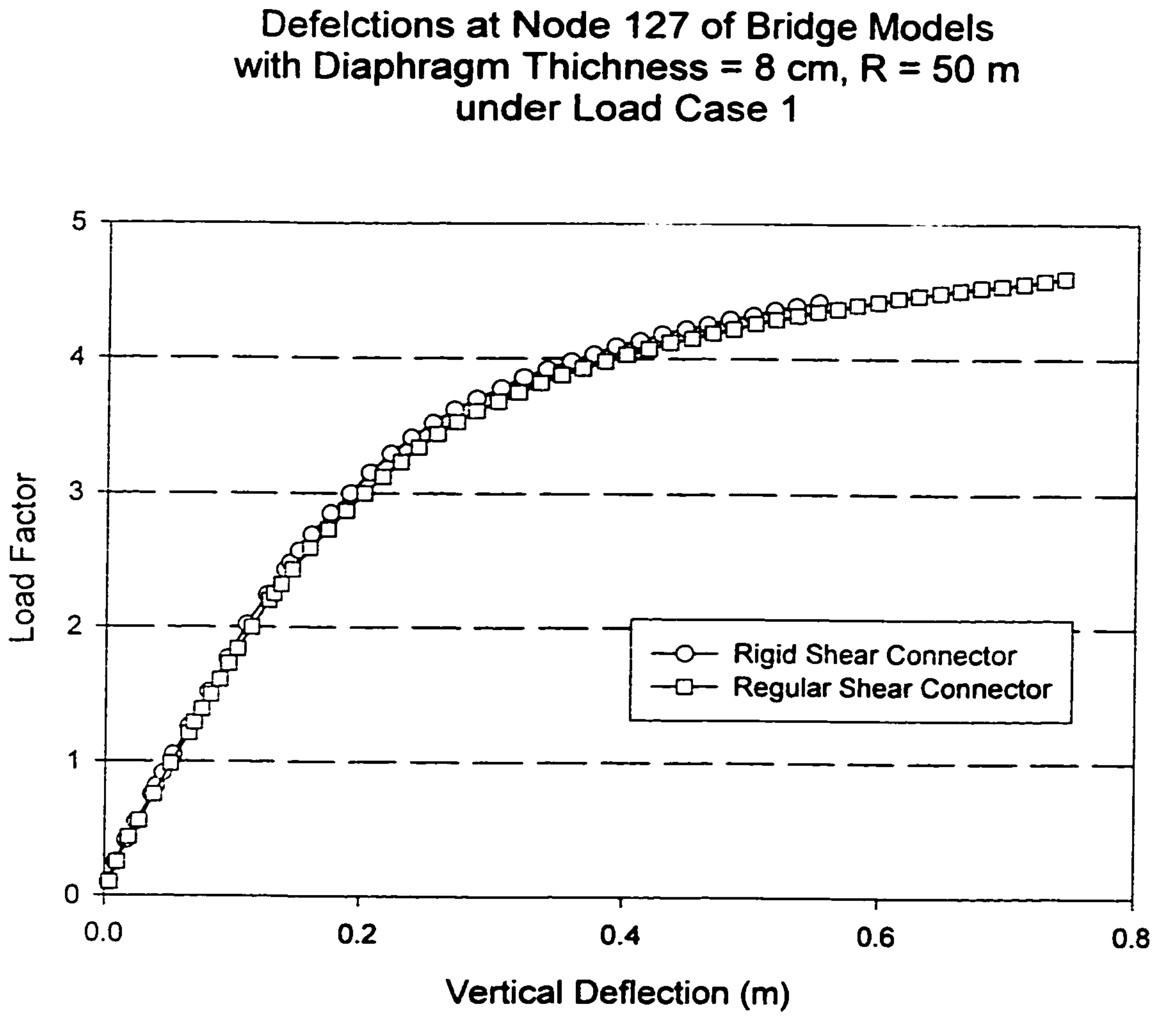

Figure 5.85 Deflections of Node 127 of Bridge Models with Various Stiffnesses of shear connectors, Diaphragm Thickness=0.08m and R=50m under Load Case 1

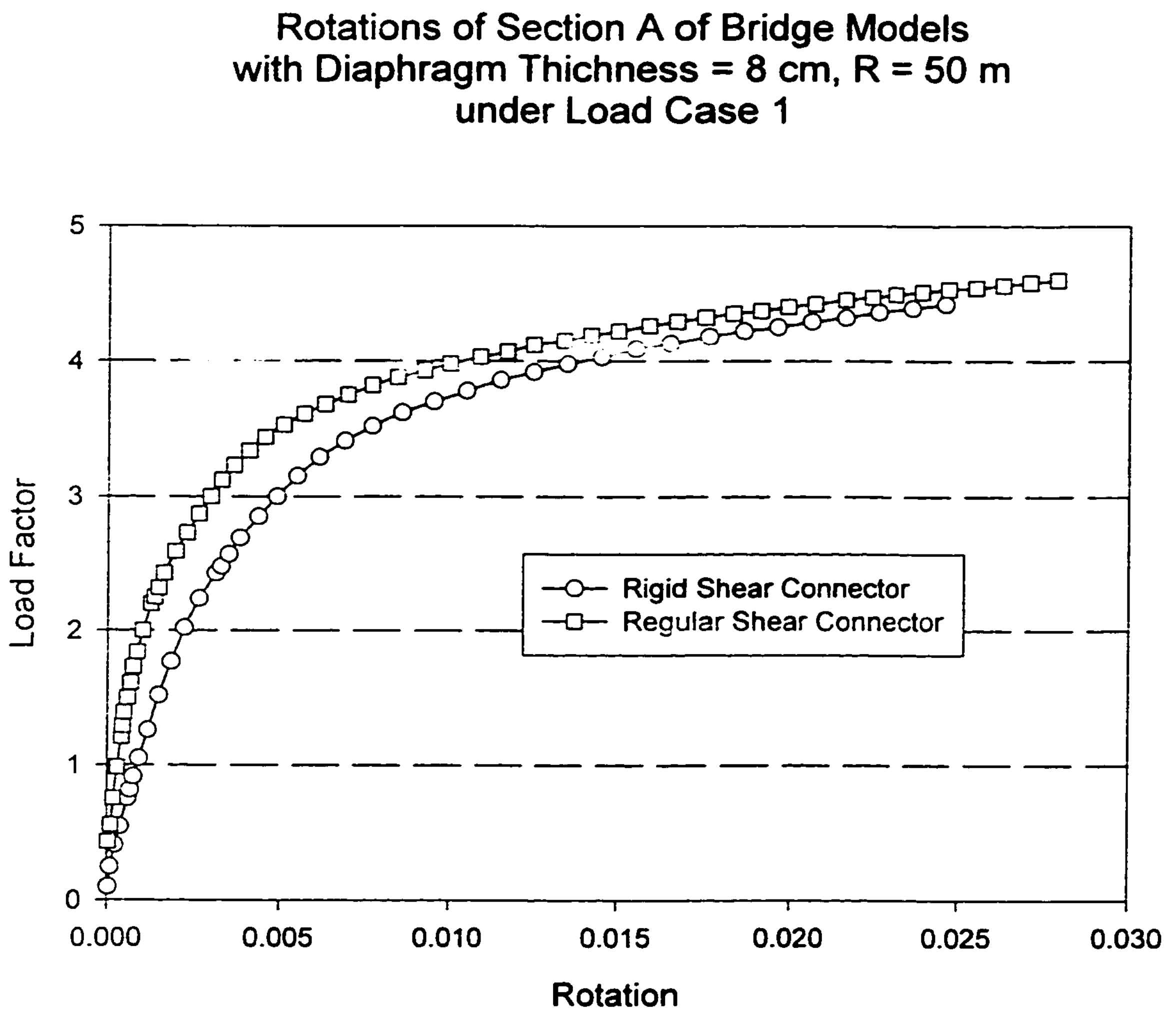

Figure 5.86. Rotations at Section A of Bridge Models with Various Stiffnesses of shear connectors, Diaphragm Thickness=0.08m and R=50m under Load Case 1

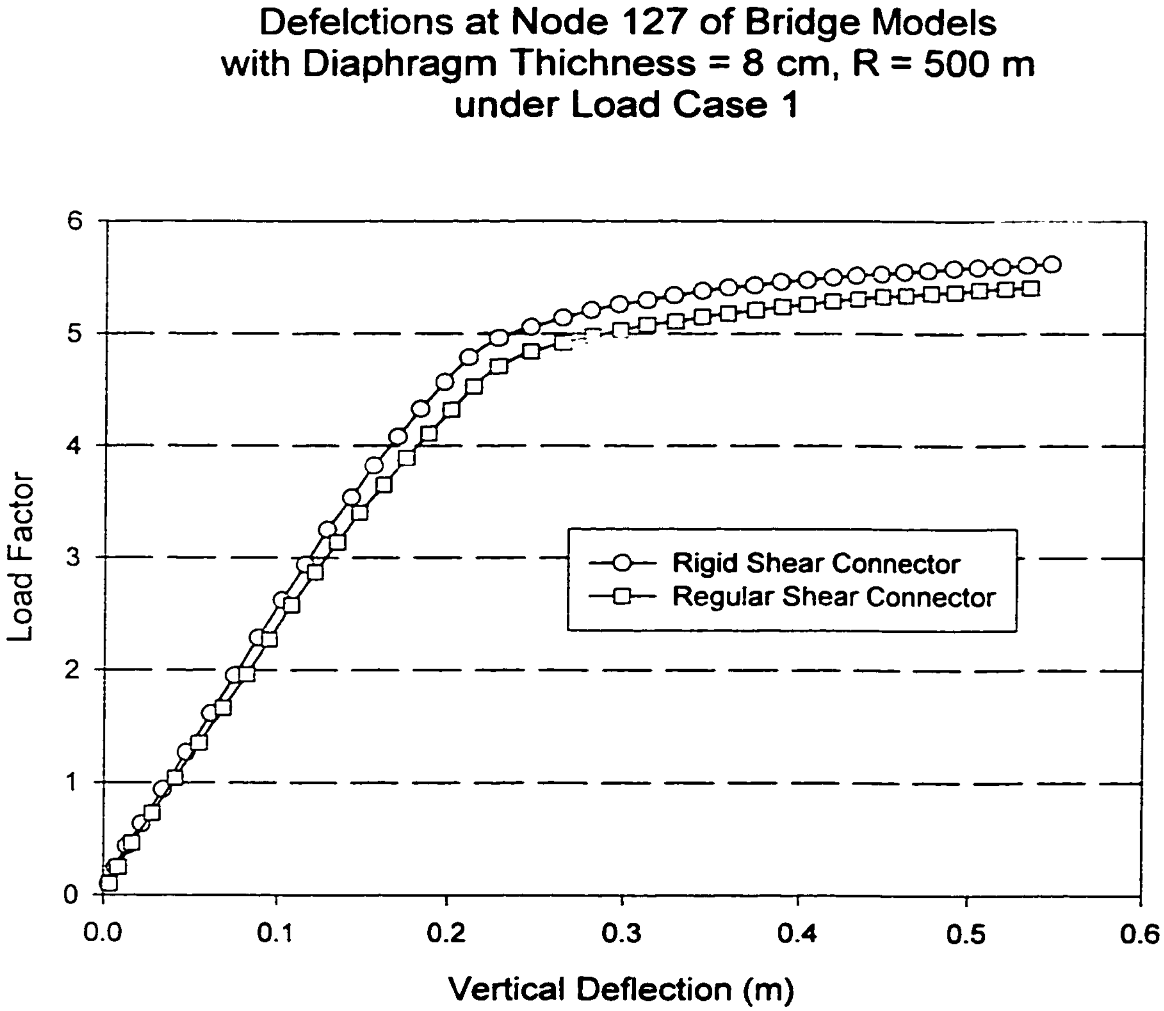

Figure 5.87 Deflections of Node 127 of Bridge Models with Various Stiffnesses of shear connectors, Diaphragm Thickness=0.08m and R=500m under Load Case 1

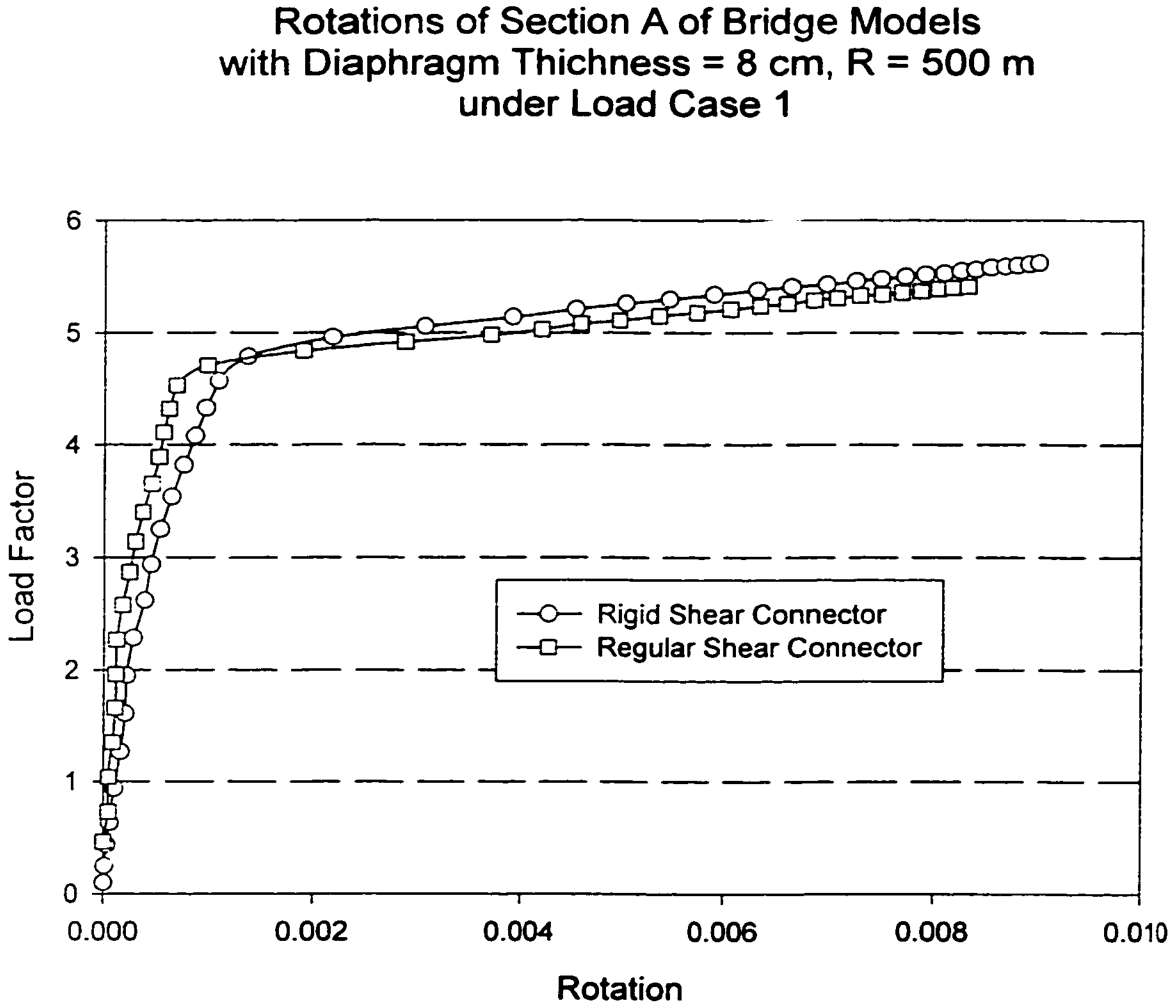

Figure 5.88. Rotations at Section A of Bridge Models with Various Stiffnesses of shear connectors, Diaphragm Thickness=0.08m and R=500m under Load Case 1

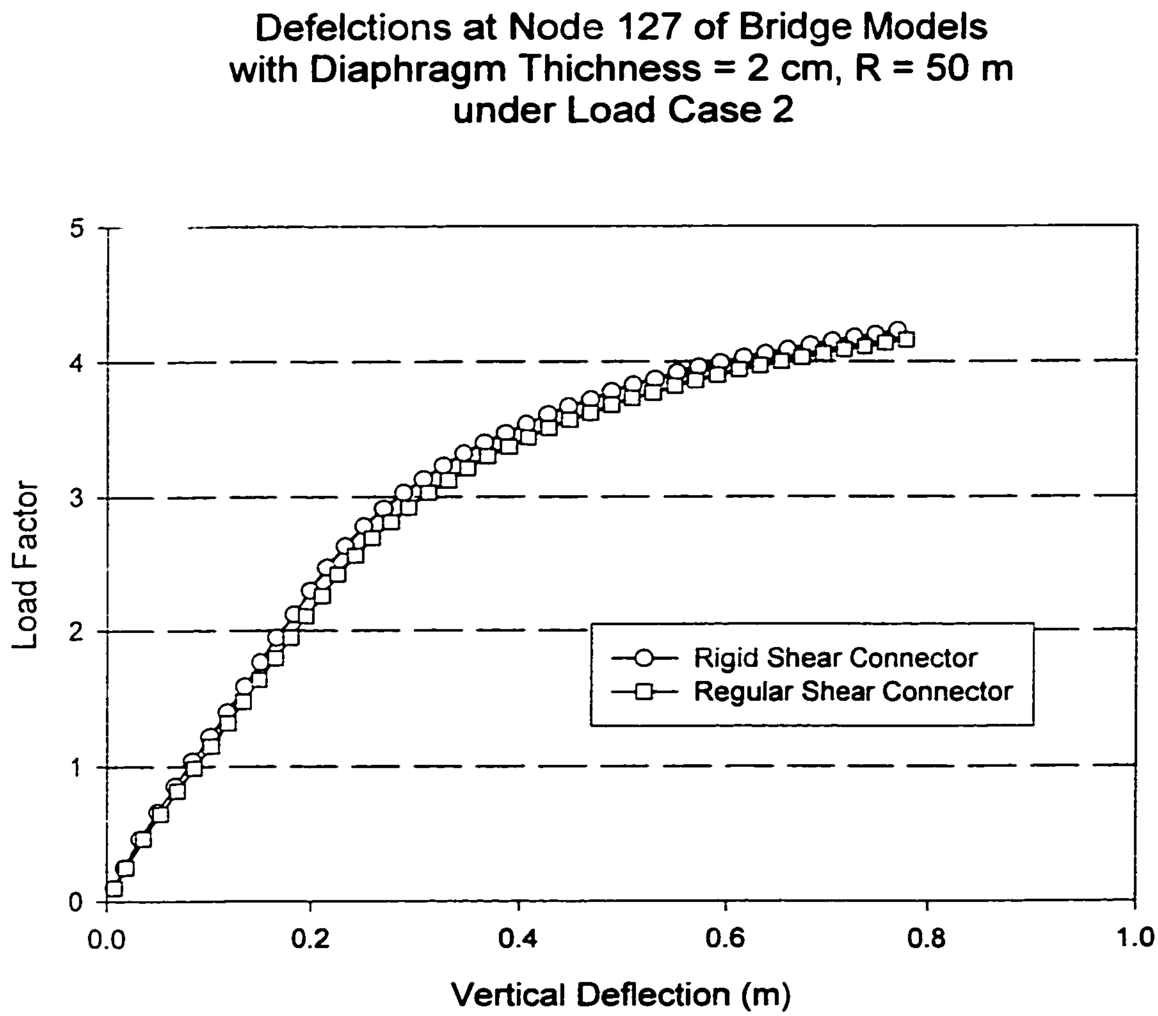

Figure 5.89 Deflections of Node 127 of Bridge Models with Various Stiffnesses of shear connectors, Diaphragm Thickness=0.02m and R=50m under Load Case 2

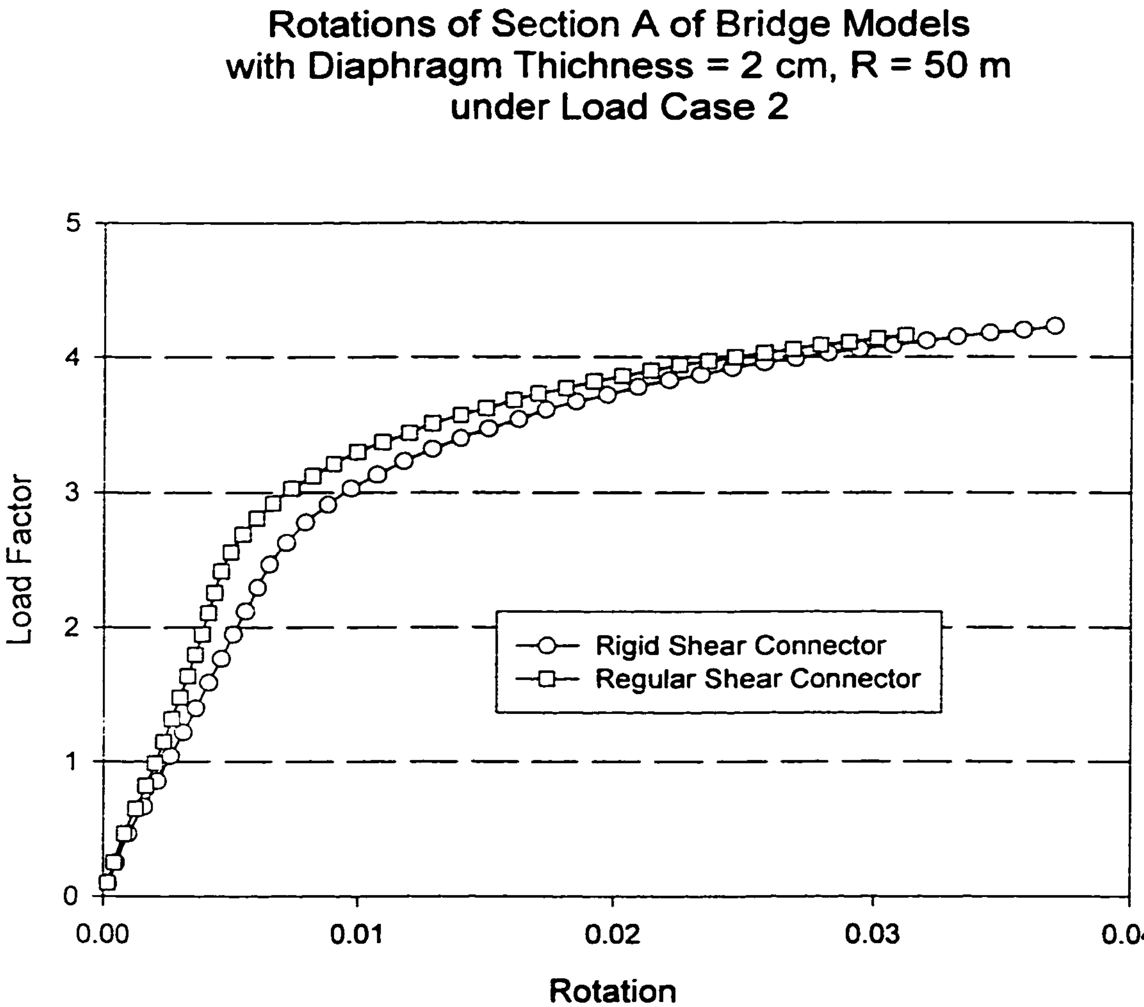

Figure 5.90. Rotations at Section A of Bridge Models with Various Stiffnesses of shear connectors, Diaphragm Thickness=0.02m and R=50m under Load Case 2

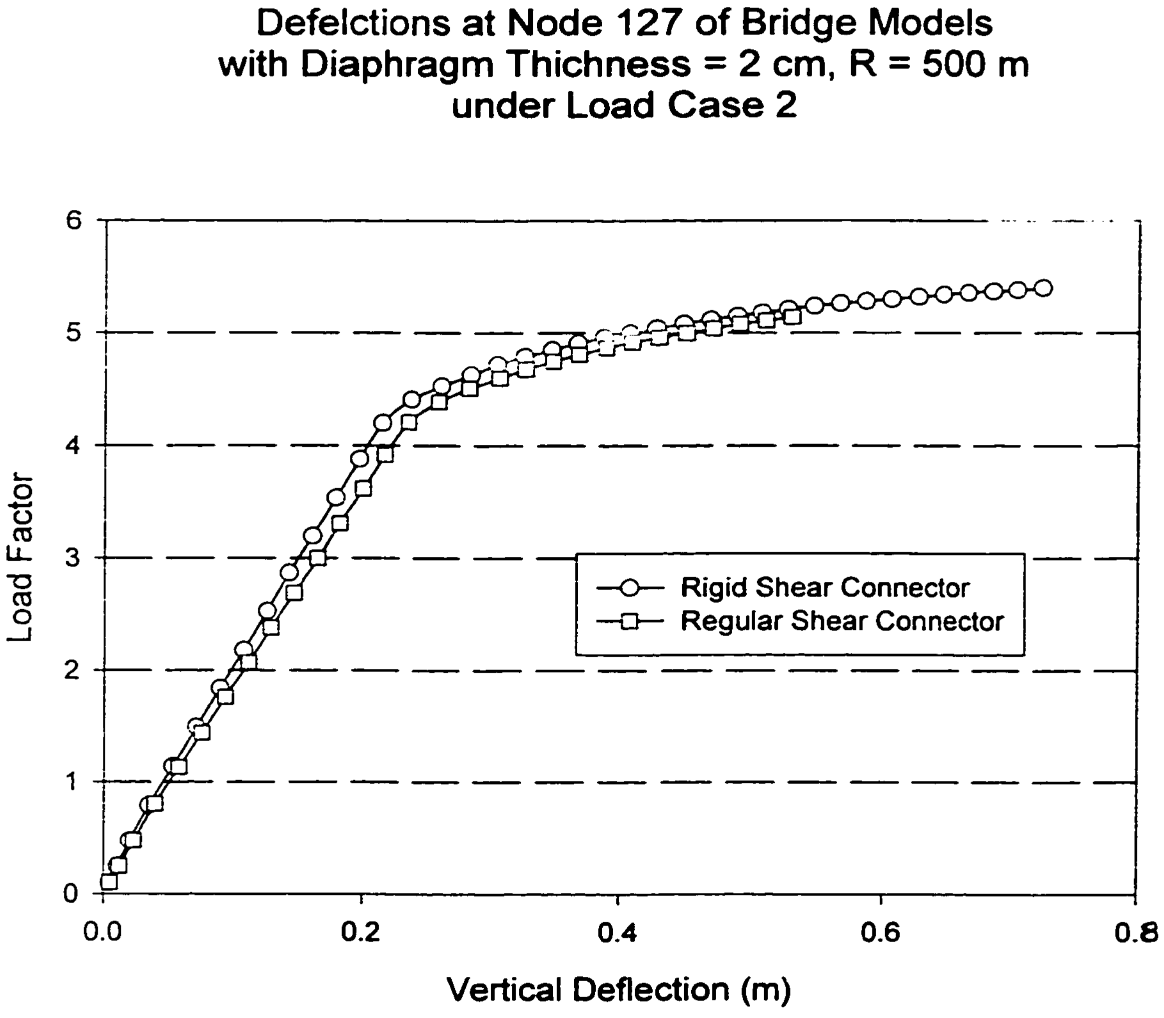

Figure 5.91 Deflections of Node 127 of Bridge Models with Various Stiffnesses of shear connectors, Diaphragm Thickness=0.02m and R=500m under Load Case 2

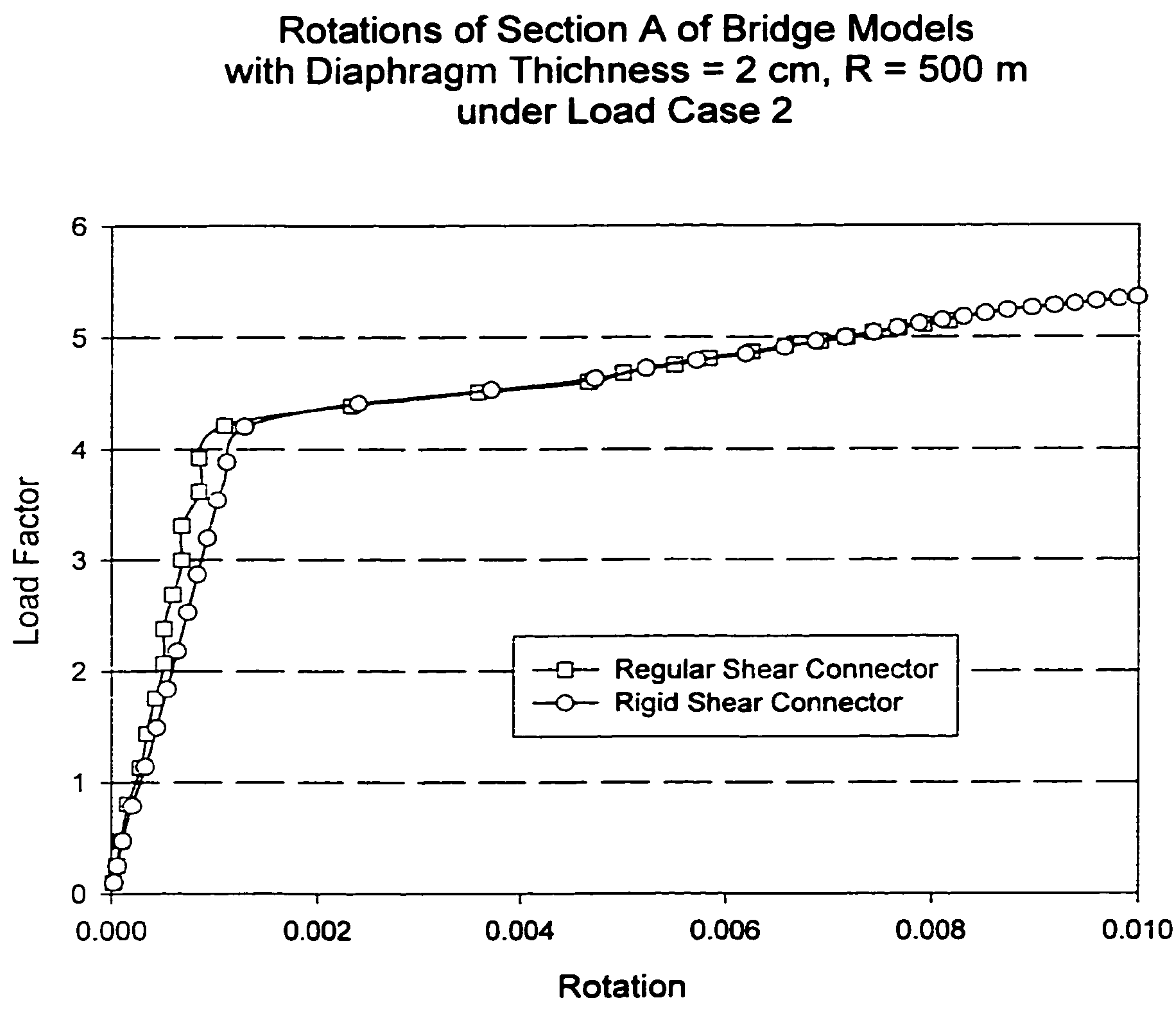

Figure 5.92. Rotations at Section A of Bridge Models with Various Stiffnesses of shear connectors, Diaphragm Thickness=0.02m and R=500m under Load Case 2

5.7.Influence of the stiffness of the middle diaphragm

With one of three different thicknesses of the plate middle diaphragm (0.02m, 0.04m and 0.08m), the height of the middle diaphragm (1.3m), and without intermediate diaphragms, bridge models were used in the nonlinear analysis. Radii of curvature (50m and 500m) were also used. Two load cases, which are Load Case 1 and Load Case 2, were employed because they are expected to induce the lower ultimate load for the bridge models based on the above parametric study observations. The stiffness of regular shear connectors and the stiffness of the middle column of 1.26×10^{11} N/m are also used in the analysis. The middle column is located at Column Location 1. The effects on the bridge models are given as follows based on each load case.

Load Case 1

For bridge models with curvature radius of 50m, vertical deflections at node 127 under Load Case 1 are shown in Figure 5.93. The rotation of section A is shown in Figure 5.94. The maximum deflection of the bridge model at section A is found at Node 127 of all bridge models with different stiffness of shear connectors under Load Case 1. In Figure 5.93, it can be seen that the bridge model with the thickness of 0.08m of the middle diaphragm has the greatest ultimate load factor of about 4.4. While the bridge model with the thickness of 0.02m of the middle diaphragm has the lowest ultimate load factor of about 3.8. In the elastic region, three bridge models have almost the same maximum deflection. However, the bridge model with less stiffness of the middle diaphragm starts to yield at the lower load factor. The bridge model with less stiffness of the middle diaphragm has the smallest rotation at section A in the elastic regions and the largest rotation at section A in the inelastic region at the same load level under Load Case 1 (Figure 5.94).

For bridge models with curvature radius of 500m, vertical deflections at node 127 under Load Case 1 are shown in Figure 5.95. The rotation of section A is shown in Figure 5.96. The maximum deflection of the bridge model at section A is found at Node 127 of all bridge models with different stiffness of shear connectors under Load Case 1. In Figure 5.95, it can be seen that the bridge model with the thickness of 0.08m of the middle diaphragm has the greatest ultimate load factor of about 5.5. While the bridge model with the thickness of 0.02m of the middle diaphragm has the lowest ultimate load factor of about 5.1. In the elastic region, three bridge models have almost the same deflection at Node 127. However, the bridge model with less stiffness of the middle diaphragm starts to yield at the lower load factor. The bridge model with less stiffness of the middle diaphragm has the smallest rotation at section A in the elastic regions and the largest rotation at section A in the inelastic region at the same load level under Load Case 1 (Figure 5.96).

Figure 5.97 shows the relationship of the ultimate load factors and the stiffnesses of the middle diaphragm of bridge models. The stiffness of the middle diaphragm was expressed as $\frac{EI}{(L/2)^3}$ (N/m), where $I = \frac{bh^3}{12}$, b and h are the width and the height of intermediate diaphragms respectively, and L is the width of the bottom plate. For both bridge models with radii of curvature of 50m and 500m, when the stiffness of the middle diaphragm is greater than 5×10^6 (N/m), the change of the ultimate load factor is within 5% compared with the straight bridge. When the stiffness of the middle diaphragm is less than 5×10^6 (N/m), the ultimate load of the bridge model decreases faster, which can be seen from Figure 5.97. When the stiffness of the middle diaphragm equals to 3×10^6 (N/m), the ultimate load of the bridge model drops by about 10% in comparison with the ultimate load of the straight bridge.

Load Case 2

For bridge models with curvature radius of 50m, vertical deflections at node 127 under Load Case 2 are shown in Figure 5.98. The rotation of section A is shown in Figure 5.99. The maximum deflection of the bridge model at section A is found at Node 127 of all bridge models with different stiffness of shear connectors under Load Case 2. In Figure 5.98, it can be seen that the bridge model with the thickness of 0.08m or 2 cm of the middle diaphragm has almost the same ultimate load factor of about 4.0. The bridge models also have the same rotation at section A in the elastic and inelastic regions under Load Case 2 (Figure 5.99). They start to yield at almost the same load factor of 26.

For bridge models with curvature radius of 500m, vertical deflections at node 127, under Load Case 2 are shown in Figure 5.100. The rotation of section A is shown in Figure 5.101. The maximum deflection of the bridge model at section A is found at Node 127 of all bridge models with different stiffness of shear connectors under Load Case 2. In Figure 5.100, it can be seen that the bridge model with the thickness of 0.08m or 2 cm of the middle diaphragm has almost the same ultimate load factor of about 4.0. The bridge models also have the same rotation at section A in the elastic and inelastic regions under Load Case 2 (Figure 5.101). They start to yield at almost the same load factor of 4.1.

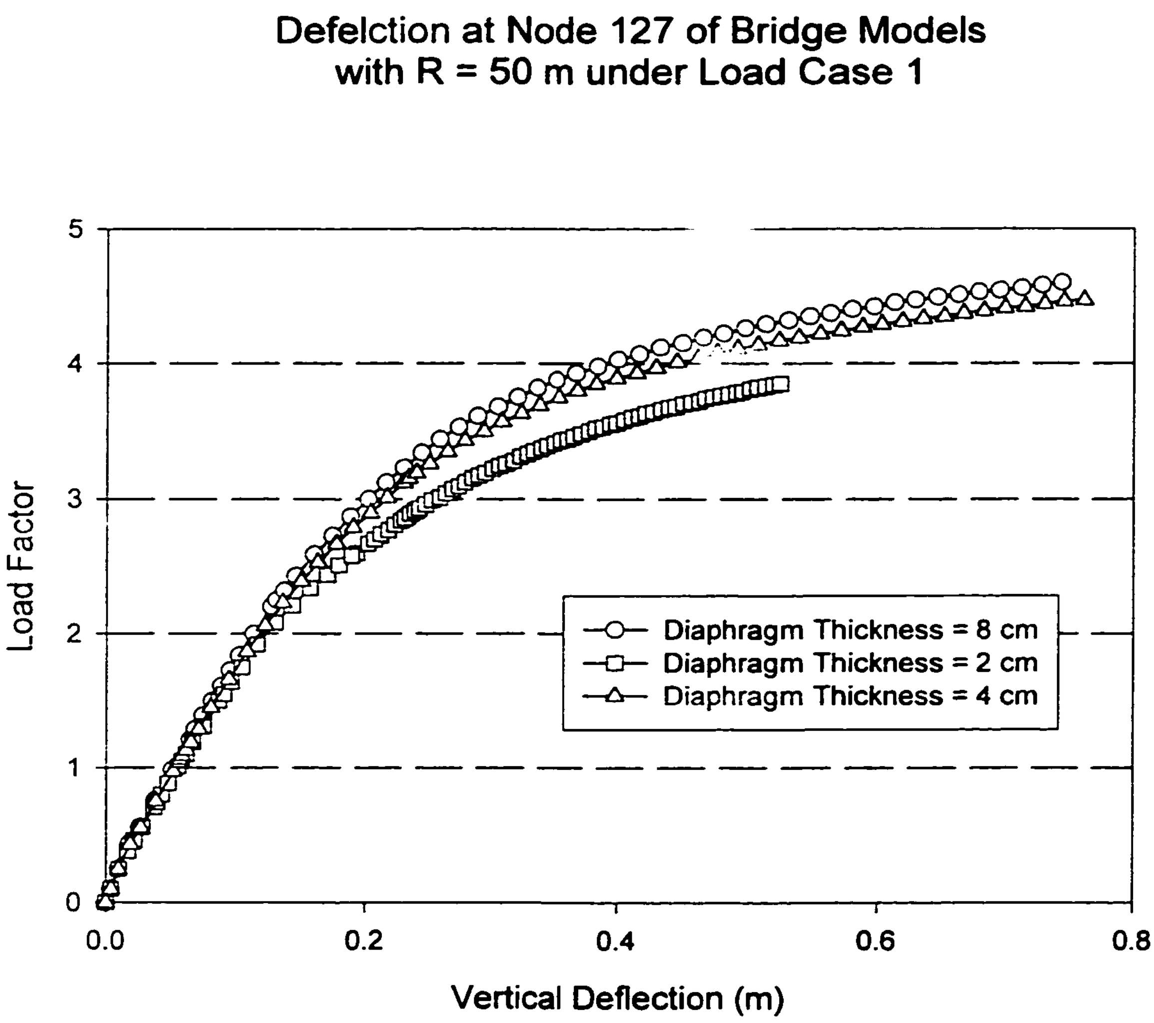

Figure 5.93 Deflections of Node 127 of Bridge Models with R=50m and Various Stiffness of Middle Diaphragm under Load Case 1

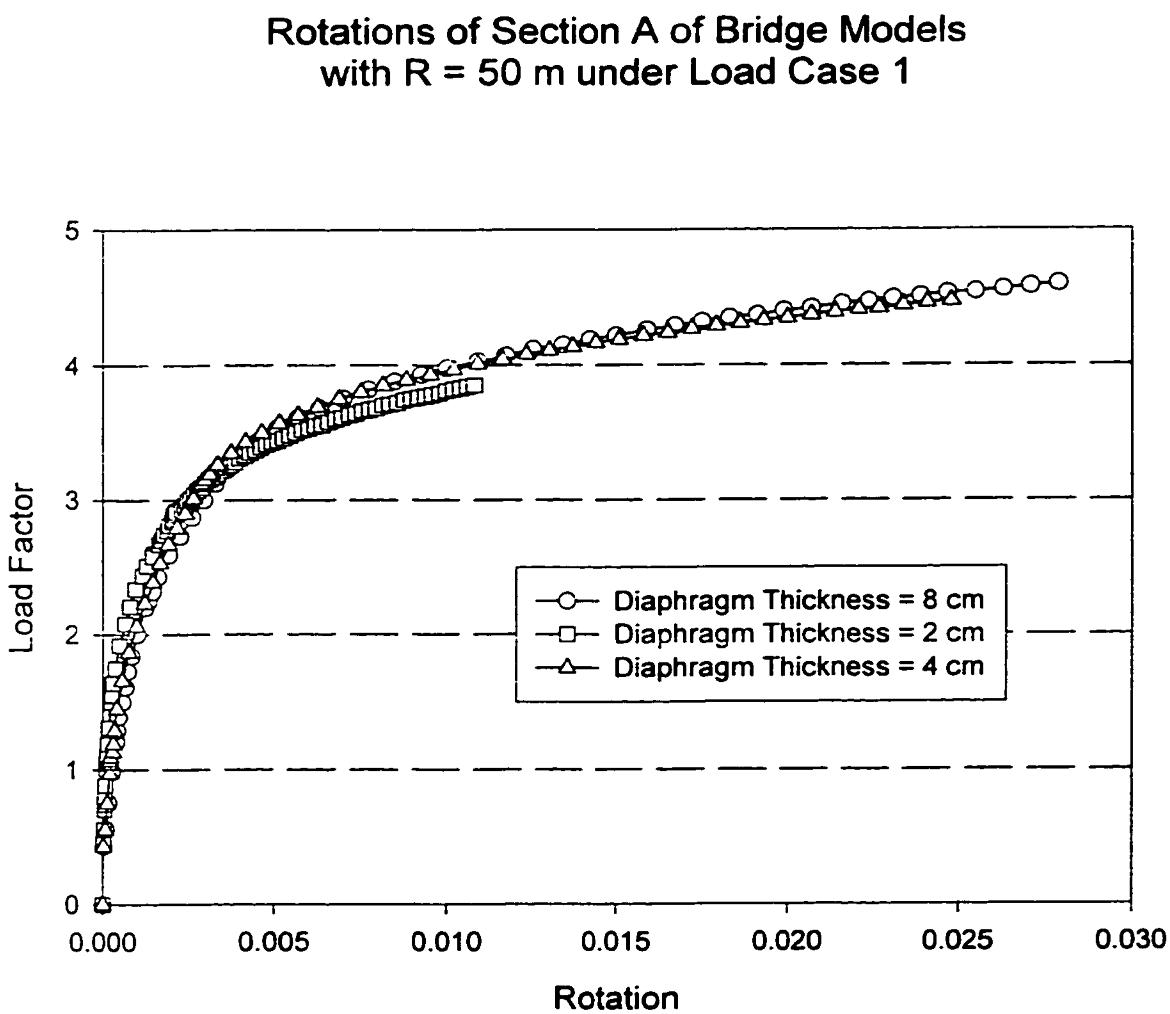

Figure 5.94. Rotations at Section A of Bridge Models R=50m and Various Stiffness of Middle Diaphragm under Load Case 1

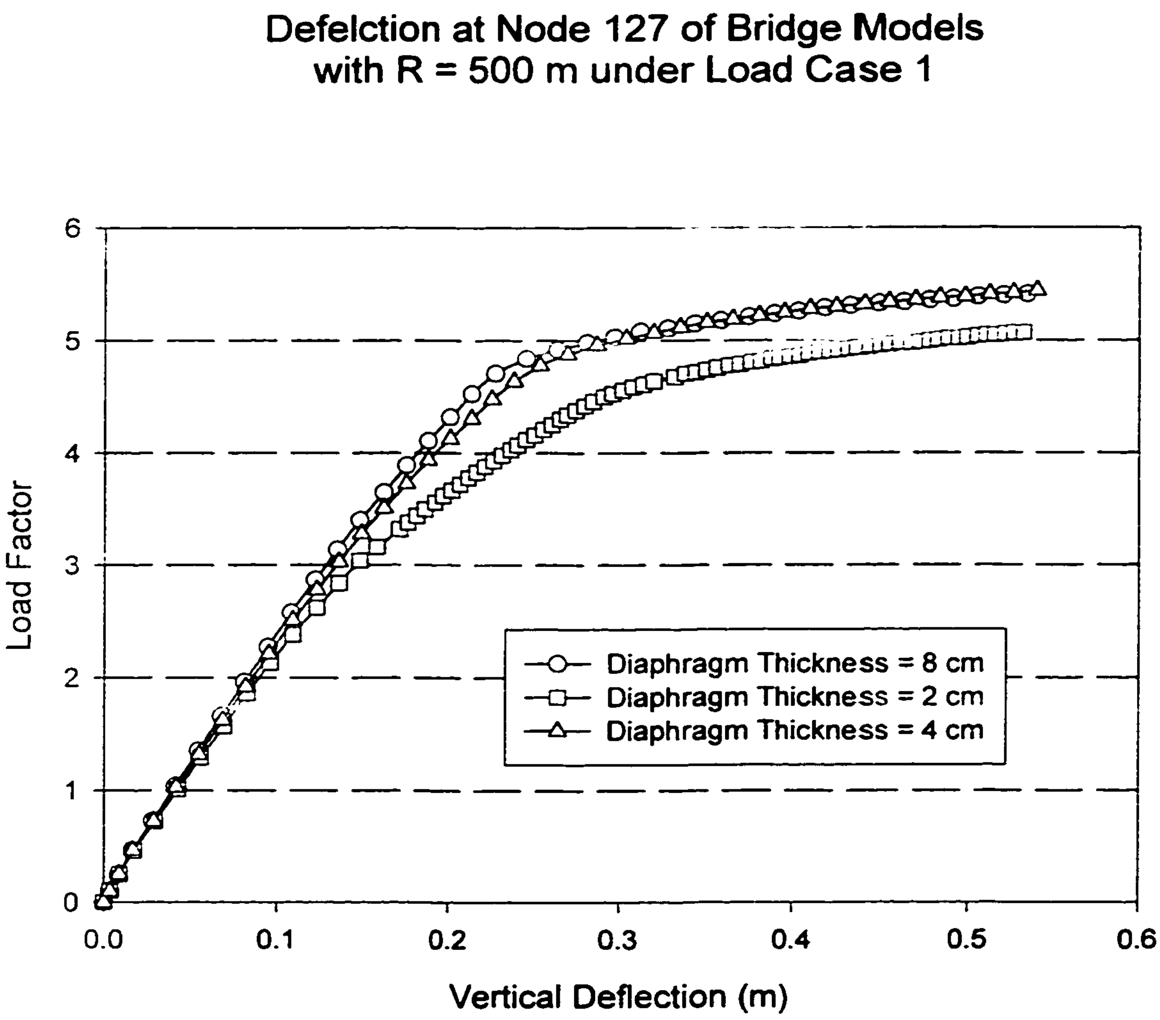

Figure 5.95 Deflections of Node 127 of Bridge Models with R=500m and Various Stiffness of Middle Diaphragm under Load Case 1

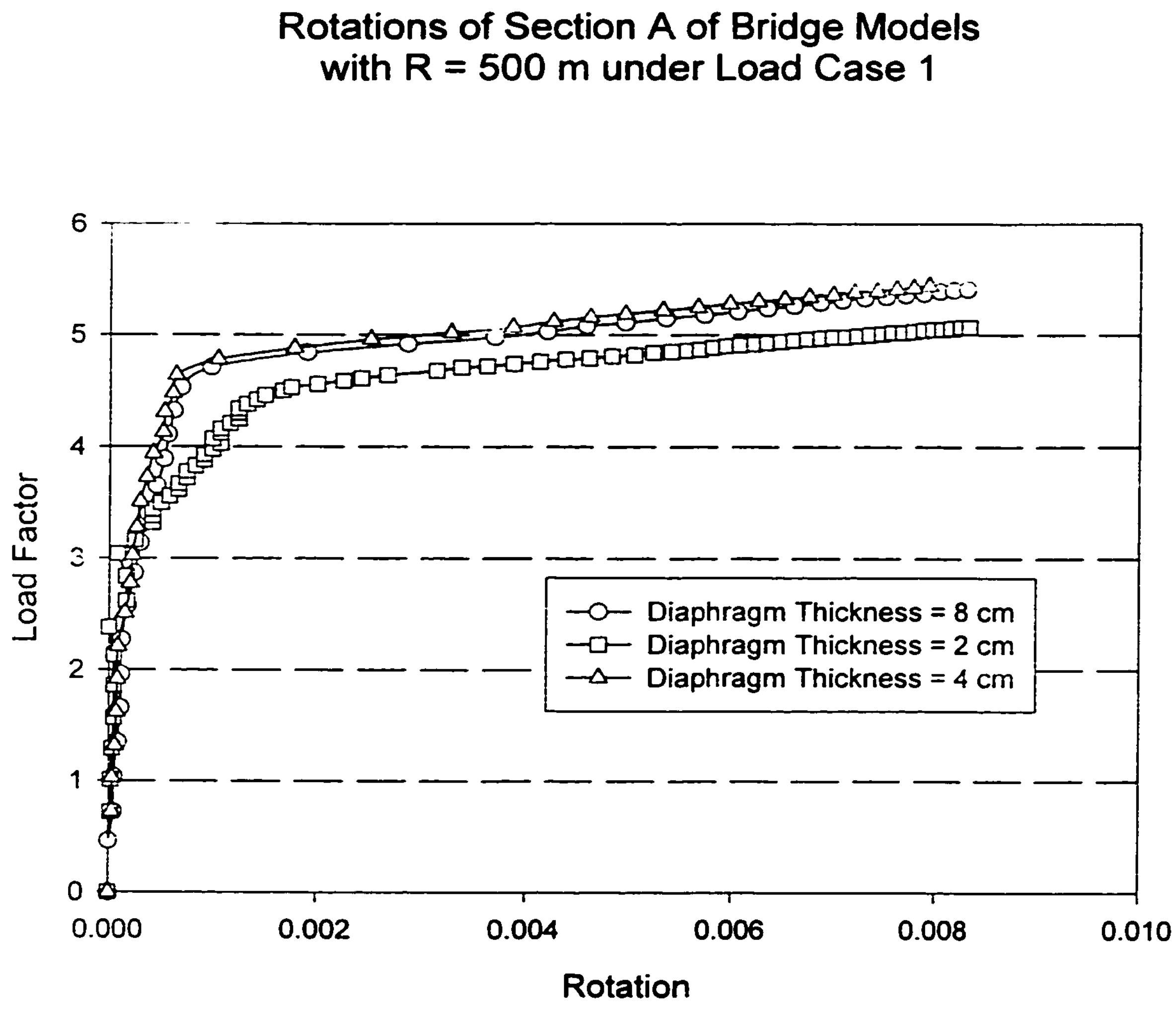

Figure 5.96. Rotations at Section A of Bridge Models with R=500m and Various Stiffness of Middle Diaphragm under Load Case 1

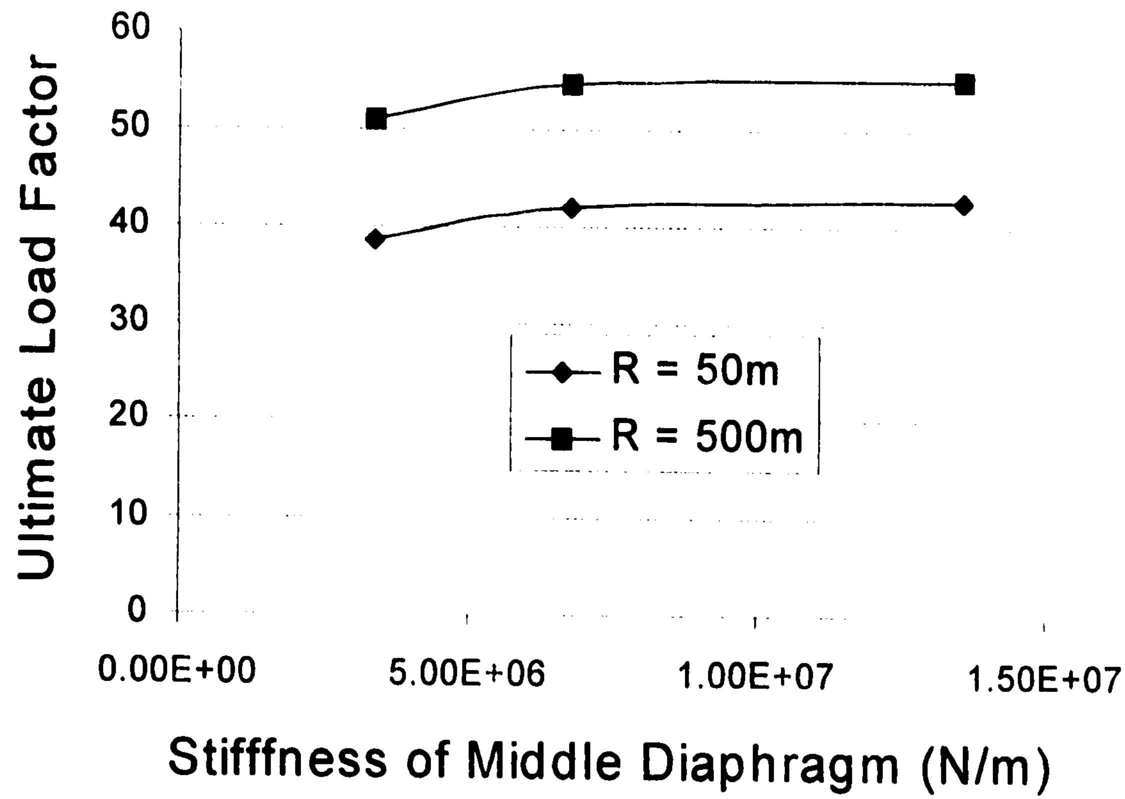

Figure 5.97 The relationship of stiffness of the middle diaphragm and ultimate load factor of the bridge models under Load Case 1

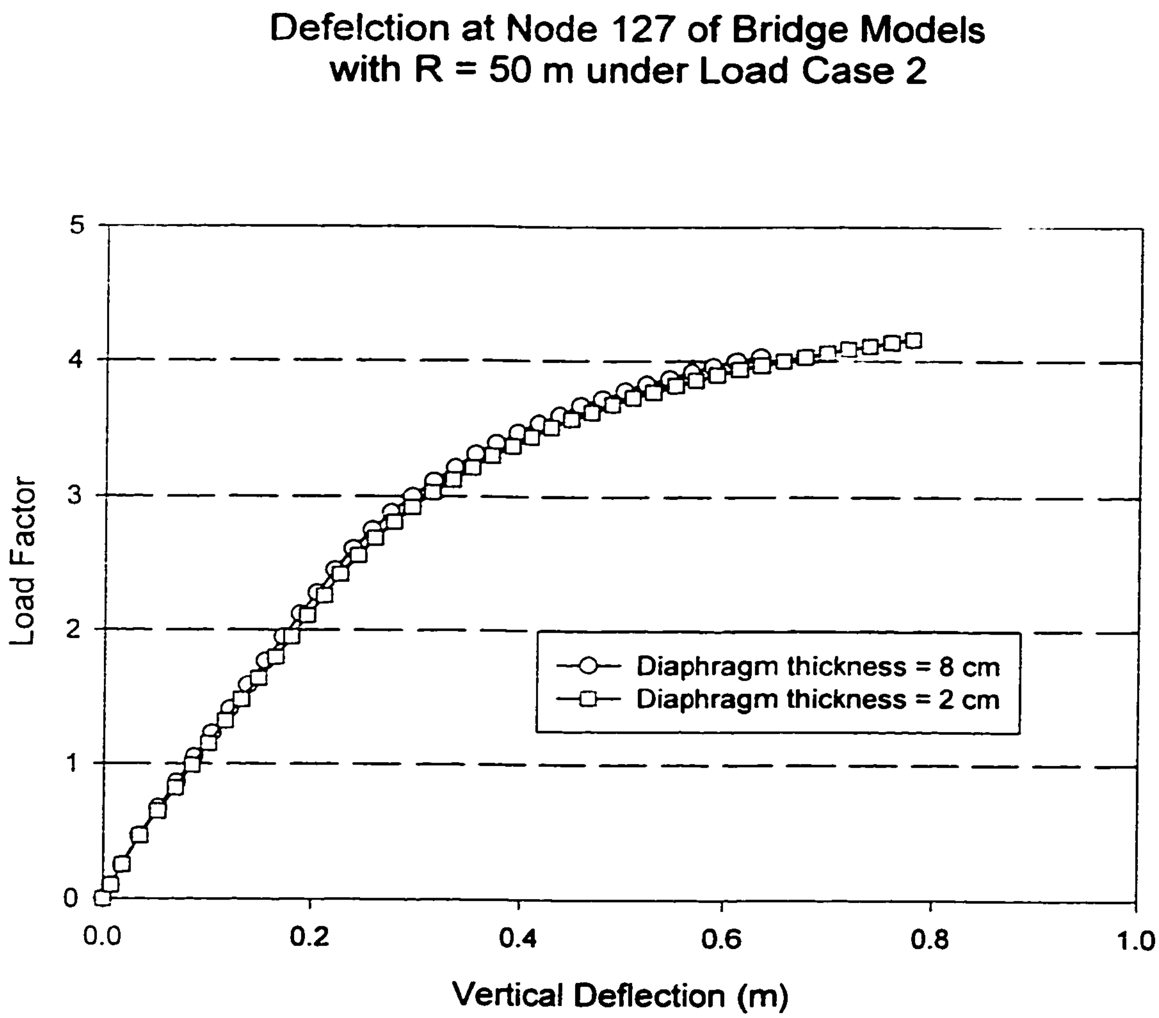

Figure 5.98 Deflections of Node 127 of Bridge Models with R=50m and Various Stiffness of Middle Diaphragm under Load Case 2

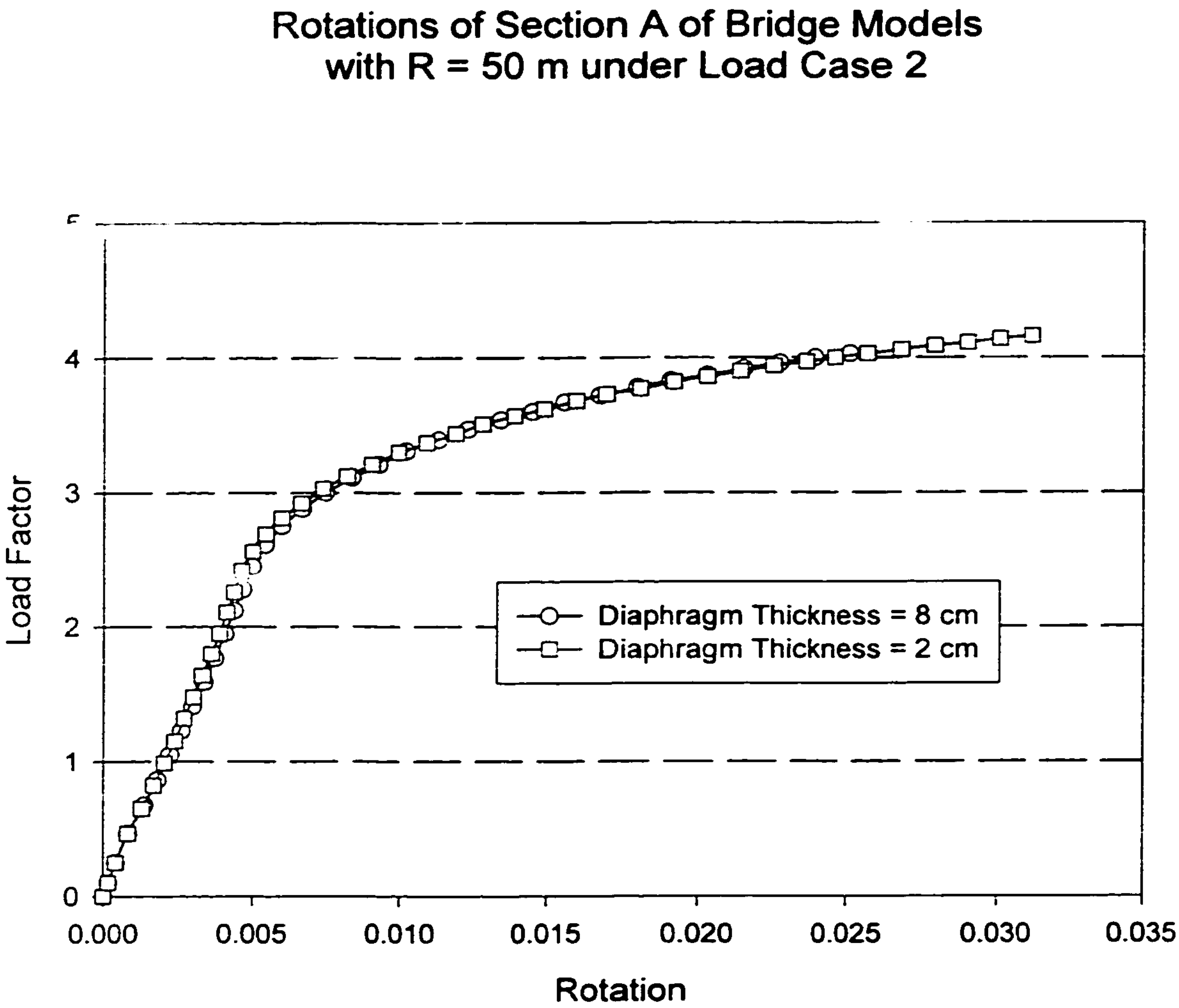

Figure 5.99. Rotations at Section A of Bridge Models R=50m and Various Stiffness of Middle Diaphragm under Load Case 2

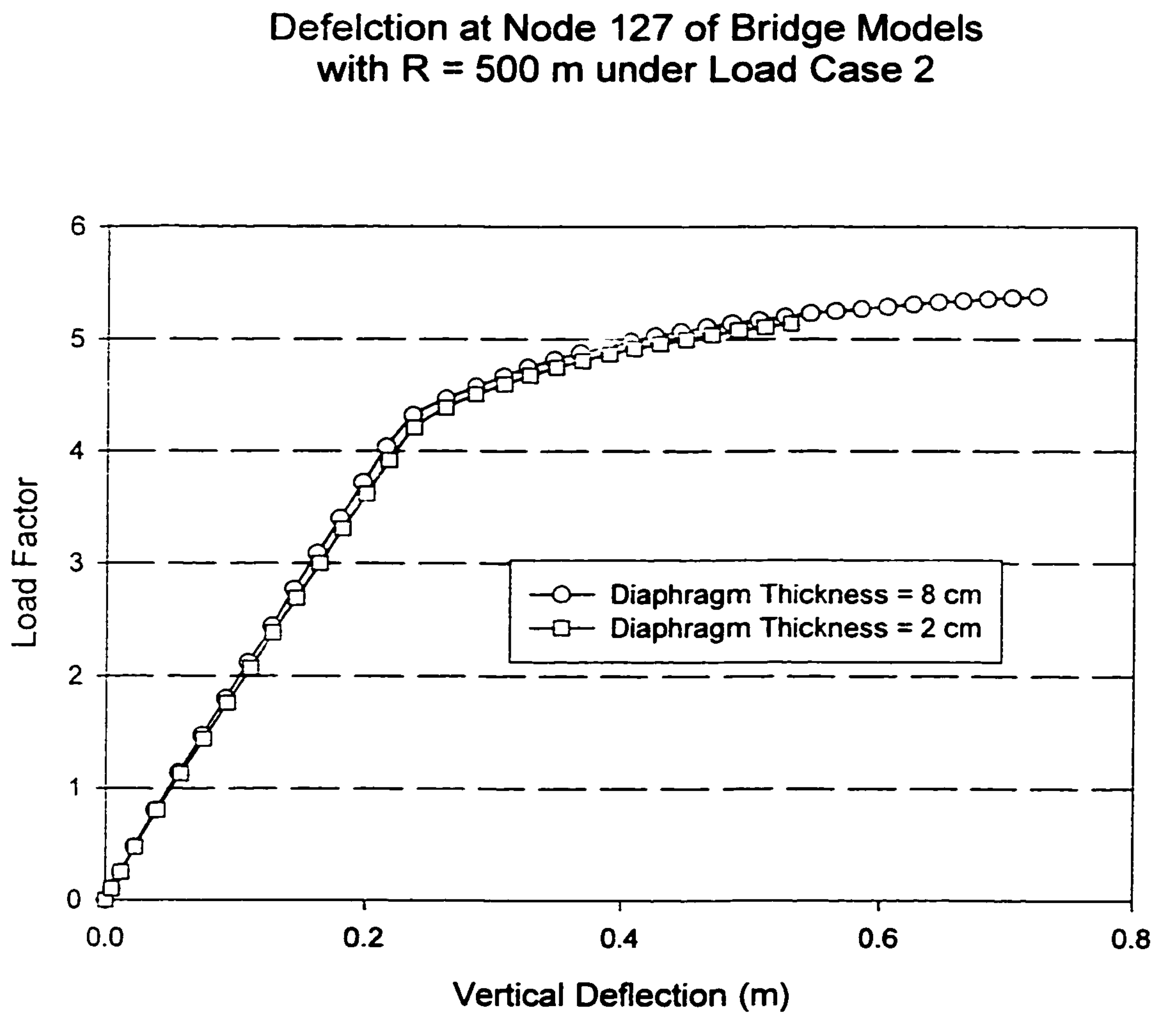

Figure 5.100 Deflections of Node 127 of Bridge Models with R=500m and Various Stiffness of Middle Diaphragm under Load Case 2

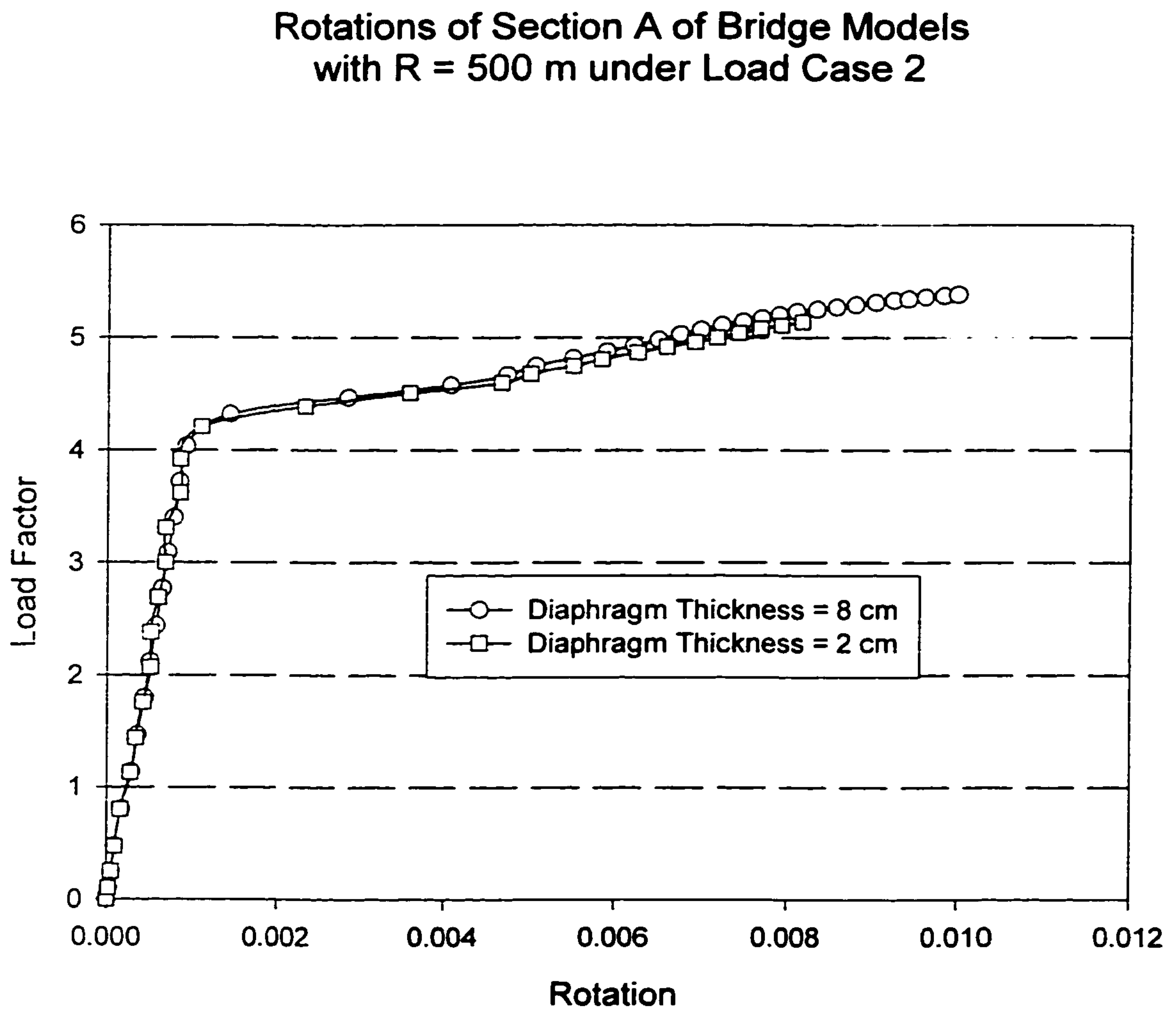

Figure 5.101. Rotations at Section A of Bridge Models with R=500m and Various Stiffness of Middle Diaphragm under Load Case 2

5.8. Influence of the stiffness of the middle support column

The bridge models without intermediate diaphragms and with one of five different stiffnesses of the middle support column with the column length of 5m and the area of its cross section of 3.14 m^2 were used in the analysis. Various elastic modulus Es are used in the analysis in order to get various stiffness of the middle column. The stiffness of the middle column is represented as L/EA. Various radii of curvature, which consist of 50m and 500m, are also used. Two load cases, which are Load Case 1 and Load Case 2, are employed because they are expected to induce the lower ultimate load for the bridge models based on the above observations. The stiffness of regular shear connectors and the thickness of the middle diaphragm of 0.02m are also used in the analysis. The middle column is located at Column Location 1. The effects on the bridge models are described as follows based on each load case.

Load Case 1

For bridge models with curvature radius of 50m, vertical deflections at node 127 under Load Case 1 are shown in Figures 5.102. The rotation of section A is shown in Figure 5.103. The maximum deflection at section A are found at Node 127 for the bridge models with the column stiffnesses of 1.26×10^{8} N/m, 1.26×10^{9} N/m, 1.26×10^{10} N/m, and 1.26×10^{11} N/m. The deflections at the middle column under the box girder of the bridges are shown in Figure 5.104. The maximum deflection at section A is found at Node 135 for bridge models with the column stiffness of 1.26×10^{7} N/m. When the column stiffness is greater than 1.26×10^{9} N/m, the bridge model has the same ultimate load factor of about 4.0. At the failure of the bridge model, the bridge model has a vertical deflection of less than 1mm at the location of the middle column. In elastic region, with the column stiffness of 1.26×10^8 N/m, the bridge model has a larger vertical deflection at Node 127 and less rotation at section A under Load Case 1. At the failure of the bridge model, the bridge model has a vertical deflection of 9mm at the location of the middle column. With the column stiffness of 1.26×10^7 N/m, the behaviors of bridge model tend to follow the behaviors of the simply supported bridge.

For bridge models with curvature radius of 500m, vertical deflections at node 127 under Load Case 1 are shown in Figure 5.105. The rotation of section A is shown in Figure 5.106. The maximum deflection at section A are found at Node 127 for the bridge models with the column stiffnesses of 1.26×10^8 N/m, 1.26×10^9 N/m, 1.26×10^{10} N/m, and 1.26×10^{11} N/m. The deflections at the middle column under the box girder of the bridges are shown in Figure 5.107. The maximum deflection at section A is found at Node 135 for bridge models with the column stiffness of 1.26×10^7 N/m. When the column stiffness is greater than 1.26×10^9 N/m, the bridge model has almost the same ultimate load factor of about 5.1. At the failure of the bridge model, the bridge model has a vertical deflection of less than 1mm at the location of the middle column. They have almost the same yielding point at the load factor of about 4.5. In elastic region, with the column stiffness of 1.26×10^8 N/m, the bridge model has a larger vertical deflection at Node 127 and less rotation at section A under Load Case 1. At the failure of the bridge model, the bridge model has a vertical deflection of 9mm at the location of the middle column. With the column stiffness of 1.26×10^7 N/m, the behaviors of bridge model tends to follow the behaviors of the simply supported bridge.

Load Case 2

For bridge models with curvature radius of 50m, vertical deflections at node 127 under Load Case 2 are shown in Figure 5.108. The rotation of section A is shown in Figure 5.109. The maximum deflection at section A are found at Node 127 for the bridge models with the column stiffnesses of 1.26×10^{8} N/m, 1.26×10^{9} N/m, and 1.26×10^{11} N/m. The deflections at the middle column under the box girder of the bridges are shown in Figure 5.110. The maximum deflection at section A is found at Node 135 for the bridge models with the column stiffness of 1.26×10^{7} N/m. When the column stiffness is greater than 1.26×10^{9} N/m, the bridge model has almost the same ultimate load factor of about 4.1. At the failure of the bridge model, the bridge model has a vertical deflection of less than 1mm at the location of the middle column. In elastic region, with the column stiffness of 1.26×10^{8} N/m, the bridge model has a larger vertical deflection at Node 127 and less rotation at section A under Load Case 2. At the failure of the bridge model, the bridge model has a vertical deflection of 4mm at the location of the middle column. With the column stiffness of 1.26×10^{7} N/m, the behaviors of bridge model tends to follow the behaviors of the simply supported bridge.

For bridge models with curvature radius of 500m, vertical deflections at node 127 under Load Case 2 are shown in Figure 5.111. The rotations of section A of the bridge models are shown in Figure 5.112. The maximum deflections at section A are found at Node 127 for the bridge models with the column stiffnesses of 1.26×10^{8} N/m, 1.26×10^{9} N/m, and 1.26×10^{11} N/m. The deflections at the middle column under the box girder of the bridges are shown in Figure 5.113. While the maximum deflection at section A are found at Node 135 for the bridge models with the column stiffness of 1.26×10^{7} N/m.

When the column stiffness is greater than 1.26×10^9 N/m, the bridge model has almost the same ultimate load factor of about 5.1. At the failure of the bridge model, the bridge model has a vertical deflection of less than 1mm at the location of the middle column. They have almost the same yielding point at the load factor of about 4.2. In elastic region, with the column stiffness of 1.26×10^8 N/m, the bridge model has a larger vertical deflection at Node 127 and less rotation at section A under Load Case 1. At the failure of the bridge model, the bridge model has a vertical deflection of 4mm at the location of the middle column. With the column stiffness of 1.26×10^7 N/m, the behaviors of bridge model tends to follow the behaviors of the simply supported bridge.

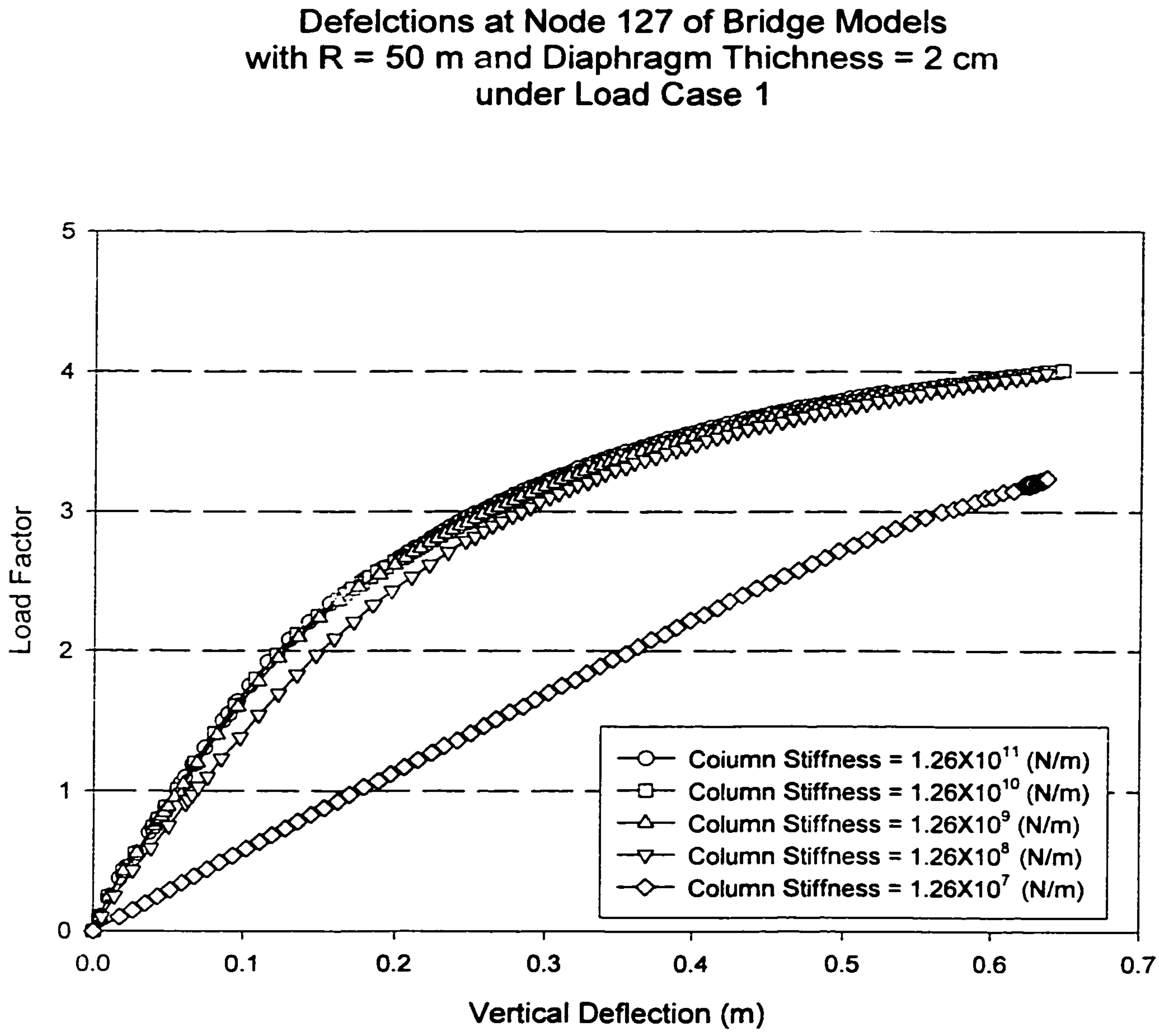

Figure 5.102 Deflections of Node 127 of Bridge Models with Various Stiffnesses of the Middle Column and R=50m under Load Case 1

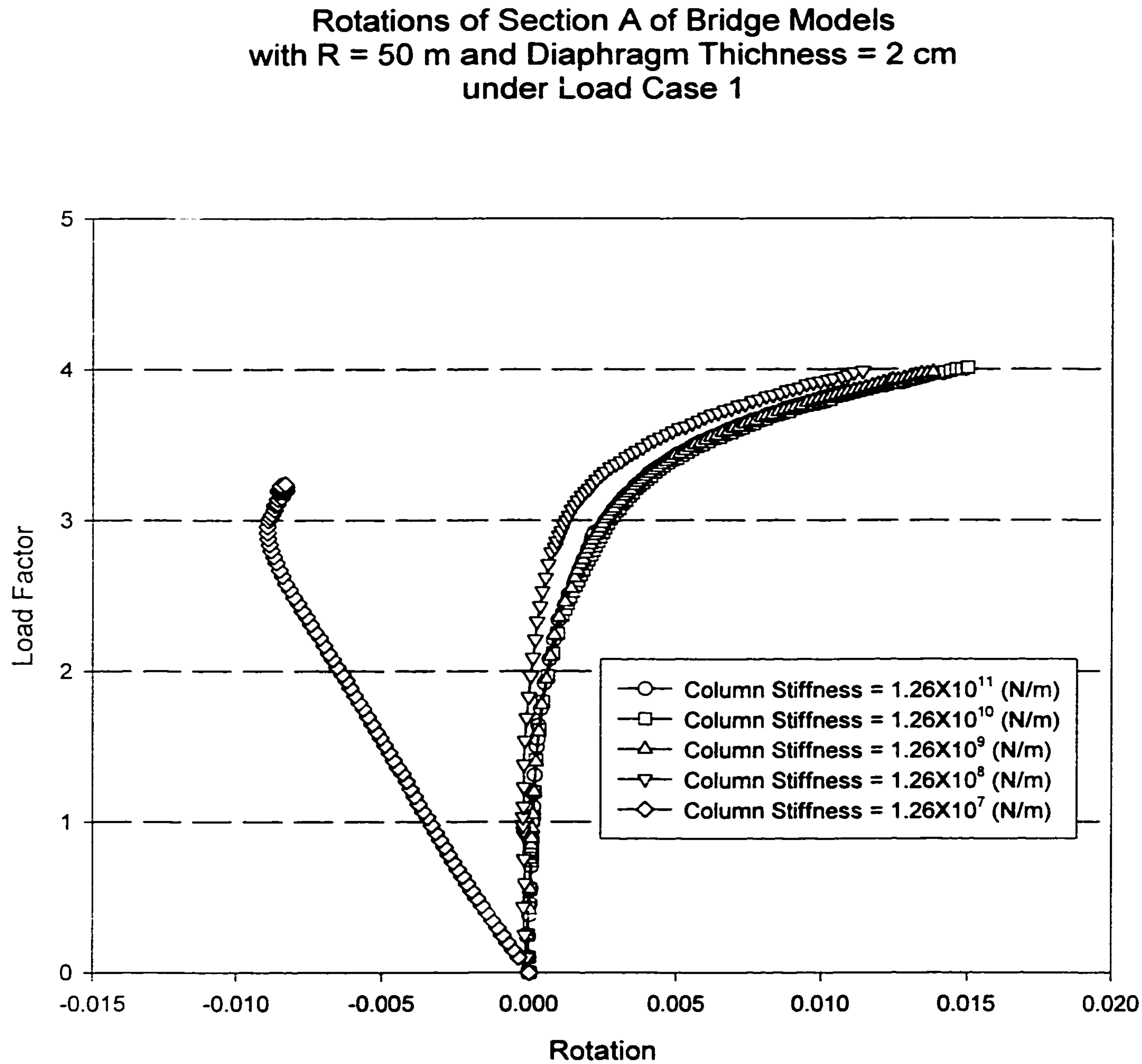

Figure 5.103. Rotations at Section A of Bridge Models with Various Stiffnesses of the Middle Column and R=50m under Load Case 1

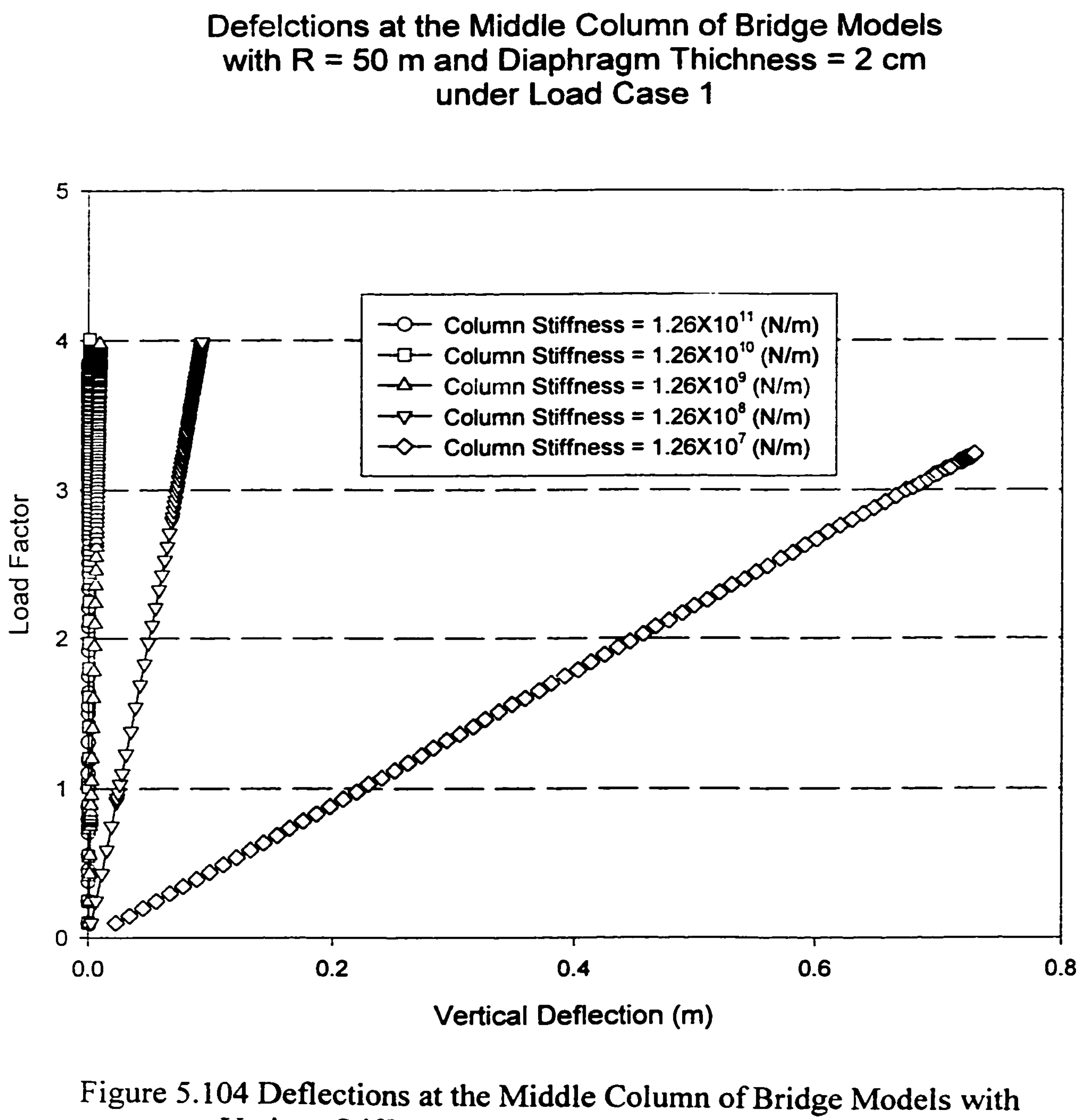

Figure 5.104 Deflections at the Middle Column of Bridge Models with Various Stiffnesses of the Middle Column and R=50m under Load Case 1

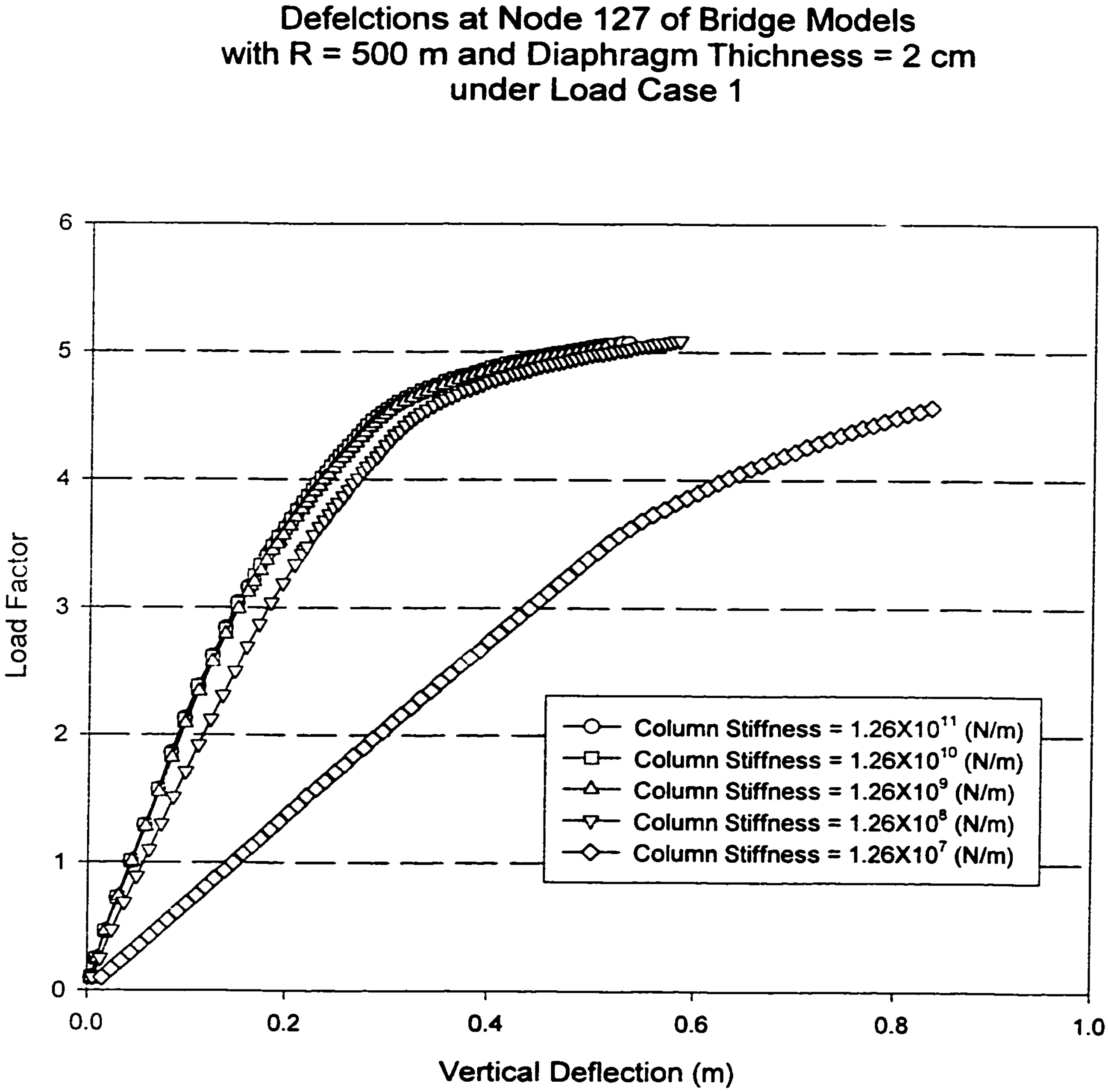

Figure 5.105 Deflections of Node 127 of Bridge Models with Various Stiffnesses of the Middle Column and R=500m under Load Case 1

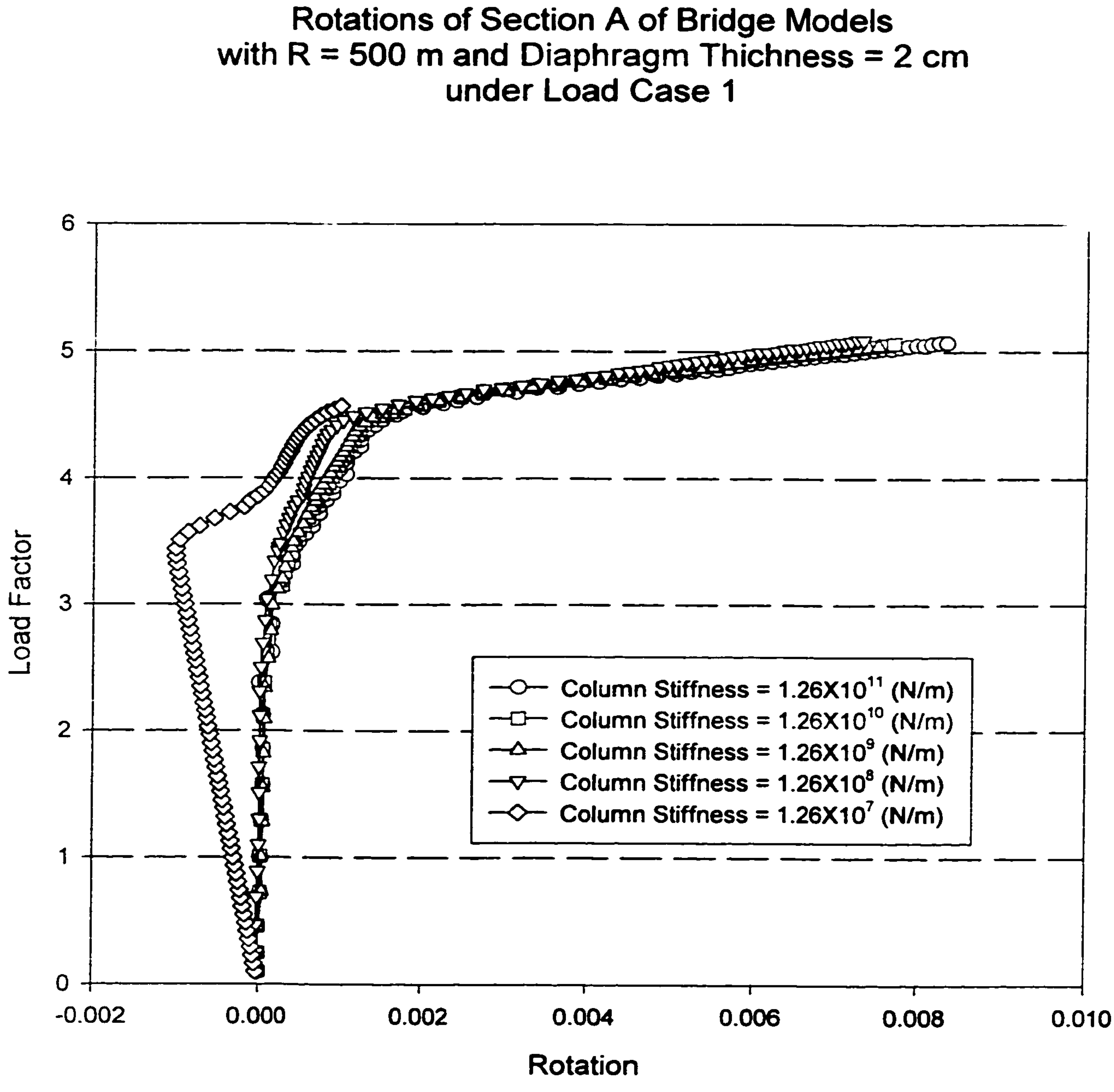

Figure 5.106. Rotations at Section A of Bridge Models with Various Stiffnesses of the Middle Column and R=500m under Load Case 1

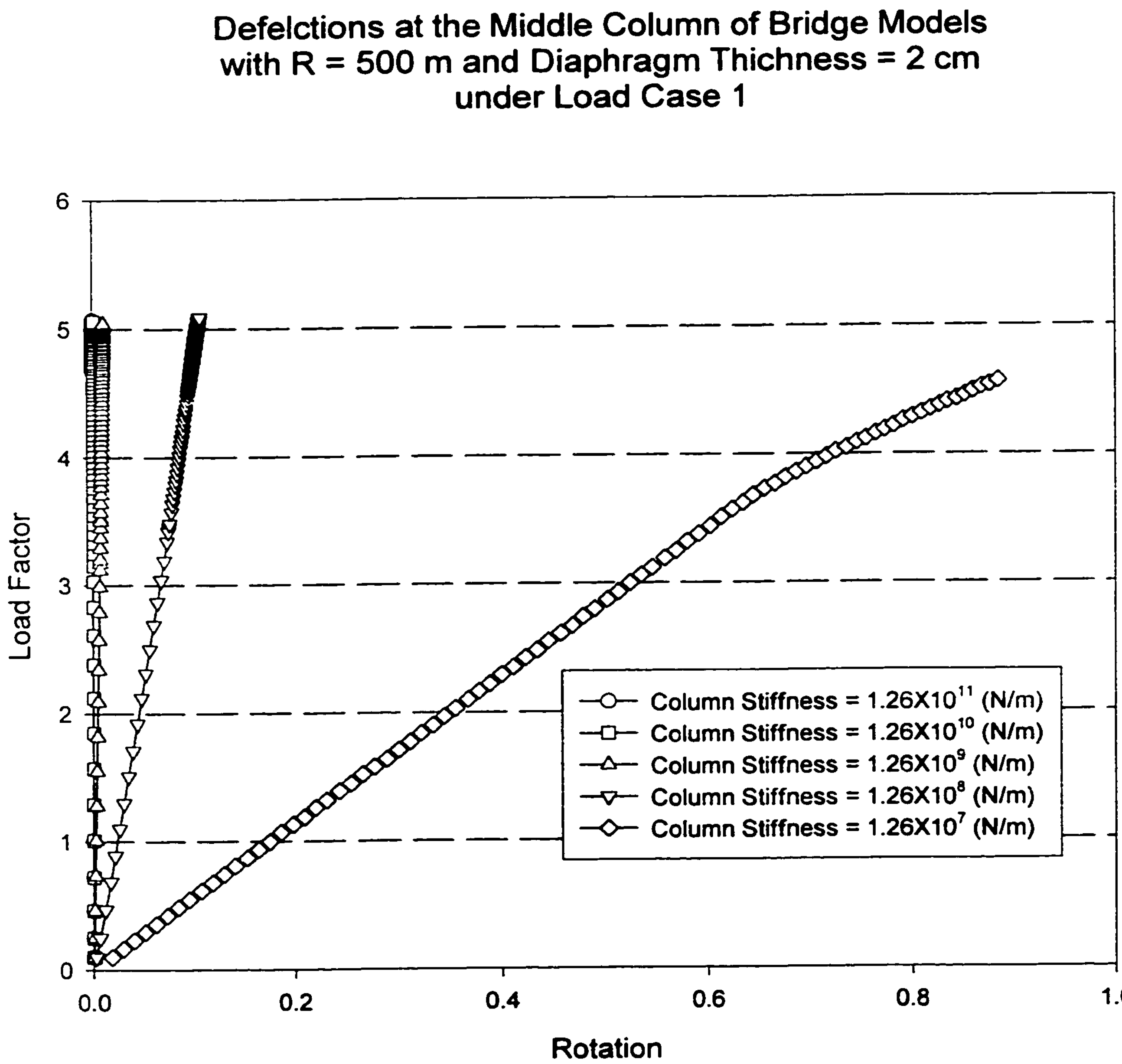

Figure 5.107 Deflections at the Middle Column of Bridge Models with Various Stiffnesses of the Middle Column and R=500m under Load Case 1

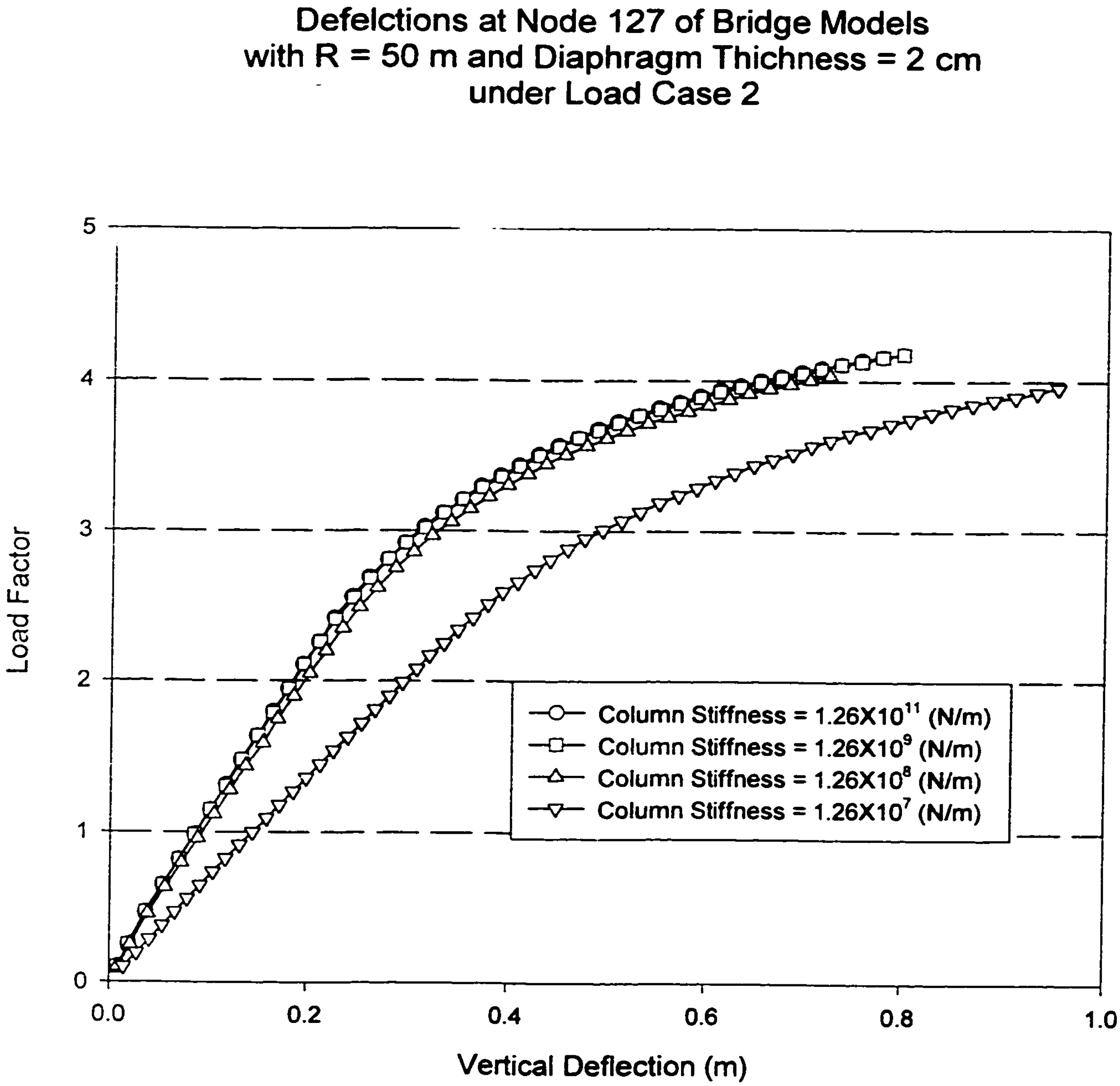

Figure 5.108 Deflections of Node 127 of Bridge Models with Various Stiffnesses of the Middle Column and R=50m under Load Case 2

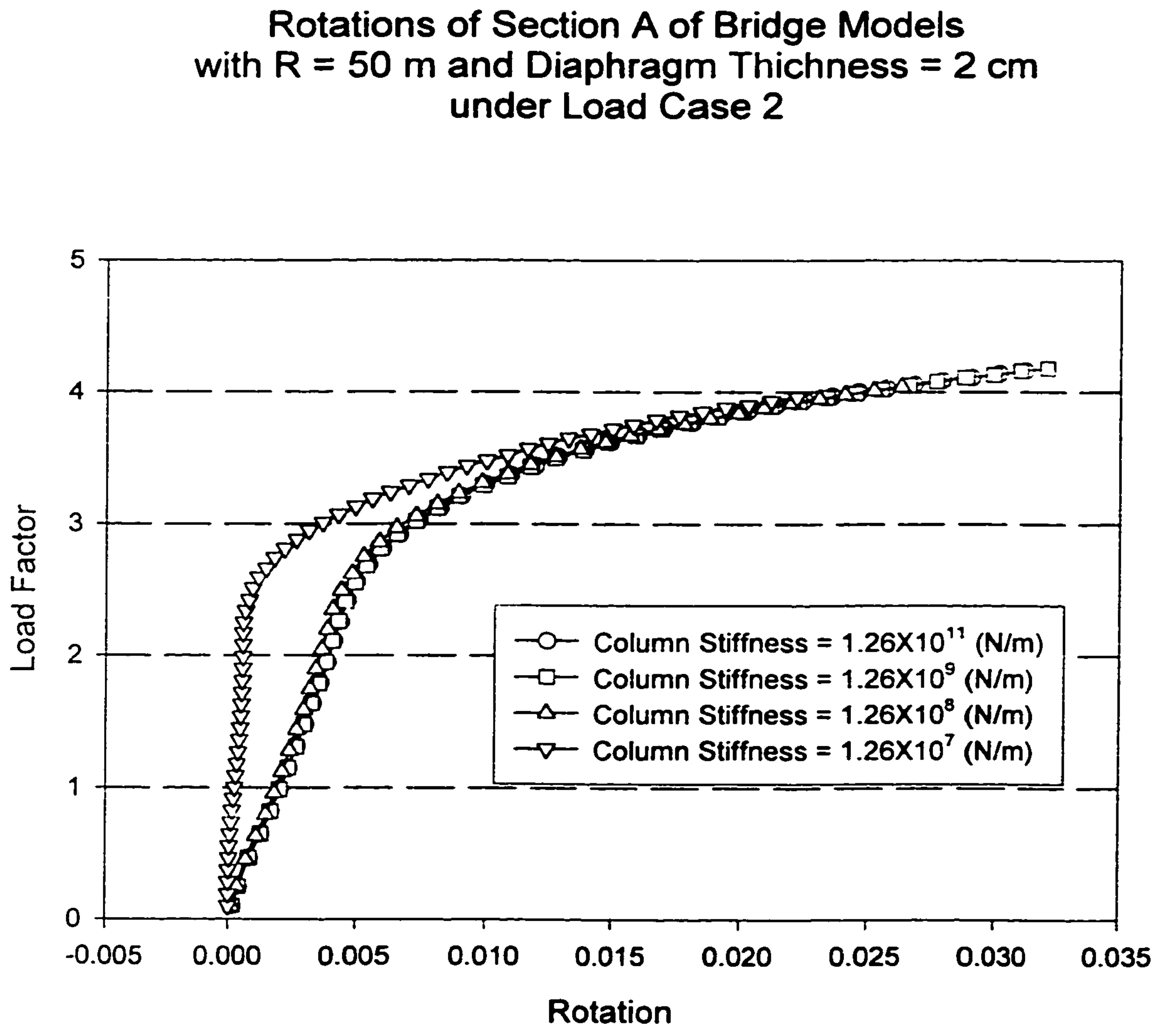

Figure 5.109. Rotations at Section A of Bridge Models with Various Stiffnesses of the Middle Column and R=50m under Load Case 2

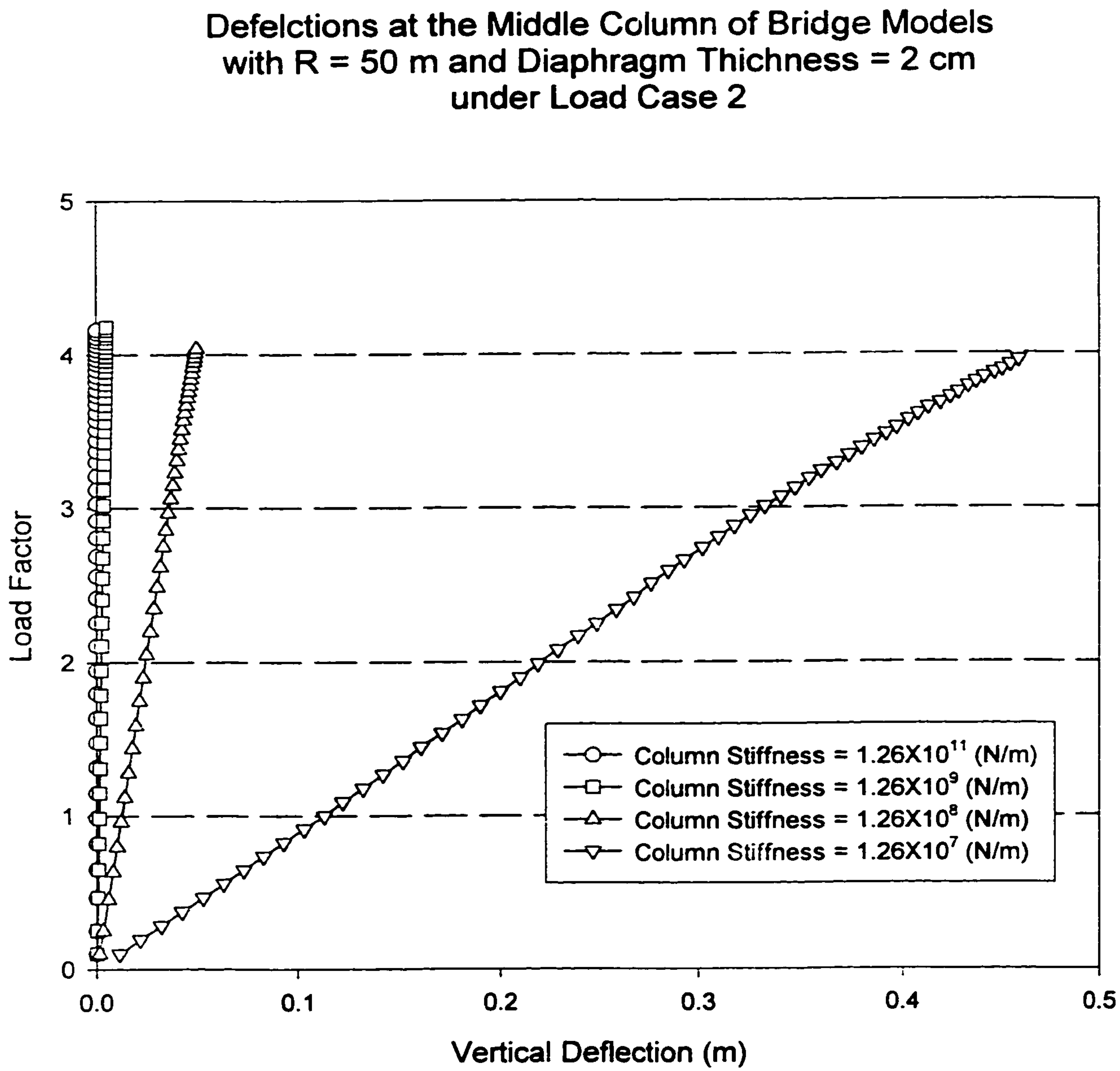

Figure 5.110 Deflections at the Middle Column of Bridge Models with Various Stiffnesses of the Middle Column and R=50m under Load Case 2

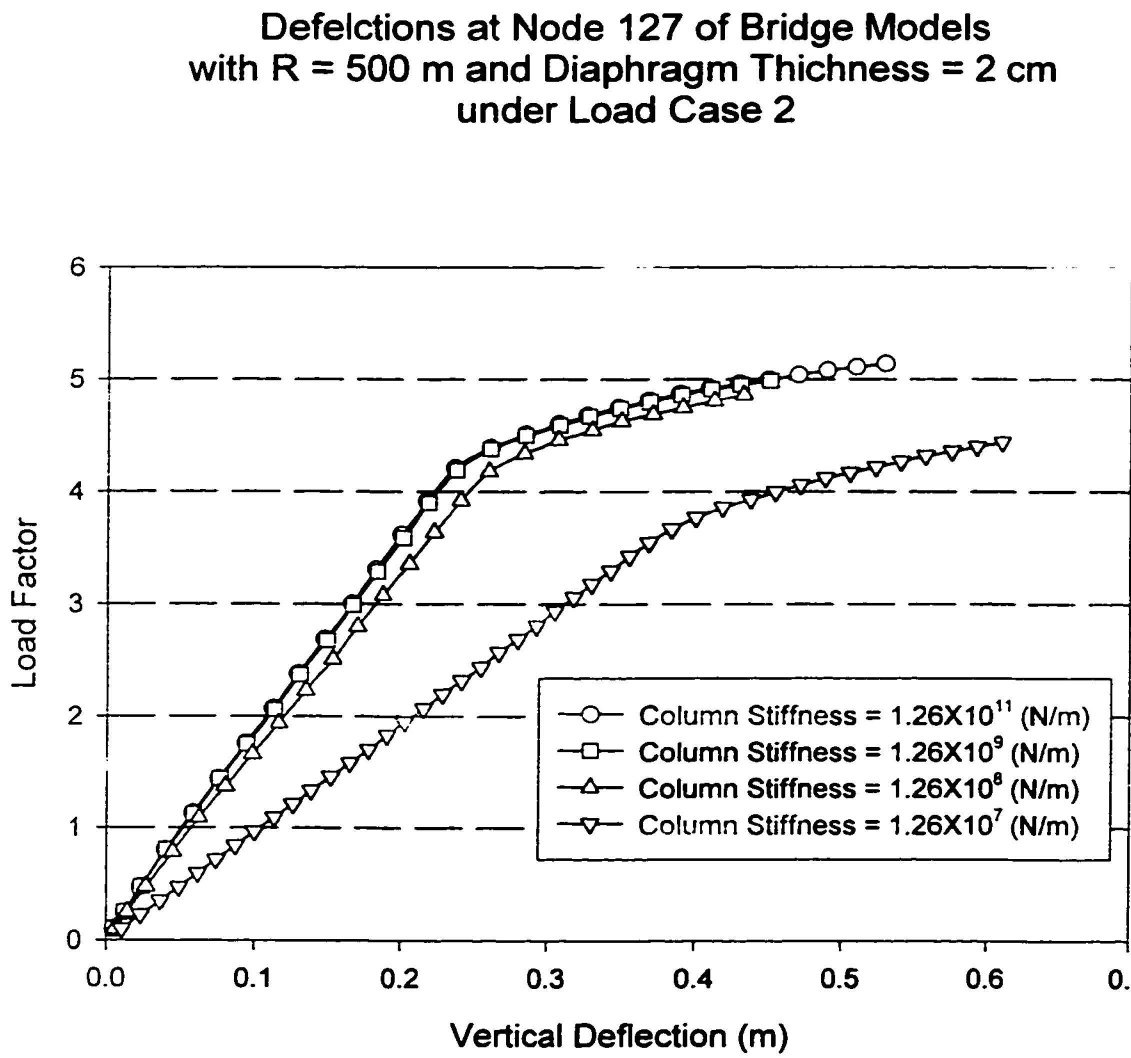

Figure 5.111 Deflections of Node 127 of Bridge Models with Various Stiffnesses of the Middle Column and R=500m under Load Case 2

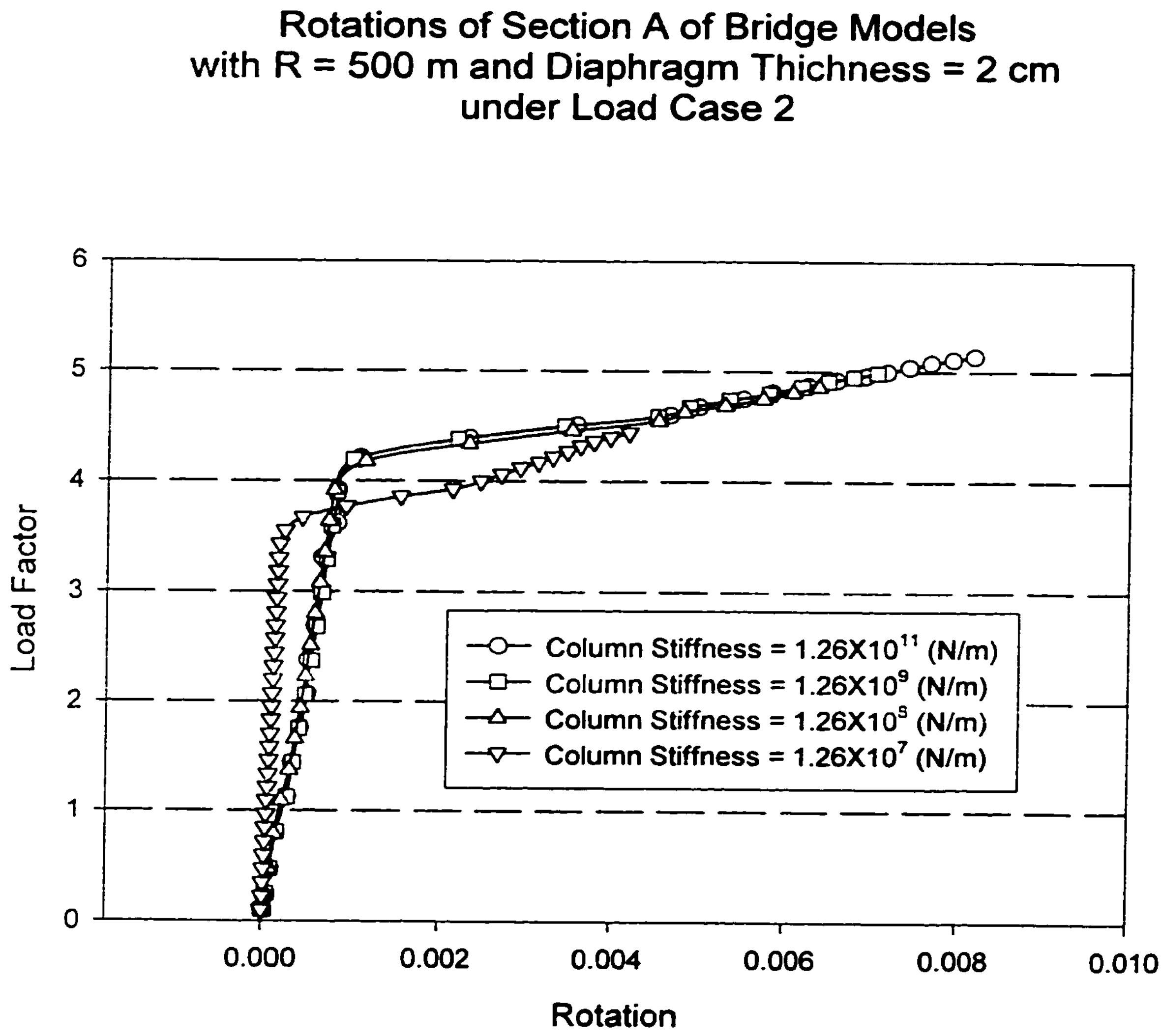

Figure 5.112. Rotations at Section A of Bridge Models with Various Stiffnesses of the Middle Column and R=500m under Load Case 2

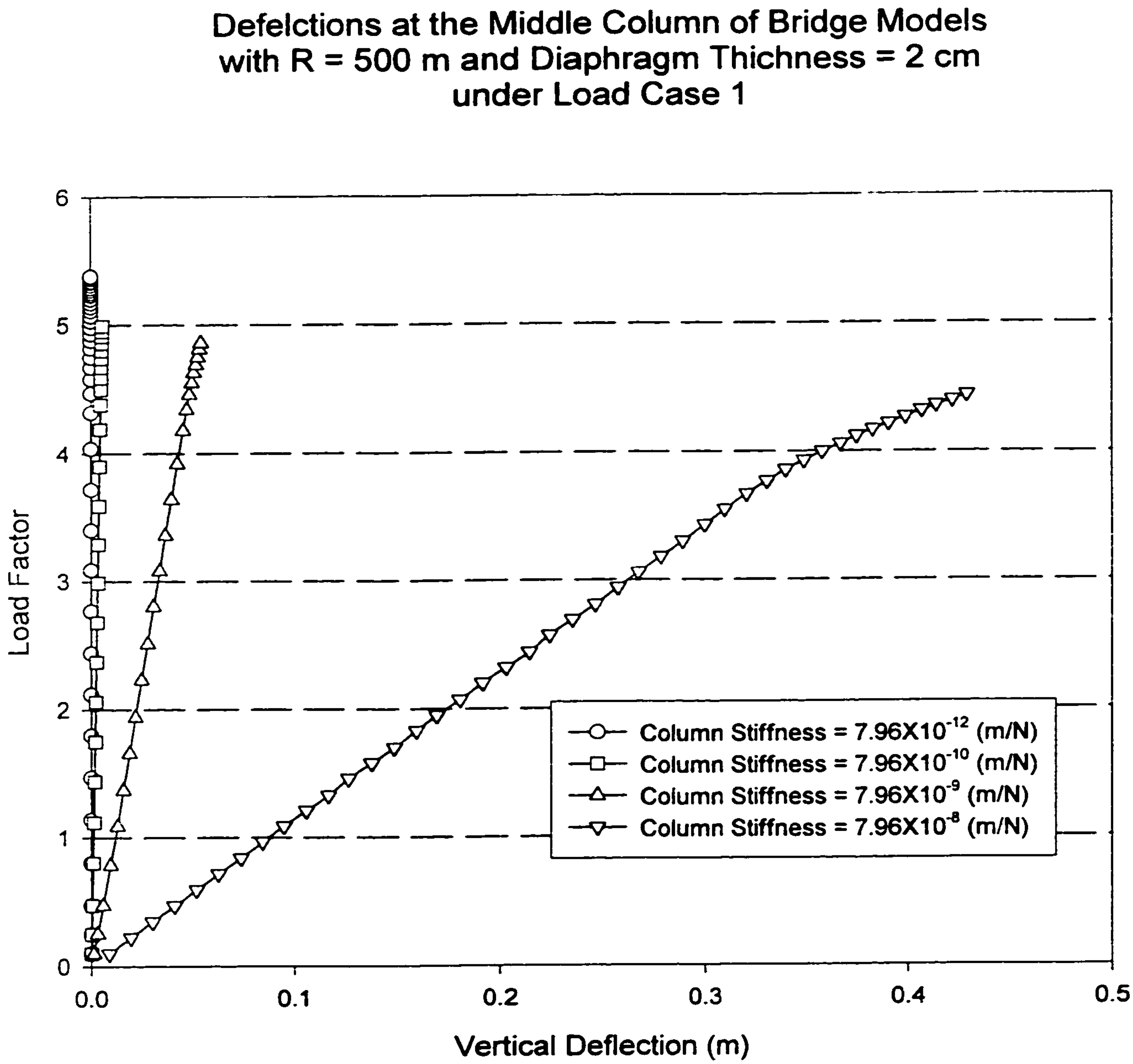

Figure 5.113 Deflections at the Middle Column of Bridge Models with Various Stiffnesses of the Middle Column and R=500m under Load Case 2

5.9. Influence of the stiffness of the intermediate diaphragms

The curved bridge models with intermediate diaphragms were analyzed. The basic dimensions of the bridge models are described section 5.2. The plate intermediate diaphragms with the height of 1.3m and various widths were used. The interval distance of the intermediate diaphragms is 7.2m. Various stiffnesses of the middle column, various locations of the middle column, various radii of curvature, various load cases, regular and rigid shear connectors, various thicknesses of the middle diaphragm, and various thicknesses of the intermediate diaphragms were also used in the nonlinear analysis.

For the bridge models with intermediate diaphragms and various middle column locations under Load Case 1, the thickness of the middle diaphragm is 0.08m, the thickness of intermediate diaphragms is 0.02m, and the regular shear connectors were used. When R=50m, vertical deflections of the bridge models at nodes 127, 131 and 135 are shown in Figures 5.114a, 5.114b and 5.114c. The rotations of section A of the bridge models are shown in Figure 5.115. From Figures, the maximum deflections of the bridge models at section A are found at Node 135. From Figures 5.114c and 5.115, the bridge model with the middle column at Column Location 2 has the greatest ultimate load factor of 5.4 approximately. The bridge model with the middle column at Column Location 1 has the ultimate load factor of about 5.2. And the bridge model with the middle column at Column Location 3 has the smallest ultimate load factor of 4.3 approximately and the greatest rotation at section A. It can also be seen that the bridge model with the middle column at Column Location 2 has the smallest maximum vertical deflection and the smallest rotation at section A in the elastic region. Obviously, the bridge model with the middle column at Column Location 1 or 2 has much greater ultimate load factor than at Column Location 3. If Column Location 3 is used in the curved bridges with 50m in radius of curvature, the capacity of the ultimate load of the bridges will decrease by more than 20%. For the bridge models with the radius of curvature 500m under load case 1, however, it is shown in Figure 5.118 that the bridge model with the middle diaphragm at Column Location 1 has a greater ultimate load factor by 5% than at Column Location 2. And it is also seen in Figure 5.119 that the bridge model with the middle diaphragm at Column Location 1 has a much smaller rotation at section A than at Column Location 2. Vertical deflections of the bridge models with R=50m at nodes 127, 131 and 135 under Load Case 2 are also shown in Figures 5.116a, 5.116b and 5.116c. The rotations of section A of the bridge models are shown in Figure 5.117. From Figures 5.116a, 5.116b and 5.116c, the maximum deflections of the bridge models at section A are found at Node 135. From Figures 5.116c and 5.117, it can be seen that the bridge model with the middle column at Column Location 1 or 2 has the same lowest ultimate load factor of 5.0 approximately under Load Case 2. It can also be seen that the bridge model with the middle column at Column Location 2 has the smaller maximum vertical deflection and the smaller rotation at section A in the elastic region.

For the bridge models with R=50m and various thicknesses of intermediate diaphragms (0.0m, 0.0002m, 0.0006m, 0.002m, and 0.02m) under Load Case 1, the thickness of the middle diaphragm is 0.08m, and the regular shear connectors were used. Vertical deflections of the bridge models at nodes 127, 131 and 135 are shown in Figures 5.120a, 5.120b and 5.120c. The rotations of section A of the bridge models are shown in Figure 5.121. The maximum deflections of the bridge models at section A are shown in

Figure 5.122. It can be seen from Figure 5.122 that when the thickness of the intermediate diaphragms is greater than 0.0006m, the bridge model with the intermediate diaphragms has almost the same ultimate load factor of approximate 5.1. The bridge model without intermediate diaphragms has only the ultimate load factor of about 4.6, hat is, the capacity of the ultimate load decreases by more than 10% in comparison with the bridge model with sufficient intermediate diaphragms. Figure 5.123 shows the relationship of the ultimate load factors and the stiffnesses of the intermediate diaphragms of bridge models. The stiffness of the intermediate diaphragms was expressed as $\frac{EI}{L^3}$(N/m), where $I = \frac{bh^3}{12}$, b and h are the width and the height of intermediate diaphragms respectively, and L is the width of the bottom plate. From Figure 5.123, it can also be observed that when the stiffness of the intermediate diaphragms is less than 1.5×10^4 N/m, the capacity of the ultimate load of the bridge model decreases rapidly. However, when the stiffness of the intermediate diaphragms is greater than 1.5×10^4 N/m, the increment of the capacity of the ultimate load of the bridge model is limited. From Figure 5.121, it can also be seen there is different behaviors for the bridge models with different stiffnesses of intermediate diaphragms. In elastic region, the outer web at section A has a larger vertical deflection than the inner web and the bridge model with more stiffness of intermediate diaphragms has a greater rotation. In ultimate state, however, when the thickness of the intermediate diaphragms is less than 0.0006m, the outer web at section A has a smaller vertical deflection than the inner web.

It is shown in Figures 5.124 and 5.125 that when the stiffness of the middle column is greater than $1.26\text{X}10^8$ (N/m), the bridge models have almost the same ultimate load factor of about 5.1. It is verified again that the capacity of the ultimate load of the bridges will be unaffected by the stiffness of the middle column if a reasonable stiffness of the middle column is used. It can also be found in the bridge models without intermediate diaphragms.

From Figures 5.126 and 5.127, it can also be seen that the ultimate load factor of bridge model may increase from 4.8 to 5.1 approximately when the thickness of the middle diaphragm increases from 0.02m to 0.08m.

From Figures 5.128 and 5.129, the bridge model with the radius of curvature from 50m to 500m has the lowest ultimate load factor under Load Case 2. It can also be seen that the bridge model with the radius of curvature 50m under Load Case 1 has almost the same ultimate load factor as under Load Case 2, although the bridge model under Load Case 2 has a larger vertical deflection than under Load Case 1.

For the bridge models with intermediate diaphragms and various radii of curvature (50m, 100m, and 500m) under Load Case 1, the thickness of the middle diaphragm is 0.08m, and the regular shear connectors were used. The maximum deflections of the bridge models at section A are found at Node 135. Vertical deflections of the bridge models at node 135 are shown in Figures 5.130. The rotations of section A of the bridge models are shown in Figure 5.131. From Figure 5.130, it can be seen that the bridge model with the radius of curvature 50m has the lowest ultimate load factor of about 5.1. The bridge model with the radius of curvature 500m has the highest ultimate load factor of about 5.7. For the bridge models under Load Case 2, the maximum deflections of the bridge models at section A are found at Node 135. Vertical deflections of the bridge models at node 135 are shown in Figures 5.132. The rotations of section A of the bridge models are shown in Figure 5.133. From Figure 5.132, it can be seen that the bridge model with the radius of curvature 50m has the lowest ultimate load factor of about 5.0. The bridge model with the radius of curvature 500m has the highest ultimate load factor of about 5.5. It is obviously seen from Figures 5.131 and 5.133 that the bridge model with the radius of curvature has the smallest rotation under either Load Case 1 or 2. From above observations, it can be found that the bridge model with smaller radius of curvature has a lower capacity of ultimate load. This phenomenon can also be found in the bridge models without intermediate diaphragms.

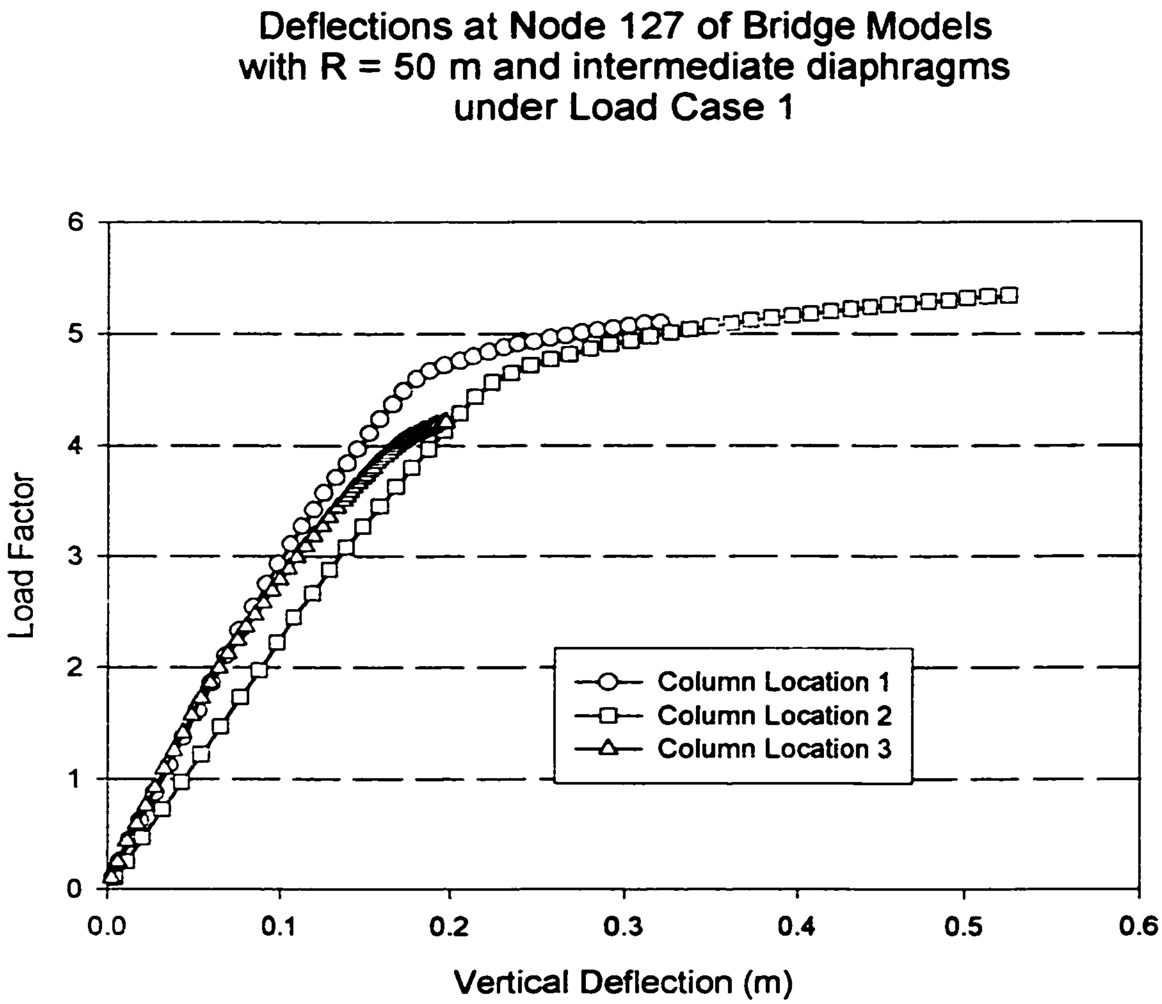

Figure 5.114a Deflections of Node 127 of Bridge Models with R=50m, intermediate diaphragms, and Various Column Locations under Load Case 1

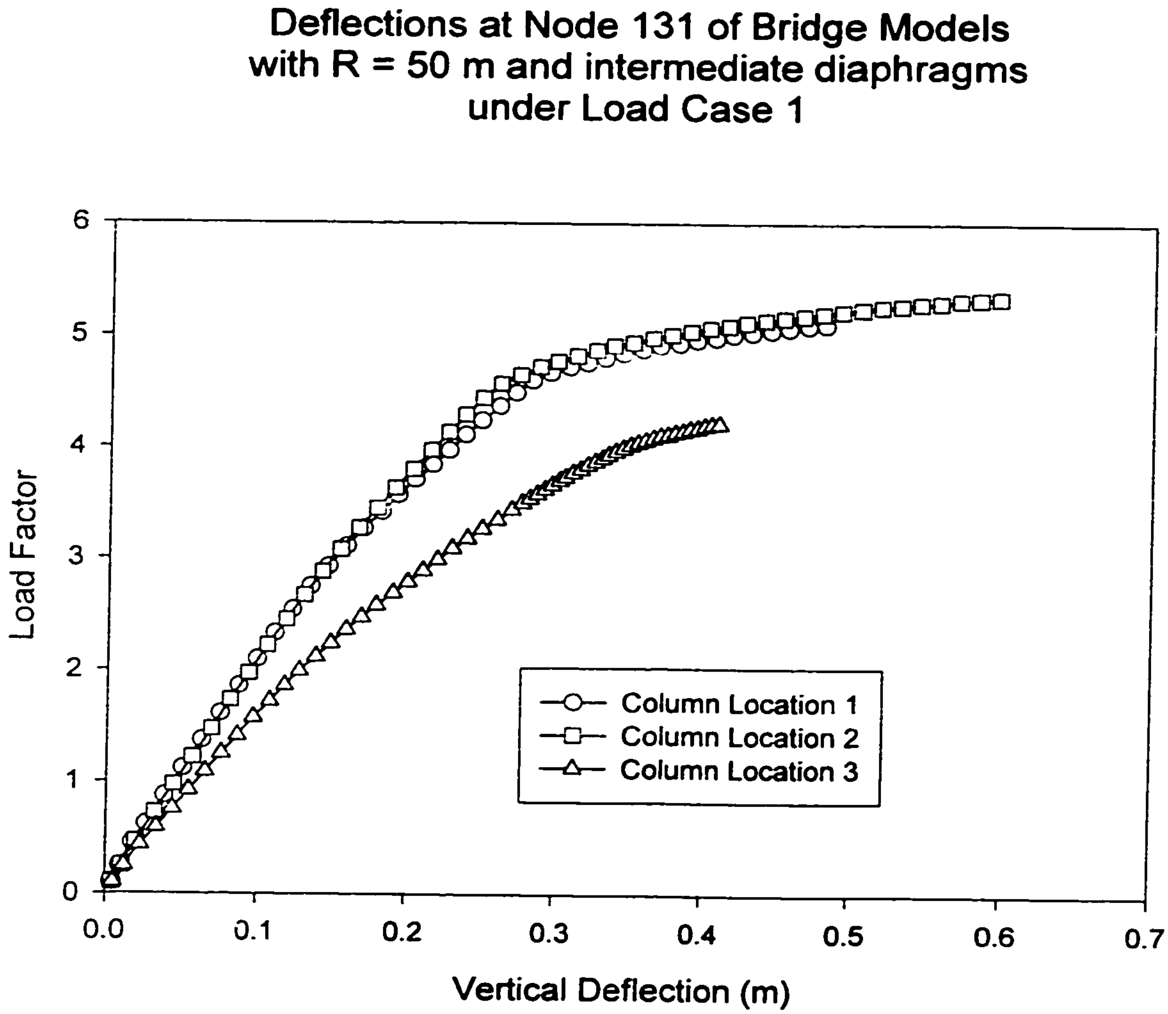

Figure 5.114b Deflections of Node 131 of Bridge Models with R=50m, intermediate diaphragms, and Various Column Locations under Load Case 1

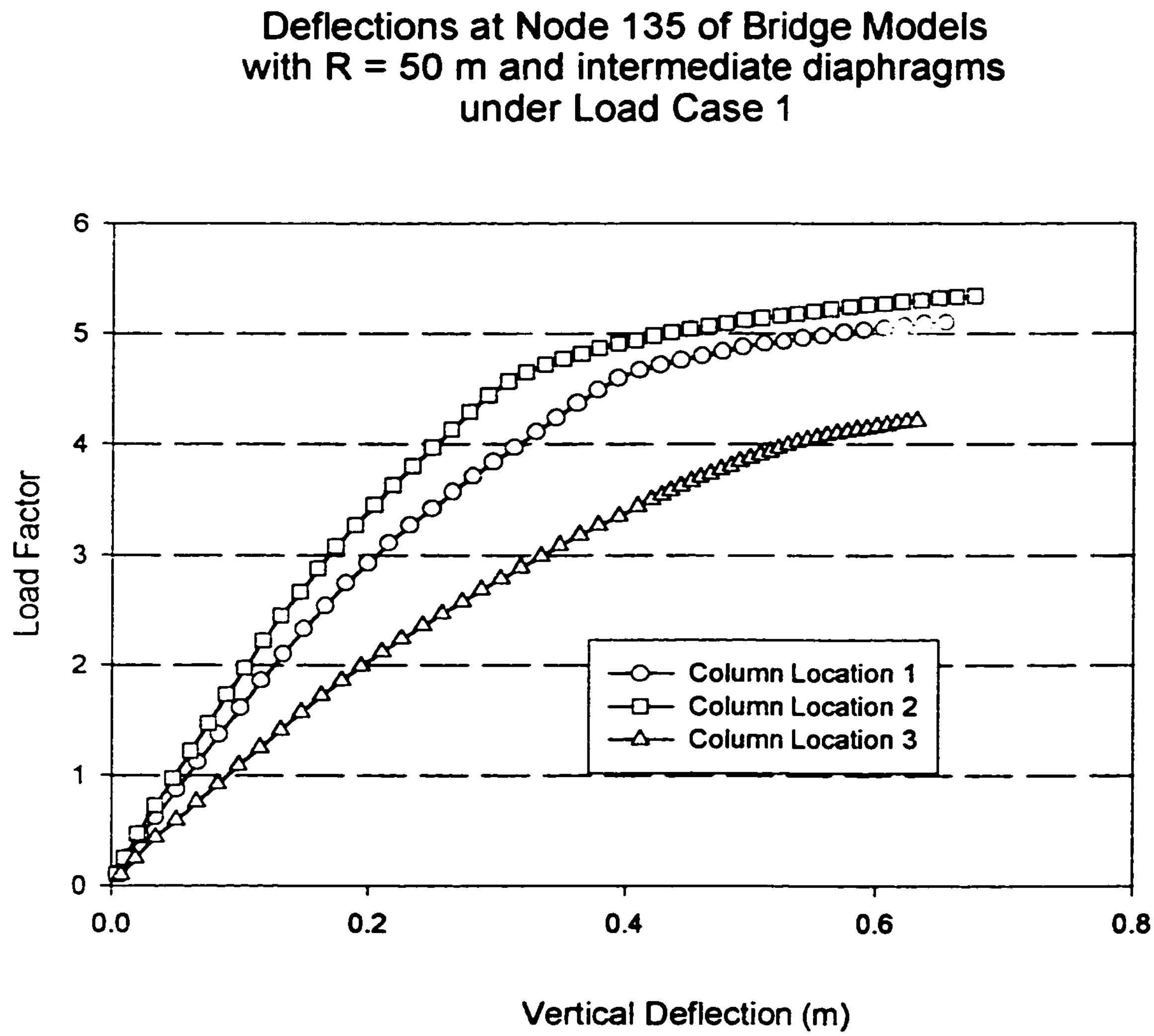

Figure 5.114c Deflections of Node 135 of Bridge Models with R=50m, intermediate diaphragms, and Various Column Locations under Load Case 1

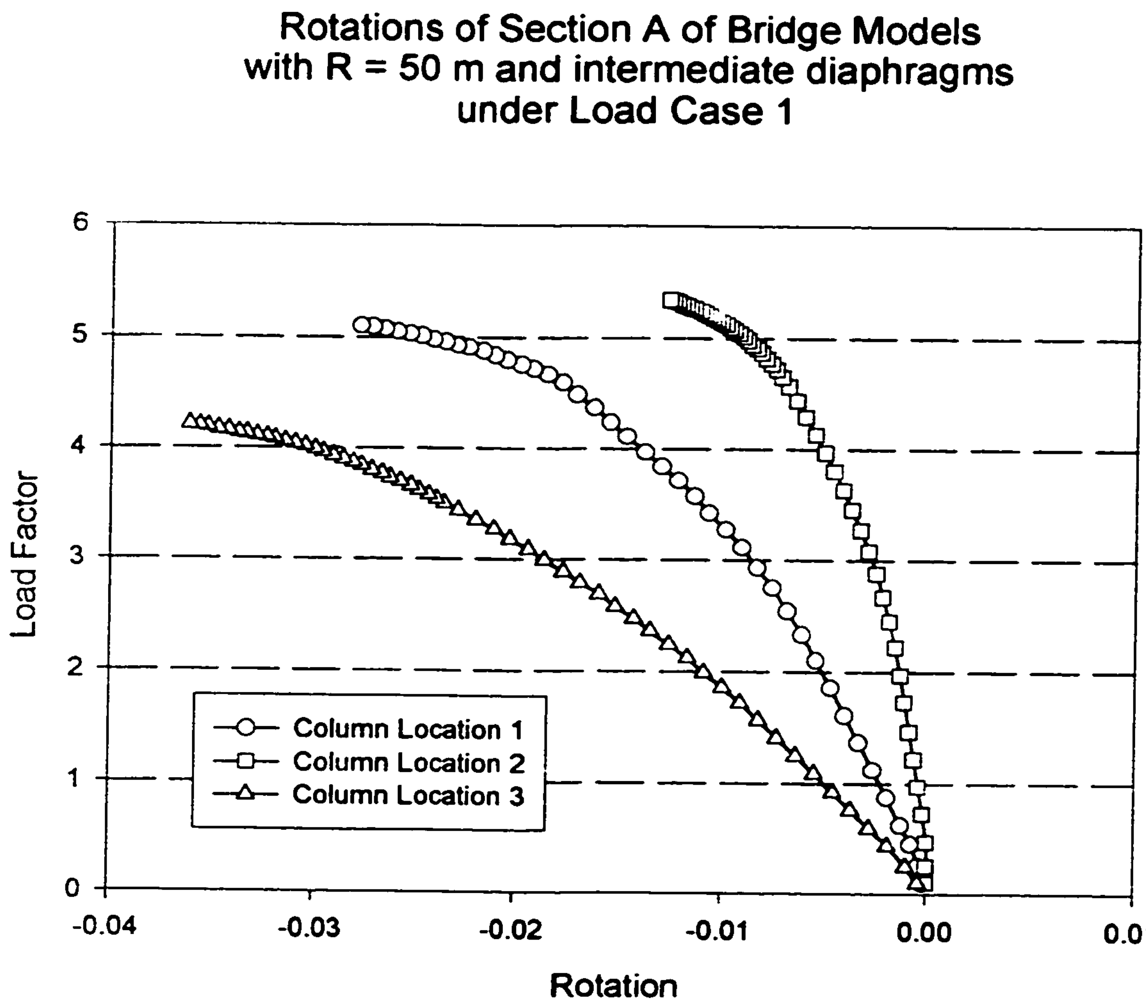

Figure 5.115. Rotations at Section A of Bridge Models with R=50m, intermediate diaphragms, and Various Column Locations under Load Case 1

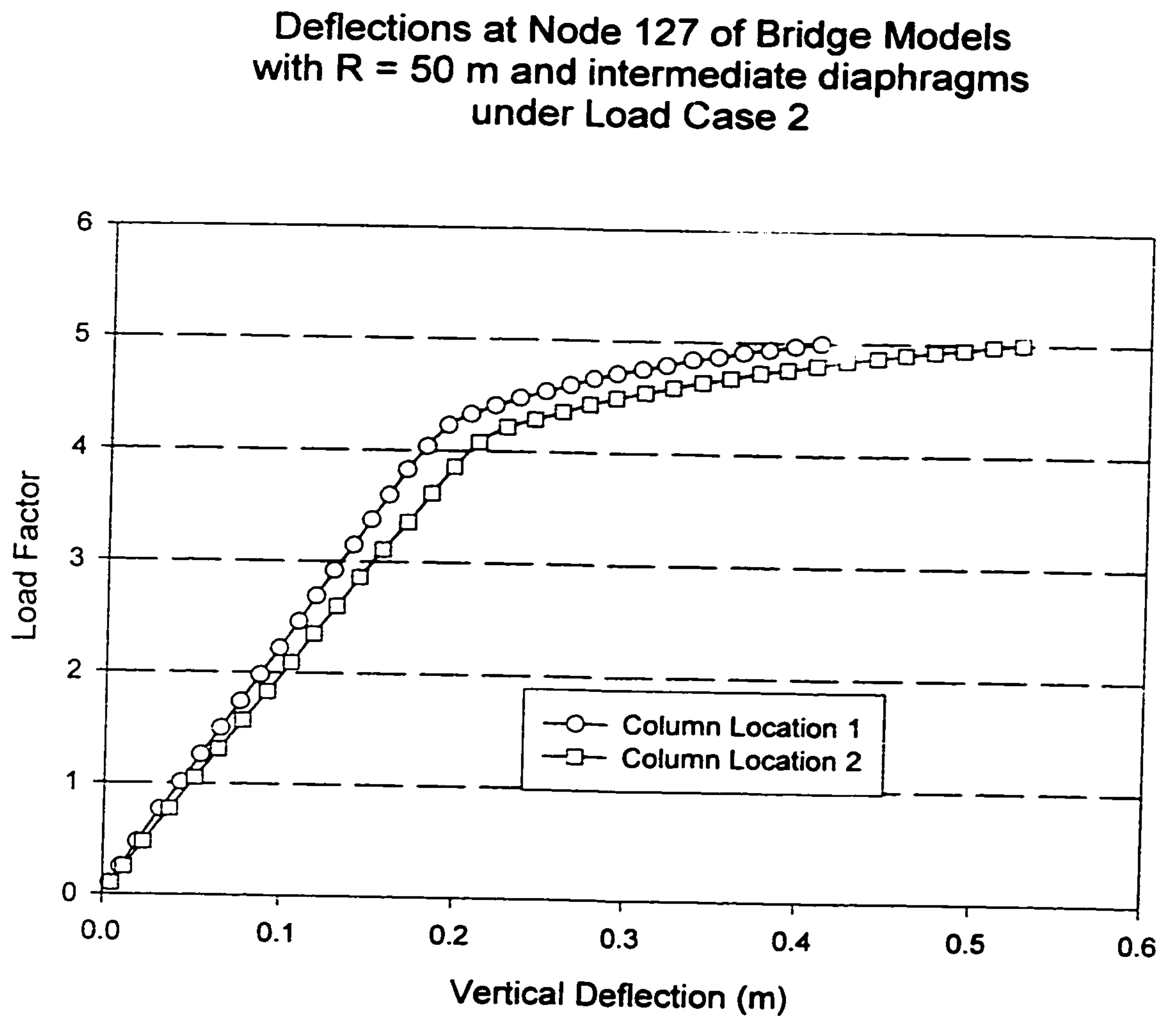

Figure 5.116a Deflections of Node 127 of Bridge Models with R=50m, intermediate diaphragms, and Various Column Locations under Load Case 2

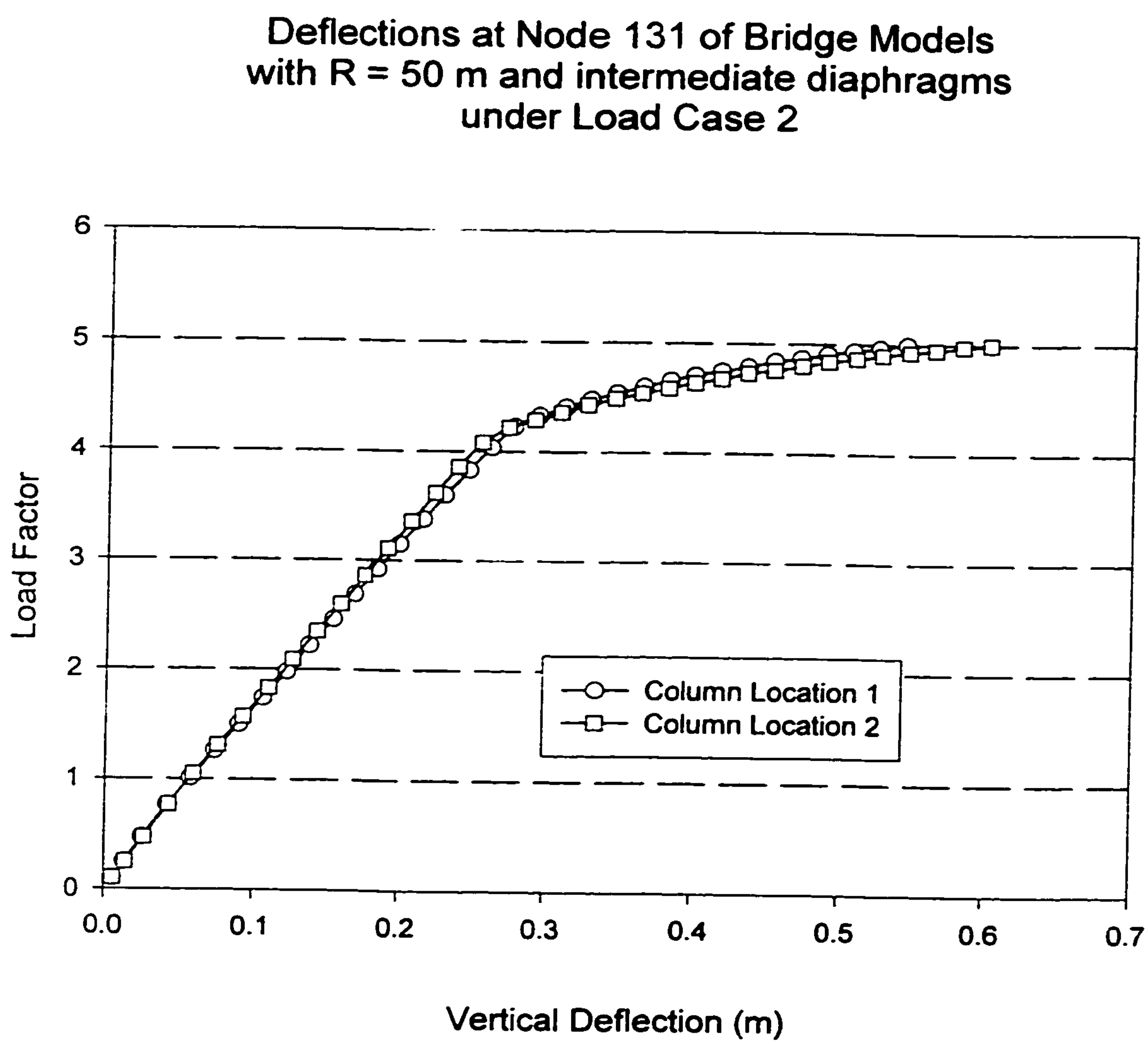

Figure 5.116b Deflections of Node 131 of Bridge Models with R=50m, intermediate diaphragms, and Various Column Locations under Load Case 2

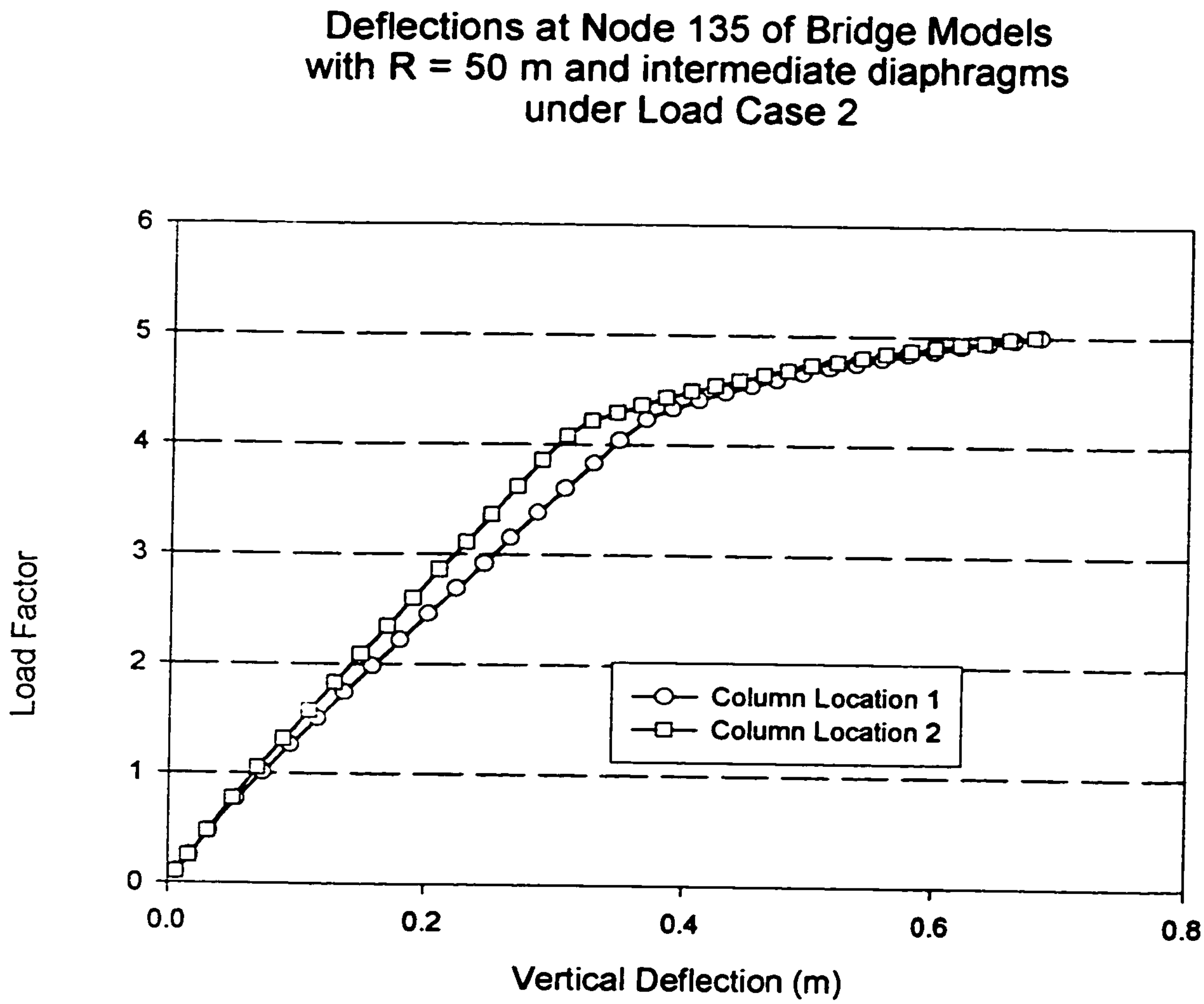

Figure 5.116c Deflections of Node 135 of Bridge Models with R=50m, intermediate diaphragms, and Various Column Locations under Load Case 2

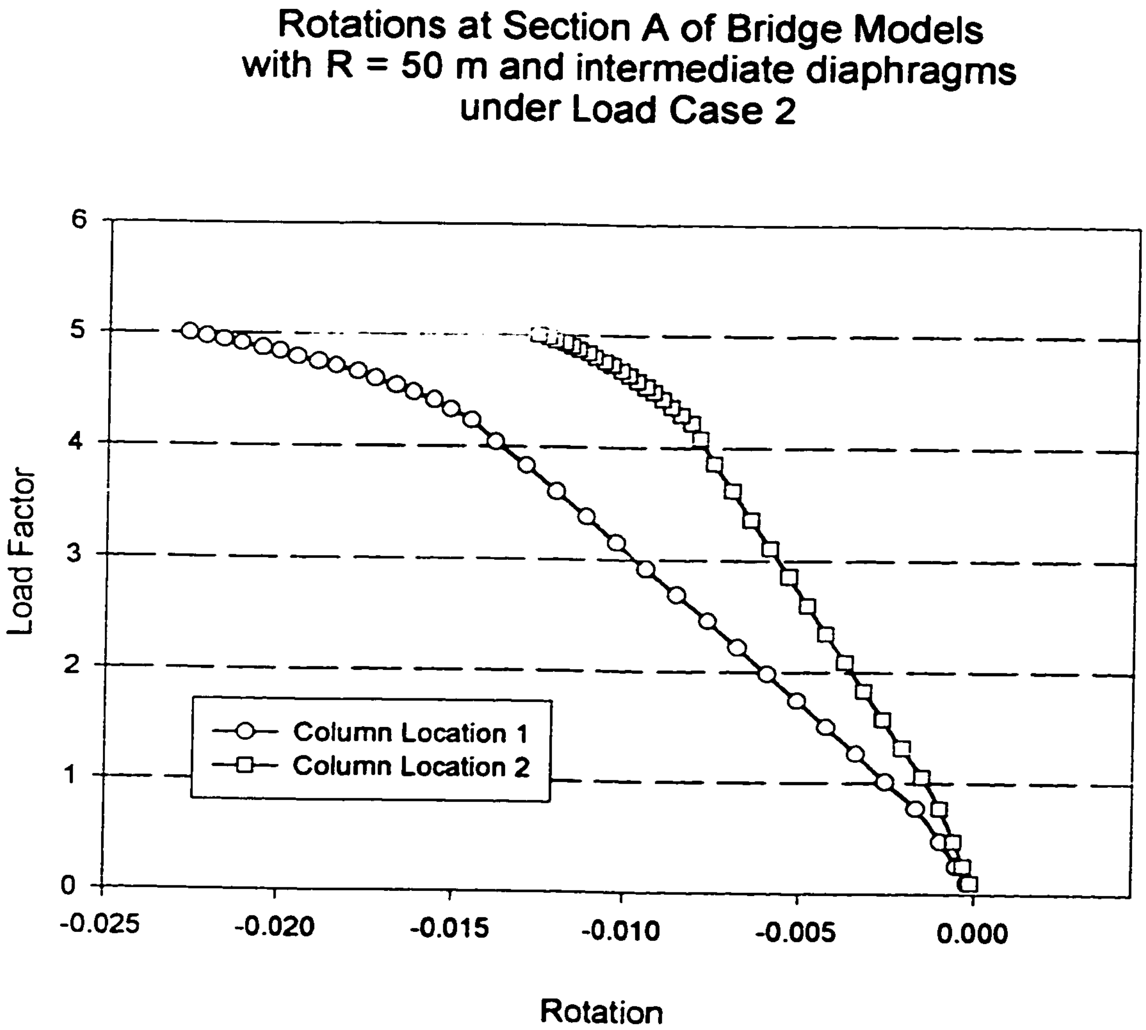

Figure 5.117. Rotations at Section A of Bridge Models with R=50m, intermediate diaphragms, and Various Column Locations under Load Case 2

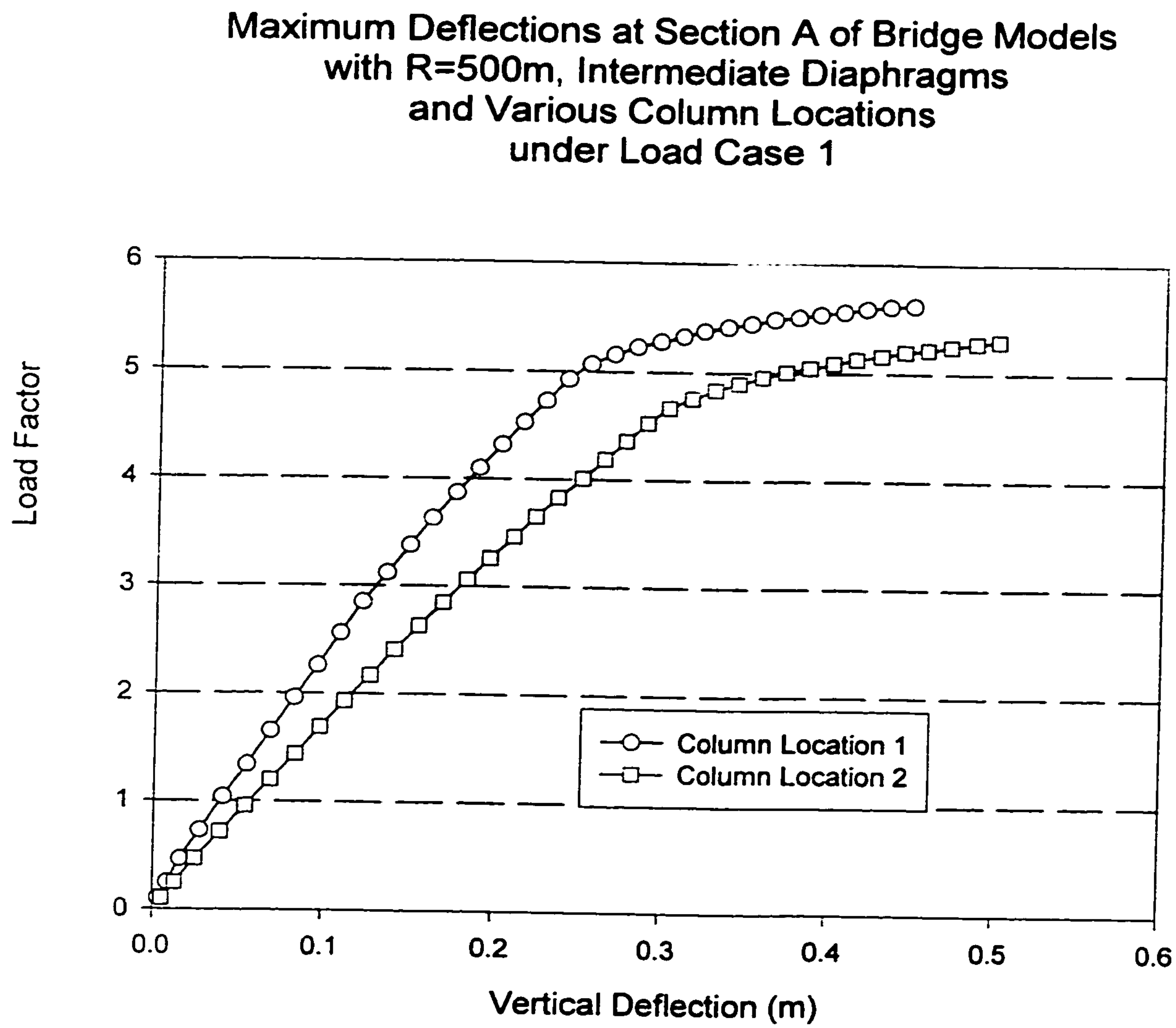

Figure 5.118 Maximum Deflections at Section A of Bridge Models with R=500m, intermediate diaphragms, and Various Column Locations under Load Case 1

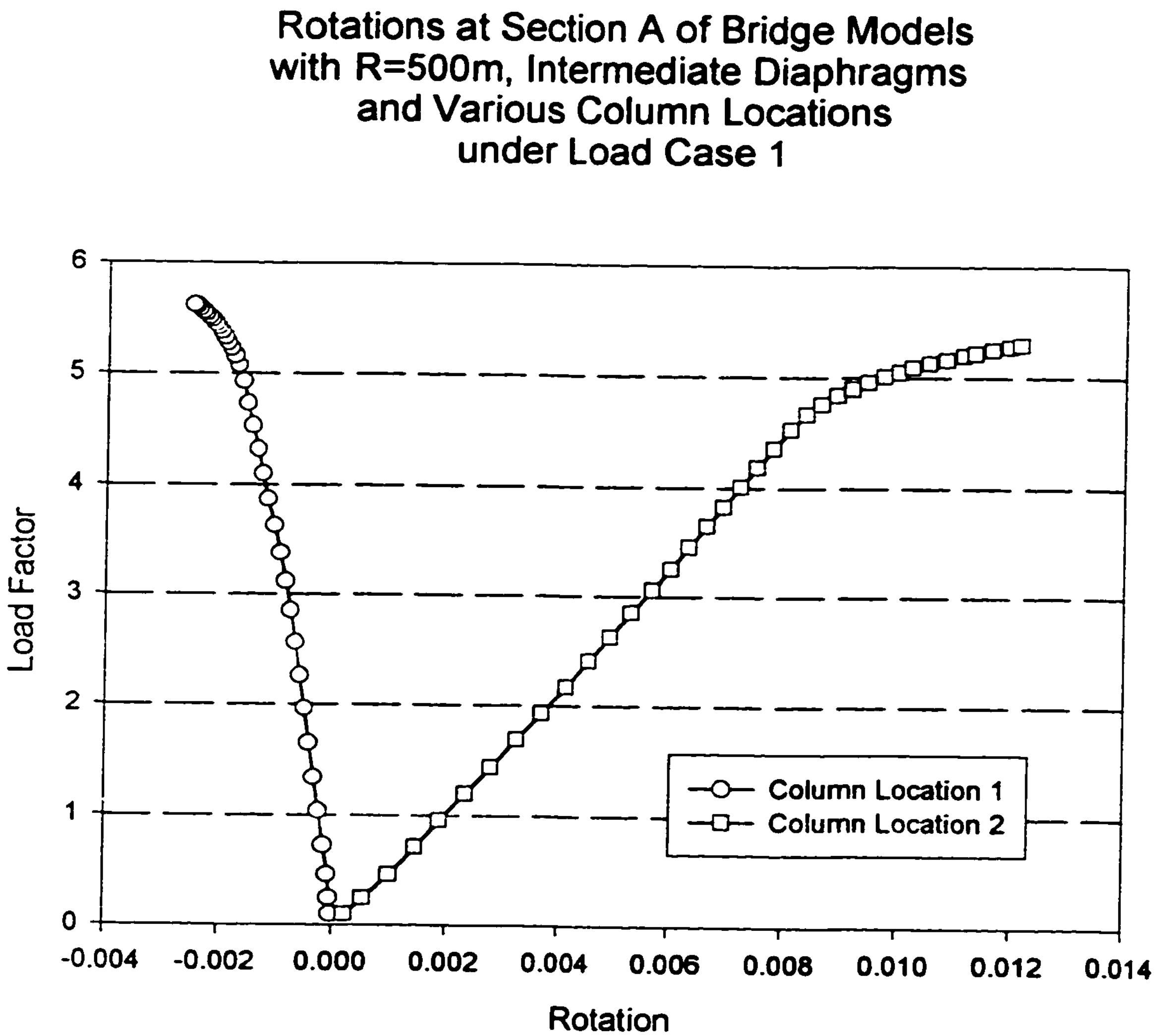

Figure 5.119. Rotations at Section A of Bridge Models with R=500m, intermediate diaphragms, and Various Column Locations under Load Case 1

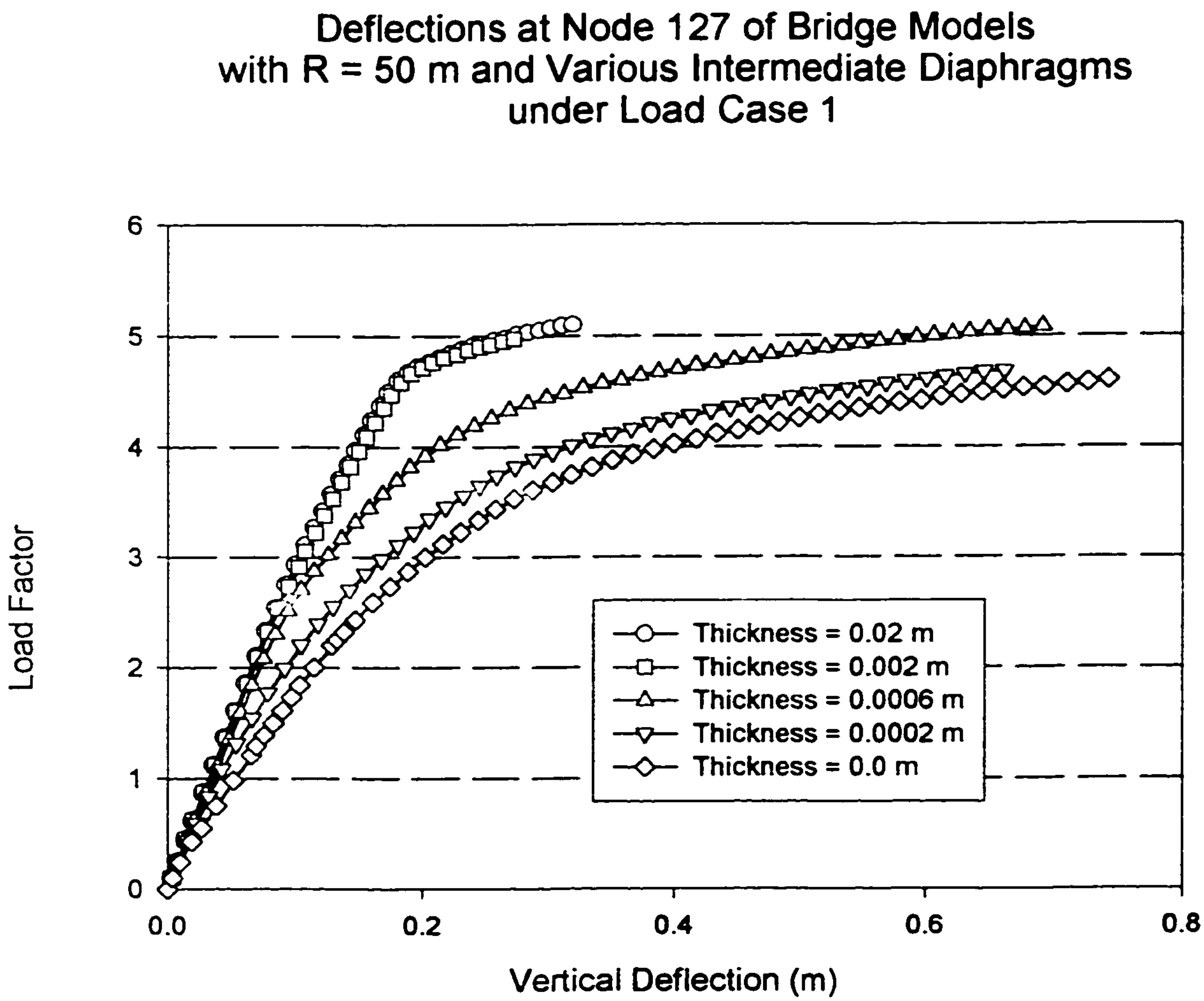

Figure 5.120a Deflections of Node 127 of Bridge Models with R=50m, various intermediate diaphragms, and Column Location 1 under Load Case 1

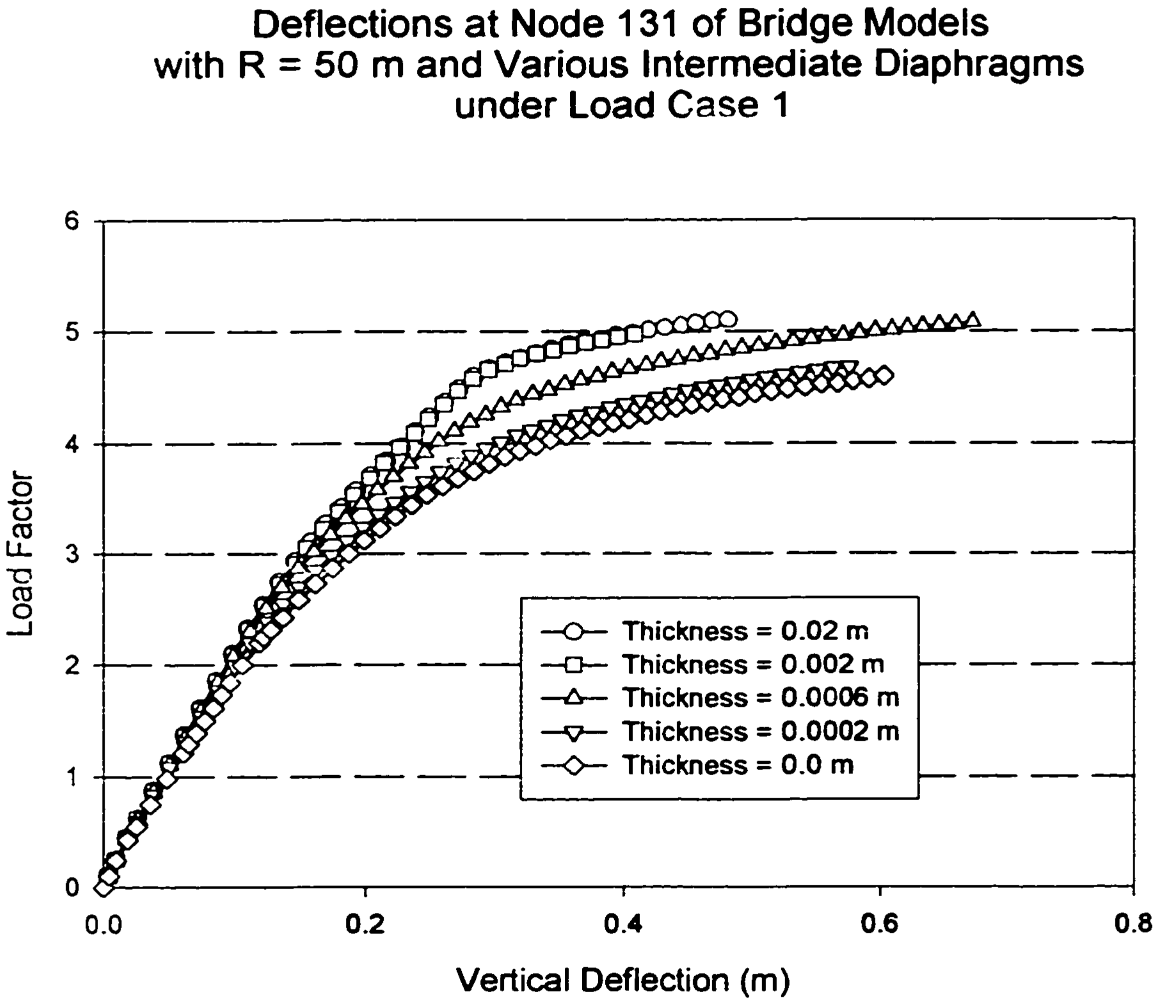

Figure 5.120b Deflections of Node 131 of Bridge Models with R=50m, various intermediate diaphragms, and Column Location 1 under Load Case 1

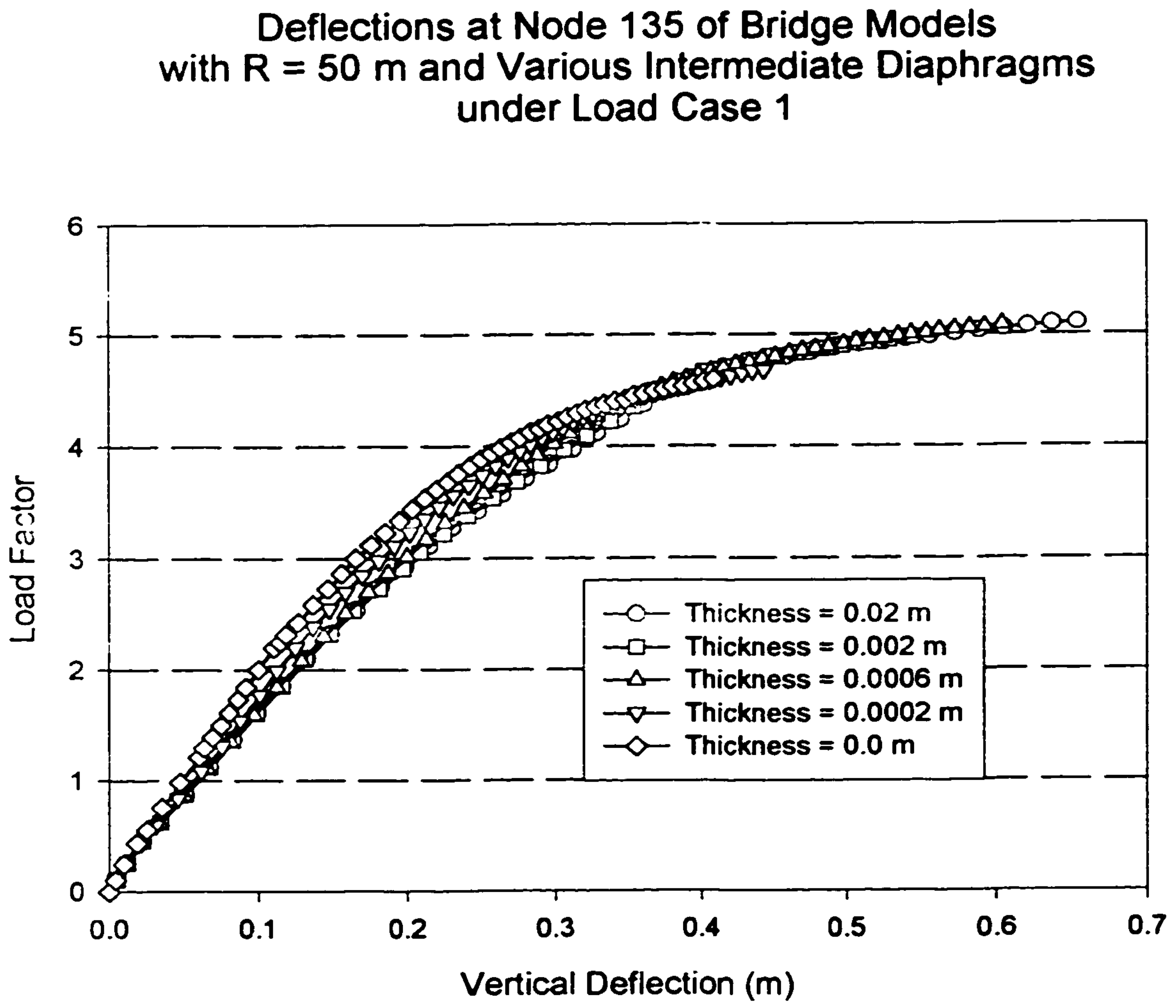

Figure 5.120c Deflections of Node 135 of Bridge Models with R=50m, various intermediate diaphragms, and Column Location 1 under Load Case 1

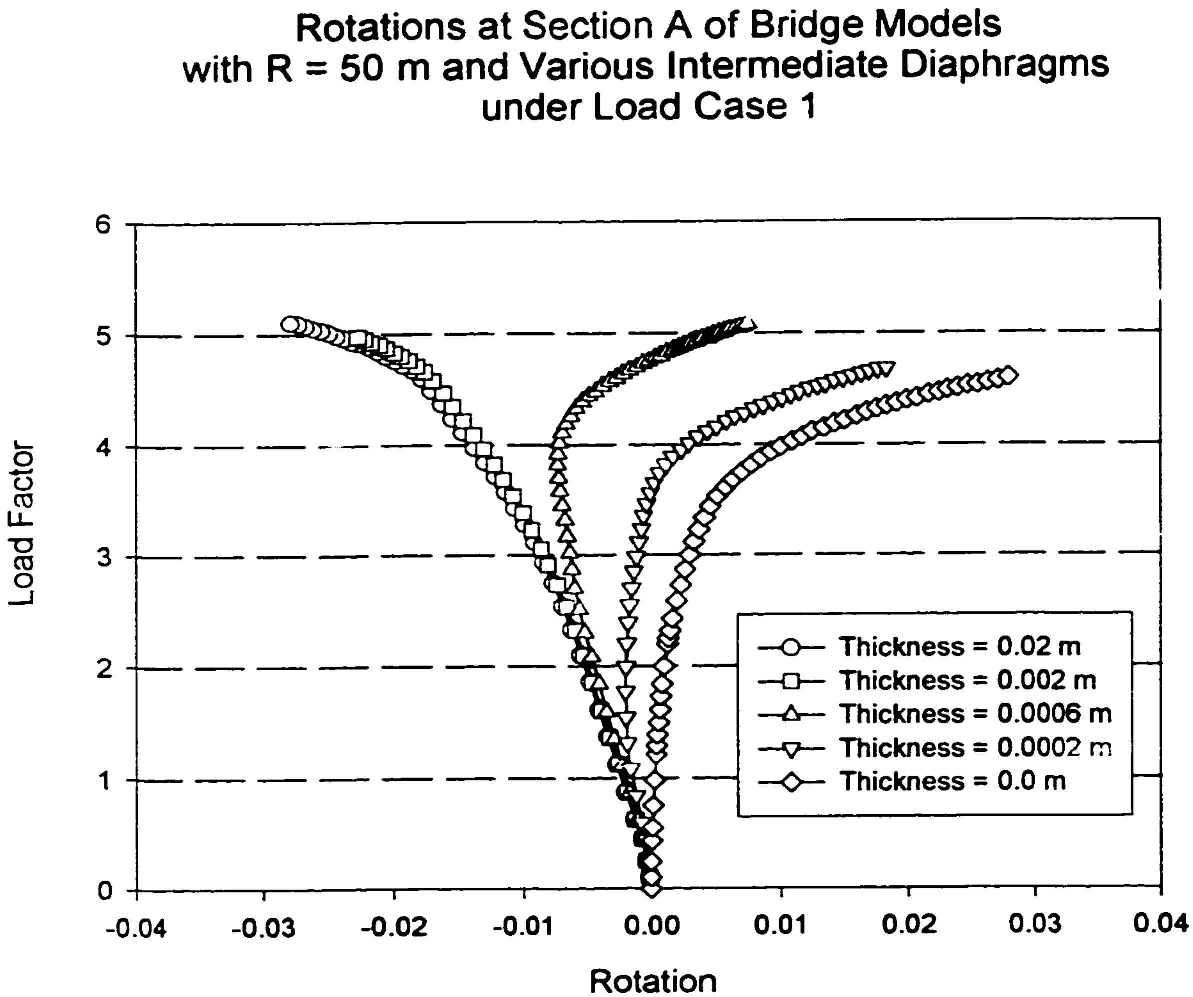

Figure 5.121. Rotations at Section A of Bridge Models with R=50m, various intermediate diaphragms, and Column Location 1 under Load Case 1

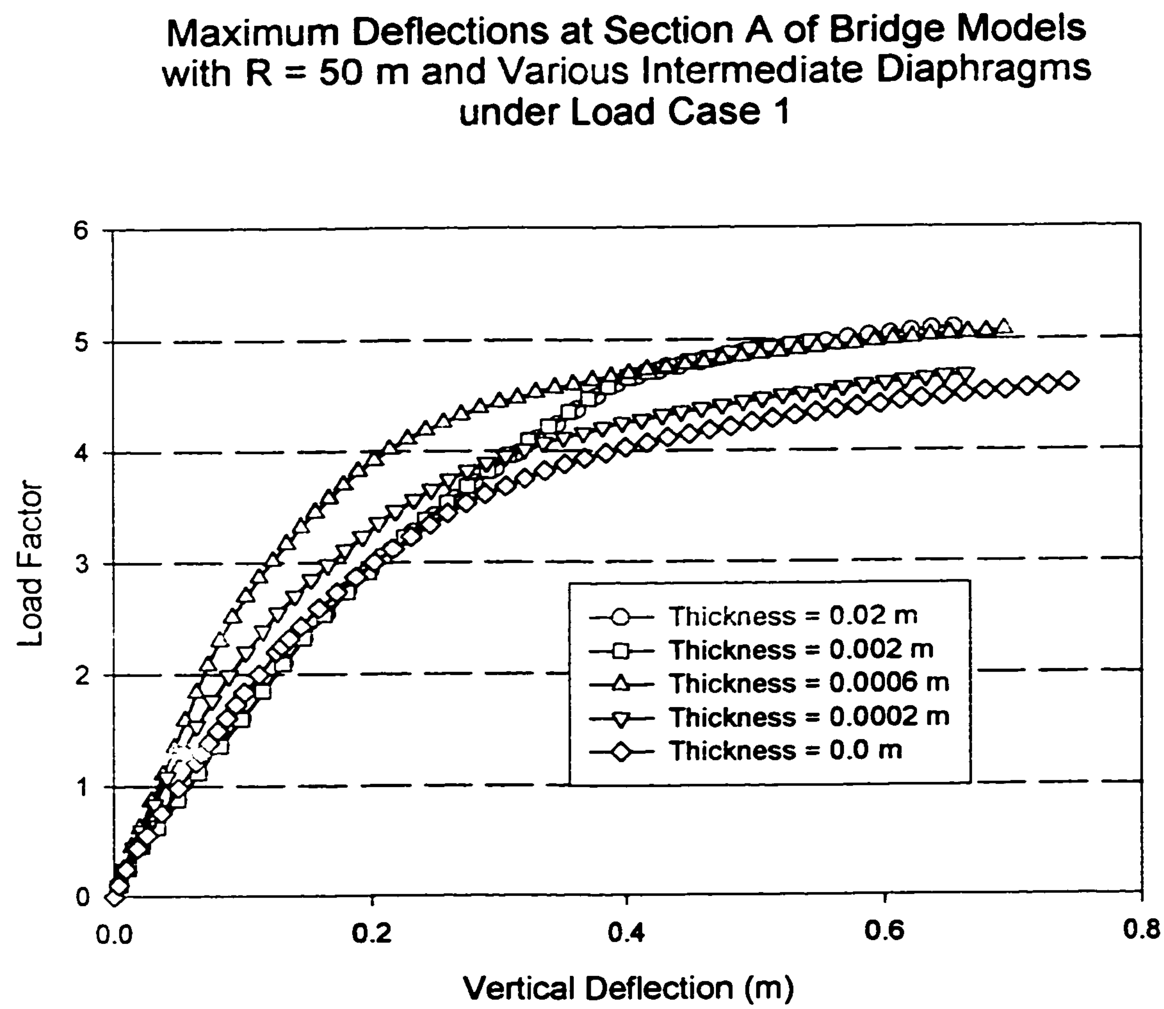

Figure 5.122 Maximum Deflections at Section A of Bridge Models with R=50m, various intermediate diaphragms, and Column Location 1 under Load Case 1

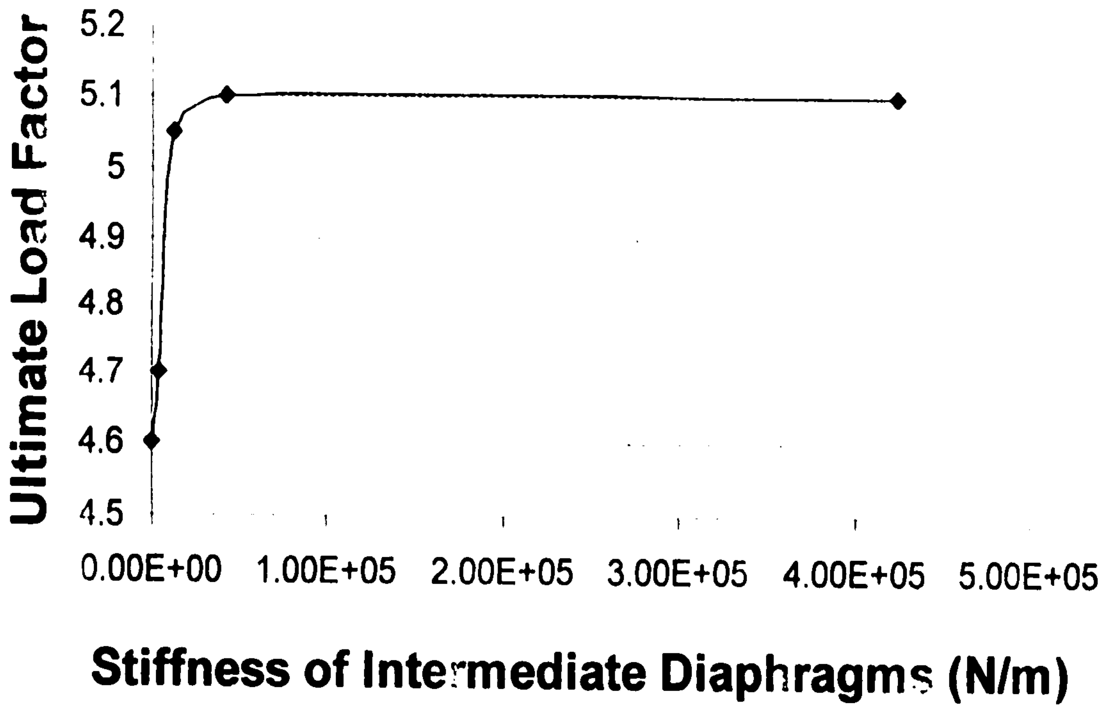

Figure 5.123 Ultimate Load Factor of bridge models vs. the stiffness of intermediate diaphragms

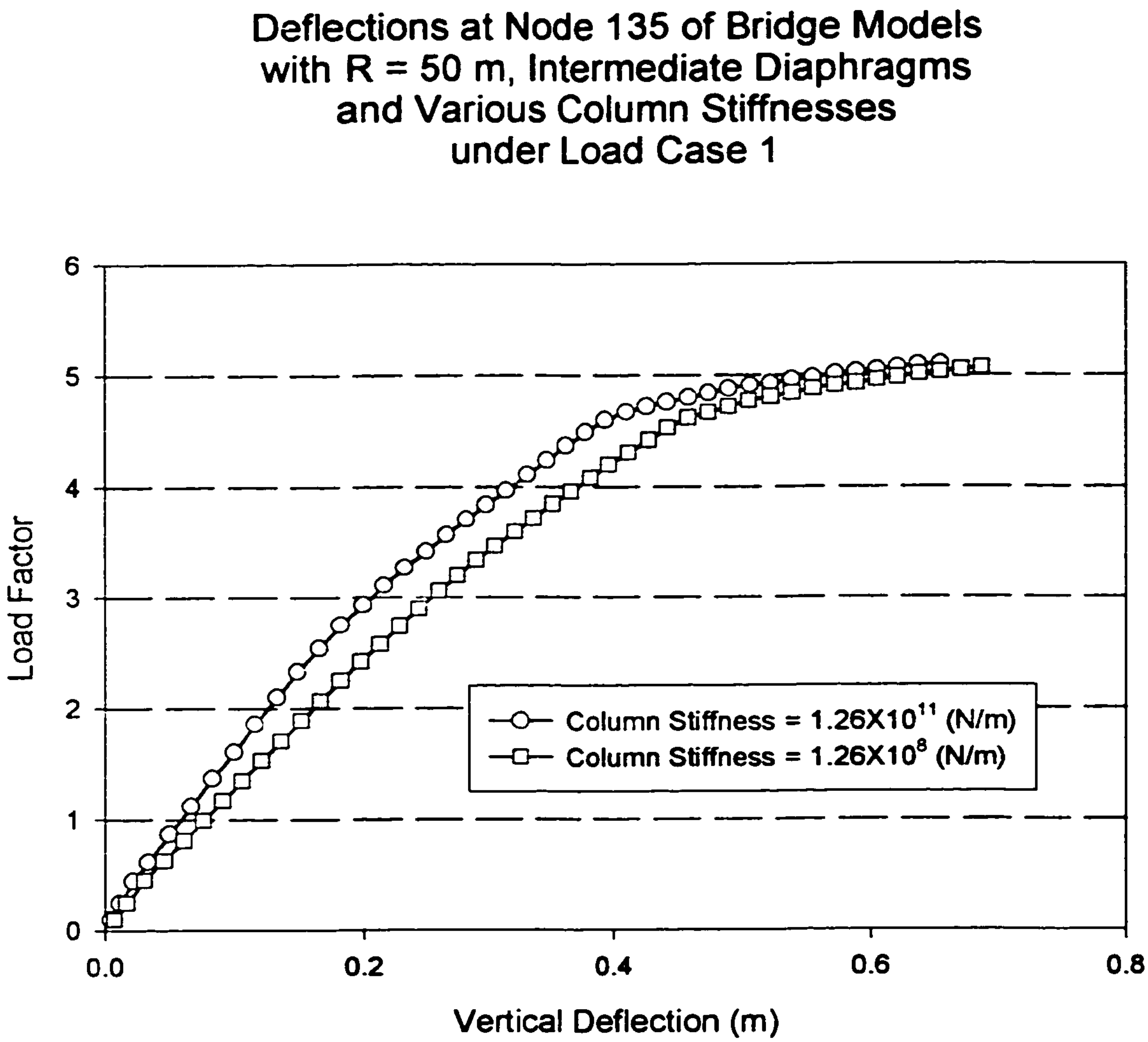

Figure 5.124 Deflections of Node 135 of Bridge Models with R=50m, intermediate diaphragms, and various column stiffnesses under Load Case 1

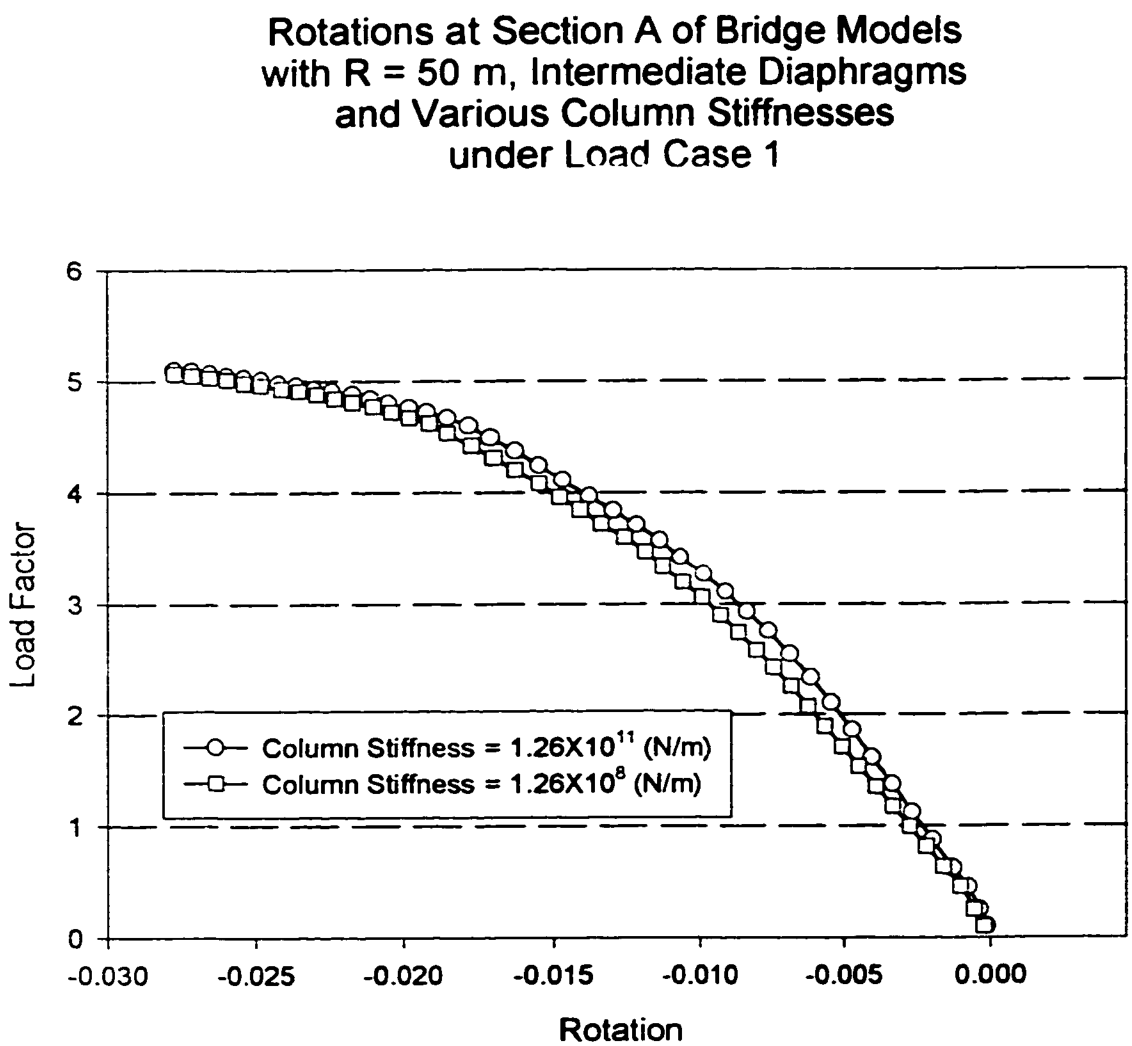

Figure 5.125. Rotations at Section A of Bridge Models with R=50m, intermediate diaphragms, and various column stiffnesses under Load Case 1

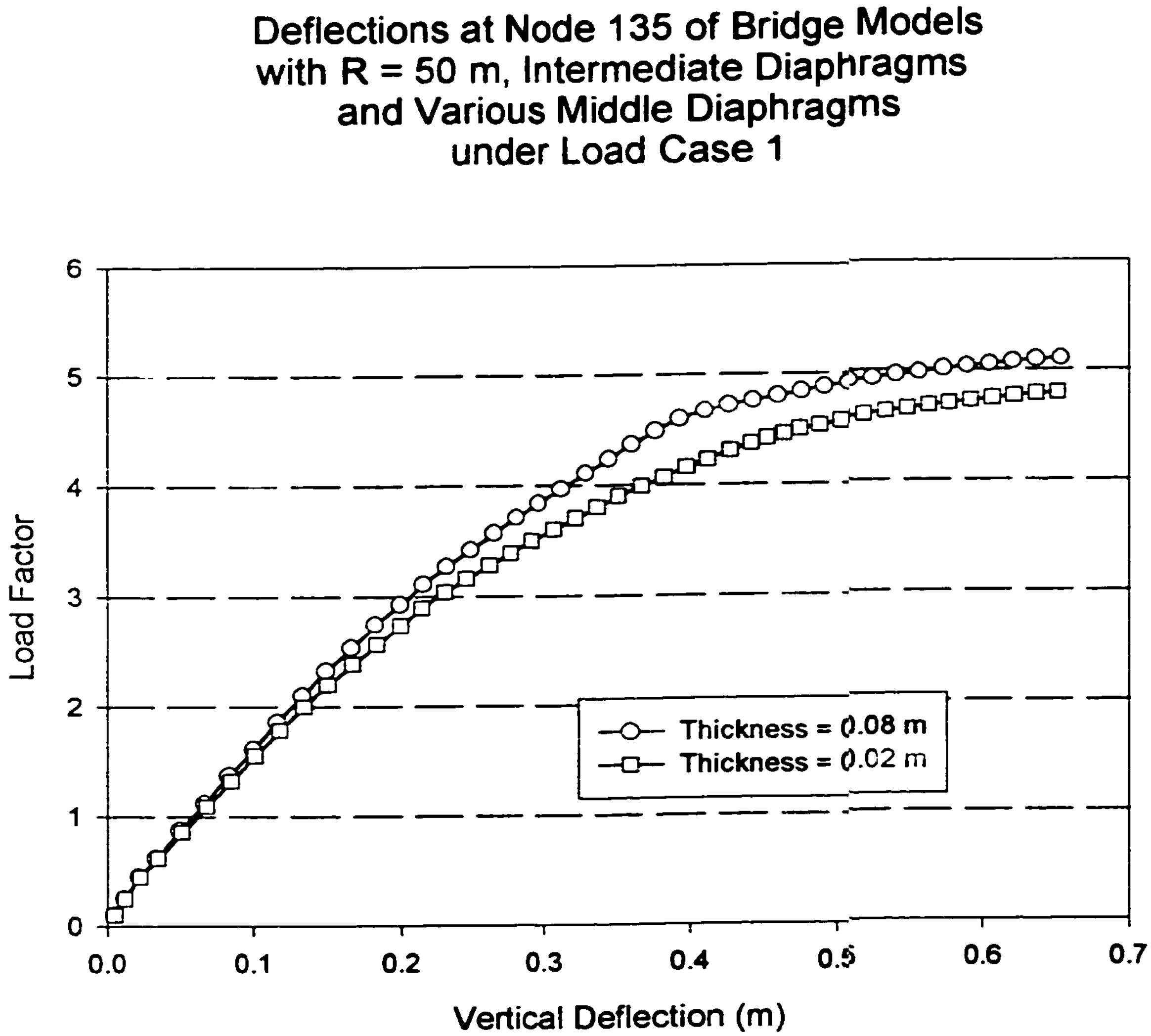

Figure 5.126 Deflections of Node 135 of Bridge Models with R=50m, intermediate diaphragms, and various middle diaphragms under Load Case 1

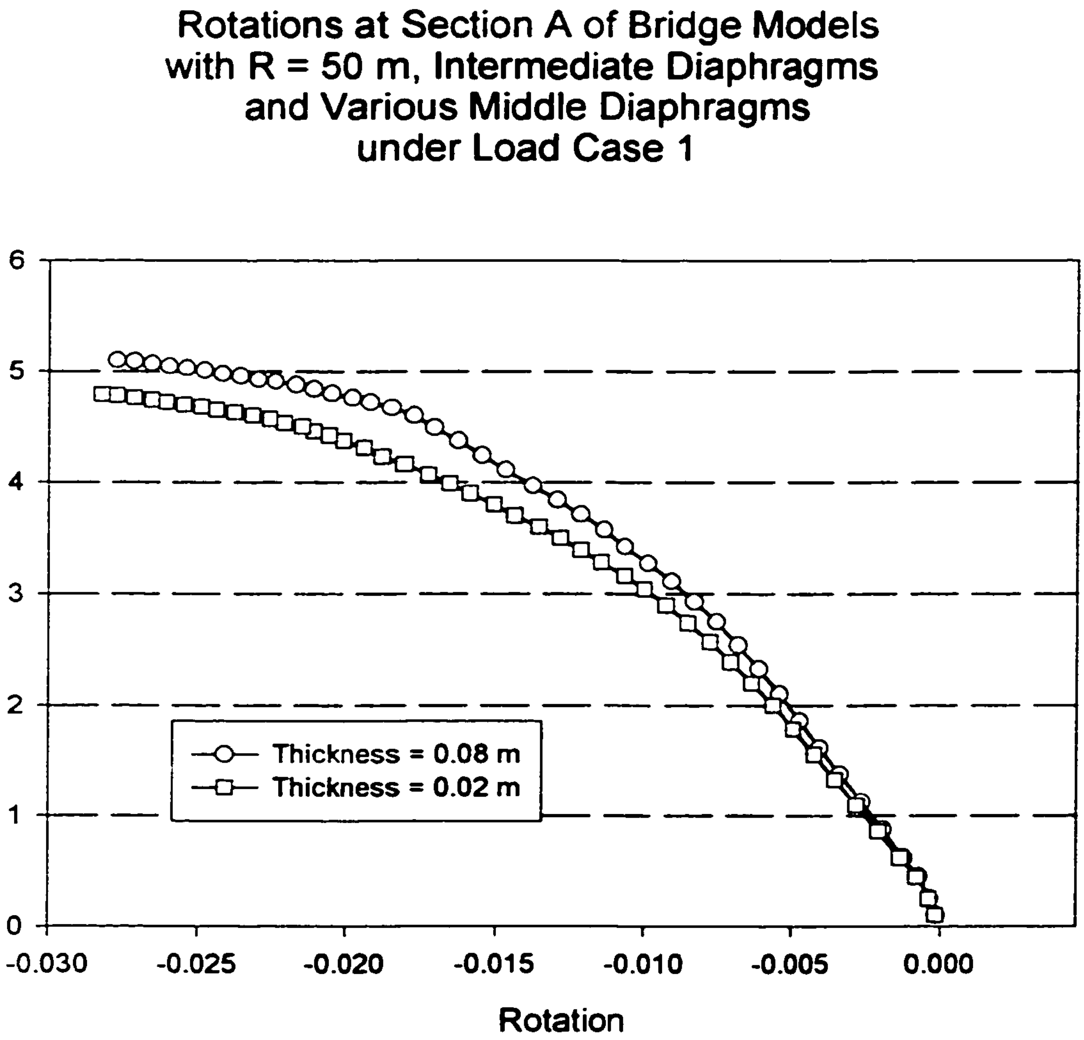

Figure 5.127. Rotations at Section A of Bridge Models with R=50m, intermediate diaphragms, and various middle diaphragms under Load Case 1

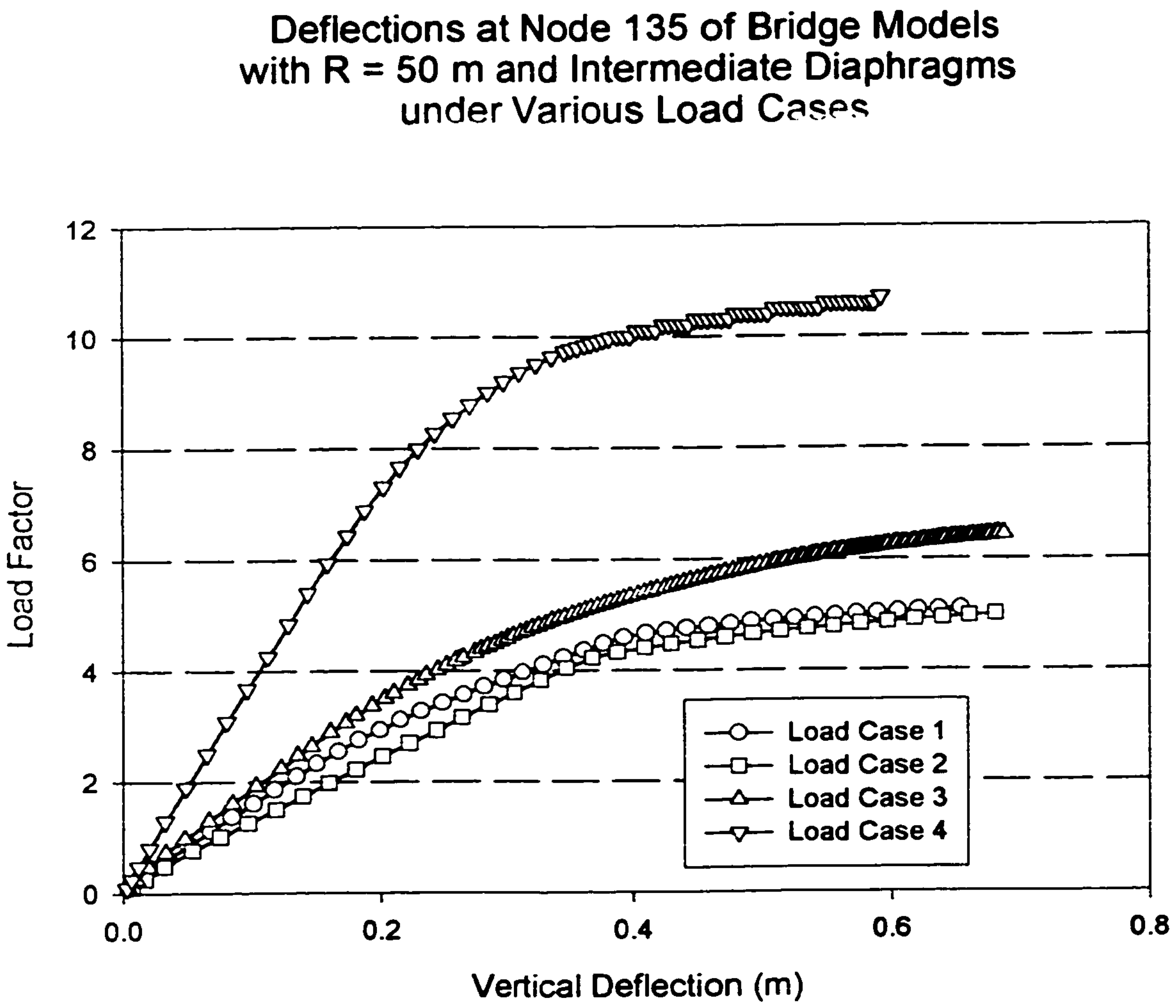

Figure 5.128 Deflections of Node 135 of Bridge Models with R=50m and intermediate diaphragms under various Load Cases

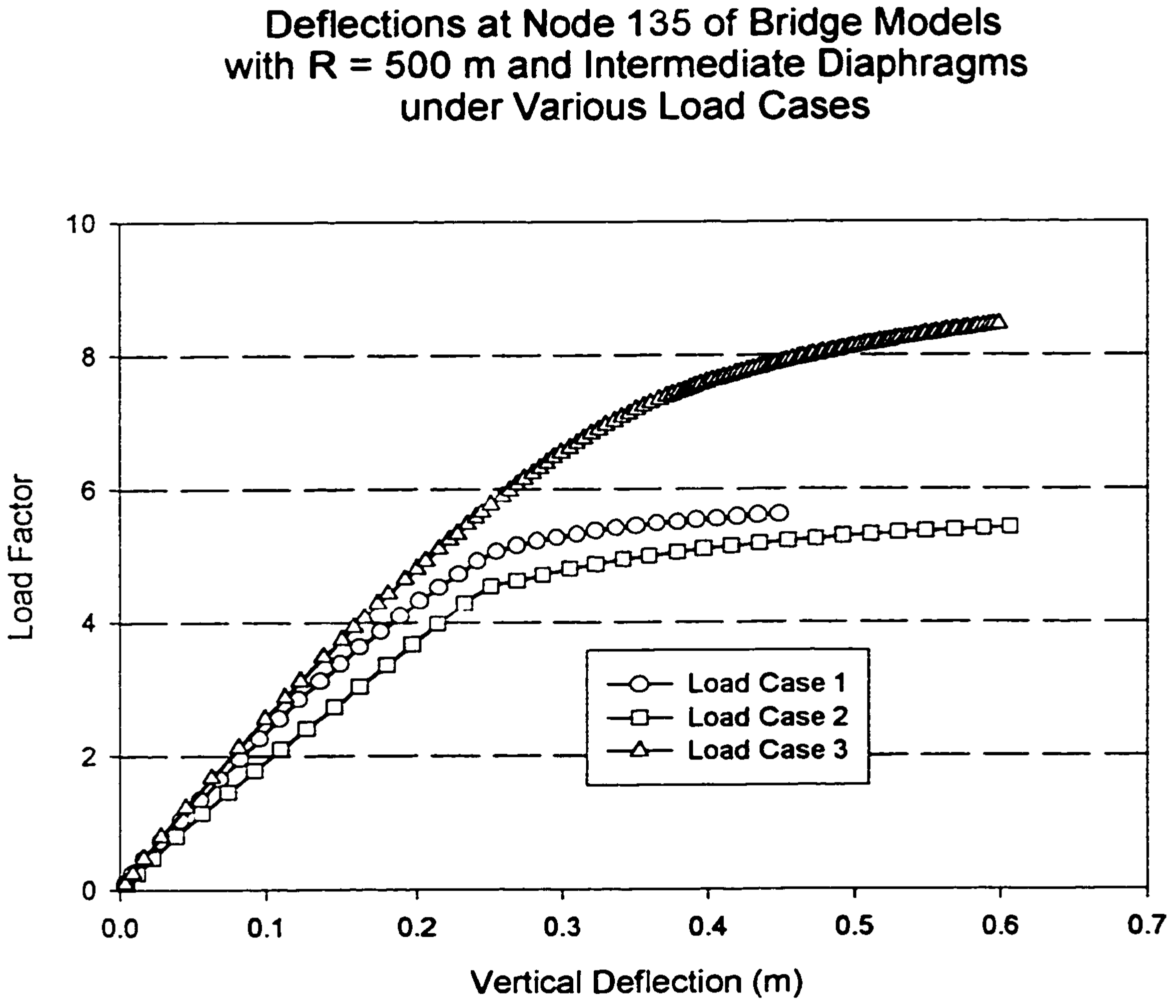

Figure 5.129. Deflections of Node 135 of Bridge Models with R=500m and intermediate diaphragms under various Load Cases

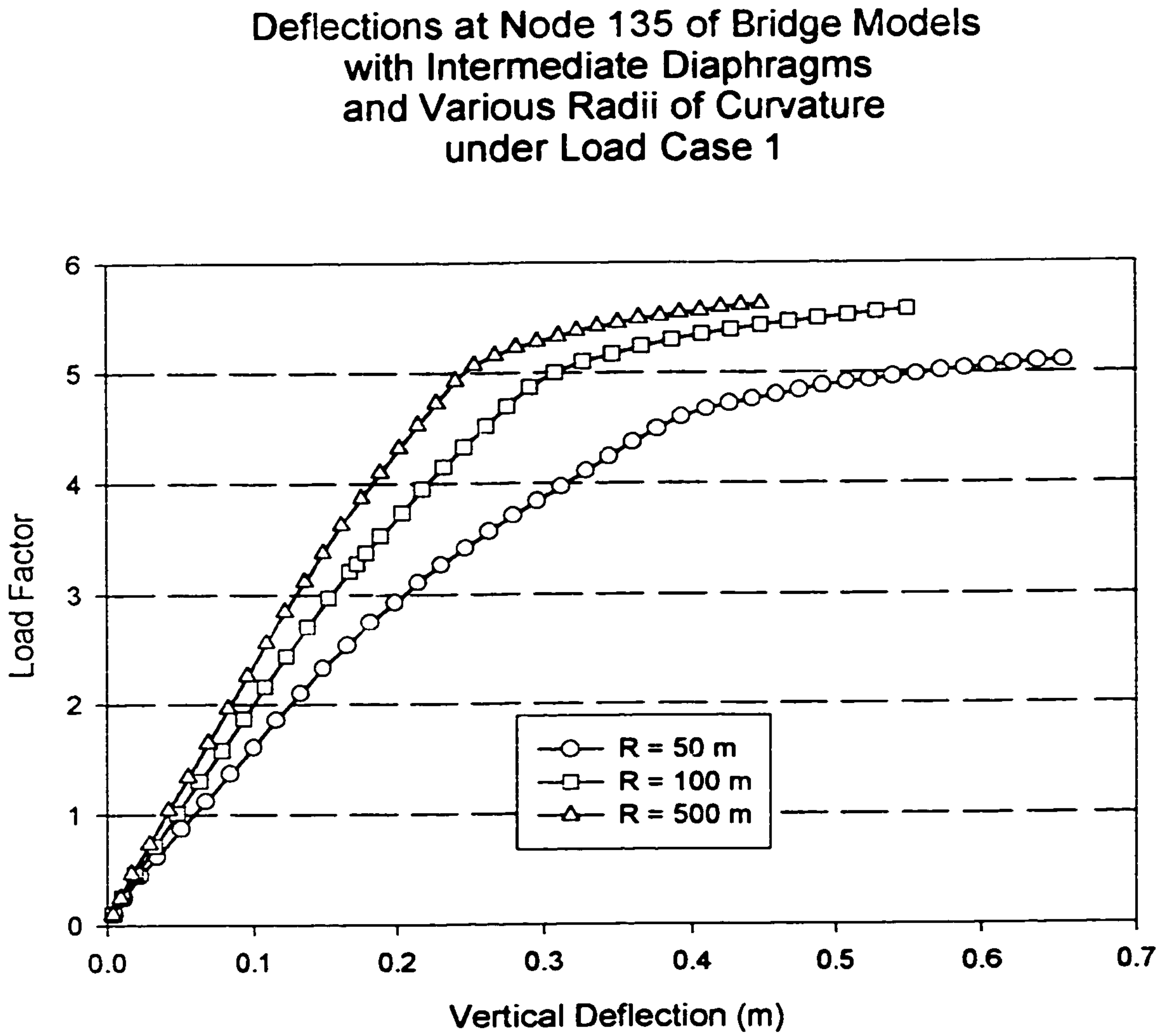

Figure 5.130 Deflections of Node 135 of Bridge Models with intermediate diaphragms, and various radii of curvature under Load Case 1

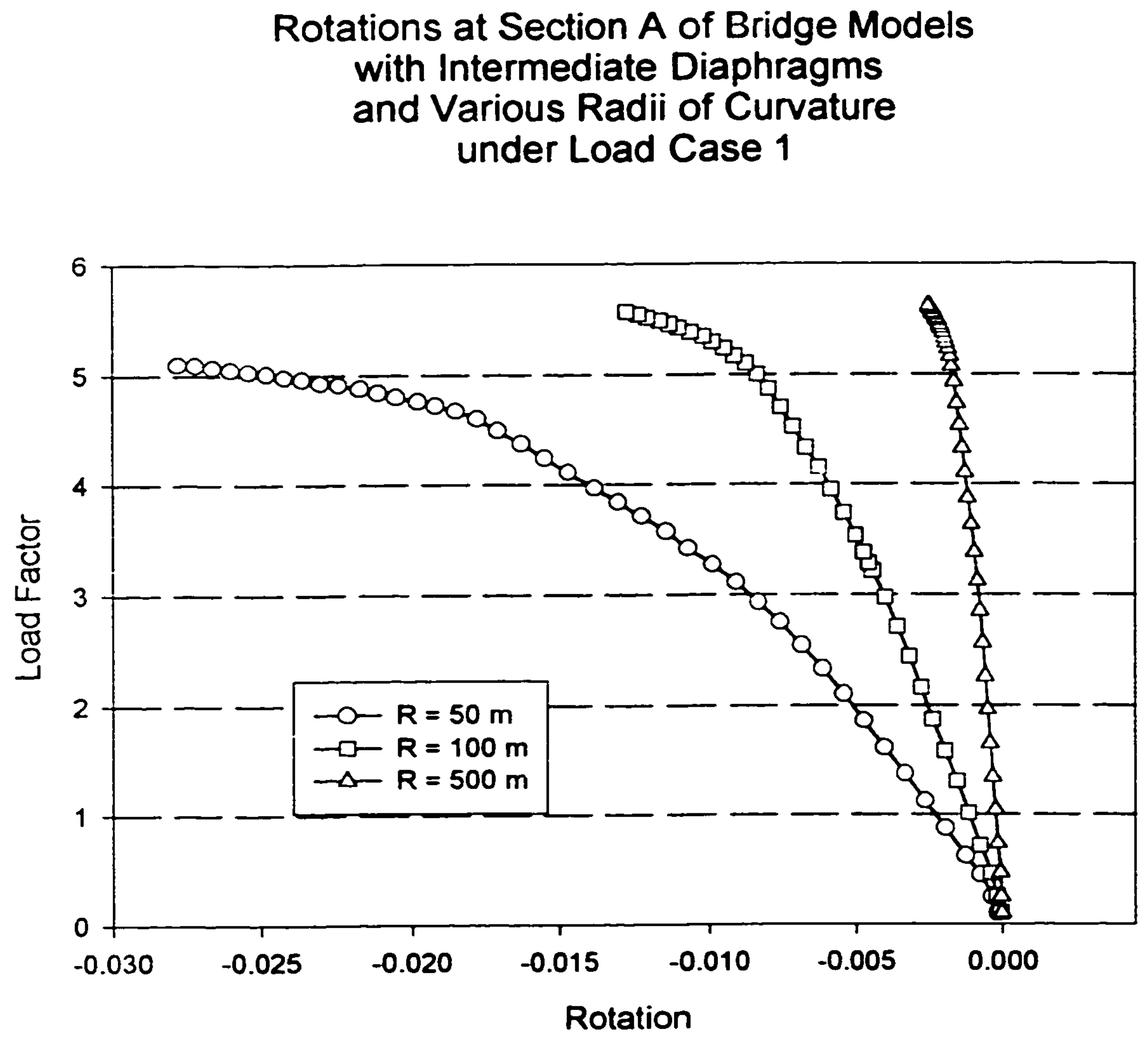

Figure 5.131. Rotations at Section A of Bridge Models with intermediate diaphragms, and various radii of curvature under Load Case 1

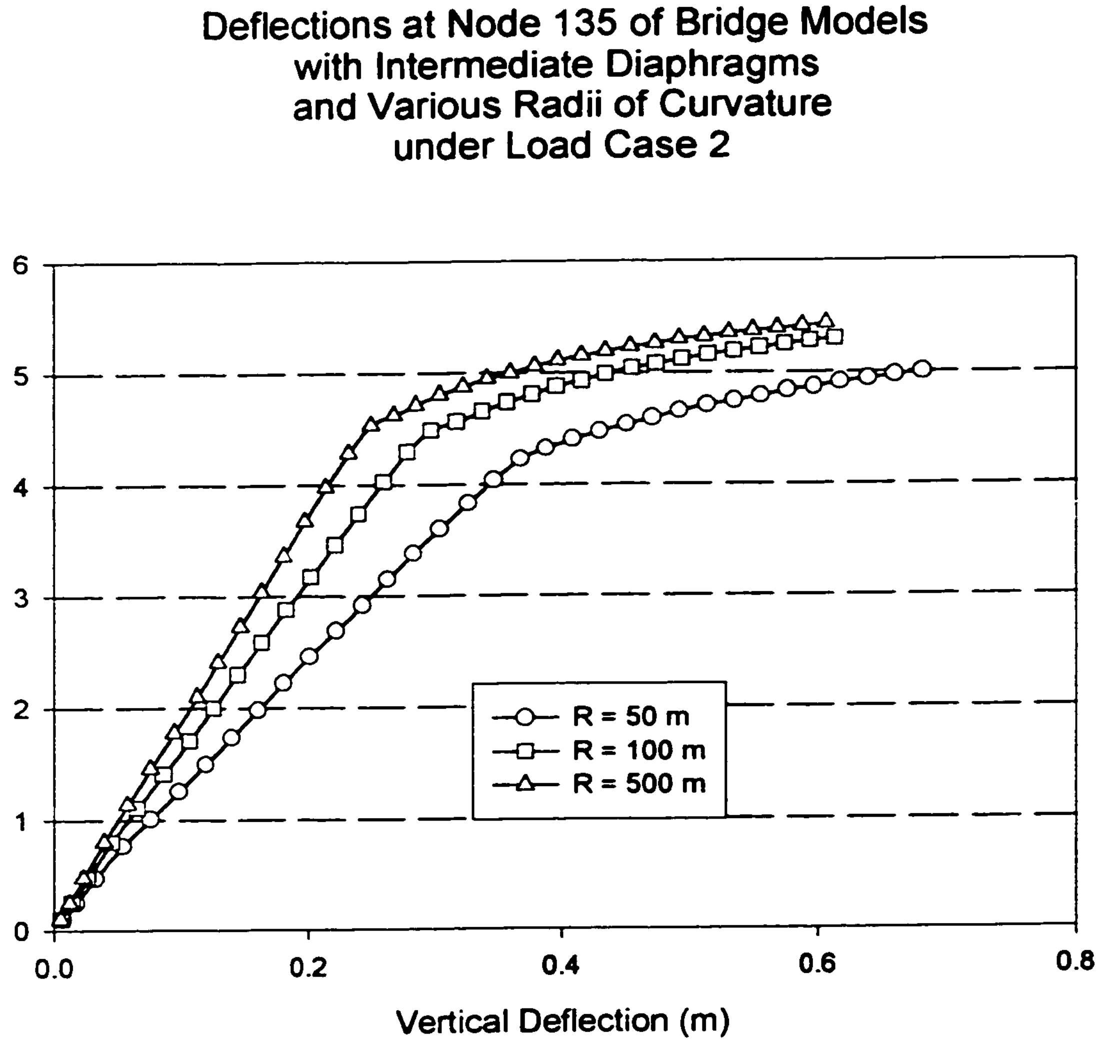

Figure 5.132 Deflections of Node 135 of Bridge Models with intermediate diaphragms, and various radii of curvature under Load Case 2

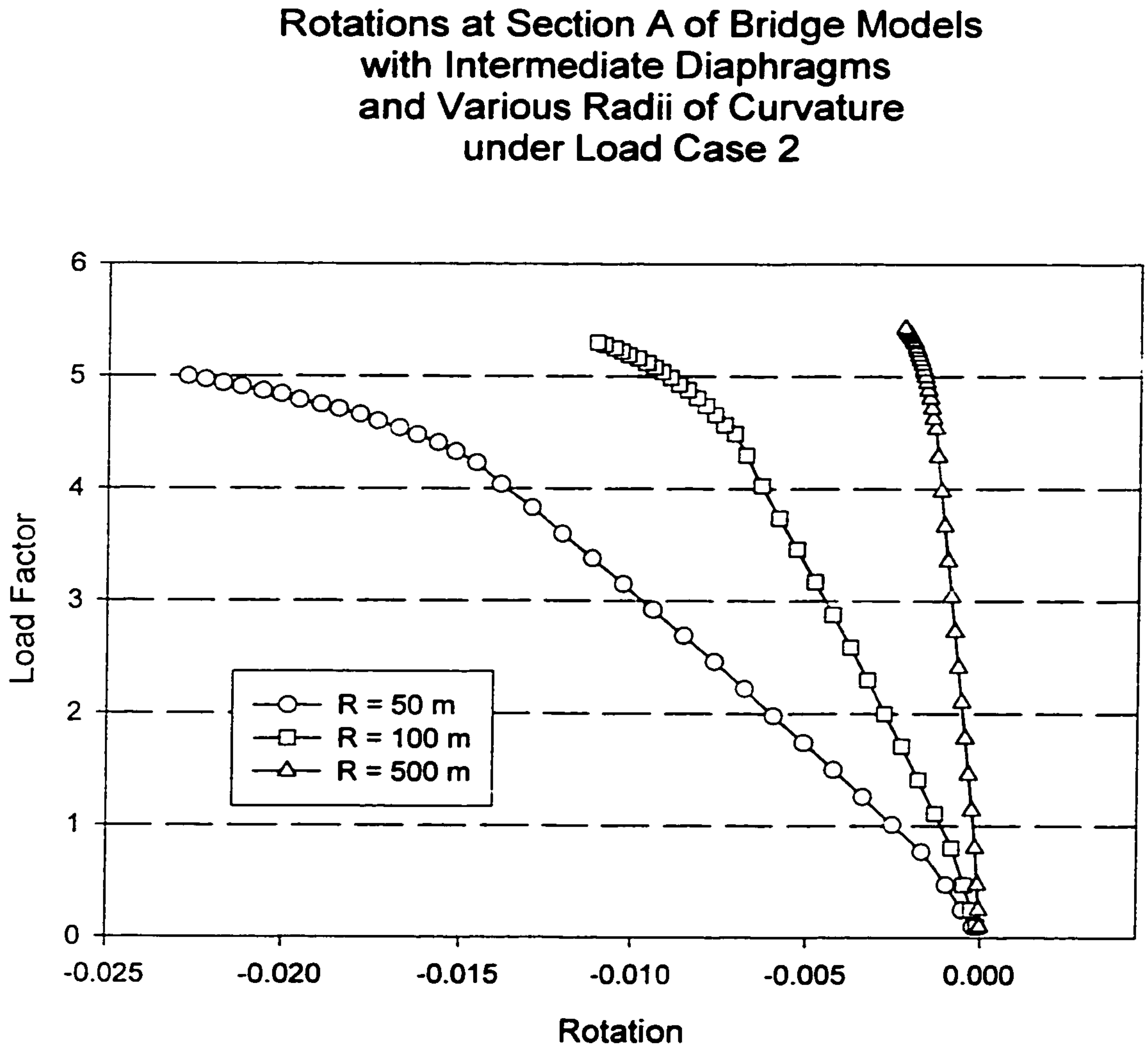

Figure 5.133. Rotations at Section A of Bridge Models with intermediate diaphragms, and various radii of curvature under Load Case 2

5.10. Discussion of research results

The nonlinear behaviors of a two-span continuous curved composite box-girder bridge model with a single column support in mid-span are investigated with various parameters. The effects of the main parameters on the ultimate loads and nonlinear behaviors of such bridges have been presented in the above sections.

Based on above observations for the bridge models with any radius of curvature, it can be concluded that the bridge models have the lowest ultimate load factor under Load Case 1; Load Case 2 will induce almost the same ultimate load factor for the bridge models as Load case 1; though Load Cases 3 and 4 will induce a larger rotation at section A of the bridge models and Load Case 2 will produce larger deflections and a smaller rotation at section A in elastic region. However, if Column Location 1 is used, it will increase the ultimate load level of the bridge models. Generally, Column Locations 2 and 3 will reduce the overall ultimate capacity of the bridge models. With a L/R value greater than 0.3 under Load Case 1 and greater than 0.2 under Load Case 2, the ultimate load capacity of bridge models decrease faster and the effect of the curvature must be taken into account in the analysis. That is, it can be concluded that when L/R is less than 0.2, the bridge models can be analyzed as straight bridges. The ultimate load capacity of the bridge models does not vary significantly when rigid shear connectors or regular shear connectors are used. In other words, the effect of the stiffness of shear connectors may be ignored in the analysis if sufficient shear connectors are used following OHBDC. It is also found that these is no significant difference of the ultimate load capacity for the bridge models when the stiffness of the middle diaphragm is greater than 5×10^6 (N/m). It is also noted that the bridge models have almost the same ultimate load capacity when the stiffness of the middle column is greater than 1.26×10^9 (N/m). In general, the stiffness of the middle column is greater than 1.26×10^9 (N/m) in practice. Therefore, it can be concluded that the ultimate load capacity of the bridge will not be significantly affected by the stiffness of the middle column.

As for effects of the stiffness of intermediate diaphragms on curved box-girder bridges, it was found in this study that when the stiffness of intermediate diaphragms is greater than 0.0006m, the capacity of the ultimate load of the bridge model will increase by 10% in comparison with the bridge model without intermediate diaphragms. That is, sufficient intermediate diaphragms will increase the capacity of the ultimate load of the curved bridges by as much as 10%. Generally, the bridge models with sufficient intermediate diaphragms have the lowest ultimate load factor under Load Case 2. However, the ultimate load factor of the bridge models under Load Case 1 is very close to the one under Load Case 2. It can be noted that Load Case 1 or 2 will govern the ultimate state of bridge models. With sufficient stiffness of intermediate diaphragms, the bridge models have the lowest ultimate load factor at Column Location 2 under both Load Cases 1 and 2. However, the bridge models with Column Location 1 have a very similar ultimate load factor compared with the bridge models with Column Location 1. Column Location 3 will reduce the capacity of the ultimate load of the bridge models with radius of curvature 50m by 20%. For the radius of curvature 500m, the capacity of the ultimate load of the bridge models at Column Location 1 is greater by 5% than that at Column Location 2.

Chapter 6

Summary and Conclusion

6.1. Summary

The increasing use of horizontally curved box girder bridges and the rather complex behaviors of these bridges especially in the nonlinear and ultimate stages have resulted in extensive research on the subject. So far very little research results on ultimate states and nonlinear behaviors of such bridges have been reported.

In this study, a two-span continuous composite curved four-cell box girder bridge model with a single middle column was used in the experimental investigation of nonlinear behaviors. Further, parametric studies were also carried out using large samples of idealized two-span continuous composite curved four-cell box girder bridge models with a single middle column similar to the bridge model in the experimental investigation.

For the experimental investigation, the bridge model with a micro concrete deck and a aluminum girder was built and tested systematically. Strains and vertical deflections of major sections were measured and investigated. A nonlinear analysis of the bridge model was carried out using the finite element method, which was used to predicate the nonlinear behaviors of the bridge model. This finite element method was used to verify the experimental results. In the finite element analysis of the bridge model, 4-node thick shell element, 3-D beam elements, and 3-D truss element were used to model the bridge. The OHBDC design truck model was used as a basic loading system applied to the bridge model. The commercial structural analysis software COSMOS/M is used in the analysis.

For the parametric study, the analysis of the ultimate state and nonlinear behavior is applied to a number of idealized two-span continuous composite curved four-cell box girder bridge models. Basic idealized curved bridges are generated based on the real bridge data. The finite element method is used in these investigations. With rather recent development of the computer giving dramatic increase in speed as well as storage capacity at reasonable cost, it is possible to investigate nonlinear behaviors of such bridges using a large amount of idealized models. Major significant parameters, which are thought to have influence on the ultimate state and nonlinear behaviors of curved box girder bridges, were used to investigate systematically the nonlinear behaviors of these bridges. The bridge models were analyzed to investigate the influences of various load cases, radii of curvature, and locations of the middle column. The influences of other parameters such as the stiffness of middle diaphragm, the stiffness of middle column, the stiffness of shear connectors, and the stiffness of intermediate diaphragms were also investigated. The vertical deflections and rotations of major sections were observed and presented. The stress distributions of some bridge models were shown graphically.

6.2. Conclusions

The following conclusions on the ultimate states and nonlinear responses of two-span continuous composite horizontally curved four-cell box girder bridges can be made from the nonlinear experimental investigation and the nonlinear finite element parametric studies, detailed in Chapters 3, 4 and 5. It should be noted that most of the following conclusions are only applicable to the experimental model referred to in the thesis and to the ideal models used for the parameter studies.

1. The analytical results of finite element method and the experimental results are in good agreement in both deflections and stresses under OHBDC design truck loading. The failure of the middle diaphragm found in the experiment could also have been predicted using the nonlinear theoretical analysis. The curved bridge model could only carry an ultimate load of 550 kN due to the failure of the middle diaphragm and the fracture failure of the shear connectors, compared with the ultimate load of 601 kN as predicted from theoretical analysis where the shear connectors and the middle diaphragm had sufficient ductility.
2. Although the fracture failure of shear connectors could not be predicted using this method, the yielding of shear connectors can be predicted using the finite element method. It is also evident from this study that the equivalent shear connector element derived from 3-D beam element can be used to model accurately the shear connectors in the material nonlinear analysis of curved composite bridges.
3. Both the experimental observation and the analytical results showed that the middle diaphragm and the shear connectors failed first. This may have caused premature failure of the bridge. In order to increase the ultimate capacity of the bridge, a stiffer middle diaphragm should be used to reduce the lateral deflections. This may also provide a more uniform stress distribution among the webs at the maximum negative moment region. Also, a greater number of shear connectors should be employed not only at the positive moment region but also at the negative moment region in order to prevent premature failure of the bridge.

4. Based on above observations for the bridge models, it may be concluded that for any radius of curvature and any location of the middle column, the bridge models without intermediate diaphragms have the lowest ultimate load factor under Load Case 1. However, the bridge models with sufficient stiffness of intermediate diaphragms have the lowest ultimate load factor under Load Case 2. It can be concluded that Load Case 1 or Load Case 2 appears to govern the nonlinear behaviors and the ultimate states of all bridge models.
5. Load Cases 3 and 4 induce a larger rotation at section A of bridge models. Load Case 2 produces larger deflections and a smaller rotation at section A in the elastic region.
6. For the bridge model without intermediate diaphragms, when the middle column is located at Column Location 1, the ultimate load level of the bridge models will be increased. Generally, Column Locations 2 and 3 will reduce the overall ultimate capacity of the bridge models without intermediate diaphragms.
7. For the bridge model with sufficient stiffness of intermediate diaphragms, Column Location 2 is better than other Column Locations for the capacity of the ultimate load of the bridge models. However, the bridge models have a very similar ultimate load factor at Column Location 1 or 2. Column Location 3 will significantly reduce the capacity of the ultimate load of the curved bridges, and is not recommended.
8. With a L/R value greater than 0.3 under Load Case 1 and greater than 0.2 under Load Case 2, the ultimate load capacity of bridge models decrease rapidly and the effect of the curvature must be taken into account in the analysis. That is, it can be concluded that when L/R less than 0.2, the bridge models may be analyzed as straight bridges.

9. The ultimate load capacity of the bridge models is little influenced whether rigid shear connectors or regular shear connectors are used. This difference can be ignored in the nonlinear analysis.

10. It is also found that there is no significant difference of the ultimate load capacity for the bridge models when the stiffness of the middle diaphragm is greater than 5×10^6 (N/m) for these bridge models.

11. All bridge models appears to have the same ultimate load capacity when the stiffness of the middle column is greater than 1.26×10^9 (N/m) and other parameters are the same. In general, the stiffness of the middle column is greater than 1.26×10^9 (N/m) in practice, unless there is a larger settlement at the middle column. Therefore, it can be concluded that the ultimate load capacity of the bridge will not be affected by the stiffness of the middle column.

12. The intermediate diaphragms play a significant role in the behaviors of curved bridges. They obviously help to distribute the applied load between the webs of bridges. Sufficient stiffness of intermediate diaphragms will also increase the capacity of the ultimate load of the curved box-girder bridges.

6.3. Recommendations for the future research

On nonlinear analysis, this study is believed to be the only reported theoretical work giving systematic effects of major parameters on the nonlinear and ultimate behaviors of horizontally curved box-girder bridges supported by a single middle column. It is recommended that more sophisticated material models be used in the analysis.

In the present study, the shear connectors are modeled using 3-D beam element with the elasto-plastic model. The equivalent shear connectors have sufficient ductility. The shear connector model with fracture failure should be developed to investigate the nonlinear behaviors of straight and curved bridges without sufficient shear connectors.

In the experimental study, the middle diaphragm has the fracture failure at the welding connection. However, the fracture failure model is not available in the analysis and the elasto-plastic model was used to model the middle diaphragm instead. The fracture failure should be modeled at the welding area of the steel girder in future research.

Only the plate type of intermediate diaphragms was used in the nonlinear analysis of curved bridges. Other different types of intermediate diaphragms should be used in the future nonlinear analysis in order to study their effects on curved bridges.

Nonlinear analysis should be performed for bridges with various compound curvatures and skewed end supports. Finally, more field experimental verification studies should be done.

References

Anija, Iph K. and Frederic, Roll (1971) Model Analysis of Curved Box-Beam Highway Bridge. ASCE, Journal of the Structural Division, 97(12), 2861-2878

ASCE_AASHTO Committee on Curved Box Girders. 1978. Curved steel box-girder bridges: state-of-the-art. ASCE Journal of the Structural Division. 104(11): 1719-1739

Aslam, M. and Godden, W.G. (1975) Model Studies of Multi-Cell Curved Box Girder Bridges. ASCE JEMD 101(3), June 207-222

Bathe Klaus-Jurgen (1982) Finite Element Procedures in Engineering Analysis. Prentice-Hall Inc., Englewood Cliffs, NewJersy.

Bazant, Z.P. and EL Nimeiri, M. (1974) Stiffness Method for Curved Box Girders at Initial Stress. ASCE Journal of the Structural Division, 100(10) 2071-2090

Cheung, M.S., Ng, S.F. and Zhong,B. (1989) Finite Strip Analysis of Beams and Plates with Material Nonlinearity, Comput. Struct. 33(1), 289-294.

Cheung, M.S. and Li,W. (1990) Finite Strip Method for Materially Nonlinear Analysis of RC Slabs, Comput. Struct., 36(2), 297-300

Cheung, M.S., Ng, S.F. and Zhao, J.Q. (1993). Analysis of Curved Reinforced Concrete Slab Bridges by the Spline Finite Strip method, Can. J. Civil Eng., 20, 855-862.

Cheung,M.S., Li,W. and Chidiac,S.E. (1996) Finite Strip Analysis of Bridges. E& FN Spon. England

Cheung, Y.K. (1969). Folded Plate Structures by Finite Strip Method. ASCE Journal of the Structural Division, 95(12), 2963-2979

Cheung, Y.K. (1968) . The Finite Strip Method in the Analysis of Elastic Plates with Two Opposite Simply Supported Ends, Proc. Inst. Civ. Eng., 40, 1-7.

Cheung, Y.K. and Fan, S.C. (1983). Static Analysis of Right Box Girder Bridges by Spline Finite Strip Method, Proc. Inst. Civ. Eng., 2, 75, 311-323.

Chu, K. J. and Jones, M. (1976) Theory of Dynamic Analysis of Box Girder Bridges. Memories of International Association of Bridge and Structural Eng. Vol. 36 II, pp. 121-145.

Chu, K. J. and Pinjarkar, S. G. (1971) Analysis of Horizontally Curved Box Girder Bridges. Journal of the Structural Division, ASCE, 2481-2501

Colville, J. 1973. Test of curved steel-concrete composite beams. Journal of Structural Engineering, ASCE, 99(7): 1555-1570

COPILOT User's Guide and Reference. Version 3.02, 1987.

Evan, H.R. and Shanmugam, N.E. 1979 An Approximate Grillage Approach to the Analysis of Cellular Structures. Institute of Civil Engineers Proceeding, part 2, vol. 67, 133-154.

Evan, H.R. and Shanmugam, N.E 1984 Simply Analysis for Cellular Structures. ASCE Journal of the Structural Division, 110(3) 531-543.

Fam, A.R. and Turkstra, C.J. (1972) Discussion of Model Analysis of Curved Box-Beam Highway Bridges. By Iph K. Anija and Roll Frederic. ASCE Journal of the Structural Division, 98(10) 2320-2323.

Fam, A.R. and Turkstra, C.J. (1975) A Finite Element Scheme for Box Bridge Analysis. Computers and Structures vol.5 179-186

Fam, A.R. and Turkstra, C.J. (1976) Model Study of Horizon tally Curved Box Girder, ASCE Journal of the Structural Division, 102(5) 1097-1108

Guo, C.M., Mufti, A.A., Jaeger, L.G. and Cheung, M.S. (1988) Nonlinear Earthquake Response Analysis of Reinforced Concrete Bridges Using the Finite Strip Mehtod, Proceedings of Ninth World Conference on Earth quake Engineering, VI, 453-458, August, Tokyo-Kyoto, Japan.

Hachem, H.M., Structural Response of Curved Box Girder Bridges, M.A.Sc. Thesis, University of Ottawa, Ottawa, Ontario. 1988.

Hambly, Edmund C. (1972) Bridge Deck Behavior. John Wiley & Sons Inc. New York

Hasebe,K., Usuki, S., and Horie, Y. 1985 Shear Lag Analysis and effective width of curved girder bridge. ASCE, JEM 111(1).

Heins, C.P., Bonakdarpour, and Bell, L.C. 1972. Multicell Curved Girder Model Stuiest. ASCE Journal of the Structural Division, 98(4) 831-843

Heins, C.P., and Oleinik, J.C., Curved Box Beam Bridge Analysis. Journal of Computers and Structures, Vol. 6, June 1976, 65-73.

Heins, C.P., and Stroczkowski, J.P. Computerized Design of Continuous Curved Tubular Girders, Journal of Computers and Structures, Vol. 6, June 1976, 273-280.

Heins, C.P. (1978) Box Girder Bridge Design- State of the Art, Engineering Journal of AISC, fourth quarter, 1978, 126-142

Kano, T. Usuki, S. and Hasebe K. 1982 Theory of Thin Walled Curved Members With Shear Deformation. Ingenieur-Archiv.

Komastu,S., Nakai. H., and Nakanishi, M. Statical Analysis of Horizontally Curved Skew Box Girder Bridges. Transactions of the Japanese Society of Civil Engineers, Vol.3, Part 2, 132-133

Konishi, I. and Komatsu, S. (1962) On Fundamental Theory of Thin Walled Curved Girder. Transactions of the Japanese Society of Civil Engineers, No.87, Nov. 1962 35-48 (in Japanese)

Konishi, I. and Komatsu, S.(1963) Three Dimensional Analysis of Simply Supported Curved Girder Bridges Transactions of the Japanese Society of Civil Engineers, No.9, Feb. 1963 11-28 (in Japanese)

Lavalle, F.H. 1976, The CUGAR 3 Algorithm, Consortium of University Research Teams, Report No.56, University of Rhode Island, Kingston, R.I., 1976

Lavalle, F.H. and Boick, J.S. (1965) Aprogram to Analyze Curved Girder Bridges, Engineering Bulletin No.8, University of Rhode Island, Dec. 1965.

Loo, Y. C. and Cusens, A. R.1978. The Finite-Strip Method in Bridge Engineering. Viewpoint Publications.

McManus, P.F., Nasir, G.A., and Culver, C.G.,(1969) Horizontally Curved Girders: State of the Art, ASCE Journal of the Structural Division, 59(5), 853-870

Meyer, C. and Scordelis, A.C. 1971. Analysis of Curved Folded Plate Structures. ASCE Journal of the Structural Division, 97(10). 2459-2480

Ng,S.F., Cheung, M.S. and Zhong,B. (1991) A Finite Strip Method for the Analysis of Structures with Material Nonlinearity, J. Struct. Eng., 117(2), 489-500.

Ng, S. F., Cheung, M. S., and Shao, R. S. 1987. Model testing of a curved continuous box girder bridge. Report, Department of Civil Engineering, University of Ottawa, Ottawa, Ontario, Canada.

Ng, S. F., Cheung, M. S., and Hachem, H. M. 1993. Study of a curved continuous composite box girder bridge. Canadian Journal of Civil Engineering, 20: 107-119.

OHBDC. 1991. Ontario highway bridge design code. Ontario Ministry of Transportation and Communications, Downsview, Ontario.

Olawale, A.O. and Plank, R.J. (1988) The Collapse Analysis of Steel Columns in Fire Using a Finite Strip Method, int. J. Num. Meth. Eng., 26(12), 2755-2764.

Oehlers, D.J. and Coughlan, C.G. 1986. The shear stiffness of stud shear connections in composite beams. Journal of Construction Steel Research, 6: 273-284

[illegible], J.C. 1974, Design Criteria for Distortional Analysis of Curved Steel Box Beams. Thesis presented to University of Maryland, at College Park, Md., in partial fulfillment of the requirements for the degree of Master of Science.

Rabizadeh, R. O. and Shore, S. (1975) Dynamic Analysis of Curved Box-Girder Bridges. Journal of the Structural Division, ASCE, Vol. 101, No. ST9, 1899-1912

Robert D. Cook (1981) Concepts and Applications of Finite Element Analysis. 2nd ed., John Wiley and Sons Inc., Toronto, Canada.

Scotrdelis, A. C., and Larsen, P. K. 1977. Structural response of curved RC box-girder bridge. ASCE Journal of the Structural Division, 103(8): 1507-1524.

Scotrdelis, A. C., Larsen, P. K and Elfgren, L.G.. 1977. Ultimate Strength of curved RC box-girder bridge. ASCE Journal of the Structural Division, 103(8): 1525-1542.

Structural Research and Analysis Corporation 1994. COSMOS/M Finite Element Analysis System, Version 1.71, Second Edition.

Schelling, D. R., Heins, C.O. and Sikes, G.H. 1978 State of The Art Curved Girder Bridge Programs. Computers and Structures. Vol.9, 27-37

The Subcommittee on the state-of-the-art survey of the task committee on composite construction of the committee on metals of the structural division 1974. Composite steel-concrete construction. Journal of Structural Engineering, ASCE, 100(5): 1085-1139

William, K.J. and Scordelis, A.C. (1972) Cellular Structures of Arbitrary Plan Geometry. ASCE, Journal of the Structural Division, 98(7) 1377-1394

G. Xi, S. F. Ng and M. S. Cheung: Nonlinear behavior of a curved continuous box-girder bridge model Seventh International Conference on Computing in Civil and Building Engineering, 19-21 August 1997, Seoul, Korea. P.p. 497-502.

Yam, L.C.P. and Chapman, J.C. 1968. The inelastic behavior of simply supported composite beams of steel and concrete. Proceedings Institutions Civil Engineers, Part 2, 41(1): 651-683

Yam, L.C.P. and Chapman, J.C. 1972. The inelastic behavior of continuous composite beams of steel and concrete. Proceedings Institutions Civil Engineers, Part 2, 53(12): 487-501

Yabuki, T., Arizumi, Y., and Vinnakota, S. 1995. Strength of thin walled box girders curved in plan. ASCE Journal of the Structural Division, 121(5): 907-914

Yoo, et al.(1975), An Analysis of a Continuous Curved Box Girder Bridge. Highway Research Record No. 579, Highway Research Board, Washington, D.C., Jan 1975.

Appendix A

Notations

A— cross-section area of the shank of the shear connector

A_D —cross-section area of a 3-D beam element

K_s —elastic stiffness of a stud

F_u—static strength of the stud shear connector, according to OHBDC

d—diameter of the shank of a shear connector

P—shear force of the shear connector

P_y—yielding shear force of the shear connector

P_u—ultimate shear force of the shear connector

D—diameter of the 3-D beam element

y—distance from the neutral axis to the point which stress is calculated

c—distance from the neutral axis to the remotest point

I—moment of inertia of the 3-D beam element

S—slip of the shear connector or the lateral displacement of the 3-D beam element

S_y—yielding slip of the shear connector or the yielding lateral displacement of the 3-D beam element

M—the bending moment of the 3-D beam element

M_y—the yielding bending moment of the 3-D beam element

ε_y—yielding strain of the 3-D beam element

σ_y—yielding stress of the 3-D beam element

E—young's modulus of the 3-D beam element

Appendix B

Equivalent shear connector element

The slip of a shear connector is assumed to be the same as the lateral displacement of a fixed-ended beam element, which is shown in Figure 8. According to a typical shear-slip relationship of a stud shear connector and the assumed deformation of a shear connector, the bilinear shear-slip relationship of the shear connector in the bridge model may be represented by means of elasto-plastic strain-stress relationship of the 3-D beam element (Figure 9).

The cross-section area of the shank and the yielding shear force of a shear connector may be expressed as equations (B.1) and (B.2) respectively.

(B.1) $A = \dfrac{\pi d^2}{4}$

(B.2) $P_y = F_u A$

The yielding shear force of the shear connector may be rewritten as

(B.3) $P_y = F_u \dfrac{\pi d^2}{4}$

According to the assumption that the stiffness of the shear connector K_s is equal to the stiffness of the 3-D beam element in the elastic region, we have

(B.4) $P = K_s S$

where $K_s = \dfrac{12}{L^3} EI$, E is Young's modulus of the 3-D beam element, I is the moment of inertia of the 3-D beam element, and L is the length of the 3-D beam element.

For the 3-D beam element, its normal stress may be expressed as

(B.5) $$\sigma_x = \frac{My}{I} = \frac{PLy}{2I}$$

where $M = P\frac{L}{2}$ according to Figure 8.

and the shear stress of the 3-D beam element may be expressed as

(B.6) $$\tau_{xy} = \frac{P}{A_D}$$

The maximum principal stress of the 3-D beam element may be expressed as

(B.7) $$\sigma = \frac{\sigma_x}{2} + \sqrt{\left(\frac{\sigma_x}{2}\right)^2 + \tau_{xy}^{\ 2}}$$

Therefore, by substituting equations (B.5) and (B.6) into equation (B.7), The maximum principal stress of the 3-D beam element may be rewritten as

(B.8) $$\sigma = \frac{PLy}{4I} + \sqrt{\left(\frac{PLy}{4I}\right)^2 + \left(\frac{P}{A_D}\right)^2}$$

In general, the effect of the shear stress is very small and may be neglected, the yielding stress of a 3-D beam element may be expressed as

(B.9) $$\sigma_y = \frac{P_y Lc}{2I}$$

The yielding stress and strain relationship of the 3-D beam element may be expressed as

(B.10) $$\sigma_y = E\varepsilon_y$$

and according to the above equations (B.4), (B.9), and (B.10), the corresponding yielding strain of a 3-D beam element may be expressed as

(B.11) $\varepsilon_y = \frac{6S_y c}{L^2} = \frac{0.3dc}{L^2}$

where $S_y = 0.05d$

If a solid round 3-D beam element is used, then c=D/2, and we have

(B.12) $I = \frac{\pi}{64} D^4$

(B.13) $\sigma_y = \frac{P_y LD}{4I} = \frac{16P_y L}{\pi D^3}$

and

(B.14) $\varepsilon_y = \frac{3S_y D}{L^2} = \frac{0.15dD}{L^2}$

Appendix C

Experimental Data

AR11(D)

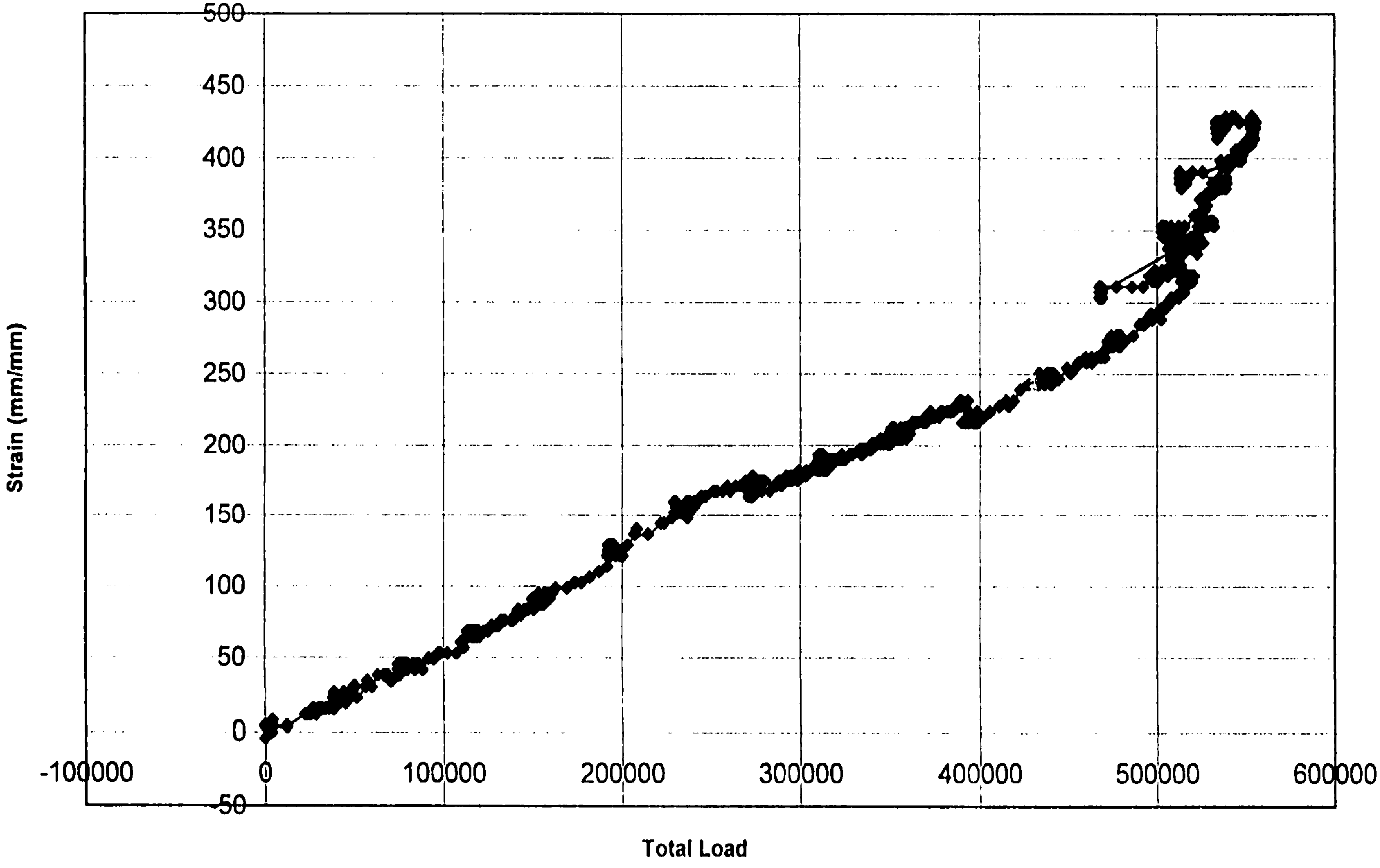

500
450
400
350
300
250
200
150
100
50
0
-50
-100000
0
100000
200000
300000
400000
500000
600000
Strain (mm/mm)
Total Load

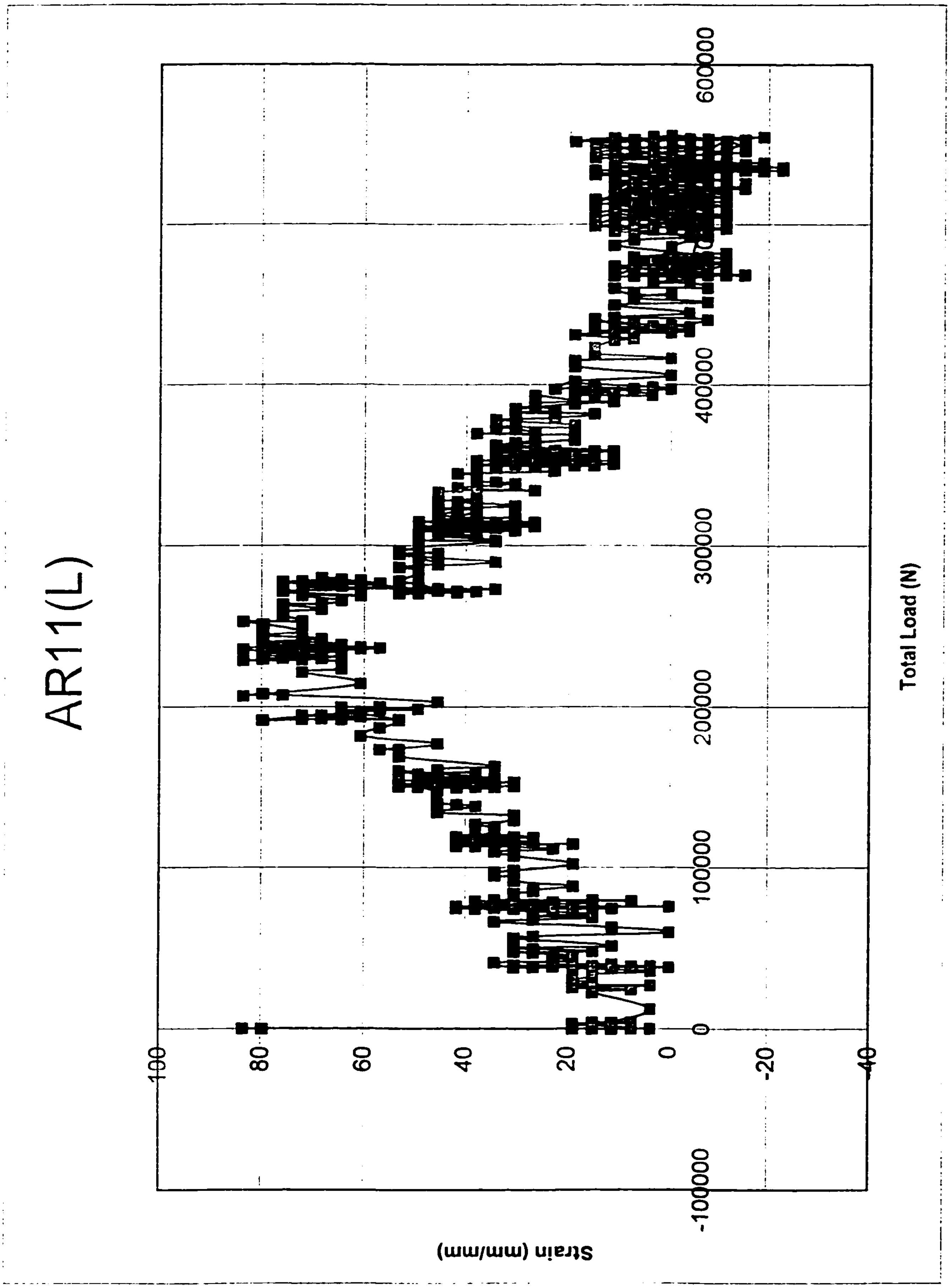
AR11(L)
Strain (mm/mm)
Total Load (N)
100
80
60
40
20
0
-20
-40
-100000
0
100000
200000
300000
400000
600000

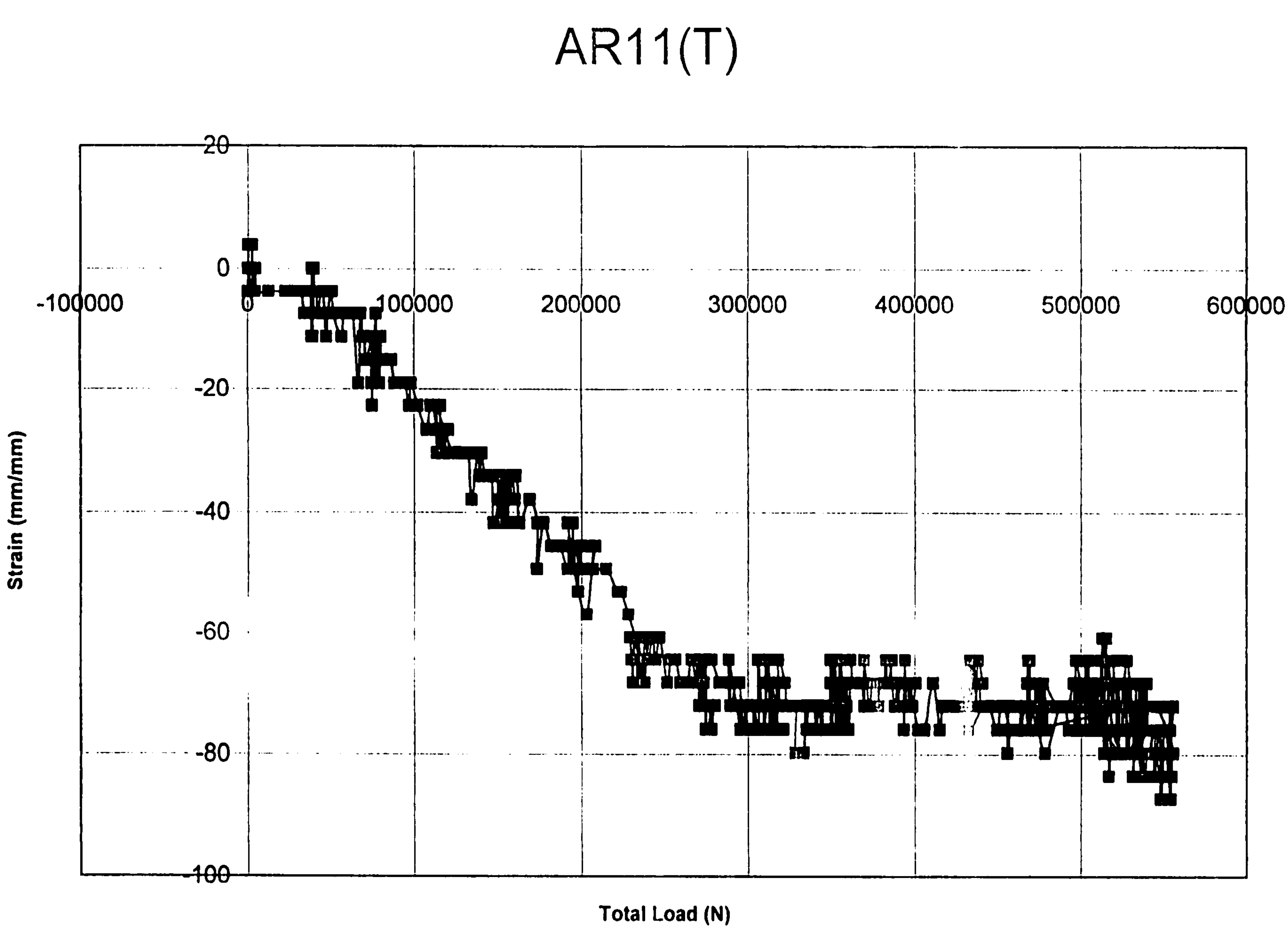
AR11(T)
20
0
-20
-40
-60
-80
-100
-100000
0
100000
200000
300000
400000
500000
600000
Strain (mm/mm)
Total Load (N)

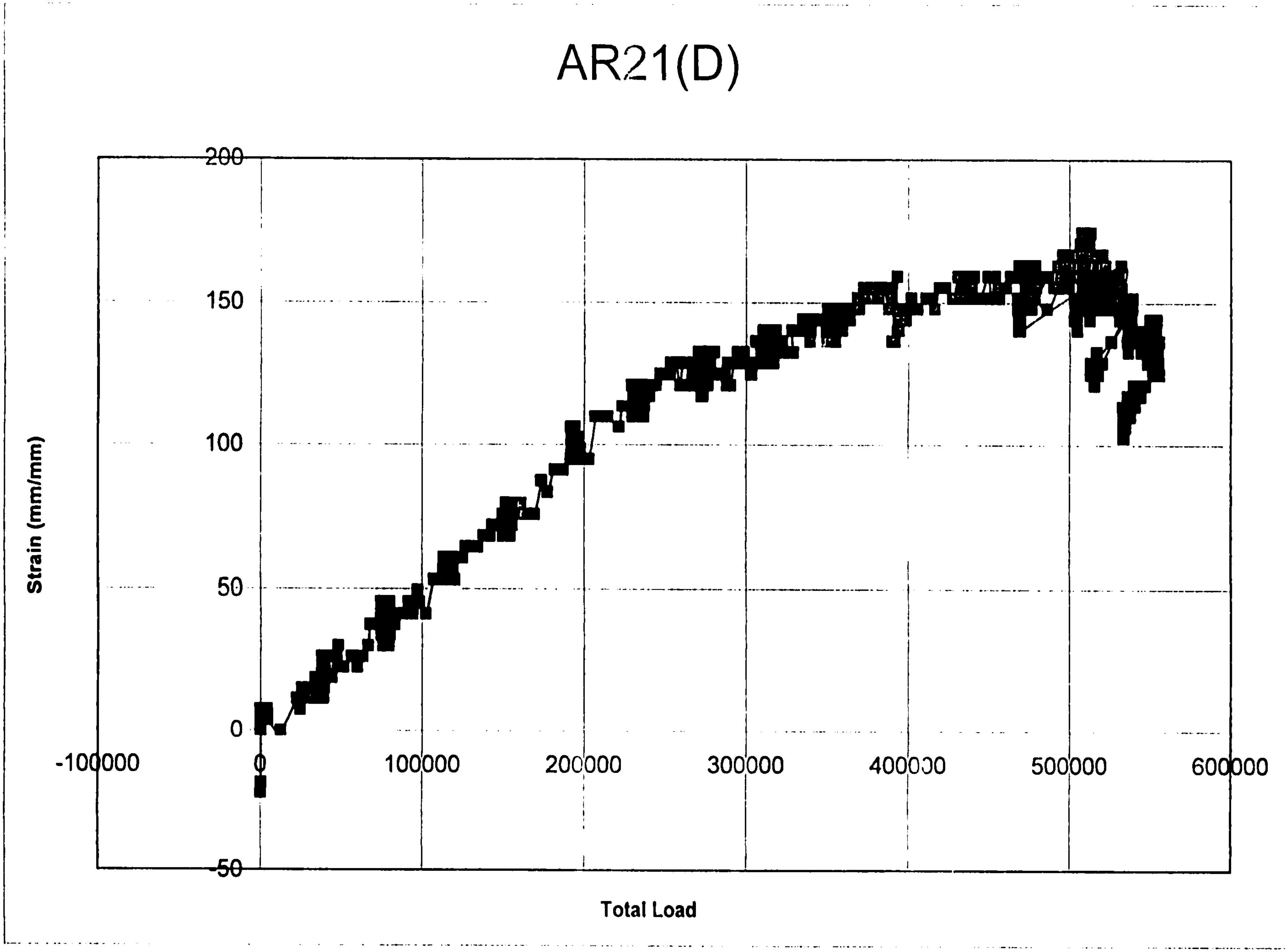
AR21(D)
Strain (mm/mm)
200
150
100
50
0
-50
-100000
0
100000
200000
300000
400000
500000
600000
Total Load

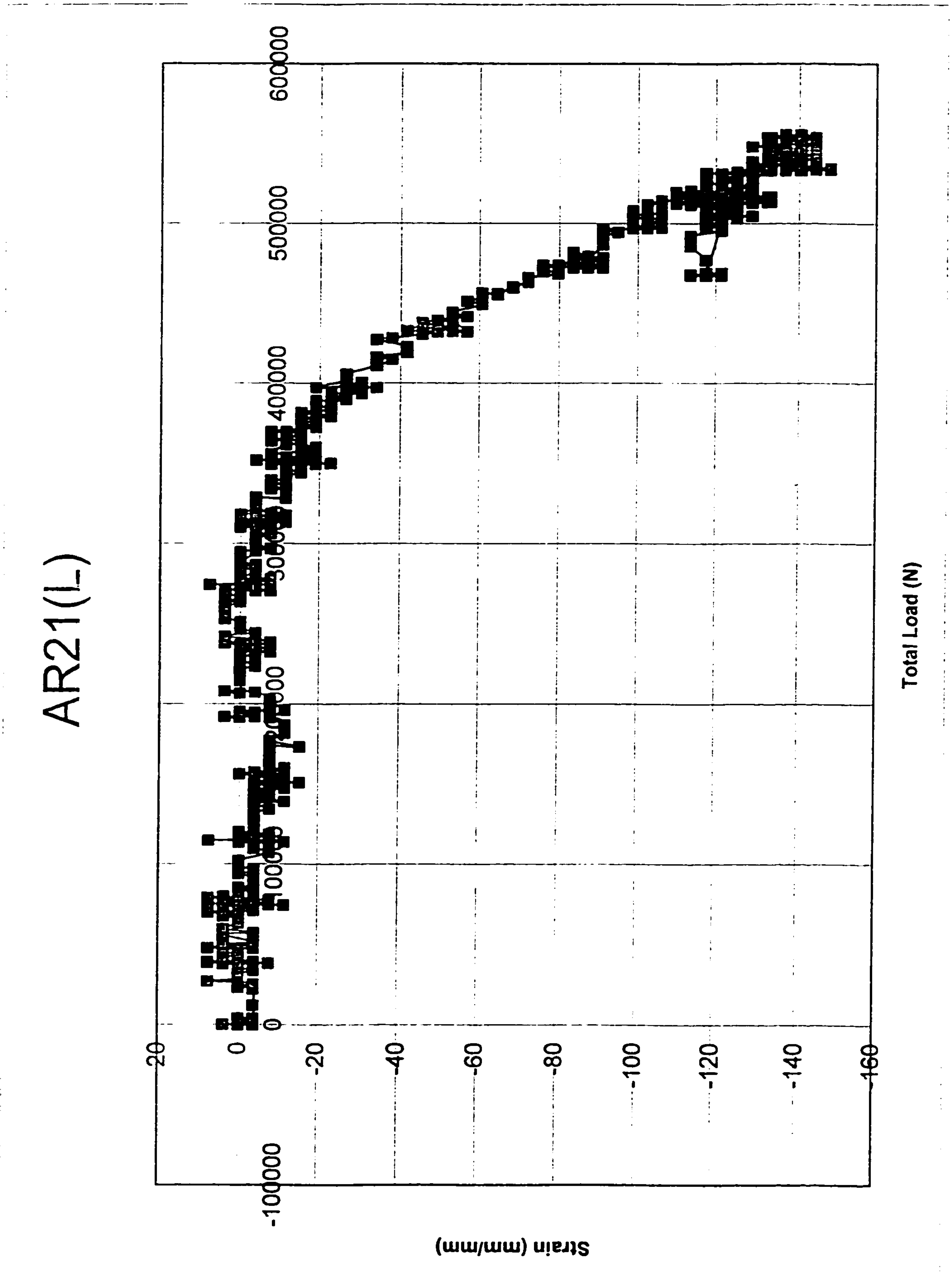
AR21(L)
Strain (mm/mm)
20
0
-20
-40
-60
-80
-100
-120
-140
-160
Total Load (N)
-100000
0
100000
200000
300000
400000
500000
600000

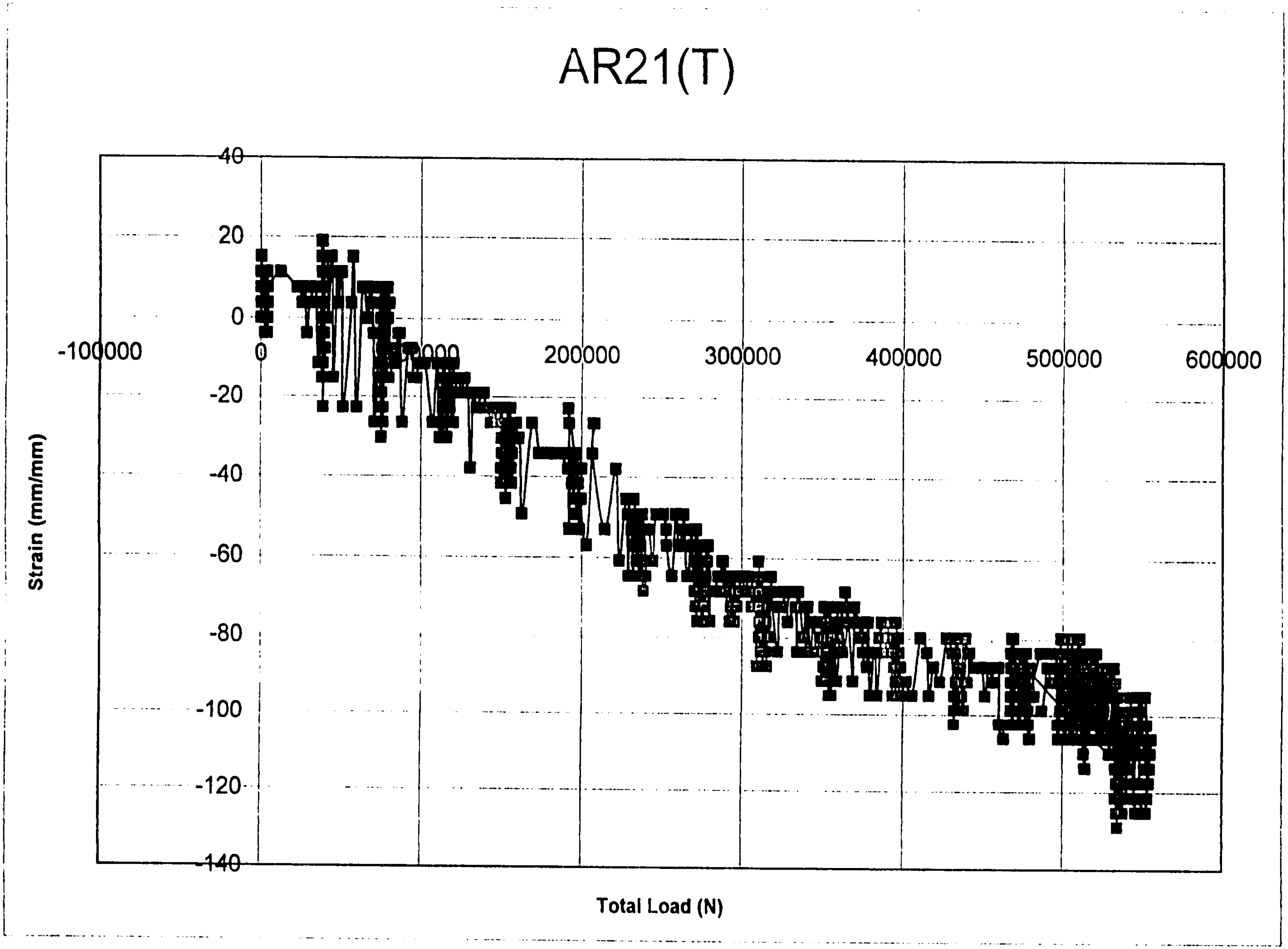
AR21(T)
40
20
0
-20
-40
-60
-80
-100
-120
-140
-100000
0
200000
300000
400000
500000
600000
Strain (mm/mm)
Total Load (N)

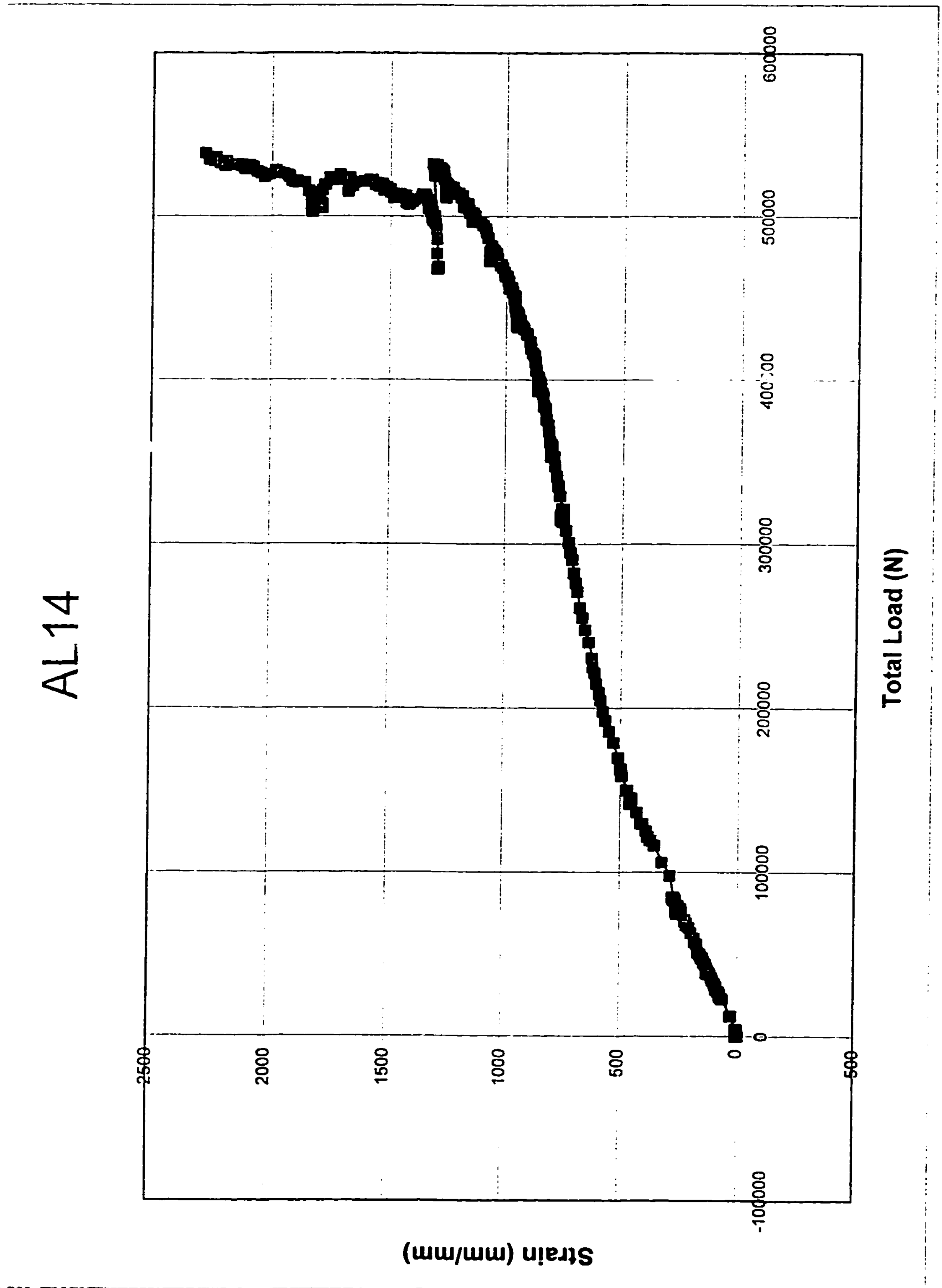
AL14
Strain (mm/mm)
Total Load (N)
2500
2000
1500
1000
500
0
-500
-100000
0
100000
200000
300000
400000
500000
600000

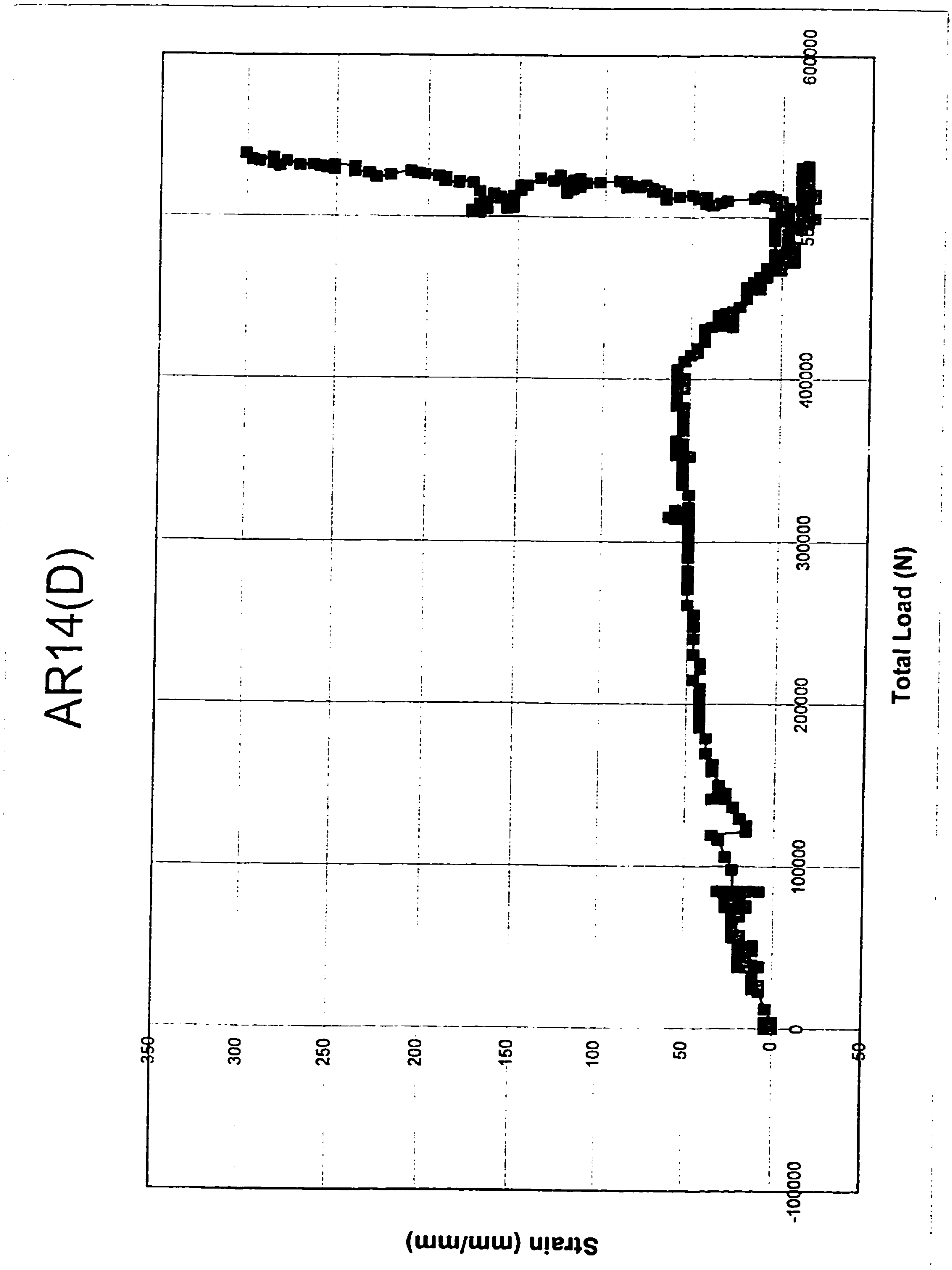
AR14(D)
Strain (mm/mm)
Total Load (N)
350
300
250
200
150
100
50
0
-50
-100000
0
100000
200000
300000
400000
500000
600000

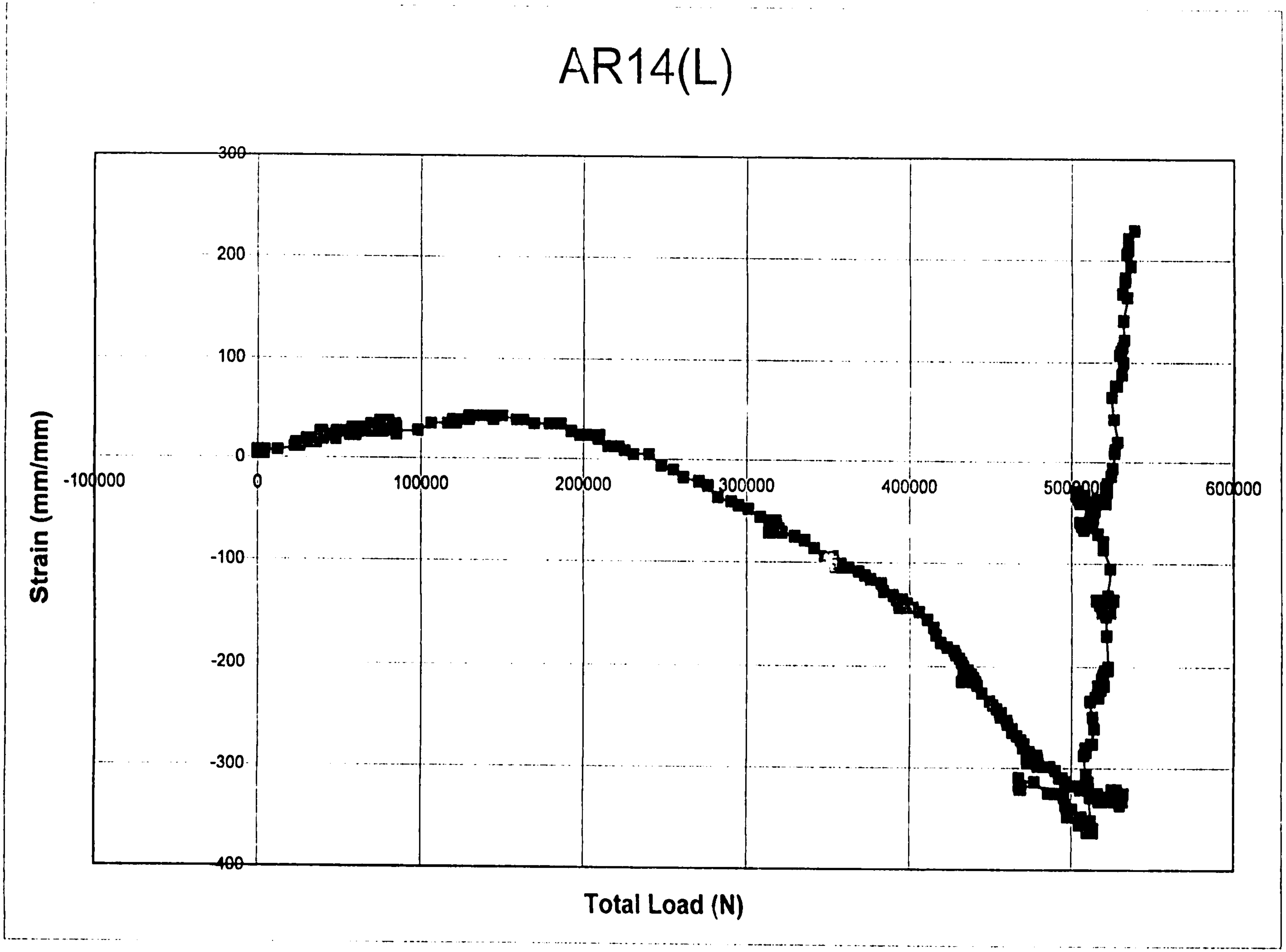
AR14(L)
Strain (mm/mm)
300
200
100
0
-100
-200
-300
-400
-100000
0
100000
200000
300000
400000
500000
600000
Total Load (N)

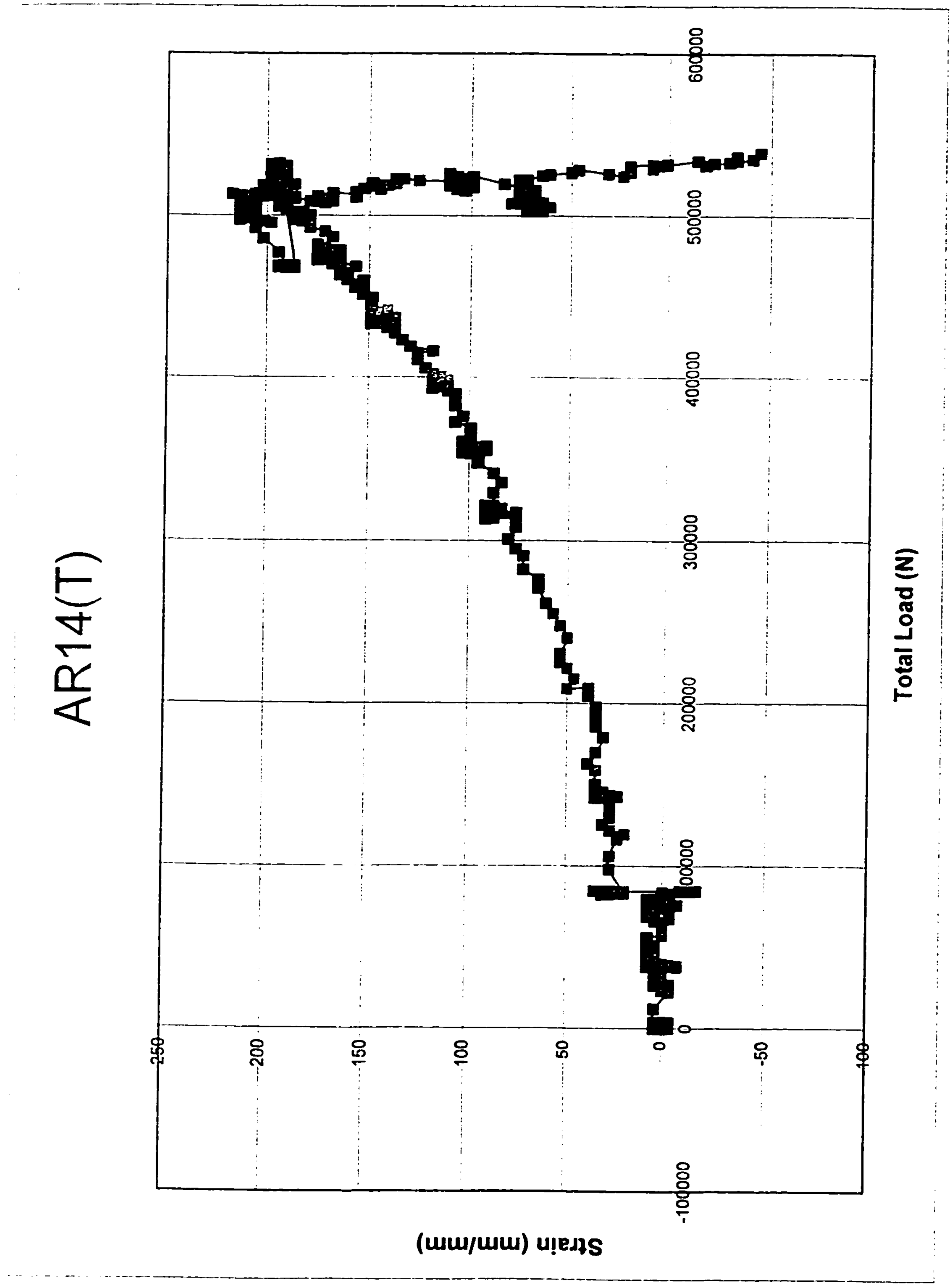
AR14(T)
Strain (mm/mm)
Total Load (N)
250
200
150
100
50
0
-50
-100
-100000
0
100000
200000
300000
400000
500000
600000

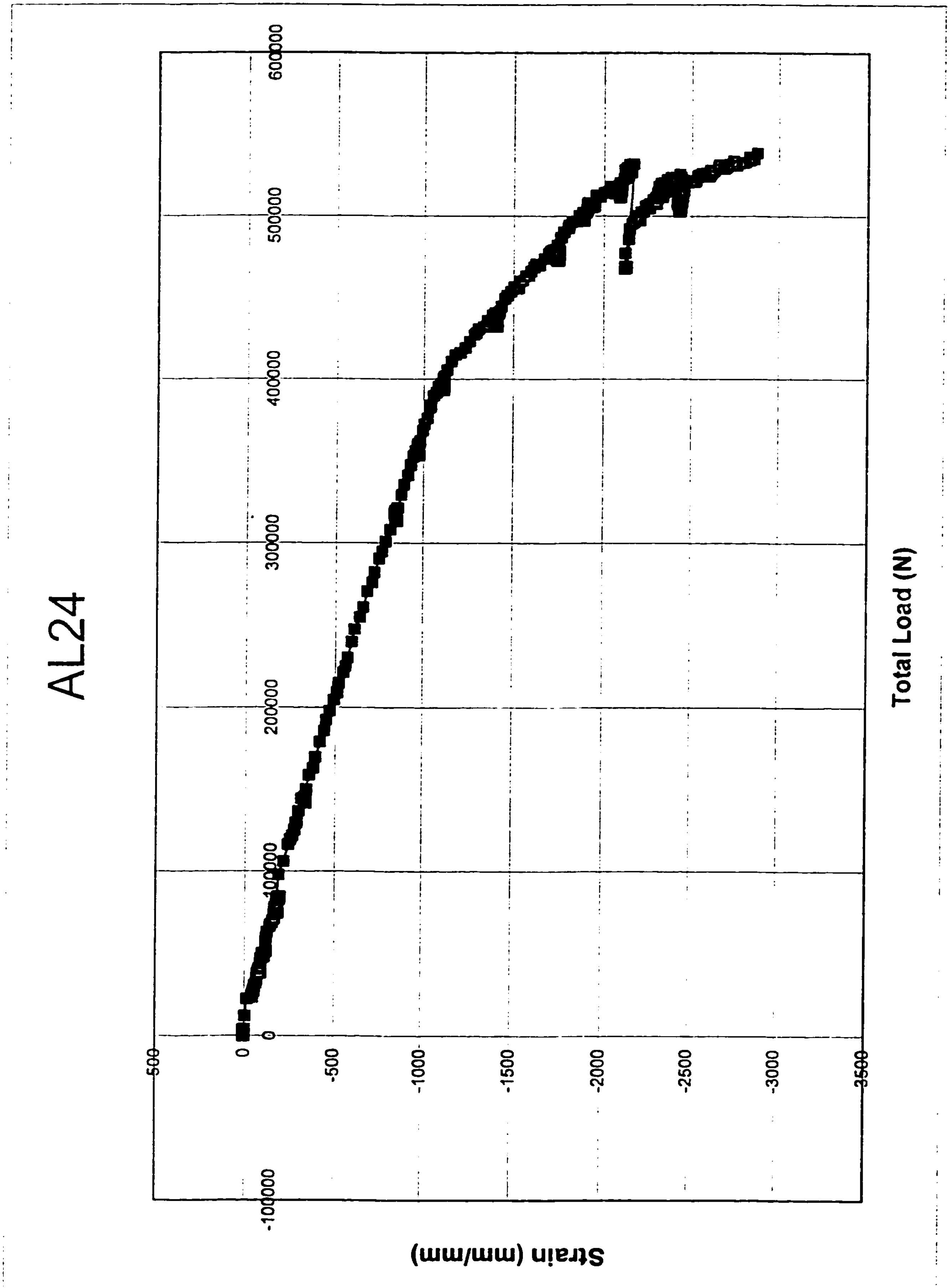

AL24
Strain (mm/mm)
Total Load (N)
-100000
0
100000
200000
300000
400000
500000
600000
500
0
-500
-1000
-1500
-2000
-2500
-3000
-3500

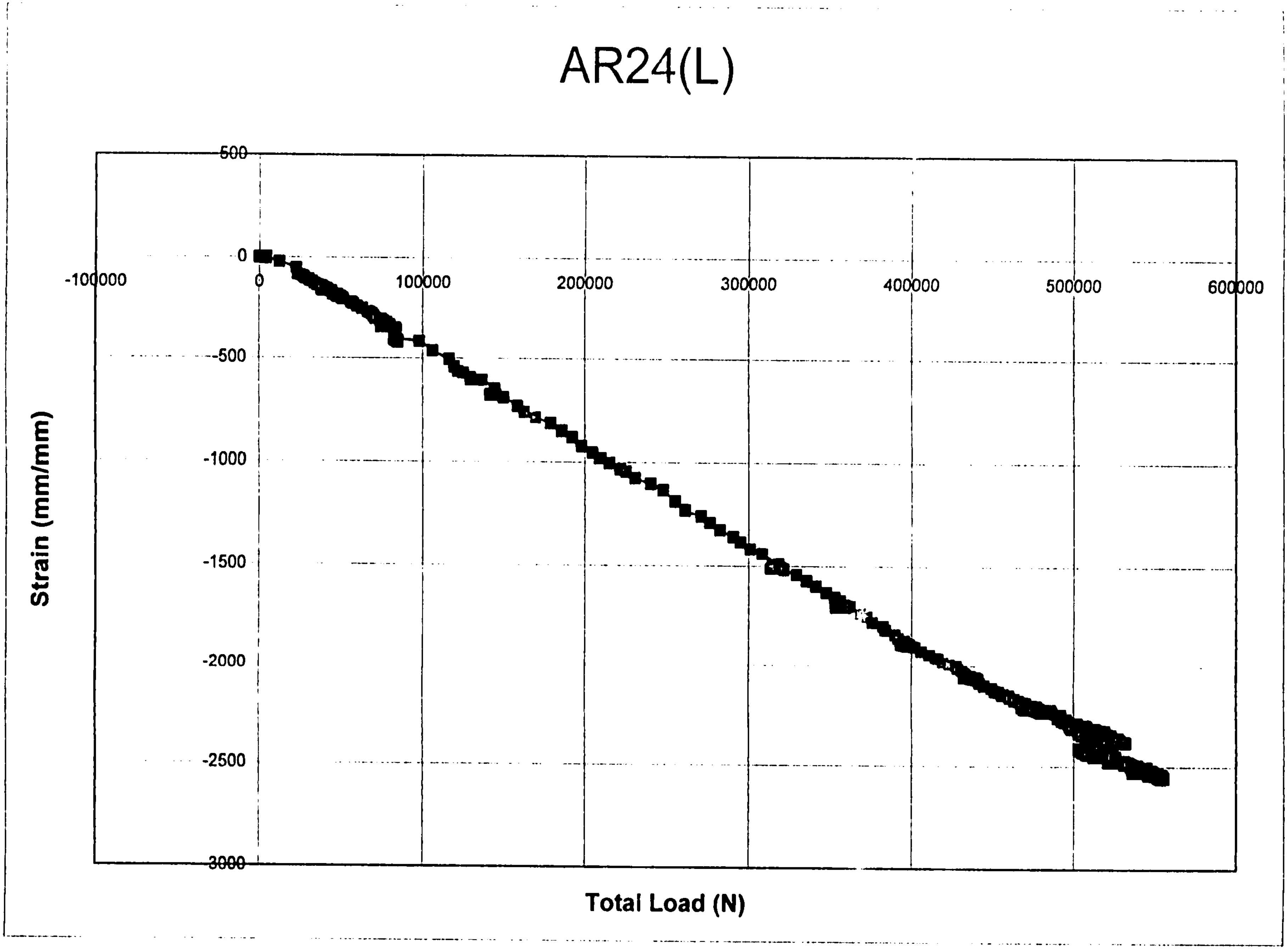
AR24(L)
Strain (mm/mm)
Total Load (N)
500
0
-500
-1000
-1500
-2000
-2500
-3000
-100000
0
100000
200000
300000
400000
500000
600000

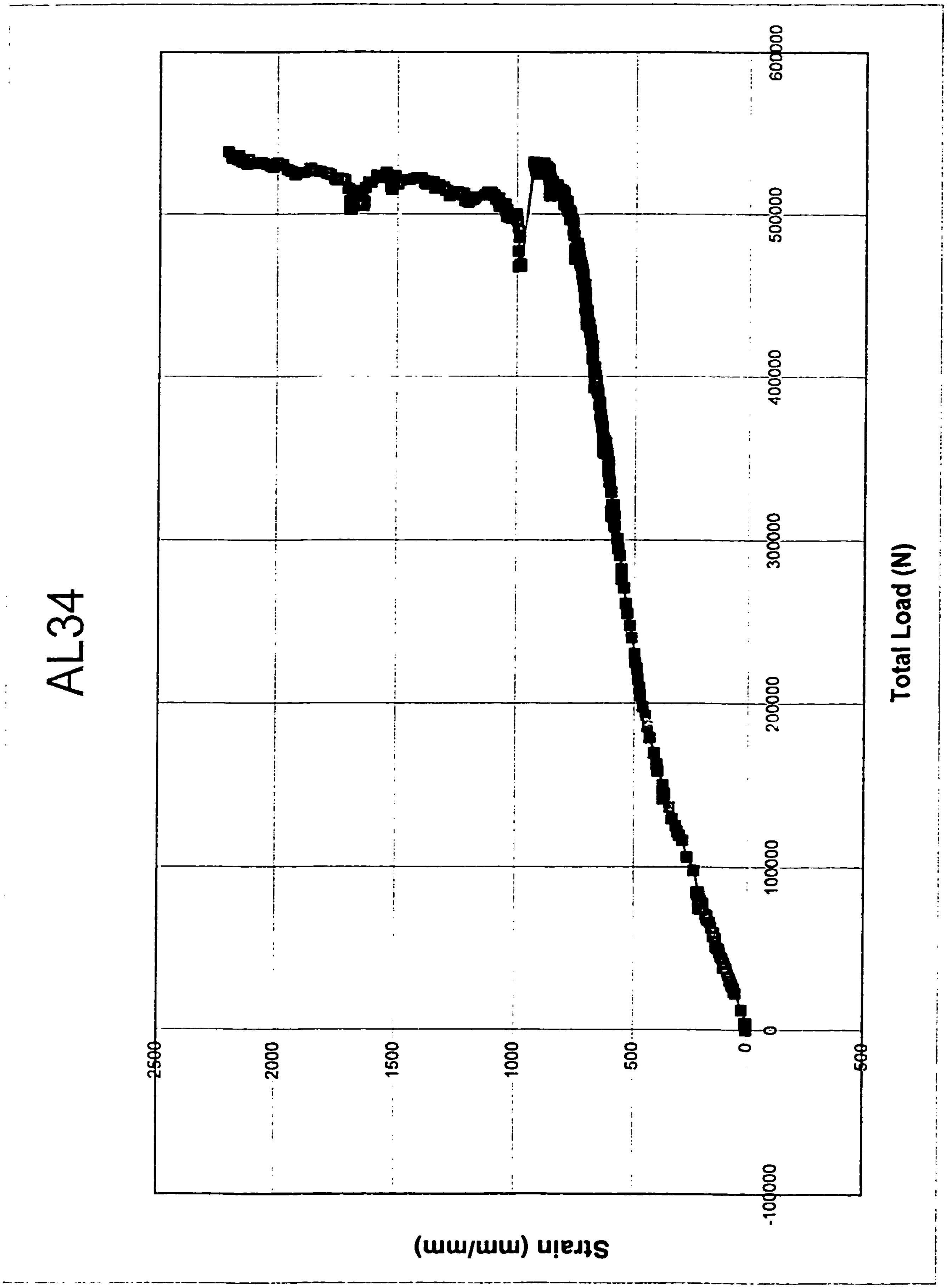
AL34
Strain (mm/mm)
Total Load (N)
2500
2000
1500
1000
500
0
-500
-100000
0
100000
200000
300000
400000
500000
600000

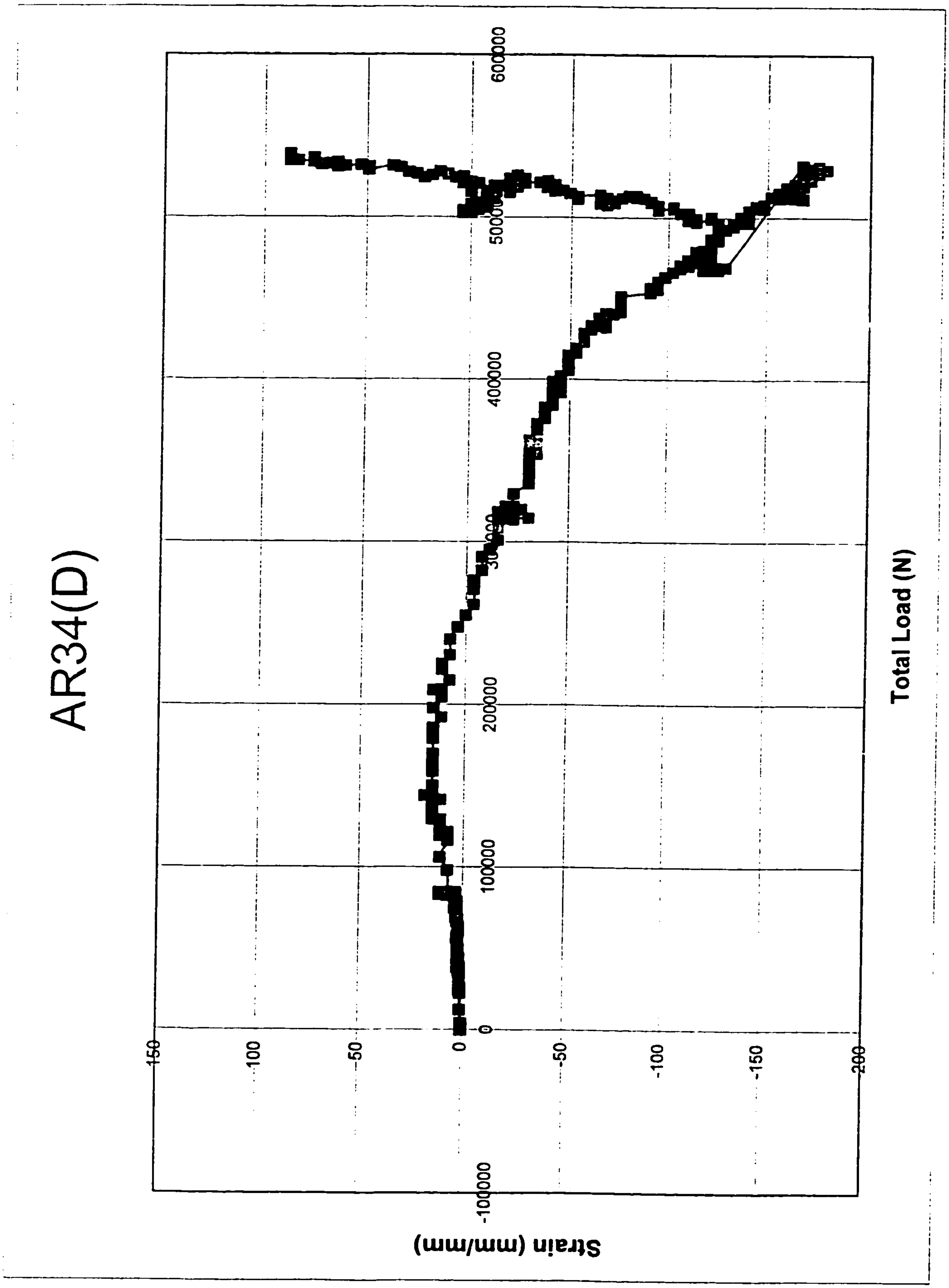
AR34(D)
Strain (mm/mm)
Total Load (N)
150
100
50
0
-50
-100
-150
-200
-100000
0
100000
200000
300000
400000
500000
600000

AR34(L)

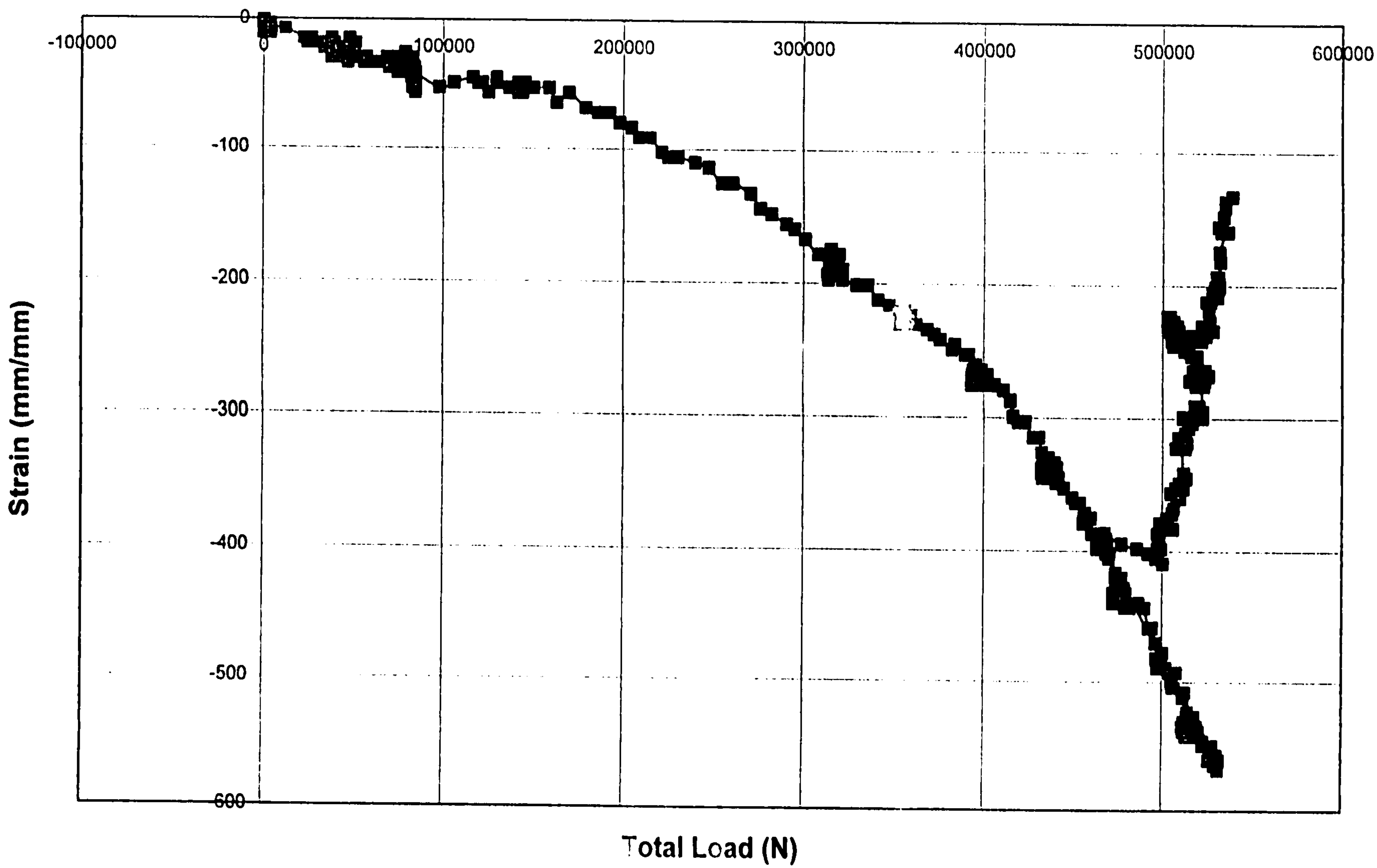
0
-100
-200
-300
-400
-500
-600
-100000
0
100000
200000
300000
400000
500000
600000
Strain (mm/mm)
Total Load (N)

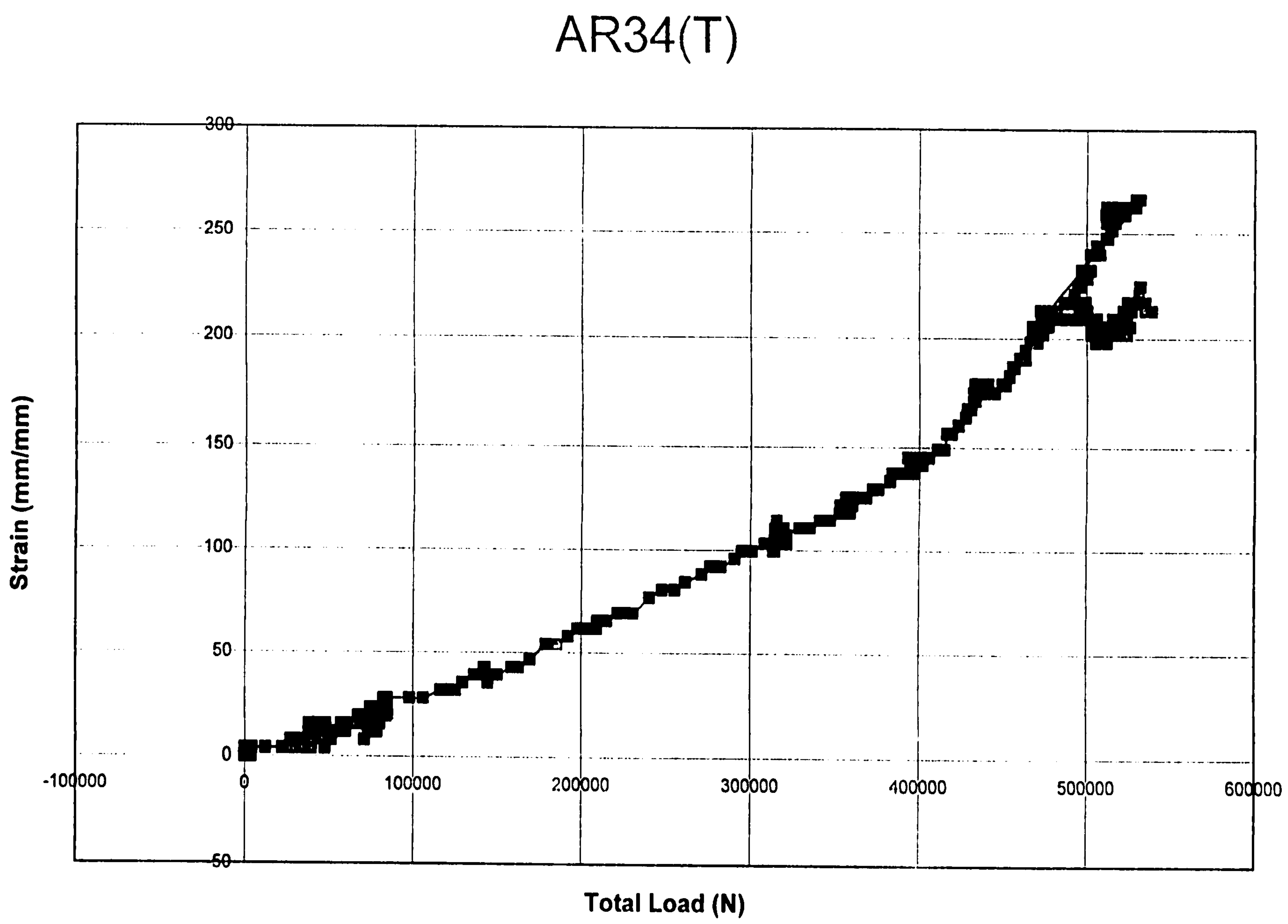
AR34(T)
Strain (mm/mm)
Total Load (N)
300
250
200
150
100
50
0
-50
-100000
0
100000
200000
300000
400000
500000
600000

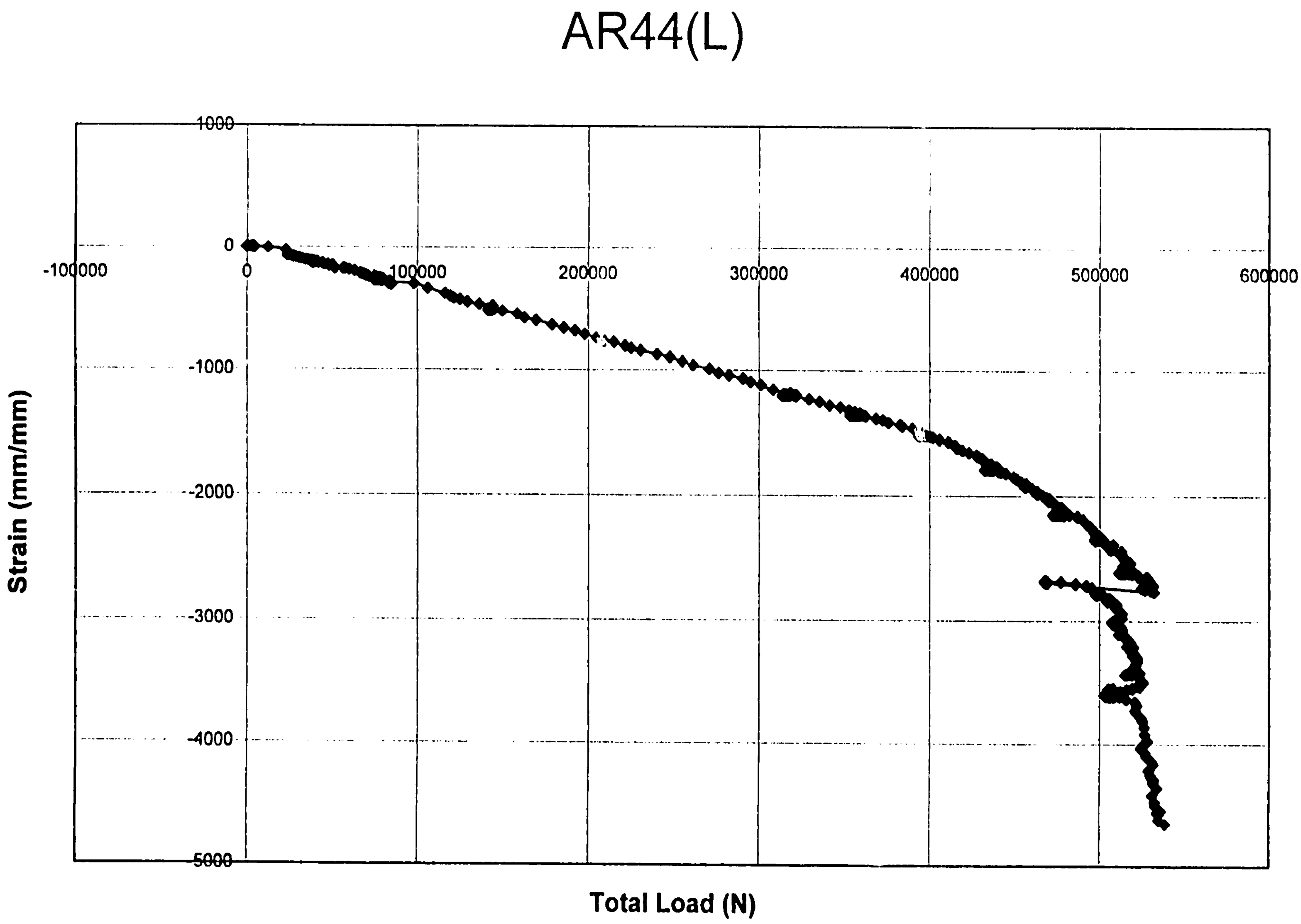
AR44(L)
1000
0
-1000
-2000
-3000
-4000
5000
-100000
0
100000
200000
300000
400000
500000
600000
Strain (mm/mm)
Total Load (N)

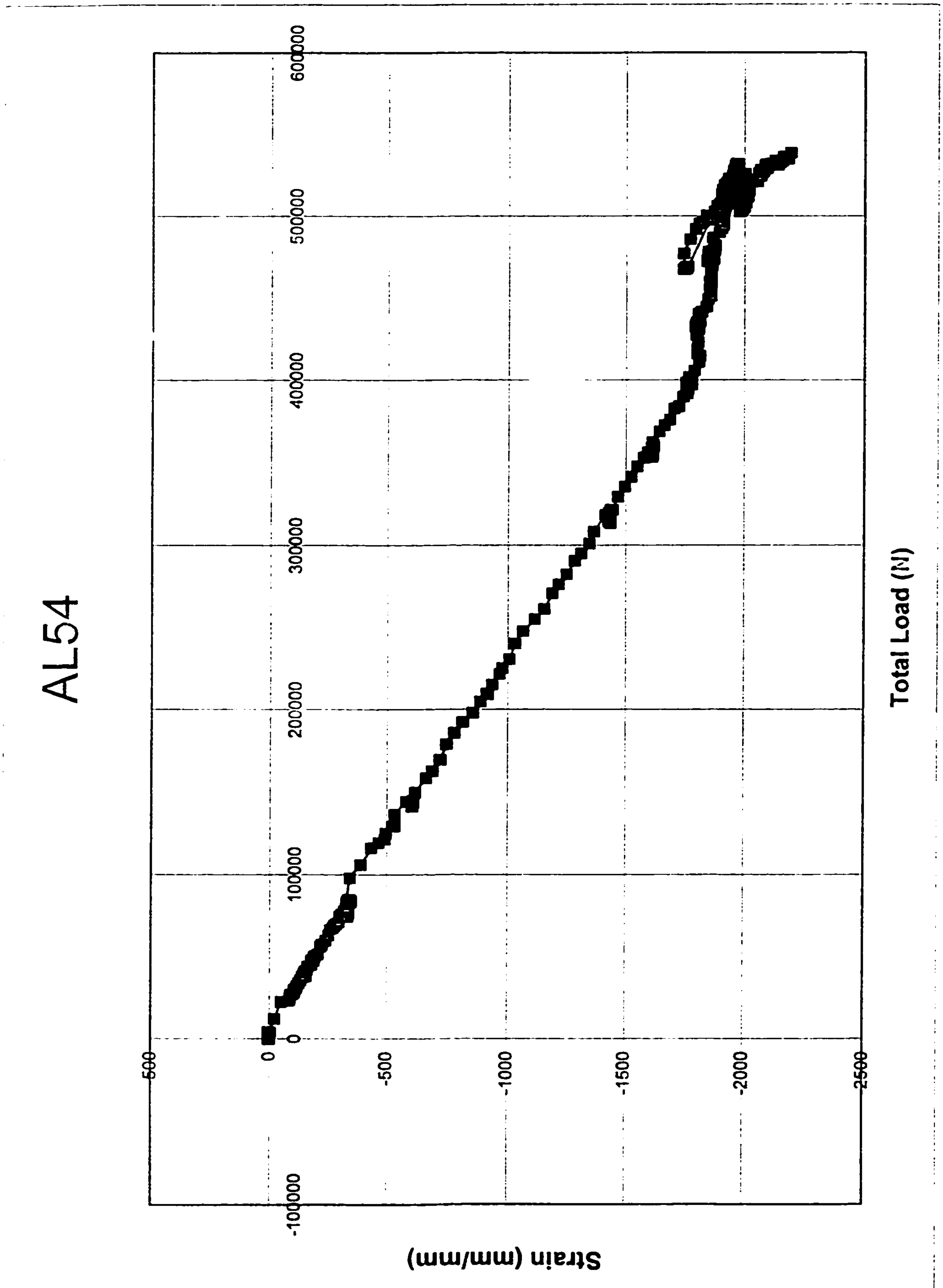
AL54
Strain (mm/mm)
Total Load (N)
-100000
0
100000
200000
300000
400000
500000
600000
500
0
-500
-1000
-1500
-2000
-2500

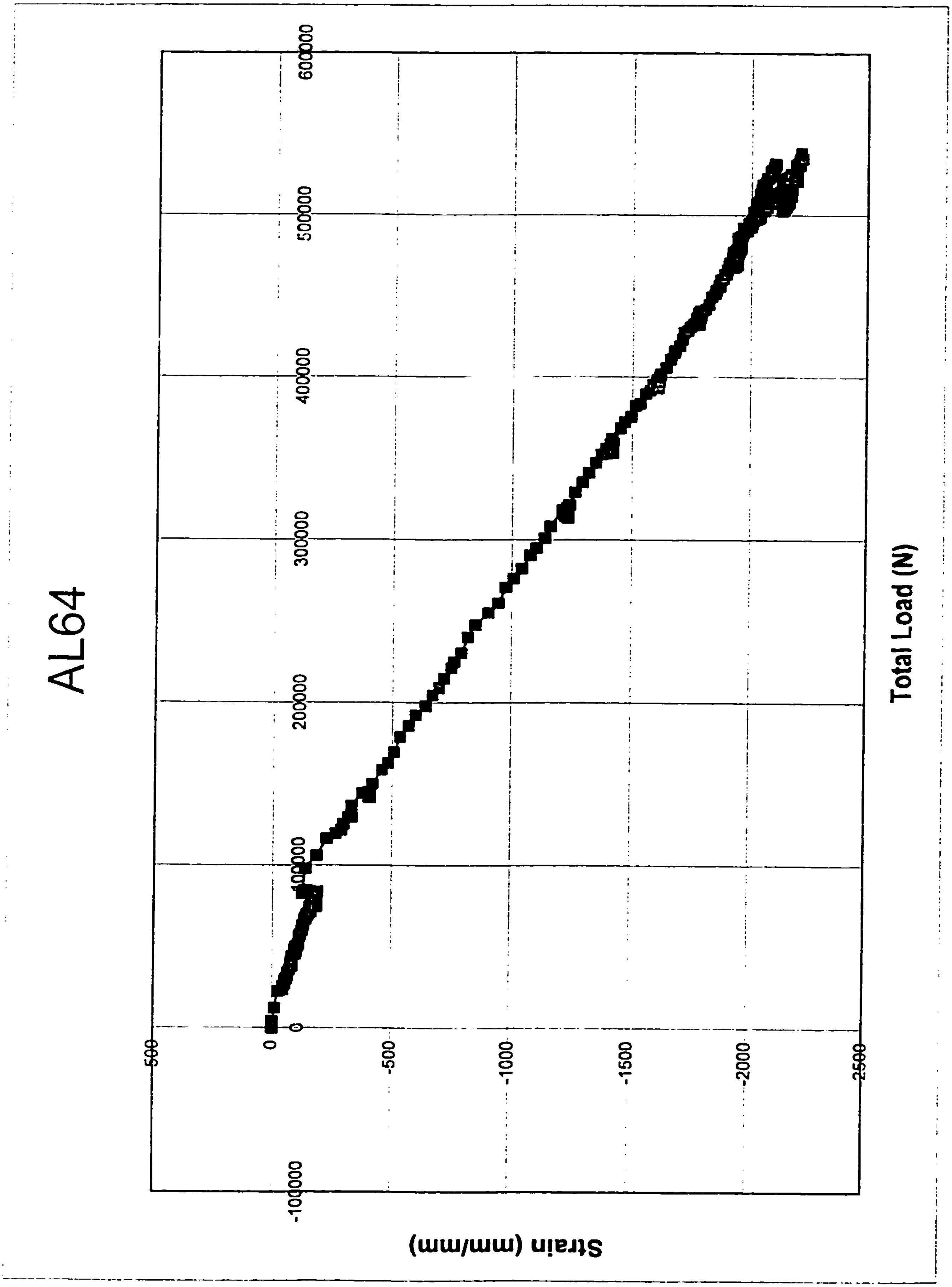
AL64
Strain (mm/mm)
Total Load (N)
-100000
0
100000
200000
300000
400000
500000
600000
500
0
-500
-1000
-1500
-2000
-2500

AL74

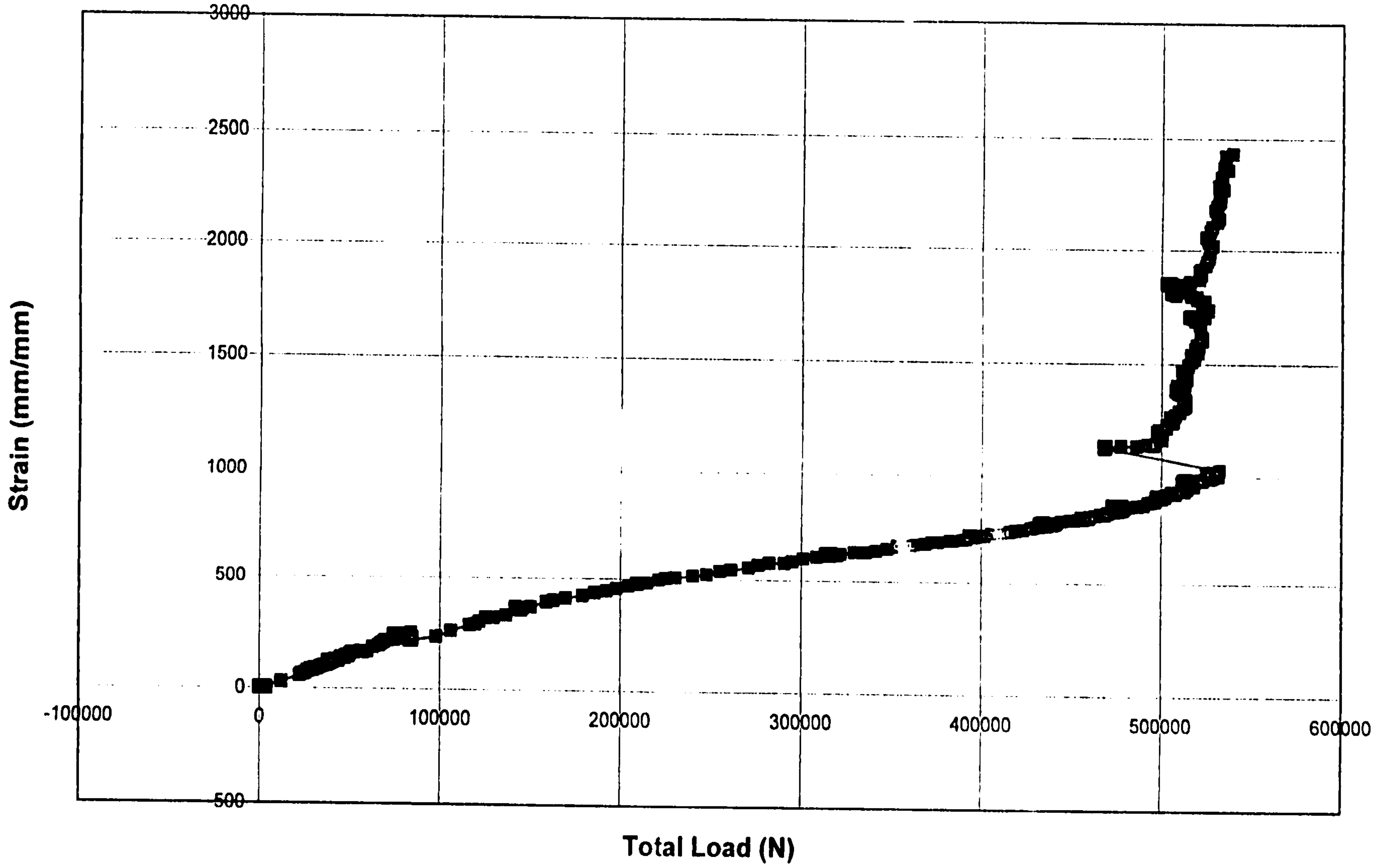

Strain (mm/mm)
3000
2500
2000
1500
1000
500
0
-500
-100000
0
100000
200000
300000
400000
500000
600000
Total Load (N)

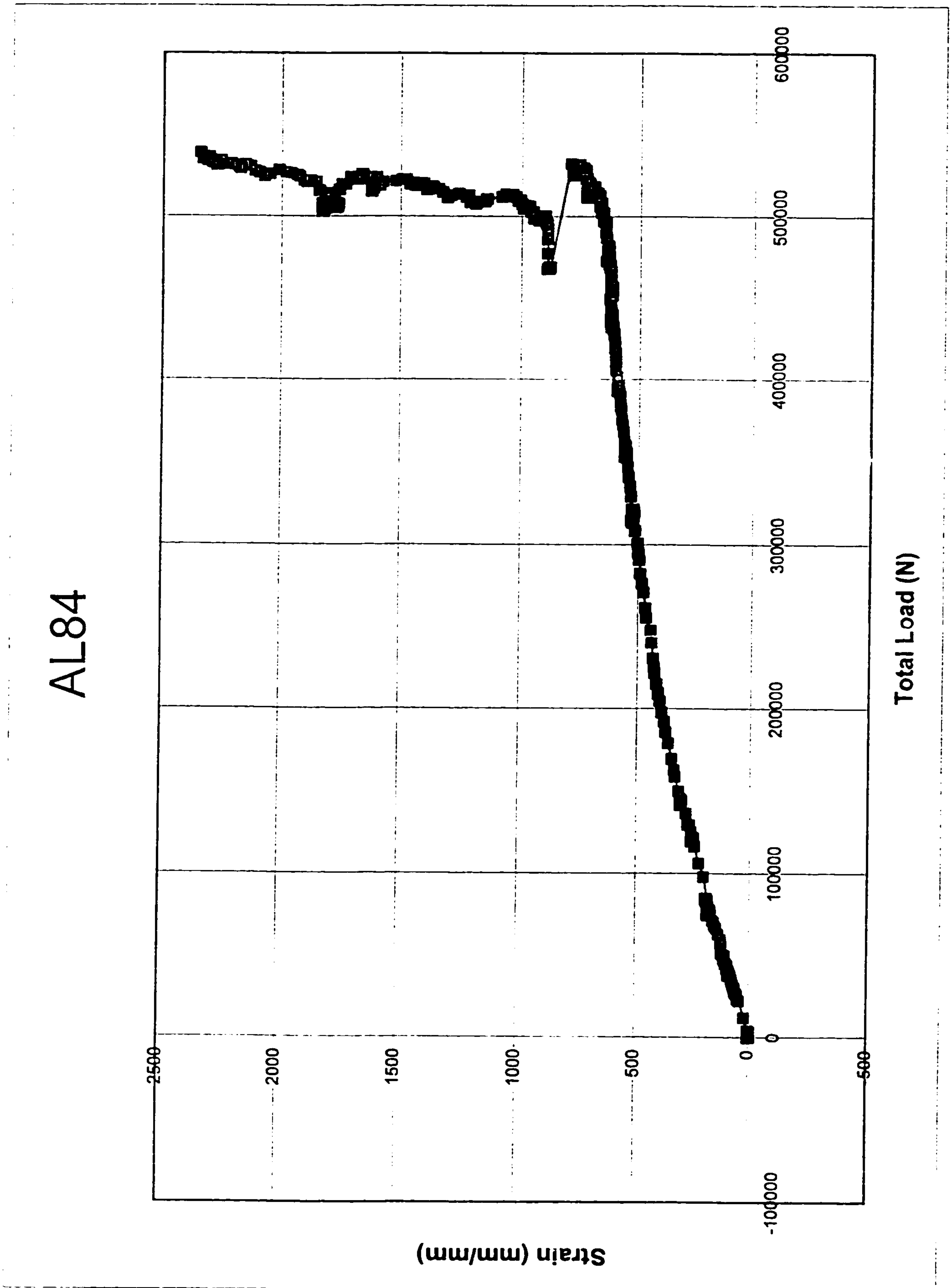
AL84
Total Load (N)
Strain (mm/mm)
-100000
0
100000
200000
300000
400000
500000
600000
2500
2000
1500
1000
500
0
-500

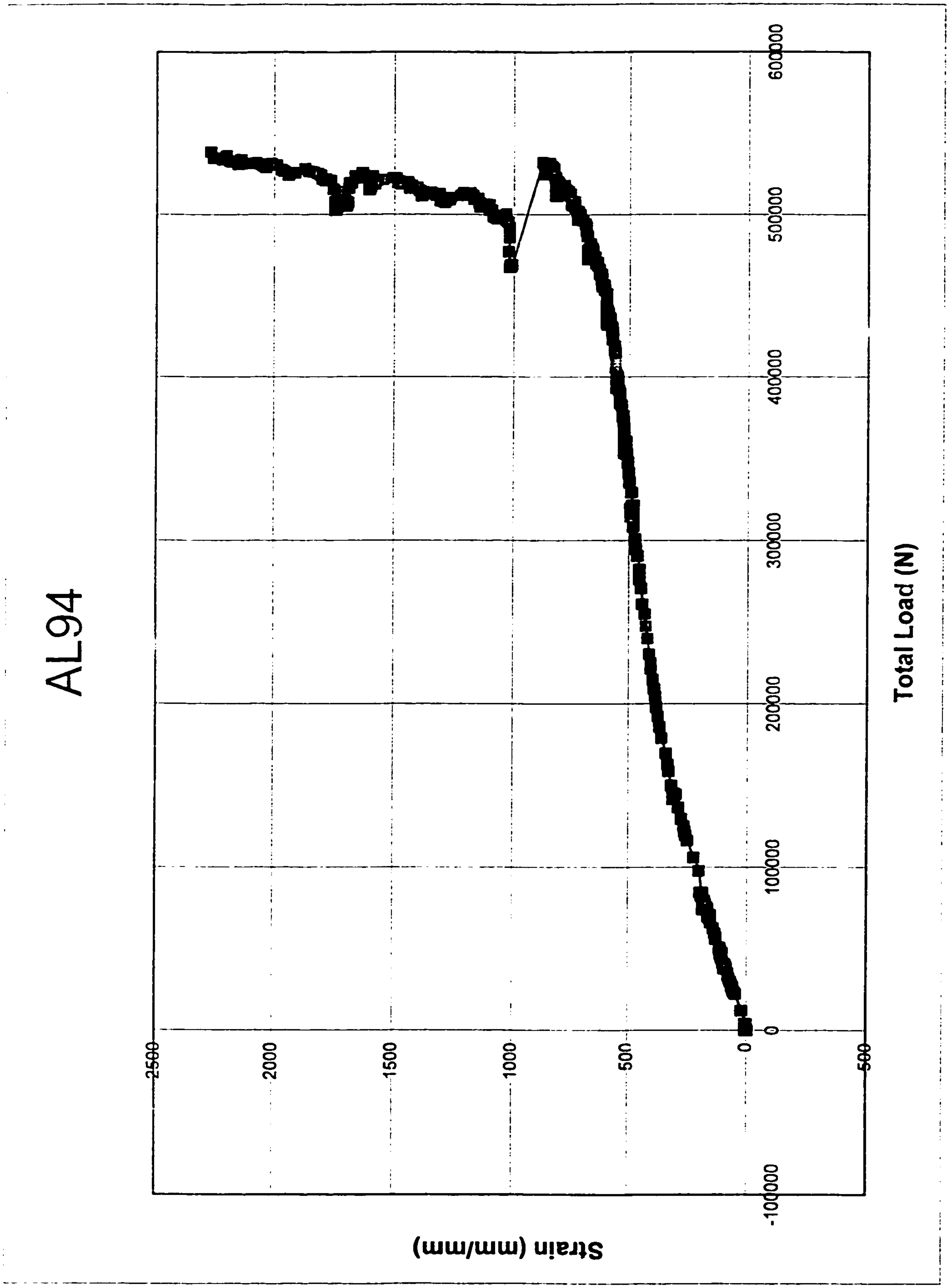
AL94
Strain (mm/mm)
Total Load (N)
2500
2000
1500
1000
500
0
-500
-100000
0
100000
200000
300000
400000
500000
600000

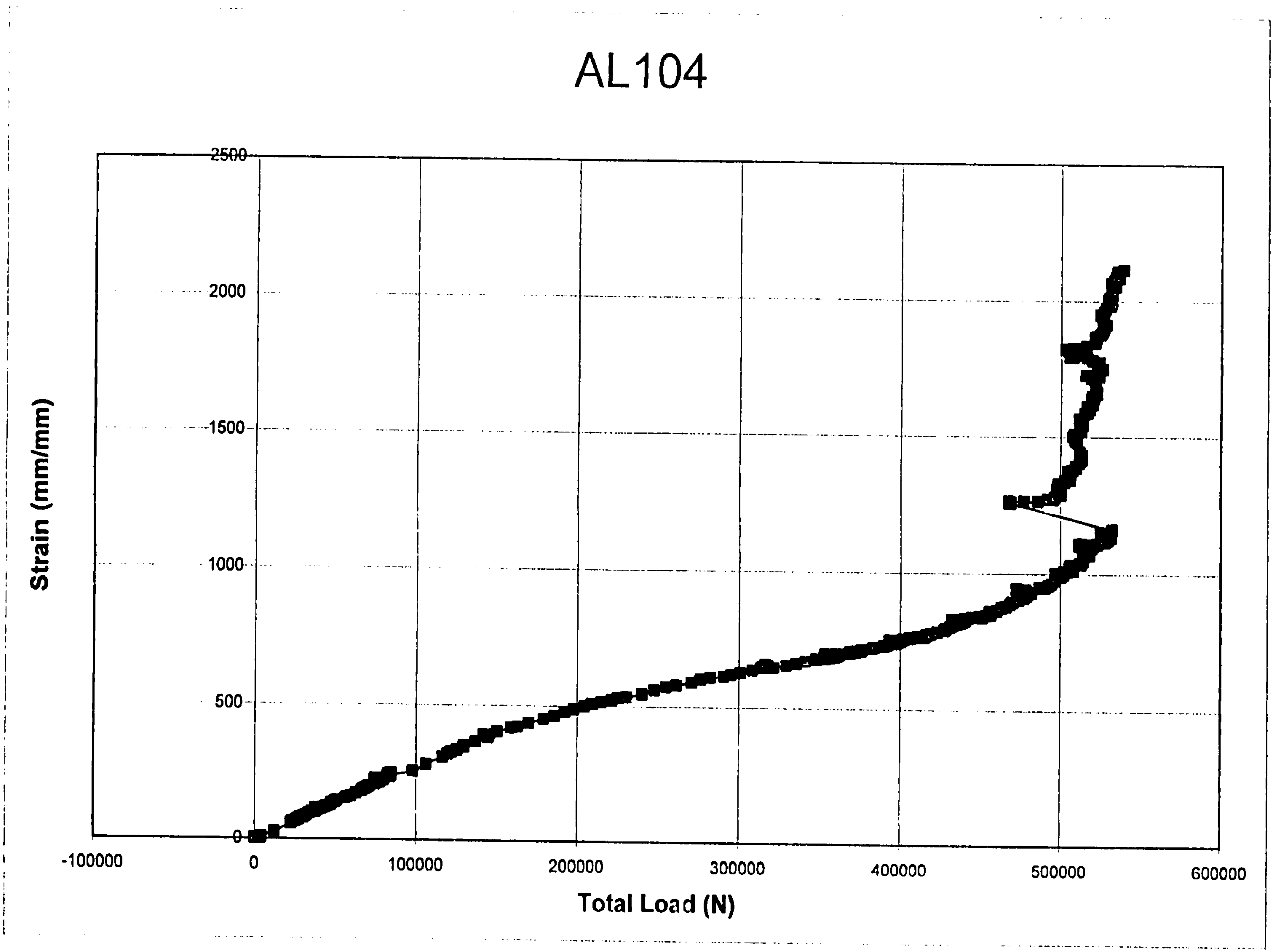
AL104
Strain (mm/mm)
2500
2000
1500
1000
500
0
-100000
0
100000
200000
300000
400000
500000
600000
Total Load (N)

AL114

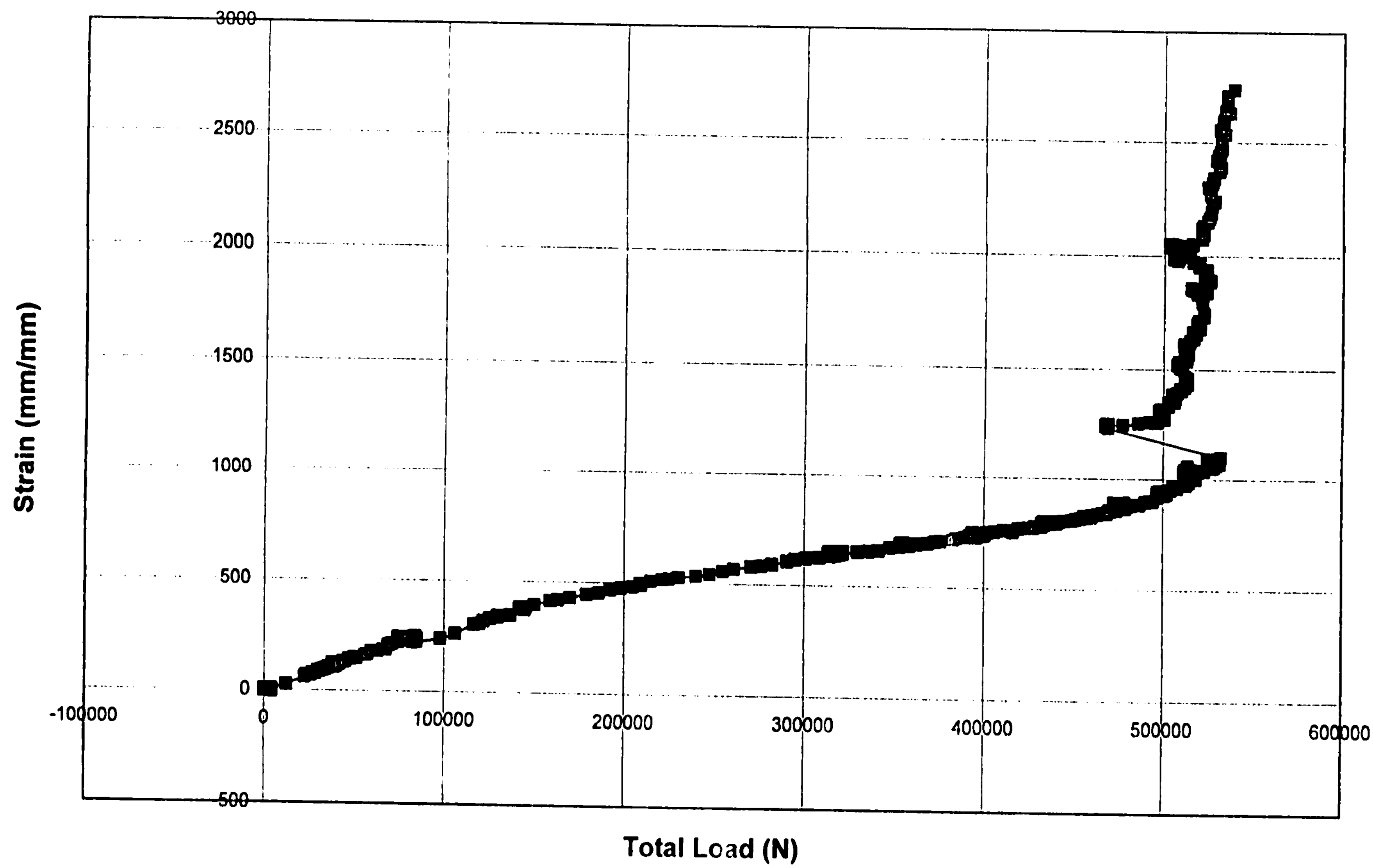
Strain (mm/mm)
Total Load (N)
3000
2500
2000
1500
1000
500
0
-500
-100000
0
100000
200000
300000
400000
500000
600000

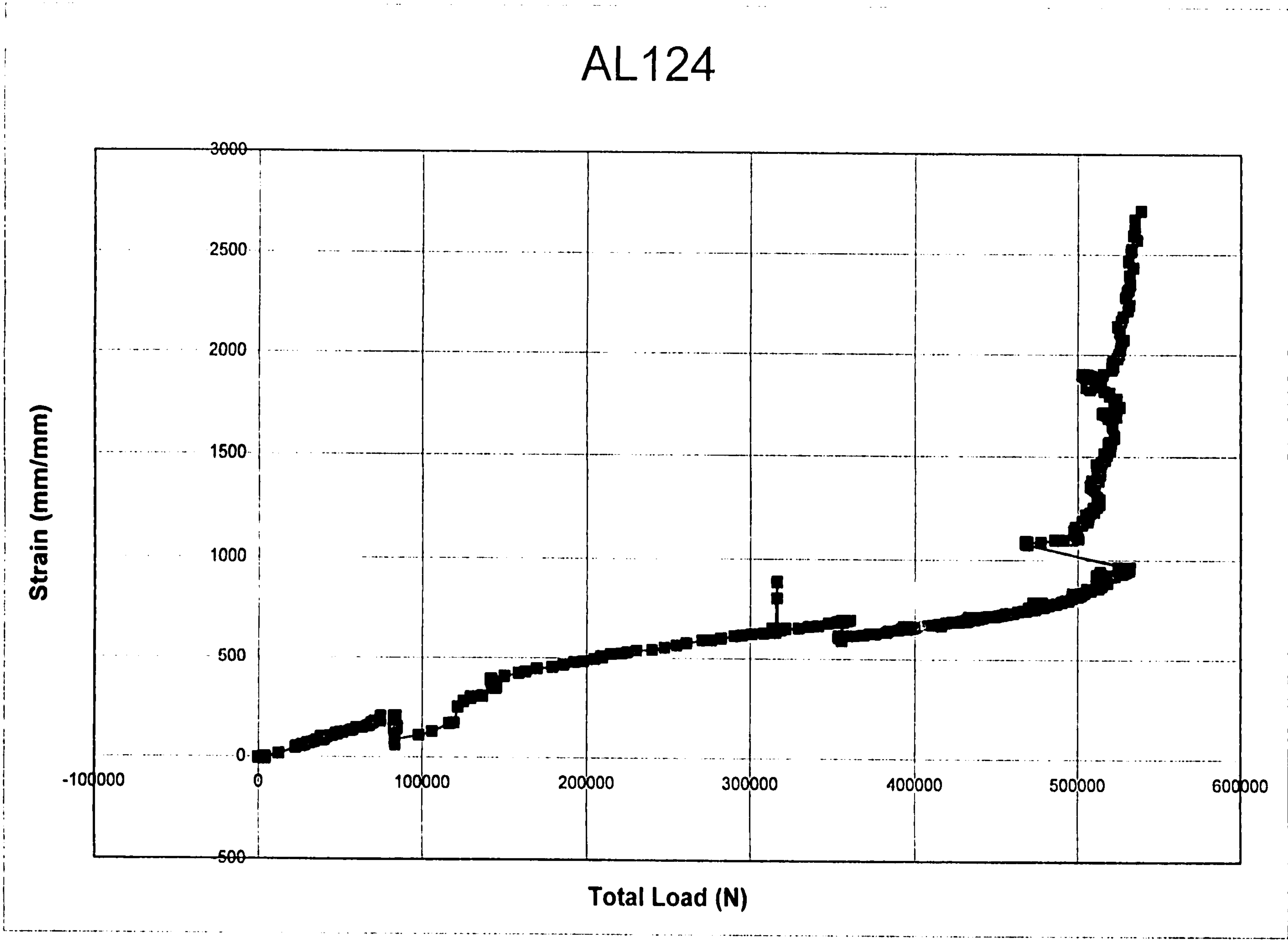

AL124
Strain (mm/mm)
3000
2500
2000
1500
1000
500
0
-500
-100000
0
100000
200000
300000
400000
500000
600000
Total Load (N)

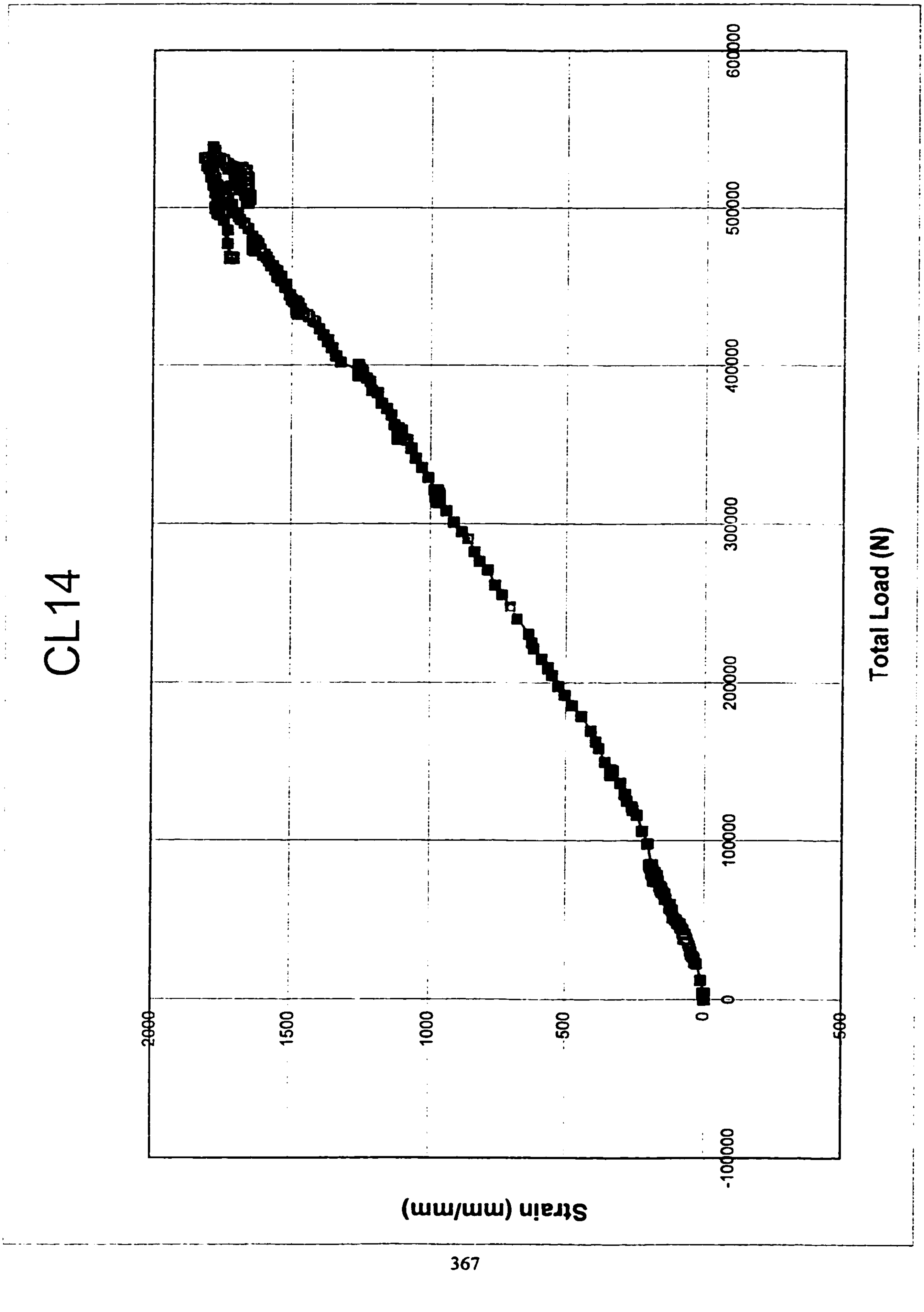
CL 14
Total Load (N)
Strain (mm/mm)
-100000
0
100000
200000
300000
400000
500000
600000
2000
1500
1000
500
0
-500

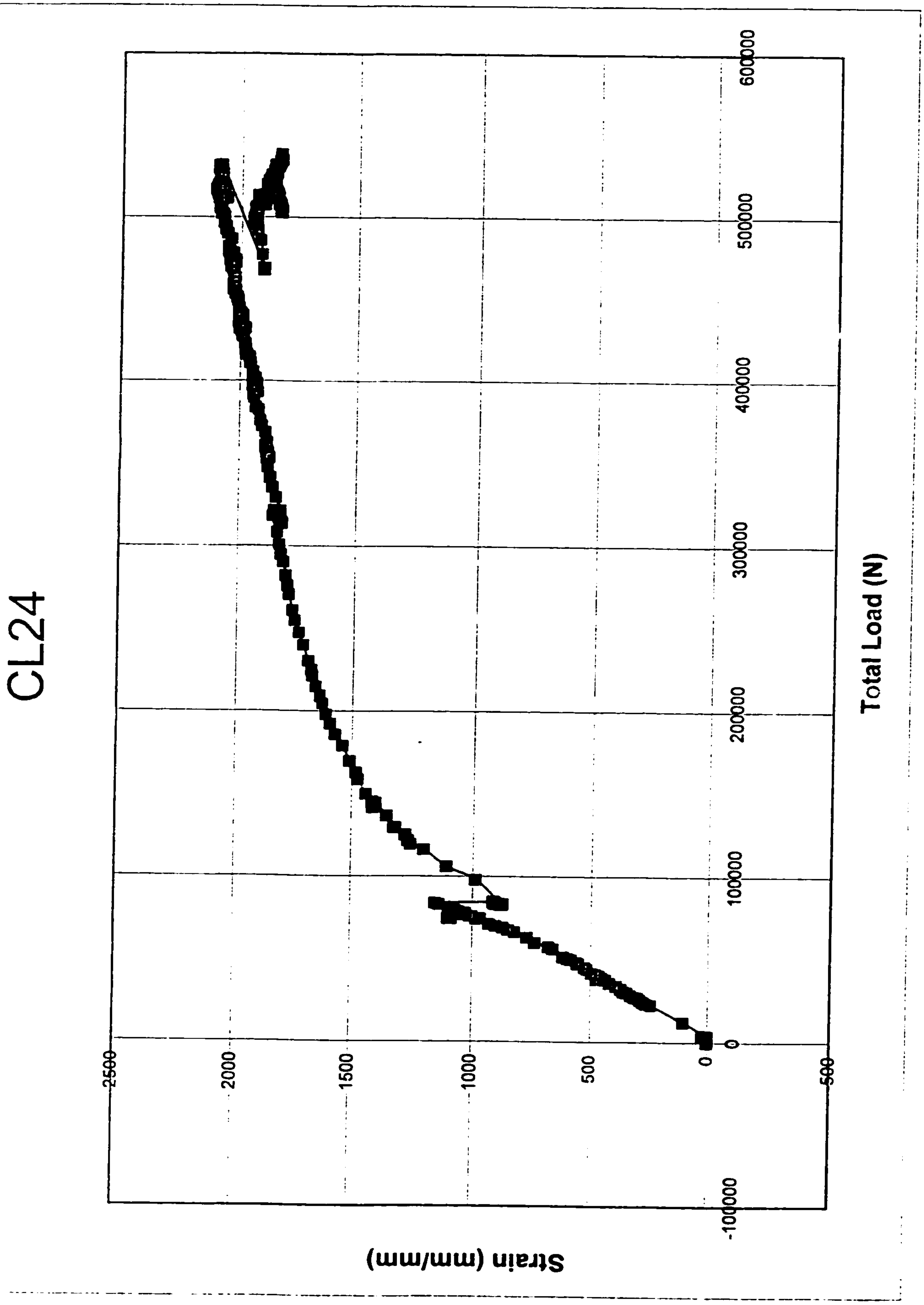

CL24
Strain (mm/mm)
Total Load (N)
2500
2000
1500
1000
500
0
-500
-100000
0
100000
200000
300000
400000
500000
600000

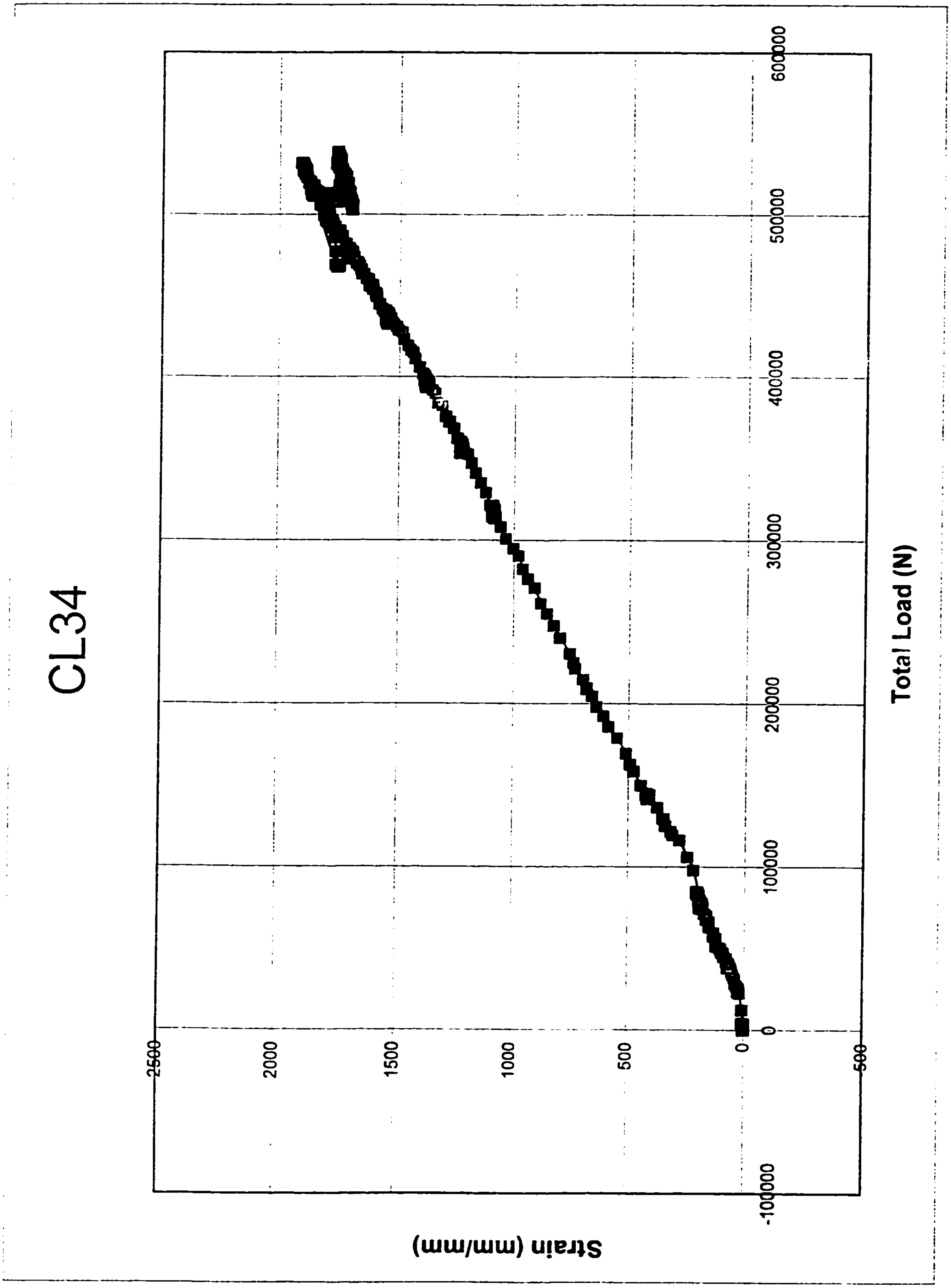
CL34
Strain (mm/mm)
Total Load (N)
-500
0
500
1000
1500
2000
2500
-100000
0
100000
200000
300000
400000
500000
600000

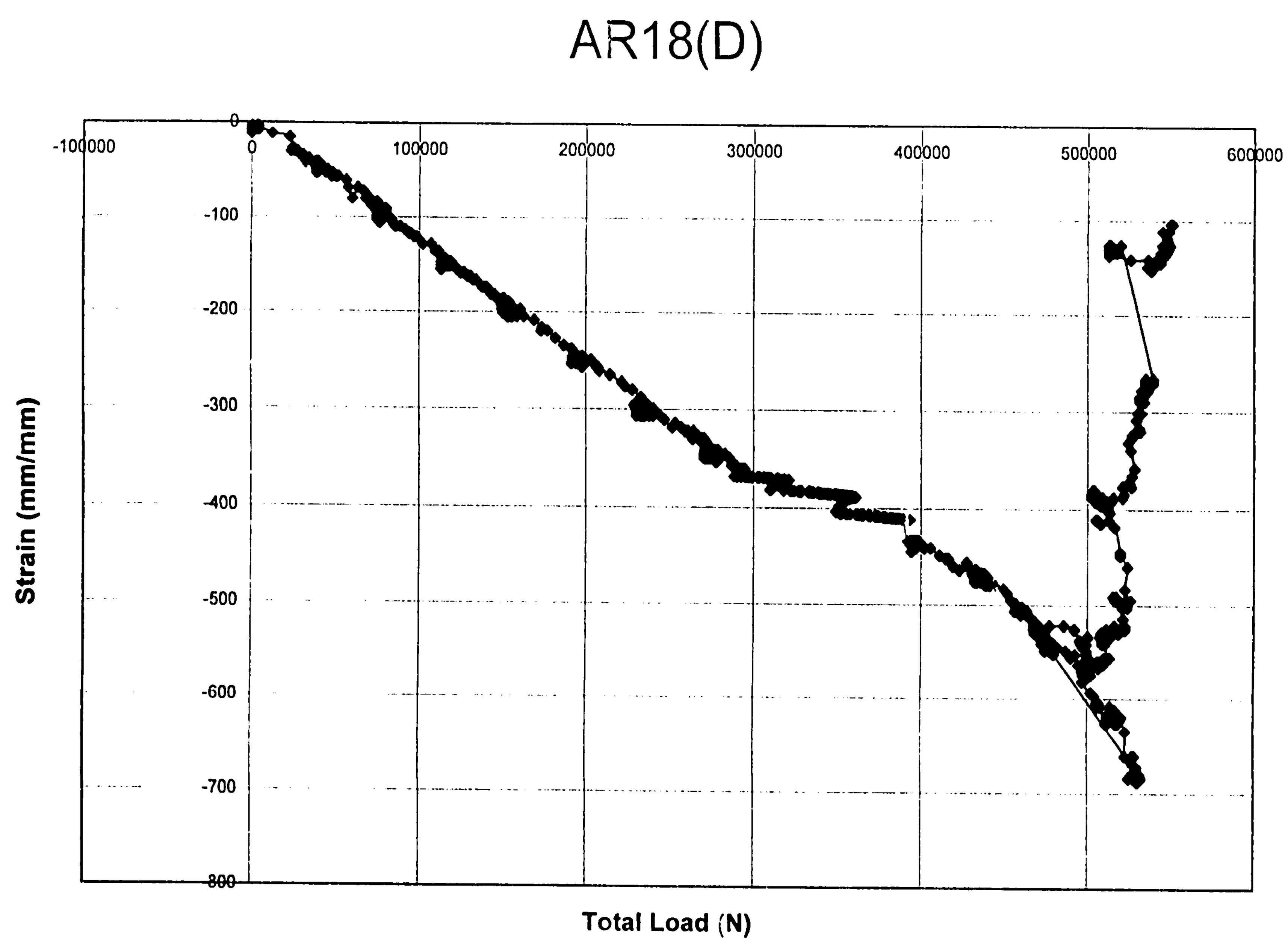
AR18(D)
Strain (mm/mm)
Total Load (N)
-100000
0
100000
200000
300000
400000
500000
600000
0
-100
-200
-300
-400
-500
-600
-700
-800

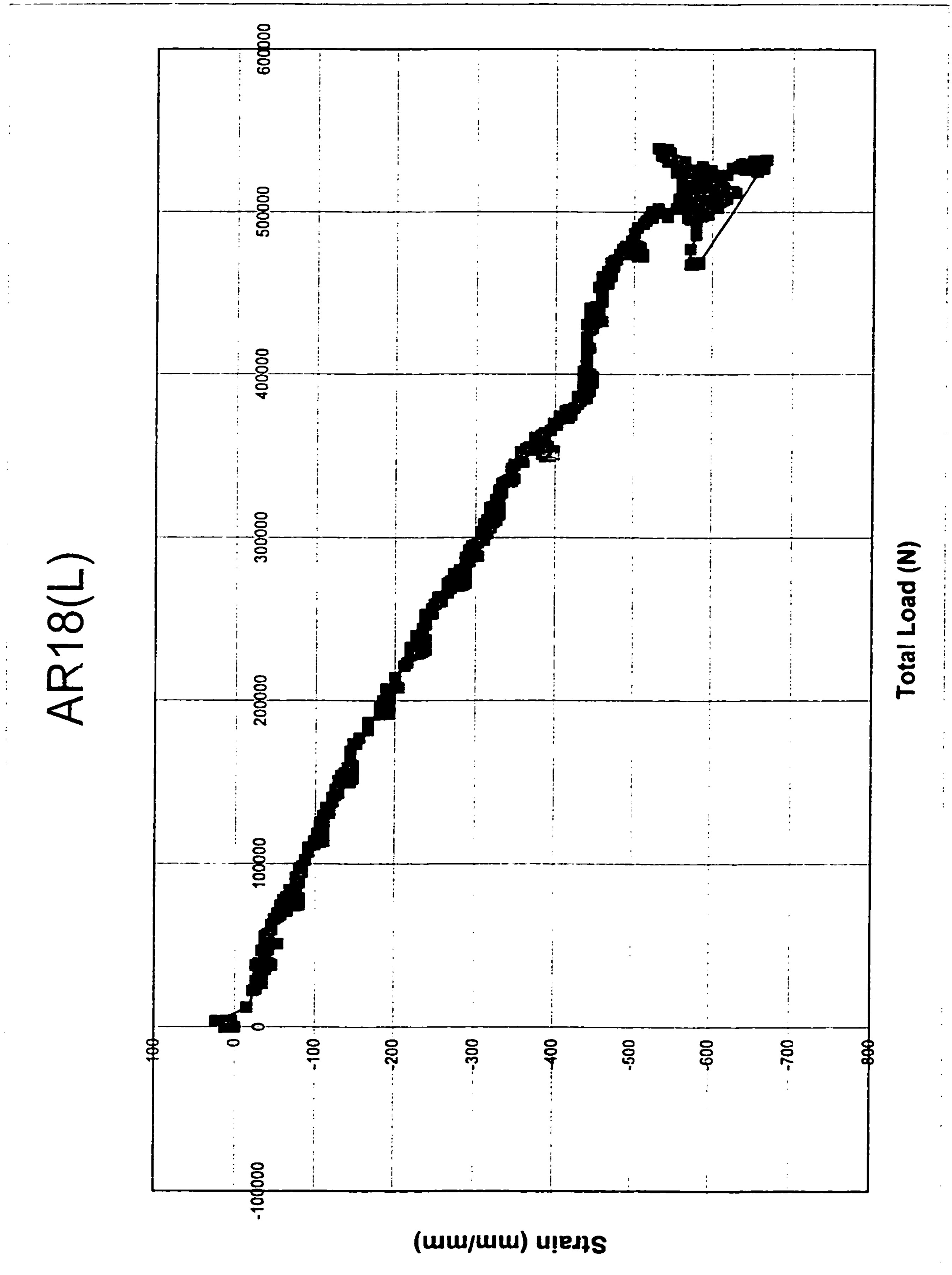
AR18(L)
Strain (mm/mm)
Total Load (N)
100
0
-100
-200
-300
-400
-500
-600
-700
-800
-100000
0
100000
200000
300000
400000
500000
600000

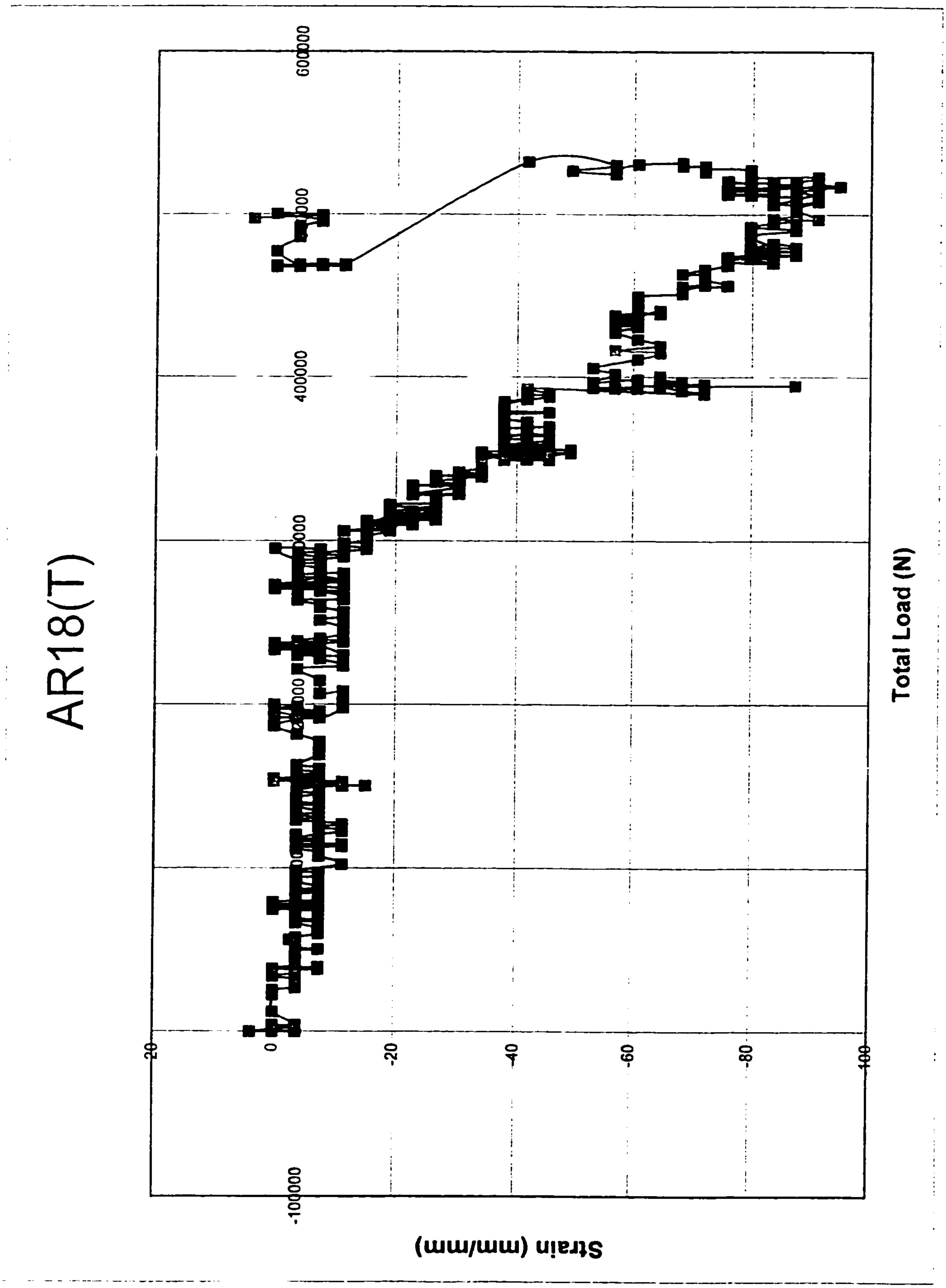
AR18(T)
Total Load (N)
Strain (mm/mm)
-100000
400000
600000
20
0
-20
-40
-60
-80
-100

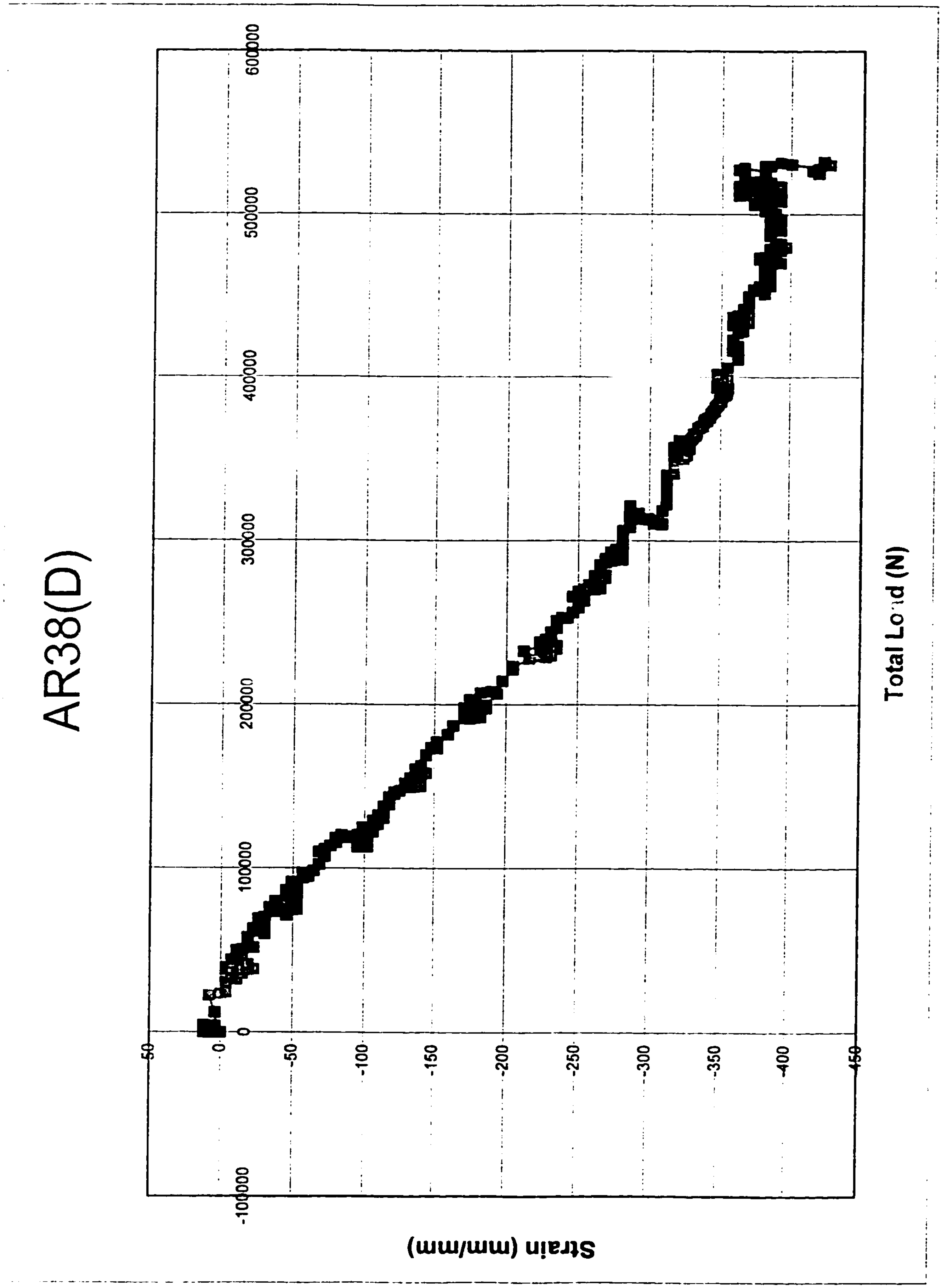
AR38(D)
Strain (mm/mm)
Total Lo d (N)
50
0
-50
-100
-150
-200
-250
-300
-350
-400
-450
-100000
0
100000
200000
300000
400000
500000
600000

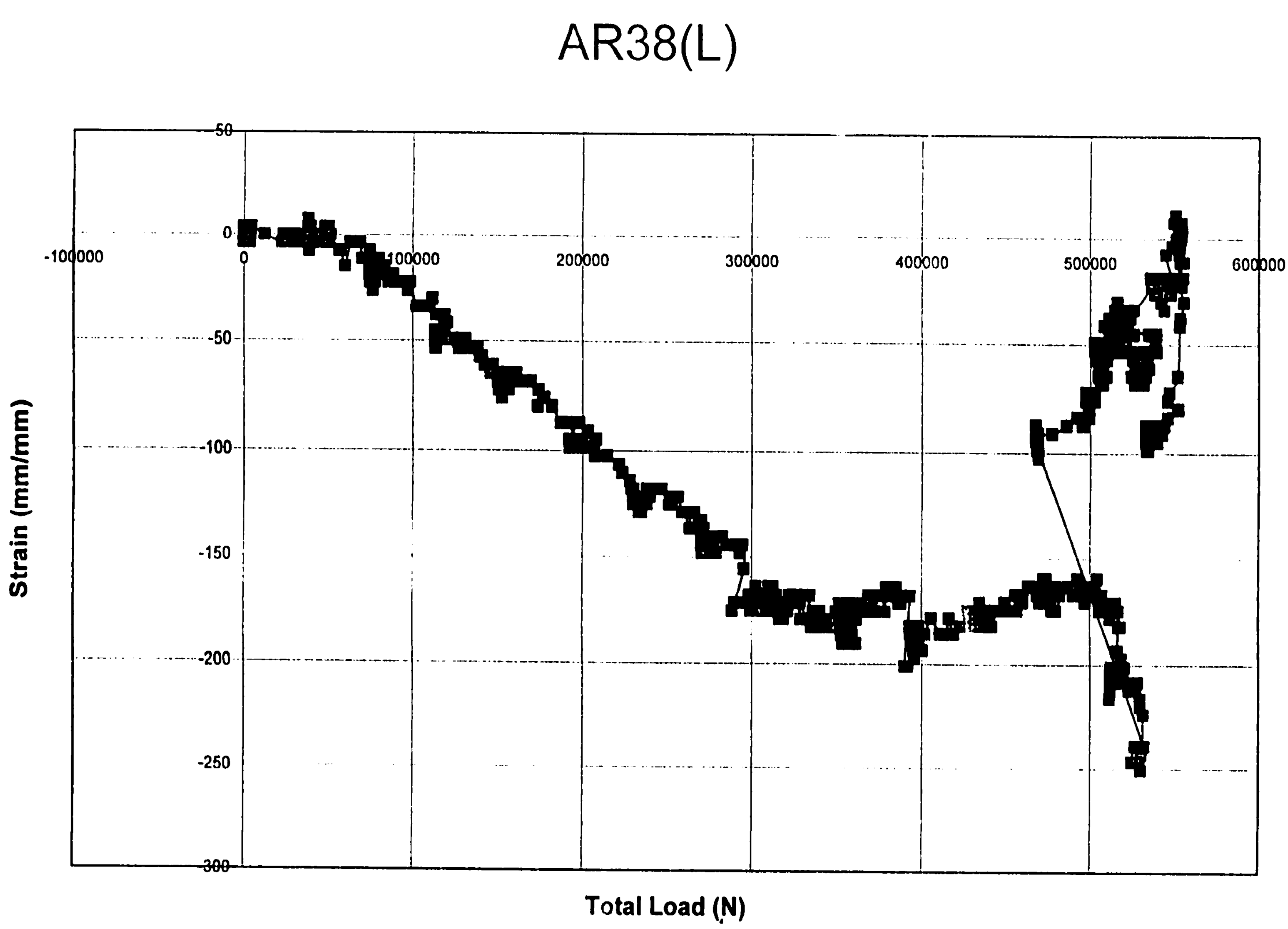
AR38(L)
Strain (mm/mm)
Total Load (N)
50
0
-50
-100
-150
-200
-250
-300
-100000
0
100000
200000
300000
400000
500000
600000

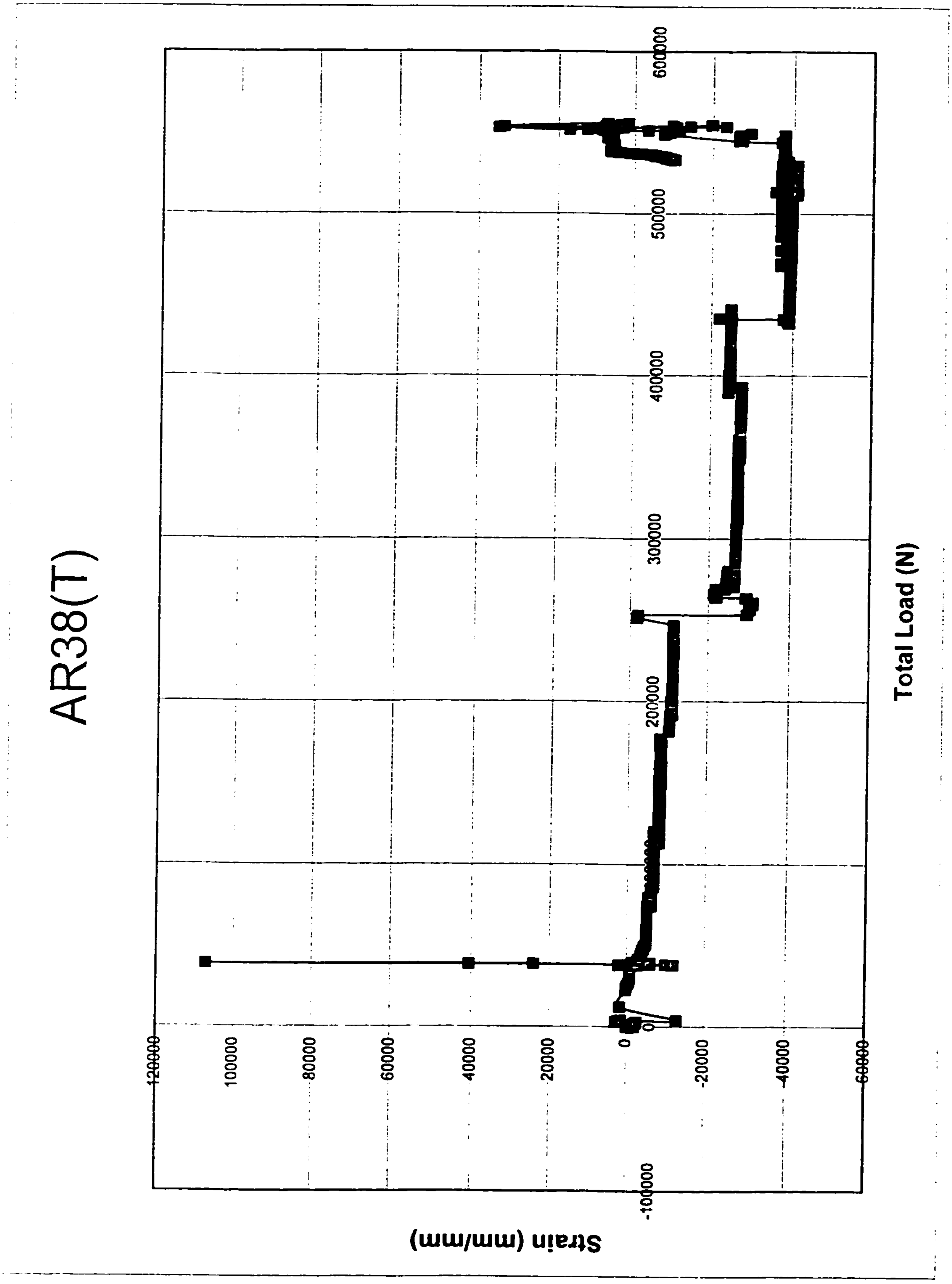
AR38(T)
Total Load (N)
Strain (mm/mm)
0
100000
200000
300000
400000
500000
600000
-100000
120000
100000
80000
60000
40000
20000
0
-20000
-40000
-60000

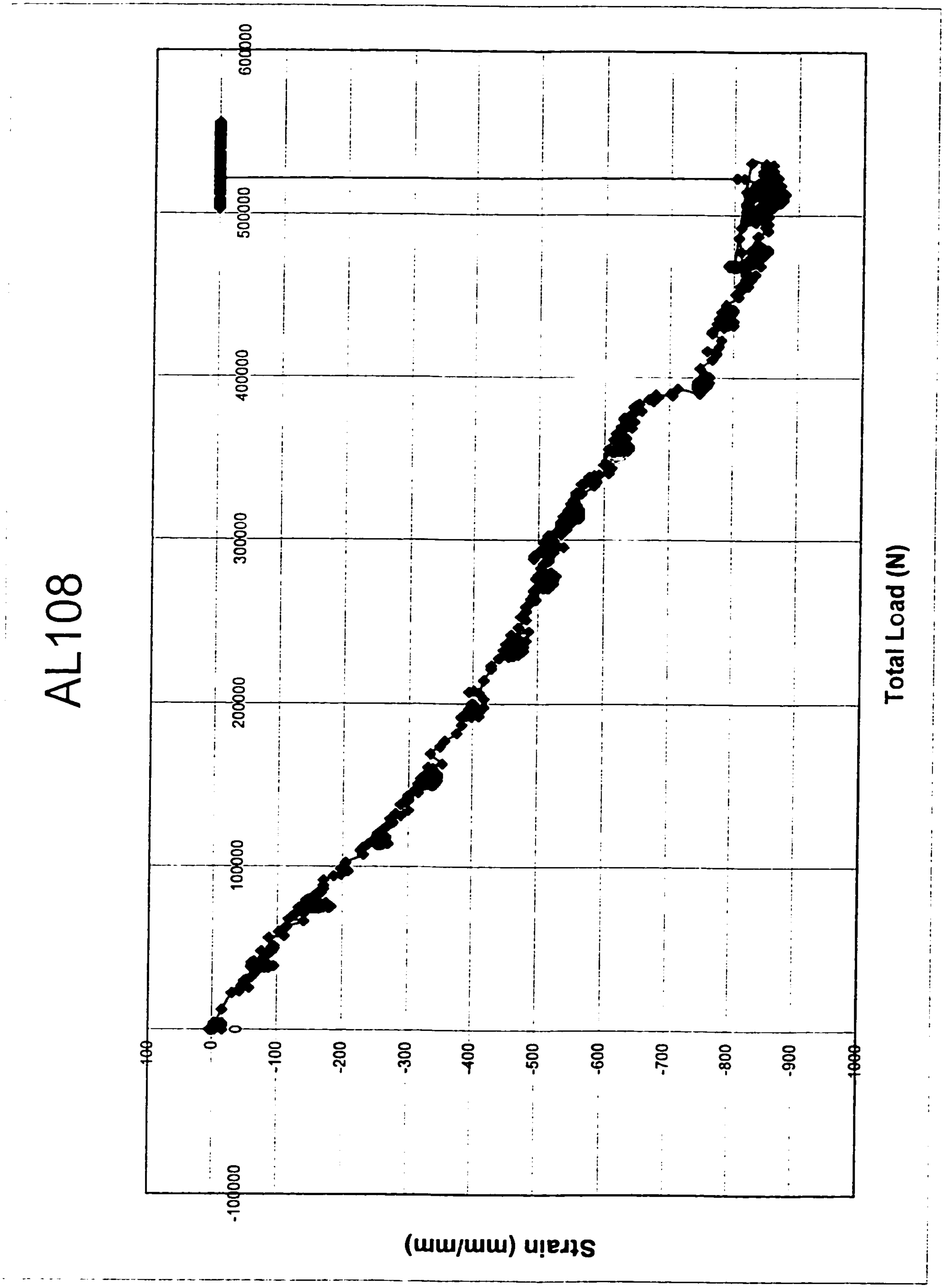

AL108
Strain (mm/mm)
Total Load (N)
100
0
-100
-200
-300
-400
-500
-600
-700
-800
-900
-1000
-100000
0
100000
200000
300000
400000
500000
600000

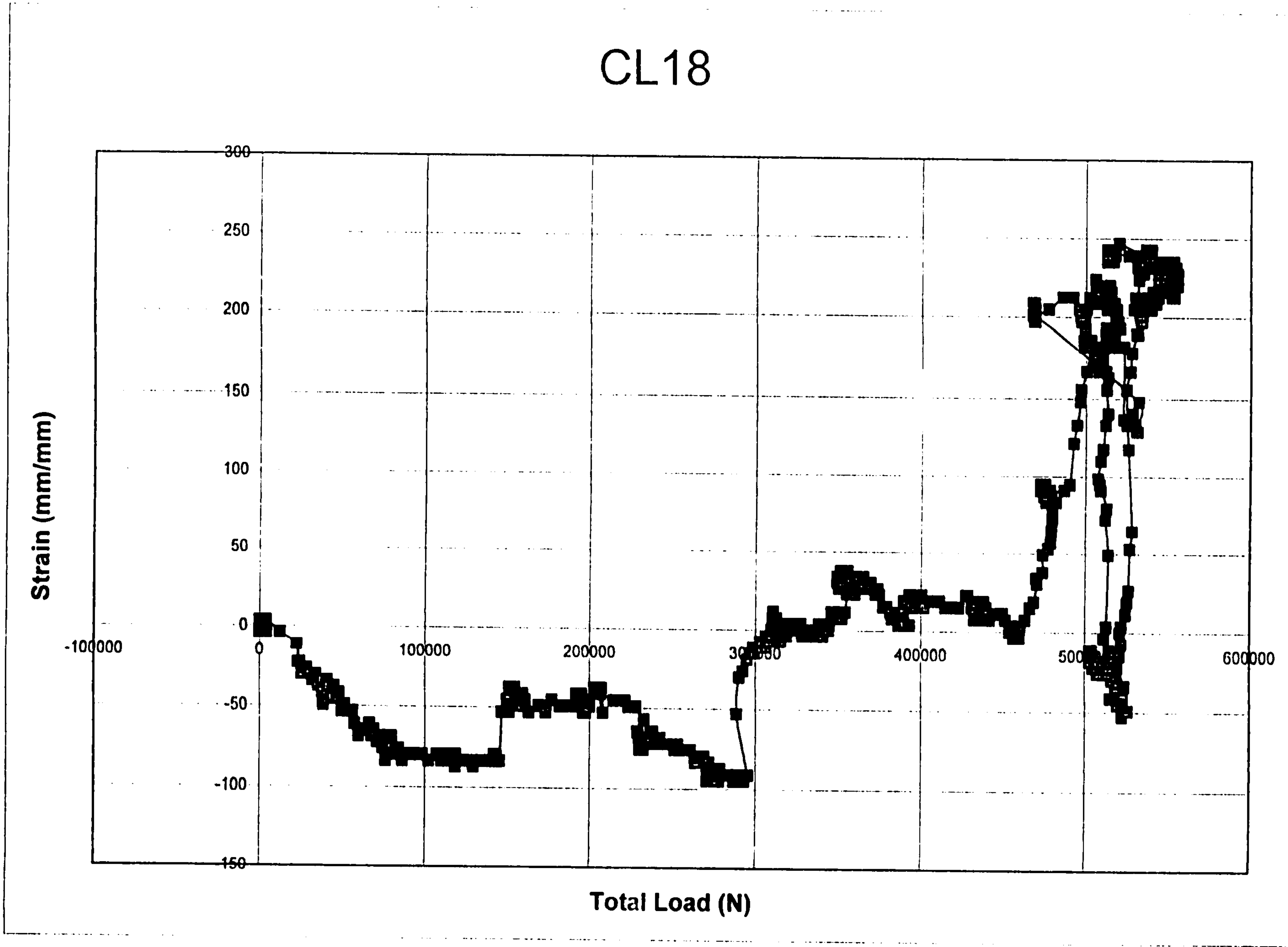
CL18
Strain (mm/mm)
300
250
200
150
100
50
0
-50
-100
-150
-100000
0
100000
200000
300000
400000
500000
600000
Total Load (N)

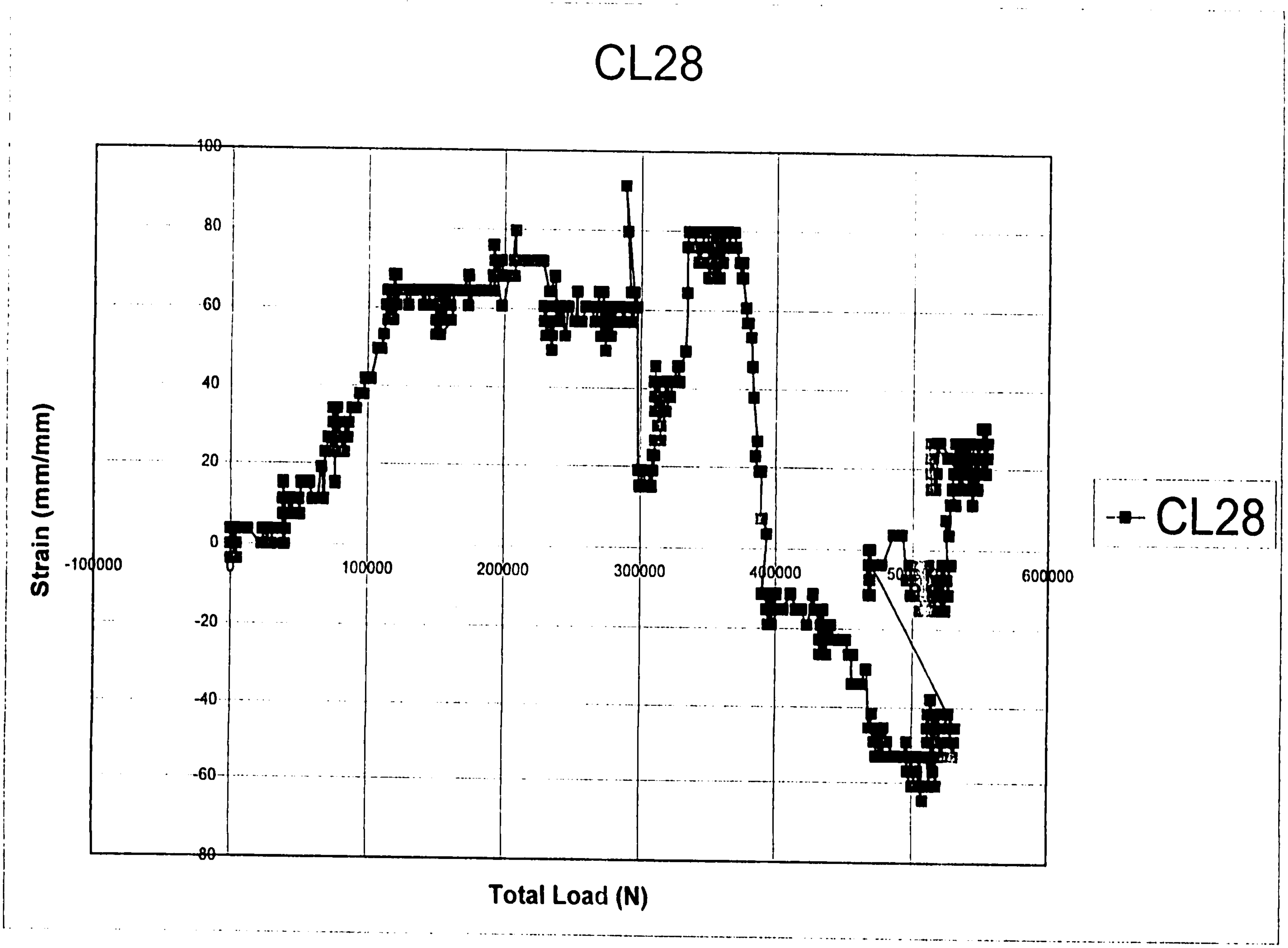
CL28
Strain (mm/mm)
100
80
60
40
20
0
-20
-40
-60
-80
-100000
0
100000
200000
300000
400000
500000
600000
Total Load (N)
CL28

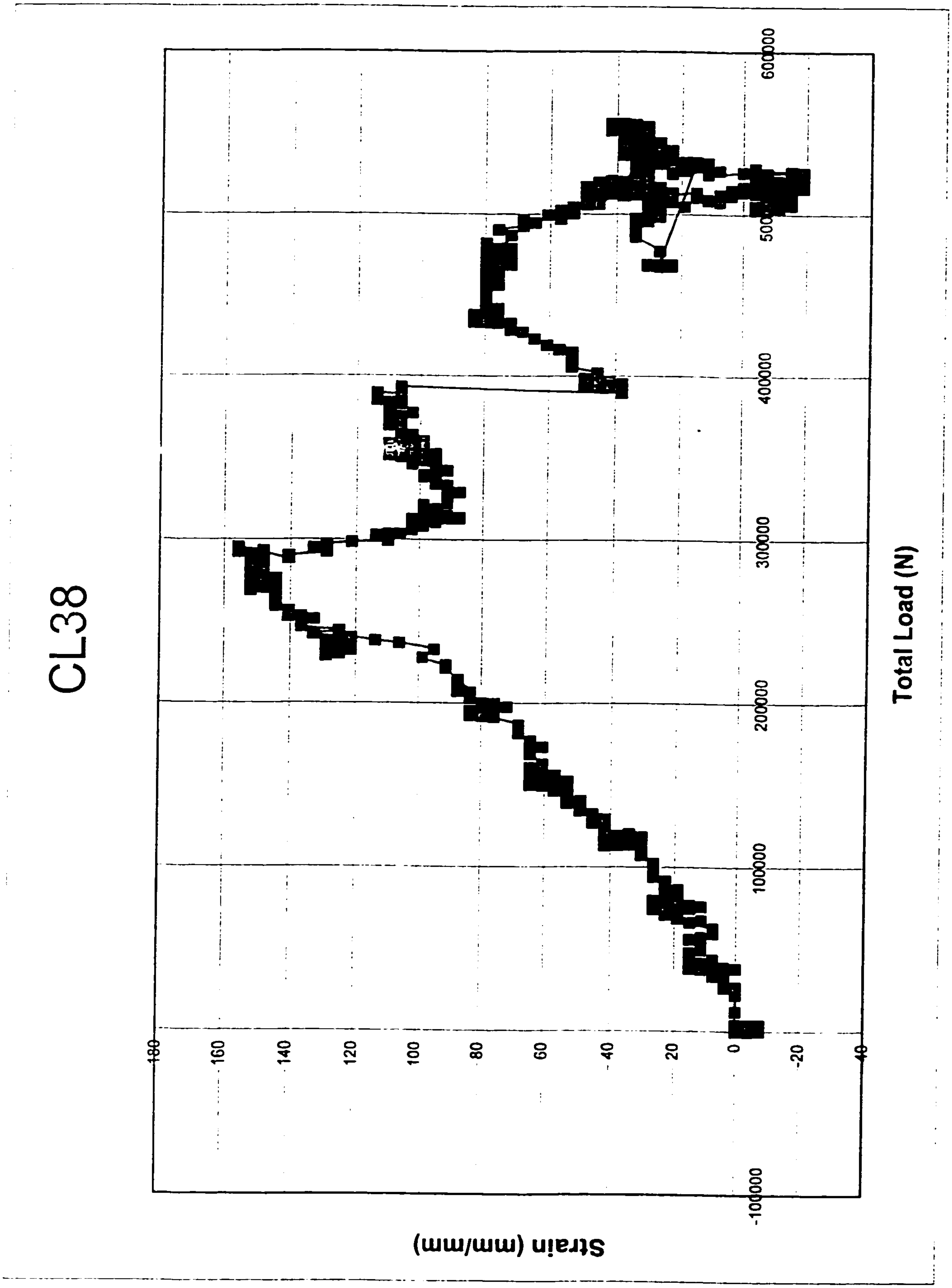
CL38
Strain (mm/mm)
Total Load (N)
-100000
100000
200000
300000
400000
500000
600000
180
160
140
120
100
80
60
40
20
0
-20
-40

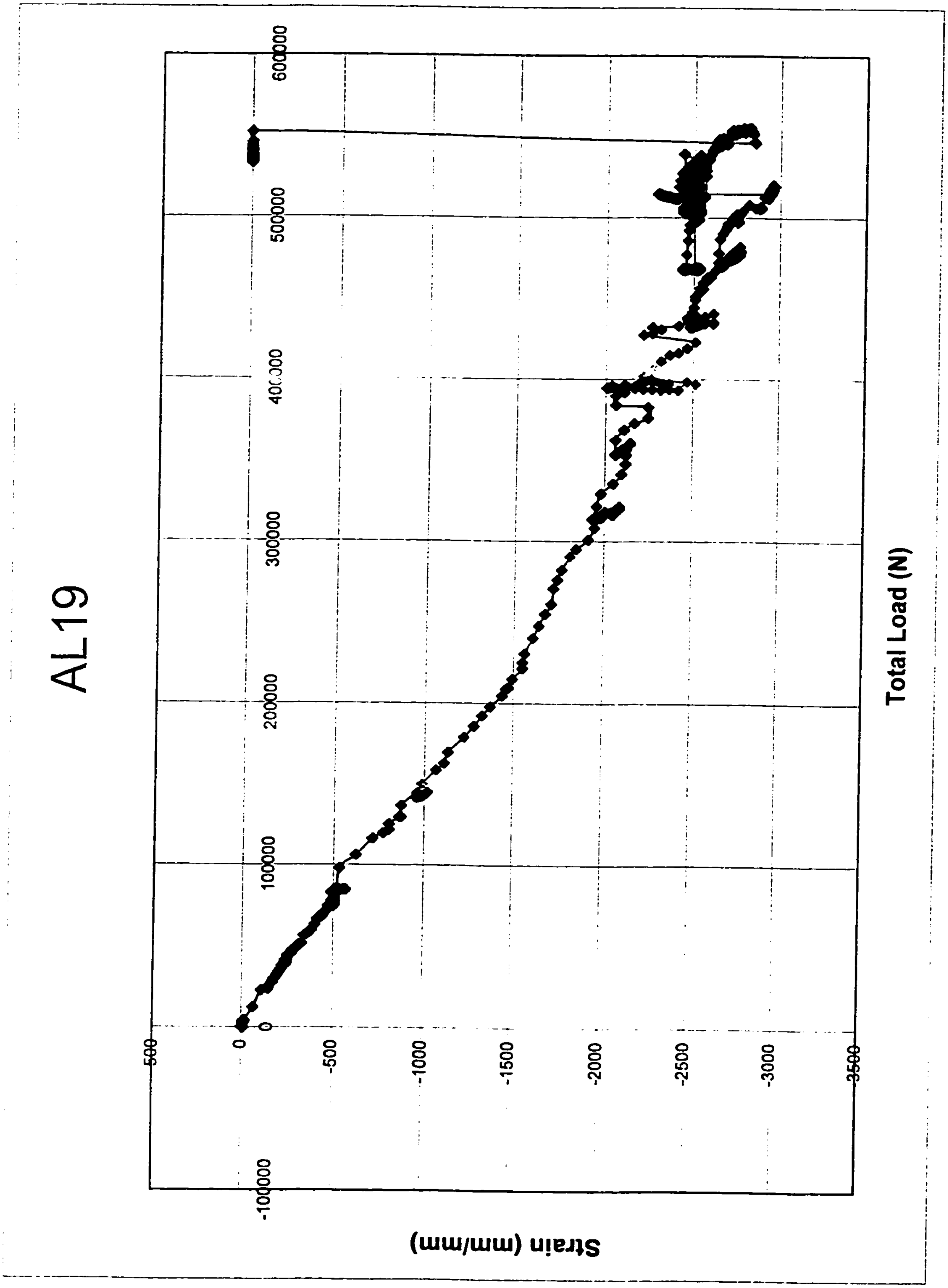
AL19
Total Load (N)
Strain (mm/mm)
-100000
0
100000
200000
300000
400000
500000
600000
500
0
-500
-1000
-1500
-2000
-2500
-3000
-3500

AL29

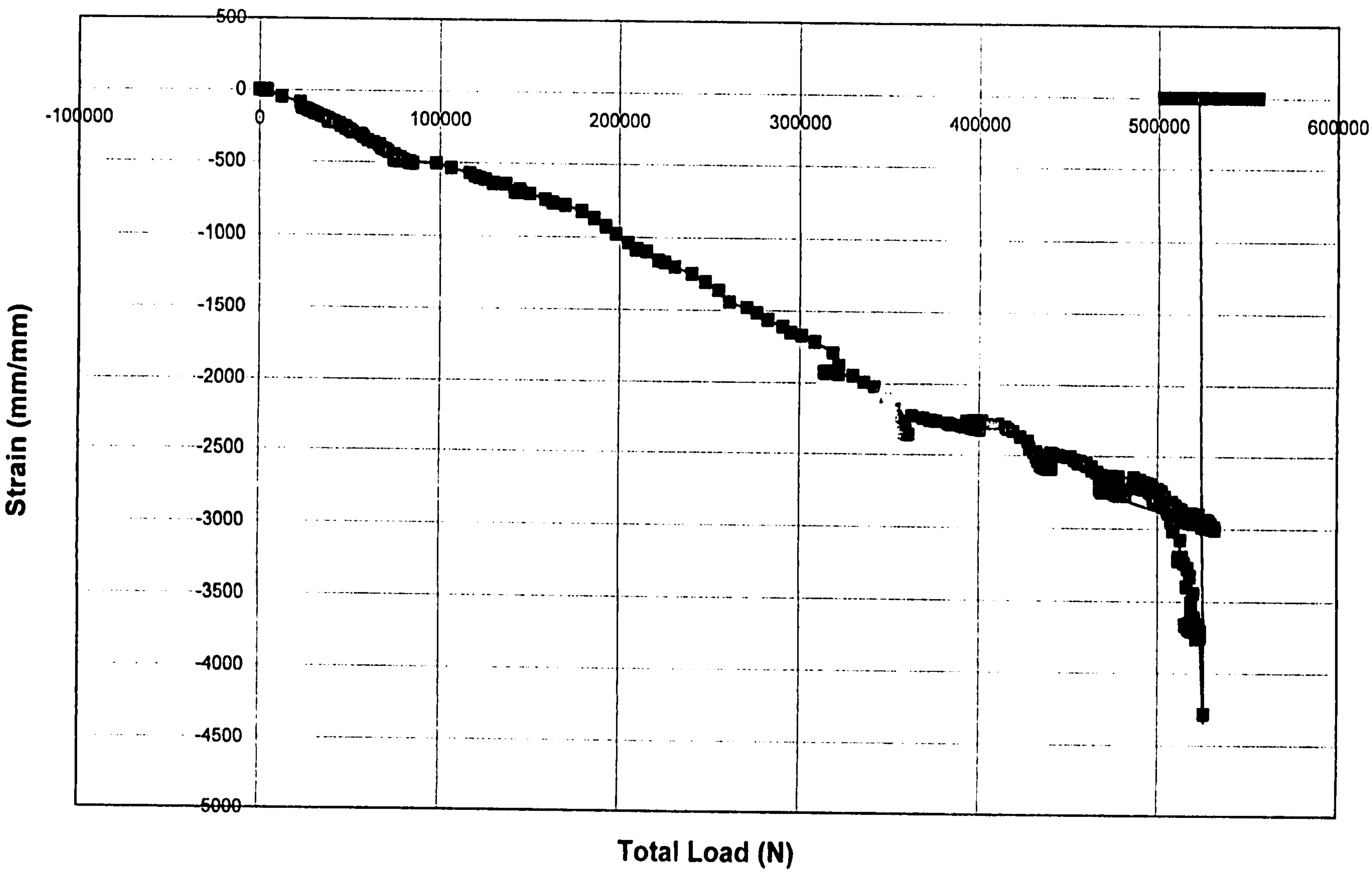

500
0
-500
-1000
-1500
-2000
-2500
-3000
-3500
-4000
-4500
-5000
-100000
0
100000
200000
300000
400000
500000
600000
Strain (mm/mm)
Total Load (N)

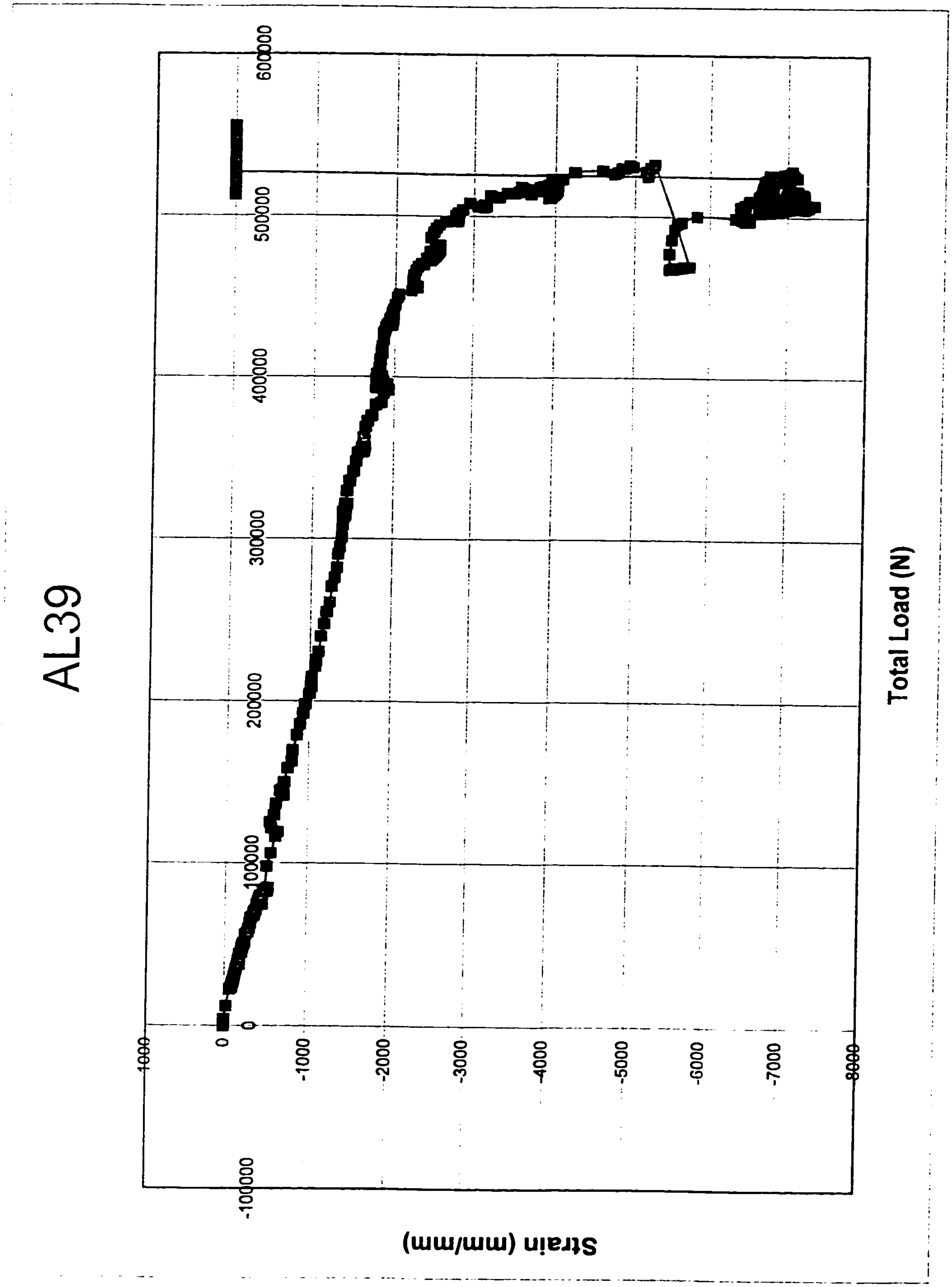
AL39
Total Load (N)
Strain (mm/mm)
-100000
0
100000
200000
300000
400000
500000
600000
1000
0
-1000
-2000
-3000
-4000
-5000
-6000
-7000
-8000

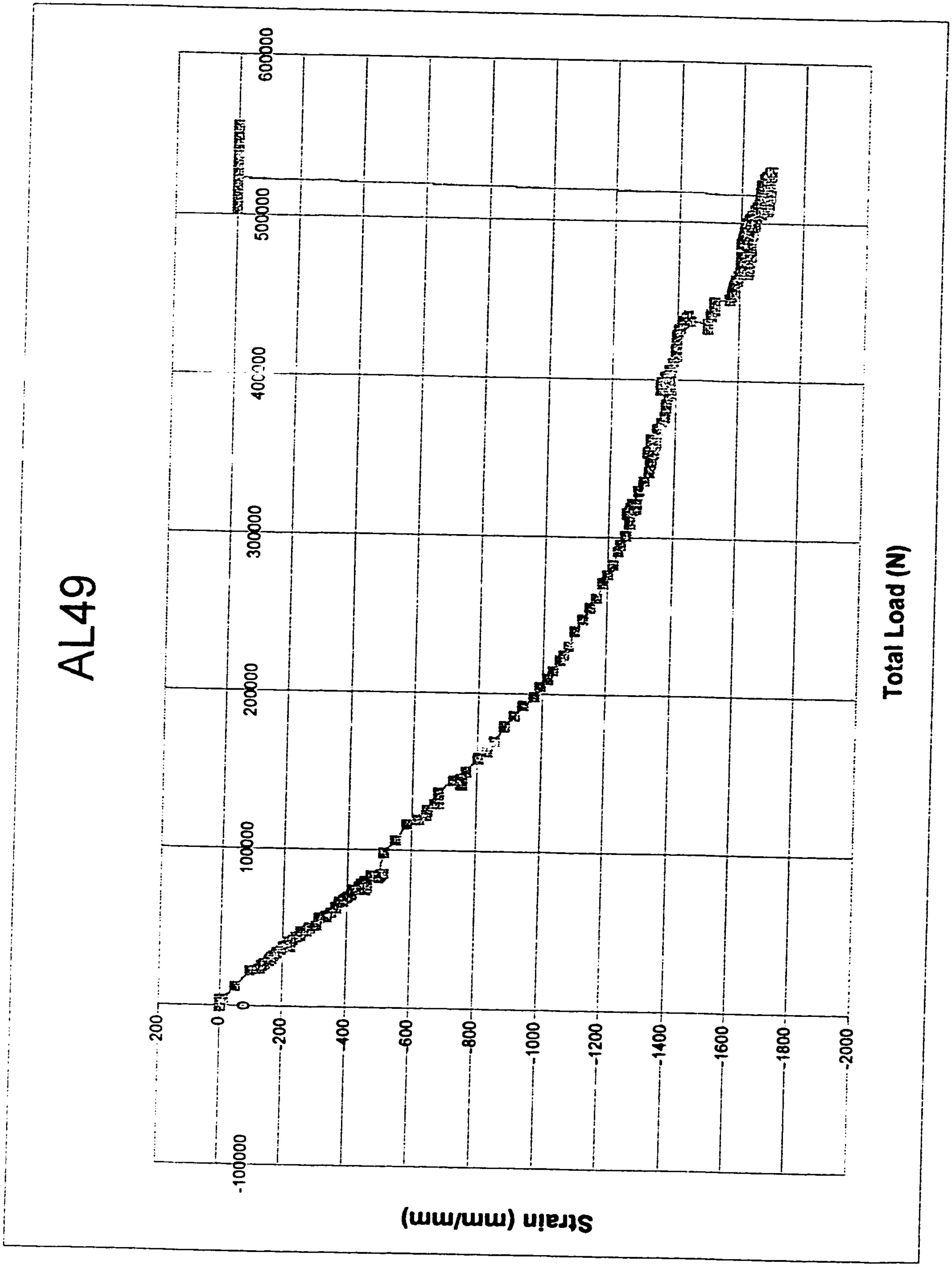
AL49
Strain (mm/mm)
Total Load (N)
200
0
-200
-400
-600
-800
-1000
-1200
-1400
-1600
-1800
-2000
-100000
0
100000
200000
300000
400000
500000
600000

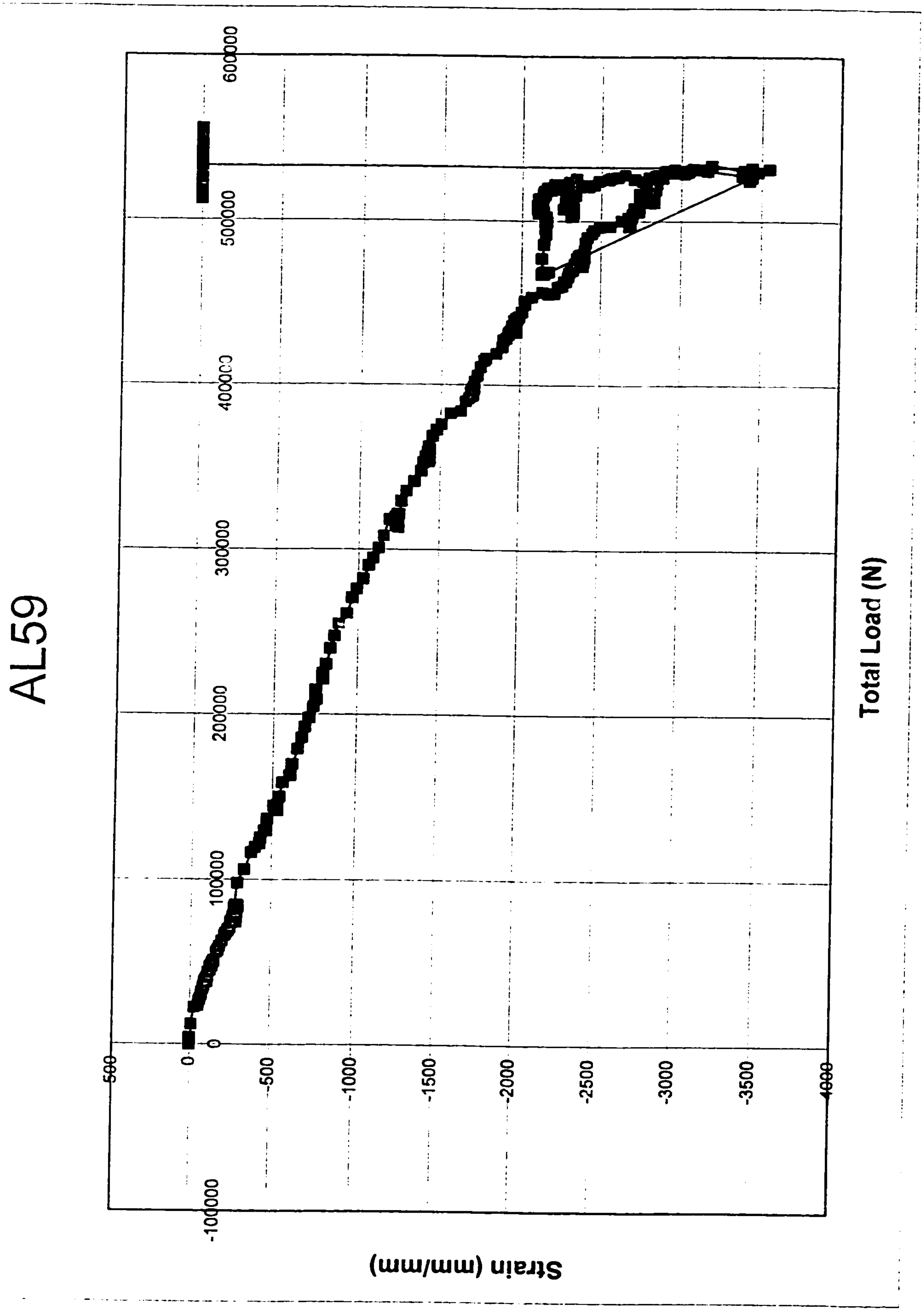
AL59
Strain (mm/mm)
Total Load (N)
-100000
0
100000
200000
300000
400000
500000
600000
500
0
-500
-1000
-1500
-2000
-2500
-3000
-3500
-4000

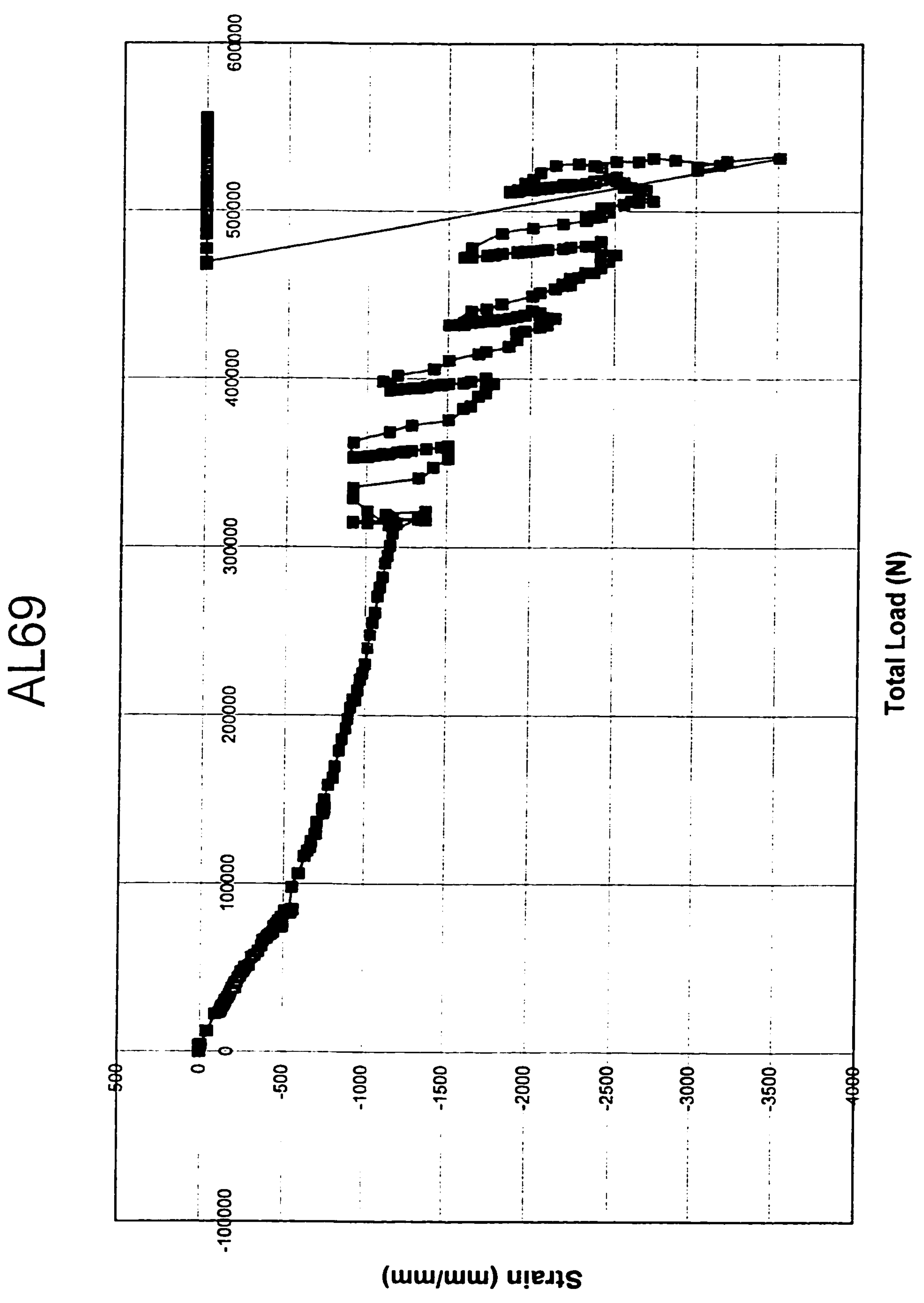
AL69
Strain (mm/mm)
Total Load (N)
500
0
-500
-1000
-1500
-2000
-2500
-3000
-3500
-4000
-100000
0
100000
200000
300000
400000
500000
600000

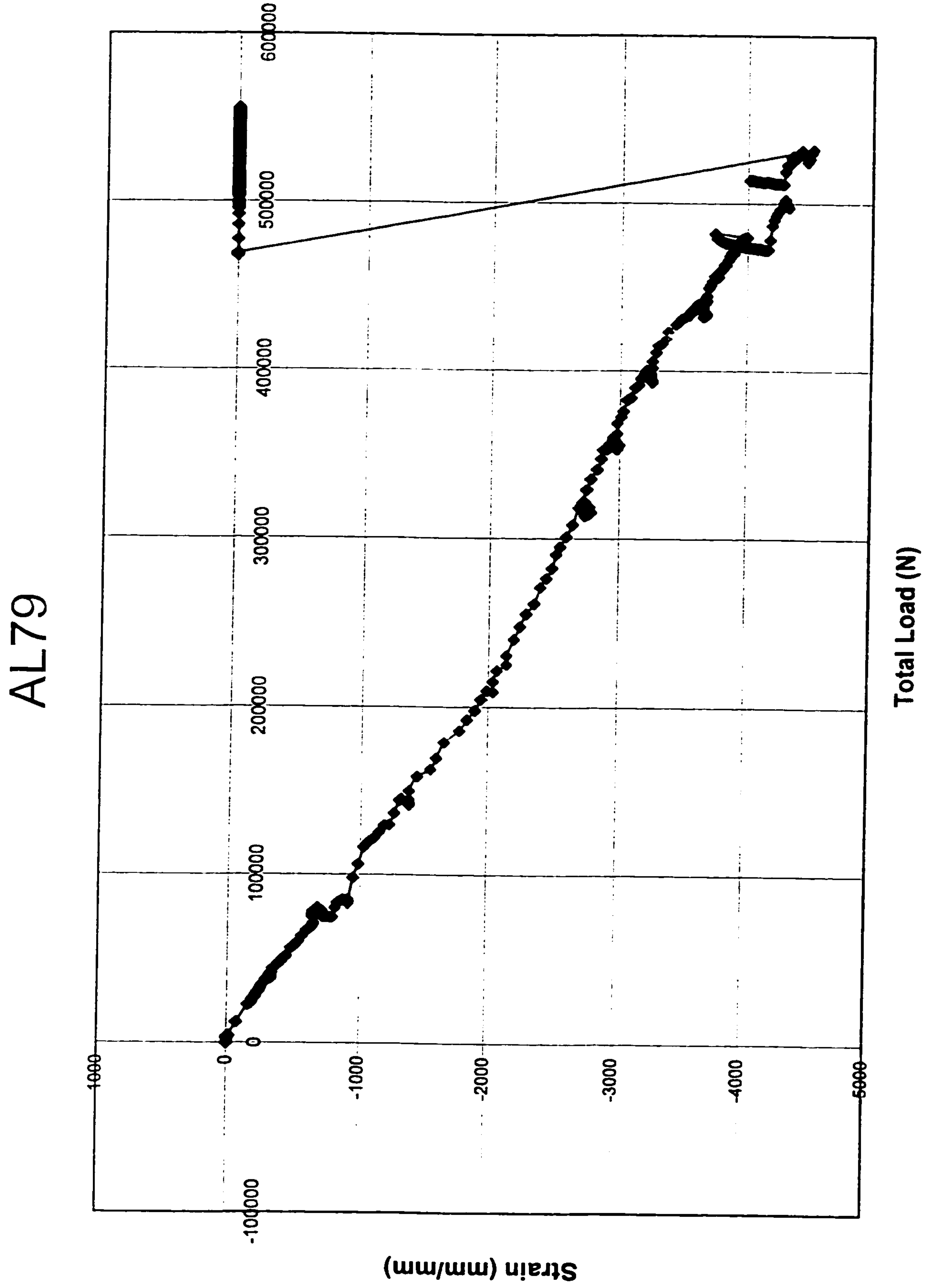
AL79
Strain (mm/mm)
Total Load (N)
1000
0
-1000
-2000
-3000
-4000
-5000
-100000
0
100000
200000
300000
400000
500000
600000

AL89

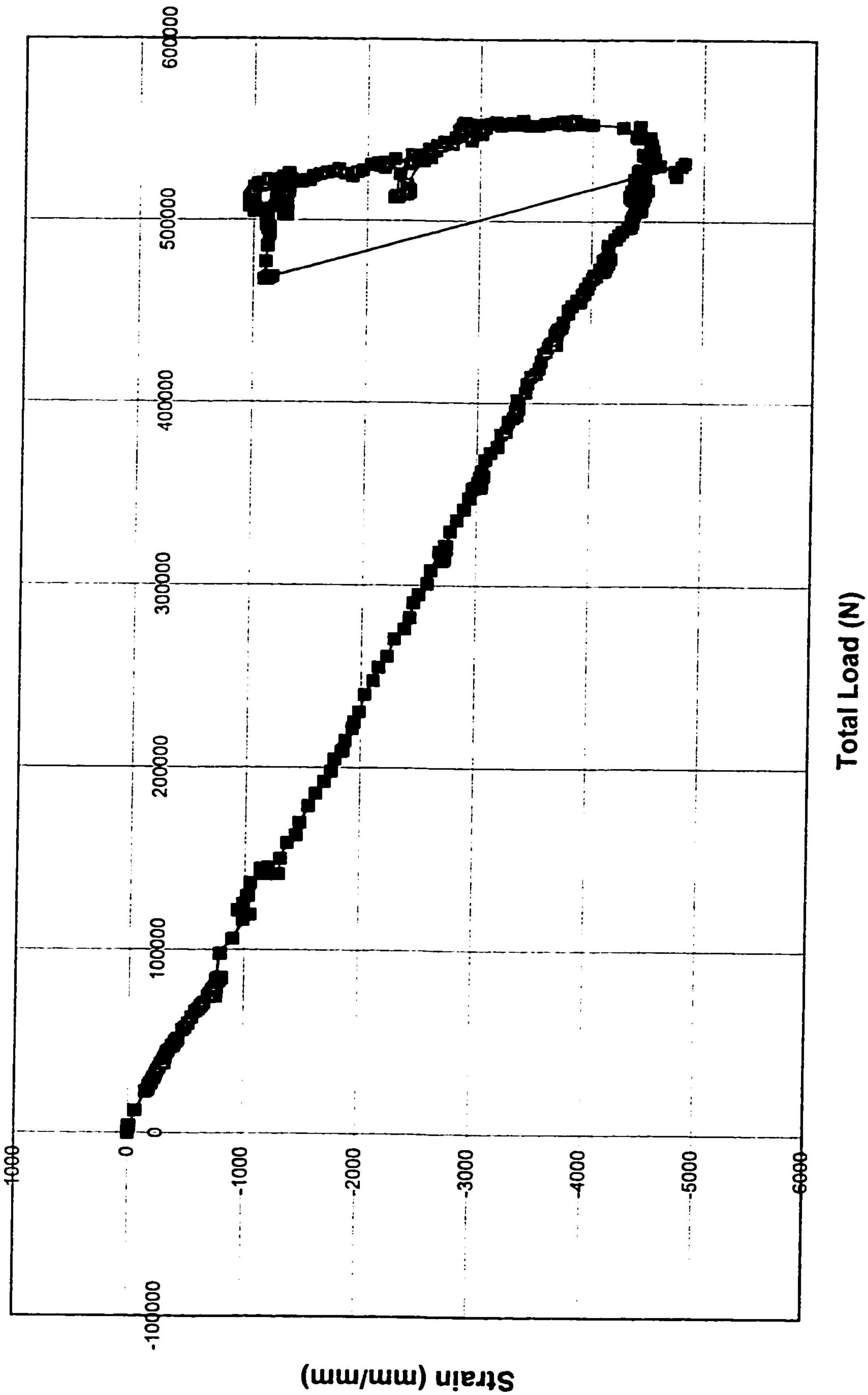

Strain (mm/mm)
Total Load (N)
-100000
0
100000
200000
300000
400000
500000
600000
1000
0
-1000
-2000
-3000
-4000
-5000
-6000

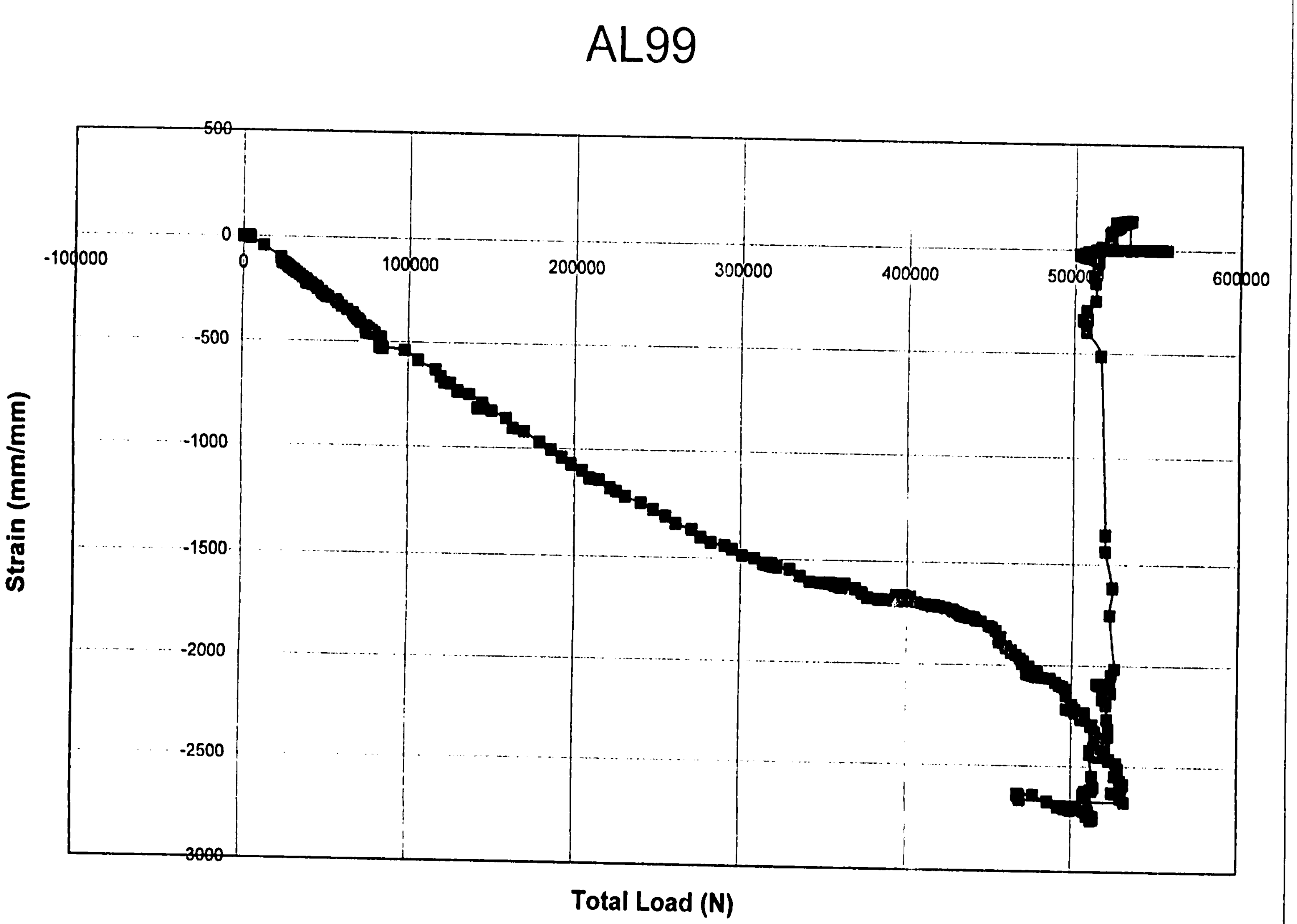
AL99
Strain (mm/mm)
500
0
-500
-1000
-1500
-2000
-2500
-3000
-100000
0
100000
200000
300000
400000
500000
600000
Total Load (N)

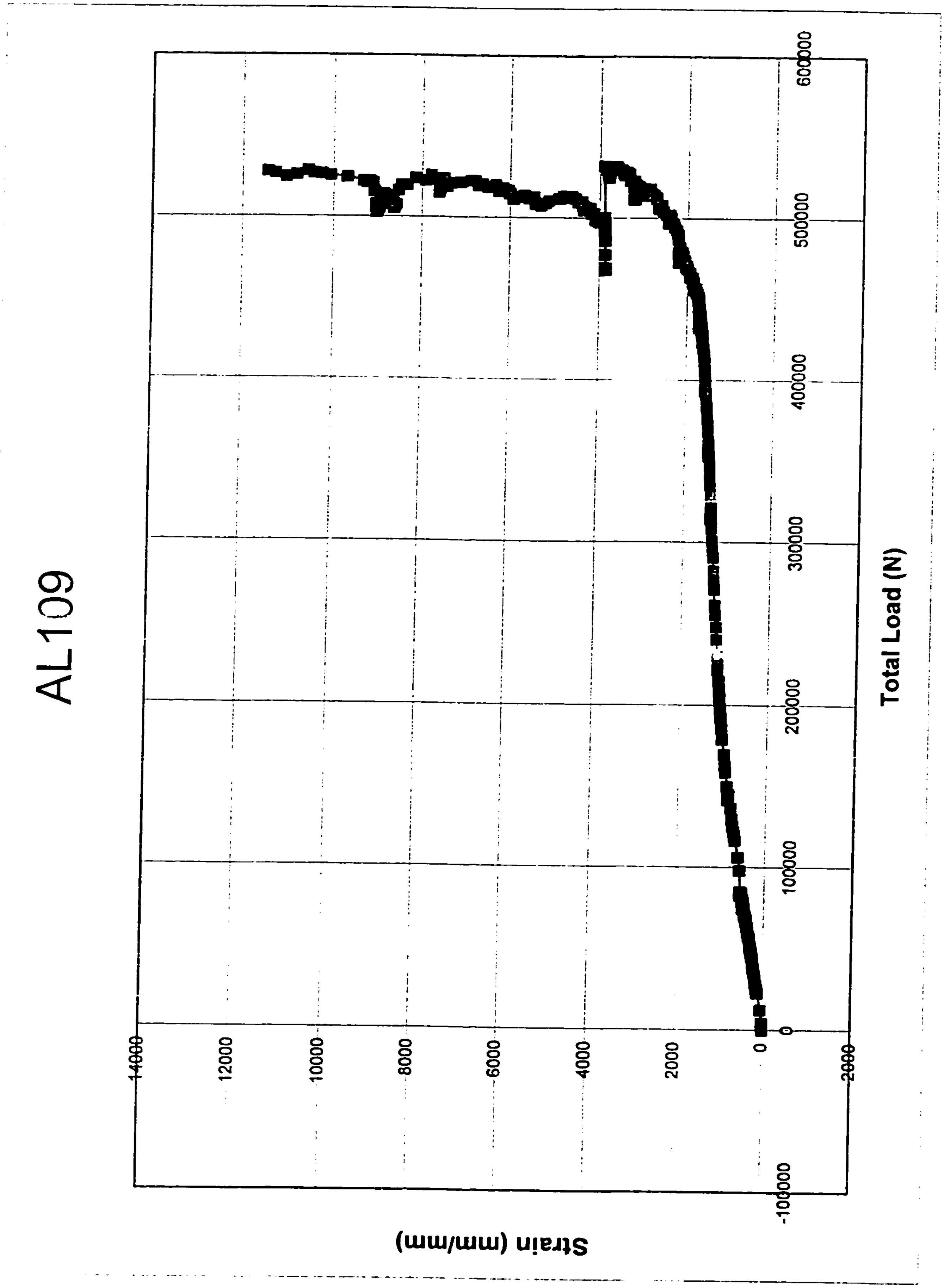
AL109
Strain (mm/mm)
14000
12000
10000
8000
6000
4000
2000
0
-2000
Total Load (N)
-100000
0
100000
200000
300000
400000
500000
600000

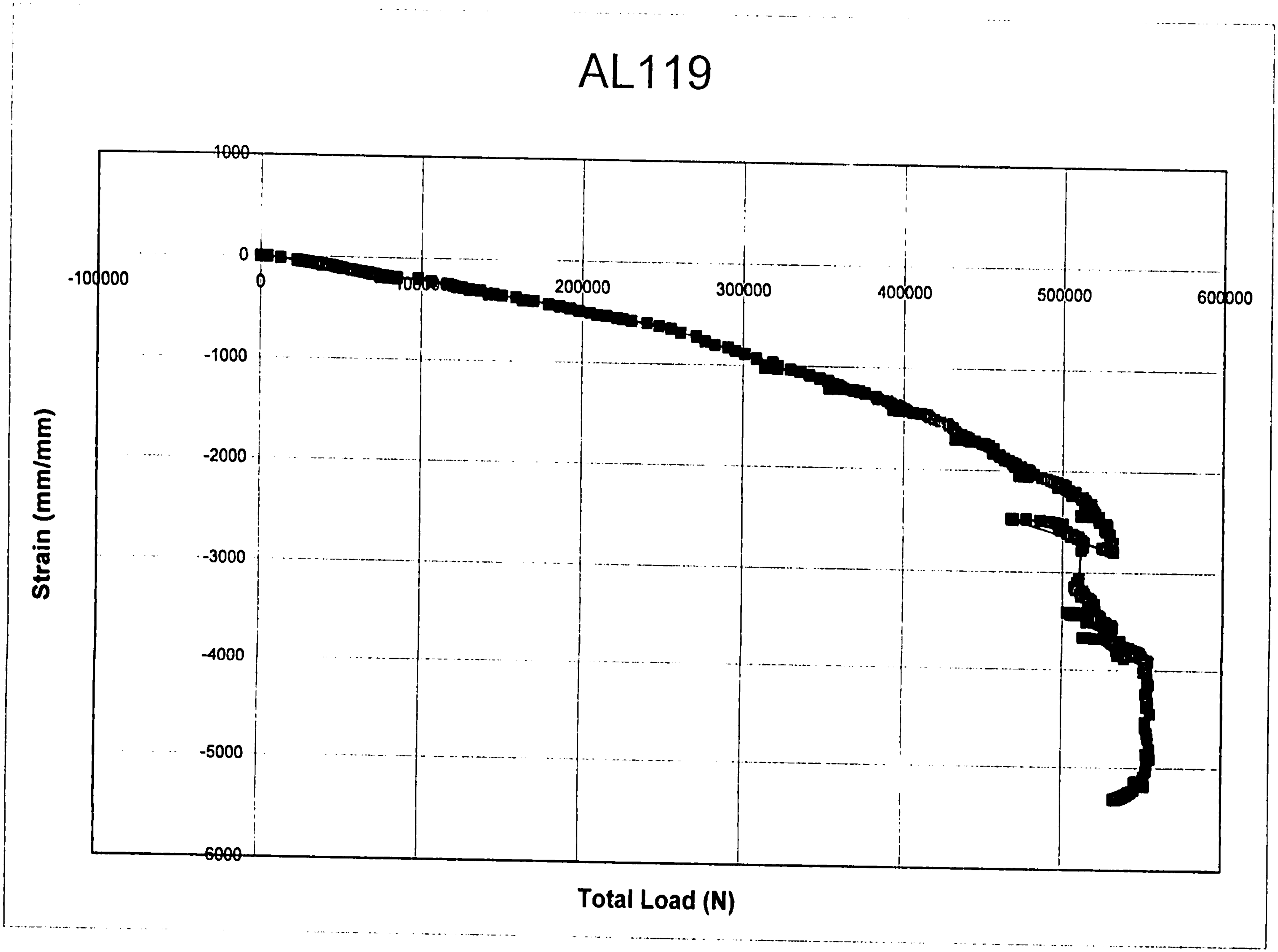
AL119
1000
0
-1000
-2000
-3000
-4000
-5000
-6000
-100000
0
100000
200000
300000
400000
500000
600000
Strain (mm/mm)
Total Load (N)

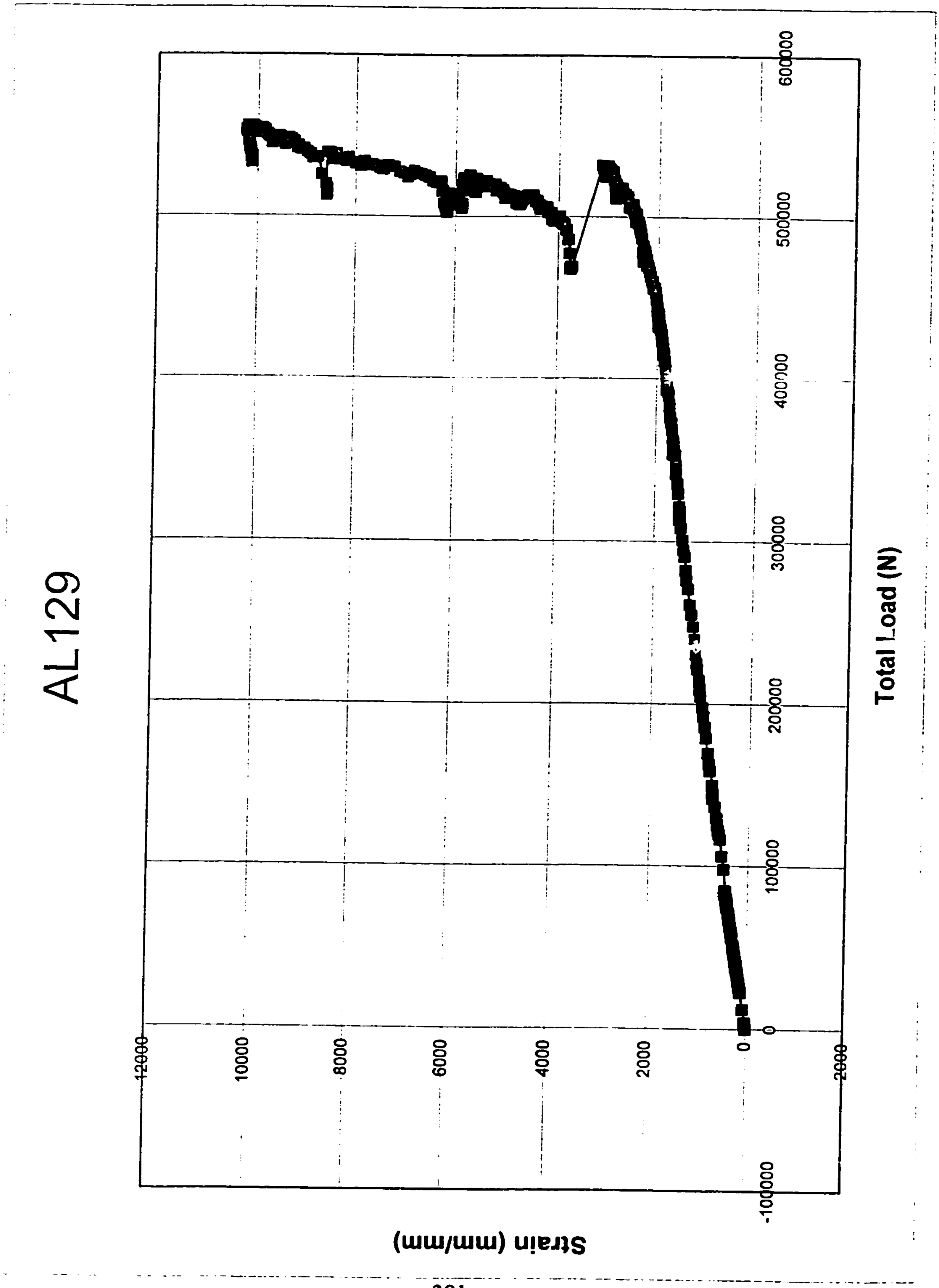
AL129
Strain (mm/mm)
Total Load (N)
-2000
0
2000
4000
6000
8000
10000
12000
-100000
0
100000
200000
300000
400000
500000
600000

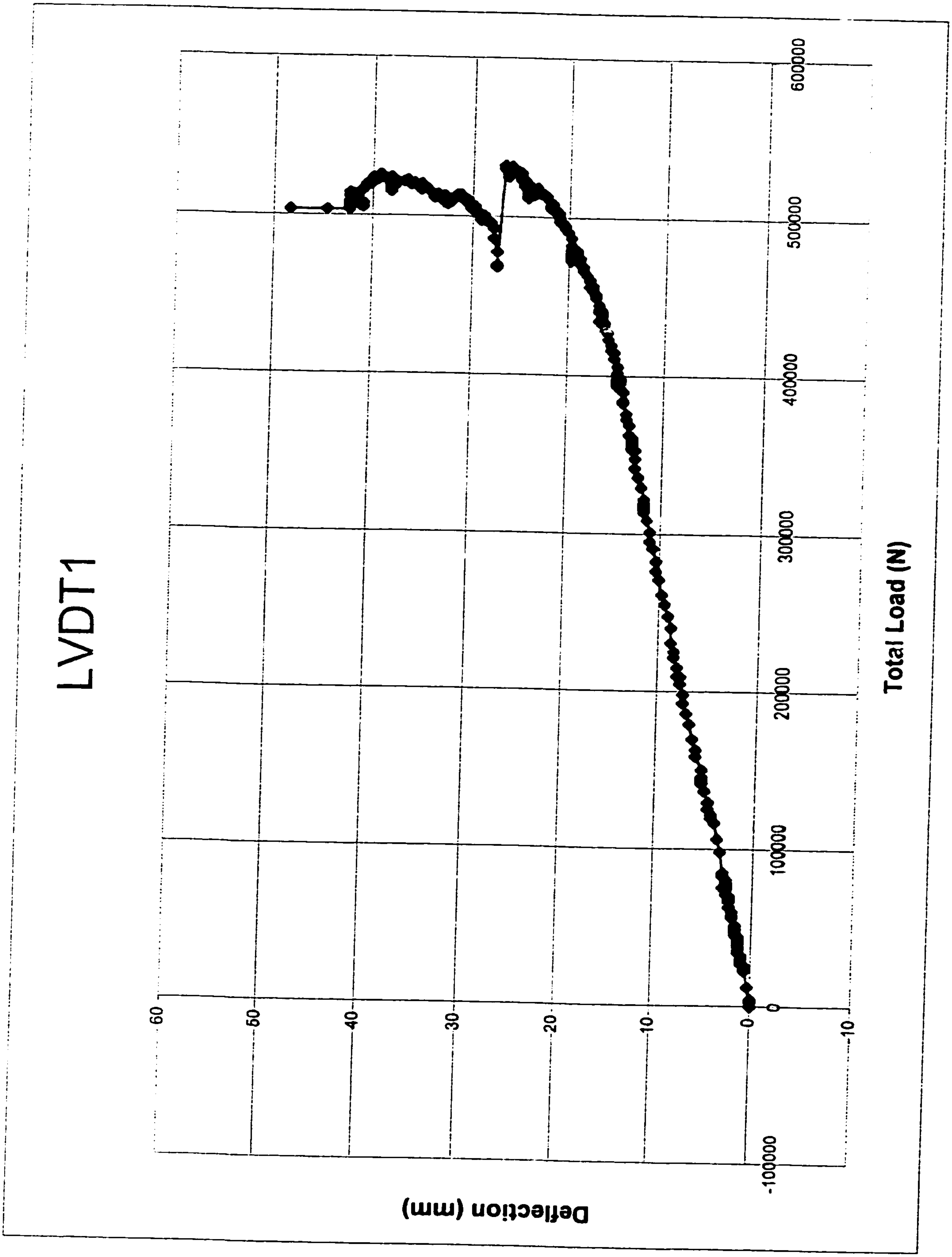
LVDT1
Deflection (mm)
Total Load (N)
60
50
40
30
20
10
0
-10
-100000
0
100000
200000
300000
400000
500000
600000

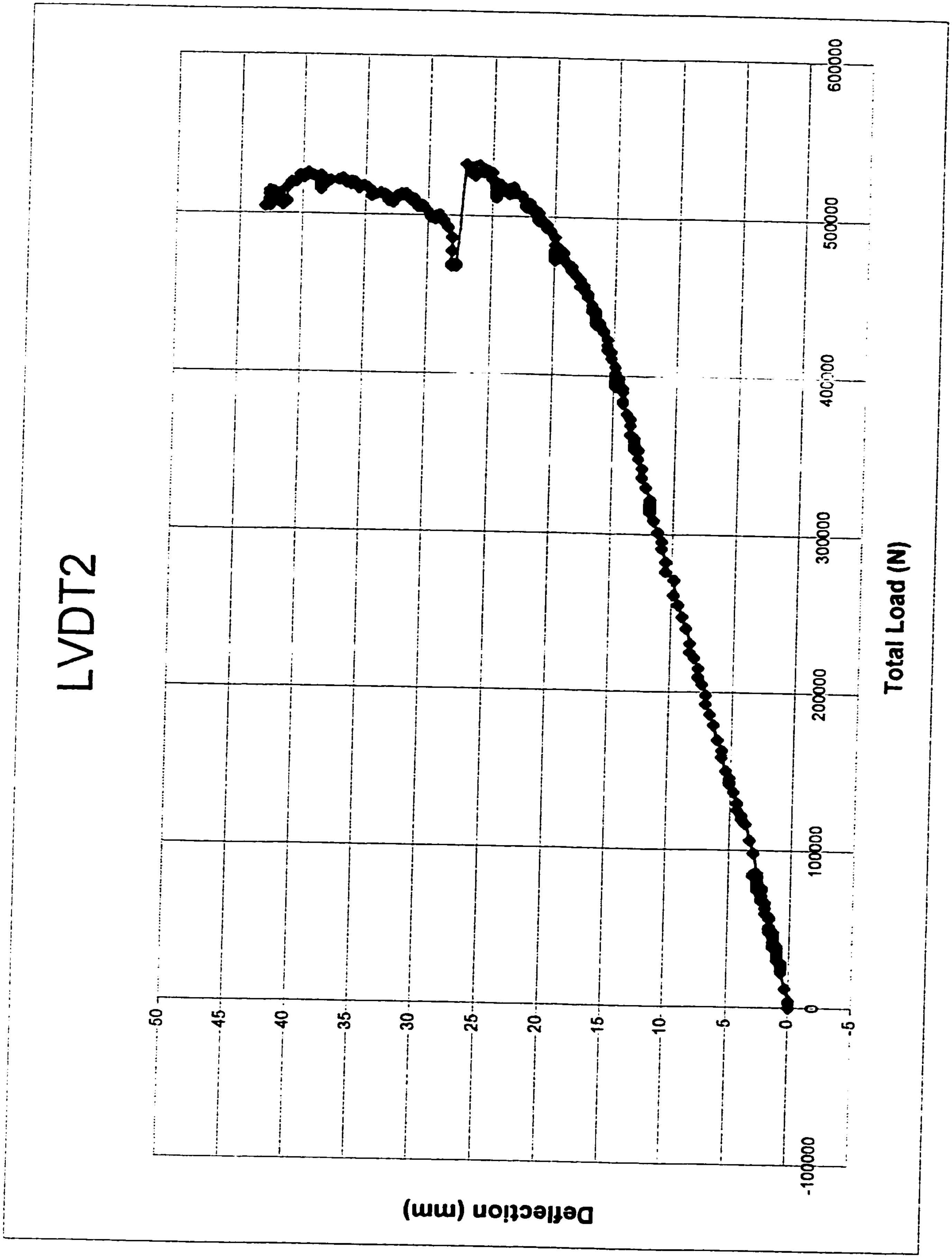
LVDT2
Deflection (mm)
Total Load (N)
50
45
40
35
30
25
20
15
10
5
0
-5
-100000
0
100000
200000
300000
400000
500000
600000

Appendix D

A Sample of Input Data of an Analytical Bridge Model

```
TITLE Nonlinear Analysis of Continuous Composite Curved Box-Girder Bridges
C*
C* COSMOS/M     Geostar V1.75
C* Problem . AL2D1        Date : 8-17-97  Time : 07:14:42
C*
C* FILE,CB4AL1D1.SES,1,1,1,1,
PT,1,-37.91461864,43.22882943,1.425,
PT,2,-28.02384856,31.95174349,1.425,
PT,3,-36.92554163,42.10112083,0,
PT,4,-34.94738761,39.84570364,0,
PT,5,-32.9692336,37.59028646,0,
PT,6,-30.99107958,35.33486927,0,
PT,7,-29.01292557,33 07945208,0,
PT,8,-36 92554163,42.10112083,1.3,
PT,9,-34.94738761,39.84570364,1.3,
PT,10,-32.9692336,37.59028646,1.3,
PT,11,-30.99107958,35.33486927,1.3,
PT,12,-29.01292557,33.07945208,1.3,
PT,13,-37.25523397,42.4770237,1.3,
PT,14,-36.59584929,41.72521797,1.3,
PT,15,-35.27[illegible]0.221[illegible]51,1.3,
PT,16,-34.61769528,39.46980078,1.3,
PT,17,-33.29892593,37.96618932,1.3,
PT,18,-32.63954126,37.21438359,1.3,
PT,19,-31.32077192,35 71077213,1.3,
PT,20,-30 66[illegible]725,34.95896[illegible],1.3,
PT,21,-29.3426179,33.45535495,1.3,
PT,22,-28.68323323,32.70354922,1.3,
PT,23,37.91461864,43.22882943,1.425,
PT,24,28.02384856,31.95174349,1.425,
PT,25,36.92554163,42.10112083,0,
PT,26,34.94738761,39.84570364,0,
PT,27,32.9692336,37.59028646,0,
PT,28,30.99107958,35.33486927,0,
PT,29,29.01292557,33.07945208,0,
PT,30,36.92554163,42 10112083,1.3,
PT,31,34.94738761,39.84570364,1.3,
PT,32,32.9692336,37.59028646,1.3,
PT,33,30.99107958,35.33486927,1.3,
PT,34,29.01292557,33.07945208,1.3,
PT,35,37.25523397,42.4770237,1.3,
PT,36,36.59584929,41.72521797,1.3,
PT,37,35.27707995,40.22160651,1.3,
PT,38,34.61769528,39.46980078,1.3,
PT,39,33.29892593,37.96618932,1.3,
PT,40,32.63954126,37.21438359,1.3,
PT,41,31.32077192,35.71077213,1.3,
PT,42,30.66138725,34.95896641,1.3,
PT,43,29.3426179,33.45535495,1.3,
PT,44,28.68323323,32.70354922,1.3,
PT,45,0,56,1.3,
PT,46,0,44,1.3,
PT,47,0,56,0,
PT,48,0,44,0,
PT,49,0,50,0,
PT,50,0,0,0,
PT,51,0,0,1.3,
PT,52,0,0,1.425,
CRARC,1,2,24,52,42.5,
CRARC,2,1,23,52,57.5,
CRARC,3,12,34,51,44,
CRARC,4,11,33,51,47,
CRARC,5,10,32,51,50,
CRARC,6,9,31,51,53,
CRARC,7,8,30,51,56,
CRARC,8,22,44,51,43.5,
CRARC,9,21,43,51,44.5,
CRARC,10,20,42,51,46.5,
CRARC,11,19,41,51,47.5,
CRARC,12,18,40,51,49.5,
```

```
CRARC,13,17,39,51,50.5,
CRARC,14,16,38,51,52.5,
CRARC,15,15,37,51,53.5,
CRARC,16,14,36,51,55.5,
CRARC,17,13,35,51,56.5,
CRARC,18,7,29,50,44,
CRARC,19,6,28,50,47,
CRARC,20,5,27,50,50,
CRARC,21,4,26,50,53,
CRARC,22,3,25,50,56,
CRLINE,23,2,1,
CRLINE,24,24,23,
CRLINE,25,7,3,
CRLINE,26,29,25,
CRLINE,27,12,7,
CRLINE,28,11,6,
CRLINE,29,10,5,
CRLINE,30,9,4,
CRLINE,31,8,3,
CRLINE,32,34,29,
CRLINE,33,33,28,
CRLINE,34,32,27,
CRLINE,35,31,26,
CRLINE,36,30,25,
CRLINE,37,22,21,
CRLINE,38,20,19,
CRLINE,39,18,17,
CRLINE,40,16,15,
CRLINE,41,14,13,
CRLINE,42,44,43,
CRLINE,43,42,41,
CRLINE,44,40,39,
CRLINE,45,38,37,
CRLINE,46,36,35,
CRLINE,47,46,45,
CRLINE,48,48,47,
CRLINE,49,46,48,
CRLINE,50,45,47,
SF4CR,1,25,18,26,22,0,
SF4CR,2,23,1,24,2,0,
SF4CR,3,27,18,32,3,0,
SF4CR,4,28,19,33,4,0,
SF4CR,5,29,20,34,5,0,
SF4CR,6,30,21,35,6,0,
SF4CR,7,31,22,36,7,0,
SF4CR,8,37,8,42,9,0,
SF4CR,9,38,10,43,11,0,
SF4CR,10,39,12,44,13,0,
SF4CR,11,40,14,45,15,0,
SF4CR,12,41,16,46,17,0,
CRLINE,51,12,8,
CRLINE,52,34,30,
SF4CR,13,27,25,31,51,0,
SF4CR,14,32,26,36,52,0,
SF4CR,15,49,48,50,47,0,
ACTSET,EG,1,
ACTSET,MP,1,
ACTSET,RC,1,
ACTSET,EG,2,
ACTSET,MP,2,
ACTSET,RC,2,
M_SF,1,1,1,4,8,60,1,1,
ACTSET,EG,3,
ACTSET,MP,3,
ACTSET,RC,3,
M_SF,3,7,1,4,4,60,1,1,
NMERGE,1,2074,1,0.002,0,0,0,
NCOMPRESS,1,2074,
ACTSET,EG,4,
ACTSET,MP,4,
```

```
ACTSET,RC,4,
M_SF,8,12,1,4,2,60,1,1,
NMERGE,1,2684,1,0.002,0,0,0,
NCOMPRESS,1,2684,
M_SF,13,15,1,4,4,8,1,1,
NMERGE,1,2514,1,0.002,0,0,0,
NCOMPRESS,1,2509,
EDELETE,2281,4000,1,
ACTSET,EG,5,
ACTSET,MP,5,
ACTSET,RC,5,
M_SF,13,15,1,4,4,8,1,1,
NMERGE,1,2514,1,0.002,0,0,0,
NCOMPRESS,1,2509,
ACTSET,EG,1,
ACTSET,MP,1,
ACTSET,RC,1,
M_SF,2,2,1,4,10,60,1,1,
ACTSET,EG,6,
ACTSET,MP,6,
ACTSET,RC,6,
EL,2977,CR,0,3,553,2429,2430,0,0,0,0,0,0,
EL,2978,CR,0,3,557,2440,2441,0,0,0,0,0,0,
EL,2979,CR,0,3,561,2451,2452,0,0,0,0,0,0,
EL,2980,CR,0,3,565,2462,2463,0,0,0,0,0,0,
EL,2981,CR,0,3,569,2473,2474,0,0,0,0,0,0,
EL,2982,CR,0,3,573,2484,2485,0,0,0,0,0,0,
EL,2983,CR,0,3,577,2495,2496,0,0,0,0,0,0,
EL,2984,CR,0,3,581,2506,2507,0,0,0,0,0,0,
EL,2985,CR,0,3,585,2517,2518,0,0,0,0,0,0,
EL,2986,CR,0,3,589,2528,2529,0,0,0,0,0,0,
EL,2987,CR,0,3,593,2539,2540,0,0,0,0,0,0,
EL,2988,CR,0,3,597,2550,2551,0,0,0,0,0,0,
EL,2989,CR,0,3,601,2561,2562,0,0,0,0,0,0,
EL,2990,CR,0,3,605,2572,2573,0,0,0,0,0,0,
EL,2991,CR,0,3,609,2583,2584,0,0,0,0,0,0,
EL,2992,CR,0,3,613,2594,2595,0,0,0,0,0,0,
EL,2993,CR,0,3,617,2605,2606,0,0,0,0,0,0,
EL,2994,CR,0,3,621,2616,2617,0,0,0,0,0,0,
EL,2995,CR,0,3,625,2627,2628,0,0,0,0,0,0,
EL,2996,CR,0,3,629,2638,2639,0,0,0,0,0,0,
EL,2997,CR,0,3,633,2649,2650,0,0,0,0,0,0,
EL,2998,CR,0,3,637,2660,2661,0,0,0,0,0,0,
EL,2999,CR,0,3,641,2671,2672,0,0,0,0,0,0,
EL,3000,CR,0,3,645,2682,2683,0,0,0,0,0,0,
EL,3001,CR,0,3,649,2693,2694,0,0,0,0,0,0,
EL,3002,CR,0,3,653,2704,2705,0,0,0,0,0,0,
EL,3003,CR,0,3,657,2715,2716,0,0,0,0,0,0,
EL,3004,CR,0,3,661,2726,2727,0,0,0,0,0,0,
EL,3005,CR,0,3,665,2737,2738,0,0,0,0,0,0,
EL,3006,CR,0,3,669,2748,2749,0,0,0,0,0,0,
EL,3007,CR,0,3,673,2759,2760,0,0,0,0,0,0,
EL,3008,CR,0,3,677,2770,2771,0,0,0,0,0,0,
EL,3009,CR,0,3,681,2781,2782,0,0,0,0,0,0,
EL,3010,CR,0,3,685,2792,2793,0,0,0,0,0,0,
EL,3011,CR,0,3,689,2803,2804,0,0,0,0,0,0,
EL,3012,CR,0,3,693,2814,2815,0,0,0,0,0,0,
EL,3013,CR,0,3,697,2825,2826,0,0,0,0,0,0,
EL,3014,CR,0,3,701,2836,2837,0,0,0,0,0,0,
EL,3015,CR,0,3,705,2847,2848,0,0,0,0,0,0,
EL,3016,CR,0,3,709,2858,2859,0,0,0,0,0,0,
EL,3017,CR,0,3,713,2869,2870,0,0,0,0,0,0,
EL,3018,CR,0,3,717,2880,2881,0,0,0,0,0,0,
EL,3019,CR,0,3,721,2891,2892,0,0,0,0,0,0,
EL,3020,CR,0,3,725,2902,2903,0,0,0,0,0,0,
EL,3021,CR,0,3,729,2913,2914,0,0,0,0,0,0,
EL,3022,CR,0,3,733,2924,2925,0,0,0,0,0,0,
EL,3023,CR,0,3,737,2935,2936,0,0,0,0,0,0,
EL,3024,CR,0,3,741,2946,2947,0,0,0,0,0,0,
EL,3025,CR,0,3,745,2957,2958,0,0,0,0,0,0,
```

EL,3026,CR,0,3,749,2968,2969,0,0,0,0,0,0,
EL,3027,CR,0,3,753,2979,2980,0,0,0,0,0,0,
EL,3028,CR,0,3,757,2990,2991,0,0,0,0,0,0,
EL,3029,CR,0,3,761,3001,3002,0,0,0,0,0,0,
EL,3030,CR,0,3,765,3012,3013,0,0,0,0,0,0,
EL,3031,CR,0,3,769,3023,3024,0,0,0,0,0,0,
EL,3032,CR,0,3,773,3034,3035,0,0,0,0,0,0,
EL,3033,CR,0,3,777,3045,3046,0,0,0,0,0,0,
EL,3034,CR,0,3,781,3056,3057,0,0,0,0,0,0,
EL,3035,CR,0,3,785,3067,3068,0,0,0,0,0,0,
EL,3036,CR,0,3,789,3078,3079,0,0,0,0,0,0,
EL,3037,CR,0,3,793,3089,3090,0,0,0,0,0,0,
EL,3038,CR,0,3,797,2431,2432,0,0,0,0,0,0,
EL,3039,CR,0,3,801,2442,2443,0,0,0,0,0,0,
EL,3040,CR,0,3,805,2453,2454,0,0,0,0,0,0,
EL,3041,CR,0,3,809,2464,2465,0,0,0,0,0,0,
EL,3042,CR,0,3,813,2475,2476,0,0,0,0,0,0,
EL,3043,CR,0,3,817,2486,2487,0,0,0,0,0,0,
EL,3044,CR,0,3,821,2497,2498,0,0,0,0,0,0,
EL,3045,CR,0,3,825,2508,2509,0,0,0,0,0,0,
EL,3046,CR,0,3,829,2519,2520,0,0,0,0,0,0,
EL,3047,CR,0,3,833,2530,2531,0,0,0,0,0,0,
EL,3048,CR,0,3,837,2541,2542,0,0,0,0,0,0,
EL,3049,CR,0,3,841,2552,2553,0,0,0,0,0,0,
EL,3050,CR,0,3,845,2563,2564,0,0,0,0,0,0,
EL,3051,CR,0,3,849,2574,2575,0,0,0,0,0,0,
EL,3052,CR,0,3,853,2585,2586,0,0,0,0,0,0,
EL,3053,CR,0,3,857,2596,2597,0,0,0,0,0,0,
EL,3054,CR,0,3,861,2607,2608,0,0,0,0,0,0,
EL,3055,CR,0,3,865,2618,2619,0,0,0,0,0,0,
EL,3056,CR,0,3,869,2629,2630,0,0,0,0,0,0,
EL,3057,CR,0,3,873,2640,2641,0,0,0,0,0,0,
EL,3058,CR,0,3,877,2651,2652,0,0,0,0,0,0,
EL,3059,CR,0,3,881,2662,2663,0,0,0,0,0,0,
EL,3060,CR,0,3,885,2673,2674,0,0,0,0,0,0,
EL,3061,CR,0,3,889,2684,2685,0,0,0,0,0,0,
EL,3062,CR,0,3,893,2695,2696,0,0,0,0,0,0,
EL,3063,CR,0,3,897,2706,2707,0,0,0,0,0,0,
EL,3064,CR,0,3,901,2717,2718,0,0,0,0,0,0,
EL,3065,CR,0,3,905,2728,2729,0,0,0,0,0,0,
EL,3066,CR,0,3,909,2739,2740,0,0,0,0,0,0,
EL,3067,CR,0,3,913,2750,2751,0,0,0,0,0,0,
EL,3068,CR,0,3,917,2761,2762,0,0,0,0,0,0,
EL,3069,CR,0,3,921,2772,2773,0,0,0,0,0,0,
EL,3070,CR,0,3,925,2783,2784,0,0,0,0,0,0,
EL,3071,CR,0,3,929,2794,2795,0,0,0,0,0,0,
EL,3072,CR,0,3,933,2805,2806,0,0,0,0,0,0,
EL,3073,CR,0,3,937,2816,2817,0,0,0,0,0,0,
EL,3074,CR,0,3,941,2827,2828,0,0,0,0,0,0,
EL,3075,CR,0,3,945,2838,2839,0,0,0,0,0,0,
EL,3076,CR,0,3,949,2849,2850,0,0,0,0,0,0,
EL,3077,CR,0,3,953,2860,2861,0,0,0,0,0,0,
EL,3078,CR,0,3,957,2871,2872,0,0,0,0,0,0,
EL,3079,CR,0,3,961,2882,2883,0,0,0,0,0,0,
EL,3080,CR,0,3,965,2893,2894,0,0,0,0,0,0,
EL,3081,CR,0,3,969,2904,2905,0,0,0,0,0,0,
EL,3082,CR,0,3,973,2915,2916,0,0,0,0,0,0,
EL,3083,CR,0,3,977,2926,2927,0,0,0,0,0,0,
EL,3084,CR,0,3,981,2937,2938,0,0,0,0,0,0,
EL,3085,CR,0,3,985,2948,2949,0,0,0,0,0,0,
EL,3086,CR,0,3,989,2959,2960,0,0,0,0,0,0,
EL,3087,CR,0,3,993,2970,2971,0,0,0,0,0,0,
EL,3088,CR,0,3,997,2981,2982,0,0,0,0,0,0,
EL,3089,CR,0,3,1001,2992,2993,0,0,0,0,0,0,
EL,3090,CR,0,3,1005,3003,3004,0,0,0,0,0,0,
EL,3091,CR,0,3,1009,3014,3015,0,0,0,0,0,0,
EL,3092,CR,0,3,1013,3025,3026,0,0,0,0,0,0,
EL,3093,CR,0,3,1017,3036,3037,0,0,0,0,0,0,
EL,3094,CR,0,3,1021,3047,3048,0,0,0,0,0,0,
EL,3095,CR,0,3,1025,3058,3059,0,0,0,0,0,0,

EL,3096,CR,0,3,1029,3069,3070,0,0,0,0,0,0,
EL,3097,CR,0,3,1033,3080,3081,0,0,0,0,0,0,
EL,3098,CR,0,3,1037,3091,3092,0,0,0,0,0,0,
EL,3099,CR,0,3,1041,2433,2434,0,0,0,0,0,0,
EL,3100,CR,0,3,1045,2444,2445,0,0,0,0,0,0,
EL,3101,CR,0,3,1049,2455,2456,0,0,0,0,0,0,
EL,3102,CR,0,3,1053,2466,2467,0,0,0,0,0,0,
EL,3103,CR,0,3,1057,2477,2478,0,0,0,0,0,0,
EL,3104,CR,0,3,1061,2488,2489,0,0,0,0,0,0,
EL,3105,CR,0,3,1065,2499,2500,0,0,0,0,0,0,
EL,3106,CR,0,3,1069,2510,2511,0,0,0,0,0,0,
EL,3107,CR,0,3,1073,2521,2522,0,0,0,0,0,0,
EL,3108,CR,0,3,1077,2532,2533,0,0,0,0,0,0,
EL,3109,CR,0,3,1081,2543,2544,0,0,0,0,0,0,
EL,3110,CR,0,3,1085,2554,2555,0,0,0,0,0,0,
EL,3111,CR,0,3,1089,2565,2566,0,0,0,0,0,0,
EL,3112,CR,0,3,1093,2576,2577,0,0,0,0,0,0,
EL,3113,CR,0,3,1097,2587,2588,0,0,0,0,0,0,
EL,3114,CR,0,3,1101,2598,2599,0,0,0,0,0,0,
EL,3115,CR,0,3,1105,2609,2610,0,0,0,0,0,0,
EL,3116,CR,0,3,1109,2620,2621,0,0,0,0,0,0,
EL,3117,CR,0,3,1113,2631,2632,0,0,0,0,0,0,
EL,3118,CR,0,3,1117,2642,2643,0,0,0,0,0,0,
EL,3119,CR,0,3,1121,2653,2654,0,0,0,0,0,0,
EL,3120,CR,0,3,1125,2664,2665,0,0,0,0,0,0,
EL,3121,CR,0,3,1129,2675,2676,0,0,0,0,0,0,
EL,3122,CR,0,3,1133,2686,2687,0,0,0,0,0,0,
EL,3123,CR,0,3,1137,2697,2698,0,0,0,0,0,0,
EL,3124,CR,0,3,1141,2708,2709,0,0,0,0,0,0,
EL,3125,CR,0,3,1145,2719,2720,0,0,0,0,0,0,
EL,3126,CR,0,3,1149,2730,2731,0,0,0,0,0,0,
EL,3127,CR,0,3,1153,2741,2742,0,0,0,0,0,0,
EL,3128,CR,0,3,1157,2752,2753,0,0,0,0,0,0,
EL,3129,CR,0,3,1161,2763,2764,0,0,0,0,0,0,
EL,3130,CR,0,3,1165,2774,2775,0,0,0,0,0,0,
EL,3131,CR,0,3,1169,2785,2786,0,0,0,0,0,0,
EL,3132,CR,0,3,1173,2796,2797,0,0,0,0,0,0,
EL,3133,CR,0,3,1177,2807,2808,0,0,0,0,0,0,
EL,3134,CR,0,3,1181,2818,2819,0,0,0,0,0,0,
EL,3135,CR,0,3,1185,2829,2830,0,0,0,0,0,0,
EL,3136,CR,0,3,1189,2840,2841,0,0,0,0,0,0,
EL,3137,CR,0,3,1193,2851,2852,0,0,0,0,0,0,
EL,3138,CR,0,3,1197,2862,2863,0,0,0,0,0,0,
EL,3139,CR,0,3,1201,2873,2874,0,0,0,0,0,0,
EL,3140,CR,0,3,1205,2884,2885,0,0,0,0,0,0,
EL,3141,CR,0,3,1209,2895,2896,0,0,0,0,0,0,
EL,3142,CR,0,3,1213,2906,2907,0,0,0,0,0,0,
EL,3143,CR,0,3,1217,2917,2918,0,0,0,0,0,0,
EL,3144,CR,0,3,1221,2928,2929,0,0,0,0,0,0,
EL,3145,CR,0,3,1225,2939,2940,0,0,0,0,0,0,
EL,3146,CR,0,3,1229,2950,2951,0,0,0,0,0,0,
EL,3147,CR,0,3,1233,2961,2962,0,0,0,0,0,0,
EL,3148,CR,0,3,1237,2972,2973,0,0,0,0,0,0,
EL,3149,CR,0,3,1241,2983,2984,0,0,0,0,0,0,
EL,3150,CR,0,3,1245,2994,2995,0,0,0,0,0,0,
EL,3151,CR,0,3,1249,3005,3006,0,0,0,0,0,0,
EL,3152,CR,0,3,1253,3016,3017,0,0,0,0,0,0,
EL,3153,CR,0,3,1257,3027,3028,0,0,0,0,0,0,
EL,3154,CR,0,3,1261,3038,3039,0,0,0,0,0,0,
EL,3155,CR,0,3,1265,3049,3050,0,0,0,0,0,0,
EL,3156,CR,0,3,1269,3060,3061,0,0,0,0,0,0,
EL,3157,CR,0,3,1273,3071,3072,0,0,0,0,0,0,
EL,3158,CR,0,3,1277,3082,3083,0,0,0,0,0,0,
EL,3159,CR,0,3,1281,3093,3094,0,0,0,0,0,0,
EL,3160,CR,0,3,1285,2435,2436,0,0,0,0,0,0,
EL,3161,CR,0,3,1289,2446,2447,0,0,0,0,0,0,
EL,3162,CR,0,3,1293,2457,2458,0,0,0,0,0,0,
EL,3163,CR,0,3,1297,2468,2469,0,0,0,0,0,0,
EL,3164,CR,0,3,1301,2479,2480,0,0,0,0,0,0,
EL,3165,CR,0,3,1305,2490,2491,0,0,0,0,0,0,

EL,3166,CR,0,3,1309,2501,2502,0,0,0,0,0,0,
EL,3167,CR,0,3,1313,2512,2513,0,0,0,0,0,0,
EL,3168,CR,0,3,1317,2523,2524,0,0,0,0,0,0,
EL,3169,CR,0,3,1321,2534,2535,0,0,0,0,0,0,
EL,3170,CR,0,3,1325,2545,2546,0,0,0,0,0,0,
EL,3171,CR,0,3,1329,2556,2557,0,0,0,0,0,0,
EL,3172,CR,0,3,1333,2567,2568,0,0,0,0,0,0,
EL,3173,CR,0,3,1337,2578,2579,0,0,0,0,0,0,
EL,3174,CR,0,3,1341,2589,2590,0,0,0,0,0,0,
EL,3175,CR,0,3,1345,2600,2601,0,0,0,0,0,0,
EL,3176,CR,0,3,1349,2611,2612,0,0,0,0,0,0,
EL,3177,CR,0,3,1353,2622,2623,0,0,0,0,0,0,
EL,3178,CR,0,3,1357,2633,2634,0,0,0,0,0,0,
EL,3179,CR,0,3,1361,2644,2645,0,0,0,0,0,0,
EL,3180,CR,0,3,1365,2655,2656,0,0,0,0,0,0,
EL,3181,CR,0,3,1369,2666,2667,0,0,0,0,0,0,
EL,3182,CR,0,3,1373,2677,2678,0,0,0,0,0,0,
EL,3183,CR,0,3,1377,2688,2689,0,0,0,0,0,0,
EL,3184,CR,0,3,1381,2699,2700,0,0,0,0,0,0,
EL,3185,CR,0,3,1385,2710,2711,0,0,0,0,0,0,
EL,3186,CR,0,3,1389,2721,2722,0,0,0,0,0,0,
EL,3187,CR,0,3,1393,2732,2733,0,0,0,0,0,0,
EL,3188,CR,0,3,1397,2743,2744,0,0,0,0,0,0,
EL,3189,CR,0,3,1401,2754,2755,0,0,0,0,0,0,
EL,3190,CR,0,3,1405,2765,2766,0,0,0,0,0,0,
EL,3191,CR,0,3,1409,2776,2777,0,0,0,0,0,0,
EL,3192,CR,0,3,1413,2787,2788,0,0,0,0,0,0,
EL,3193,CR,0,3,1417,2798,2799,0,0,0,0,0,0,
EL,3194,CR,0,3,1421,2809,2810,0,0,0,0,0,0,
EL,3195,CR,0,3,1425,2820,2821,0,0,0,0,0,0,
EL,3196,CR,0,3,1429,2831,2832,0,0,0,0,0,0,
EL,3197,CR,0,3,1433,2842,2843,0,0,0,0,0,0,
EL,3198,CR,0,3,1437,2853,2854,0,0,0,0,0,0,
EL,3199,CR,0,3,1441,2864,2865,0,0,0,0,0,0,
EL,3200,CR,0,3,1445,2875,2876,0,0,0,0,0,0,
EL,3201,CR,0,3,1449,2886,2887,0,0,0,0,0,0,
EL,3202,CR,0,3,1453,2897,2898,0,0,0,0,0,0,
EL,3203,CR,0,3,1457,2908,2909,0,0,0,0,0,0,
EL,3204,CR,0,3,1461,2919,2920,0,0,0,0,0,0,
EL,3205,CR,0,3,1465,2930,2931,0,0,0,0,0,0,
EL,3206,CR,0,3,1469,2941,2942,0,0,0,0,0,0,
EL,3207,CR,0,3,1473,2952,2953,0,0,0,0,0,0,
EL,3208,CR,0,3,1477,2963,2964,0,0,0,0,0,0,
EL,3209,CR,0,3,1481,2974,2975,0,0,0,0,0,0,
EL,3210,CR,0,3,1485,2985,2986,0,0,0,0,0,0,
EL,3211,CR,0,3,1489,2996,2997,0,0,0,0,0,0,
EL,3212,CR,0,3,1493,3007,3008,0,0,0,0,0,0,
EL,3213,CR,0,3,1497,3018,3019,0,0,0,0,0,0,
EL,3214,CR,0,3,1501,3029,3030,0,0,0,0,0,0,
EL,3215,CR,0,3,1505,3040,3041,0,0,0,0,0,0,
EL,3216,CR,0,3,1509,3051,3052,0,0,0,0,0,0,
EL,3217,CR,0,3,1513,3062,3063,0,0,0,0,0,0,
EL,3218,CR,0,3,1517,3073,3074,0,0,0,0,0,0,
EL,3219,CR,0,3,1521,3084,3085,0,0,0,0,0,0,
EL,3220,CR,0,3,1525,3095,3096,0,0,0,0,0,0,
EL,3221,CR,0,3,1529,2437,2438,0,0,0,0,0,0,
EL,3222,CR,0,3,1533,2448,2449,0,0,0,0,0,0,
EL,3223,CR,0,3,1537,2459,2460,0,0,0,0,0,0,
EL,3224,CR,0,3,1541,2470,2471,0,0,0,0,0,0,
EL,3225,CR,0,3,1545,2481,2482,0,0,0,0,0,0,
EL,3226,CR,0,3,1549,2492,2493,0,0,0,0,0,0,
EL,3227,CR,0,3,1553,2503,2504,0,0,0,0,0,0,
EL,3228,CR,0,3,1557,2514,2515,0,0,0,0,0,0,
EL,3229,CR,0,3,1561,2525,2526,0,0,0,0,0,0,
EL,3230,CR,0,3,1565,2536,2537,0,0,0,0,0,0,
EL,3231,CR,0,3,1569,2547,2548,0,0,0,0,0,0,
EL,3232,CR,0,3,1573,2558,2559,0,0,0,0,0,0,
EL,3233,CR,0,3,1577,2569,2570,0,0,0,0,0,0,
EL,3234,CR,0,3,1581,2580,2581,0,0,0,0,0,0,
EL,3235,CR,0,3,1585,2591,2592,0,0,0,0,0,0,

```
EL,3236,CR,0,3,1589,2602,2603,0,0,0,0,0,0,
EL,3237,CR,0,3,1593,2613,2614,0,0,0,0,0,0,
EL,3238,CR,0,3,1597,2624,2625,0,0,0,0,0,0,
EL,3239,CR,0,3,1601,2635,2636,0,0,0,0,0,0,
EL,3240,CR,0,3,1605,2646,2647,0,0,0,0,0,0,
EL,3241,CR,0,3,1609,2657,2658,0,0,0,0,0,0,
EL,3242,CR,0,3,1613,2668,2669,0,0,0,0,0,0,
EL,3243,CR,0,3,1617,2679,2680,0,0,0,0,0,0,
EL,3244,CR,0,3,1621,2690,2691,0,0,0,0,0,0,
EL,3245,CR,0,3,1625,2701,2702,0,0,0,0,0,0,
EL,3246,CR,0,3,1629,2712,2713,0,0,0,0,0,0,
EL,3247,CR,0,3,1633,2723,2724,0,0,0,0,0,0,
EL,3248,CR,0,3,1637,2734,2735,0,0,0,0,0,0,
EL,3249,CR,0,3,1641,2745,2746,0,0,0,0,0,0,
EL,3250,CR,0,3,1645,2756,2757,0,0,0,0,0,0,
EL,3251,CR,0,3,1649,2767,2768,0,0,0,0,0,0,
EL,3252,CR,0,3,1653,2778,2779,0,0,0,0,0,0,
EL,3253,CR,0,3,1657,2789,2790,0,0,0,0,0,0,
EL,3254,CR,0,3,1661,2800,2801,0,0,0,0,0,0,
EL,3255,CR,0,3,1665,2811,2812,0,0,0,0,0,0,
EL,3256,CR,0,3,1669,2822,2823,0,0,0,0,0,0,
EL,3257,CR,0,3,1673,2833,2834,0,0,0,0,0,0,
EL,3258,CR,0,3,1677,2844,2845,0,0,0,0,0,0,
EL,3259,CR,0,3,1681,2855,2856,0,0,0,0,0,0,
EL,3260,CR,0,3,1685,2866,2867,0,0,0,0,0,0,
EL,3261,CR,0,3,1689,2877,2878,0,0,0,0,0,0,
EL,3262,CR,0,3,1693,2888,2889,0,0,0,0,0,0,
EL,3263,CR,0,3,1697,2899,2900,0,0,0,0,0,0,
EL,3264,CR,0,3,1701,2910,2911,0,0,0,0,0,0,
EL,3265,CR,0,3,1705,2921,2922,0,0,0,0,0,0,
EL,3266,CR,0,3,1709,2932,2933,0,0,0,0,0,0,
EL,3267,CR,0,3,1713,2943,2944,0,0,0,0,0,0,
EL,3268,CR,0,3,1717,2954,2955,0,0,0,0,0,0,
EL,3269,CR,0,3,1721,2965,2966,0,0,0,0,0,0,
EL,3270,CR,0,3,1725,2976,2977,0,0,0,0,0,0,
EL,3271,CR,0,3,1729,2987,2988,0,0,0,0,0,0,
EL,3272,CR,0,3,1733,2998,2999,0,0,0,0,0,0,
EL,3273,CR,0,3,1737,3009,3010,0,0,0,0,0,0,
EL,3274,CR,0,3,1741,3020,3021,0,0,0,0,0,0,
EL,3275,CR,0,3,1745,3031,3032,0,0,0,0,0,0,
EL,3276,CR,0,3,1749,3042,3043,0,0,0,0,0,0,
EL,3277,CR,0,3,1753,3053,3054,0,0,0,0,0,0,
EL,3278,CR,0,3,1757,3064,3065,0,0,0,0,0,0,
EL,3279,CR,0,3,1761,3075,3076,0,0,0,0,0,0,
EL,3280,CR,0,3,1765,3086,3087,0,0,0,0,0,0,
EL,3281,CR,0,3,1769,3097,3098,0,0,0,0,0,0,
DND,1,UZ,0,9,2,,
DND,541,UZ,0,549,2,,
DND,275,UZ,0,275,1,RZ,UX,UY,,
ACTSET,EG,7,
ACTSET,MP,7,
ACTSET,RC,7,
EL,3282,CR,0,3,569,2473,2474,0,0,0,0,0,0,
EL,3283,CR,0,3,813,2475,2476,0,0,0,0,0,0,
EL,3284,CR,0,3,1057,2477,2478,0,0,0,0,0,0,
EL,3285,CR,0,3,1301,2479,2480,0,0,0,0,0,0,
EL,3286,CR,0,3,1545,2481,2482,0,0,0,0,0,0,
EL,3287,CR,0,3,593,2539,2540,0,0,0,0,0,0,
EL,3288,CR,0,3,837,2541,2542,0,0,0,0,0,0,
EL,3289,CR,0,3,1081,2543,2544,0,0,0,0,0,0,
EL,3290,CR,0,3,1325,2545,2546,0,0,0,0,0,0,
EL,3291,CR,0,3,1569,2547,2548,0,0,0,0,0,0,
EL,3292,CR,0,3,613,2594,2595,0,0,0,0,0,0,
EL,3293,CR,0,3,857,2596,2597,0,0,0,0,0,0,
EL,3294,CR,0,3,1101,2598,2599,0,0,0,0,0,0,
EL,3295,CR,0,3,1345,2600,2601,0,0,0,0,0,0,
EL,3296,CR,0,3,1589,2602,2603,0,0,0,0,0,0,
EL,3297,CR,0,3,617,2605,2606,0,0,0,0,0,0,
EL,3298,CR,0,3,861,2607,2608,0,0,0,0,0,0,
EL,3299,CR,0,3,1105,2609,2610,0,0,0,0,0,0,
```

```
EL,3300,CR,0,3,1349,2611,2612,0,0,0,0,0,0,
EL,3301,CR,0,3,1593,2613,2614,0,0,0,0,0,0,
EL,3302,CR,0,3,629,2638,2639,0,0,0,0,0,0,
EL,3303,CR,0,3,873,2640,2641,0,0,0,0,0,0,
EL,3304,CR,0,3,1117,2642,2643,0,0,0,0,0,0,
EL,3305,CR,0,3,1361,2644,2645,0,0,0,0,0,0,
EL,3306,CR,0,3,1605,2646,2647,0,0,0,0,0,0,
EL,3307,CR,0,3,717,2880,2881,0,0,0,0,0,0,
EL,3308,CR,0,3,961,2882,2883,0,0,0,0,0,0,
EL,3309,CR,0,3,1205,2884,2885,0,0,0,0,0,0,
EL,3310,CR,0,3,1449,2886,2887,0,0,0,0,0,0,
EL,3311,CR,0,3,1693,2888,2889,0,0,0,0,0,0,
EL,3312,CR,0,3,729,2913,2914,0,0,0,0,0,0,
EL,3313,CR,0,3,973,2915,2916,0,0,0,0,0,0,
EL,3314,CR,0,3,1217,2917,2918,0,0,0,0,0,0,
EL,3315,CR,0,3,1461,2919,2920,0,0,0,0,0,0,
EL,3316,CR,0,3,1705,2921,2922,0,0,0,0,0,0,
EL,3317,CR,0,3,733,2924,2925,0,0,0,0,0,0,
EL,3318,CR,0,3,977,2926,2927,0,0,0,0,0,0,
EL,3319,CR,0,3,1221,2928,2929,0,0,0,0,0,0,
EL,3320,CR,0,3,1465,2930,2931,0,0,0,0,0,0,
EL,3321,CR,0,3,1709,2932,2933,0,0,0,0,0,0,
EL,3322,CR,0,3,753,2979,2980,0,0,0,0,0,0,
EL,3323,CR,0,3,997,2981,2982,0,0,0,0,0,0,
EL,3324,CR,0,3,1241,2983,2984,0,0,0,0,0,0,
EL,3325,CR,0,3,1485,2985,2986,0,0,0,0,0,0,
EL,3326,CR,0,3,1729,2987,2988,0,0,0,0,0,0,
EL,3327,CR,0,3,777,3045,3046,0,0,0,0,0,0,
EL,3328,CR,0,3,1021,3047,3048,0,0,0,0,0,0,
EL,3329,CR,0,3,1265,3049,3050,0,0,0,0,0,0,
EL,3330,CR,0,3,1509,3051,3052,0,0,0,0,0,0,
EL,3331,CR,0,3,1753,3053,3054,0,0,0,0,0,0,
EGROUP,1,SHELL4T,1,0,0,0,4,0,0,0,
EGROUP,2,SHELL4T,1,0,0,0,1,0,0,0,
EGROUP,3,SHELL4T,1,0,0,0,1,0,0,0,
EGROUP,4,SHELL4T,1,0,0,0,1,0,0,0,
EGROUP,5,SHELL4T,1,0,0,0,1,0,0,0,
EGROUP,6,BEAM3D,0,0,0,0,1,0,0,0,
EGROUP,7,TRUSS3D,0,0,0,0,1,0,0,0,
RCONST,1,1,1,6,0.25,0,0,0,0,0,
RCONST,2,2,1,6,0.01,0,0,0,0,0,
RCONST,3,3,1,6,0.01,0,0,0,0,0,
RCONST,4,4,1,6,0.006,0,0,0,0,0,
RCONST,5,5,1,6,0.02,0,0,0,0,0,
BMSECDEF,6,6,2,1,8,0.0574,0,0,0,0,0,0,0,
RCONST,7,7,1,4,0.04,0,0,0,
MPROP,1,NUXY,0.2,
MPROP,2,NUXY,0.2,
MPROP,3,NUXY,0.2,
MPROP,4,NUXY,0.2,
MPROP,5,NUXY,0.2,
MPROP,6,NUXY,0.2,
MPROP,7,NUXY,0.2,
MPROP,1,DENS,2500,
MPROP,2,DENS,7800,
MPROP,3,DENS,7800,
MPROP,4,DENS,7800,
MPROP,5,DENS,7800,
MPROP,6,DENS,7800,
MPROP,7,DENS,0,
MPCTYP,1,0,
MPCTYP,2,1,
MPCTYP,3,1,
MPCTYP,4,1,
MPCTYP,4,1,
MPCTYP,5,1,
MPCTYP,6,1,
MPCTYP,7,1,
MPC,7,0,1,0.00175,3.5E8,0.4,3.8E8,
MPC,6,0,1,0.044,4.1E8,0.4,4.1E8,
```

```
MPC,5,0,1,0.00175,3.5E8,0.4,3.8E8,
MPC,4,0,1,0.00175,3.5E8,0.4,3.8E8,
MPC,3,0,1,0.00175,3.5E8,0.4,3.8E8,
MPC,2,0,1,0.00175,3.5E8,0.4,3.8E8,
MPC,1,0,1,-4E-2,-3E7,-2.5E-3,-4E7,-1.25E-3,-4E7,0,0,2E-4,1E6,4E-2,1E4,&

ACTSET,EG,8,
ACTSET,MP,8,
ACTSET,RC,8,
EGROUP,8,BEAM3D,0,0,0,0,0,0,0,0,
MPROP,8,EX,2E11,NUXY,0.2,
RCONST,8,8,1,10,3.14,0.049,0.049,1,1,0,0,0,0.9,0.9,
PTGEN,1,49,49,1,0,0,0,5,
PTDEL,53,53,1,
PTGEN,1,49,49,1,0,0,0,-5,
CRLINE,53,49,53,
MA_CR,53,53,1,1,3,48,
NMERGE,275,3099,2824,0.01,0,0,0,
NCOMPRESS,1,3105,
EDELETE,3332,3336,1,
M_CR,53,53,1,3,1,1,48,
NMERGE,3099,275,2824,0.01,0,0,0,
NCOMPRESS,1,3101,
EGROUP,8,BEAM3D,0,0,0,0,0,0,0,0,
RCONST,8,8,11,4,0,0,0,1,
RCONST,8,8,4,10,1,1,1,0,1,0.9,0.9,0,0,0,
RESTART,0,
DNDEL,275,AL,275,1,
DND,3099,AL,0,3099,1,
NDELETE,3100,3100,1,
NCOMPRESS,1,3100,
FNDEL,1,AL,4000,1,
FND,2481,FZ,-7896,2473,8,
FND,2480,FZ,-6704,2474,6,
FND,2479,FZ,-6584,2475,4,
FND,2478,FZ,-5632,2476,2,
FND,2477,FZ,-10368,2477,1,
FND,2547,FZ,-9870,2539,8,
FND,2546,FZ,-8380,2540,6,
FND,2545,FZ,-8230,2541,4,
FND,2544,FZ,-7040,2542,2,
FND,2543,FZ,-12960,2543,1,
FND,2602,FZ,-7896,2594,8,
FND,2601,FZ,-6704,2595,6,
FND,2600,FZ,-6584,2596,4,
FND,2599,FZ,-5632,2597,2,
FND,2598,FZ,-10368,2598,1,
FND,2613,FZ,-7896,2605,8,
FND,2612,FZ,-6704,2606,6,
FND,2611,FZ,-6584,2607,4,
FND,2610,FZ,-5632,2608,2,
FND,2609,FZ,-10368,2609,1,
FND,2646,FZ,-2961,2638,8,
FND,2645,FZ,-2514,2639,6,
FND,2644,FZ,-2469,2640,4,
FND,2643,FZ,-2112,2641,2,
FND,2642,FZ,-3888,2642,1,
FND,2888,FZ,-2961,2880,8,
FND,2887,FZ,-2514,2881,6,
FND,2886,FZ,-2469,2882,4,
FND,2885,FZ,-2112,2883,2,
FND,2884,FZ,-3888,2884,1,
FND,2921,FZ,-7896,2913,8,
FND,2920,FZ,-6704,2914,6,
FND,2919,FZ,-6584,2915,4,
FND,2918,FZ,-5632,2916,2,
FND,2917,FZ,-10368,2917,1,
FND,2932,FZ,-7896,2924,8,
FND,2931,FZ,-6704,2925,6,
FND,2930,FZ,-6584,2926,4,
```

```
FND,2929,FZ,-5632,2927,2,
FND,2928,FZ,-10368,2928,1,
FND,2987,FZ,-9870,2979,8,
FND,2986,FZ,-8380,2980,6,
FND,2985,FZ,-8230,2981,4,
FND,2984,FZ,-7040,2982,2,
FND,2983,FZ,-12960,2983,1,
FND,3053,FZ,-7896,3045,8,
FND,3052,FZ,-6704,3046,6,
FND,3051,FZ,-6584,3047,4,
FND,3050,FZ,-5632,3048,2,
FND,3049,FZ,-10368,3049,1,
RCONST,5,5,1,1,0.08,
EGROUP,9,SHELL4T,1,0,0,0,1,0,0,0,
MPROP,9,NUXY,0.2,
RCONST,9,9,1,6,0.02,0,0,0,0,0,
MPCTYP,9,1,
MPC,9,0,1,1.75E-3,3.5E8,0.4,3.8E8,
PTND,54,54,
PTND,55,1549,
PTND,54,63,
PTND,55,1553,
PTND,56,55,
PTND,57,577,
PTND,58,117,
PTND,59,1577,
PTND,60,109,
PTND,61,601,
PTND,62,171,
PTND,63,1601,
PTND,64,163,
PTND,65,625,
PTND,66,225,
PTND,67,1625,
PTND,68,217,
PTND,69,649,
SF4PT,16,54,55,57,56,0,
SF4PT,17,58,59,61,60,0,
SF4PT,18,62,63,65,64,0,
SF4PT,19,66,67,69,68,0,
PTND,70,495,
PTND,71,1744,
PTND,71,1745,
PTND,72,487,
PTND,73,769,
PTND,74,441,
PTND,75,1721,
PTND,76,433,
PTND,77,745,
PTND,78,387,
PTND,79,1697,
PTND,80,379,
PTND,81,721,
PTND,82,333,
PTND,83,1673,
PTND,84,325,
PTND,85,697,
SF4PT,20,82,83,85,84,0,
SF4PT,21,78,79,81,80,0,
SF4PT,22,74,75,77,76,0,
SF4PT,23,70,71,73,72,0,
M_SF,16,23,1,4,4,8,1,1,
NMERGE,1,4000,1,0.005,0,0,0,
NCOMPRESS,1,3455,
ECOMPRESS,1,3588,
FNDEL,2790,AL,4000,1,
DND,275,UX,0,275,1,UY,RZ,,
PRINT_OPS,1,0,0,1,0,1,0,0,0,0,
NL_PRINT,1,0,0,0,0,0,0,
MPC,1,0,1,-4E-2,-4.2E7,-2.5E-3,-4.2E7,-1.25E-3,-4E7,0,0,2.5E-5,8E5,4E-&
```

```
2,8E5,
PRINT_NDSET,1,1,300,
PRINT_ELSET,1,100,100,
NL_CONTROL,2,0,100,1,150,5,1,0,0.5,
NL_AUTOSTEP,1,1E-008,0.5,5,
NL_PLOT,1,150,1,0,
A_NONLINEAR,S,1,1,20,0.004,0,N,0,0,1e+010,0.001,0.01,0,1,
REACTION,1,
RESTART,0,
```